NASA CR-135356
RI/RD78-114

NASA

FINAL REPORT

PREBURNER OF STAGED COMBUSTION ROCKET ENGINE

(NASA-CR-135356) PREBURNER OF STAGED COMBUSTION ROCKET ENGINE Final Report, Jul. 1975 - Dec. 1977 (Rocketdyne) 280 p
HC A13/MF A01 CSCL 21H

N78-24279

Unclas
G3/20 20766

by

M. C. Yost

Rockwell International

Rocketdyne Division

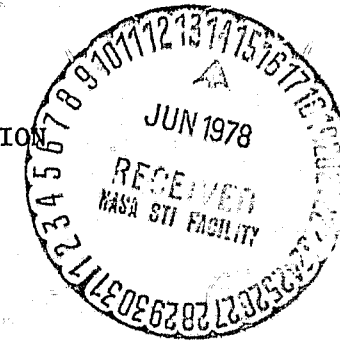

Prepared for

NATIONAL AERONAUTICS AND SPACE ADMINISTRATION

NASA-Lewis Research Center
Contract NAS3-19713
A. Pavli and H. Price
Project Manager

1. Report No.	2. Government Accession No.	3. Recipient's Catalog No.
NASA CR-135356		

4. Title and Subtitle	5. Report Date
PREBURNER OF STAGED COMBUSTION ROCKET ENGINE	February 1978
	6. Performing Organization Code

7. Author(s)	8. Performing Organization Report No.
M. C. Yost	RI/RD78-114
	10. Work Unit No.

9. Performing Organization Name and Address	11. Contract or Grant No.
Rockwell International Rocketdyne Division 6633 Canoga Avenue Canoga Park, CA 91304	NAS3-19713
	13. Type of Report and Period Covered Final (July 1975 - December 1977)

12. Sponsoring Agency Name and Address	14. Sponsoring Agency Code
National Aeronautics and Space Administration Washington, D.C. 20546	

15. Supplementary Notes

Project Managers, Albert Pavli and Harold Price
NASA-Lewis Research Center
Cleveland, Ohio 44135

16. Abstract

The components required for a high-pressure preburner, including injector, combustor, and ducting, were designed, fabricated, and tested with LOX and hydrogen. These components were then assembled with existing injector, thrust chamber, and nozzle components for testing as a staged combustion assembly. Testing at 400:1 nozzle expansion area ratio was conducted at simulated altitude conditions utilizing a self-pumping diffuser and a heated gaseous nitrogen ejector; testing at 8:1 expansion area ratio was at ground-level conditions. Diffuser/ejector operation was successful, and measured specific impulse performance, 4688 N-s/kg (478 sec), exceeded design goals. Nozzle boundary layer pressure and temperature measurements were made to evaluate boundary layer drag.

17. Key Words (Suggested by Author(s))		18. Distribution Statement
Staged combustion	Altitude simulation	
Preburner	Concentric element injection	
Spark ignition	Pressure rake	
Diffuser	Thrust chamber	
Ejector		
Nozzle flow		

19. Security Classif. (of this report)	20. Security Classif. (of this page)	21. No. of Pages	22. Price*
Unclassified	Unclassified	280	

* For sale by the National Technical Information Service, Springfield, Virginia 22151

Staged Combustion Engine Assembly

FOREWORD

The work herein was conducted by the Advanced Propulsion Engineering and the Engineering Test personnel at Rocketdyne, a division of Rockwell International, under Contract NAS3-19713 from July 1975 to December 1977. Mr. Albert Pavli and Mr. Harold Price, NASA Lewis Research Center, were NASA Project Managers, Mr. Harold Diem was Rocketdyne Program Manager, Mr. Anthony T. Zachary was Rocketdyne Project Manager, and Mr. Paul C. Dennies, Senior Project Engineer, and Mr. Max C. Yost, Project Engineer, were responsible for the technical direction of the program.

Important contributions to the conduct of the program and to the preparation of the report material were made by the following Rocketdyne personnel with their indicated area of responsibility:

Engineering Test	Mr. J. Pulte
Advanced Design	Mr. H. Marker
Aerothermodynamics	Mr. J. Shoji
Aerothermodynamics	Mr. W. Wagner

CONTENTS

ILLUSTRATIONS

TABLES

SUMMARY

The objective of this program was to provide the analysis, design, fabrication assembly and test of a regeneratively cooled LOX/hydrogen Staged Combustion Assembly System with a 400:1 expansion area ratio nozzle utilizing an 89 000 Newton (20 000 pound) thrust regeneratively cooled thrust chamber and 175:1 tubular nozzle fabricated and tested during an earlier program. The components for this assembly included two spark/torch oxygen-hydrogen igniters, two servo-controlled LOX valves, a preburner injector, a preburner combustor, a main propellant injector, a regeneratively cooled combustion chamber, a regeneratively cooled tubular nozzle with an expansion area ratio of 175:1, an uncooled heavy-wall steel nozzle with an expansion area ratio of 400:1, and interconnecting ducting. The analytical effort was performed to optimize the thermal and structural characteristics of each of the new components and the ducting, and to reverify the capabilities of the previously fabricated components.

The testing effort provided a demonstration of the preburner/combustor chamber operation, chamber combustion efficiency and stability, and chamber and nozzle heat transfer. Separate bypass cooling of the chamber and nozzle was performed to reduce test operations complexities and to provide for adequate component cooling during the chamber pressure start transient when the exhaust gas flow was separated from the nozzle wall. Measurement of the combustion performance indicated that chamber characteristic velocity efficiency (η_{c^*}) was 99.3%; specific impulse with the 400:1 nozzle was 4690 N-sec/kg (478.2 seconds).

The spark/torch oxygen-hydrogen igniter concept was established under NASA/LeRC direction and further developed by Rocketdyne. A small quantity of gaseous oxygen and gaseous hydrogen, introduced into a hydrogen cooled duct, are ignited by a high-energy spark to provide to the preburner and main combustion chambers a jet of hot gas capable of igniting the main propellant flows to each chamber.

The preburner injector was designed for liquid oxygen and gaseous hydrogen propellants with coaxial injection elements and a solid copper faceplate. The injector elements were designed to use hydrogen at 239 K (431 R), equivalent to the mixed mean temperature of the chamber and nozzle coolant outlet.

The preburner combustor was an Inconel 625 cylindrical shell with a gaseous hydrogen cooled inner liner. At the preburner exit the exhaust gas flow was divided into two ducts leading to the two high-pressure propellant turbopumps, or for the test series conducted on this program, to two turbine simulation orifices, and thence into the main combustion chamber injector.

The main propellant injector was a coaxial injection element unit with a porous Rigimesh faceplate, fabricated during a prior NASA/LeRC sponsored thrust chamber technology program. The injection elements were modified to utilize the fuel rich preburner exhaust gases as the fuel together with the remainder of the system liquid oxygen.

The regeneratively cooled combustion chamber was a zirconium copper alloy liner with machined longitudinal grooves for coolant passages and an electroformed nickel closeout shell that had been fabricated during the prior NASA/LeRC sponsored program. The chamber included a small part of the expansion nozzle to an area ratio of 8:1. The coolant manifolding provides capability for either regenerative or separate cooling.

The nozzle with the 175:1 expansion area ratio was fabricated with A286 tapered tubing with two-pass cooling and was capable of either regenerative or separate cooling. This component also was fabricated on the prior NASA/LeRC sponsored program.

The 400:1 nozzle extension was fabricated from mild steel sheet rolled to shape and butt welded. After welding and stress relieving, the nozzle inner contour and the exterior were machined to approximately 6.4 mm (0.25 inch) thickness. Pressure taps were provided in two rows along the length of the nozzle for measuring the static pressure profile. The nozzle was fabricated by NASA/LeRC and supplied to Rocketdyne for these tests.

The testing effort was performed in "building block" fashion, with each test series providing a foundation of understanding and preparation for the succeeding series. The initial testing was a series of 18 tests of the preburner igniter and preburner assembly to establish igniter operation and preburner sequencing and operation.

Staged combustion assembly testing was then performed to establish the operation of the preburner and main chamber operating as a unit. Combustion chamber performance, heat transfer characteristics, and thrust chamber starting transients were determined to provide a basis for establishing the start and operating sequences and parameters for the nozzle testing with the diffuser/ejector system. During these tests, final modification to the spark igniters was made to enhance their reliability and capability to function with minimum between-test inspection.

A series of blowdown tests of the diffuser/ejector system was performed to establish the ejector sequence timing, ejector pump-out capability, and GN_2 pressure and heater temperature capabilities. The completion of these blowdowns and the prior staged combustion assembly tests signalled the readiness to proceed into the 400:1 nozzle testing. The two nozzle components were installed on the staged combustion assembly and the entire system was aligned with the diffuser inlet.

The test series with the 400:1 nozzle started with an igniter system checkout, followed by a test of the preburner only and then a mainstage test of very short duration, 0.25 seconds. Staged combustion assembly system operation was satisfactory as was the GN_2 ejector operation, although the main chamber operating duration was too short for the diffuser to pump out the altitude capsule and the nozzle flow was separated from the wall throughout this test.

Three tests of 2.15, 2.65, and 2.80 seconds main chamber duration were performed during which full unseparated flow in the nozzle was realized and

steady-state capsule altitude pressures as low as 0.23 N/cm^2a (0.33 psia) were achieved. Main chamber pressures for these tests were as high as 1582 N/cm^2a (2294 psia), approximately 15% above the chamber rated chamber pressure. System operation was satisfactory during these tests and an average specific impulse of 478.2 seconds was measured. All three tests were of sufficient duration for all performance parameters to reach steady state, or very nearly so, and stabilized heat transfer, nozzle pressure, and diffuser measurements were obtained.

Additional testing, including three tests of 4.0, 5.0, and 5.2 seconds duration, was performed to obtain further performance, nozzle aerodynamics, and thrust chamber heat transfer information. Bypass cooling, with the hydrogen coolant passing first through the combustion chamber coolant jacket and then, in series, through the nozzle tubes, was used to obtain the extended duration testing. Main chamber pressures as high as 1376.6 N/cm^2a (2286.6 psia) were attained. Test data confirmed the specific impulse value achieved and heat transfer measurements conformed to prior test results.

INTRODUCTION

System studies conducted to determine the feasibility of developing a reusable vehicle for future NASA and Air Force orbital transfer and deep space maneuvering missions have shown that high-pressure, staged combustion cycle engines offer the highest specific impulse and payload capability. A review of the vehicle and engine system studies indicates that a single high area ratio bell nozzle, high chamber pressure, staged combustion cycle engine at 89 000 Newtons (20 000 pounds) thrust level is near optimum for the NASA and DOD mission requirements. The engine designed to meet these requirements has been designated the Advanced Space Engine (ASE).

This program was initiated to provide the required technology base for the subsequent development of a high performance, high expansion area ratio nozzle and staged combustion cycle rocket engine using a single fuel preburner and a liquid hydrogen cooled thrust chamber assembly.

Liquid hydrogen cooled and fueled rocket engine assemblies and components have been studied and developed by Rocketdyne and other agencies for many years. The particular design parameters utilized for this program were established by extrapolating from the Rocketdyne Space Shuttle Main Engine designs and the J-2 engine program to the ASE operating conditions. The thrust chamber operating conditions for this engine are shown in Table 1.

TABLE 1. THRUST CHAMBER OPERATING CONDITIONS

	Nominal Design Point
Thrust, N (pounds)	88 900 (20 000)
Chamber Pressure, N/cm^2a (psia)	1380 (2000)
Mixture Ratio (overall)	6.0
Nozzle Expansion Ratio	
Regeneratively Cooled	175:1
Uncooled	400:1
Propellant Inlet Temperature, K (R)	
Hydrogen	
To Injector	~278 (~500)
To Chamber	~50 (~90)
Oxygen	78 (140)
Propellant Inlet Pressure	
Hydrogen	TBD
Oxygen	TBD
Energy Release Efficiency (ERE), %	98

Technology items of interest developed during the course of the program include continued evaluation of the design parameters for the spark/torch igniter, the multielement preburner propellant injector, and the hydrogen cooled combustion chamber; installation and use of boundary layer pressure and temperature measurement devices at the exit of the 400:1 nozzle; and diffuser/ejector design and operation with the high expansion area ratio nozzles.

This report presents the design and analysis effort conducted on each component and subsystem; the fabrication effort; the testing of the preburner assembly, the staged combustion assembly, and the high area ratio nozzle with the diffuser/ejector system; the results from each phase of the testing; and analysis of the major and significant events of the program.

DISCUSSION

The Advanced Space Engine system uses a single preburner to provide the hot gas to power the high-pressure fuel and oxidizer turbopumps. The preburner receives liquid oxygen from the high-pressure oxygen turbopump and high-pressure gaseous hydrogen from the discharge of the thrust chamber upper coolant jacket, oxidizer boost pump turbine, and fuel boost pump turbine. The preburner injector introduces the well mixed propellants into the combustor and produces high performance and stable combustion. The preburner is directly attached to the inlet of the turbine on the high-pressure fuel turbopump. The hot-gas flow from the preburner is routed through a transition section where hot-gas flow for the high-pressure oxidizer turbopump is tapped off through a branching elbow. The balance of the hot gas flows into the turbine manifold on the high-pressure fuel turbopump. During this program, orifices were used to simulate the turbines and to provide the necessary pressure drop prior to distribution of the hot, fuel-rich gas to the main injector.

This section describes the design of the preburner injector, combustor, system ducting and assembly, and the design modifications to the igniters and the main propellant injector, including heat transfer and performance analyses necessary to complete the final designs.

DESIGN AND ANALYSIS

The preburner assembly (Fig. 1) is designed to operate through a tank-head, idle-mode start into mainstage at any operating point defined within the limits of the engine mixture ratio excursion from 5.5 to 6.5. The design point preburner operating parameters (mainstage engine mixture ratio 6.5) are given in Table 2.

The structural features of the preburner have been designed to meet the requirements of a service-free life of 60 thermal cycles or 2 hours accumulated run time, and a service life between overhauls of 300 thermal cycles or 10 hours accumulated run time.

TABLE 2. PREBURNER NOMINAL OPERATING PARAMETERS

Chamber Pressure, N/cm^2a (psia)	2328	(3377)
Combustion Temperature, K (R)	1053	(1896)
Mixture Ratio (o/f)		0.82
Total Flowrate, kg/s (lb/sec)	4.16	(9.18)
Fuel Inlet Temperature, K (R)	239	(431)
Oxidizer Inlet Temperature, K (R)	91	(163)

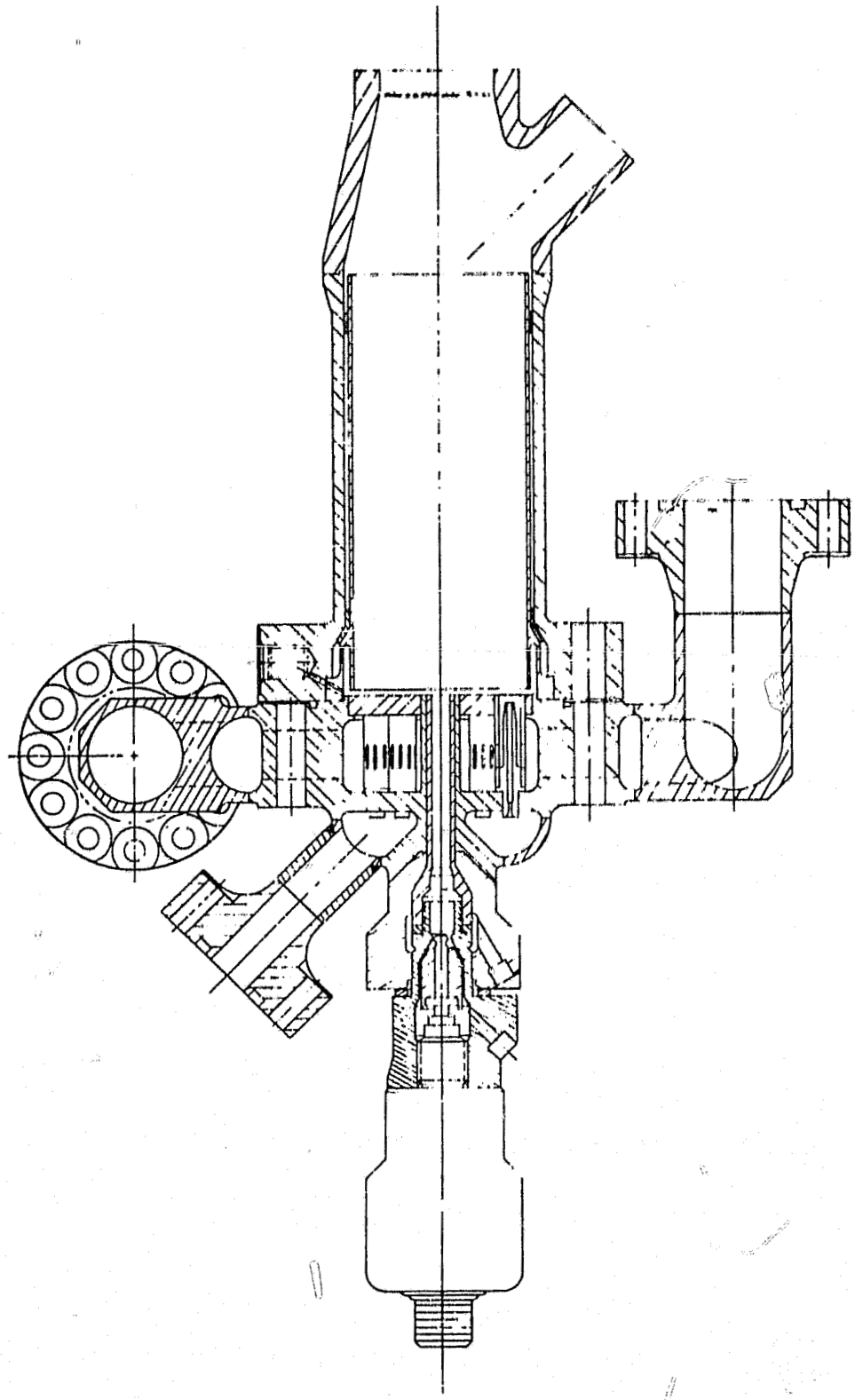

Figure 1. Preburner of Staged Combustion Rocket Engine

Ignition Systems

The ignition source for the preburner is a spark/torch igniter, Fig. 2, mounted in the center of the injector. This igniter location was selected over an igniter location in the combustor wall because it will not: (1) impinge high-temperature hot gas against the combustor wall, (2) interfere with the flow streams of the injector elements, (3) require an envelope in a high strain region of the preburner structure, and (4) compromise the use of a cooled liner and acoustic absorbers. The principal disadvantage of using a center mounted igniter is the potential for directing the high-temperature ignition flame into the turbine. To prevent this, the igniter was designed to operate at an overall mixture ratio equal to the preburner mixture ratio and a coaxial igniter exhaust nozzle was used to enhance mixing.

Igniter Design and Operation. A spark/torch ignition system was selected after a comprehensive review of the state-of-the-art ignition systems. The primary requirements of the ignition system are: (1) the igniters are to be capable of operating at start with cold propellants supplied at tank head/idle mode pressures producing repeatable, reliable ignition of the preburner and thrust chamber, and (2) the igniters are to be of a configuration which can meet the life requirements of the engine. The ignition systems considered to be the most applicable were the combustion wave igniter, the ASI (augmented spark igniter), and the spark/torch igniter. Each of these systems appeared to have potential for meeting the ignition system requirements; however, the spark/torch igniter appeared to be superior because of the potential for high spark electrode durability, predictable and repeatable ignition conditions at the spark electrode, and a higher temperature downstream of the igniter exit to enhance main propellant ignition. The igniters used in the preburner and thrust chamber were basically the same configuration.

The spark/torch igniter uses a spark plug, Fig. 3, and exciter assembly, Fig. 4, for ignition, an integral oxygen/hydrogen injector, and combustor/nozzle for ducting the hot gas to the injector, Fig. 5. Gaseous oxidizer is injected from an annular manifold around the spark electrode. A small amount of gaseous fuel is injected into the igniter combustor/nozzle where it mixes with the oxidizer downstream of the electrode producing an oxidizer-rich combustion (MR $\approx$ 40:1). The bulk of the igniter fuel flows around the nozzle, or tube liner, and is discharged at the injector face.

The igniter has the capability for rapid-reignition with minimum delay in the event of a flameout during the start transition. It also provides a high mixture ratio near the electrode for reliable ignition and produces a hot core for main propellant ignition. The extremely high mixture ratio of the hot core is also advantageous for main propellant ignition because combustion of the coolant hydrogen discharged from the liner drives the hot core temperature higher through the stoichiometric point before it is totally mixed with the igniter flow. Other advantages of the spark/torch igniter are: (1) the oxidizer flow around the electrode provides cooling for the electrode and minimizes the potential for erosion from combustion, and (2) the injection technique using impinging fuel streams below the electrode produces repeatable conditions for ignition.

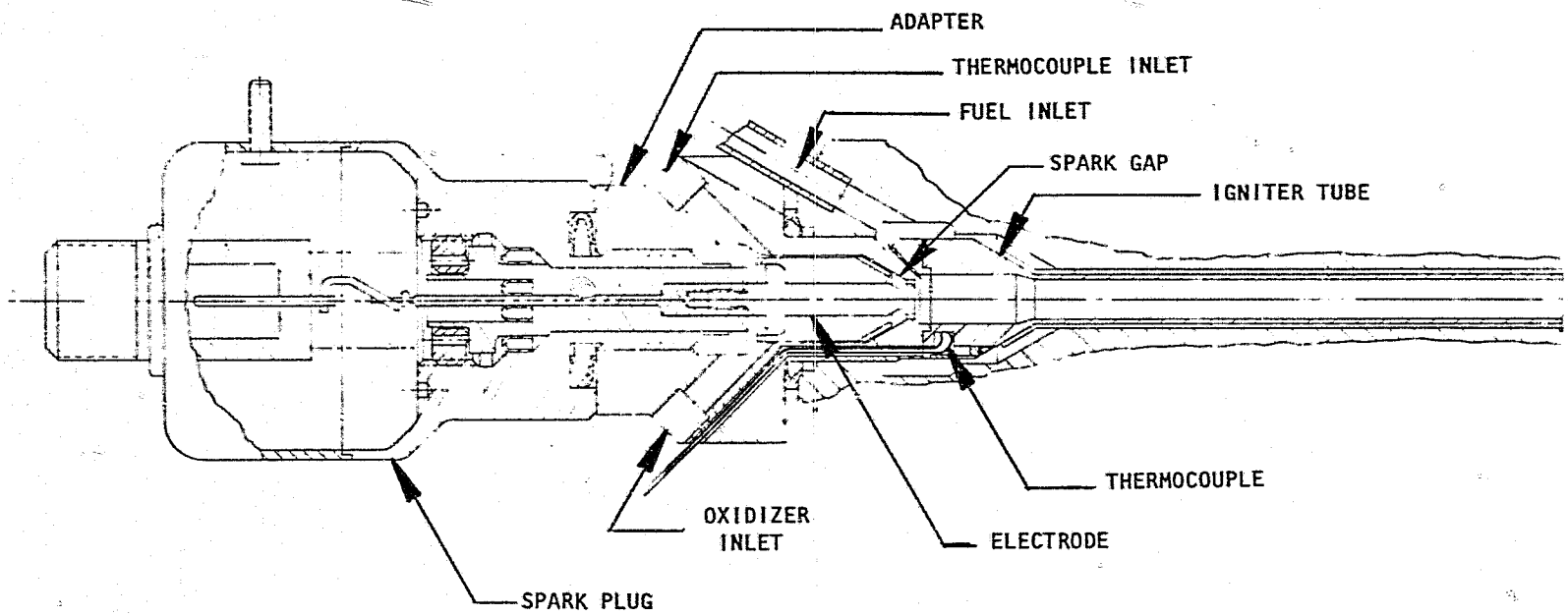

Figure 2. 20K Advanced Thrust Chamber Igniter Assembly

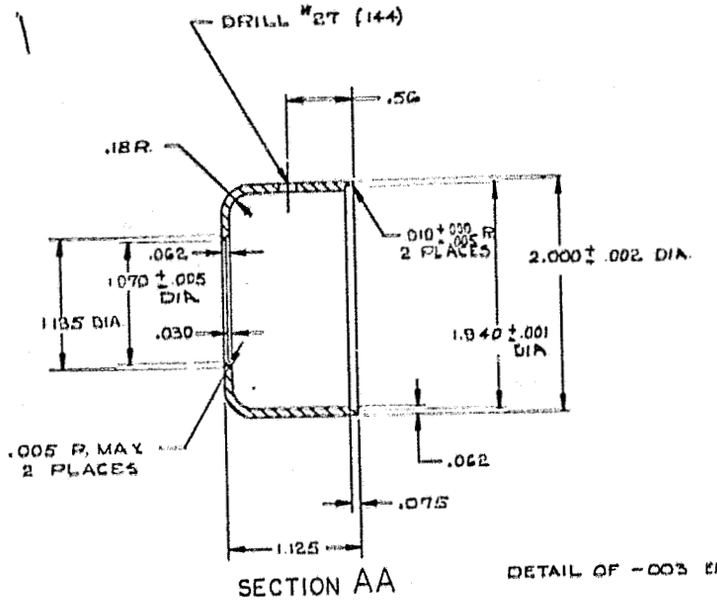

SECTION AA

DETAIL OF -003 ENCLOSURE

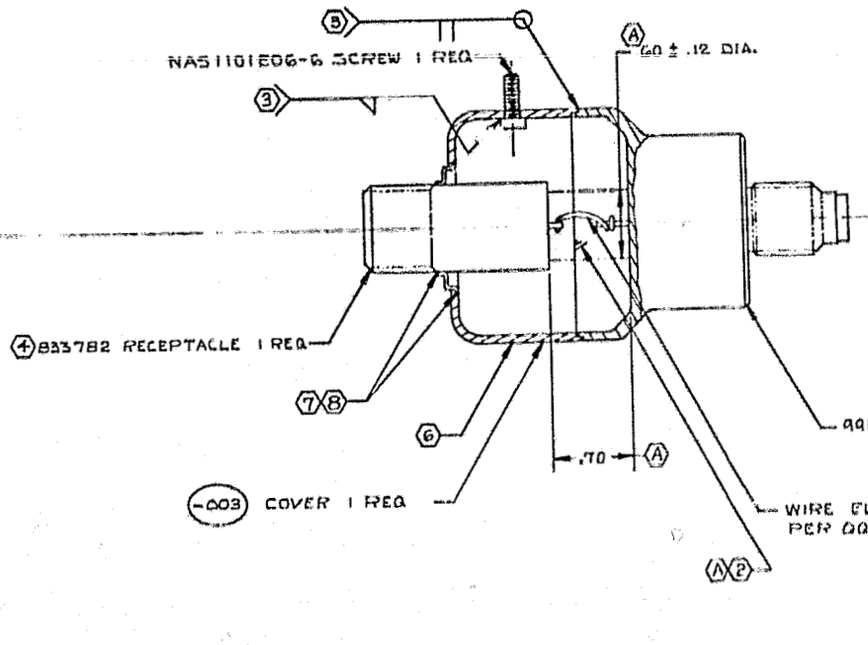

(3) PURGE WITH DRY NI
PRIOR TO SOLDERING
(7) SOLDER PER MIL-S-6
(6) ELECTROCHEMICAL ETC
(5) SOLDER PER RAD
(4) AMP INC CAPITRO
(3) WELD PER RADIC
(2) ENCAPSULATE PER
TYP III CLASS A
1. MACHINE PER RAD
NOTE: UNLESS

REVISIONS

ZONE	LTR	DESCRIPTION	DATE	APPROVED
		1. MAY BE REWORKED 3. RECORD CHANGE 2. CANNOT BE REWORKED 4. NOW SHOP PRACTICE 5. PARTS MADE OK		

FOLDOUT FRAME

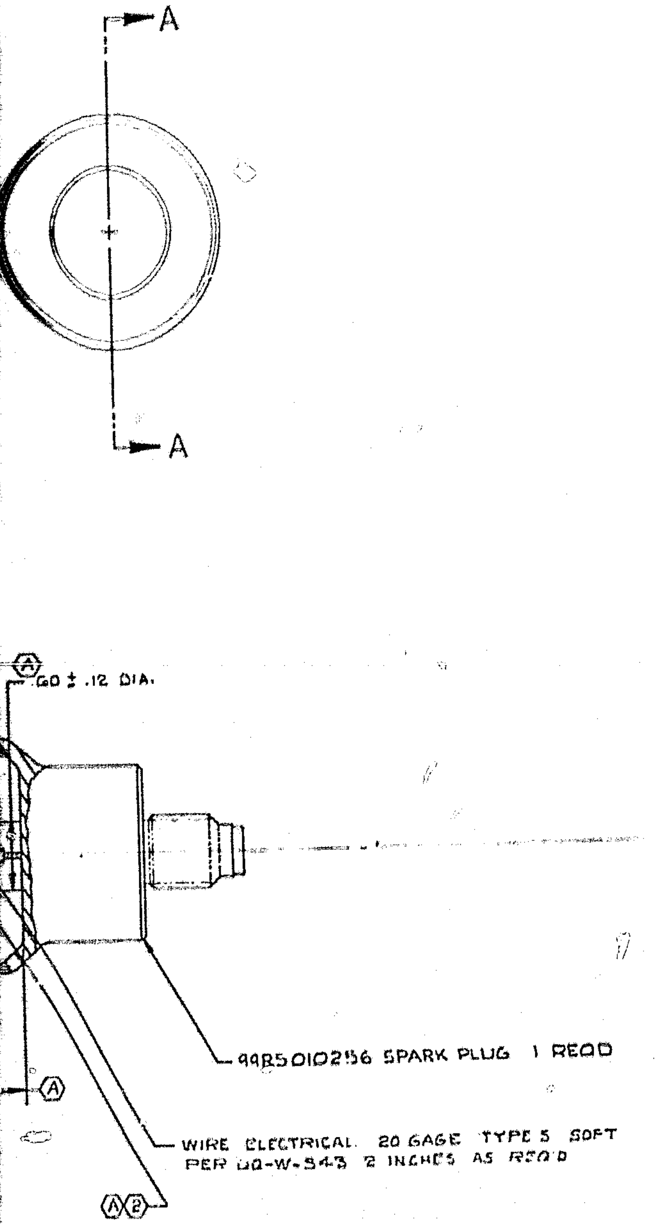

ORIGINAL PAGE IS OF POOR QUALITY

Figure 3

11

8. PURGE WITH DRY NITROGEN PER MIL-P-27401 IMMEDIATELY PRIOR TO SOLDERING RECEPTACLE BUT AFTER WELDING
7. SOLDER PER MIL-S-6872 USING Sn60 WRAP2 SOLDER.
6. ELECTROCHEMICAL ETCH ASSY PER RF0004-001
5. SOLDER PER RA0115-006
4. AMP INC CAPITRON DIVISION ELIZABETH PA.
3. WELD PER RA0107-042 CLASS II
2. ENCAPSULATE PER RA0116-006 USING RB0120-005 TYP XII CLASS A
1. MACHINE PER RA0115-002

NOTE: UNLESS OTHERWISE SPECIFIED

-003	304L CRES	.80 x 4.25	
NO	MATERIAL	SIZE	SPECIFICATION

-001 NO

HEAT TREAT

FINISH

MATL NOTED

DO NOT SCALE PRINT

Rockwell International Corporation
Rocketdyne Division
Canoga Park, Ca

SIZE E CODE IDENT NO 02602 DRAWING NO.

1. SCOPE: THIS SPECIFICATION ESTABLISHES THE REQUIREMENTS FOR A MULTIPLE-PURPOSE SPARK EXCITER.

2. OPERATIONAL CHARACTERISTICS

2.1 ELECTRICAL

2.1.1 EXCITATION - THE EXCITER SHALL BE CAPABLE OF OPERATING WITHIN SPECIFIED PERFORMANCE LIMITS WHEN SUPPLIED WITH 24 TO 32 VOLTS D.C. THE APPLICATION OR REMOVAL OF 28 VDC POWER WILL NOT CAUSE A SPARK. THE POWER CIRCUIT SHALL BE ISOLATED FROM CASE GROUND.

2.1.2 SPARK COMMAND - THE APPLICATION OF 24 TO 32 VOLTS DC TO THE SPARK COMMAND CIRCUIT SHALL INITIATE OUTPUT WITHIN 10 MILLISECONDS.

2.1.3 SPARK MONITOR - A PULSE SIGNAL OF 1 TO 5 VOLTS SHALL BE PROVIDED FOR EACH SPARK OUTPUT. THE EXTERNAL LOAD WILL BE GREATER THAN 10 K OHMS.

2.1.4 OUTPUT ENERGY - THE EXCITER SHALL DELIVER A MINIMUM OF 100 MILLIJOULES OF ENERGY PER SPARK INTO A 1.27 ±.13 mm (0.050 ±0.005 INCH) AIR GAP THROUGH 18 ±.15m (6 ±0.5 FEET) OF INTEGRAL COAXIAL TRANSMISSION CABLE.

2.1.5 OUTPUT VOLTAGE - THE EXCITER SHALL BE CAPABLE OF DELIVERING A BREAKDOWN VOLTAGE OF 25,000 VOLTS.

2.1.6 REPETITION RATE - THE ENERGY SHALL BE DELIVERED AT THE RATE OF 200 ±10 SPARKS PER SECOND.

2.1.7 OUTPUT ISOLATION - THE OUTPUT CIRCUIT SHALL BE ISOLATED FROM CASE AND POWER GROUNDS. THE LEAKAGE CURRENT BETWEEN CASE OR POWER GROUND AND THE OUTPUT RETURN SHALL BE LESS THAN 1 MILLIAMP. THE EXCITER IS NOT REQUIRED TO FUNCTION WITH A FLOATING OUTPUT AND WILL BE GROUNDED BY WAY OF THE ATTACHED SPARK PLUG.

2.2 ENVIRONMENT - THE EXCITER SHALL BE OPERATIONAL IN A TEMPERATURE RANGE OF 272 K TO 311 K (30 F TO 100 F). THE UNIT SHALL BE SEALED AGAINST THE EFFECTS OF HUMIDITY.

2.3 ACCESS - THE INTERNAL COMPONENTS SHALL BE ACCESSABLE WHEN THE UNIT IS MOUNTED.

2.4 CONFIGURATION - THE UNIT SHALL BE CONSTRUCTED AS ILLUSTRATED BELOW. UNLESS OTHERWISE SPECIFIED, DIMENSION AS REQUIRED.

3.0 ACCESSORIES - EACH UNIT SHALL INCLUDE A SCHEMATIC AND PARTS LIST.

PIN	INPUT
A	+28 VDC POWER
B	+28 VDC SPARK COMMAND
C	SPARK MONITOR SIGNAL
D	28 VDC RETURN

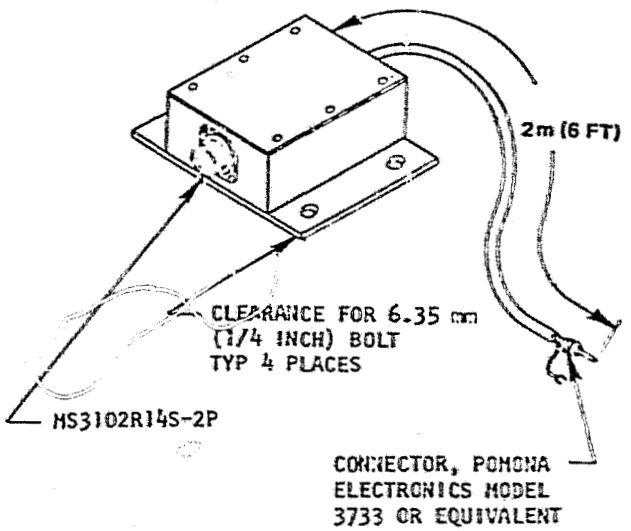

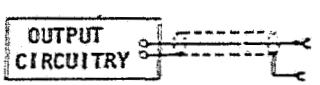

OUTPUT CIRCUIT
SCHEMATIC

Figure 4. Capacitance Exciter Specifications

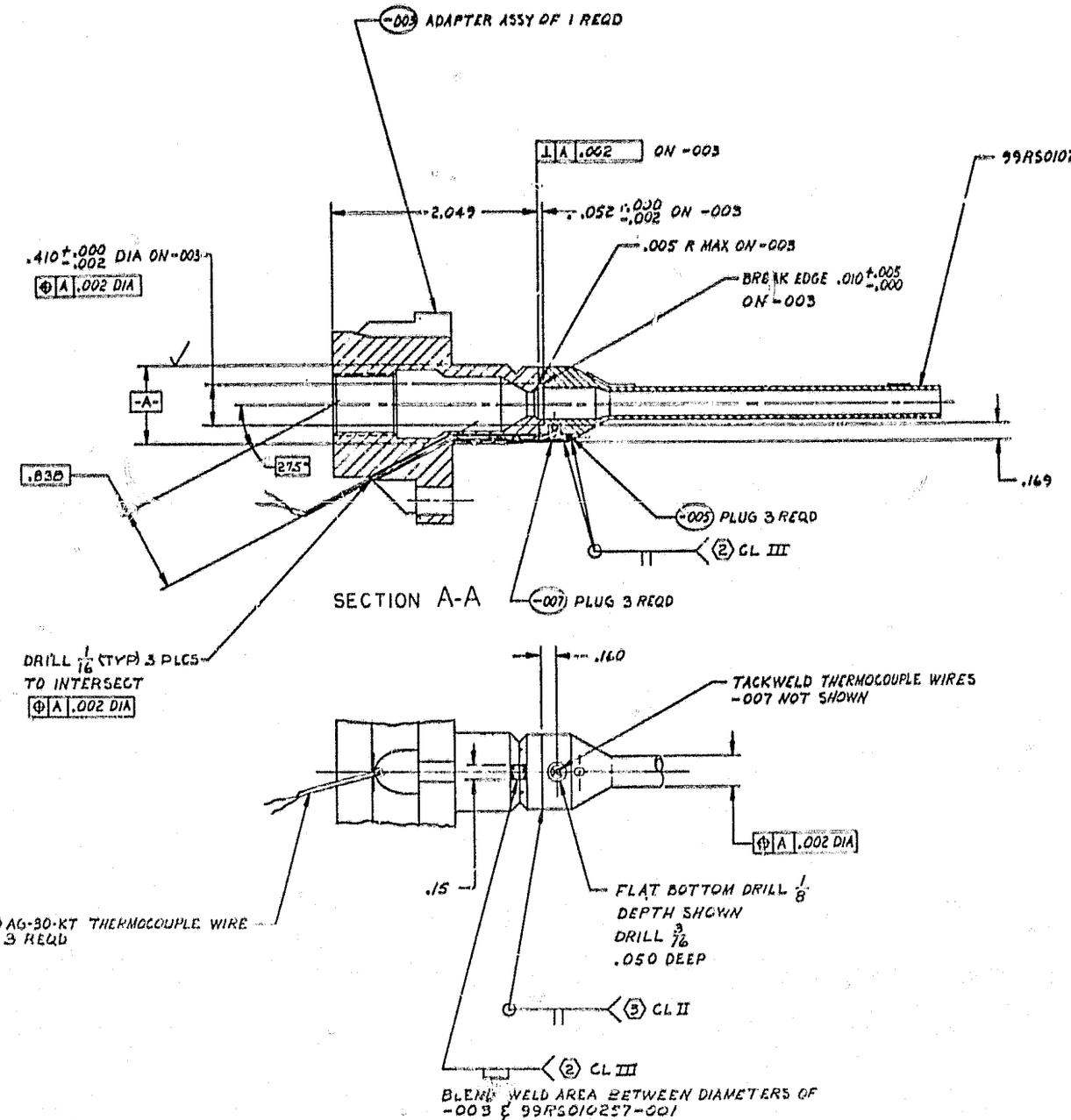

ORIGINAL PAGE IS
OF POOR QUALITY

⟨5⟩ CALIFORNIA ALLOY CO, 1475 POTRERO AVE, SOUTH EL MONTE, CA 91733
⟨4⟩ DEEP ELECTROCHEMICAL ETCH IDENTIFY PER RA0104-008.
⟨3⟩ ELECTRON BEAM WELD PER RA0107-042.
⟨2⟩ WELD PER RA0107-027.
1. MACHINE PER RA0103-016.

NOTE: UNLESS OTHERWISE SPECIFIED

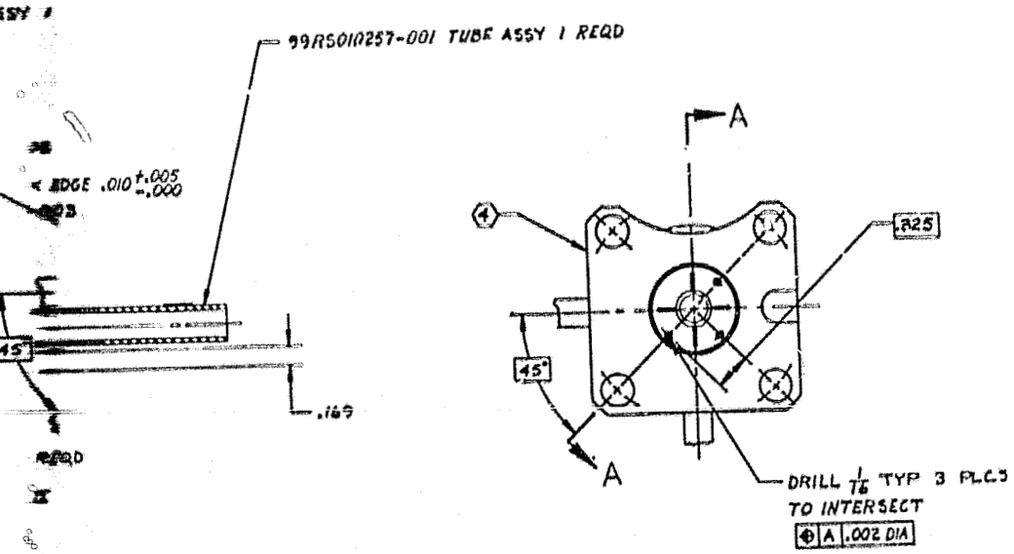

WELD THERMOCOUPLE WIRES
NOT SHOWN

A .002 DIA

1/8

OF

PER

ORIGINAL PAGE IS
OF POOR QUALITY

Figure 5

13

NO	MATERIAL	SIZE	SPECIFICATION
-007	NICKEL 200 SHEET	.18 DIA X.031	ASTM B160
-005	NICKEL 200 SHEET	.060 DIA X.00	ASTM B160
-003	MAKE FROM R[illegible]6191F		

-001
NO

(5) CALIFORNIA ALLOY CO, 142[illegible] POTRERO AVE, SOUTH EL MONTE, CA 9[illegible]
(4) DEEP ELECTROCHEMICAL ETC / IDENTIFY PER RA0104-028.
(3) ELECTRON BEAM WELD PER RA0107-042.
(2) WELD PER RA0107-027.
1. MACHINE PER RA0109-016.

NOTE: UNLESS OTHERWISE SPECIFIED

HEAT TREAT	NONE
FINISH	NONE
MATL	NOTED

UNLESS OTHERWISE SPECIFIED DIMENSIONS ARE IN INCHES AND APPLY PRIOR TO PLATING
125 MICRO INCH MAX. SURF. ROUGHNESS
TOLERANCES ON 2 PLACE DECIMALS XX ± .01 .XXX ± .010
HOLES NOTE'S "DRILL"

OVER	THRU	TOLERANCE
.000	.062	+.0015 -.0000
.062	.125	+.0020 -.0000
.125	.250	+.0025 -.0000
.250	.500	+.0030 -.0000
.500	.750	+.0035 -.0000
.750	1.000	+.0040 -.0000
1.000	1.500	+.0050 -.0000

DO NOT SCALE PRINT

DRAWN DATE
CHK DATE
ENGR
MATL
STRESS
DESIGN ACTIVITY APPVD DATE

Rockwell International Corporation
Rocketdyne Division
Canoga Park, California

ADAPTER
2CR SPARK IGNITER
ASSY OF

SIZE	CAGE IDENT NO.	DRAWING NO.
E	02602	99RS010258

SCALE 2/1 SHEET

99RS010258

1 of 1

The spark plug is attached to the igniter with a threaded joint and the seal at this point is integral with the spark plug. The igniter body was fabricated from Inconel 625 and the liner, or tube, was made of nickel and welded to the igniter body.

In an actual engine system, the propellants for the preburner and thrust chamber igniters would be supplied from the discharge of the high-pressure fuel and oxidizer turbopumps. Consequently, the igniter was designed to operate with ambient temperature gaseous propellants.

A detailed discussion of the igniter design, fabrication, and evaluation testing is presented in the Advanced Thrust Chamber Technology Final Report (Ref. 1).

Preburner Injector

The preburner injector is an assembly consisting of a one-piece body, 15 self-contained coaxial injection elements, a faceplate, a fuel manifold with two inlets, and an oxidizer manifold and inlet, Fig. 6 and 7. The self-contained coaxial injection elements discharge liquid oxygen from a center post whose exit is recessed behind the plane of the injector face. Gaseous hydrogen is injected from an annulus around each oxidizer post. Each element is a unit in which oxidizer and fuel metering is provided. The oxidizer flow is controlled primarily by the sudden expansion orifice at the upstream end of the oxidizer post. A rounded entrance minimizes entrance effects so that the pressure drop is accurately controlled by the relationship between the orifice and the post diameters. The fuel flow is metered by the annulus area between the oxidizer post and fuel sleeves. The entrance slots that feed the annulus are designed so that the width, 0.89 mm (0.035 inch), is less than the minimum width of the fuel annulus, 1.50 mm (0.059 inch), to provide a filtering capability to prevent contamination from plugging the fuel annulus. Cold-flow tests on the SSME preburner elements, designed using the same basic criteria, have shown that a 6% restriction of the slot entrance area results in only a 2% reduction in flowrate. Special consideration to prevent a reduction in element fuel flowrate is warranted because a reduction in element fuel flowrate raises the element mixture ratio and produces the potential for high temperature streaks in the combustor.

The preburner injector is a lightweight design. The self-contained elements, brazed to the injector body and faceplate, provide a path through which the pressure loads across the faceplate are carried to the injector body. This reduces faceplate distortion and allows a thinner faceplate to be used. Low weight also results from the use of a braze/welded injector assembly since bolts, flanges, and seals are not required.

Performance Analysis. The preburner has been designed to produce high combustion efficiency and thoroughly mixed, uniform temperature exhaust gas. The key feature of the preburner design which controls performance is the coaxial element design. Although the main emphasis is placed on designing injection characteristics of the coaxial elements to produce performance and mixing, consideration is also given to factors which control the element pattern, number of elements, and element spacing.

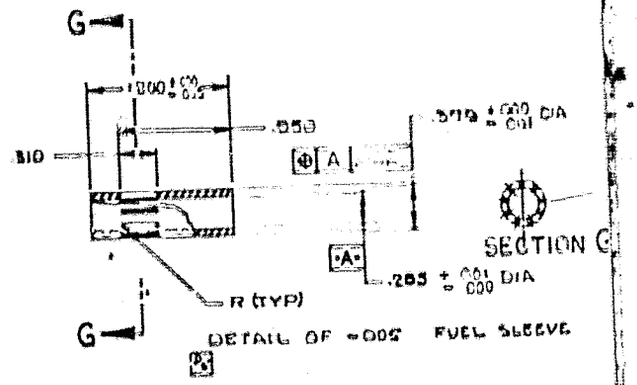

DETAIL OF -005 FUEL SLEEVE

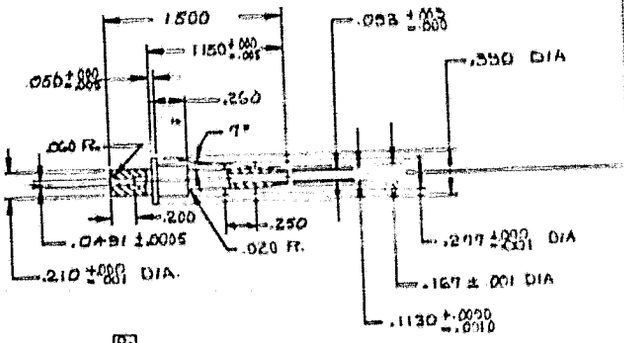

DETAIL OF -007 POST

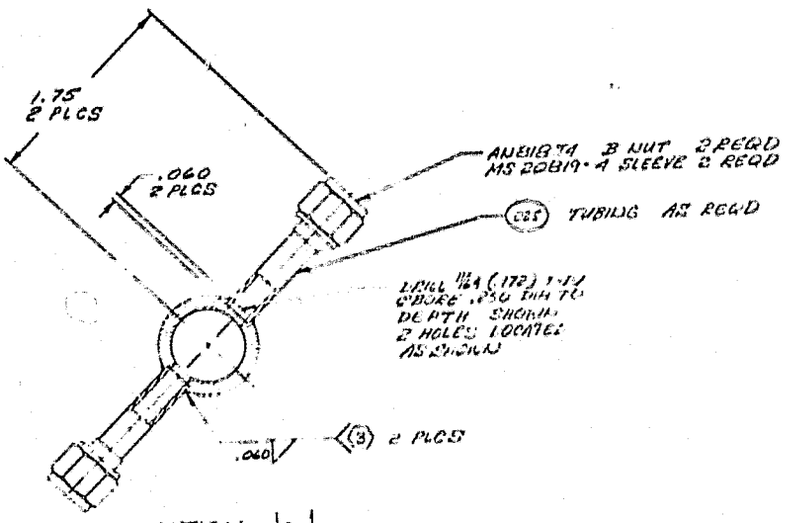

SECTION J-J

SECTION G-G

.035 TYP 9 PLCS
EQUALLY SPACED
WITHIN 0° 30'

Rockwell International Corporation
Rocketdyne Division

CODE IDENT 07407			
99PS010247		CHNG	SHEET 1

MICROFILM OVERLAY AREA

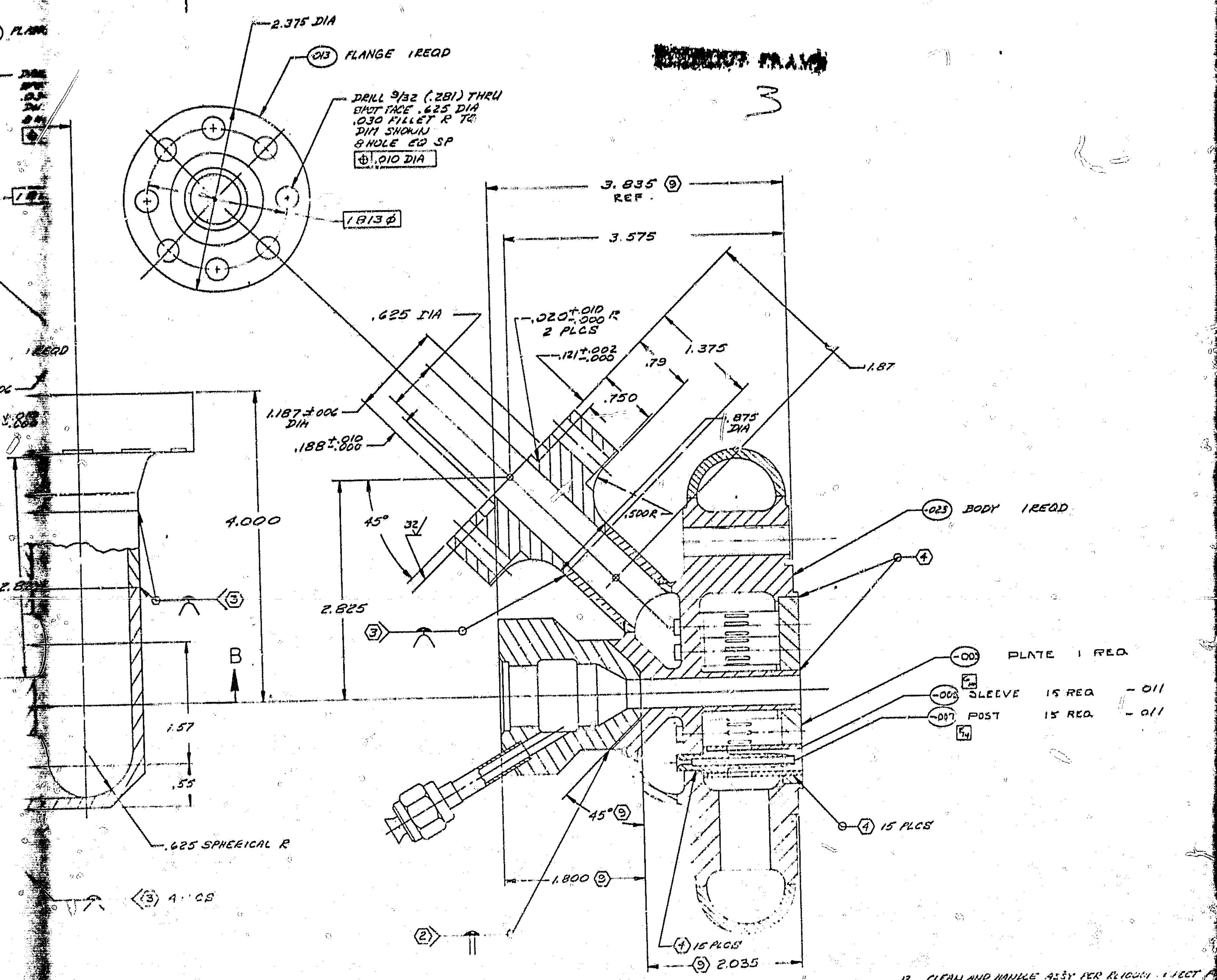

SECTION A-A

13 CLEAN AND HANDLE ASSY PER ... SERVICE AND IDENTIFY ...

(12) CLEAN DETAILS PER RA0110-018

11. BRAZE PER RA0107-004 WITH ... BRAZE ALLOY

10 PROOF PRESSURE TEST ... REPEAT ...

(9) ... -023 INJECTOR BODY AS ...

(8) GOLD PLATE .0004 TO ...

(7) DUCTILE NICKEL PLATE .0002 TO ... THKK PER ...

(6) COORDINATE ... HOLES ... PLATE

(5) DIMENSIONS TO APPLY AFTER PLATING

(4) BRAZE PER RA0107-015 WITH ... BRAZE

(3) WELD PER RA0107-027

(2) WELD PER RA0107-04?

1 MACHINE PER RA0103-016

NOTE UNLESS OTHERWISE SPECIFIED

Rockwell International Corporation
Rocketdyne Division
Canoga Park California

CODE IDENT 02602			
99PS010247			1-2

MICROFILM OVERLAY AREA

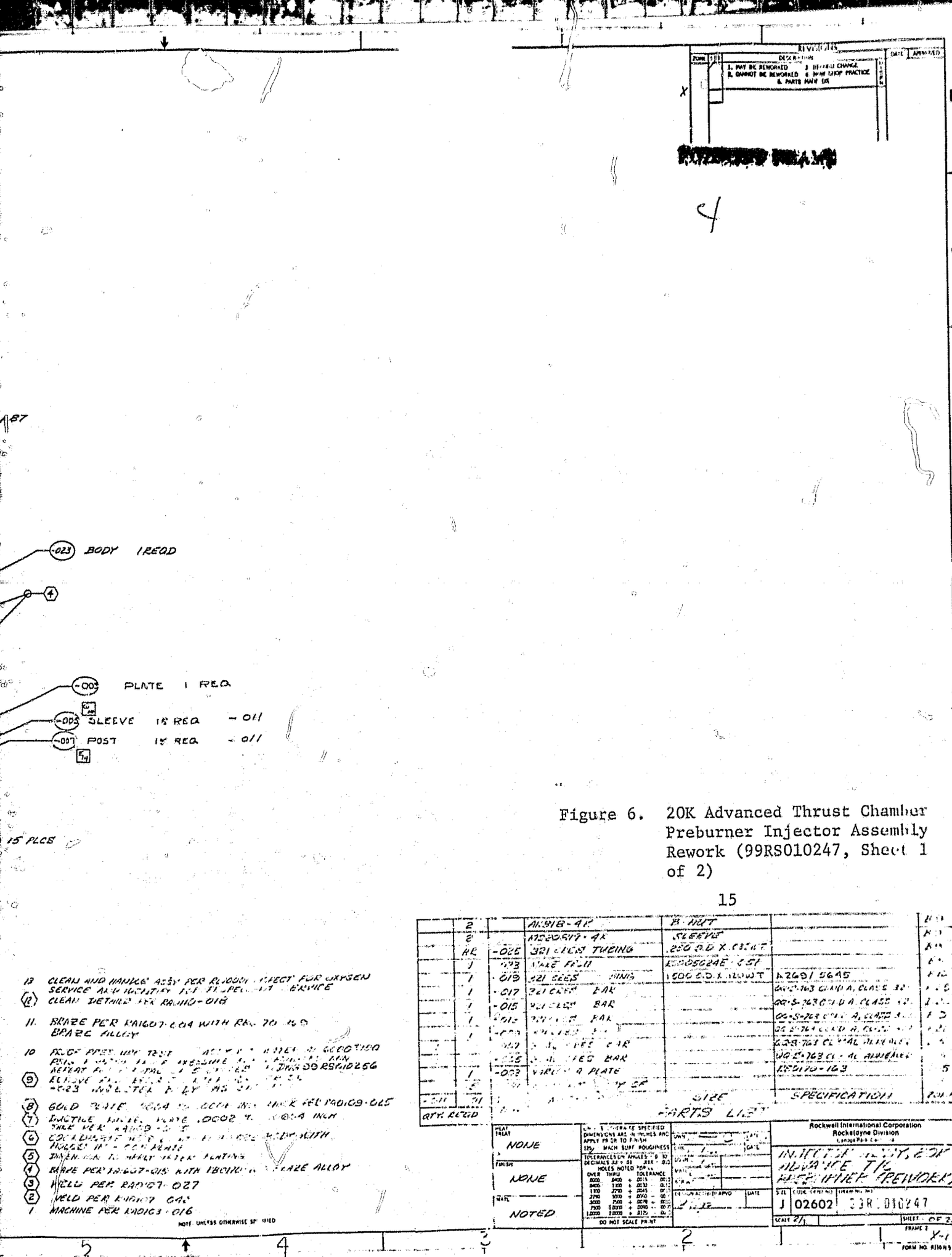

Figure 6. 20K Advanced Thrust Chamber Preburner Injector Assembly Rework (99RS010247, Sheet 1 of 2)

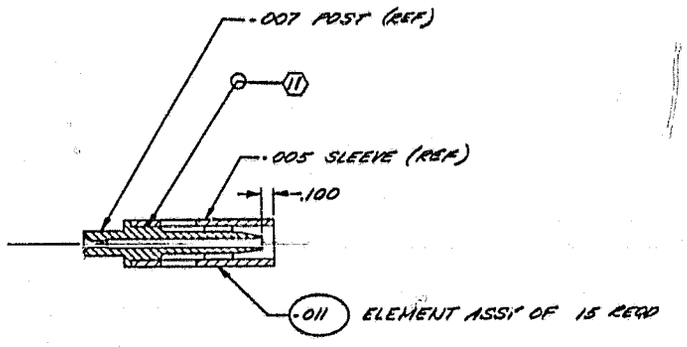

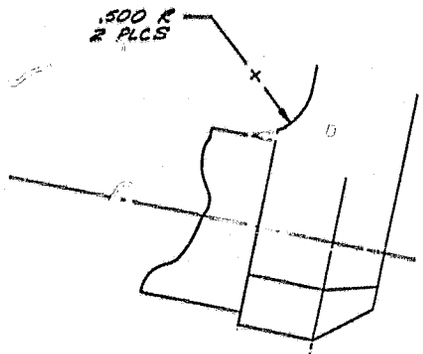

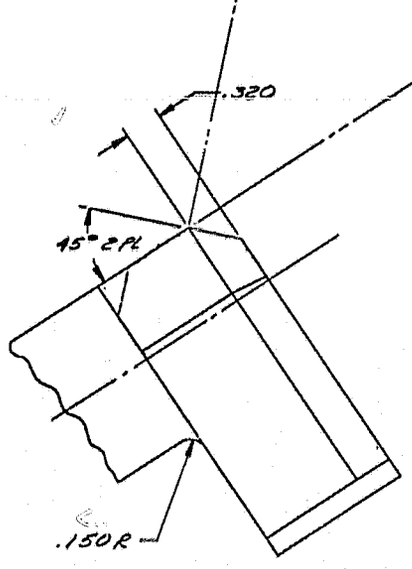

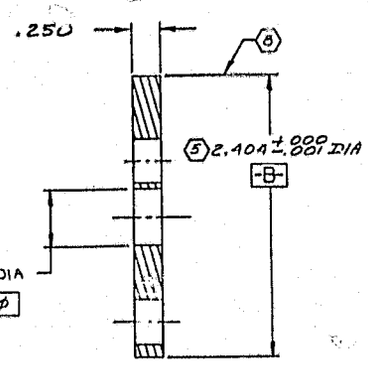

SECTION F-F

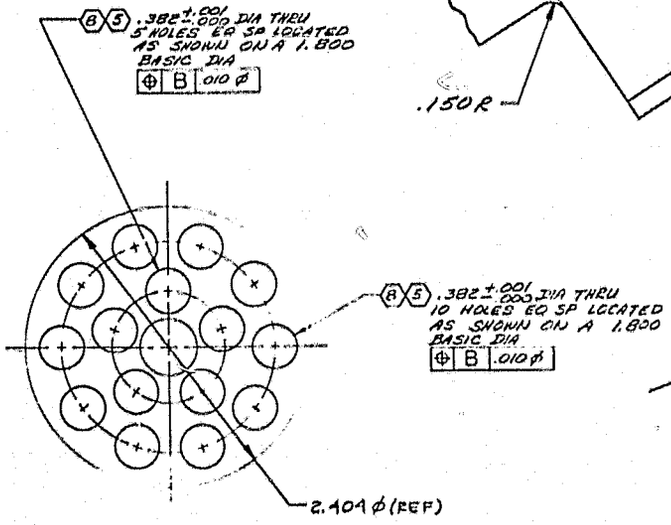

DE :F -003 FACEPLATE
[15]

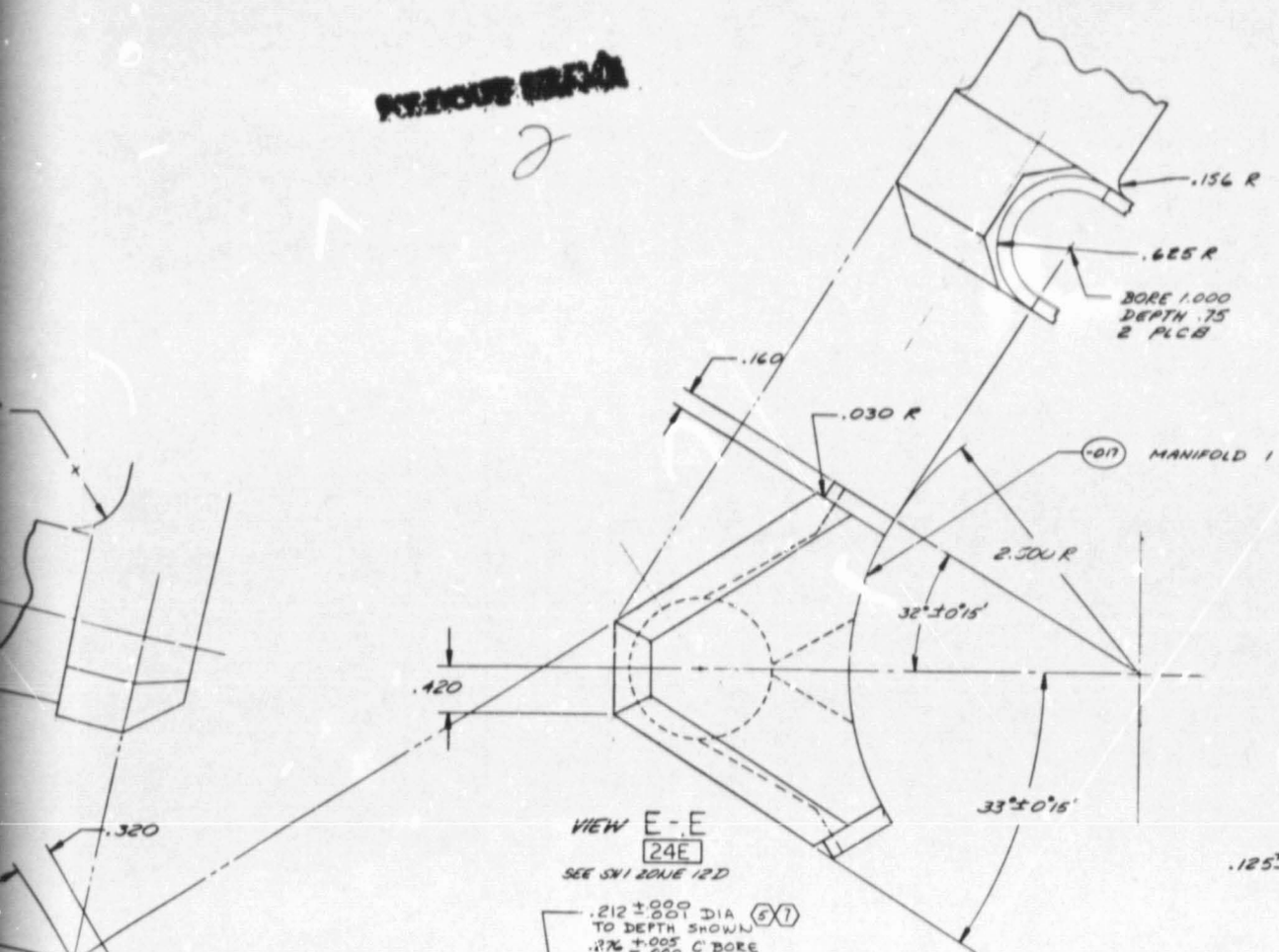

VIEW E-E
24E
SEE SW1 ZONE 12D

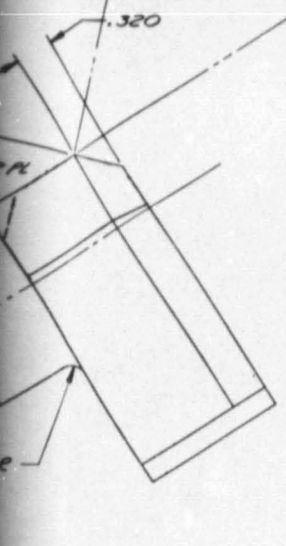

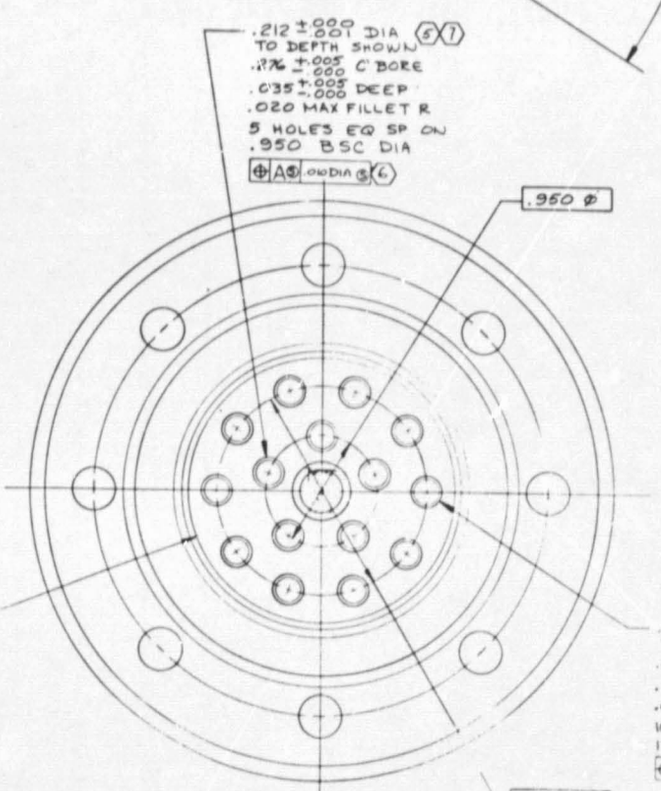

VIEW H-H 23D

27E E

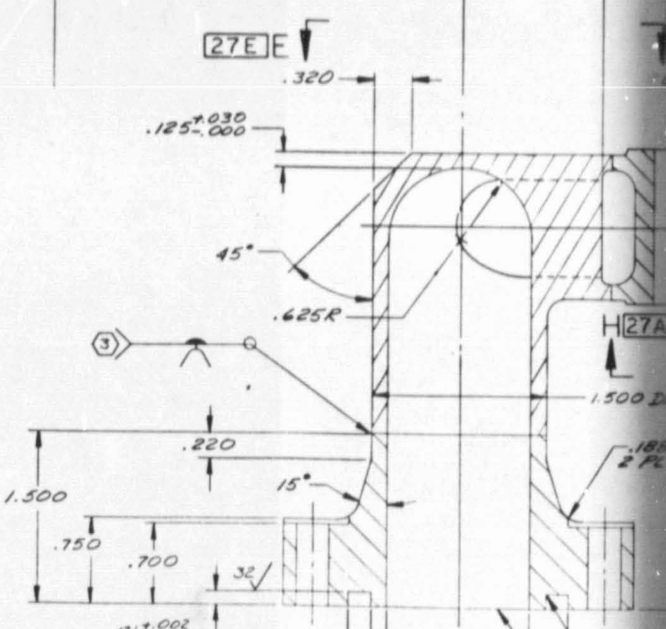

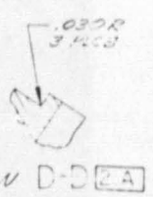

VIEW D-D 24A

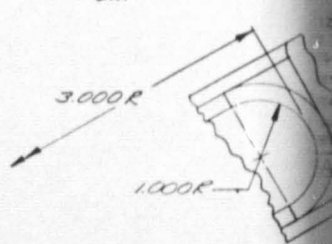

VIEW C-C

Rockwell International Corporation
Rocketdyne Division

CODE IDENT	DWG NO.	REV
99RS010247		2

[redacted]

3

.156 R

.625 R

BORE 1.000
DEPTH .75
2 PLCS

-011 MANIFOLD 1 REQD

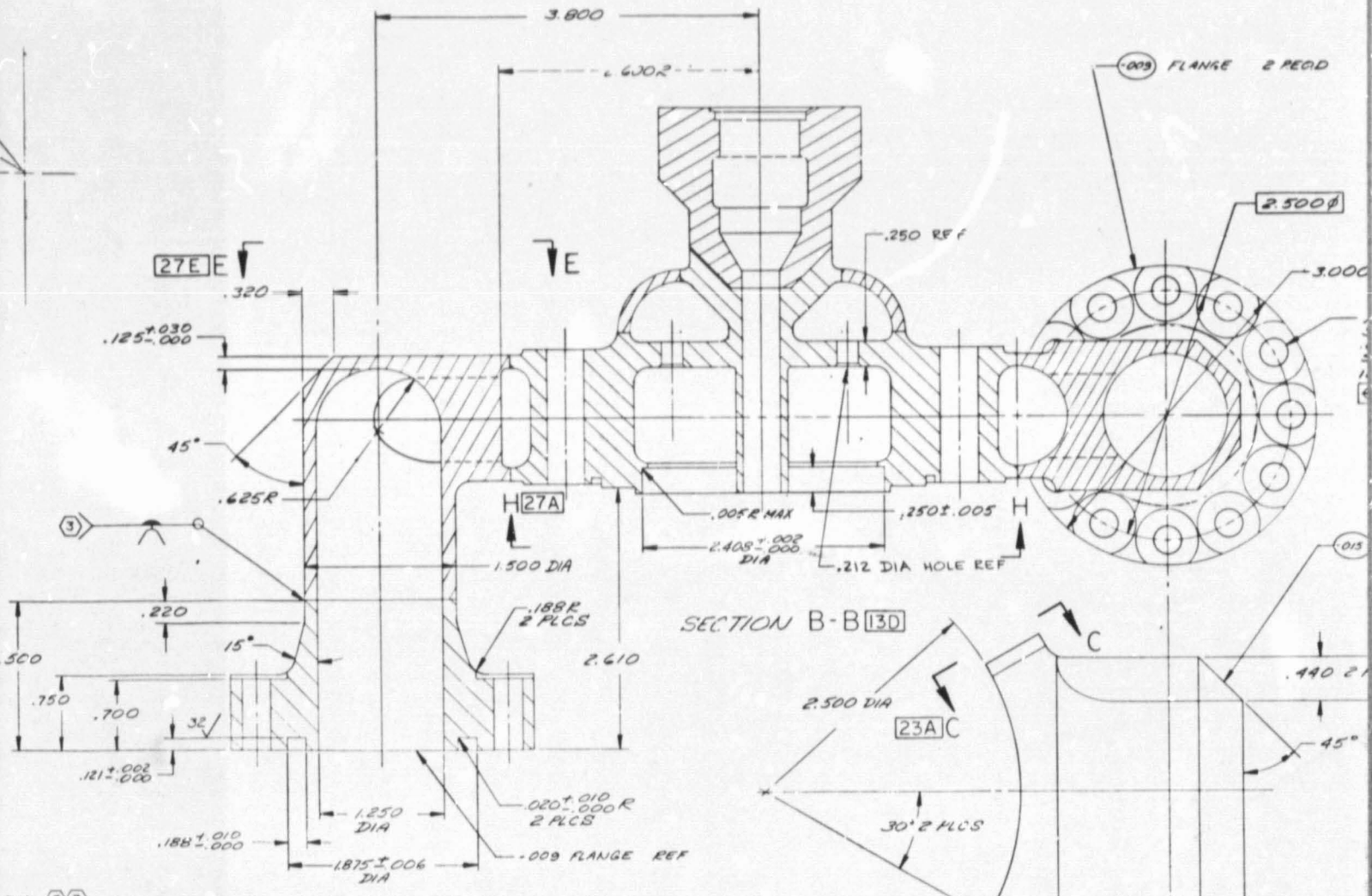

.009 ±.001 DIA (5) (7)
DEPTH SHOWN
.005 C'BORE
.000 ±.005 DEEP
.000 MAX FILLET R
ES EQUALLY
2 PLCS DIA
(6)

Rockwell International Corporation
Rocketdyne Division

CODE IDENT NO.	FRAME
99RS010247	

CHNG	SHEET
	2

25 24 23 22 21

MICROFILM OVERLAP AREA

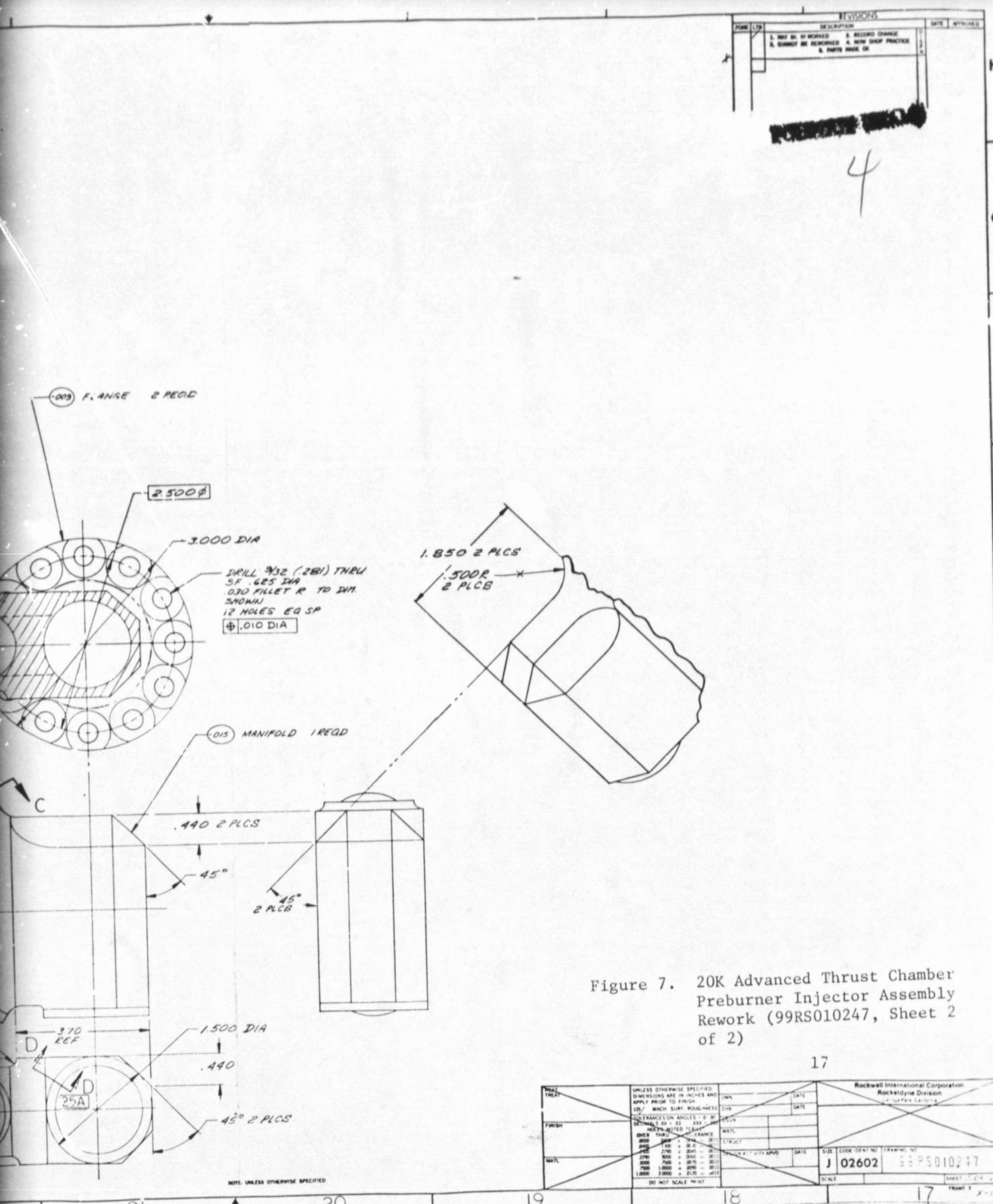

Figure 7. 20K Advanced Thrust Chamber Preburner Injector Assembly Rework (99RS010247, Sheet 2 of 2)

The preburner injection pattern has 15 elements approximately equally spaced in a pattern of two concentric circles. The selection of the injection pattern and number of elements was based on the minimum practical spacing between elements that fabricational limits would allow, the minimum element flowrate that can be metered with reasonably sized orifices and annuli, and the number of elements that would complete a concentric circular pattern with nearly equal spacing.

Low element flowrate and close element spacing are design objectives for the preburner because of performance and weight considerations. The element flowrate must be selected such that the diameter of the oxidizer jet is small enough to allow the oxidizer to be completely atomized before the surrounding annular jet of gaseous hydrogen has fully expanded into the combustion chamber. The mechanisms through which the coaxial element produces atomization, vaporization, and mixing are a function of the relative velocity between the low-velocity liquid oxidizer and the high-velocity gaseous fuel. Atomization of the oxidizer in a region of high relative velocity is desirable since the atomization rate increases with relative velocity while the oxidizer drop size decreases. Small drops increase the rate of vaporization by providing more available surface area per unit mass for heat transfer. A high velocity fuel stream also enhances vaporization because the heat transfer film coefficient on the surface of the drops increases with the relative velocity between the drops and the fuel stream.

Two techniques were used in the design of the preburner element to ensure high performance: (1) a recessed oxidizer post was used to increase the atomization rate and minimize the oxidizer drop size by forcing the hydrogen to remain at a high velocity around the oxidizer jet for the length of the recess, and (2) the element was designed for complete atomization of the oxidizer in the high fuel velocity region of the element flow field.

Vaporization and reaction efficiency of coaxial elements have been extensively studied and modeled at Rocketdyne, and a very comprehensive combustion model, the Coaxial Injection Combustion Model (CICM, Ref. 2) has been developed. The performance of the preburner coaxial element was evaluated using this model.

The preburner coaxial element has an oxidizer post recess of 2.5 mm (0.100 inch), a total flowrate of 0.284 kg/sec (0.626 lb/sec) at the design point, an oxidizer jet velocity of 26.2 m/sec (85.9 ft/sec), and an expanded fuel velocity in the recess of 213 m/sec (700 ft/sec). The selection of the recess depth and propellant velocities was based on the successful SSME full-scale preburner coaxial element design. The results of this analysis are summarized in Fig. 8 through 10. It can be seen from Fig. 8 that total vaporization and reaction of the oxidizer is predicted within 7.62 cm (3.0 inches) from the injector face. Figure 9 shows that the fuel velocity remains high in the recess and decreases rapidly within the first 1.27 cm (0.5 inch) from the injector face. The recess produces 11% atomization and complete atomization occurs within the first 1.27 cm (0.5 inch), Fig. 8; the drops produced are small, ranging from 60 - 104 microns in diameter, Fig. 10. The remaining 6.35 cm (2.5 inches) are required for complete vaporization and reaction.

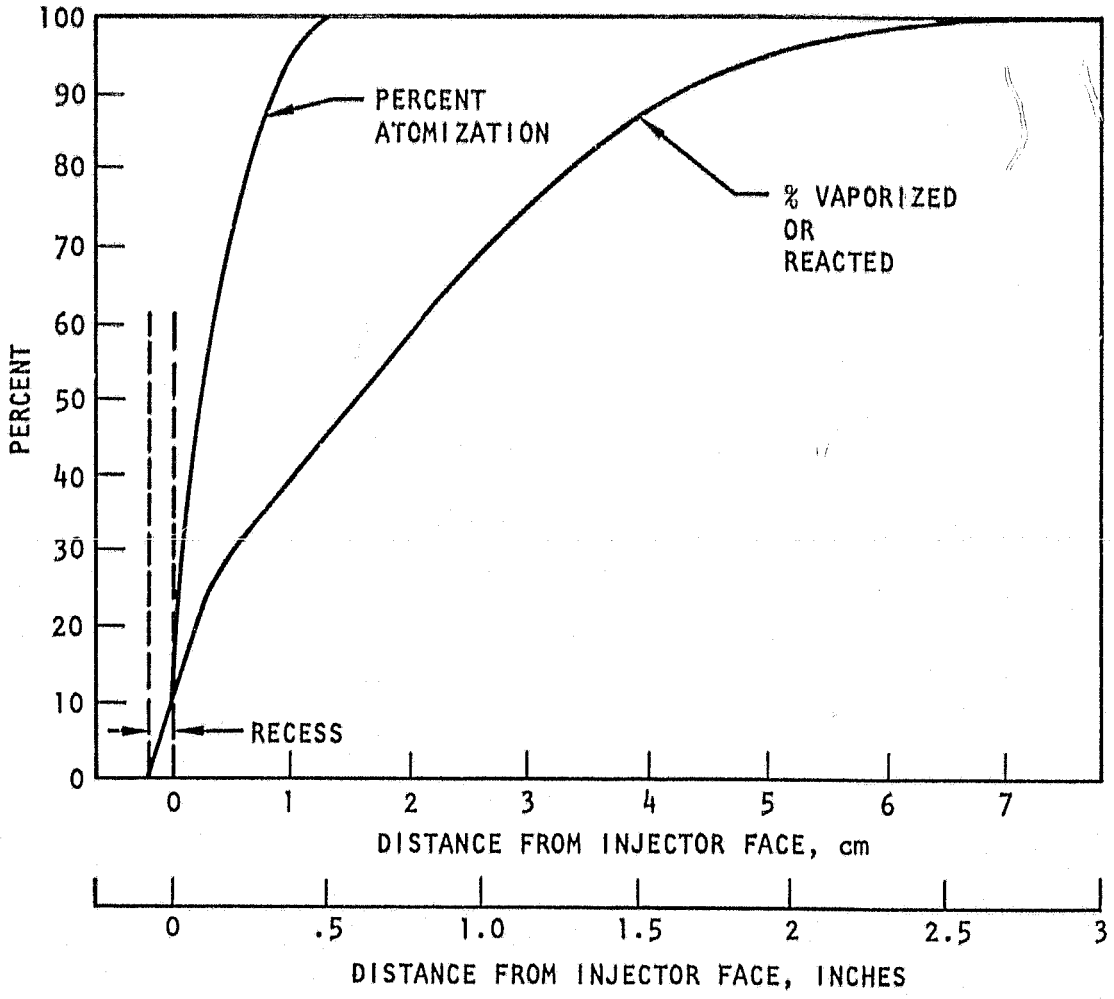

Figure 8. Preburner Coaxial Element

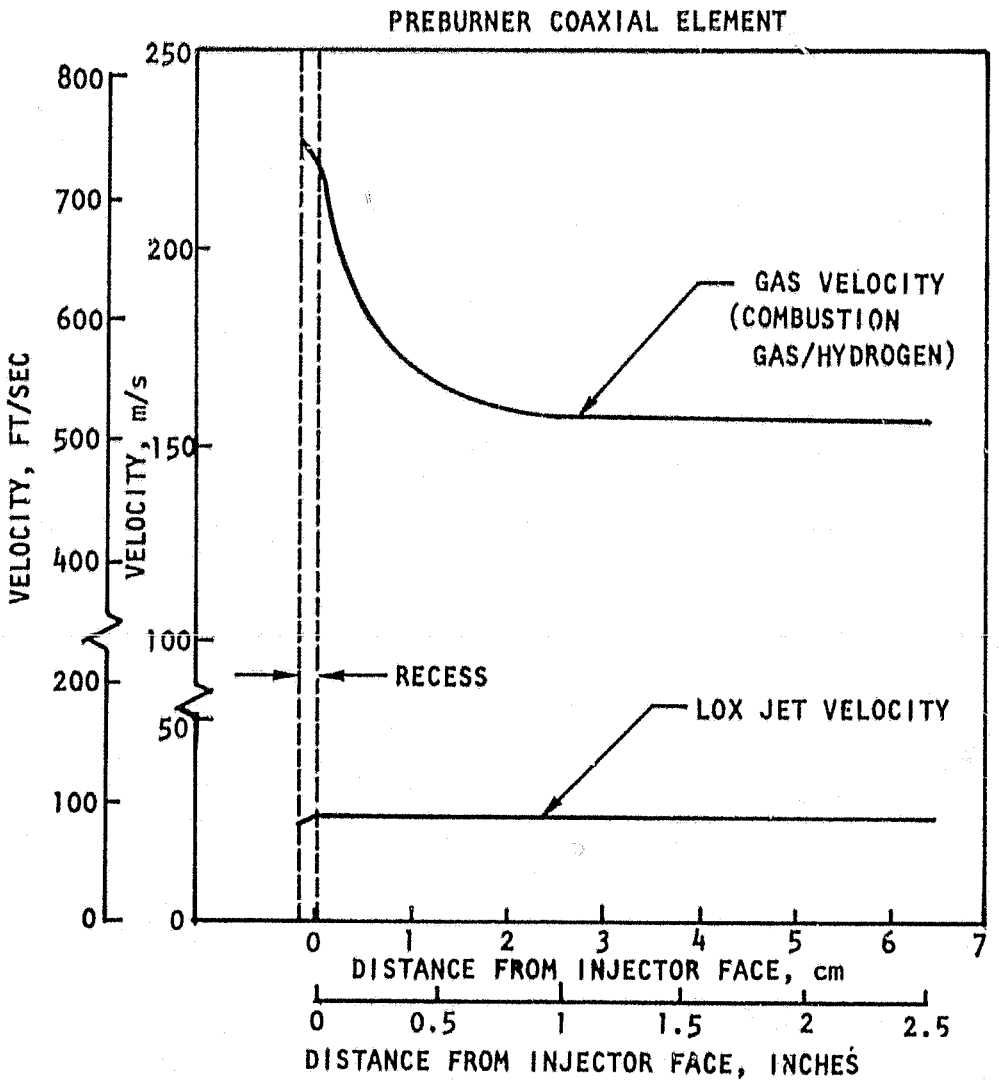

Figure 9. Preburner Axial Element Velocity vs Distance From Injector Face

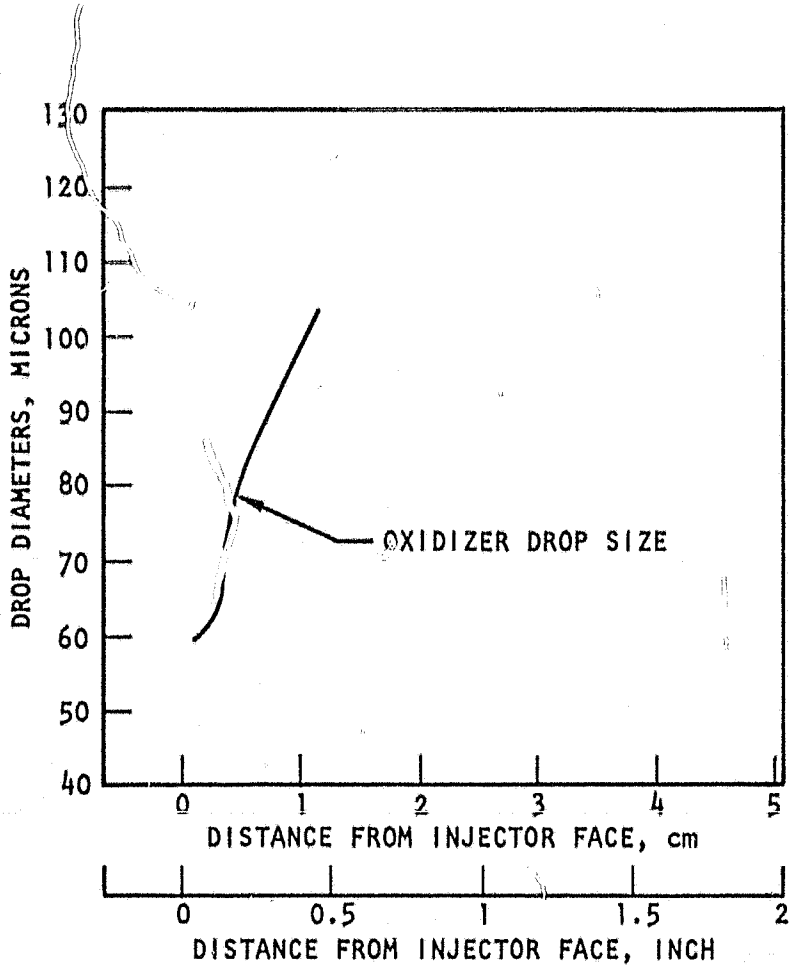

Figure 10. Preburner Coaxial Element Oxidizer Drop Diameter vs Distance from Injector Face

The mixing capability of the element design was evaluated using design criteria acquired during cold-flow testing of the SSME preburner coaxial elements, conducted according to Ref. 3. From the results of this testing, a mixing uniformity parameter, E_m, representing a mass-weighted measure of the deviation of the mixture ratio distribution across the element flow field from the overall element mixture ratio has been developed. The mixing uniformity parameter, E_m, is defined below:

$$E_m = 100 \times \left[1 - \sum_{i}^{n} \frac{\dot{w}_i}{\dot{w}_t} \frac{\left(R - r_i\right)}{R} - \sum_{i}^{n} \frac{\dot{w}_i}{\dot{w}_t} \frac{\left(R - \overline{r}_i\right)}{(R-1)} \right]$$

where

$\dot{w}_i/\dot{w}_t$ = mass fraction in the ith stream tube

R = ratio of total oxidizer to total oxidizer plus fuel (total flow)

r_i = ratio of local oxidizer flow in a stream tube to the total flow in stream tubes for which $r_i < R$

$\overline{r}_i$ = ratio of local oxidizer flow in a stream tube to the total flow in stream tubes for which $r_i > R$

The mixing uniformity factor was found to correlate with the ratio of the injected propellant densities and injected velocities, Fig. 11. The cold-flow distribution data from which this plot was prepared was measured at a location 12.70 cm (5 inches) from the injector face. It can be seen that for the preburner nondimensionless density/velocity parameter of 0.5, the design point, the predicted mixing uniformity parameter is approximately 95%. This indicated that the element would produce thorough mixing and uniform temperature exhaust gas.

A comparison of the ASE preburner element design features with three types of SSME preburner elements is shown in Table 3. Study of this comparison shows that the ASE element design has closely followed the proven SSME element configurations; the only significant deviation shows the element fuel sleeve gap to be significantly larger than SSME counterparts, but this is principally the result of higher temperature of the fuel at the inlet to the ASE preburner. Table 4 summarizes the significant features of the ASE preburner injector elements.

Thermal and Structural Analysis. A heat transfer analysis of the injector was conducted to support the structural analysis of the injector and to ensure that local overheating would not occur on the injector face or in the igniter ducting. The temperatures at various locations on the injector are shown in Fig. 12. As noted, the maximum injector face temperature is predicted to be 478 K (500 F) and the maximum igniter tube temperature is predicted to be 839 K (1050 F) neither of which is excessive.

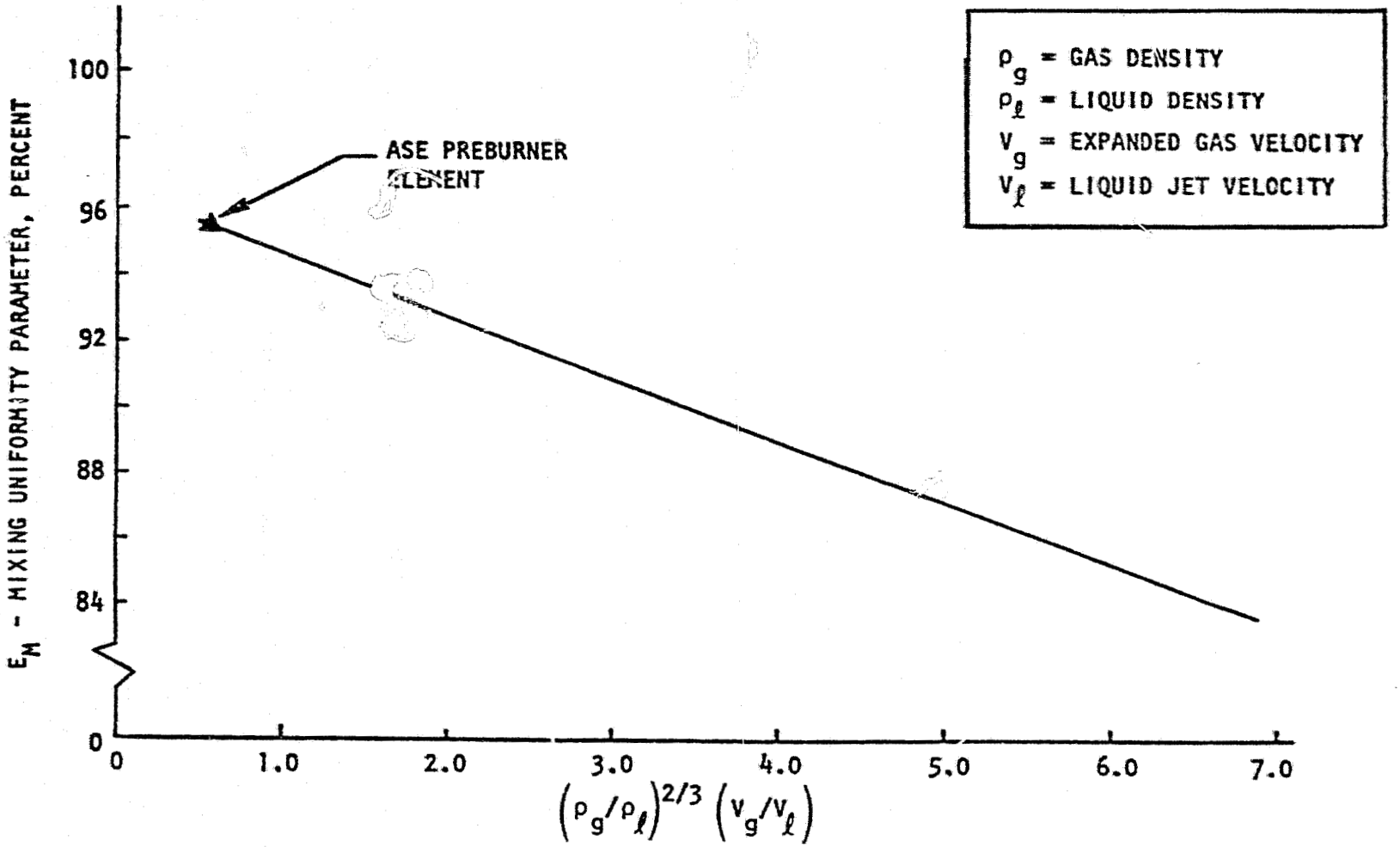

Figure 11. SSME Preburner Coaxial Element Cold-Flow Mixing Tests

TABLE 3. COMPARISON OF ASE AND SSME PREBURNER INJECTOR ELEMENTS OPERATING CHARACTERISTICS

Operating Characteristics	SSME		Phase B Full-Scale Preburner	ASE
	OPB	FPB		
Flowrate per Element, kg/s (lb/sec)	0.204 (0.450)	0.204 (0.525)	0.330 (0.728)	0.284 (0.626)
Fuel Inlet Temperature, K (R)	164 (296)	164 (296)	69 (125)	239 (431)
Oxidizer Inlet Temperature, K (R)	114 (205)	114 (205)	106 (190)	108 (195)
Chamber Pressure, N/cm^{2}a (psia)	3623 (5254)	3570 (5178)	2413 (3500)	2335 (3386)
Oxidizer Post Velocity, m/s (ft/sec)	25.1 (82.4)	24.3 (79.7)	24.4 (80)	26.2 (85.9)
Fuel Sleeve Velocity, m/s (ft/sec) (1)	358 (1176)	369 (1210)	364 (1195)	290 (953)
Fuel Post end Velocity, m/s (ft/sec) (2)	255 (836)	262 (860)	259 (849)	227 (745)
Fuel Recess Velocity, m/s (ft/sec) (3)	210 (689)	216 (709)	213 (700)	213 (700)
Geometry				
Oxidizer Control Orifice Diameter, mm (inch)	0.914 (0.0360)	1.031 (0.0406)	1.27 (0.050)	1.247 (0.0491)
LOX Post Thickness, mm (inch)	0 724 (0.0285)	0.749 (0.0295)	0.46 (0.018)	0.94 (0.037)
LOX Post ID, mm (inch)	1.96 (0.077)	2.26 (0.089)	2.64 (0.104)	2.36 (0.093)
LOX Post Recess, mm (inch)	2.54 (0.100)	2.54 (0.100)	2.54 (0.100)	2.54 (0.100)
Fuel Sleeve ID, mm (inch)	4.70 (0.185)	4.93 (0.194)	4.95 (0.195)	7.24 (0.285)
Fuel Sleeve Gap, mm (inch)	0.648 (0.0255)	0.58 (0.023)	0.69 (0.027)	1.50 (0.059)
Effective Injector Face Area per Element, mm^2 (in.^{2})	160.6 (0.249)	162.6 (0.252)	192.9 (0.299)	194.8 (0.302)

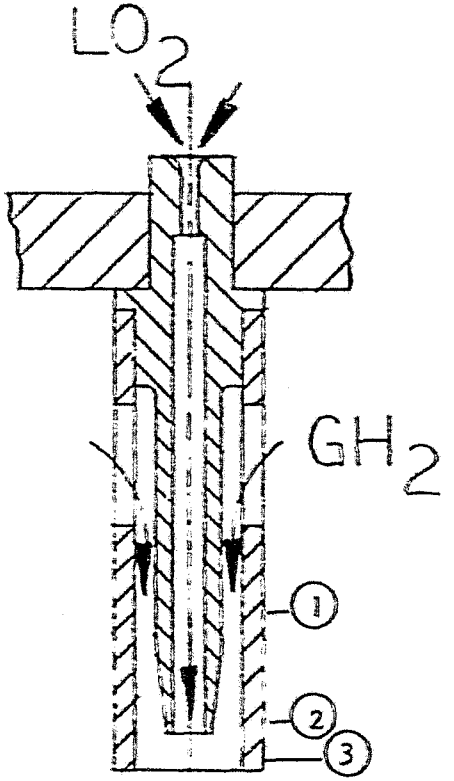

TABLE 4. PREBURNER INJECTOR ELEMENT FEATURES

- The ASE preburner elements have the same design features as the SSME preburners
  - High relative velocity between the propellant streams in the recess, $V_O \approx 25$ m/s, $V_F \approx 213$ m/s, recess depth = 2.5 mm ($V_O \approx 80$ ft/sec, $V_F \approx 700$ ft/sec, recess depth = 0.100 inch)
  - Low flowrate per element, $V \approx 0.23$ (≈ 0.5 lb/sec) and close element spacing, $V \approx 12.5$ mm, (≈ 0.5 inch)
  - Rounded entrance oxidizer control orifice
  - Narrow feed slots at entrance to fuel side of element
  - Elements fabricated as separate subassemblies
- The rationale and substantiation used in selecting these design features are the same as used for the SSME preburner elements

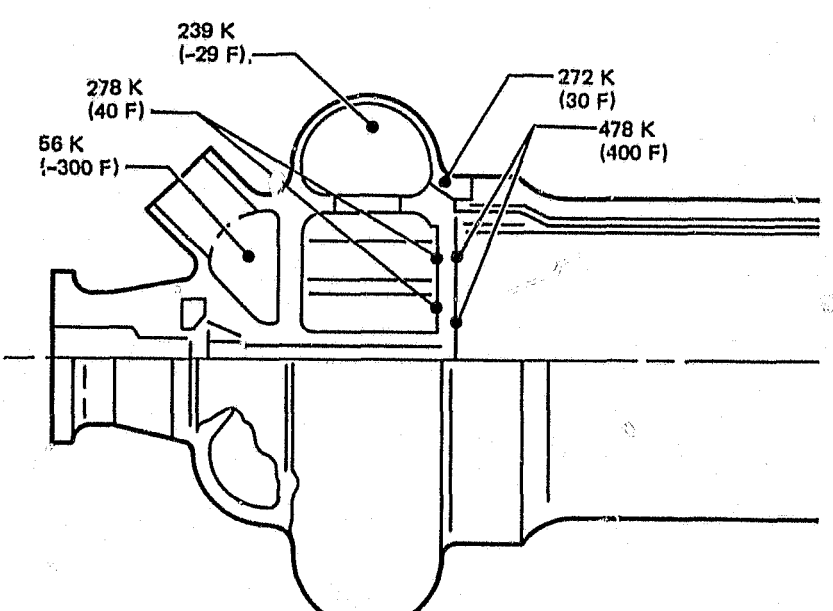

Figure 12. Preburner Injector Temperature Distribution

For purposes of modeling, the preburner was divided into three physical parts: (1) the igniter, (2) the injector body, and (3) the combustor body. The igniter was modeled as an axisymmetric thin shell of revolution; the injector body was modeled as an axisymmetric finite element model. The sections of the injector and igniter considered to be most critical or of most interest are shown on Fig. 13, and the basic strength and life values are shown in Tables 5 and 6. Figure 14 shows the deflection of the injector faceplate with the maximum relative displacement of 0.01 mm (0.004 inch).

The injector body and propellant manifolds and lines were fabricated from Inconel 625 because of its high strength and resistance to hydrogen embrittlement. The injector faceplate was fabricated from copper to facilitate heat transfer to the hydrogen in the injector manifold. CRES 304L was used for the self-contained injector elements because it had adequate strength for this application and was more easily machined and brazed.

Preburner Combustor

The preburner combustor (Fig. 15) is a cylindrical combustion chamber with an exhaust transition section to interface with the turbine manifold on the fuel turbopump and a branch elbow to split off flow to the oxidizer turbopump. A fuel-cooled liner is used within the cylindrical combustor body to limit the wall temperature of the structural shell and to extend the combustor life, enhance the durability, and reduce overall weight by allowing thinner walls.

Coolant flow for the liner is supplied from the injector fuel inlet manifold through 12 orifices. The liner produces an effective thermal barrier for the structural outer wall with only 2% of the preburner fuel flow. The coolant flow is dumped into the exhaust gas flow at the exit of the combustor.

Wires, brazed onto the liner, center the liner within the combustor body to maintain a constant area annulus for the coolant flow. Six acoustic absorber cavities are provided in the liner below the injector face for increased combustion stability margin.

A heavy flange was provided at the forward end for bolting the injector to the combustor body. Flexibility to change the injector, or to remove the injector for inspection of either injector or combustor and lines was thus retained.

Thermal and Structural Analysis. A steady-state heat transfer analysis of the preburner combustor wall temperature profile was conducted to support the structural analysis. The combustor wall temperature profile was determined for the worst case preburner operating conditions corresponding to a preburner combustion temperature of 1383 K (2030 R) at the maximum engine operating point. The resulting temperature profile is given in Fig. 16. The maximum temperature of the combustor wall under the most severe case was calculated to be 450 K (350 F) although the wall temperature in the transition section downstream of the coolant sleeve exceeded this value.

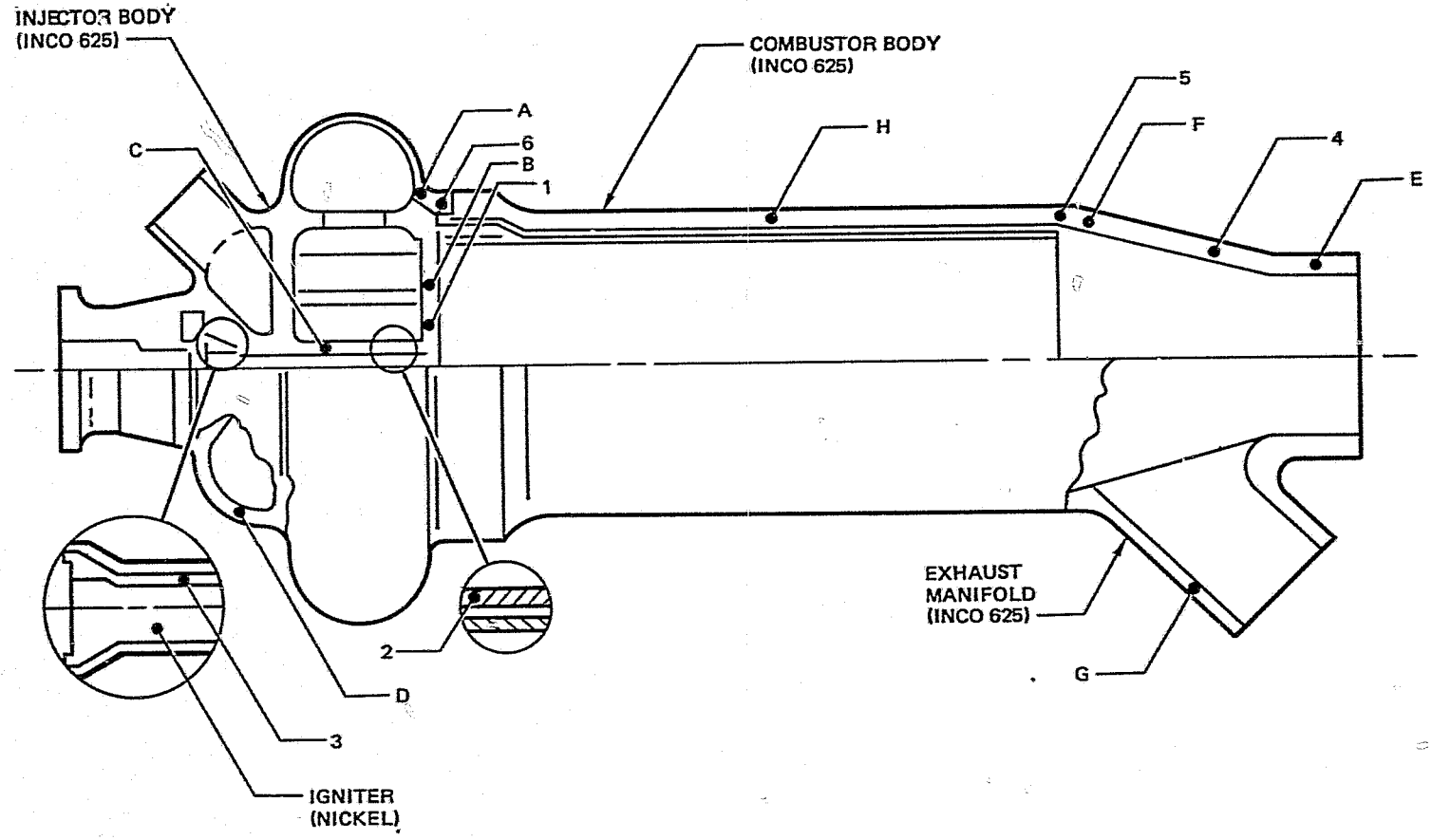

Figure 13. Preburner Structural Analysis

TABLE 5. PREBURNER INJECTOR BASIC STRENGTHS

Point (1)	Temperature, K (F)	σ_{eff} (2) N/cm^2 (lb/in.^{2})	Stress		Safety Factor	
			Yield (3) N/cm^2 (lb/in.^{2})	Ultimate, (4) N/cm^2 (lb/in.^{2})	On Yield Strength	On Ultimate (Strength)
A	272 (30)	27 400 (39,744)	38 610 (56,000)	79 980 (116,000)	1.41	2.92
B	403 (265)	14 650 (22,700)	33 100 (48,000)	73 090 (106,000)	2.31	4.67
C	184 (-129)	13 510 (19,600)	41 370 (60,000)	85 500 (124,000)	3.06	6.33
D	89 (-300)	16 130 (23,400)	50 330 (73,000)	99 980 (145,000)	3.12	6.20

(1) Points shown on Fig. 10

(2) Effective stress

(3) Tensile yield strength at operating temperature

(4) Tensile ultimate strength at operating temperature

TABLE 6. PREBURNER INJECTOR LIFE DATA

Point (1)	Fatigue				Creep			
	Temperature K (F)	σ_{eff} (2) cm/cm	N_f (3)	$\phi_f = \left(\frac{300}{N_f}\right)$	σ_{eff} (4) N/cm^2 (psi)	tr, (5) hours	$\phi_c = \left(\frac{10}{tr}\right)$	$4\ (\phi_f + \phi_c)$
1	453 (355)	0.003 0	10^5	0.003	3960 (5744)			
2	144 (-200)	0.001 3	10^6	Negligible	Negligible	Negligible	Negligible	Negligible
3	561 (550)	0.010 1	15,000	0.020	Negligible			

(1) Points shown on Figure 10

(2) Effective strain range

(3) Cycles to failure at operating temperature and effective strain

(4) Effective stress

(5) Time to rupture at operating temperature and effective stress

NOTE: Operating cycles = 300, and exposure time = 10 hours

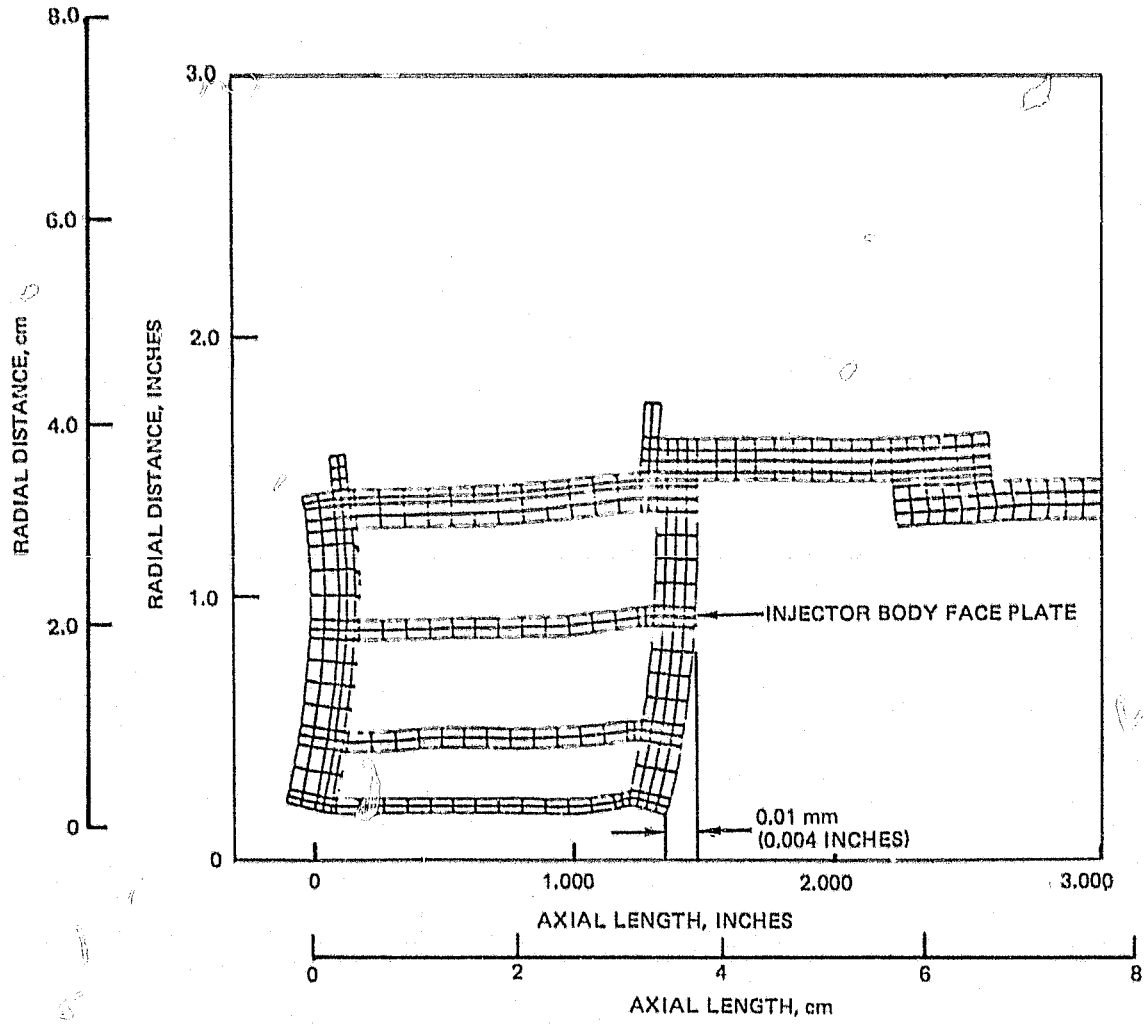

Figure 14. Preburner Injector Faceplate Deflection Model

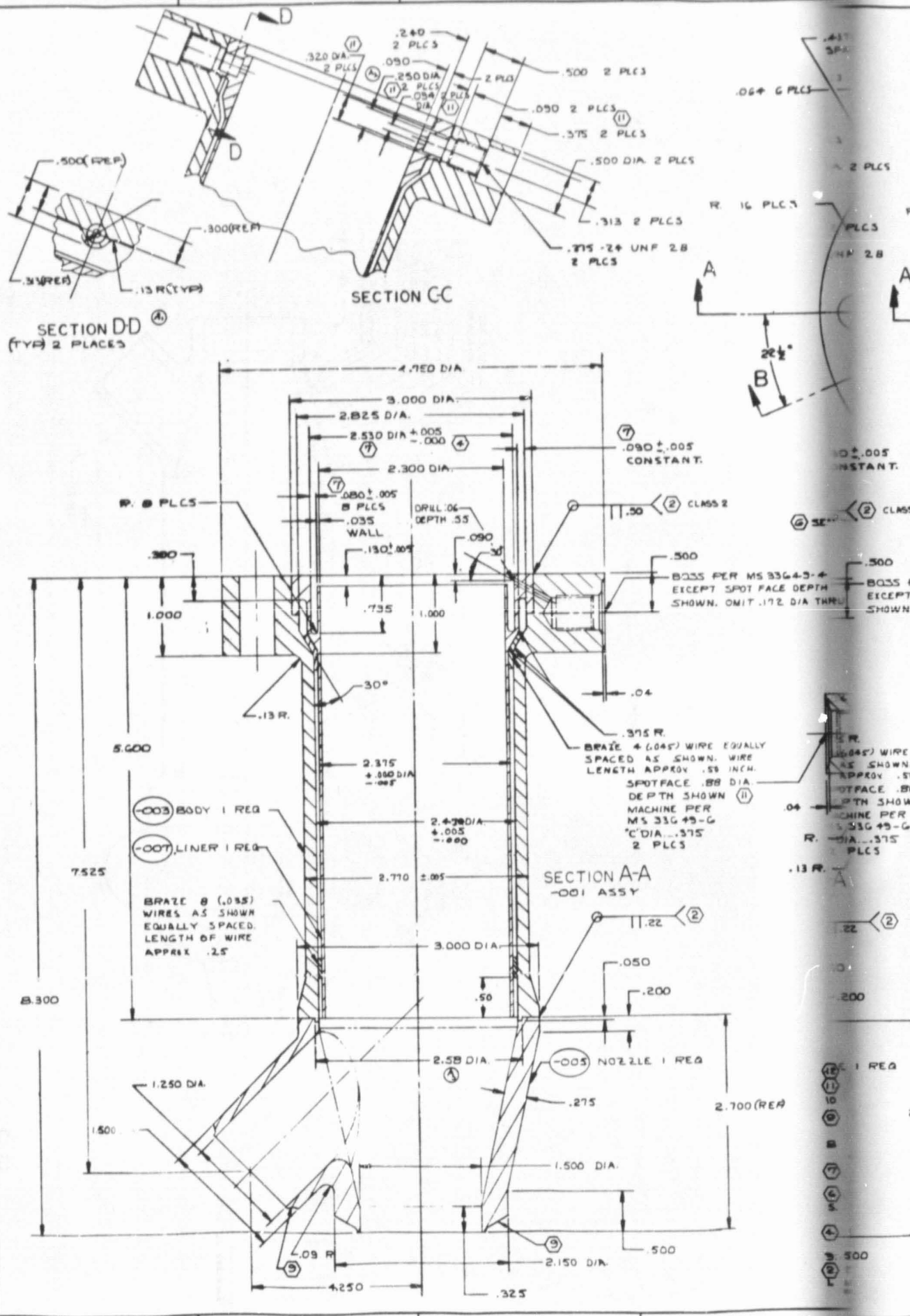
SECTION C-C
SECTION D-D
(TYP) 2 PLACES
SECTION A-A
-001 ASSY
4.760 DIA
3.000 DIA
2.825 DIA
2.530 DIA +.005 -.000
2.300 DIA
.090 ±.005
CONSTANT
.080 ±.005
8 PLCS
.035
WALL
DRILL .06
DEPTH .55
CLASS 2
.130 ±.005
.380
1.000
.735
.500
BOSS PER MS 33643-4
EXCEPT SPOT FACE DEPTH
SHOWN. OMIT .172 DIA THRU
30°
.13 R.
.04
.375 R.
BRAZE 4 (.045) WIRE EQUALLY
SPACED AS SHOWN. WIRE
LENGTH APPROX .55 INCH.
SPOTFACE .88 DIA.
DEPTH SHOWN
MACHINE PER
MS 33649-6
"C" DIA. .375
2 PLCS
5.600
2.375 +.000 -.005 DIA
-003 BODY 1 REQ
-007 LINER 1 REQ
2.438 DIA +.005 -.000
7.525
2.770 ±.005
BRAZE 8 (.035)
WIRES AS SHOWN
EQUALLY SPACED.
LENGTH OF WIRE
APPRX .25
8.300
3.000 DIA
.050
.200
.50
2.58 DIA
-005 NOZZLE 1 REQ
1.250 DIA
.275
2.700 (REF)
1.500
1.500 DIA
.09 R
2.150 DIA
.500
4.250
.325
.320 DIA
2 PLCS
.240
2 PLCS
.090
.250 DIA
2 PLCS
.054 DIA
2 PLCS
.500 2 PLCS
.090 2 PLCS
.375 2 PLCS
.500 DIA 2 PLCS
.313 2 PLCS
.875 -24 UNF 2B
2 PLCS
.500 (REF)
.300 (REF)
.13 R (TYP)
.064 6 PLCS
R. 16 PLCS
22½°

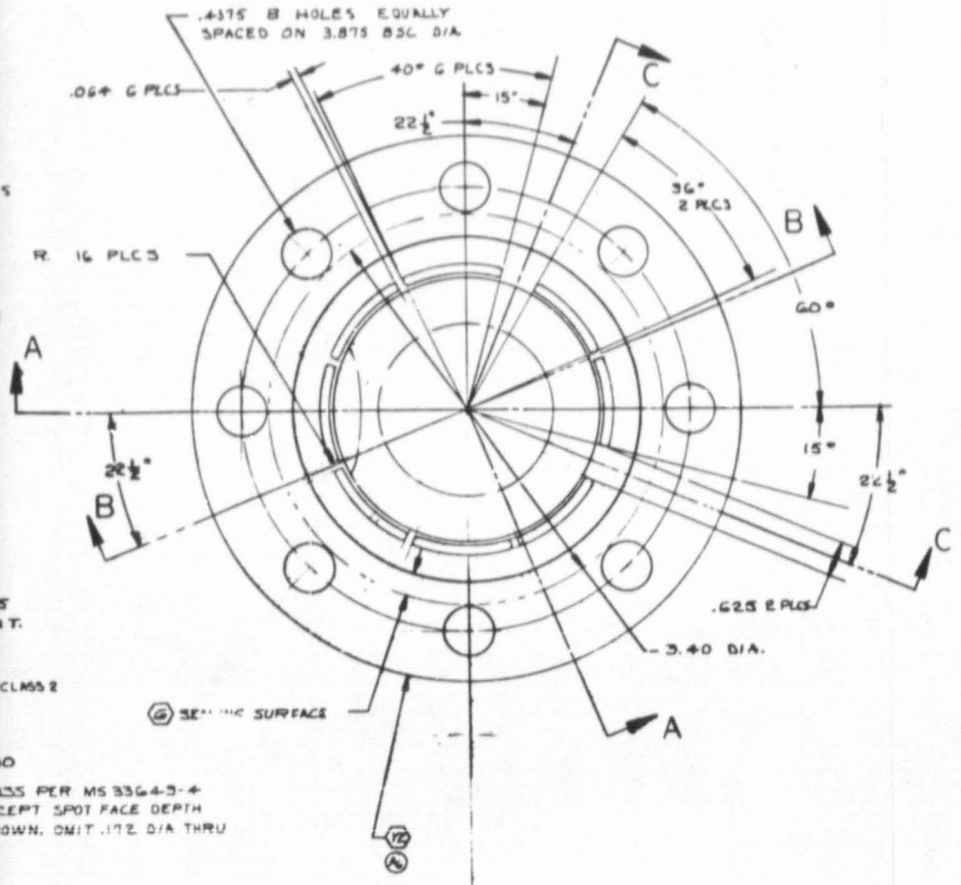

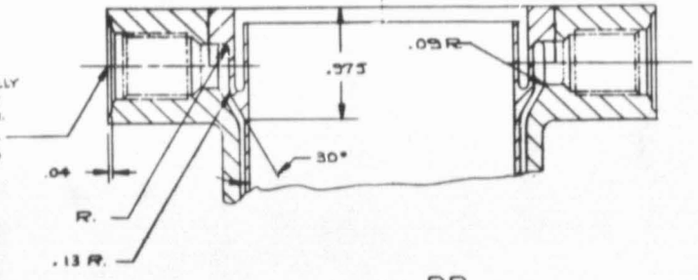

SECTION BB

REVISIONS				
ZONE	LTR	DESCRIPTION	DATE	APPROVED
	A	1. ADDED SECTION DD FOR CLARITY. 2. ADDED NOTE 11 3. 2.58 DIA WAS 2.58 4. CHANGED NOTE 10 99RS010250 WAS 99RS010256 5. CHANGED NOTE 1 RA0103-002 WAS RA0103-016 6. ADDED NOTE # 12.		

[redacted]

2

ORIGINAL PAGE IS
OF POOR QUALITY

(12) IDENTIFY BY ELECTICAL CHEMICAL ETCHING
(11) MACHINE AFTER E.B. WELDING
10 PRESSURE TEST ON 99RS010250 ASSY.
(9) PREP FOR FULL PENETRATION J-GROVE WELD
8 PROOF PRESS AS AN ASSY WITH P/N 99RS010249, 99RS010252, 99RS010253 DUCTING.
(7) ELECTRICAL DISCHARGING MACHINING PERMITTED ON THIS SURFACE.
(6) FLAT WITHIN 4 HELIUM LIGHT BANDS
5. PROOF PRESS TEST -001 ASSY WITH WATER AT 6000 PSIG ± 100 HOLD 3 MIN EACH FOR 5 CYCLES
(4) ELECTRICAL DISCHARGE MACHINING ACCEPTABLE ON THIS SURFACE.
3. CLEAN PER RA0110-018
(2) E.B. WELD PER RA0107-042 CLASS I
1 MACHINE PER RA0103-016

NOTES: UNLESS OTHERWISE SPECIFIED

Figure 15

31

DASH NO	MATERIAL	SIZE	SPECIFICATION	ZONE
-007	INCONEL 625		AMS 5666	
-005	INCONEL 625		AMS 5666	
-003	INCONEL 625		AMS 5666	

-001 ASSY

NEXT ASSY | USED ON | APPLICATION

UNLESS OTHERWISE SPECIFIED DIMENSIONS ARE IN INCHES AND APPLY PRIOR TO FINISH. SURFACE ROUGHNESS MACH TURF. TOLERANCES ± ANGLES ± 0° 30' DECIMALS .XX ± .03 .XXX ± .010 HOLES LISTED "TRUE" GIVEN THRU TOLERANCE

DRAWN | DATE | CHK | DESIGN | MATL | STRUCT | DESIGN APPROVED | DATE

DO NOT SCALE PRINT

Rocketdyne Division
Canoga Park, California

PREBURNER BOLT, 20K AXIAL THRUST

NEXT ASSY OF

SIZE E | CODE IDENT NO. 02602 | DRAWING NO. 99RS010246

SCALE 2/1 | SHEET 1 OF 1

99RS010246

X-1

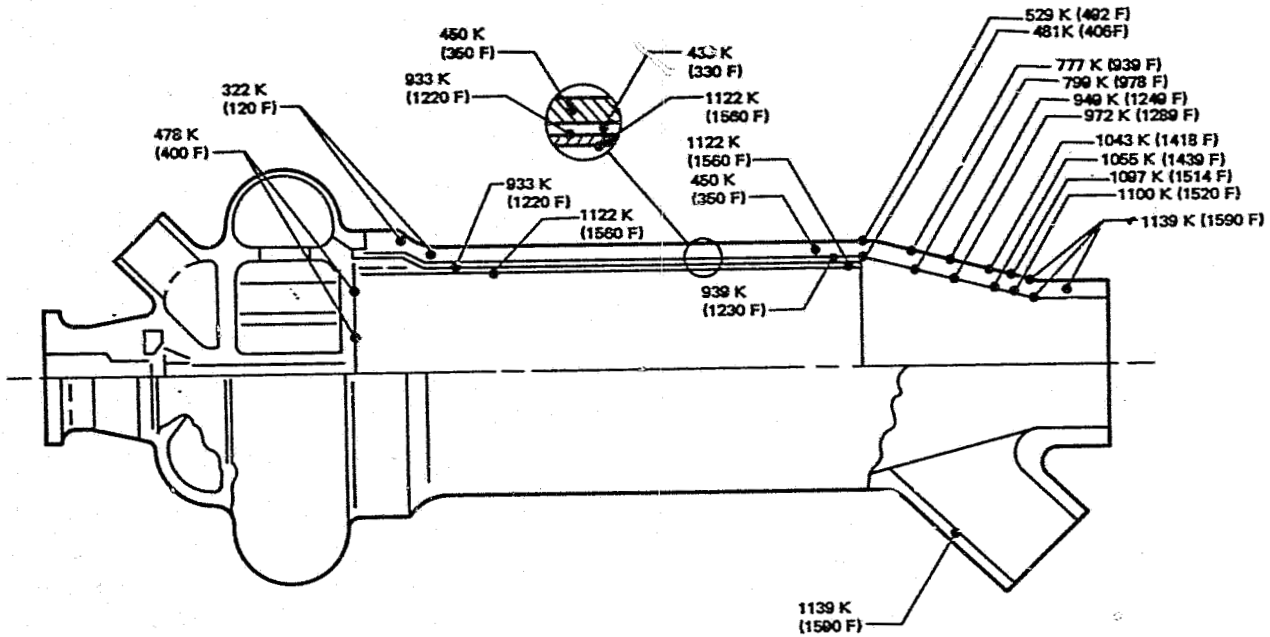

Figure 16. Preburner Combustor Temperature Distribution

A one-dimensional thermal analysis was performed on the preburner liner both at the end of the liner at the coolant exit and at the forward end near the injector. The gas-side heat transfer coefficient was determined using a standard pipe flow equation with a 20% safety factor:

$$h_g = 0.026 \frac{c_p \mu^{0.2} G^{0.8}}{D_H^{0.2} Pr^{0.6}}$$

where

c_p = specific heat

μ = viscosity

G = mass velocity

D_H = hydraulic diameter

Pr = Prandtl number

The coolant-side heat transfer coefficient was determined using the McCarthy-Wolf correlation:

$$h_c = 0.025 \left(\frac{k}{D_H}\right) (Re)^{0.8} (Pr)^{0.4} \left(\frac{T_b}{T_{wc}}\right)^{0.55} \phi_c$$

where

k = thermal conductivity

and

D_H = hydraulic diameter

Re = Reynolds number

Pr = Prandtl number

T_b = coolant bulk temperature

T_{wc} = coolant sidewall temperature

ϕ_c = curvature enhancement

The liner material thermal conductivity variation with temperature was included and the hydrogen gas coolant bulk temperature rise was calculated using average values of the wall temperature and film coefficients over the total liner surface area. The operating conditions used in the analysis are shown in Table 7.

As previously noted, the preburner was divided into three physical parts: (1) the combustor body, (2) the igniter, and (3) the injector body for modeling purposes. The combustor body was modeled as an axisymmetric thin shell of revolution and analyzed for stresses, strains, and deflections by the computer.

Those areas of the preburner considered most critical or of the most interest are shown on Fig. 13 and the basic strength and life values are shown on Table 8 and 9.

The combustor body and combustor exhaust manifolds were fabricated from Inconel 625. This material was selected primarily because of its high strength in the range of temperatures which were expected to occur on the preburner, and its low susceptibility to hydrogen embrittlement. In addition, Rocketdyne has established machining, brazing, and welding techniques for this material.

A structural and life analysis was conducted on the preburner for the most critical combinations of pressure and thermal loading. The temperatures and pressures used are shown in Fig. 16 and 17. Minimum safety factors of 1.1 on yield strength, 1.4 on ultimate strength, and 4.0 on life were used while limiting total creep to 1.0%.

The fundamental theory used in life prediction analysis is that failure depends on the accumulation of creep damage and fatigue damage. Data obtained from material fatigue specimens and test data of actual hardware, or, if test data are unavailable, the method of universal slopes is used in the life analysis.

The life analysis is based on a definition of the stress-strain-time temperature history during each operating cycle. Creep damage is evaluated from the stress-time-temperature cycle and fatigue damage from the strain-time-temperature cycle.

The increment of creep damage, $\Delta\phi_c$, is determined by the ratio of the time spent at a particular stress level, t, to the time-to-rupture at that stress level, t_r. This is presented mathematically as:

$$\Delta\phi_c = \frac{t}{t_r}$$

where

$\Delta\phi_c$ = Creep damage increment

t = time at stress σ

t_r = time to rupture at the stress σ

TABLE 7. PREBURNER LINER THERMAL ANALYSES CONDITIONS ANALYZED

- Coolant Inlet
  - P = 3402 N/cm^2 (4934 psi)
  - T = 281 K (506 R)
  - $\dot{W}_{H_2}$ = 45 g/s (0.1 lb/sec)
- Hot Gas
  - P_c = 3034 N/cm^2 (4400 psi)
  - T_c = 1129 K (2050 R)
  - W_{TOT} = 5.153 kg/s (11.36 lb/sec)
- Geometry
  - $D_{Hot\ Gas}$ = 6.032 cm (2.375 inches)
  - Linear
    - Inconel 625
    - 0.89 mm (0.035 inch) Thickness
  - Coolant Annulus = 0.76 mm (0.03 inch)

TABLE 8. PREBURNER COMBUSTOR BASIC STRENGTHS

Point (1)	Temperature, K (F)	σ_{eff} (2) N/cm^2 (psi)	Stress		Safety Factor	
			Yield, (3) N/cm^2 (psi)	Ultimate, (4) N/cm^2 (psi)	On Yield Strength	On Ultimate Strength
E	1139 (1590)	8 690 (12 600)	15 500 (22 500)	22 800 (33 000)	1.79	2.62
F	672 (750)	20 070 (29 090)	26 900 (39 000)	67 600 (98 000)	1.34	3.37
G	1139 (1590)	8 690 (12 600)	15 500 (22 500)	22 800 (33 000)	1.79	2.62
H	529 (492)	26 500 (38 427)	29 300 (42 500)	70 330 (102 000)	1.11	2.65

(1) Points shown on Fig. 13

(2) Effective stress

(3) Tensile yield strength at operating temperature

(4) Tensile ultimate strength at operating temperature

TABLE 9. PREBURNER COMBUSTOR LIFE DATA

Point(1)	Fatigue				Creep			
	Temperature K (F)	σ_{eff},(2) cm/cm	N_f(3)	$\phi_f = \frac{300}{N_f}$	σ_{eff},(4) N/cm^2 (psi)	t_r,(5) hours	$\phi_c = \frac{10}{t_r}$	$4\phi_f + \phi_c$
4	1078 (1480)	0.003 4	10,000	0.03	11 476 (16,644)	200	0.05	0.32
5	644 (700)	0.003 7	10,000	0.03	20 058 (29,090)	Negligible	Negligible	Negligible
6	278 (40)	0.001 0	10^6	Negligible	6534 (9476)			

(1) Points shown on Fig. 13

(2) Effective strain range

(3) Cycles to failure at operating temperature and effective strain

(4) Effective stress

(5) Time to rupture at operating temperature and effective stress

NOTE: Operating cycles = 300; exposure time = 10 hours

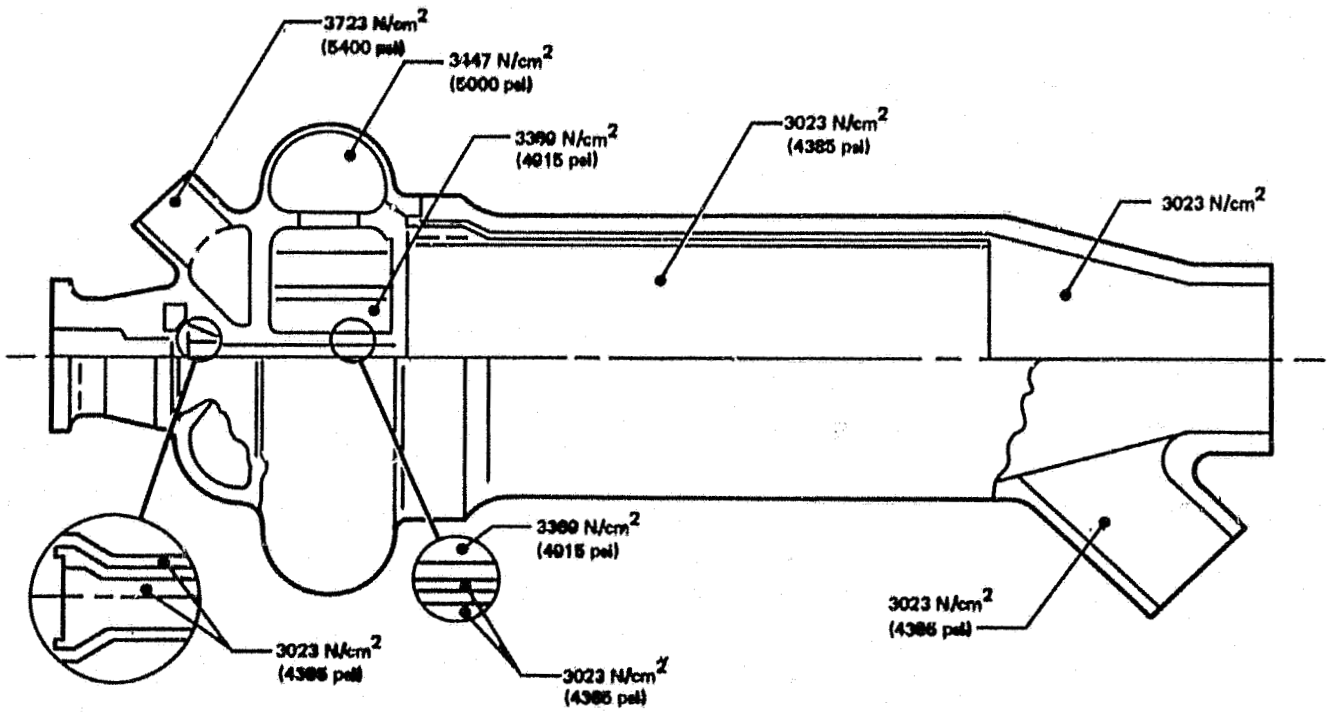

Figure 17. Preburner Pressure Distribution

The total creep damage, ϕ_c, is given by:

$$\phi_c = \sum \Delta \phi_c$$

Fatigue damage, ϕ_f, is determined by the ratio of the actual number of cycles (starts and stops), applied at a particular strain range, to the number of cycles which would cause failure at that strain range.

A generalized life equation used to consider the total damage caused by the interaction of low-cycle fatigue and creep rupture takes the following form:

$$4\ (\phi_f + \phi_c) = 1.0$$

The safety factor of 4 is applied to the typical fatigue and creep rupture life.

Main Injector

The main injector (Fig. 18) was modified from an injector previously fabricated on NASA Contract NAS3-17825, Advanced Thrust Chamber Technology. The design and analysis of the injector is fully described in the final report of that program, NASA CR135221 (Ref. 1). The injector was modified to flow the hot gas effluent from the preburner through the fuel manifold and fuel sleeves of the injection elements. The modification consisted of replacing the existing fuel sleeve design with sleeves with a larger internal diameter. The larger annulus thus created was designed to pass the lower density higher preburner gas flowrate at, or near, the optimum injection velocity. The modified injection element configuration is shown in Fig. 19.

A summary of the main injector element design parameter is presented in Table 10 for the modified injector as well as for the original injector. For comparison purposes the design features of the SSME main injector are also shown. These comparisons illustrate that the main injector, as modified, compares favorably with existing, tested injectors. Although the fuel injection (cup) velocity was higher than the fuel velocity in the original injector, it was still less than the corresponding velocity in the SSME injector.

The injector manifold housing was modified to include the fuel ducting leading from the simulated oxidizer and fuel turbine outlets as shown in Fig. 20. While no turbopumps were used during the assembly or test phases, the use of flight configuration ducting was considered desirable to permit assessment of the injector operation with preburner exhaust products flowing into the injector manifold as though from the turbine exhausts.

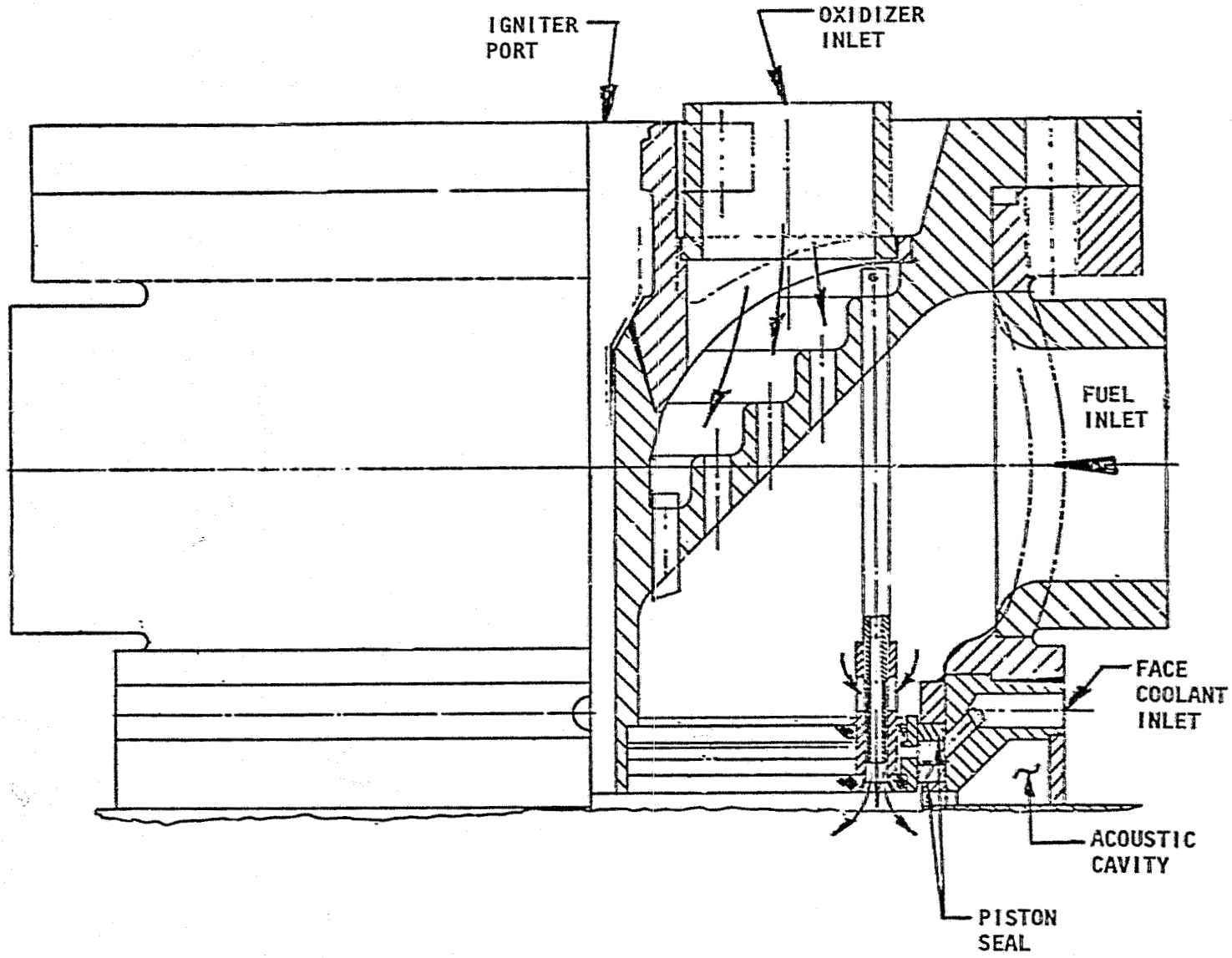

Figure 18. Flanged Injector No. 2

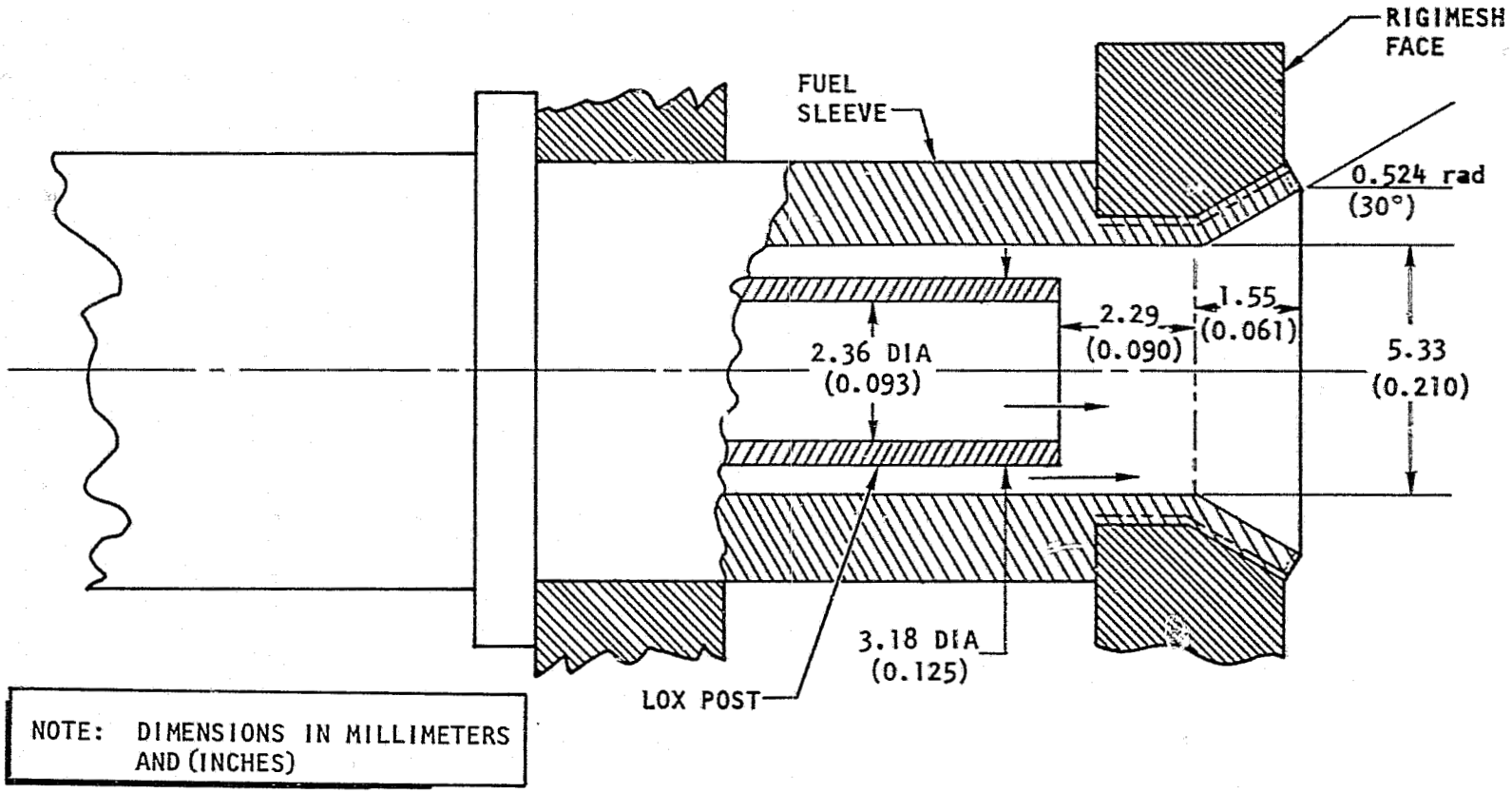

Figure 19. Main Injector Element Configuration

TABLE 10. MAIN INJECTOR ELEMENT DESIGN PARAMETERS

Parameters	Main Injector for Preburner Program		Main Injector for 89K Thrust Chamber Program (Ref. 1)		SSME Main Injector	
	SI	English	SI	English	SI	English
Sleeve ID, D, mm (inch)	5.33	0.210	4.22	0.166	8.84	0.348
Fuel Sleeve Gap, mm (inch)	1.08	0.0425	0.52	0.0205	1.52	0.060
Recess, L, mm (inch)	2.29	0.090	2.29	0.090	5.08	0.200
Recess Ratio, L/D	0.429		0.542		0.570	
Fuel Gap Velocity, m/s (ft/sec)	414.5	1360	338.3	1110	457.2	1500
Fuel Cup Velocity, m/s (ft/sec)	332.8	1092	211.8	695	367.9	1207
Cup ΔP, estimated, N/cm^2 (psi)	44	64	45	65	41	60
Fuel Flowrate per Element, kg/s (lb/sec)	0.039	0.087*	0.022	0.049	0.178*	0.392*
LOX Post OD, mm (inch)	3.18	0.125	3.18	0.125	5.84	0.230
LOX Post ID, mm (inch)	2.36	0.093	2.36	0.093	4.78	0.188
LOX Post Wall Thickness, mm (inch)	4.06	0.016	4.06	0.016	0.53	0.021
LOX Post Velocity, m/s (ft/sec)	27.0	89	30.5	100	32.0	105
LOX Flowrate per Element, kg/s (lb/sec)	0.134	0.296	0.152	0.334	0.686	1.513

*Preburner exhaust products

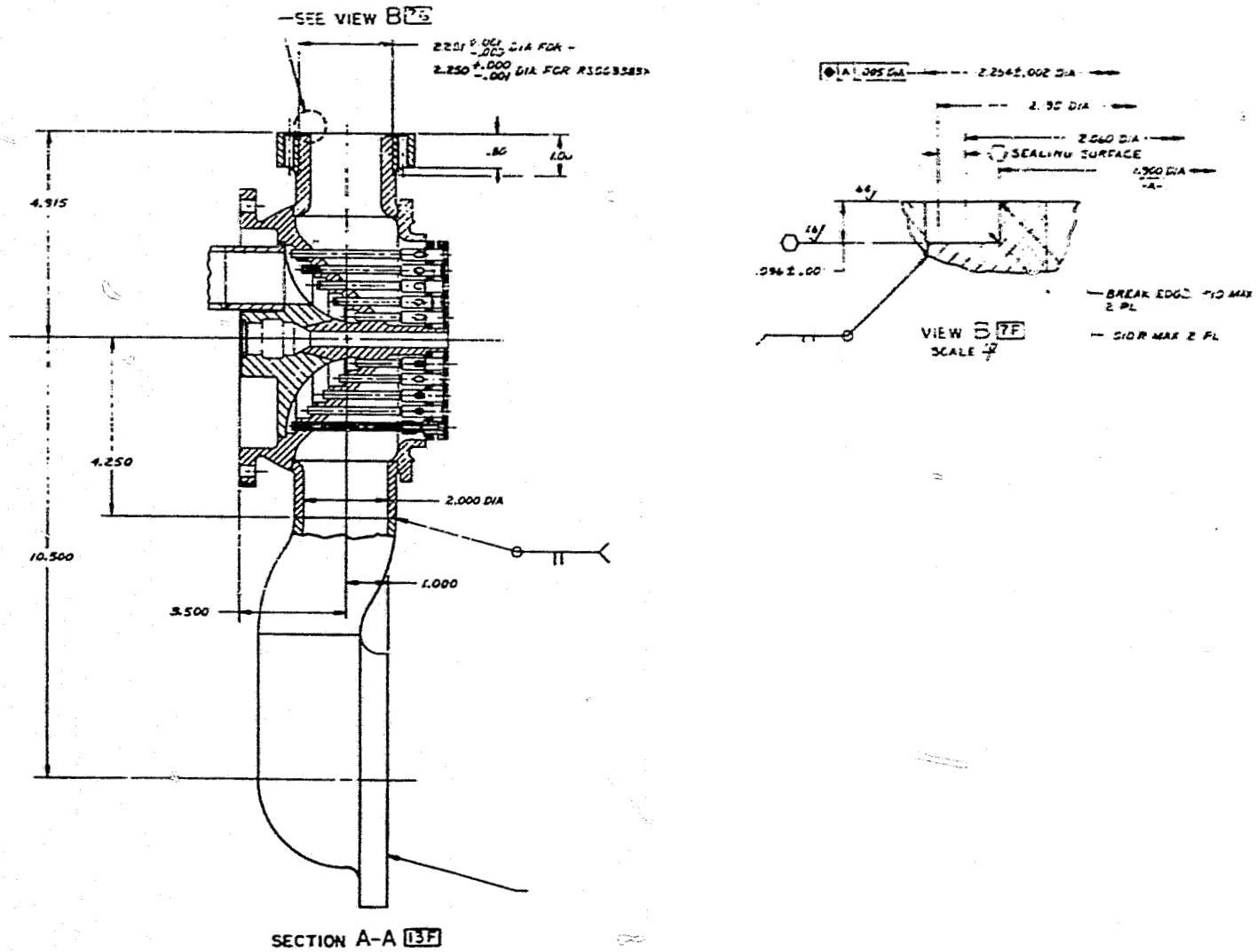

Figure 20. Main Injector Element Design Parameters

Performance Analysis. Comparative history of various injectors and local mixing efficiencies versus a velocity-related mixing parameter is shown in Fig. 21. This shows that the main burner injector, as modified by the sleeve change, was operating in a region of high mixing efficiency similar to, or better than, the SSME main injection element.

For the modified main injector, at a mixing parameter value of 15 and a cup recess/liquid jet diameter ratio of 0.429, a mixture ratio uniformity factor (E_m) of nearly 100 is shown on Fig. 21. A generalized plot of E_m versus $\eta_{c*,\ mix}$ obtained from SSME and other injector cold-flow data in the mixture ratio range of 5.0 to 7.0 (Fig. 22) led to a predicted $\eta_{c*,\ mix}$ for the injector in excess of 99.5%.

The Coaxial Injection Combustion Model (CICM) was used as a performance prediction tool, and the main injector design configuration was analyzed using the CICM model, at three system mixture ratios of interest: 5.5, 6.0, and 6.5. Results shown in Fig. 23 indicate high vaporization/reaction efficiencies for all mixture ratios of interest. The vaporization/reaction efficiency ($\eta_{c*,\ vap}$) represents the percentage of propellant vaporized and reacted in the combustion chamber assuming perfect mixture ratio distribution. It includes drop size vaporization characteristics and reaction rates.

Overall injection characteristic velocity efficiency is normally expressed as the product of the mixing efficiency, and the vaporization/reaction efficiency:

$$\eta_{c*,\ pred} = \eta_{c*,\ mix} \times \eta_{c*,\ vap}$$

For the main injector design, the overall predicted characteristic velocity efficiency values were as shown in Table 11.

TABLE 11. MAIN INJECTOR η_{c*} VALUES

Mixture Ratio, o/f	Characteristic Velocity Efficiency η_{c*}, %
5.85	99.5
6.38	99.43
6.92	98.42

Injector Life. The main injector fabricated for the Advanced Thrust Chamber Technology program (NAS3-17825) fully met the cycle life requirements of that program since ambient hydrogen gas was the fuel used in injector operation. However, this effort required injector operation using the hot products of

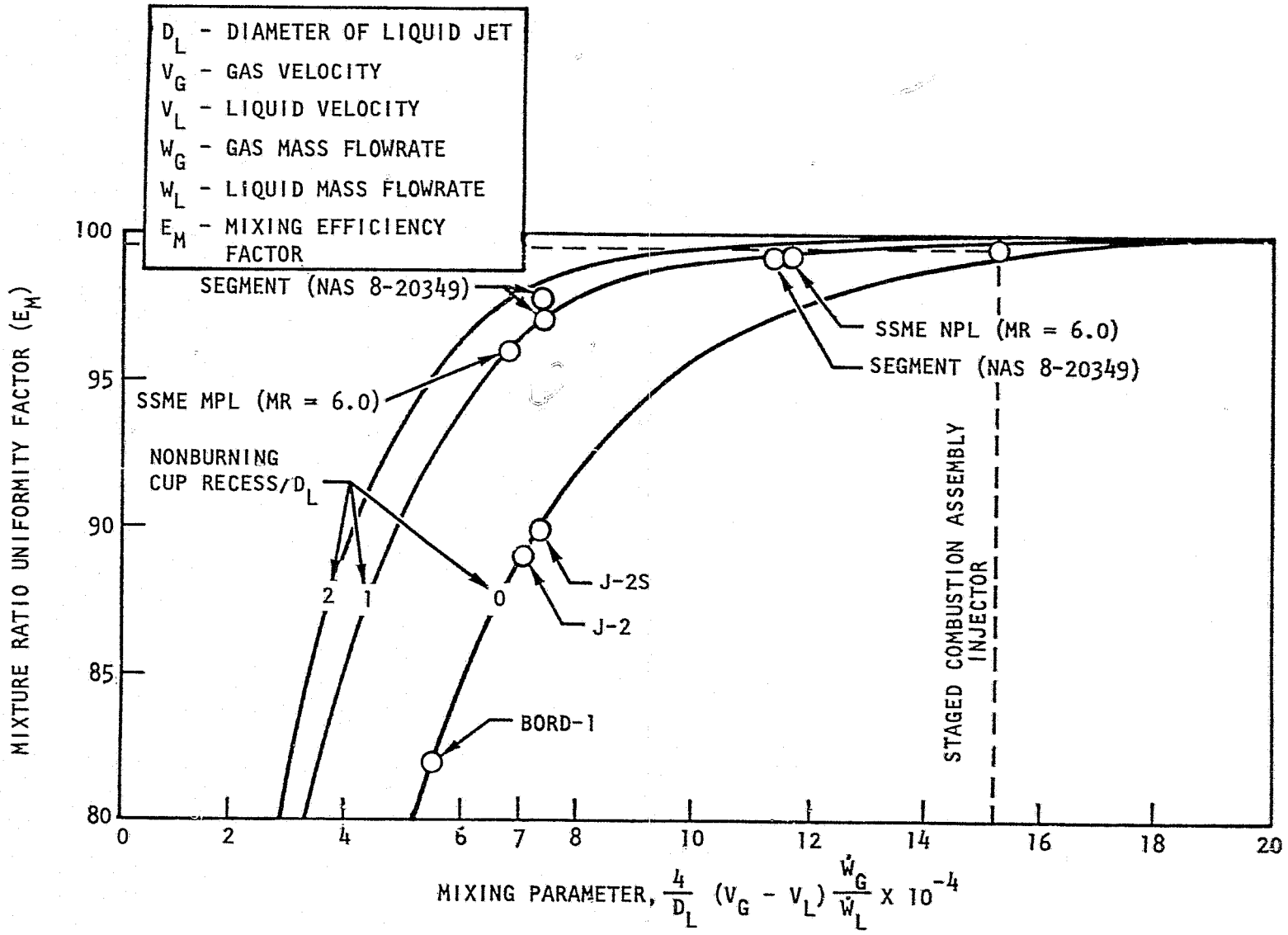

Figure 21. Injector Mixing Efficiency Comparison

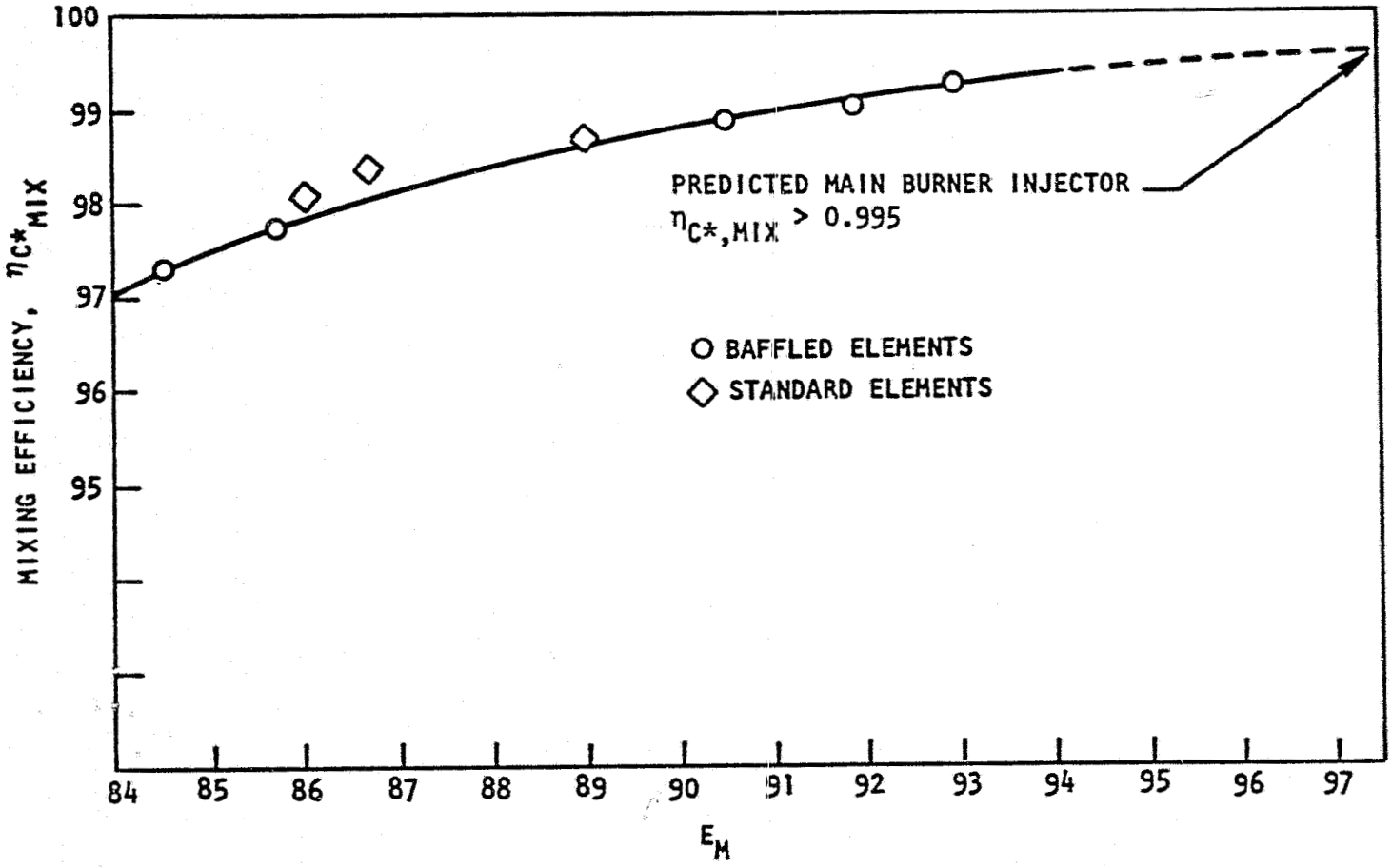

Figure 22. Generalized Plot of Mixing Efficiency (E_m) and ηc^*_{mix}, Based on SSME and Other Cold-Flow Data (o/f = 5 to 7)

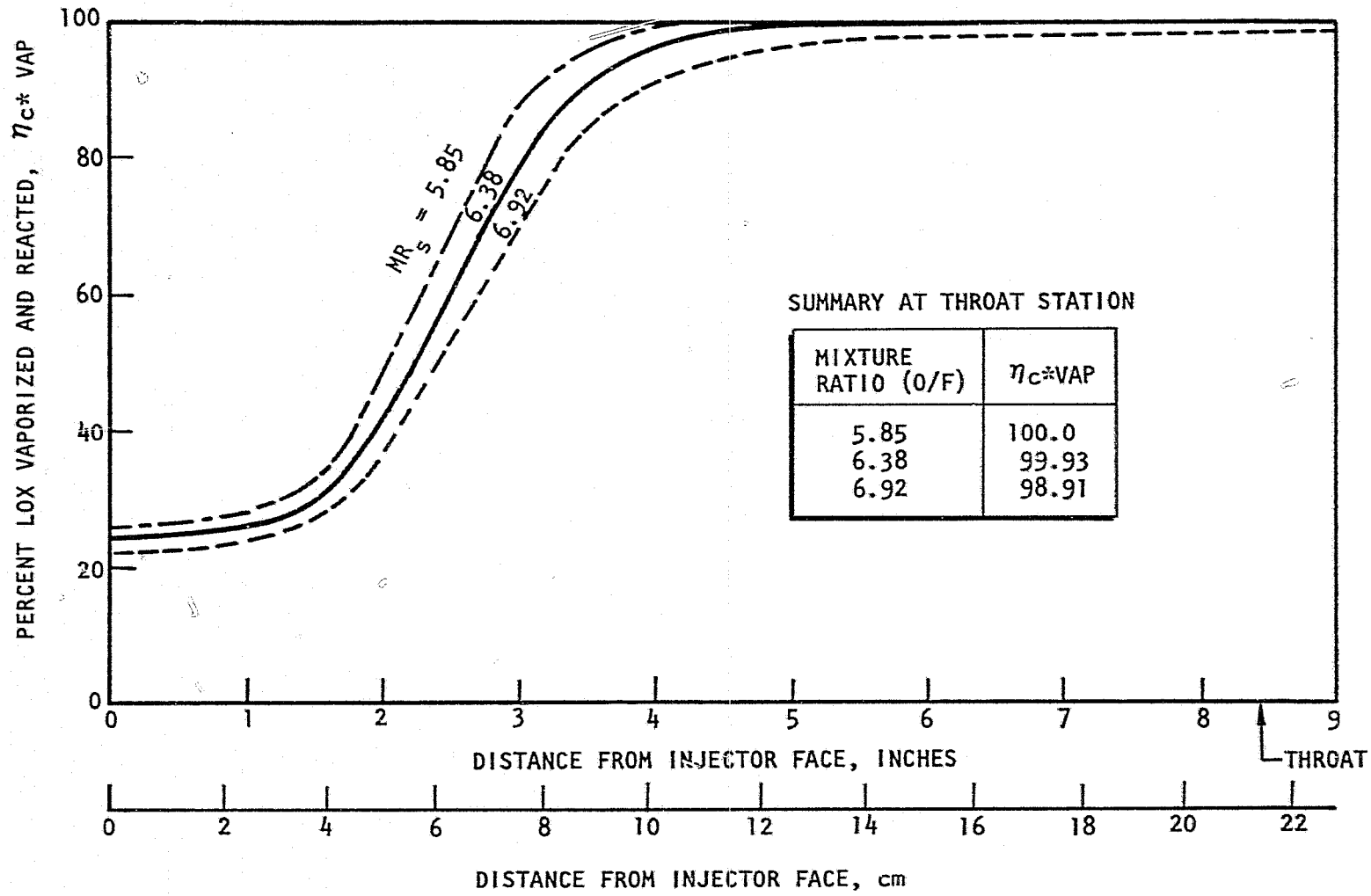

Figure 23. Main Burner Injector Performance per CICM Computer Analysis

combustion from the preburner; the net result is a substantial temperature differential, ~780 K (~1400 F), across the common wall between the fuel and oxidizer injection manifolds.

The cycle life of the injector in this area can also be greatly influenced by the transient thermal behavior during an engine start and shutdown with liquid hydrogen coolant flow used for preburner fuel. During a typical engine start, the temperature differential ($T_{hot\text{-}gas\ side} - T_{LOX\ side}$) through the interpropellant structure would rise to the mainstage value. On shut-down, since liquid hydrogen is colder than liquid oxygen, and the fuel flow lags the oxidizer flow, the temperature differential might be negative. This transient thermal gradient behavior would increase the effective strain range encountered by the injector and could decrease its cyclic life capability. However, since near-ambient temperature hydrogen was used for the preburner fuel during this test program, a less severe impact on cyclic life was expected.

Injector Simulator

During the initial testing of the preburner assembly, it was necessary to duct the hot, fuel-rich preburner gases away from the test stand and toward the facility flame duct. For this purpose, a main injector simulator was created to which the preburner, ducting, and turbine simulators could be attached. This simulator was fabricated from a heavy endpiece suitable for bolting to the test stand and a section of 15.2 cm (6 inch) Schedule 80 pipe (Fig. 24). The simulator was designed for use during the early testing so that possible difficulties encountered with the untested and untried preburner assembly would not pose unnecessary hazards to the more costly injector and cooled combustion chamber. Comparatively thin walled pipe was used for the simulator body because the pressure within the body was expected to be low, with the simulator body principally providing flow direction for the exhaust gases.

Combustion Stability

All features of the preburner design which have a potential effect on combustion stability were controlled to provide maximum preburner stability. The recessed coaxial element injector design is inherently stable, because the stripping action of the high velocity hydrogen produces small oxidizer droplets which are vaporized so rapidly that they are relatively insensitive to transverse acoustic disturbances. This was verified by performing a Priem analysis (Ref. 4) on the preburner, Fig. 25. Although the results of this analysis indicated that the preburner should be dynamically stable, an acoustic absorber was included in the design for additional stability margin. The absorber has 11% open area relative to the combustor cross section and consists of six L-shaped quarter wave cavities spaced along the periphery of the injector end of the combustion chamber. Figure 26 shows the damping provided by the preburner absorber as a function of absorber depth. The optimized depth of 15.5 mm (0.61 inches) was selected. The absorber is tuned for primary damping of the first tangential mode of instability, approximately 16 000 Hz, although it will provide damping for other, higher frequency, transverse modes.

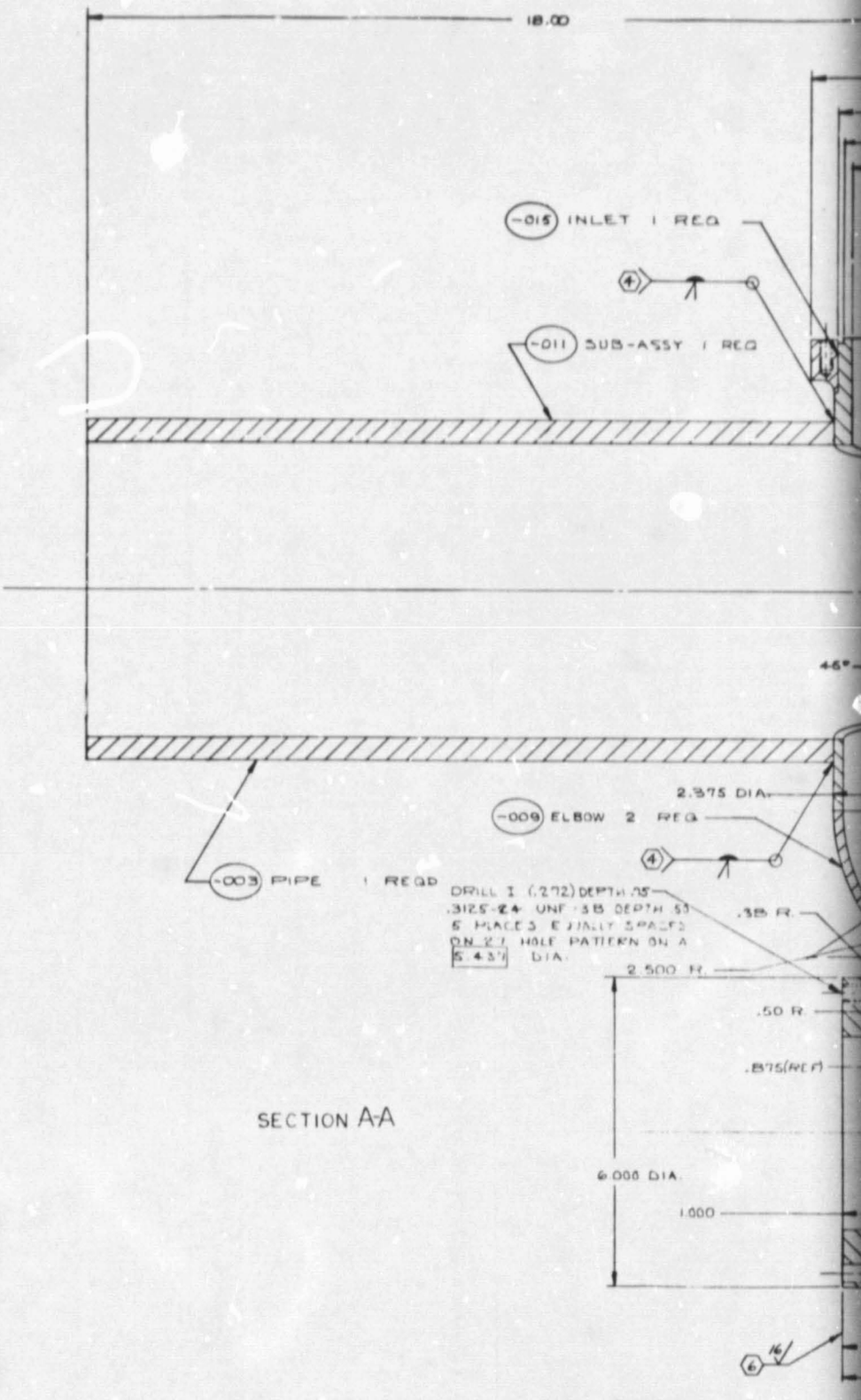
18.00
-015 INLET 1 REQ
4
-011 SUB-ASSY 1 REQ
45°
2.375 DIA.
-009 ELBOW 2 REQ
4
-003 PIPE 1 REQD
DRILL 1 (.272) DEPTH .75
.3125-24 UNF-3B DEPTH .53
6 PLACES EQUALLY SPACED
ON 2.1 HOLE PATTERN ON A
5.437 DIA.
.38 R.
2.500 R.
.50 R.
.875(REF)
6.000 DIA.
1.000
6
16

SECTION A-A

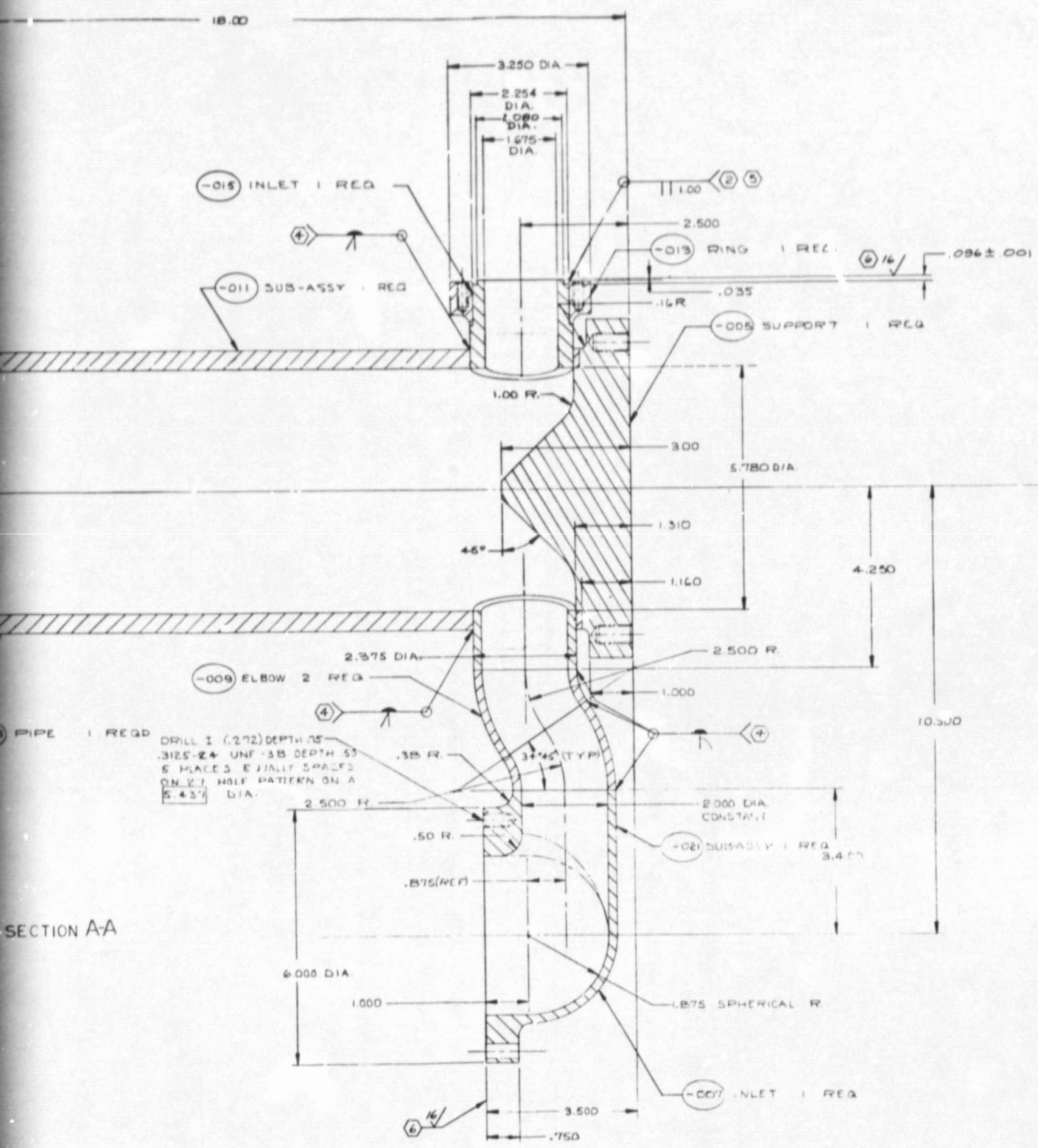

Rockwell International Corporation
Rocketdyne Division
Canoga Park, California

CODE IDENT 82602	FRAME 1	
99RS010249		CHNG SHEET

MICROFILM OVERLAP AREA

FOLDOUT FRAME

3

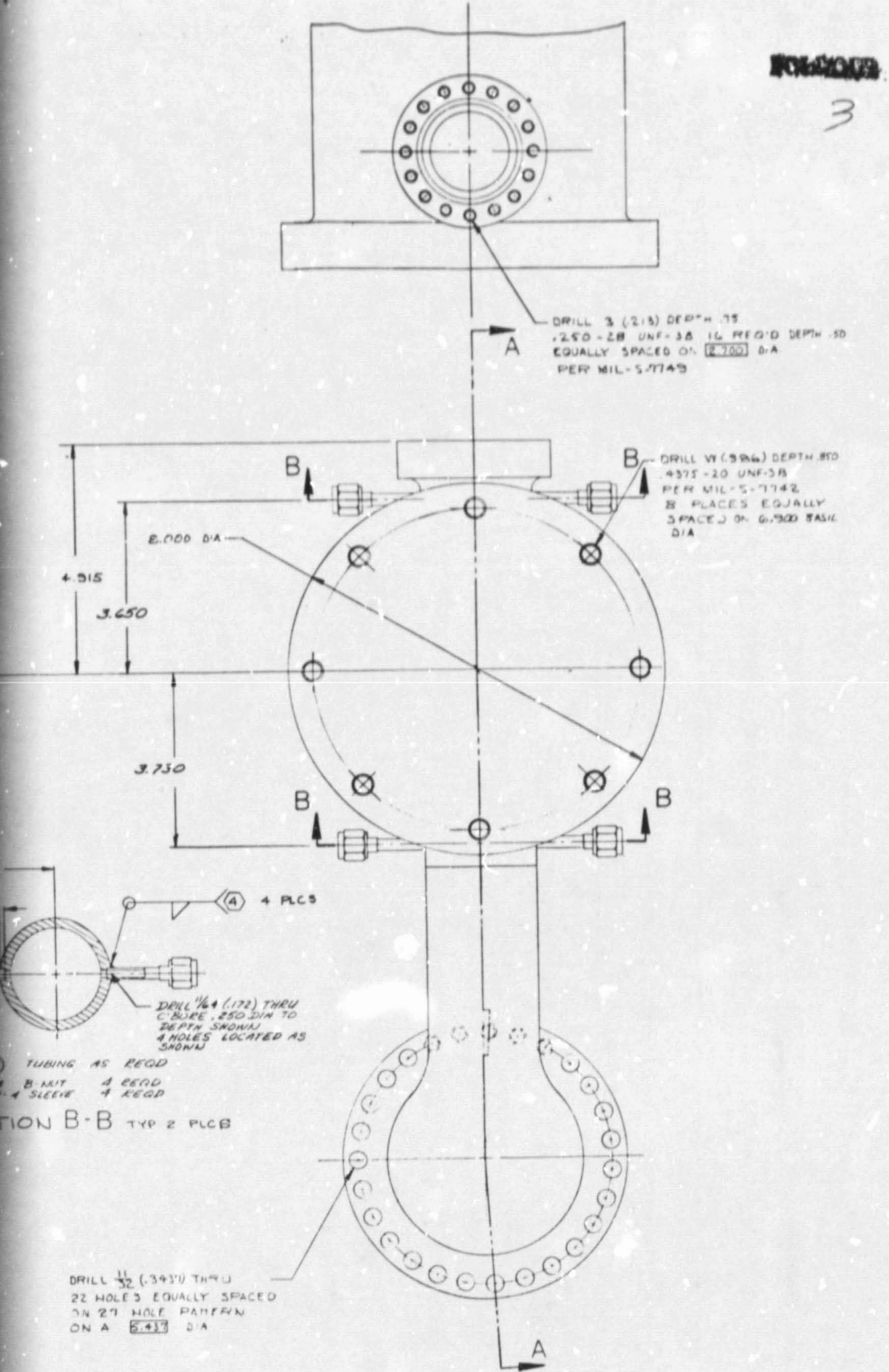

-021
-011
-001
ASSY

6. FLAT WITHIN 4 HELIUM LIGHT BANDS
5. WELD PRIOR TO MACHINING
4. WELD PER RA0107-027
3. CLEAN PER RA0110-018
2. EB WELD PER RA0107-042
1. MACHINE PER RA0103-016

NOTE: UNLESS OTHERWISE SPECIFIED

FILM OVERLAP AREA

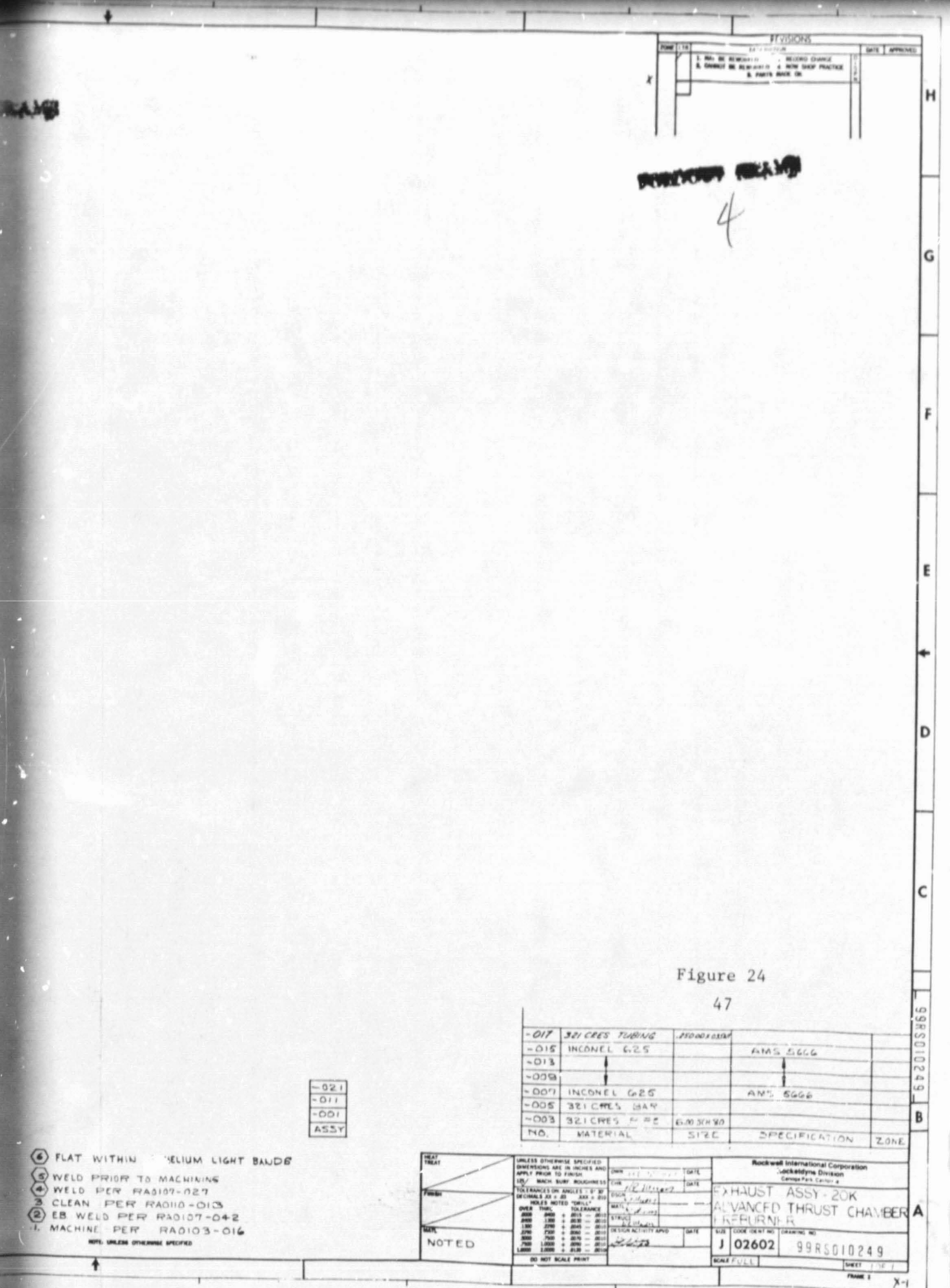

NO.	MATERIAL	SIZE	SPECIFICATION	ZONE
-017	321 CRES TUBING	.250 OD x .035W		
-015	INCONEL 625		AMS 5666	
-013	↕		↕	
-009	↕		↕	
-007	INCONEL 625		AMS 5666	
-005	321 CRES BAR			
-003	321 CRES PIPE	6.00 SCH 80		

-021
-011
-001
ASSY

(6) FLAT WITHIN .XXX SELIUM LIGHT BAUDE
(5) WELD PRIOR TO MACHINING
(4) WELD PER RA0107-027
(3) CLEAN PER RA0110-013
(2) EB WELD PER RA0107-042
(1) MACHINE PER RA0103-016

NOTE: UNLESS OTHERWISE SPECIFIED

HEAT TREAT
FINISH
SIZE NOTED

UNLESS OTHERWISE SPECIFIED DIMENSIONS ARE IN INCHES AND APPLY PRIOR TO FINISH
125 MICRO INCH BURY ROUGHNESS
TOLERANCES ON ANGLES ± 0° 30'
DECIMALS .XX ± .03 .XXX ± .010
HOLES NOTED "DRILL" TOLERANCE
OVER THRU TOLERANCE
.000 .999 + .015 — .000
1.000 1.999 + .020 — .000
2.000 2.999 + .025 — .000
3.000 3.999 + .030 — .000
4.000 4.999 + .035 — .000
5.000 5.999 + .040 — .000
6.000 6.999 + .045 — .000
DO NOT SCALE PRINT

DWN DATE
CHK DATE
DSGN
MATL
STRUC
DESIGN ACTIVITY APVD DATE

Rockwell International Corporation
Rocketdyne Division
Canoga Park, California

EXHAUST ASSY - 20K
ADVANCED THRUST CHAMBER
REGENERATOR

SIZE J | CODE IDENT NO. 02602 | DRAWING NO. 99RS010249
SCALE FULL | SHEET 1 OF 1
FRAME 2 X-1

99RS010249

Figure 24

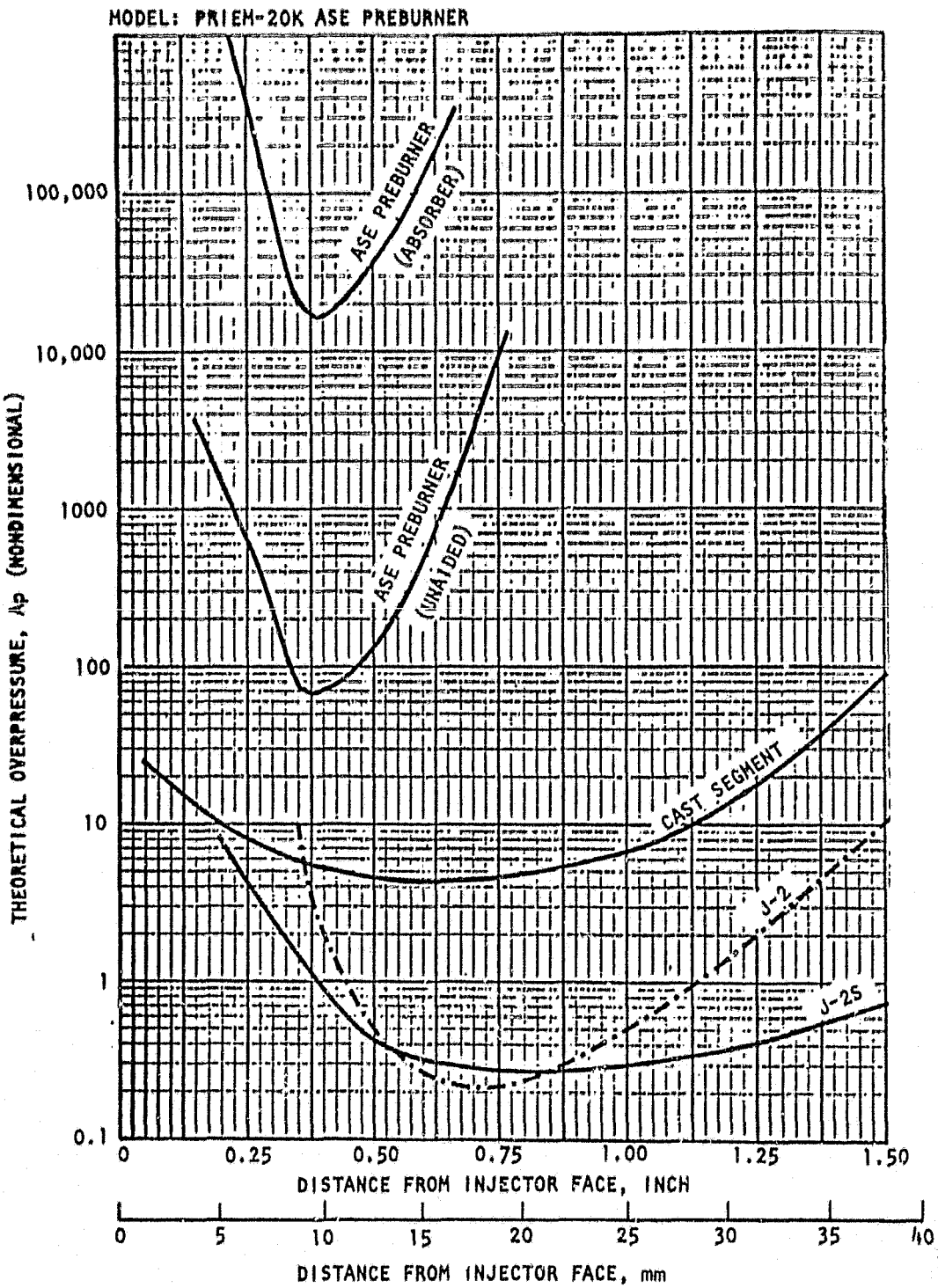

Figure 25. Priem Analysis With Preburner Combustor

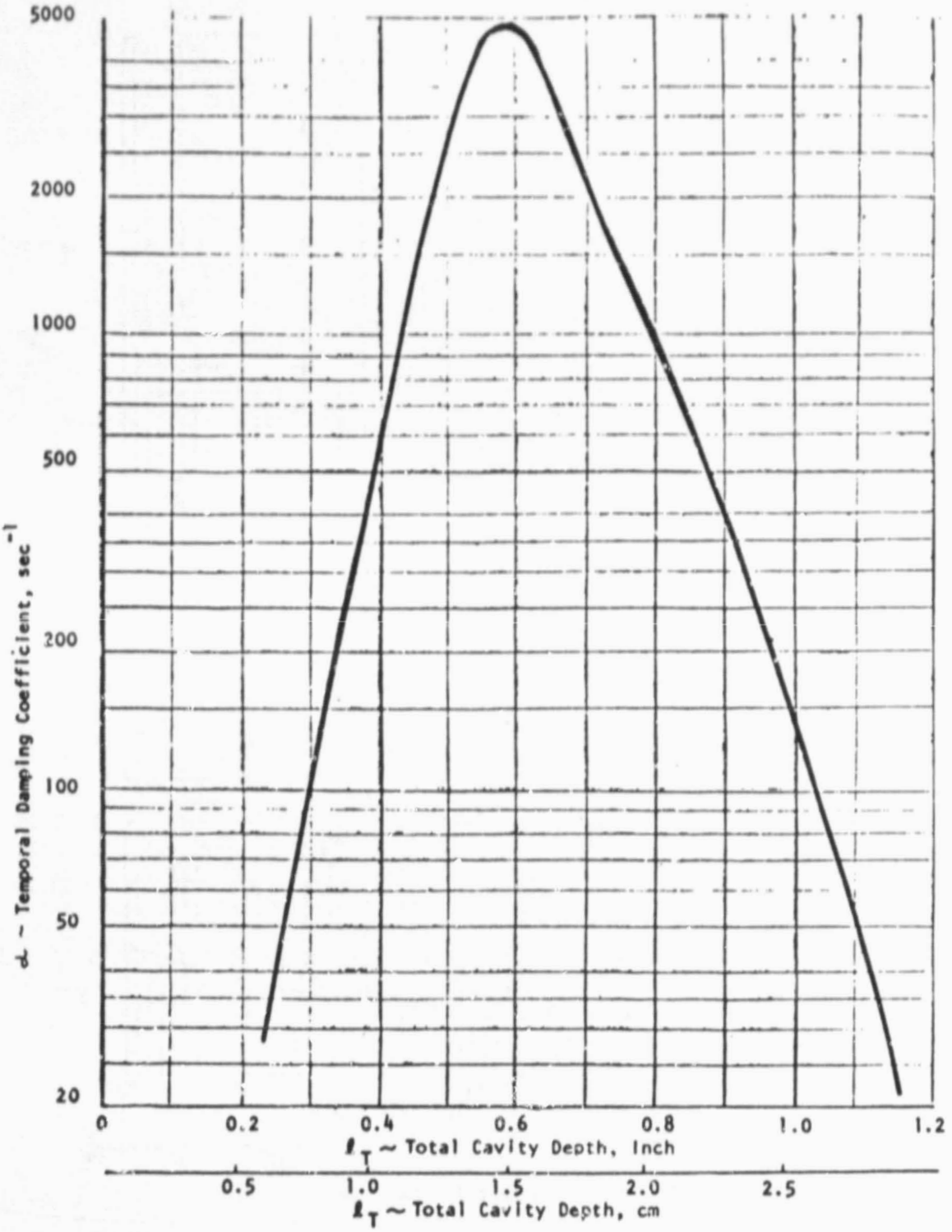

Figure 26. Preburner Acoustic Cavity Design, First Tangential Mode

Figure 28a, shows an industry-wide survey of test results with acoustic damping devices. Figure 28b shows that the preburner injector with the acoustic cavities is well within the stable region, the large open area to the right. Although the acoustic absorber would have been effective with a significantly lower open area, a larger open area was incorporated into the design to maintain a more reasonable slot width of 2.03 mm (0.080 inch).

The feed-system coupled stability of the preburner was evaluated using two approaches: (1) an analysis of the response characteristics of the major elements capable of coupling in an unstable feedback loop, and (2) an analysis using a "double dead-time" analog simulation of the engine which allowed for a detailed evaluation of the interaction of the engine components in a closed-loop operational environment.

The basic mechanism of feed-system coupling is as shown in Fig. 27. For an oscillation to grow or sustain, the total loop gain must be greater than unity and the phase shift must be proper. One way to ensure against coupling of this type is to design the various components such that there are no common frequencies where each has significant gain. This approach was carried out in the design of the ASE.

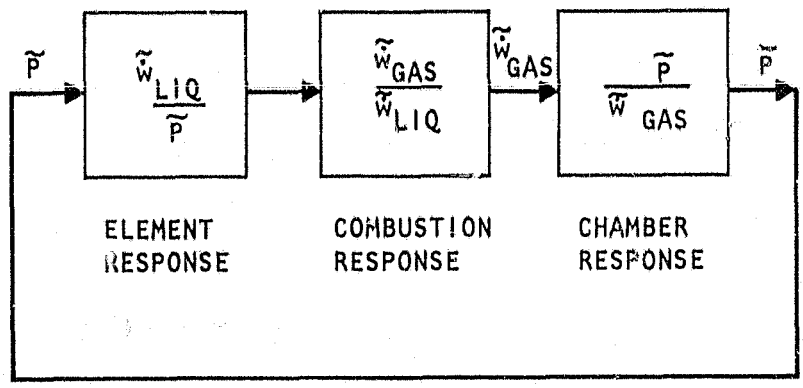

Figure 27. Feedback Loop/Feed-System Coupling

As a result of the open-loop analysis, the preburner was designed such that the hydraulic response, the combustion response (determined using the Rocketdyne Coaxial Injection Combustion Model, CICM, Ref. 2), and the combustor response have no common frequencies where each has a significant gain.

To accomplish the closed loop analysis, a nonlinear mathematical model of the engine system was constructed for the ASE system. This model represented the dynamics of the thrust chamber and preburner and their liquid and gaseous feed systems. The model was mechanized for closed-loop solution on the analog computer and used to parametrically study the engine system stability in the frequency range of 0 to 3000 Hz.

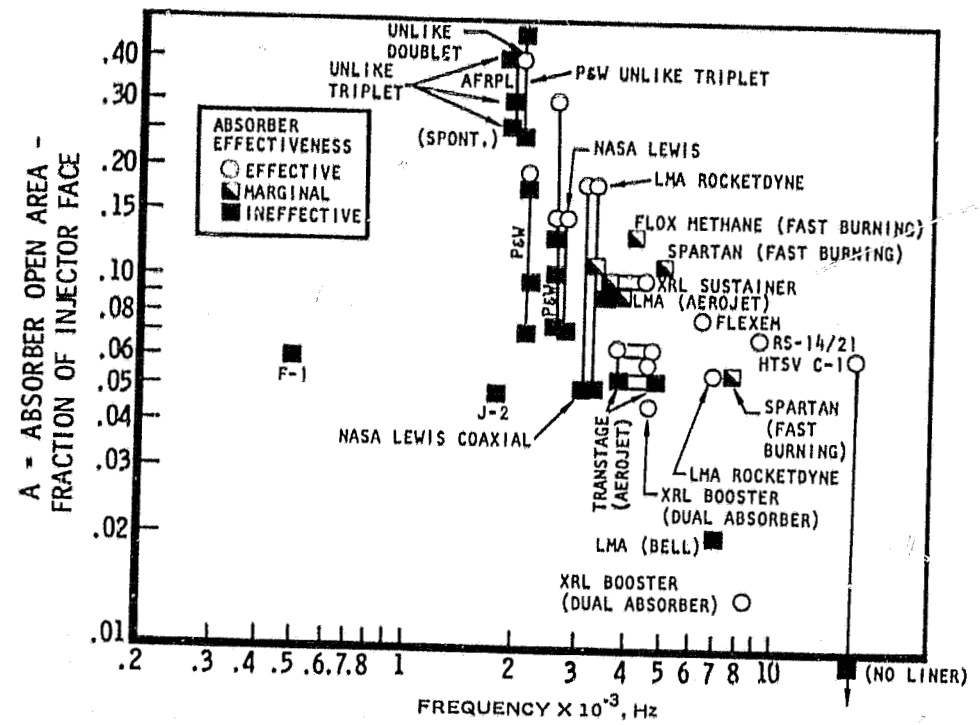

(a)

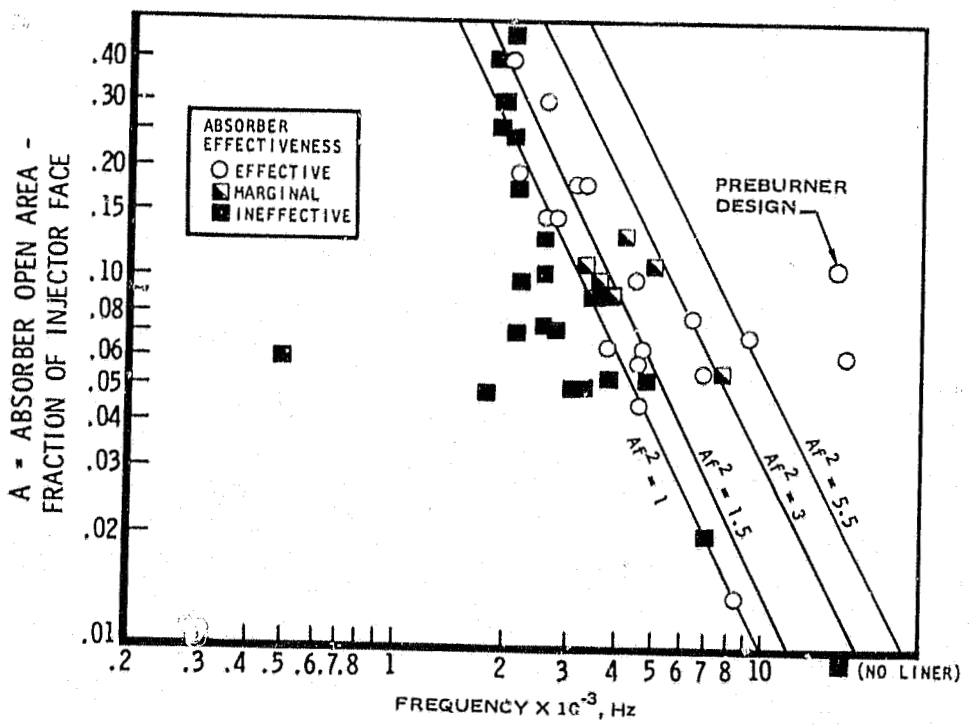

(b)

Figure 28. Absorber Experience

A simplified schematic of the model is shown in Fig. 29. Somewhat further detail of the preburner system (Fig. 30) and main combustion chamber (Fig. 31) are also shown. The possibility of coupling between the preburner and the main chamber was allowed through the mechanization of the hot-gas system as shown in Fig. 32.

The general formulation (Fig. 33) allowed for variation of both a time delay and klystron (clumping) lead term for each propellant. The model, therefore, may be described as a double dead-time model with klystron lead. The description was repeated for both the preburner and main chamber, and the two systems were coupled together through the hot-gas system.

A stability map for the preburner was generated to depict the system stability margin, Fig. 34. This map plots the boundary of incipient instability as a function of the oxidizer injector transport time delay and the oxidizer clumping time constant for fixed similar fuel parameters. In this manner, the stability boundary can be compared to the probable operating region of the preburner to assess the degree of stability margin present. The thrust chamber map obtained from previous study is presented in Fig. 35.

Areas above the boundary of incipient instability are unstable, while those below are stable. The separation of the incipient instability boundary from the probable operating region is the best indicator of the stability margin.

Results of the analog model studies showed no modes of instability because of coupling of either the preburner or the main chamber with the fuel or oxidizer feed systems. The lowest stability margin of the engine is associated with the preburner (Fig. 34). It should be noted that, even in this instance, the clumping lead time constant would have to be more than doubled from the probable operational region to cause instability.

The preburner design was reviewed for susceptibility to longitudinal instability by comparing the power transmission factors of the ASE preburner and the SSME preburners (Table 12).

The power transmission factor is defined as:

$$P_t = \frac{4 \times S_1 \times S_2}{(S_1 + S_2)^2}$$

where

S_1 = Chamber cross-sectional area

S_2 = Throat or nozzle block cross-sectional area

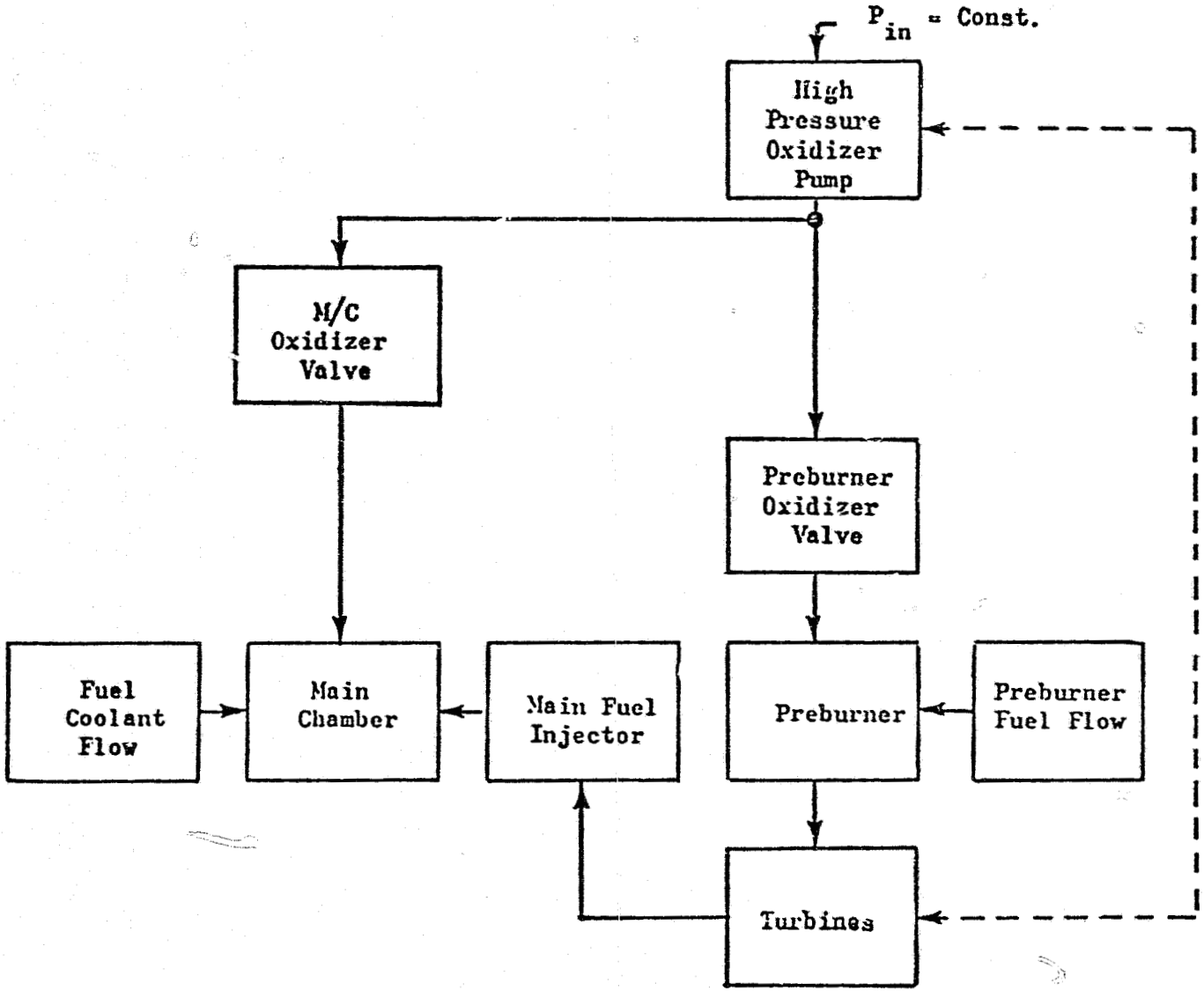

Figure 29. Analog Model Simplified Schematic

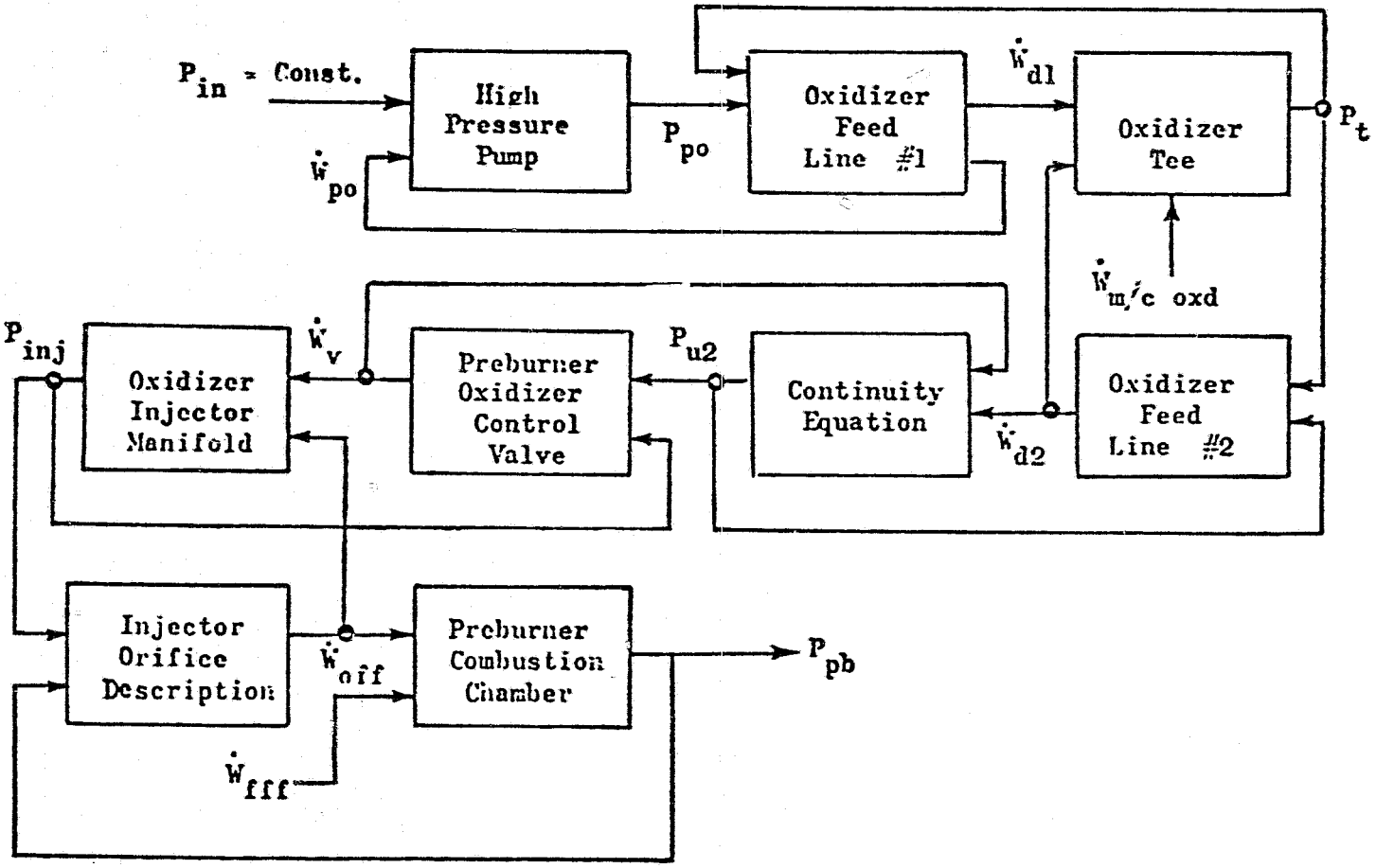

Figure 30. Preburner Model

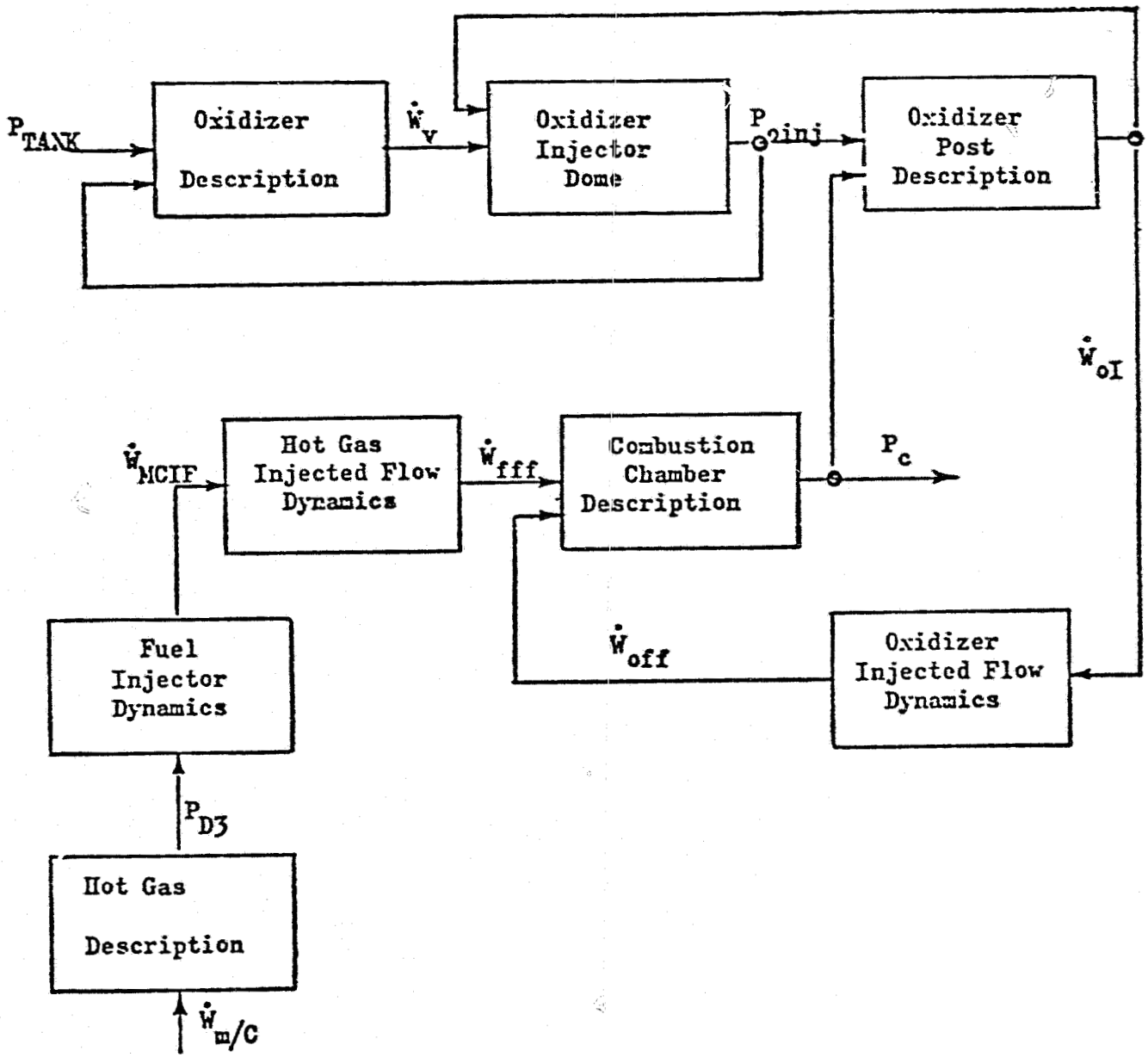

Figure 31. Main Chamber Model

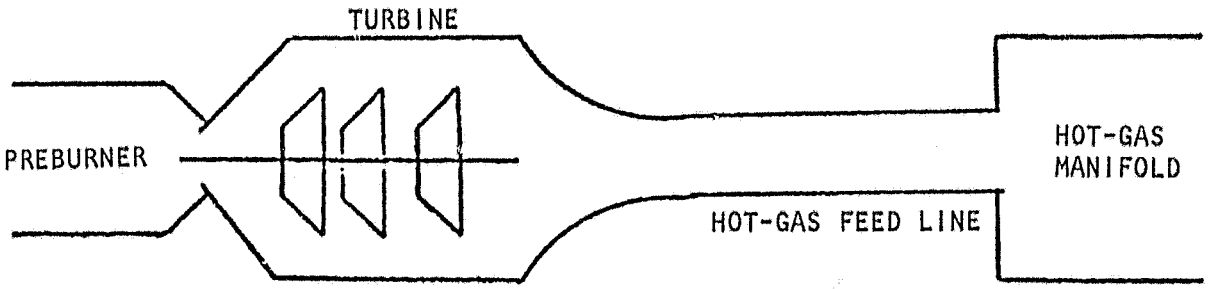

Figure 32. Hot-Gas System Model

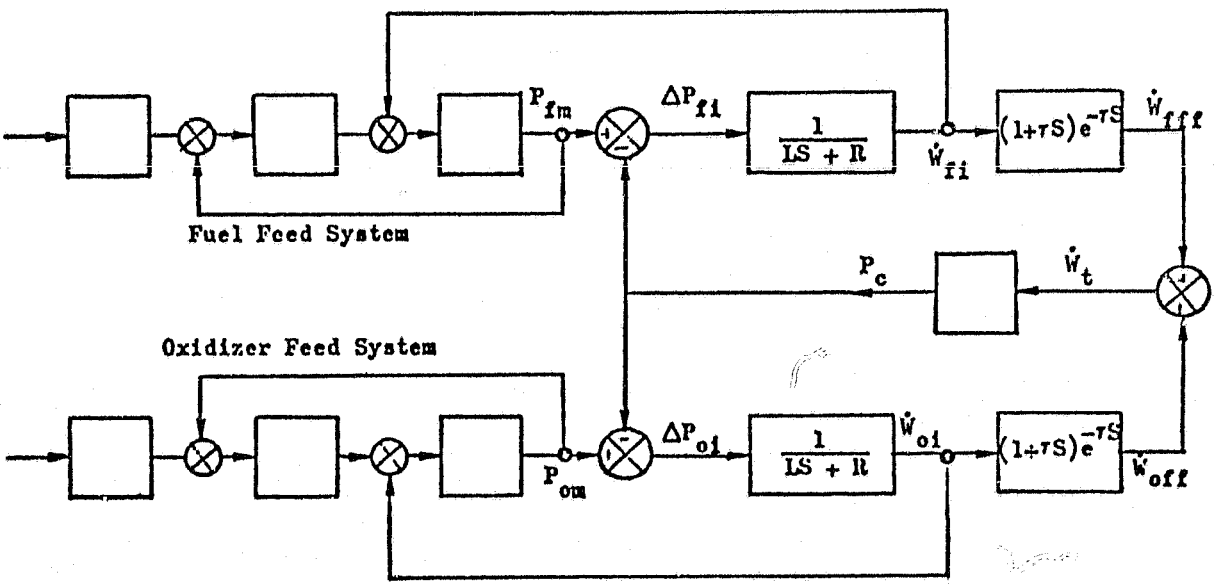

Where P_{fm}, P_{om} = Fuel & Oxidizer Manifold Pressure

$\dot{W}_{fi}$, $\dot{W}_{oi}$ = Fuel & Oxidizer Injector Flowrate

$\dot{W}_{fff}$, $\dot{W}_{off}$ = Fuel & Oxidizer Flowrate at Flame Front

P_c = Combustion Chamber Pressure

Figure 33. Typical Closed-Loop Feed System/ Engine-Coupled Block Diagram

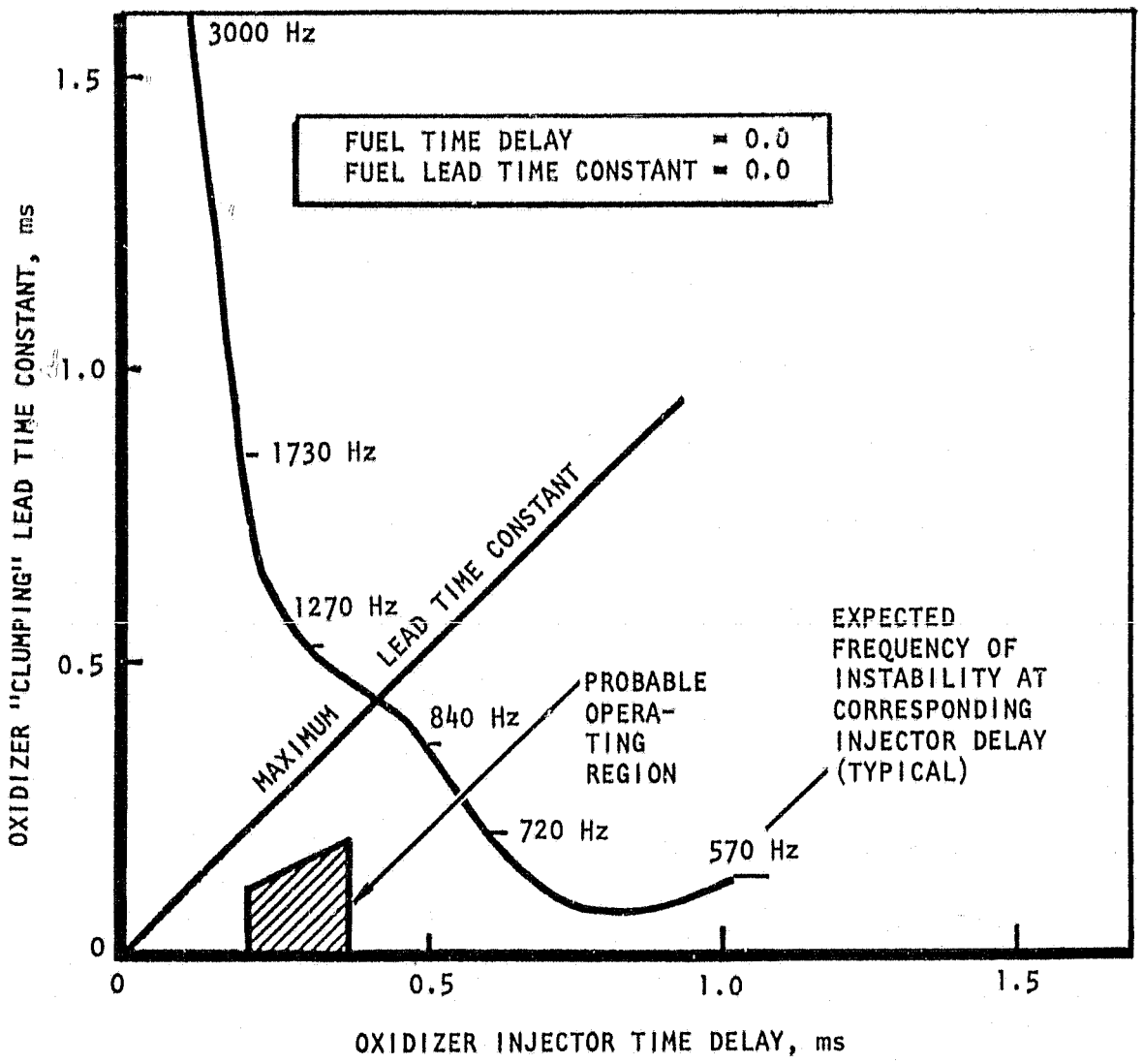

Figure 34. Stability Map for the Preburner

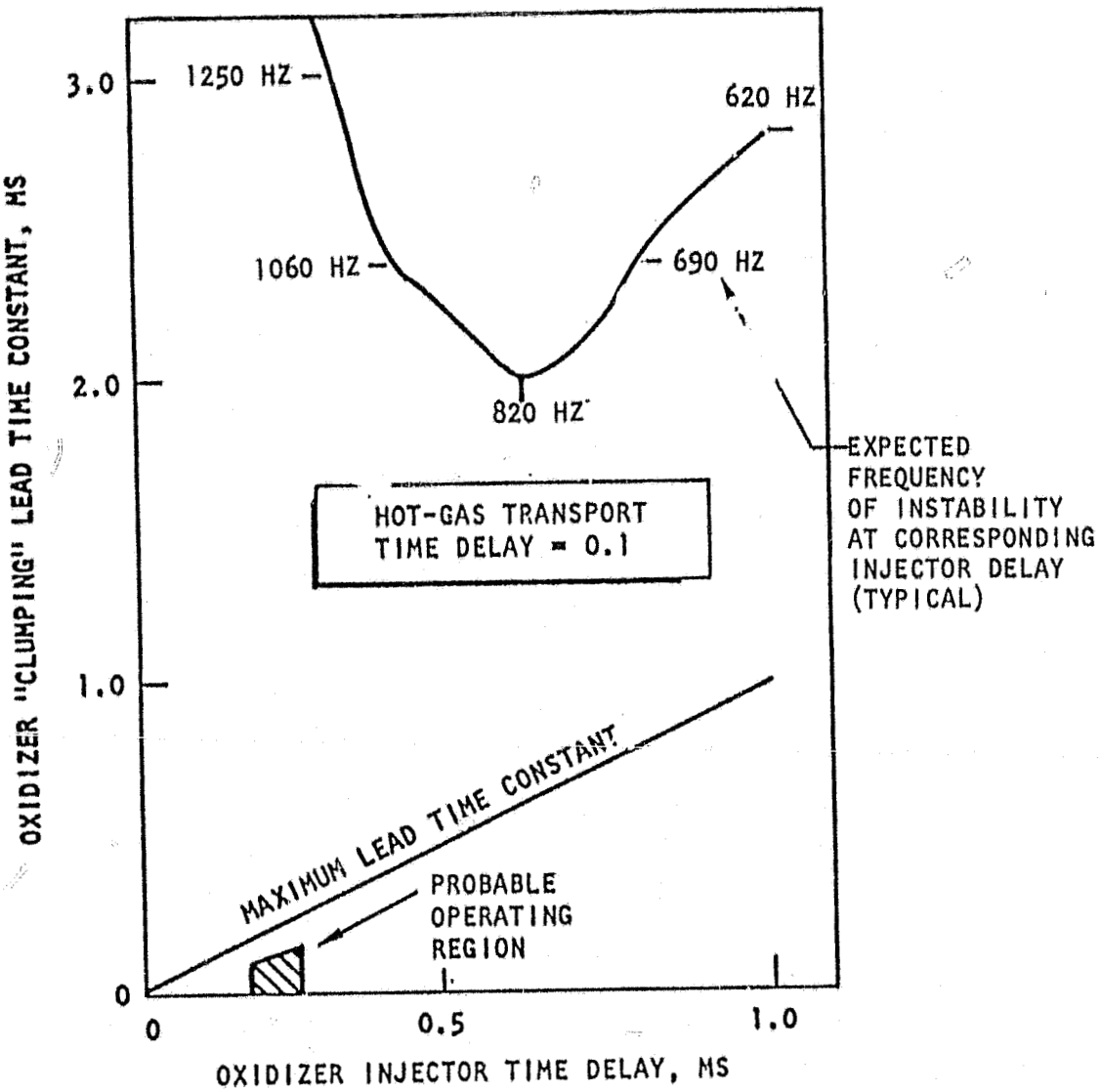

Figure 35. Stability Map for the Advanced Thrust Chamber

TABLE 12. COMPARISON OF POWER TRANSMISSION FACTORS FOR ASE AND SSME PREBURNERS

Preburner	ASE		SSME (ox)		SSME (fuel)	
	SI	English	SI	English	SI	English
Chamber Diameter, cm(inches)	5.84	2.3	18.87	7.43	26.49	10.43
Turbine Nozzle Block Area, $cm^2(in.^2)$	6.252	0.969	14.84	2.3	40.00	6.2
Mixture Ratio (O_2/H_2)	0.80	-	0.55-0.88	-	0.55-0.88	-
Power Transmission Factor	0.61	-	0.19	-	0.25	-

The power transmission factor of the ASE preburner was shown to be quite high, 0.61, providing a higher resistance to this instability mode than is found in the SSME units.

The dynamic stability of the main chamber during idle mode was reviewed by comparison with the J-2S engine operating at similar conditions, Table 13. The injected propellants were assumed to be gaseous oxygen and gaseous hydrogen. At the idle mode operating chamber pressure of 4.14 N/cm^2a (6 psia), the ASE is inherently more stable than the J-2S because the injector P/P_c ratio is more favorable. However, even if instability occurred, expected oscillation amplitudes would not exceed 2.07 N/cm^2 (3 psi) peak-to-peak (Table 14).

LOX Control Valves

The LOX preburner and main injector values were specifically designed and fabricated for an engine assembly and were used during the staged combustion assembly test series to provide system control. The valves are hydraulically actuated using facility servovalves and a pair of controllers. The valves were designed as a part of a company-sponsored effort to evaluate controls requirements and controls components for Space Engine application. Use of the valves during the test program was intended to provide the benefit of characterizing the requirements for electric motor actuated valves for engine operation, and to provide close control of LOX volumes.

A valve design layout is shown in Fig. 36. The details of valve body, ball, seals, and bearings are of a design suitable for use on a breadboard engine assembly. The hydraulic actuators were available from another program. In this component application the valves could be ramped open to a preset position to control the rate of preburner and main chamber pressure buildup with the option of switching to a parameter control to provide the correct flowrate for the main chamber injector and the preburner injector. Both are ball valves using similar details except for differences in the ball diameters and related details.

The injector valve incorporates a 2.54 cm (1 inch) spherical diameter ball with a 1.27 cm (0.50 inch) diameter flow passage and the preburner valve incorporates a 1.59 cm (0.625 inch) spherical diameter ball with 0.76 cm (0.300 inch) diameter flow passage. The shaft and ball seals are made from SP211 (Dupont) material, triangle shape design, spring loaded for high-pressure sealing. The shaft seal design is similar to the SSME valve shaft seal design; however, this is the first application where this design concept has been incorporated for the valve ball seal.

Figure 37 shows a plot of the calculated valve hydraulic actuation pressure required versus valve inlet (upstream) pressure for both valves. The test facility can provide 1380 N/cm^2 (2000 psi) hydraulic actuation pressure so adequate margin is available.

TABLE 13. COMPARISON OF ASE AND J-2S IDLE MODE CONDITION

Propellants	ASE (Full Thrust) LOX/GH_2	ASE (Idle Mode) GOX/GH_2	J-2S (Full Thrust) LOX/GH_2	J-2S (Idle Mode) GOX/GH_2
P_c, N/cm^2a (psia)	1420 (2060)	4.12 (5.98)	827 (1200)	18.4 (26.7)
MR (o/f)	6.4	1.5	5.5	2.6
$P_{inj\ ox}$, N/cm^2a (psia)	2089 (3030)	8.1 (11.7)	972 (1410)	23-31 (33-45)
$P_{inj\ f}$, N/cm^2a (psia)	1614 (2341)	4.4 (6.4)	917 (1330)	18-23 (27-34)
$(\Delta P/P_c)$ Oxidizer	0.471	0.957	0.175	0.24-0.69
$(\Delta P/P_c)$ Fuel	0.136	0.070	0.108	0.01-0.27
Stability	Predicted dynamically stable		Sensitive in transition to intermediate bomb sizes	Some occurrence of chug at 1 kHz, and up to 9 N/cm^2 p-p (13 psi p-p)

TABLE 14. COMBUSTION STABILITY OF ASE MAIN CHAMBER DURING IDLE MODE

- Comparison with J-2S engine
- ASE idle-mode operation inherently more stable than J-2S idle-mode operation
  - Some possibility of chug
  - Oscillation amplitude $\leq$ 2.07 N/cm^2 (3 psi)
- Instability during ASE idle-mode operation should not adversely affect engine operation if indeed instability occurs at all

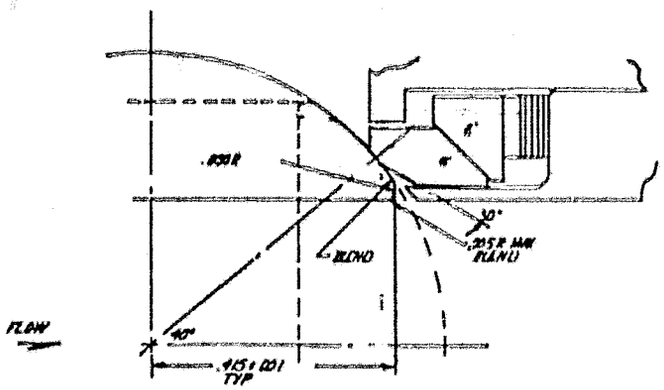

BALL DETAIL (INJ)
SCALE 10:1

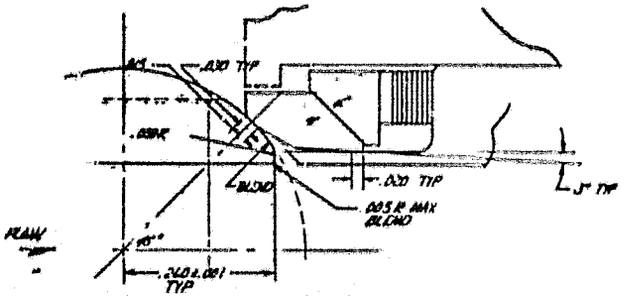

BALL DETAIL (PRECHAMBER)
SCALE 10:1

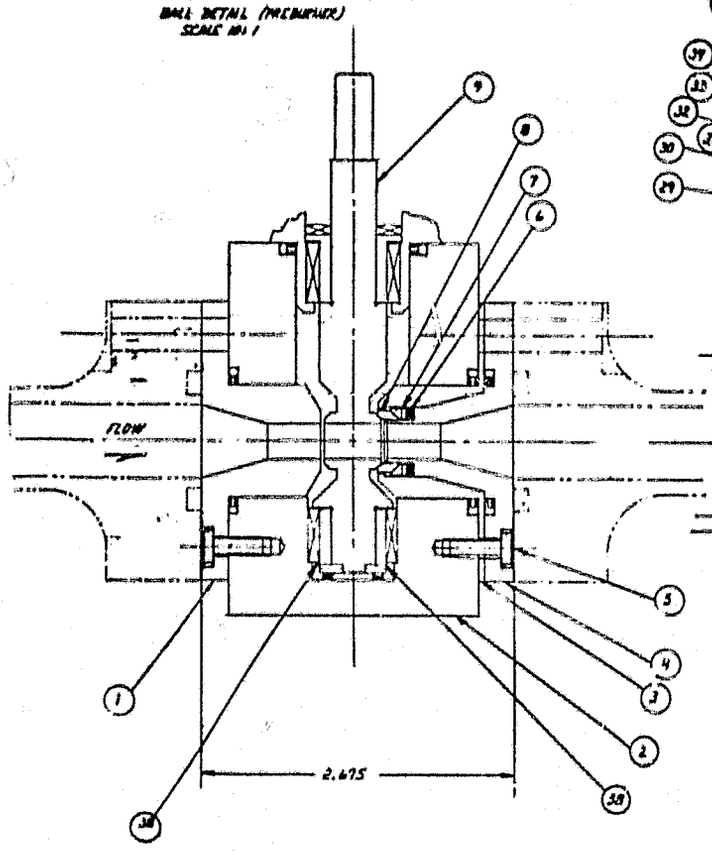

PRECHAMBER VALVE

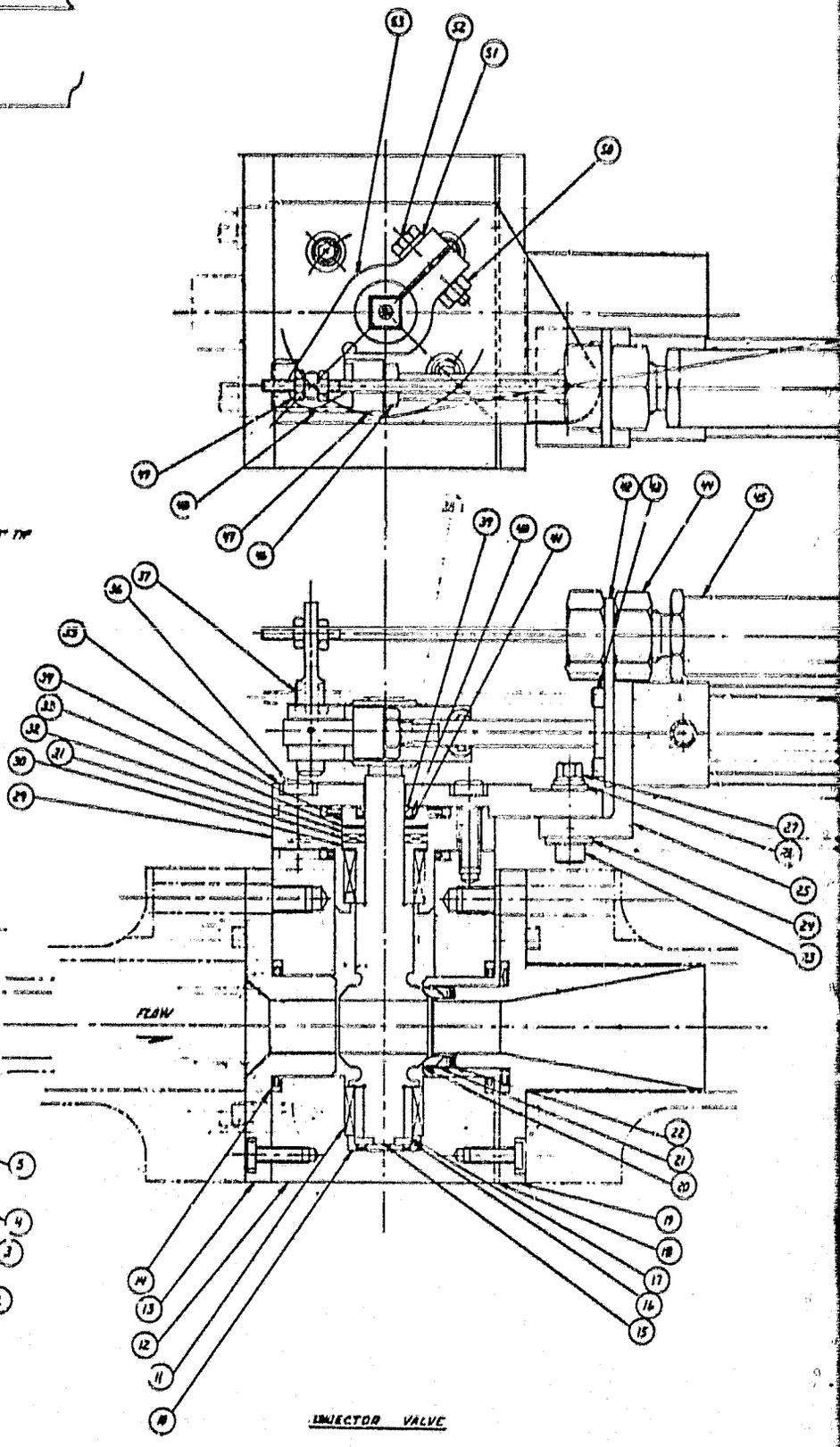

INJECTOR VALVE

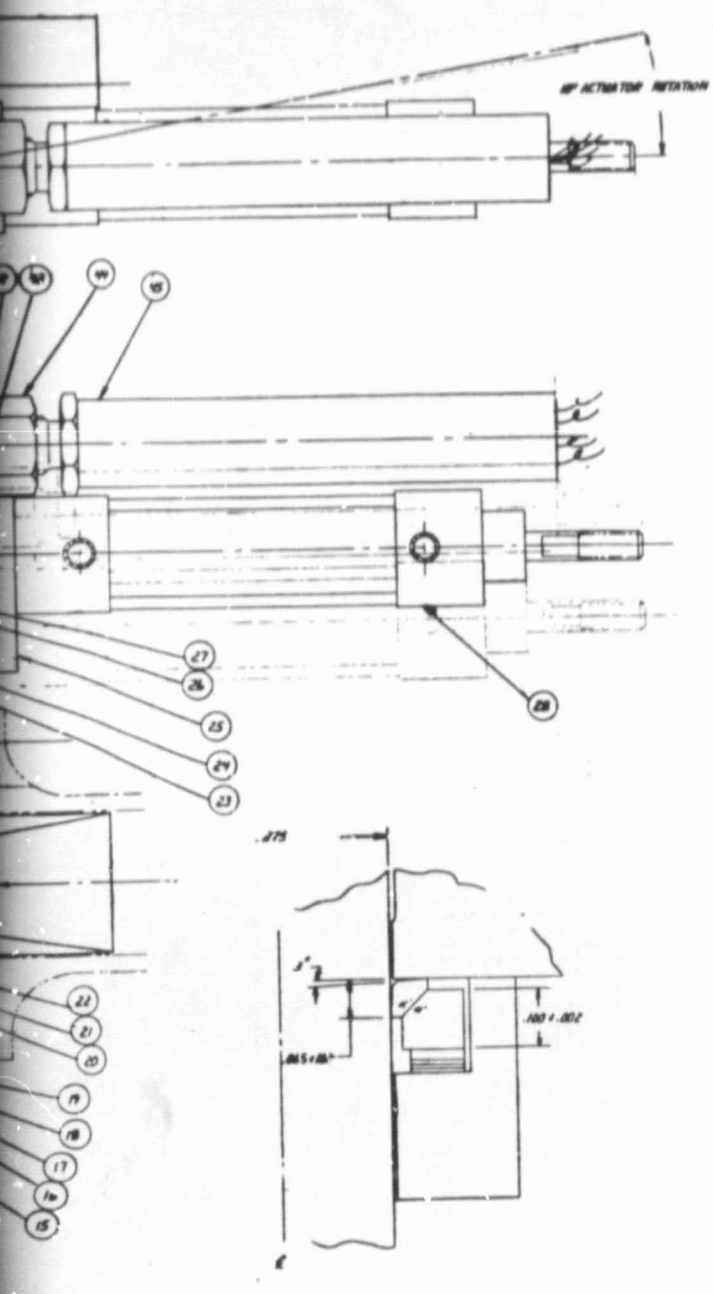

SHAFT SEAL DETAIL
SCALE 10:1

NO.	QTY	PART NO.	DESCRIPTION	MATERIAL
52	1		SEAL WASHER	304 CRES
54	1		SEAL WASHER	304 CRES
53	2	AP74-0114	LEVER	
52	2	RD11-4BFF-0946	BOLT	
51	2	RD1518-5M2-08PV	WASHER	
50	2	NAS679C4W	NUT	
49	4	MS20391-6A	NUT	
48	2	MS16362-6	PIN	
47	2	1-1875-1	EYE, ROD	
46	2	AN315-4R	NUT	
45	2	55-408	POS. IND. (COLLINS)	
44	4	AN315-8R	NUT	
43	8	NAS1101-08-8	SCREW	
42	4	AP74-042	BRACKET	
41	8	316-4 (PIC)	WAVE SPRING	302
40	2	AP74-012-003	LOADER	303
39	2	AP74-013-001	SEAL	SP211 (DUPONT)
38	2	AP74-025	BRG RACE	440 C
37	2	AP74-043	PIN	
36	8	NAS1101-C3-16	SCREW	
35	2	AP74-038	CAP	304L
34	2	AP74-022	SPACER	303
33	VAR	AP74-014-005	SHIM	302
32	2	AP74-014-005	BRG RACE	440 C
31	2	NTN-613	BEARING (TORRINGTON)	
30	2	AP74-015	BRG RACE	440C
29	2	AP74-009	FLANGE	304
28	2	DAMER $\frac{1}{4}$ × 4.5	ACTUATOR	
27	2	MS21043-3	NUT	
26	2	AJ-3-W	WASHER (PIC)	
25	2	AP74-01	BRACKET	
24	2	AJ-3-W	WASHER (PIC)	
23	2	4931	SHOULDER BOLT (PIC)	
22	9	D6-6	WAVE SPRING	302
21	1	AP74-028-009	LOADER	303
20	1	AP74-024-003	SEAL	SP211 (DUPONT)
19	1	AP74-016	FLANGE	321
18	1	AP74-018	SEAL RETAINER	321
17	2	AP74-021-005	WASHER	TFE
16	2	AP74-021-003	WASHER	303
15	1	AP74-004	BALL (INJECTOR)	INCO 718
14	10	R2023AA-1250	K-SEAL	A286 GOLD PLATED
13	1	AP74-017	FLANGE	321
12	1	AP74-010-	BODY (INJECTOR)	
11	4	AG 22923	ROLLER BRG (TORRINGTON)	
10	9	D6-9	WAVE WASHER (PIC)	
9	1	AP74-007	BALL (PREBURNER)	INCO 718
8	1	AP74-024-005	SEAL	SP211 (DUPONT)
7	1	AP74-023-005	LOADER	303
6	18	D6-6 (PIC)	SPRING, WAVE	302
5	28	MS 1101E08-9	SCREW	
4	1	AP74-019	FLANGE	321
3	1	AP74-020	SEAL RETAINER	321
2	1	AP74-010-005	BODY (PREBURNER)	321 CRES
1	1	AP74-011	FLANGE	321

Figure 36

ADVANCED DESIGN

Rockwell International

Rocketdyne Division
6633 Canoga Avenue
Canoga Park, California 91304

LAYOUT - ASE PREBURNER & INJECTOR
LOX VALVES

Drawn	APVD	Code Ident No.
		02602
SCALE 2/1	DATE	AP-

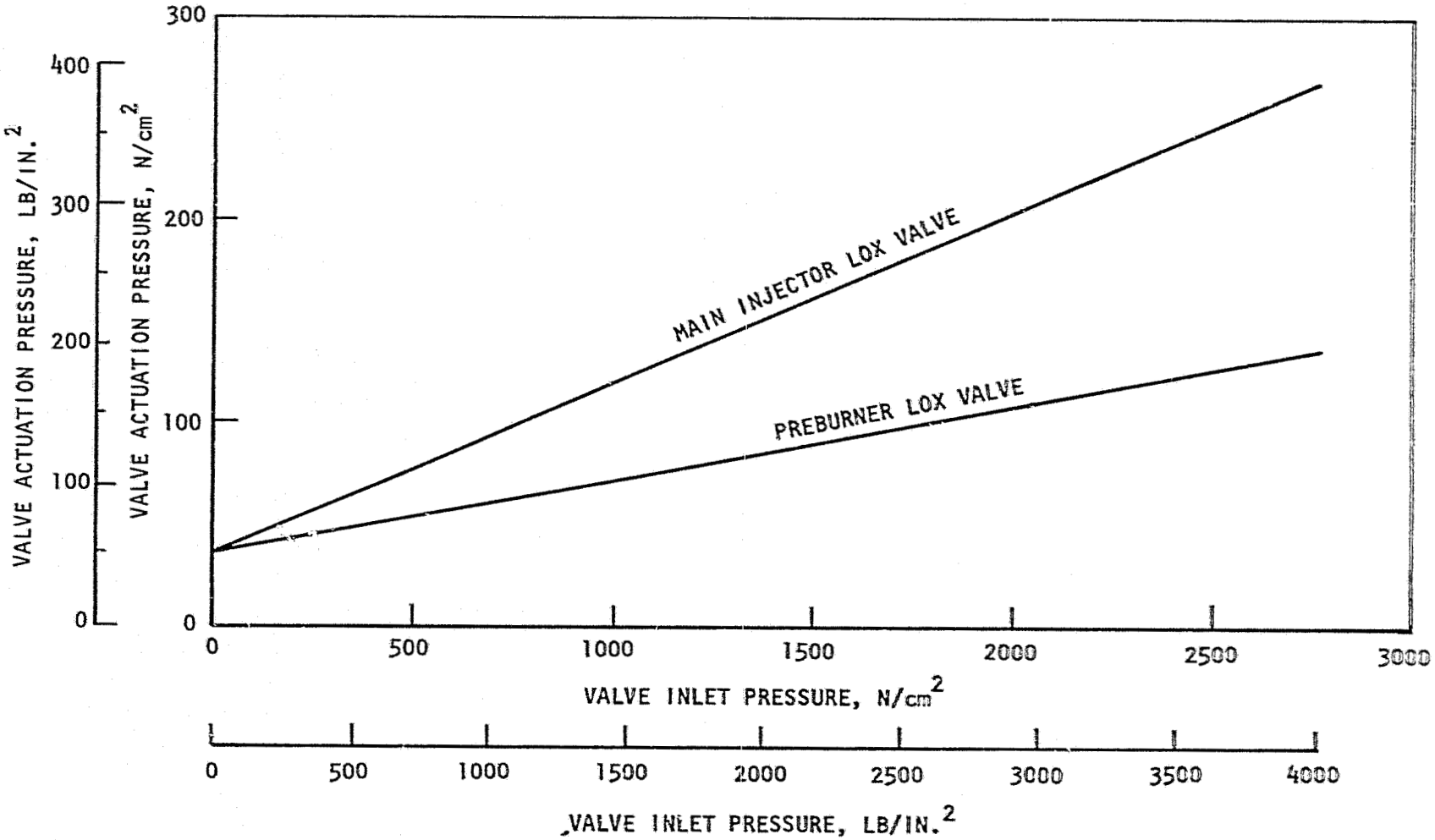

Figure 37. Valve Actuation Pressure vs Valve Inlet Pressure

Combustion Chamber

The combustion chamber for the staged combustion system assembly was a zirconium copper, electroformed nickel chamber, Fig. , designed and fabricated as an integral part of the Advanced Thrust Chamber Technology Program, NAS3-17825. A complete discussion of the analytical, design, and fabrication effort for this component can be found in the final report of that program (Ref. 1).

Regeneratively Cooled Nozzle

The Regeneratively cooled 175:1 nozzle for the staged combustion system assembly was a two-pass A286 tubular nozzle, Fig. 39, designed and fabricated as an integral part of the Advanced Thrust Chamber Technology program, NAS3-17825. A complete discussion of the analytical, design, and fabrication effort for this component can be found in the final report of that program (Ref. 1).

400:1 Nozzle Extension

An uncooled nozzle extension was designed by NASA personnel to mate with the 175:1 regeneratively cooled nozzle and to continue the nozzle contour out to a 400:1 area ratio. Figure 40 shows the nozzle configuration with the wall static pressure taps for nozzle pressure profile recording. Thermal analyses were performed to ensure that the uncooled nozzle wall would not be harmed by the expected high heat flux during the start transient when the exhaust gas flow would be separated from the nozzle wall, as well as to ensure that the nozzle would function satisfactorily during steady-state testing of extended duration with the exhaust gases attached to the nozzle wall. Figures 41 through 43 show the results of this analytical study.

The heat flux to the nozzle during separated flow was estimated at eight times the nominal steady-state heat flux; the predicted nozzle wall temperature as a function of time is shown in Fig. 41. Shown parametrically on this plot are several thicknesses of steel nozzle wall. Thus with 6.35 mm (0.25 inch) wall thickness the maximum gas side wall temperature would be about 950 K (1250 F) at the end of 5 seconds of testing. With this margin, no difficulty with wall burning was expected; any planned test would be automatically cut off if the nozzle were flowing separated for the duration.

The nozzle wall temperature versus time during nominal operation with full nozzle flow is shown for two axial locations in Fig. 42 and 43. The maximum expected wall temperature does not exceed 530 K (500 F) during 5 seconds of testing.

Staged Combustion Assembly System

The staged combustion assembly system (Fig. 44) is composed of the spark/torch igniters, preburner injector, preburner combustion chamber, hot gas ducts, oxygen and hydrogen turbine simulators, main propellant injector, zirconium copper LH_2 cooled combustion chamber, LH_2 cooled tubular nozzle and uncooled

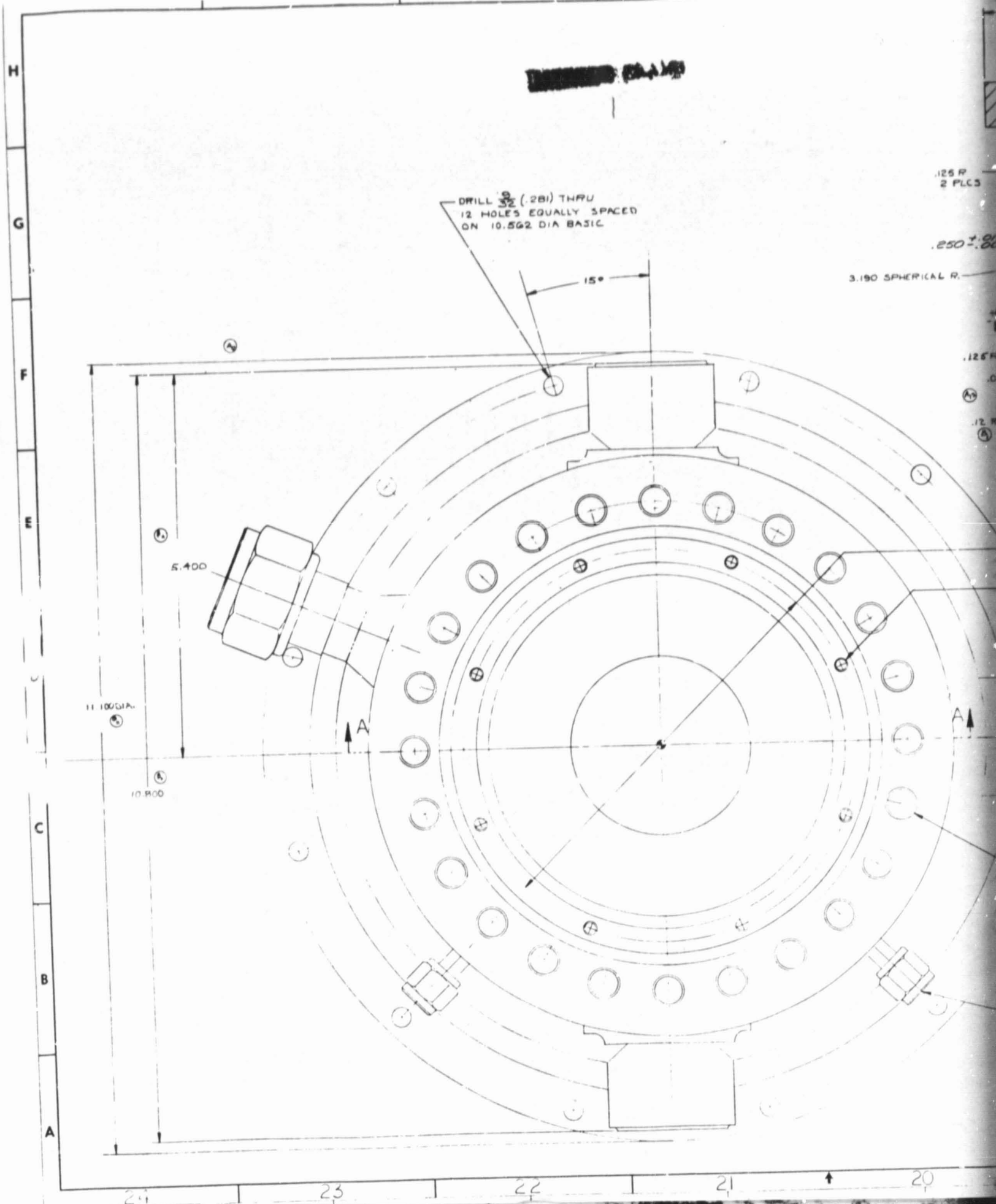
DRILL 9/32 (.281) THRU
12 HOLES EQUALLY SPACED
ON 10.562 DIA BASIC
15°
.125 R
2 PLCS
3.190 SPHERICAL R.
5.400
11.100 DIA.
10.800
A
A
H
G
F
E
C
B
A
23
22
21
20

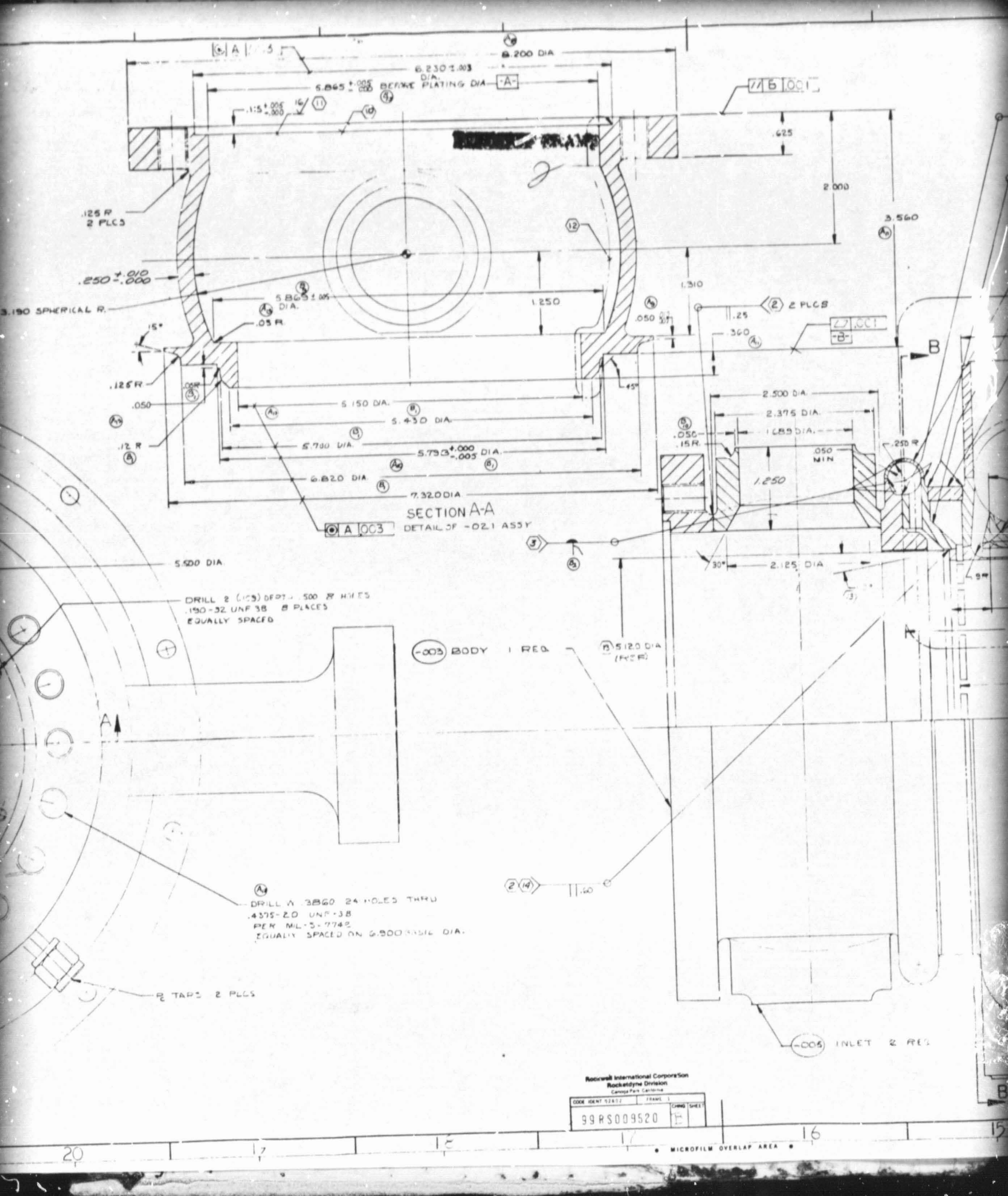
8.200 DIA
6.230 ±.003 DIA.
5.865 +.005 -.000 BEFORE PLATING DIA -A-
.625
2.000
3.560
.125 R 2 PLCS
.250 +.010 -.000
3.190 SPHERICAL R.
5.863 ±.005 DIA.
1.250
1.310
.050
2 PLCS
.25
.360
B
.15°
.05 R
.125 R
.050
.12 R
5.150 DIA.
5.430 DIA.
5.780 DIA.
5.793 +.000 -.005 DIA.
6.820 DIA
7.320 DIA
45°
2.500 DIA.
2.375 DIA.
1.689 DIA.
.050
.15 R.
.250 R
.050 MIN
1.250
SECTION A-A
A 003
DETAIL OF -021 ASSY
5.500 DIA
30°
2.125 DIA
DRILL 2 (-003) DEPTH .500 R HOLES
.190-32 UNF 3B 8 PLACES
EQUALLY SPACED
-003 BODY 1 REQ
5.120 DIA (REF R)
A
DRILL 24 .3860 HOLES THRU
.4375-20 UNF-3B
PER MIL-S-7742
EQUALLY SPACED ON 6.900 BASIC DIA.
.60
2 TAPS 2 PLCS
-005 INLET 2 REQ
Rocketdyne Division
99RS009520
MICROFILM OVERLAP AREA

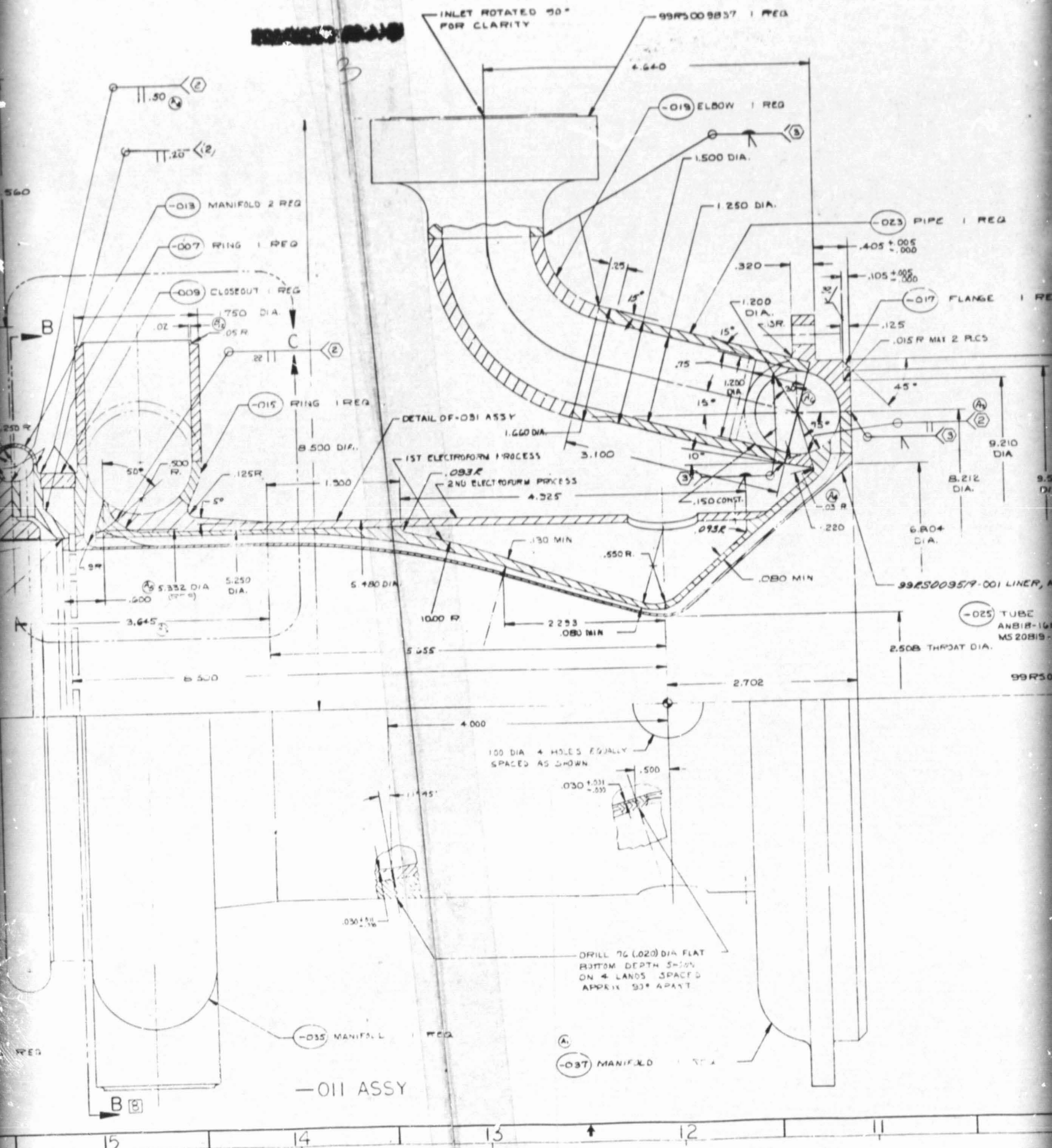
INLET ROTATED 90° FOR CLARITY
99RS009837 1 REQ
4.640
-019 ELBOW 1 REQ
1.500 DIA.
1.250 DIA.
-023 PIPE 1 REQ
.405 +.005 -.000
.320
.105 +.005 -.000
-017 FLANGE 1 REQ
.125
.015 R MAX 2 PLCS
1.200 DIA.
.3R.
.25
15°
.75
45°
9.210 DIA
8.212 DIA.
6.804 DIA.
-013 MANIFOLD 2 REQ
-007 RING 1 REQ
-009 CLOSEOUT 1 REQ
.750 DIA.
.02
.05 R
-015 RING 1 REQ
DETAIL OF -031 ASSY
1.660 DIA.
3.100
8.500 DIA.
1ST ELECTROFORM PROCESS
.093R
2ND ELECTROFORM PROCESS
4.325
.150 CONST.
.220
.125R.
1.300
.500 R.
50°
5°
.130 MIN
.550 R.
.080 MIN
99RS009579-001 LINER,
5.332 DIA
5.250 DIA.
5.480 DIA
.600
3.645
10.00 R
2.293
.080 MIN
5.055
2.508 THROAT DIA.
-025 TUBE
AN818-16
MS 20819-
99RS0
5.500
2.702
4.000
.100 DIA 4 HOLES EQUALLY SPACED AS SHOWN
.500
.030 +.031 -.000
.030 +.011 -.000
DRILL 76 (.020) DIA FLAT BOTTOM DEPTH .5-.6 ON 4 LANDS SPACED APPROX 90° APART
-035 MANIFOLD 1 REQ
-037 MANIFOLD 1 REQ
-011 ASSY
B
C
15
14
13
12
11

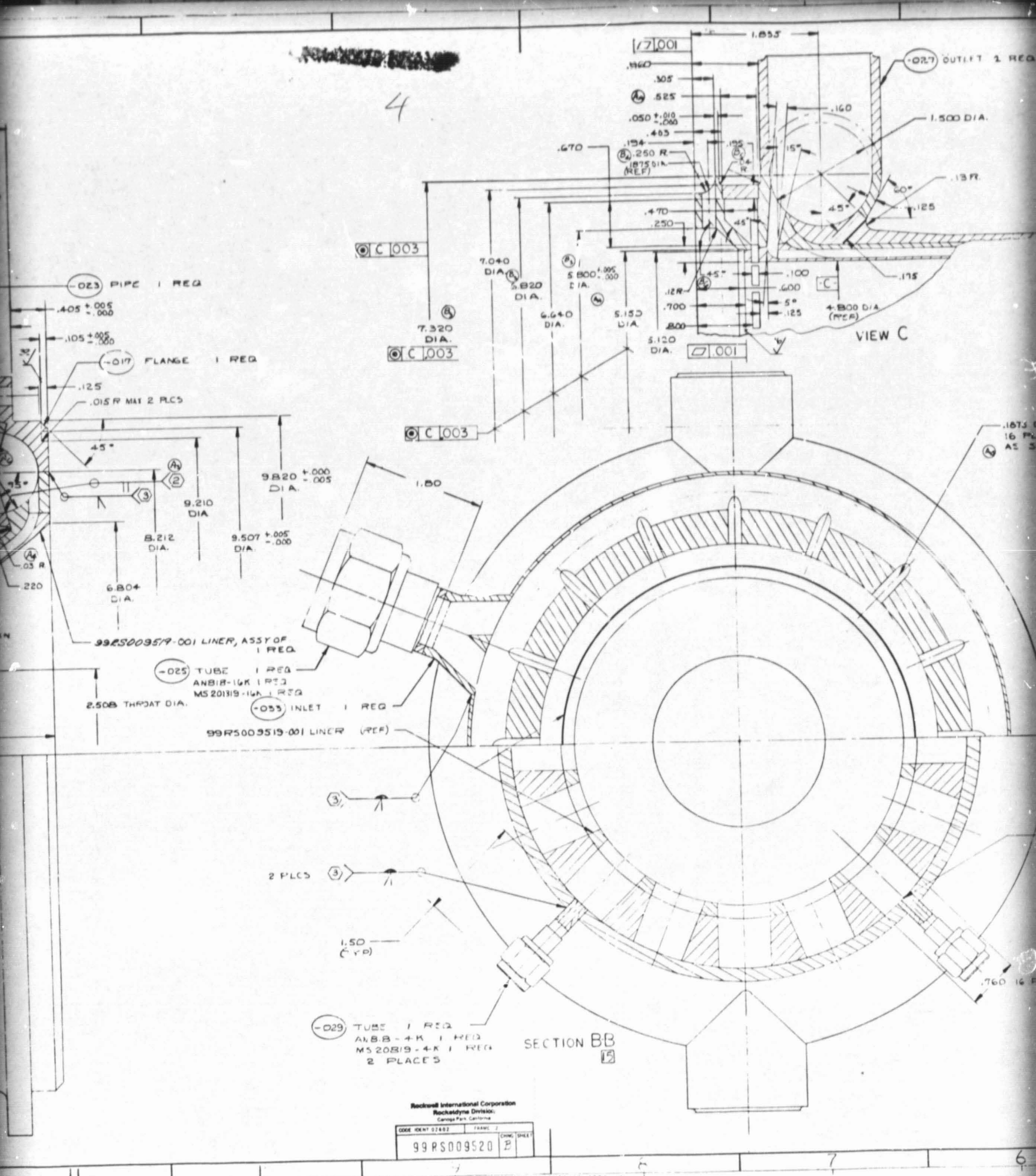

Rockwell International Corporation
Rocketdyne Division
Canoga Park, California

CODE IDENT 07602	FRAME 1		
99RS009520		CHNG B	SHEET

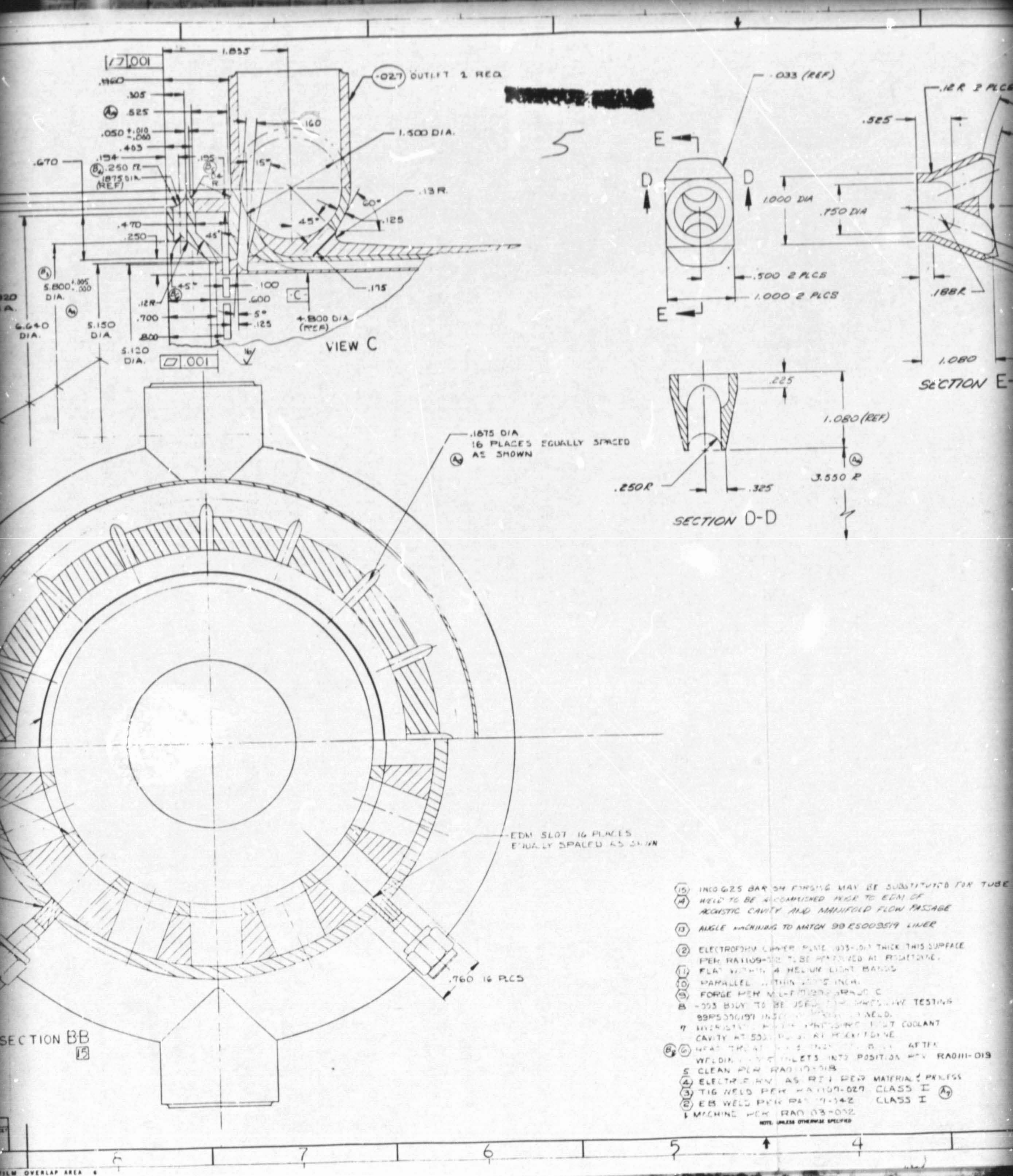

.027 OUTLET 1 REQ
[redacted]
5
VIEW C
1.855
1.500 DIA.
.13 R.
4.800 DIA. (REF)
6.640 DIA.
5.800 DIA.
5.150 DIA.
5.120 DIA.
.033 (REF)
1.000 DIA
.750 DIA
.500 2 PLCS
1.000 2 PLCS
SECTION D-D
.225
1.080 (REF)
3.550 R
.250 R
.325
.525
.12 R 2 PLCS
.188 R
1.080
SECTION E-
.1875 DIA
16 PLACES EQUALLY SPACED
AS SHOWN
EDM SLOT 16 PLACES
EQUALLY SPACED AS SHOWN
.760 16 PLCS
SECTION BB
15
INCO 625 BAR OR FORGING MAY BE SUBSTITUTED FOR TUBE
WELD TO BE ACCOMPLISHED PRIOR TO EDM OF ACOUSTIC CAVITY AND MANIFOLD FLOW PASSAGE
ANGLE MACHINING TO MATCH 99R5009519 LINER
ELECTROFORM COPPER PLATE THICK THIS SURFACE
FLAT WITHIN 4 HELIUM LIGHT BANDS
PARALLEL WITHIN INCH.
TESTING
COOLANT
WELDING INLETS INTO POSITION PER RA0111-019
CLEAN PER RA0
TIG WELD PER RA1109-027 CLASS I
EB WELD PER CLASS I
MACHINE PER RA0 03-002
NOTE: UNLESS OTHERWISE SPECIFIED
FILM OVERLAP AREA

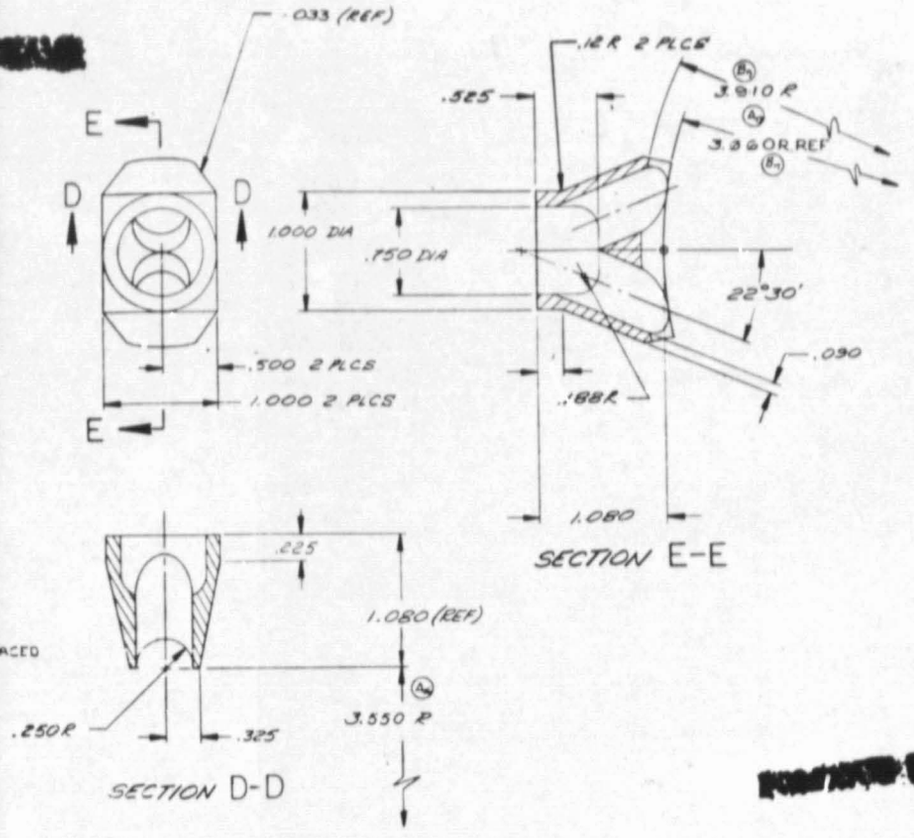

REVISIONS

ZONE	LTR	DESCRIPTION	DATE	APPROVED
		1. MAY BE REWORKED 2. RECORD CHANGE 3. CANNOT BE REWORKED 4. NOW SHOP PRACTICE 5. PARTS MADE OR		
	A			
3C		1) ON FACE OF DWG -037 WAS -035 ADDED -037 TO MATERIAL		
5B		2) ADDED GEN NOTE = 5		
11E		3) CHANGED WELD D ES		
11E		4) ADDED .03 R.		
15E		5) ADDED .00 DIM & 5.335 DIA (REF)		
11E		6) ADDED 30° ANGLE		
6A		7) CHANGED WELDS TO		
15G		8) .50 WELD DEPTH WAS		
17F		9) .050 +.010 -.000 DIM WAS .05		
16E		10) 7.100 DIA WAS 7.250 DIA, 6.750 DIA WAS 6.750 DIA, 5.590 +.005 -.003 WAS 5.650 ±.005 DIA		
15G		11) 3.560 WAS 3.740, 360 WAS		
11F		12) REMOVED: SECT F-F, .250 R 4 PLACES, DIM .175 AND .213 ADDED 15° AND .050 DIM; .125R WAS		
19E				
20F				
15D		13) 3.645 WAS 3.465		
7H		14) 1.833 WAS 1.655		
8F		.700 WAS .520, .800 WAS		
8G		.125R WAS .09R, 5.595 WAS 5.655; ADDED .1875 DIA REF		
4H		.403 WAS .445, .305 WAS		
9G		7.100 WAS 7.250, 6.600 WAS 6.750 DIA		
6F		15) .1875 DIA 16 PLACES WAS .250 DIA DEPTH .75 8 PLACES		
4E		16) 3.550R WAS 3.626R		
3G,H		17) 3.800R WAS 3.875R, 3.550R REF WAS 3.688R		
17H		18) 8.200 DIA WAS 8.00		
19C		DRILL W (.3680) WAS .4375-20 WAS .375-24		
19F		6.900 DIA WAS 6.700		
		19) ADDED .03 R. EFFECT ON: EXPERIMENTAL		
	B			
18E		1. 6.920 DIA WAS 6.600 ADDED .12R, 7.320 DIA WAS 7.180 DIA., ADDED .25R, ADDED 5.430 DIA., 5.798 WAS 5.590, 5.700 DIA WAS 5.460		
11E		2. R WAS		
9G		3. 5.800 WAS 5.595, 6.920 DIA WAS 6.600 DIA, 7.320 DIA WAS 7.280 DIA REMOVED 7.180 DIA		
8G		4. .25R WAS .12R		
8G		5. .04 R. WAS .09R		
8G		6. ADDED 45° .660 WAS .425		
3H		7. 3660R REF WAS 3.510 REF, 3.910 R. WAS 3.8		
5A		8. CHANGED HEAT TREAT CALLOUT RA111-019 WAS RA111-009		
18F		9. ADDED 5.863 ±.005		
19F		10. ADDED 3 GROOVE & DIMEN		
24C		11. ADD 11.180 DIA, 13.831 & 5.43		
19E		12. ADDED .02 DIM & .15 R		
		13. 5.865 +.005 -.000 BEFORE FLAT WAS 5.835 ±.005		
		EFF: ALL PARTS MADE		

Figure 38

65

-037	INCO G25 TUBE	[illegible]	AMS [illegible]	12A
-035	INCO G25 TUBE	1.75 [illegible]	AMS [illegible]	14A
-033	304L CRES BAR	1.250 D X 1.05	[illegible]	10D
-029	304L CRES TUBE	1.250 [illegible]	[illegible]	10A
-027	INCO G25 TUBE	1.75 [illegible]	AMS [illegible]	6H
-025	304L CRES TUBE	1.03 [illegible]	[illegible]	10D
-023	304L CRES PIPE	14 DIA SCH Y 310	[illegible]	11G
-019	304L CRES FLEXW	5 [illegible]	RBOI [illegible]	12G
-017	INCO G25 FORGING	11.250 DIA X 1.03	AMS 5666	11F
-015	INCO G25 BAR	2.35 X .75 X .53	AMS 5666	14F
-013	INCO G25 BAR	2.5 X .75 X .50	AMS 5666	15F
-009	INCO G25 BAR	2.8 X .5 X .2	AMS 5666	15F
-007	INCO G25 FORGING	7.50 X 5 X 1.5	AMS 5666	15F
-005	INCO G25 FORGING	2.750 X 1.25	AMS 5666	16A
-003	INCO TIG FILLER WIRE	.040 DIA	RBOI [illegible] (9)	17C
NO	MATERIAL	SIZE	SPECIFICATION	ZONE

(15) INCO G25 BAR OR FORGING MAY BE SUBSTITUTED FOR TUBE MATL
(14) HELD TO BE ACCOMPLISHED PRIOR TO SEAL OF ACOUSTIC CAVITY AND MANIFOLD FLOW PASSAGE
(13) ANGLE MACHINING TO MATCH 99RS003519 LINER
(12) ELECTROFORM COPPER PLATE .033-.037 THICK THIS SURFACE PER RA1109-002 TO BE RESTRICTED AT ROCKETDYNE
(11) FLAT WITHIN .4 HELIUM LIGHT BANDS
(10) PARALLEL WITHIN .005 INCH
(9) FORGE PER MIL-F-[illegible] GRADE C
(8) -003 BUY TO BE USED FOR [illegible] TESTING 99RS003519 [illegible] WELD.
(7) [illegible] CAVITY AT 550 PSIG AT ROCKETDYNE.
(6) HEAT TREAT AS [illegible] AFTER WELDING [illegible] INLETS INTO POSITION PER RA0111-019
(5) CLEAN PER RA0110-018
(4) ELECTRICALLY AS REQ PER MATERIAL & PROCESS
(3) TIG WELD PER RA1109-027 CLASS I (A7)
(2) EB WELD PER RA1109-042 CLASS I
(1) MACHINE PER RA0103-032

NOTE: UNLESS OTHERWISE SPECIFIED

-031	
-021	
-011	-001
SUB ASSY	ASSY

HEAT TREAT: NOTED
FINISH:
MATL: NOTED

UNLESS OTHERWISE SPECIFIED DIMENSIONS ARE IN INCHES AND APPLY PRIOR TO FINISH
125/ MACH SURF ROUGHNESS
TOLERANCES ON ANGLES ± 0° DECIMALS .XX ± .01 .XXX ± .010

HOLES NOTED "DRILL" OVER	THRU	TOLERANCE
.0000	.0400	+ .0015 — .0010
.0401	.1360	+ .0020 — .0010
.1361	.2790	+ .0045 — .0010
.2791	.5000	+ .0060 — .0010
.5001	.7500	+ .0075 — .0010
.7501	1.0000	+ .0090 — .0010
1.0001	2.0000	+ .0120 — .0010

DO NOT SCALE PRINT

DRAWN [illegible] DATE
CHK [illegible] DATE
ENGR [illegible]
MATL [illegible]
STANDARDS [illegible]
DESIGN ACTIVITY APVD DATE

Rocketdyne Division
Rockwell International Corporation
Canoga Park California

COMBUSTION CHAMBER, 20K-ADVANCED THRUST CHAMBER, ASSY OF

SIZE J | CODE IDENT NO 02602 | DRAWING NO 99RS003520

SCALE [illegible] SHEET [illegible]

FRAME 3

FORM NO. 81844 REV. 7-73

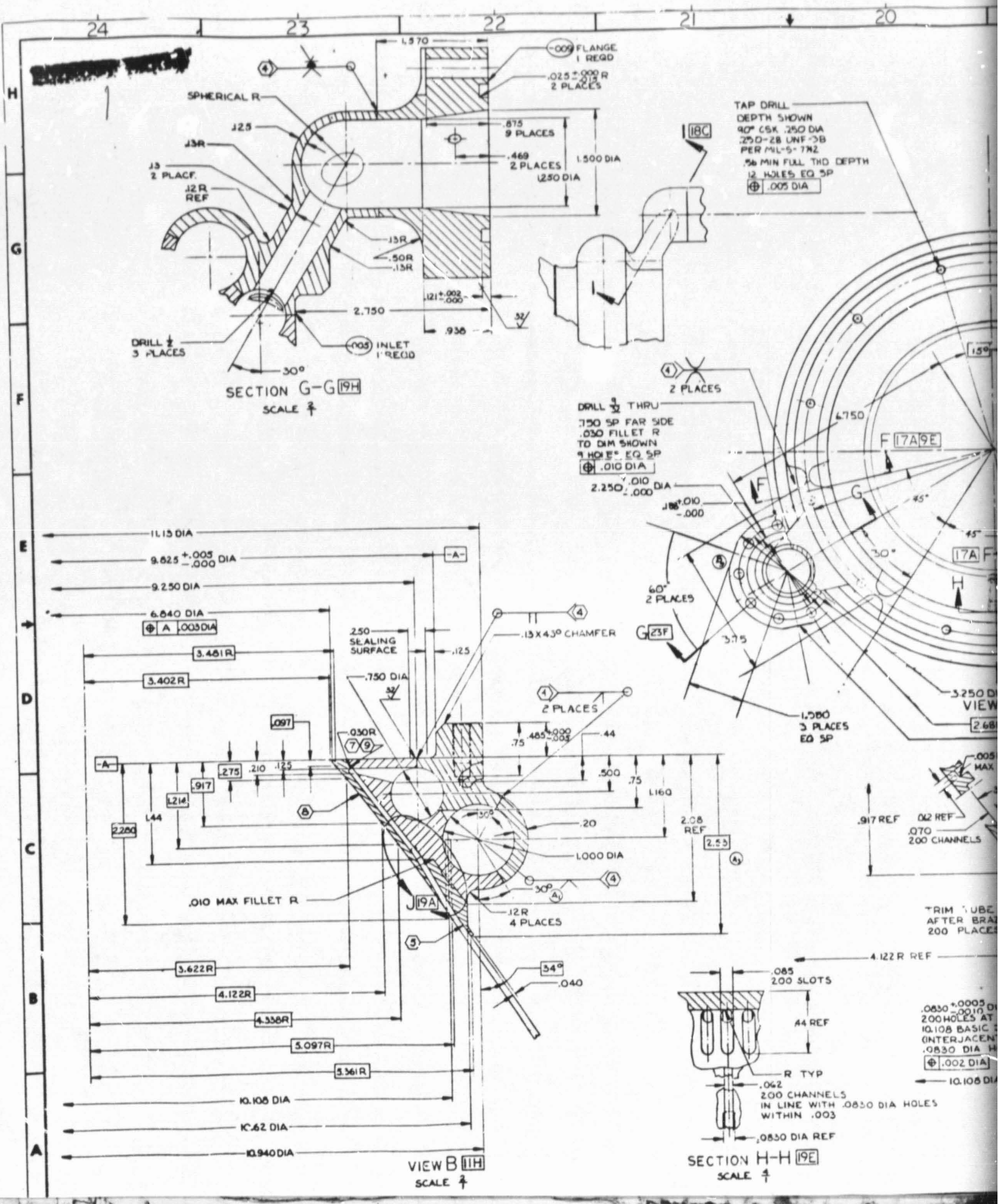

SECTION G-G 19H
SCALE 2/1
SPHERICAL R
FLANGE 1 REQD
.025 +.000 -.015 R 2 PLACES
.875 9 PLACES
.469 2 PLACES
1.500 DIA
1.250 DIA
DRILL 1/8 3 PLACES
INLET 1 REQD
2.750
.938
30°
TAP DRILL DEPTH SHOWN
90° CSK .250 DIA
.250-28 UNF-3B PER MIL-S-7742
.56 MIN FULL THD DEPTH
12 HOLES EQ SP
.005 DIA
2 PLACES
DRILL 9/32 THRU
.750 SP FAR SIDE
.030 FILLET R TO DIM SHOWN
9 HOLES EQ SP
.010 DIA
2.250 +.010 -.000 DIA
60° 2 PLACES
1.580 3 PLACES EQ SP
6.750
11.13 DIA
9.825 +.005 -.000 DIA
9.250 DIA
6.840 DIA
A .003 DIA
3.481R
3.402R
.250 SEALING SURFACE
.125
.750 DIA
.13 X 43° CHAMFER
2 PLACES
.030R
1.000 DIA
.010 MAX FILLET R
.12R 4 PLACES
3.622R
4.122R
4.338R
5.097R
5.361R
10.108 DIA
10.62 DIA
10.940 DIA
34°
.040
VIEW B 11H
SCALE 2/1
.085 200 SLOTS
.44 REF
R TYP
.062 200 CHANNELS IN LINE WITH .0830 DIA HOLES WITHIN .003
.0830 DIA REF
SECTION H-H 19E
SCALE 4/1
.917 REF
.070 200 CHANNELS
TRIM TUBE AFTER BRAZ 200 PLACES
4.122 R REF
10.108 DIA

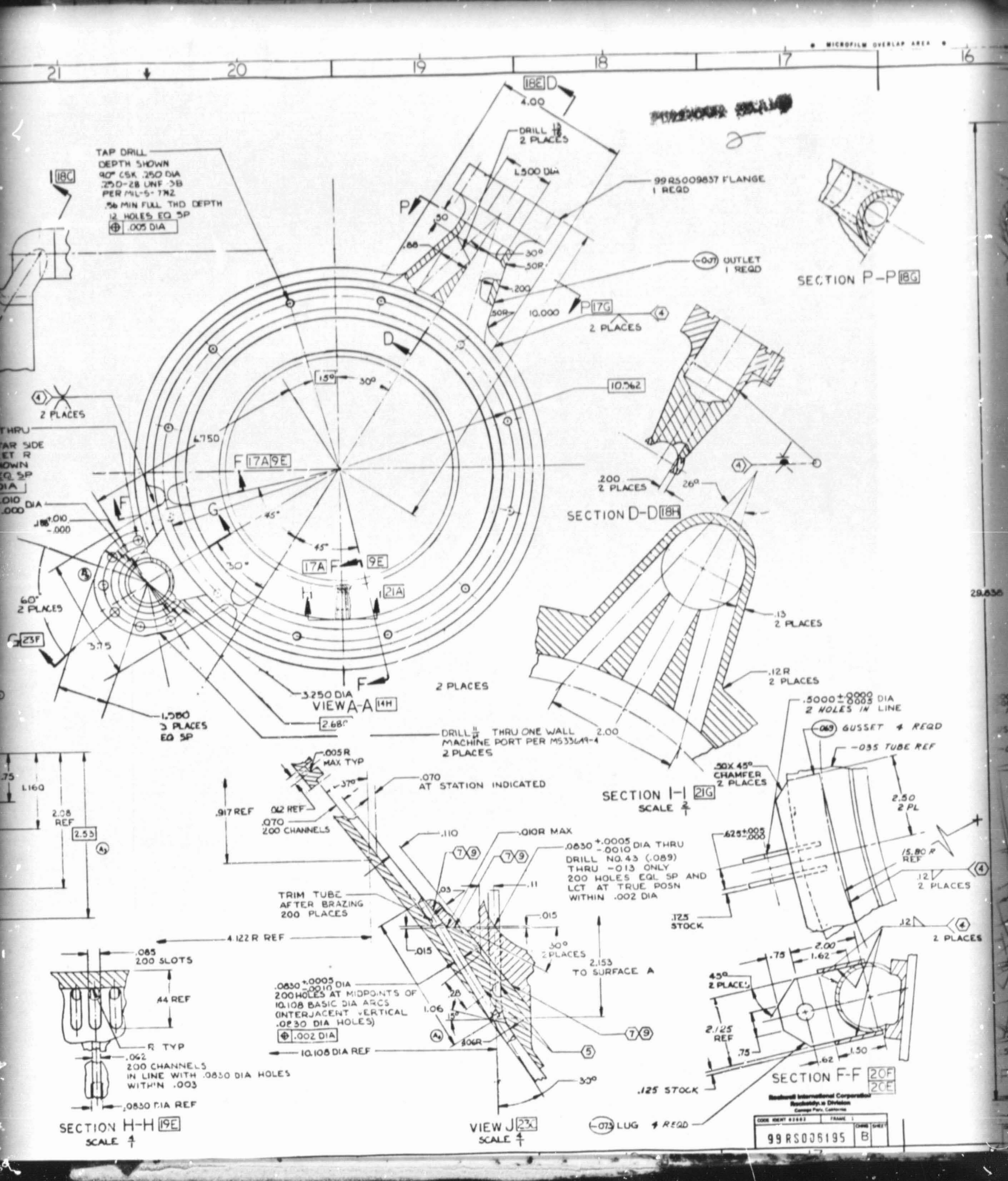
TAP DRILL
DEPTH SHOWN
90° CSK .250 DIA
.250-28 UNF-3B
PER MIL-S-7742
.56 MIN FULL THD DEPTH
12 HOLES EQ SP
.005 DIA
DRILL 13/16
2 PLACES
4.500 DIA
99RS009837 FLANGE
1 REQD
-037 OUTLET
1 REQD
SECTION P-P 18G
10.562
2 PLACES
.200
2 PLACES
SECTION D-D 18H
.13
2 PLACES
.12R
2 PLACES
.5000 +.0005 -.0000 DIA
2 HOLES IN LINE
-069 GUSSET 4 REQD
-035 TUBE REF
.50 X 45° CHAMFER
2 PLACES
SECTION I-I 21G
SCALE 2/1
2.50
2 PL
.625 +.005 -.000
15.80 R
REF
.12
2 PLACES
.125
STOCK
.12
2 PLACES
2.00
1.62
.75
45°
2 PLACES
2.125
REF
.75
1.50
.62
.125 STOCK
SECTION F-F 20F 20E
-073 LUG 4 REQD
4.750
3.250 DIA
VIEW A-A 14H
1.580
3 PLACES
EQ SP
2.68°
2 PLACES
DRILL 11/64 THRU ONE WALL
MACHINE PORT PER MS33649-4
2 PLACES
2.00
.005 R
MAX TYP
.37°
.070
AT STATION INDICATED
.917 REF
.042 REF
.070
200 CHANNELS
.110
.010R MAX
.0830 +.0005 -.0010 DIA THRU
DRILL NO. 43 (.089)
THRU -013 ONLY
200 HOLES EQL SP AND
LCT AT TRUE POSN
WITHIN .002 DIA
TRIM TUBE
AFTER BRAZING
200 PLACES
.03
.11
.015
.015
4.122 R REF
30°
2 PLACES
2.153
TO SURFACE A
.085
200 SLOTS
.44 REF
R TYP
.062
200 CHANNELS
IN LINE WITH .0830 DIA HOLES
WITHIN .003
.0830 DIA REF
.0830 +.0005 -.0010 DIA
200 HOLES AT MIDPOINTS OF
10.108 BASIC DIA ARCS
(INTERJACENT VERTICAL
.0830 DIA HOLES)
.002 DIA
.28
1.06
15°
.106R
10.108 DIA REF
30°
SECTION H-H 19E
SCALE 4/1
VIEW J 23X
SCALE 4/1
1.160
2.08
REF
2.53
.375
29.836
Rockwell International Corporation
Rocketdyne Division
Canoga Park, California
CODE IDENT 02647
FRAME 1
99RS006195
CHNG
B
SHEET

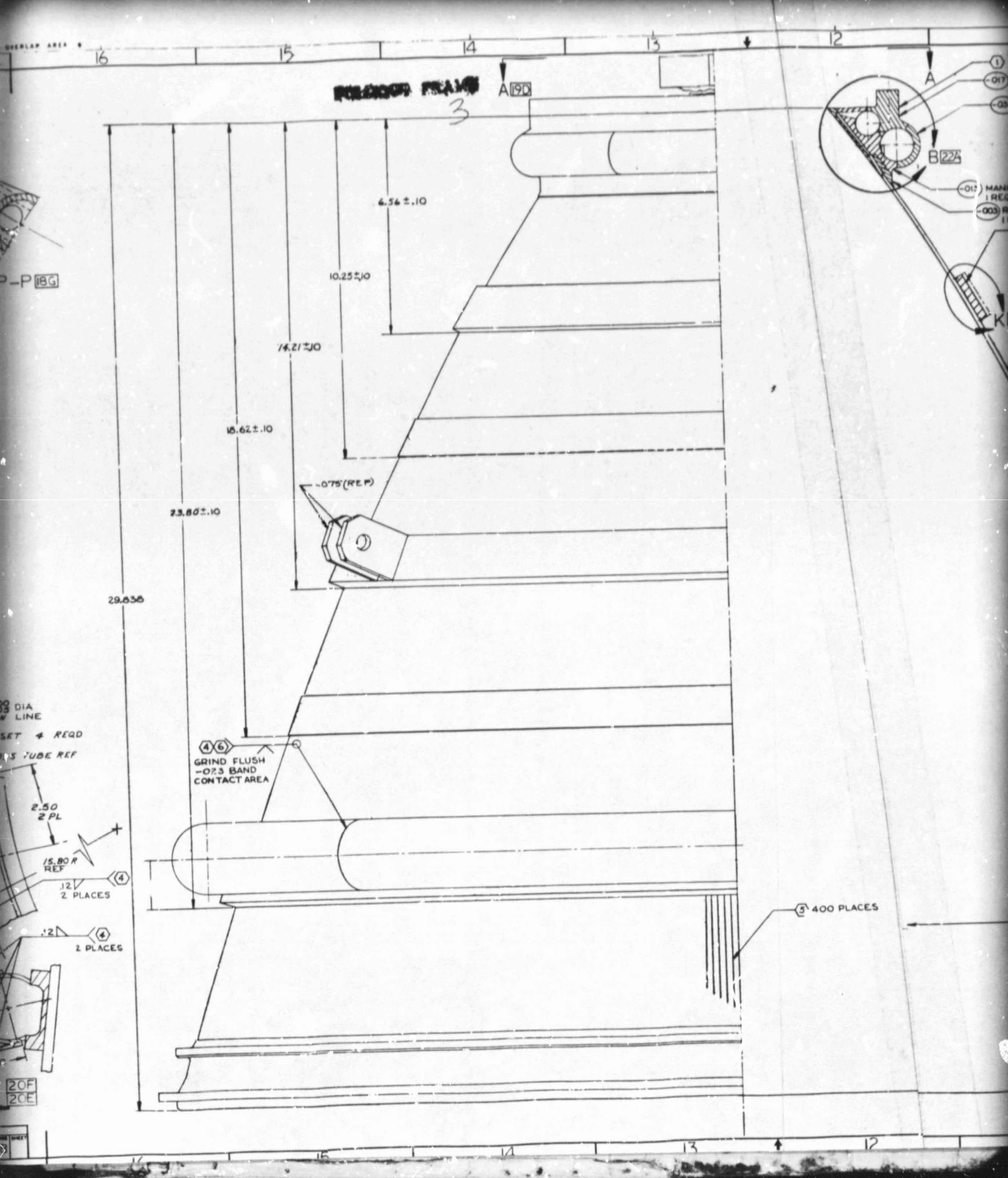

OVERLAP AREA
16
15
14
13
12
A 19D
3
A
B 22A
-017
-013 MAN
1 REQ
-003
K
6.56 ± .10
10.25 ± .10
14.21 ± .10
18.62 ± .10
23.80 ± .10
29.838
-.075 (REF)
P-P 18G
DIA
LINE
SET 4 REQD
TUBE REF
2.50
2 PL
15.80 R
REF
.12
2 PLACES
.12
2 PLACES
4
6
GRIND FLUSH
-023 BAND
CONTACT AREA
5 400 PLACES
20F
20E

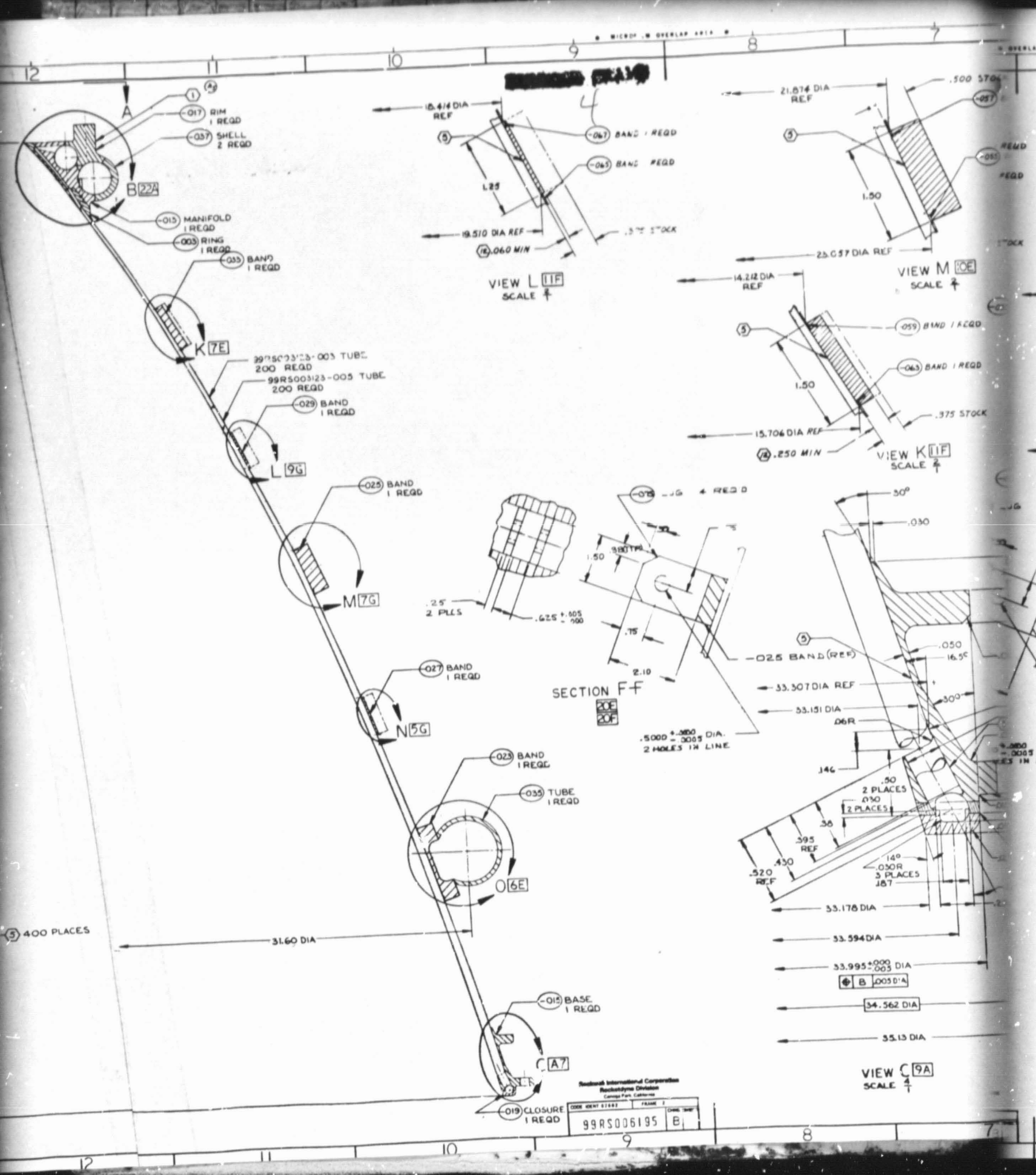
-017 RIM 1 REQD
-037 SHELL 2 REQD
-013 MANIFOLD 1 REQD
-003 RING 1 REQD
-033 BAND 1 REQD
-029 BAND 1 REQD
-025 BAND 1 REQD
-027 BAND 1 REQD
-023 BAND 1 REQD
-035 TUBE 1 REQD
-015 BASE 1 REQD
-019 CLOSURE 1 REQD
99RS003123-003 TUBE 200 REQD
99RS003123-005 TUBE 200 REQD
B 22A
K 7E
L 9G
M 7G
N 5G
O 6E
C A7
VIEW L 11F
SCALE 4
VIEW M 10E
SCALE 4
VIEW K 11F
SCALE 4
SECTION F-F 20F 20F
VIEW C 9A
SCALE 4
31.60 DIA
33.178 DIA
33.594 DIA
34.562 DIA
35.13 DIA
99RS006195
B

13 HYDROSTATIC PRESSURE TEST AT 4800 PSI ± 125 PER ENGR INSTRUCTIONS.
12 MACHINE AFTER BRAZING.
11 LEAK AND PRESS. PROOF TEST PER ENGR INSTRUCTIONS
10 ELECTRON BEAM WELD PER RA0107-042
9 DUCTILE NICKEL PLATE -013 .0001 TO .0002 THICK PER RA1109-005 ON SURFACES INDICATED
8 SURFACE OF -003 MUST BE WITHIN .010 OF BASIC CONTOUR
7 FURNACE BRAZE (SECOND CYCLE) PER RA1607-014 AND ENGINEERING INSTRUCTIONS
6 WELD JOINTS ON BANDS AND TUBES MUST BE STAGGERED ON CIRCUMFERENCE OF NOZZLE
5 FURNACE BRAZE AND HEAT TREAT PER RA1607-014 AND ENGR INSTRUCTIONS TO OBTAIN A286 MATL PROPERTIES: F_{tu} = 140,000 lb/in², F_{ty} = 95,000 lb/in², e = 15 % MIN
4 WELD PER RA0107-027 CLASS 1
3 ~~MAY BE FABRICATED FROM MULTIPLE PIECES~~
2 MACHINE PER RA0103-002
1 IDENTIFY PER RA0104-008

NOTE: UNLESS OTHERWISE SPECIFIED

[redacted]

6

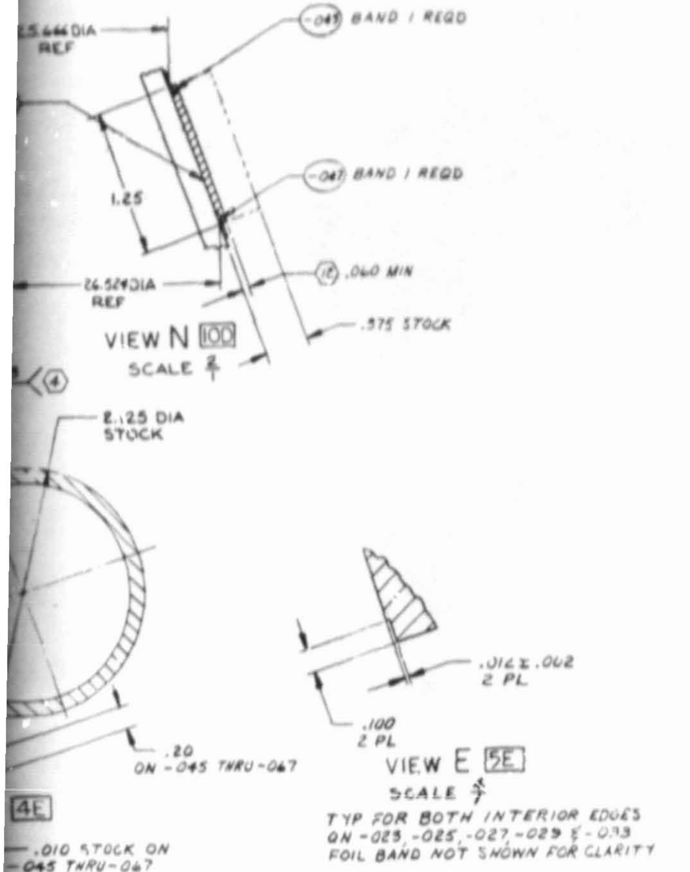

REVISIONS

ZONE	LTR	DESCRIPTION		DATE	APPROVED
22C	A	1) ADDED 30°	4		
23A		2) 10.108 DIA WAS 10.108 DIA	3		
21C		3) (2.53) WAS 2.53	3		
19A		4) ADDED .406R AND 15°	4		
11 H		5) ADDED (1)	3		
6B		6) 308 LC WAS 308 ELC	4		
7&C		7) .090 WAS .060, ADDED .030R 3 PLACES	4		
8C		8) ADDED .595 REF	3		
2B		9) -019 WAS MADE FROM 321 CRES PL MIL-S-6721 COMP 321	4		
	B				
10-11		1) REMOVED -039 & -043	1		
10-11		2) REVISED -023, -025, -027, -029, -033 & -035	2		
		3) (-025 THRU -033) 347 CRES FORG WAS 347 CRES SHEET	2		
4-9		4) ADDED -045 THRU -067 & VIEW E	3		
4E					
17-18		5) ADDED -069, -073 & SECT F-F	3		
		6) ADDED NOTE (12)	3		
		7) DELETED NOTE (3)			
18		8) ADDED 31.60 DIA	3		
20E		9) CHANGED LOCATION OF -005 & -009 INLET ON MANIFOLD 120° COUNTERCLOCKWISE VIEW A-A LOOKING AFT			
9E		10) ADDED -073 LUGS	1		
		11) ADDED PRESS TEST NOTE 13			
		EFF: ALL PARTS MADE			

Figure 39

67

NO.	MATERIAL	SIZE	SPECIFICATION	ZONE
-075	321 CRES PLATE			9E
-073	347 CRES SH		MIL-S-6721 COMP 347	18A
-069	347 CRES SH		MIL-S-6721 COMP 347	17C
-067	NICKEL 200 FOIL		COML GRADE	9H
-065				9H
-063				7F
-059				7F
-057				7H
-055				7H
-053				7F
-049				7E
-047				4H
-045	NICKEL 200 FOIL		COML GRADE	4H
~~-043~~	~~347 CRES TUBE~~	~~.375 O.D. X .028~~	~~MIL-T-8808, TYPE II~~	~~11G~~
~~-039~~	~~347 CRES TUBE~~	~~1.000 O.D. X .058~~	~~MIL-T-8808, TYPE II~~	~~10E~~
-037	INCO 625 TUBE	1.375 O.D. X .188	RB0170-128	11H
-035	347 CRES TUBE	2.125 O.D. X .120	MIL-T-8808, TYPE II	9C
-033	347 CRES FORGING	———	QQ-S-763 CLASS 347 COND A	11G
-029		———		11F
-027		———		10D
-025		———		10E
-023	347 CRES FORGING	———	QQ-S-763 CLASS 347 COND A	10C
-019	INCO 625 PL	———	AMS 5599	10A
-017	INCO 625 PL	———	AMS 5599	11H
-015	347 CRES PL	———	MIL-S-6721 COMP 347	9B
-013	INCO 625 PL	———	AMS 5599	11G
-009	347 CRES BAR	———	QQ-S-763 CLASS 347 COND A	22H
-007		———		17G
-005	347 CRES BAR	———	QQ-S-763 CLASS 347 COND A	23F
-003	OFHC COP PL	———	RB0170-047 OFHC	11G

13 HYDROSTATIC PRESSURE TEST AT 4800 PSI ± 25 PER ENGR INSTRUCTIONS.
(12) MACHINE AFTER BRAZING.
11 LEAK AND PRESS. PROOF TEST PER ENGR. INSTRUCTIONS
(10) ELECTRON BEAM WELD PER RA0107-042
(9) DUCTILE NICKEL PLATE -013 .0001 TO .0002 THICK PER RA1109-005 ON SURFACES INDICATED
(8) SURFACE OF -003 MUST BE WITHIN .010 OF BASIC CONTOUR
(7) FURNACE BRAZE (SECOND CYCLE) PER RA1607-014 AND ENGINEERING INSTRUCTIONS
(6) WELD JOINTS ON BANDS AND TUBES MUST BE STAGGERED ON CIRCUMFERENCE OF NOZZLE
(5) FURNACE BRAZE AND HEAT TREAT PER RA1607-014 AND ENGR INSTRUCTIONS TO OBTAIN A286 MATL PROPERTIES: F_{tu} = 140,000 LB/IN², F_{ty} 15,000 LB/IN², e 15% MIN
(4) WELD PER RA0107-027 CLASS II
~~(3) MAY BE FABRICATED FROM MULTIPLE PIECES~~
2. MACHINE PER RA0103-002
(1) IDENTIFY PER RA0104-008

NOTE: UNLESS OTHERWISE SPECIFIED

-001
NO

HEAT TREAT	(5)
FINISH	(9)
SEAL	NOTED

UNLESS OTHERWISE SPECIFIED DIMENSIONS ARE IN INCHES AND APPLY PRIOR TO FINISH

NAS3-17825

Rockwell International Corporation
Rocketdyne Division
Canoga Park, California

NOZZLE, REGENERATIVELY COOLED ADVANCED THRUST CHAMBER, 20K, ASSY OF

SIZE J | CODE IDENT NO 02602 | DRAWING NO 99RS006195

SCALE 1/1

DO NOT SCALE PRINT

99RS006195

CONTOUR COORDINATES SEE NOTE 3	
X	Yr
0.000	16.580 REF
1.690	17.060
4.122	17.722
6.686	18.347
12.380	19.648
18.721	20.927
22.678	21.661
31.659	23.116
35.409	23.675
46.331 REF	25.050 REF

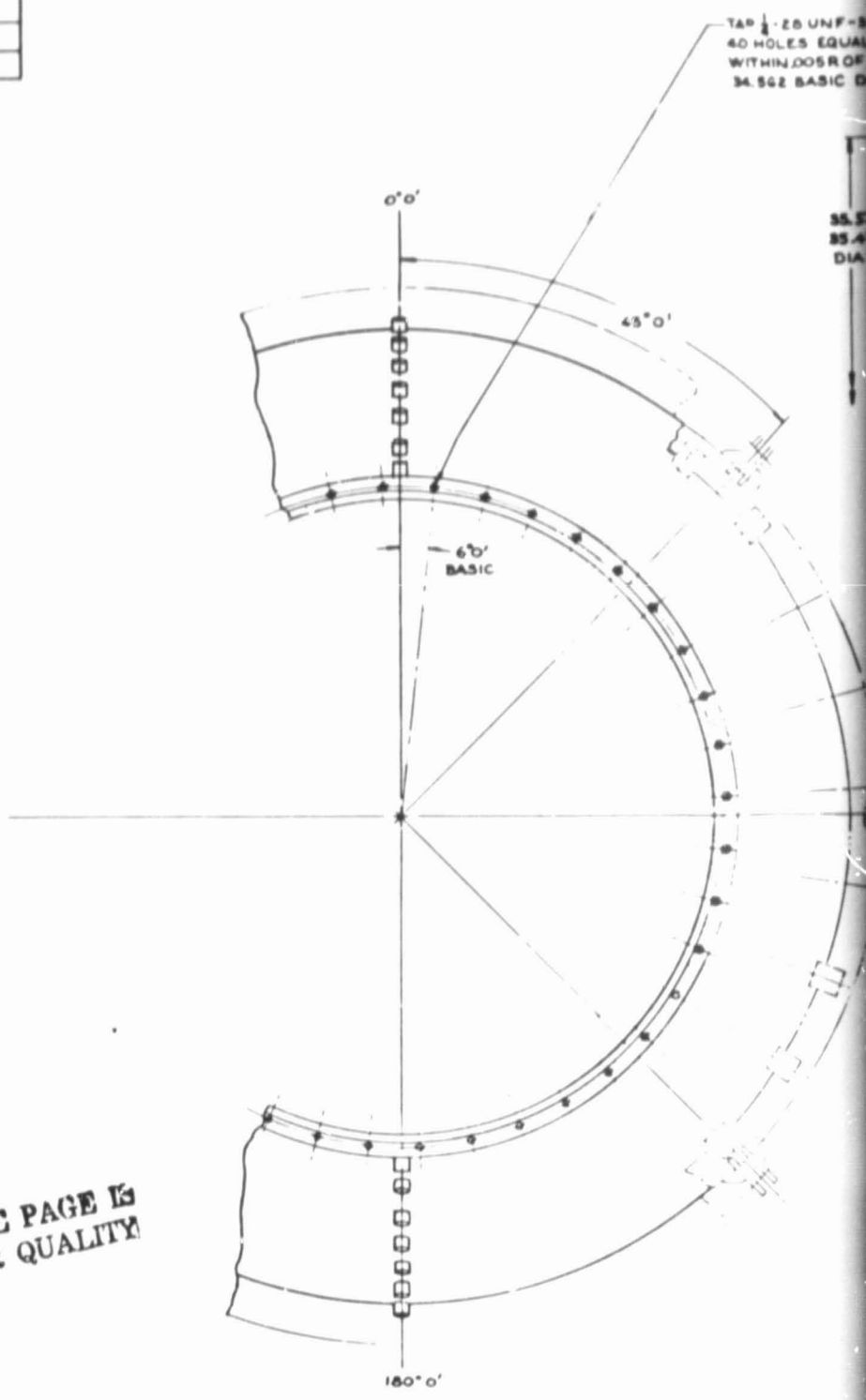

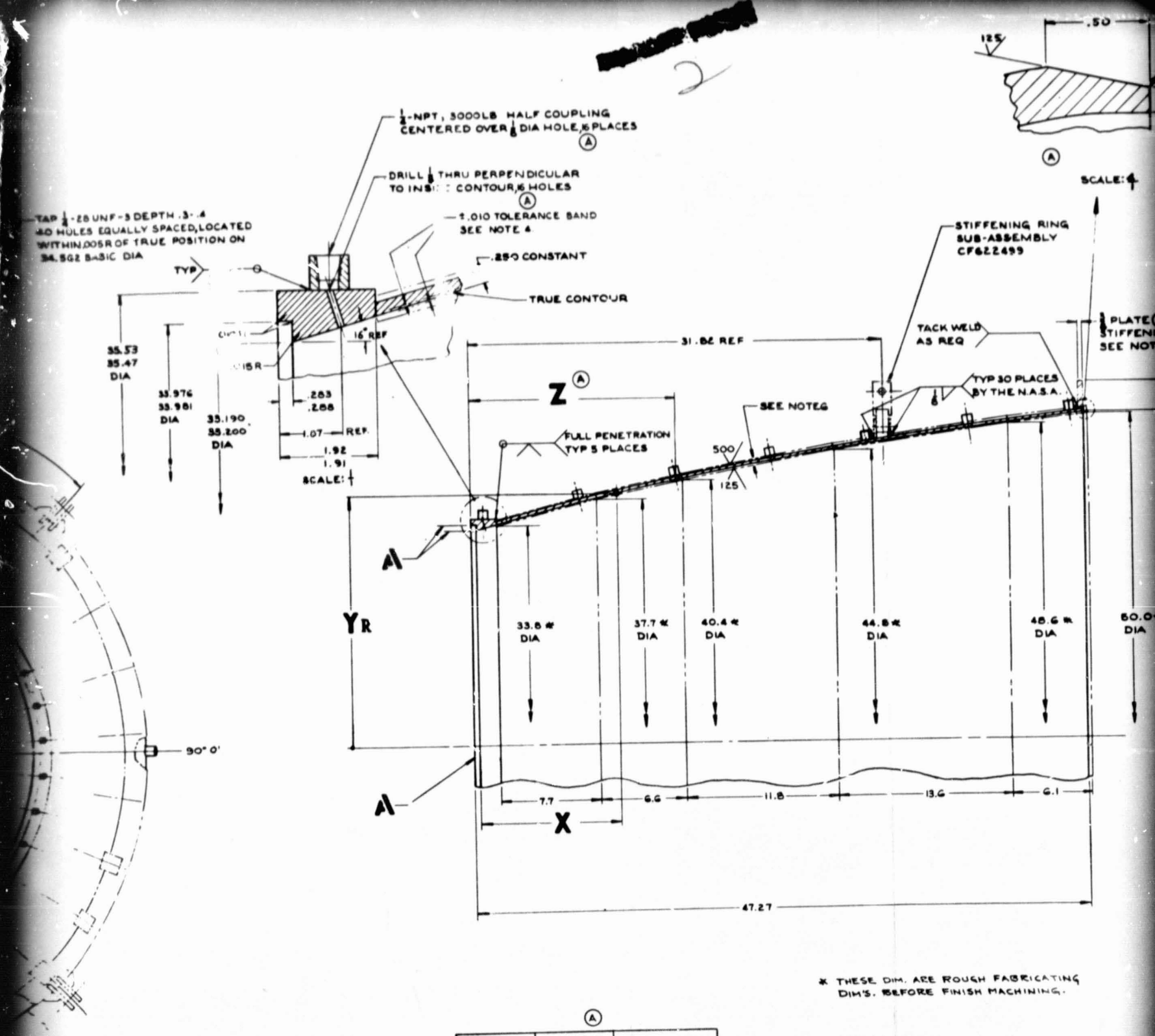

* THESE DIM. ARE ROUGH FABRICATING DIM'S. BEFORE FINISH MACHINING.

(A)

Z	NUMBERS OF TAPS	ORIENTATION
1.00	2	0°0', 180°0'
8.38	2	0°0', 180°0'
15.76	2	0°0', 180°0'
23.14	2	0°0', 180°0'
30.52	2	0°0', 180°0'
38.40	2	0°0', 180°0'
46.28	4	0°0', 90°0', 180°0', 270°0'

SCALE ½ & NOTED

UNLESS OTHERWISE SPECIFIED
.X DEC. DIM. TOLT. ± .03
.XX DEC. DIM. TOLT. ± .01
.XXX DEC. DIM. TOLT. ± .005
ANGULAR DIM. DIM. TOLT. ± 0°30'
____ DEC. DIM. TOLT. ±
BREAK SHARP EDGES .01-.02

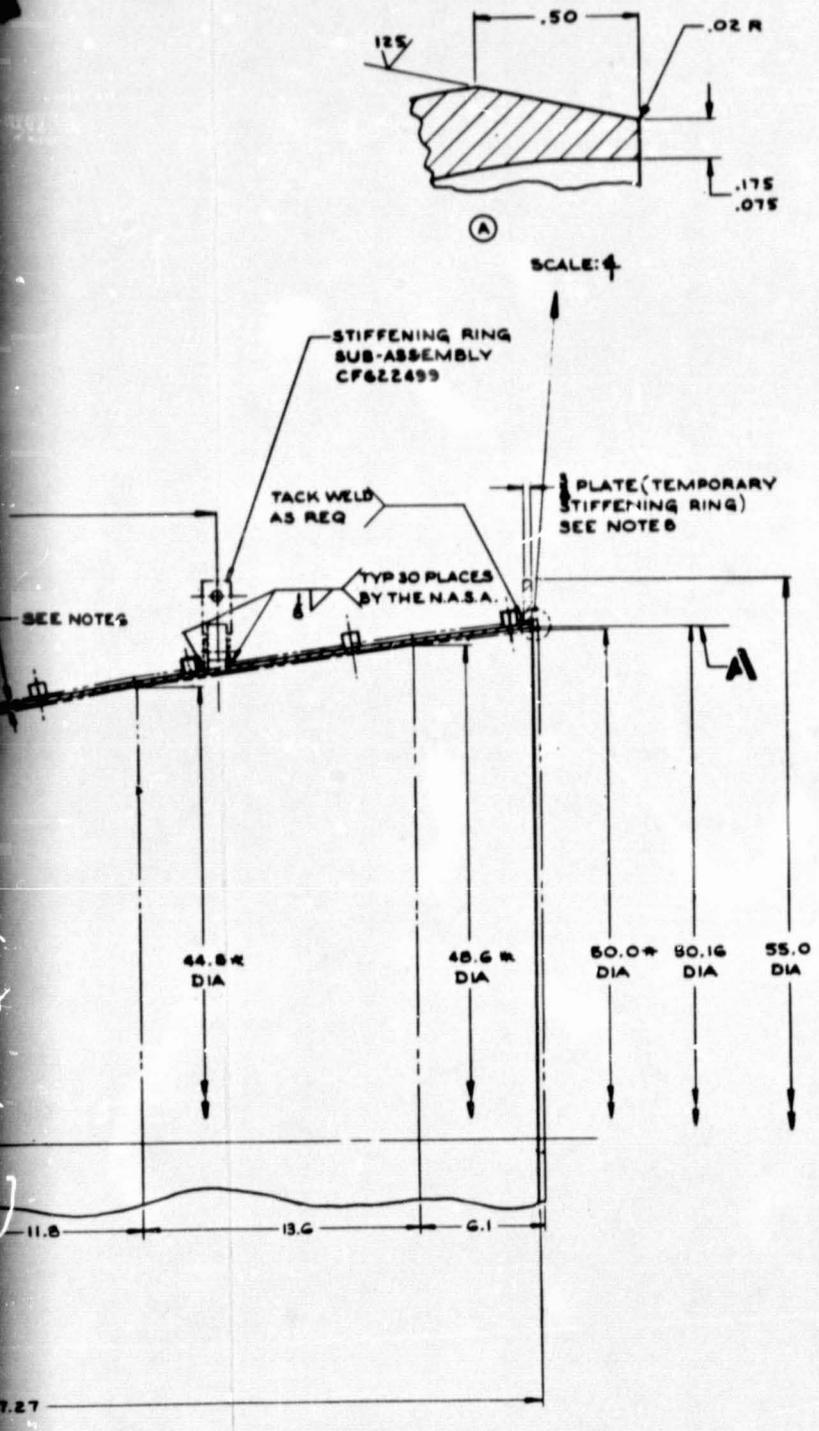

* THESE DIM. ARE ROUGH FABRICATING DIM'S. BEFORE FINISH MACHINING.

1. A SURFACES MUST BE CONCENTRIC, PARALLEL, FLAT, SQUARE AND TRUE (AS APPLICABLE) TO EACH OTHER WITHIN .010 F.I.R.
2. 64 √ ALL OVER UNLESS OTHERWISE NOTED.
3. CONTOUR COORDINATES ARE BASIC AND DEFINE THE TRUE CONTOUR.
4. CONTOUR IS PRODUCED BY FAIRED LINES BETWEEN STATIONS FROM END TO END. CONTOUR TO BE SMOOTH AND CONTINUOUS WITHIN TOLERANCE SPECIFIED.
5. MATERIAL: S.A.E. 1010 - 1030.
6. INITIAL WELDMENT TO BE MADE OF ½ INCH THICK PLATE. ALL WELDS TO BE GTAW OR GMAW PER MIL-W-8611.
7. THERMAL STRESS RELIEVE AFTER WELDING AND BEFORE FINISH MACHINING BY HEATING TO 1100°-1150°F IN AIR, HOLD FOR ONE HOUR AND THEN AIR COOL.
8. TEMPORARY STIFFENING RING TO BE REMOVED AFTER FINISH MACHINING AND INSTALLATION OF STIFFENING RING SUB-ASSEMBLY CF 622499.

[redacted]

3

Figure 40
69

SCALE: ½ & NOTED	REFERENCE	INITIAL	DATE
UNLESS OTHERWISE SPECIFIED	1 REQ	DR.	
X DEC. DIM. TOLT. ± .03		CK.	D.A.R. 8-6
XX DEC. DIM. TOLT. ± .01		E. ENGR.	8-13-72
XXX DEC. DIM. TOLT. ± .005		A. ENGR.	
ANGULAR DIM. TOLT. ± 0°30'		P. ENGR.	
___ DEC. DIM. TOLT. ±		G. E. CO.	8-17-72
BREAK SHARP EDGES .01-.02		G. E. CO.	
		G. E. CO.	8-13-72
		G. E. CO.	8-17-72

CHANGE	NO.	REVISION (M)	DATE	CK. APP.
(M)	A	GENERAL REVISIONS	2-11-77	E.K. Cat GTR. Gmk.

HEAT SINK EXHAUST NOZZLE

ADVANCED THRUST CHAMBER TESTS,

NATIONAL AERONAUTICS AND SPACE ADMINISTRATION
LEWIS RESEARCH CENTER
CLEVELAND, OHIO

CF622498

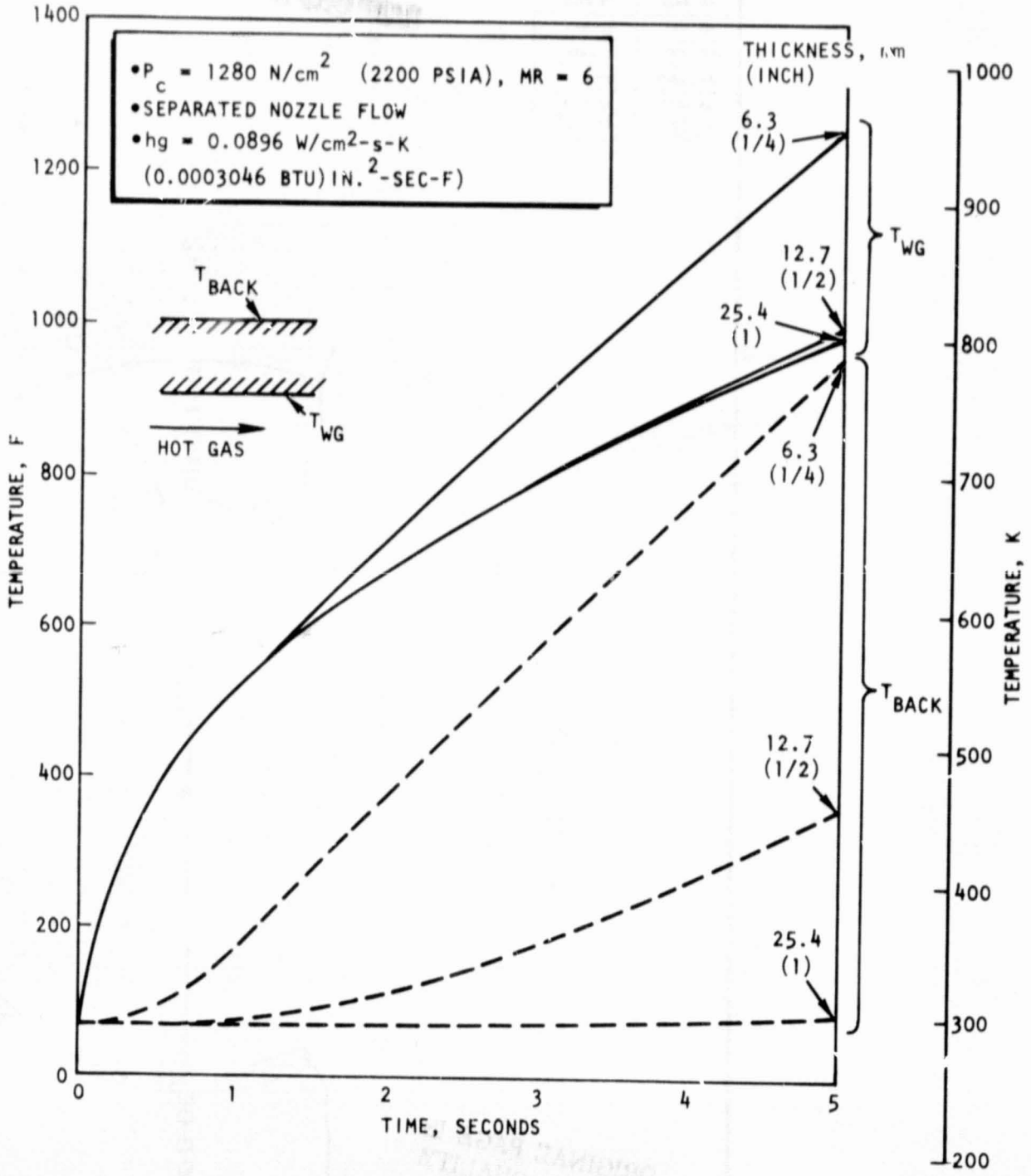

Figure 41. Separated Nozzle Flow Temperature vs Time

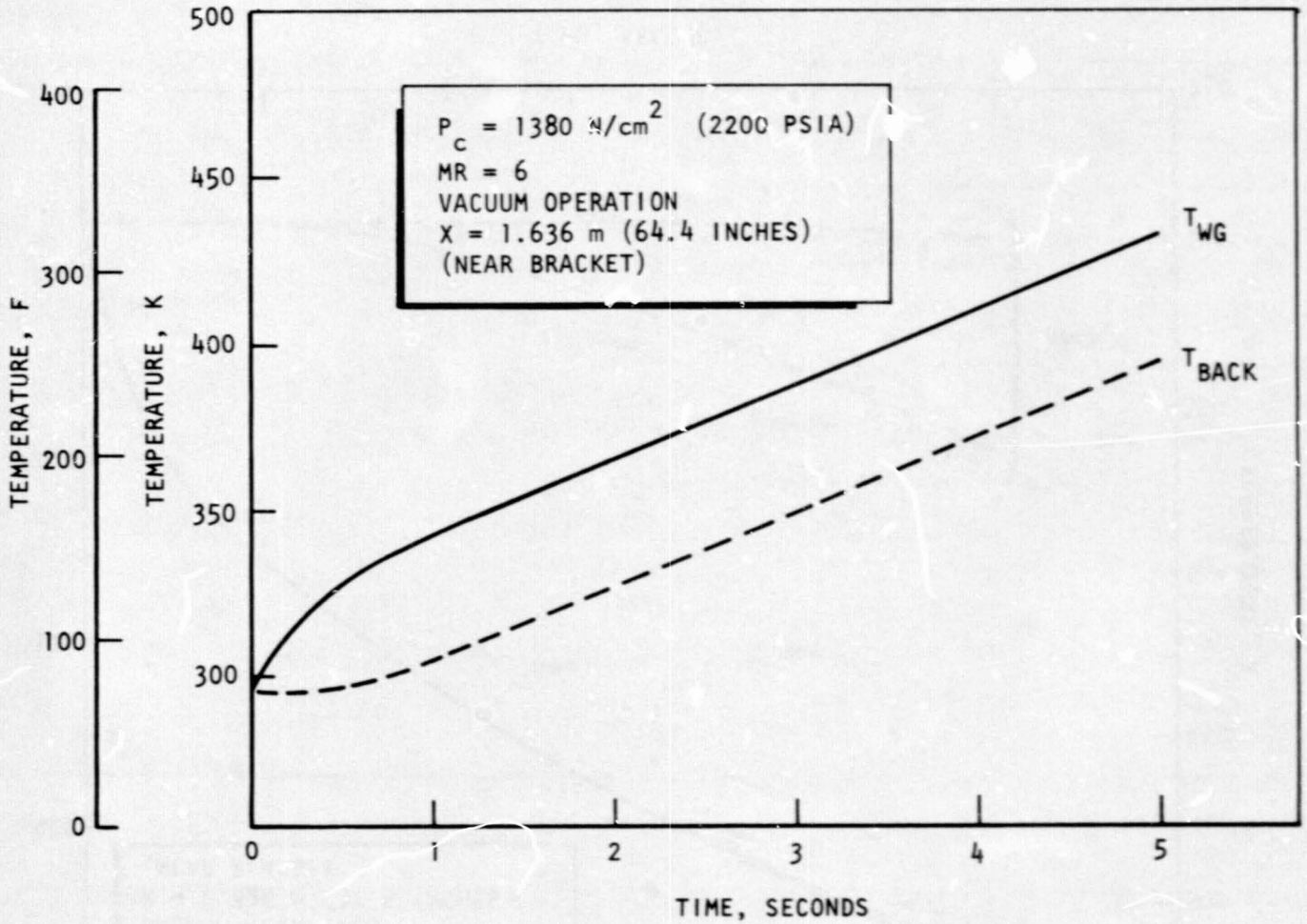

Figure 42. Nozzle Wall Temperature Near Bracket vs Time

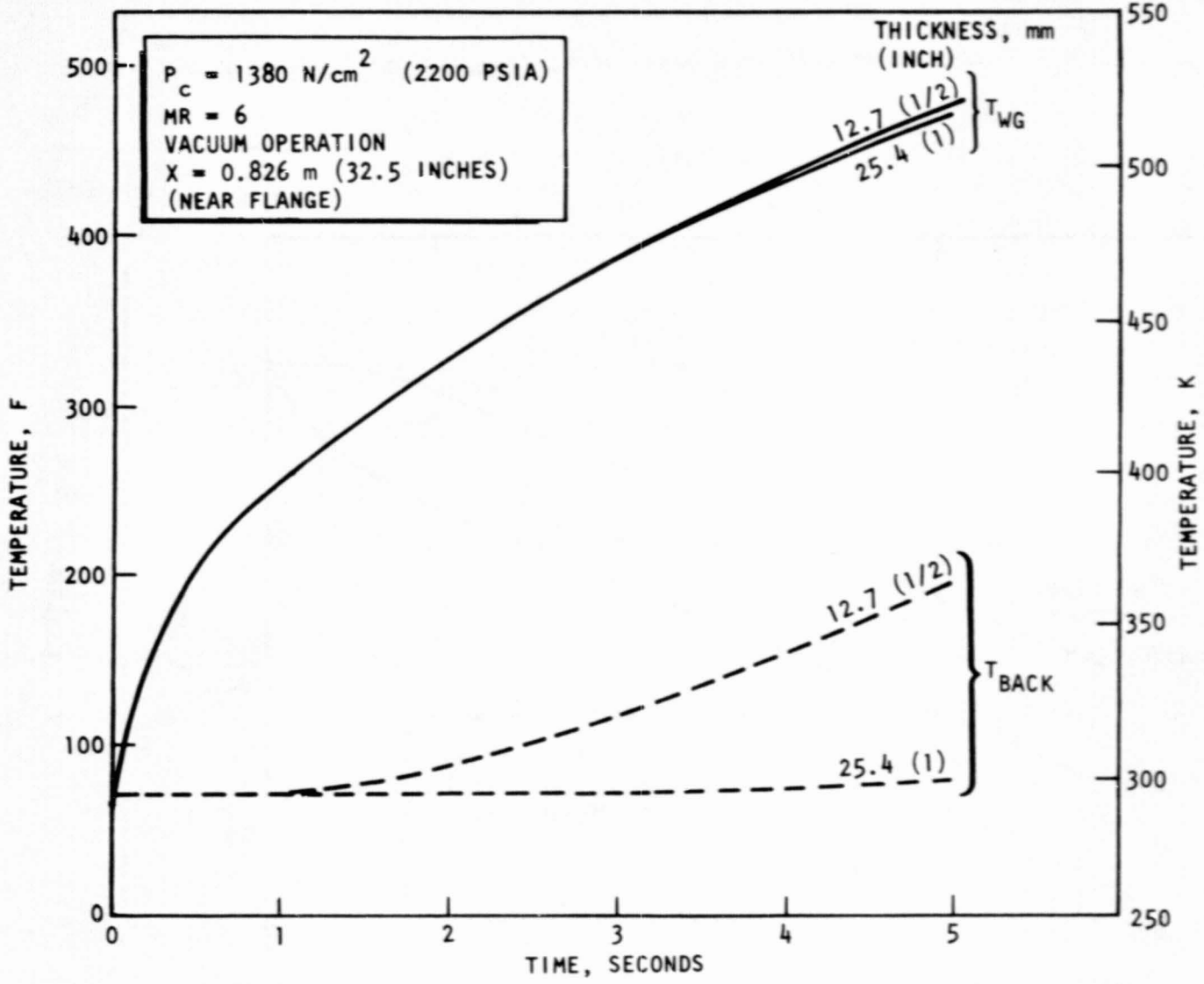

Figure 43. Nozzle Wall Temperature Near Flange vs Time

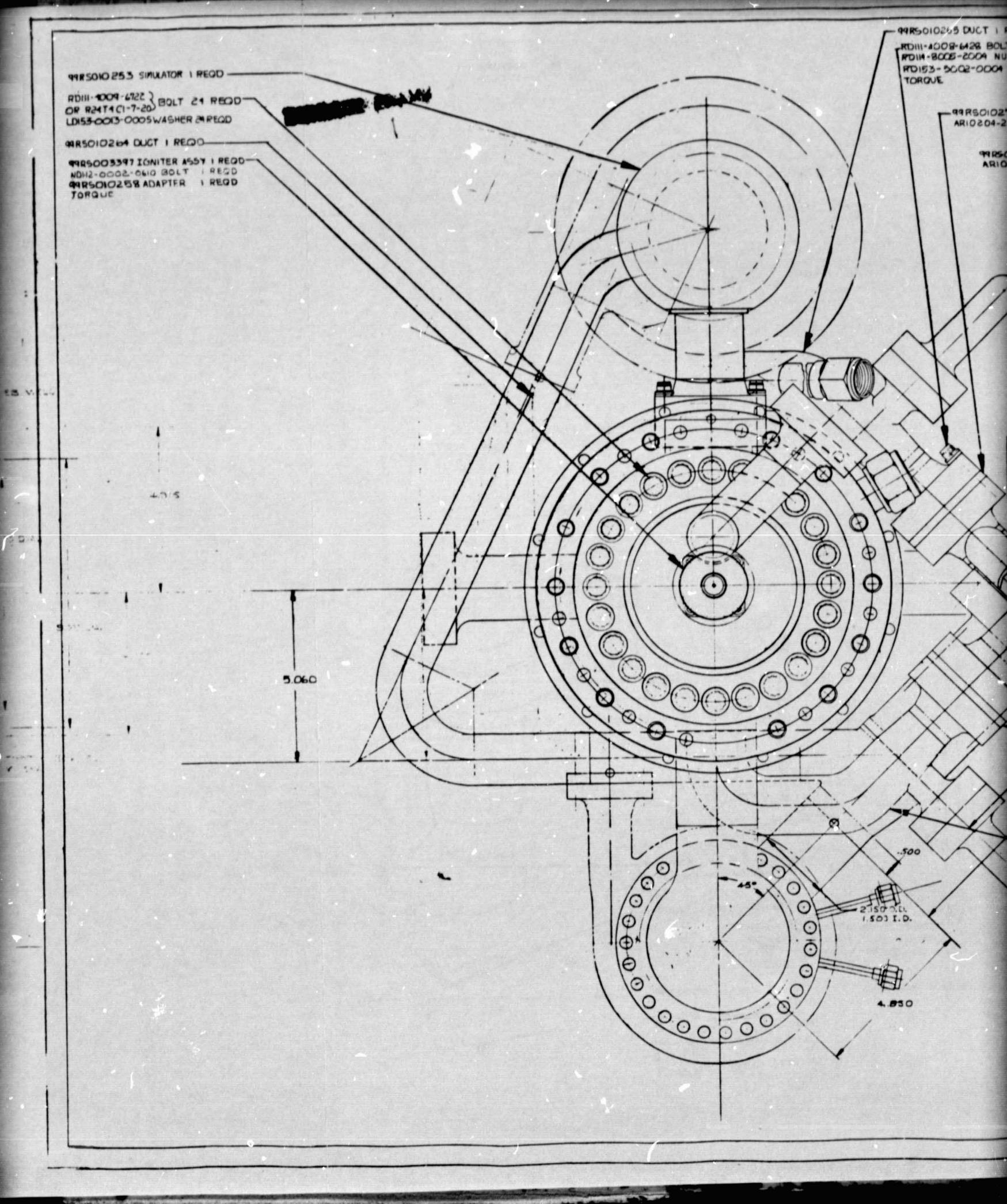
99RS010253 SIMULATOR 1 REQD
RD111-1009-6722
OR R24T4C1-7-20 BOLT 24 REQD
LD153-0003-0005 WASHER 24 REQD
99RS010264 DUCT 1 REQD
99RS003397 IGNITER ASSY 1 REQD
ND112-0002-0610 BOLT 1 REQD
99RS010258 ADAPTER 1 REQD
TORQUE
99RS010265 DUCT 1
RD111-4008-6428 BOL
RD114-8005-2009 NU
RD153-5002-0009
TORQUE
5.060
.500
45°
2.150 I.D.
1.503 I.D.
4.850

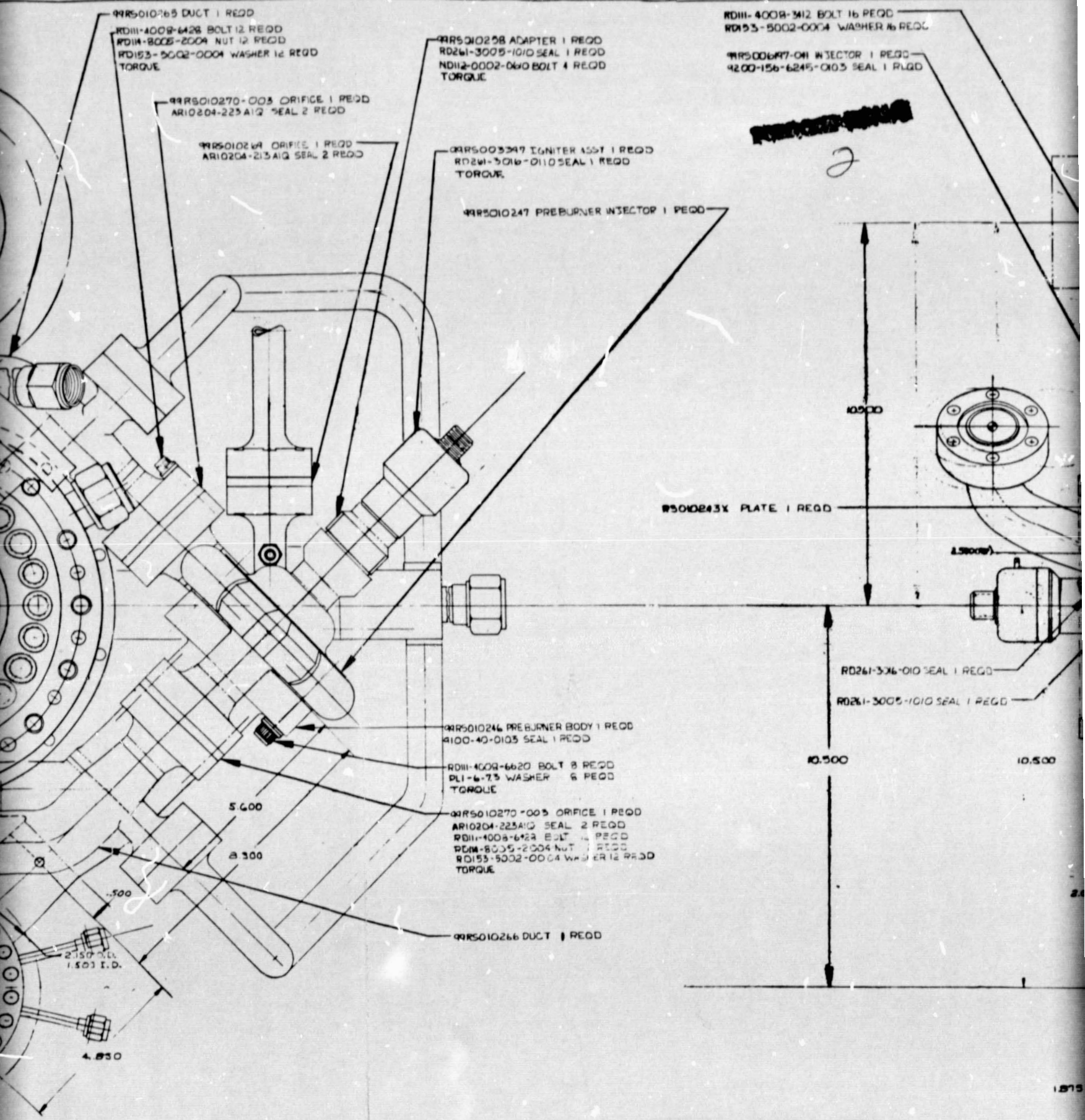
RR5010265 DUCT 1 REQD
RD111-4008-6428 BOLT 12 REQD
RD114-8008-2004 NUT 12 REQD
RD153-5002-0004 WASHER 12 REQD
TORQUE
RR5010270-003 ORIFICE 1 REQD
AR10204-223AIQ SEAL 2 REQD
RR5010269 ORIFICE 1 REQD
AR10204-213AIQ SEAL 2 REQD
RR5010258 ADAPTER 1 REQD
RD261-3005-1010 SEAL 1 REQD
ND112-0002-0660 BOLT 4 REQD
TORQUE
RR5003397 IGNITER ASSY 1 REQD
RD261-5016-0110 SEAL 1 REQD
TORQUE
RR5010247 PREBURNER INJECTOR 1 REQD
RR5010246 PREBURNER BODY 1 REQD
4100-40-0103 SEAL 1 REQD
RD111-4008-6620 BOLT 8 REQD
PL1-6-7.5 WASHER 8 REQD
TORQUE
RR5010270-003 ORIFICE 1 REQD
AR10204-223AIQ SEAL 2 REQD
RD111-4008-6428 BOLT 12 REQD
RD114-8005-2004 NUT 12 REQD
RD153-5002-0004 WASHER 12 REQD
TORQUE
RR5010266 DUCT 1 REQD
5.600
8.300
.500
2.150 O.D.
1.501 I.D.
4.850
RD111-4008-3412 BOLT 16 REQD
RD153-5002-0004 WASHER 16 REQD
RR5006R7-041 INJECTOR 1 REQD
4200-156-6245-0103 SEAL 1 RLQD
10.500
R5010243X PLATE 1 REQD
RD261-336-010 SEAL 1 REQD
RD261-3005-1010 SEAL 1 REQD
10.500
10.500

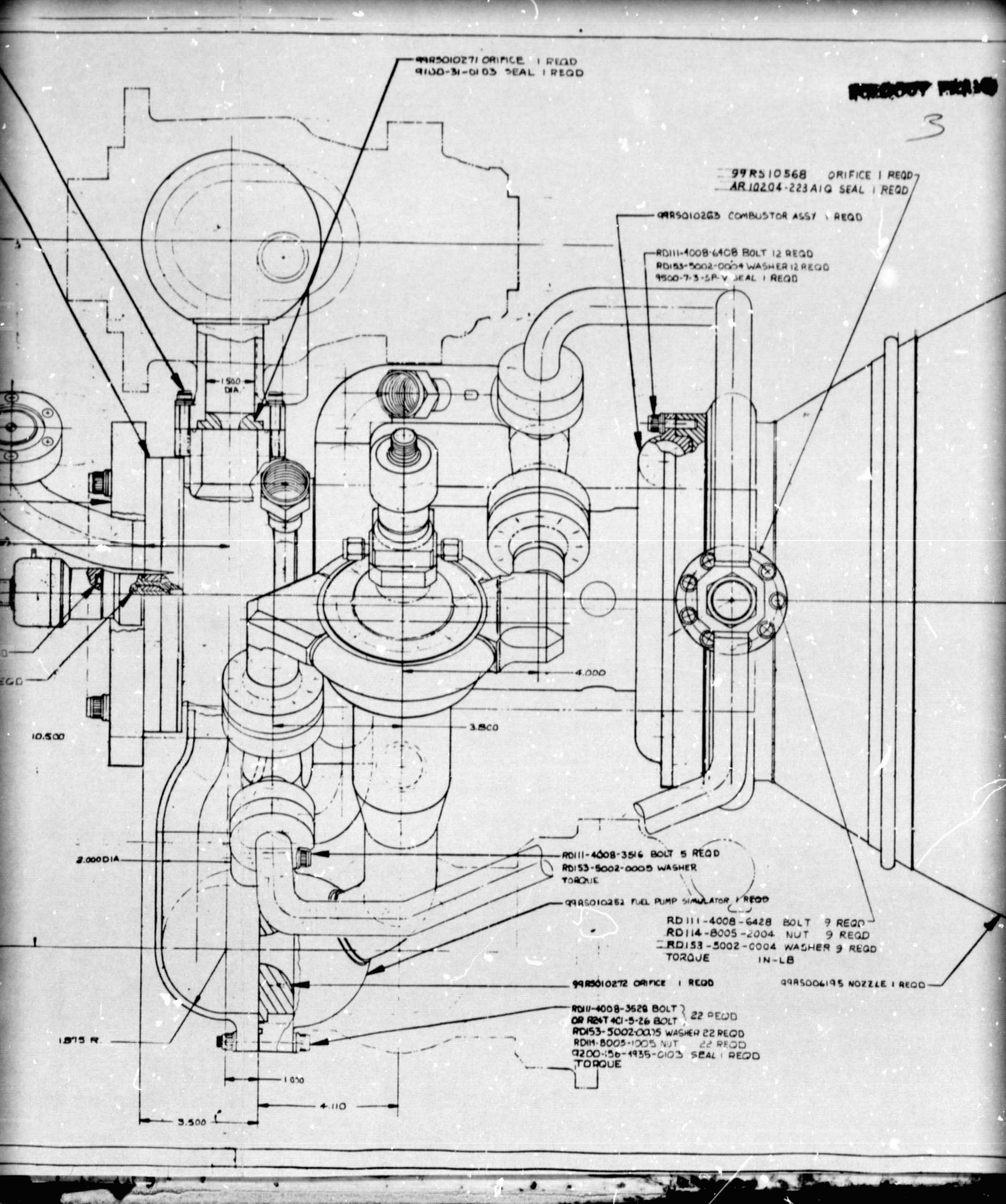
99RS010271 ORIFICE 1 REQD
9130-31-0103 SEAL 1 REQD
99RS10568 ORIFICE 1 REQD
AR10204-223A1Q SEAL 1 REQD
99RS010263 COMBUSTOR ASSY 1 REQD
RD111-4008-6408 BOLT 12 REQD
RD153-5002-0004 WASHER 12 REQD
9500-7-3-SP-V SEAL 1 REQD
1.500 DIA
4.000
3.800
10.500
2.000 DIA
RD111-4008-3516 BOLT 5 REQD
RD153-5002-0005 WASHER
TORQUE
99RS010262 FUEL PUMP SIMULATOR 1 REQD
RD111-4008-6428 BOLT 9 REQD
RD114-8005-2004 NUT 9 REQD
RD153-5002-0004 WASHER 9 REQD
TORQUE IN-LB
99RS010272 ORIFICE 1 REQD
99RS006195 NOZZLE 1 REQD
RD111-4008-3528 BOLT
OR R26T4C1-5-26 BOLT 22 REQD
RD153-5002-0015 WASHER 22 REQD
RD114-8005-1005 NUT 22 REQD
9200-156-1935-0103 SEAL 1 REQD
TORQUE
1.875 R
1.030
4.110
3.500

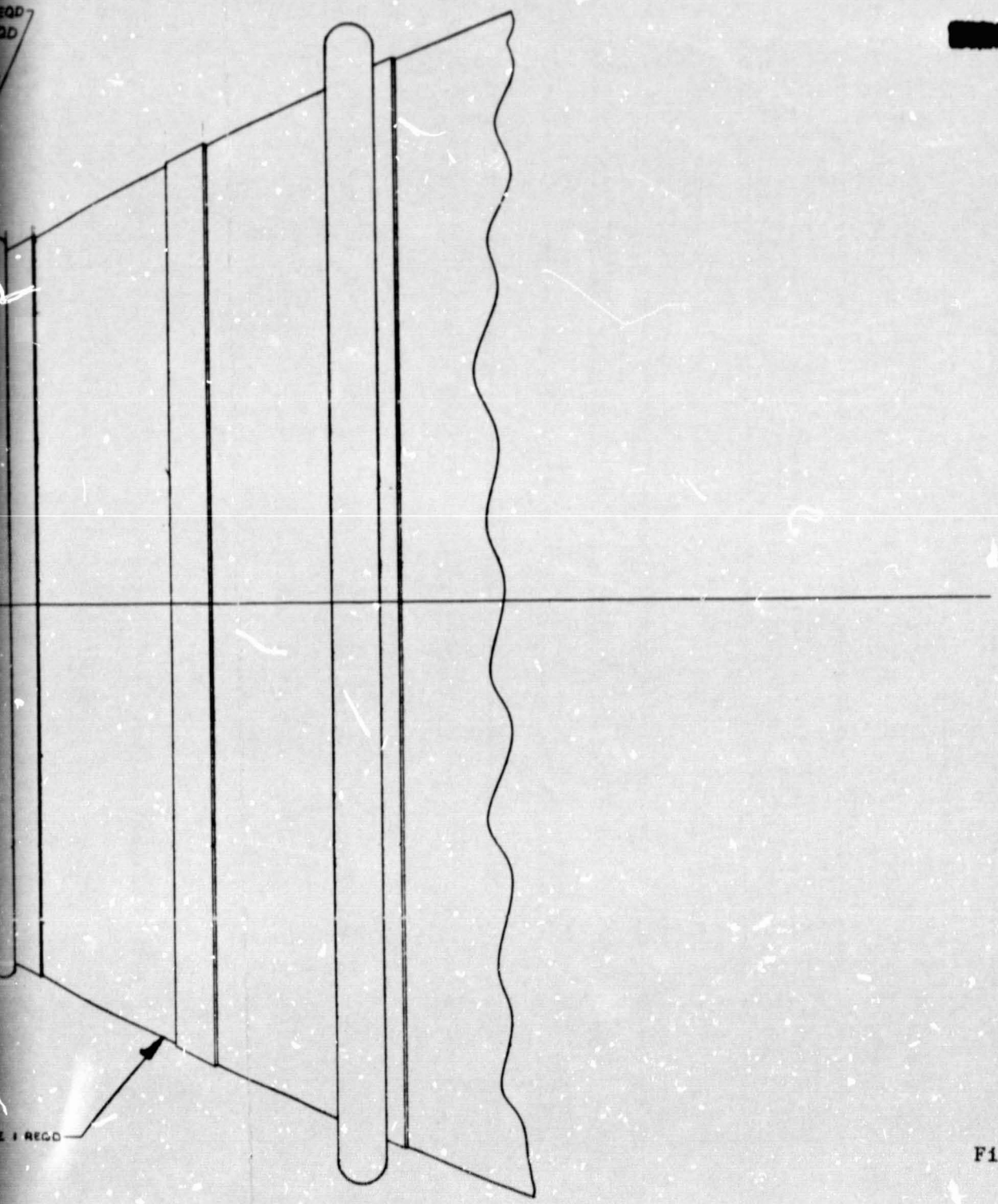

Figure 44

STAGED COMBUSTION
SYSTEM ASSY - 20K ADV
THRUST CHAMBER

02602

nozzle extension to the 400:1 area ratio. The preburner components, ducting, fuel turbine simulators, and the nozzle extension were fabricated new for this program; the remainder of the components were transferred from the Advanced Thrust Chamber Technology program.

Design layouts were established to locate the various components as they would be located in an engine system package. The initial layout and subsequent component fabrication were based on assembling the staged combustion assembly as a regeneratively cooled system for the testing effort. Thus, the layouts shown, and the flanged and fitting connnection locations reflect this original intent. Figure 45 shows a partially sectioned layout of the staged combustion assembly with the interconnecting fuel ducting and turbine simulators. Figure 46 shows the same assembly view with the preburner removed to illustrate the ducting arrangement more clearly. This view shows the coolant ducts from the single nozzle outlet connecting to the two coolant ducts from the combustion chamber coolant outlet. The combined coolant flow was then to proceed on to the preburner injector at the two flanged connections. Also shown on these two views are two of three threaded fittings to provide an overboard dump of excess coolant flow, thus providing an option during the testing effort of supplying excess coolant flow to both the chamber and nozzle.

A complete layout of the coolant system and assembly is shown in Fig. 47. The oxidizer turbine simulator (Fig. 48) with the hot-gas ducting (Fig. 49) provided the transport passageway for the fraction of the preburner exhaust gas which would be required to drive the oxidizer turbopump. Provision has been made for an orifice at the flange which connects to one side of the main injector to simulate the turbine pressure drop and to meter the hot gas flow to the required 32%. Iteration of the thermal and structural analysis of the ducting and its routing was required to achieve a system configuration which could withstand the loads imposed by thermal growth of the ducting.

Table 15 is a summary of two of the configurations reviewed and analyzed for thermal loads. Model 1 is representative of a compact ducting system which was acceptable because of the high loads imposed on the injector body and the turbopump assemblies. Model 3 is the final configuration which was released for fabrication. The loads transmitted to the injector housing and to the two turbopump assemblies were significantly lower for this model because of the combination of smaller diameter and thinner wall ducting and greater length of ducting as noted in the first part of Table 15.

Figure 45. Staged Combustion Assembly

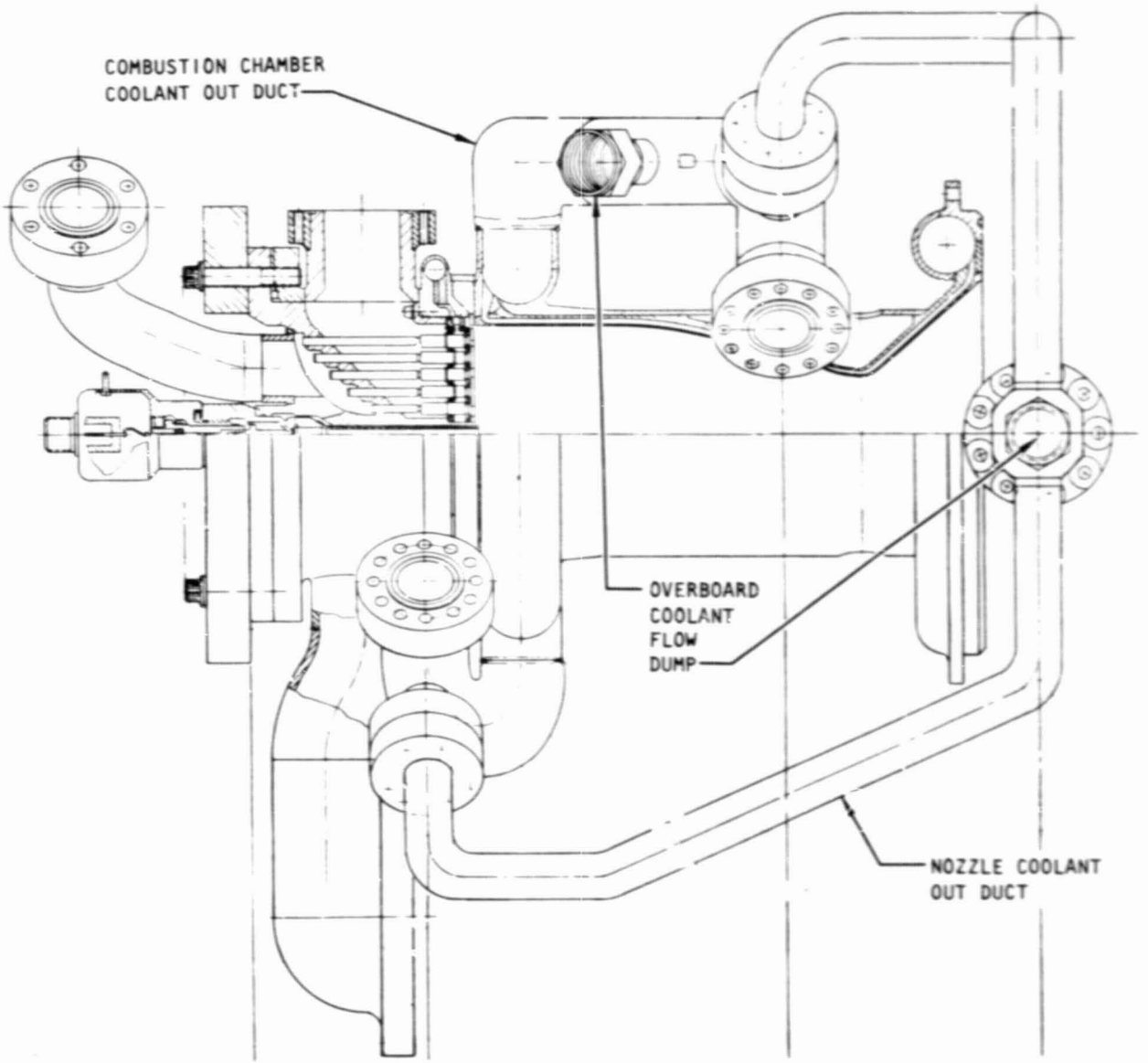

Figure 46. Staged Combustion Assembly With Preburner Removed

TABLE 15. DUCT LOADS

PREBURNER MODEL DIFFERENCES

Preburner Fuel Inlet Lines		
	Line Size	
	Straights	Elbow
Model 1	43.2 mm OD x 5.6 mm wall (1.7-in. OD x 0.22-in. wall)	43.2 mm OD x 5.6 mm wall (1.7-in. OD x 0.22-in. wall)
Model 3	38.1 mm OD x 1.65 mm wall (1.5-in. OD x 0.065-in. wall)	43.2 mm OD x 3.0 mm wall (1.7-in. OD x 0.12-in. wall)

Preburner-to-Oxidizer-Turbopump Hot-Gas Duct		
	Line Size	Remarks
Model 1	38.1 mm OD x 3.8 mm wall (1.5-in. OD x 0.15-in. wall)	
Model 3	38.1 mm OD x 3.18 mm wall (1.5 in. OD x 0.125-in. wall)	Length of pipe increased

TRANSIENT THERMAL LOADS

Main Injector Body - Oxidizer Pump Side				
	Fuel Inlet Loading			
	F_{axial}, N (pounds)	F_{shear}, N (pounds)	M_{torque}, N · cm (in.-lb)	$M_{bending}$, N · cm (in.-lb)
Model 1	6672 (1500)	3928 (883)	45 420 (4020)	81 270 (7193)
Model 3	3216 (723)	2135 (480)	28 670 (2538)	48 620 (4303)
Turbine Hot-Gas Inlets				
	Fuel Turbopump			
Model 1	6805 (1530)	4470 (1005)	37 170 (3290)	146 210 (12,941)
Model 3	4804 (1080)	4297 (966)	30 660 (2714)	113 940 (10,085)
	Oxidizer Turbopump			
Model 1	476 (107)	7731 (1738)	13 330 (1180)	91 400 (8090)
Model 3	418 (94)	3843 (864)	8575 (759)	60 240 (5332)

NOTE: Loads given as magnitudes only; no signs are given, since directions for F_{shear} and $M_{bending}$ do not necessarily coincide.

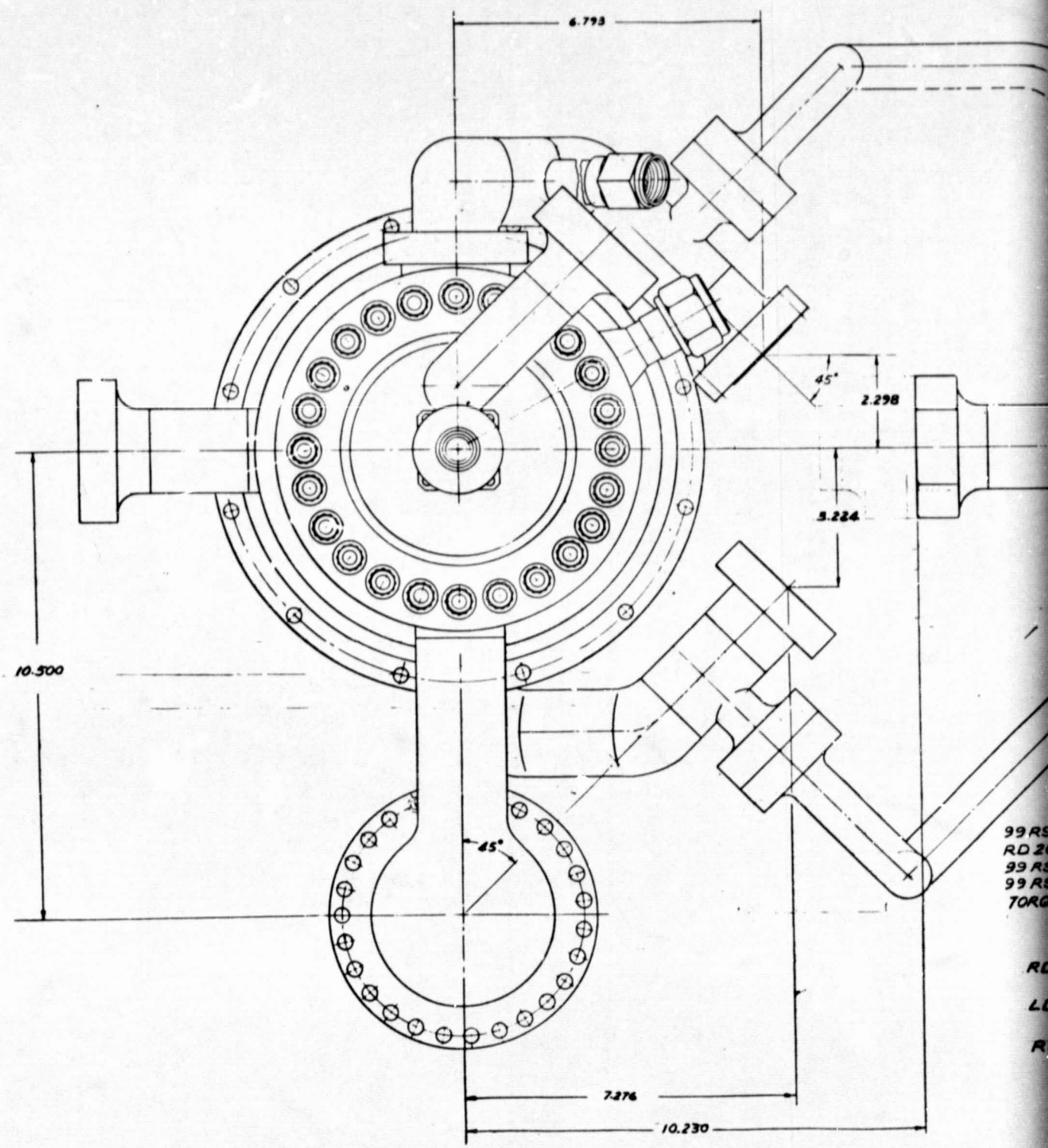
99RS006
6.793
45°
2.298
5.224
10.500
45°
7.276
10.230

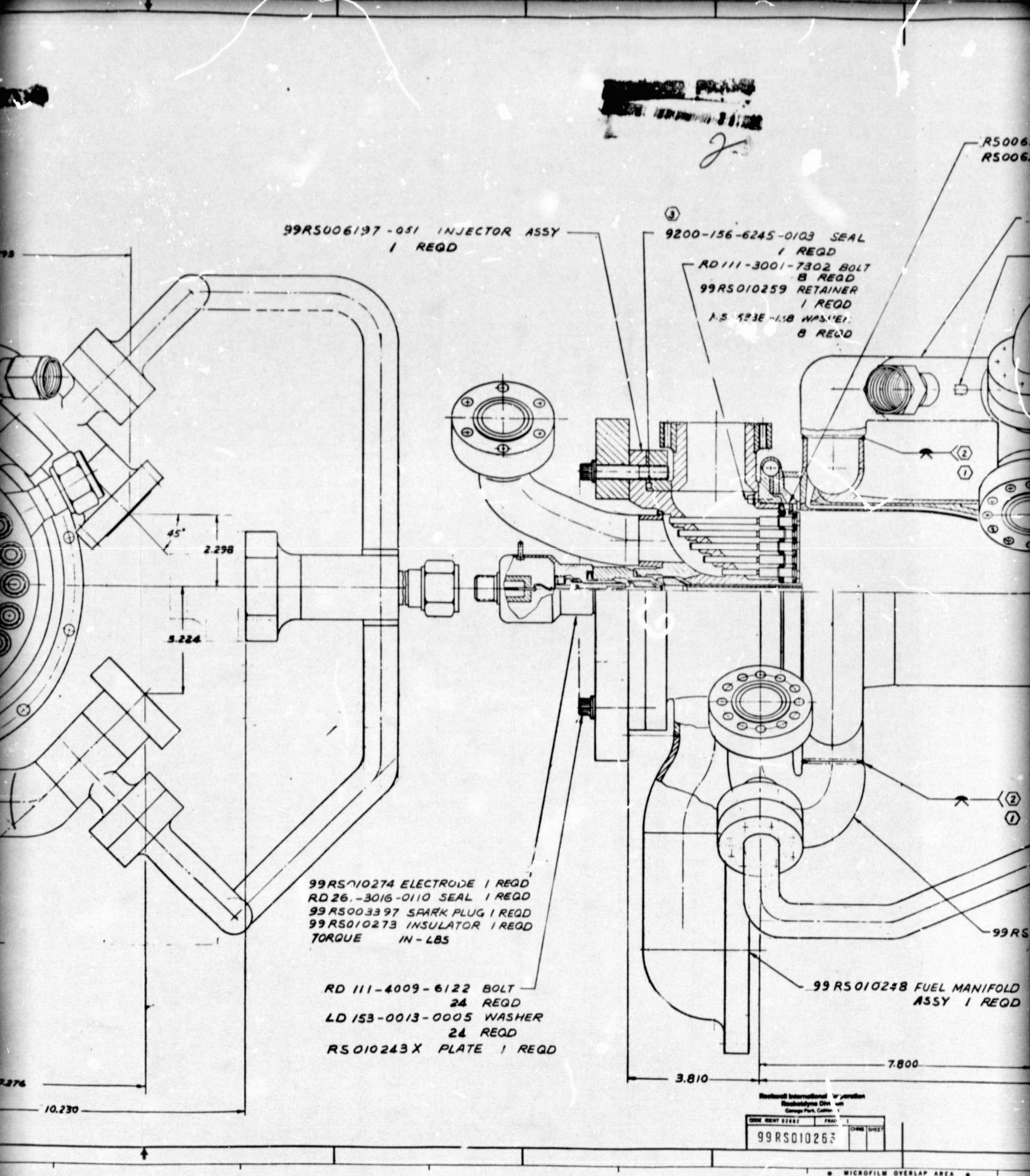
99RS006197-051 INJECTOR ASSY
1 REQD
9200-156-6245-0103 SEAL
1 REQD
RD111-3001-7302 BOLT
8 REQD
99RS010259 RETAINER
1 REQD
8 REQD
45°
2.298
3.224
99RS010274 ELECTRODE 1 REQD
RD26,-3016-0110 SEAL 1 REQD
99RS003397 SPARK PLUG 1 REQD
99RS010273 INSULATOR 1 REQD
TORQUE IN-LBS
RD111-4009-6122 BOLT
24 REQD
LD153-0013-0005 WASHER
24 REQD
RS010243X PLATE 1 REQD
99RS010248 FUEL MANIFOLD
ASSY 1 REQD
7.800
3.810
10.230
99RS010263
MICROFILM OVERLAP AREA

[redacted]

3

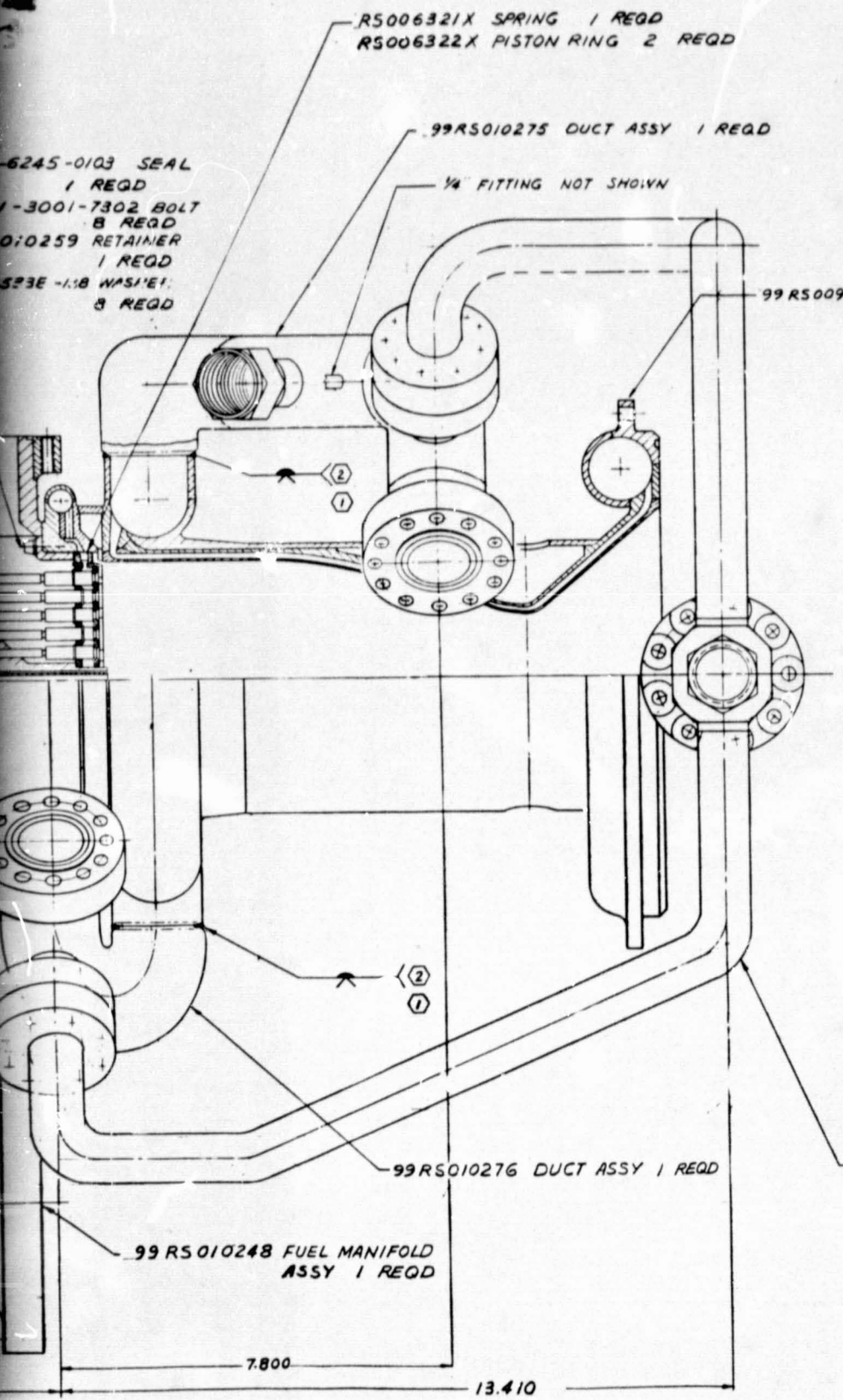

-6245-0103 SEAL
1 REQD
1-3001-7302 BOLT
8 REQD
0;0259 RETAINER
1 REQD
523E-1.18 WASHER
8 REQD

4. LEA
③ MA
HY
NO
② WE
① ASS

Rocketdyne International Corporation
Rocketdyne Division
Canoga Park, California

CODE IDENT 07407	FRAME 1		
99RS010263		CHANG	SHEET

REVISIONS

ZONE	LTR	DESCRIPTION	DATE	APPROVED
		1. MAY BE REWORKED 2. RECORD CHANGE 3. CANNOT BE REWORKED 4. NEW SHOP PRACTICE 5. PARTS MADE OK		

[redacted]

4

REQD

1 REQD
8 REQD
8 REQD
16 REQD

4. LEAK TEST PER ENGINEERING INSTRUCTION
③ MAY BE PURCHASED FROM HYDRODYNE, 7041 ½ VINELAND AVE NORTH HOLLYWOOD, CALIF 91605
② WELD PER RA0107-027
① ASSEMBLY PER SPEC

NOTE: UNLESS OTHERWISE SPECIFIED

Figure 47

UNLESS OTHERWISE SPECIFIED: DIMENSIONS ARE IN INCHES AND APPLY PRIOR TO FINISH.
MACH. SURF. ROUGHNESS
TOLERANCES ON: ANGLES ± 0° 30' DECIMALS .XX ± .03 .XXX ± .010
HOLES NOTED "DRILL" ①
DO NOT SCALE PRINT

NAS3-17825

Rockwell International Corporation
Rocketdyne Division
Canoga Park, California

COMBUSTION CHAMBER ASSY
20K THRUST CHAMBER
PREBURNER

SIZE	CODE IDENT NO.	DRAWING NO.
J	02602	99RS010263

99RS010263

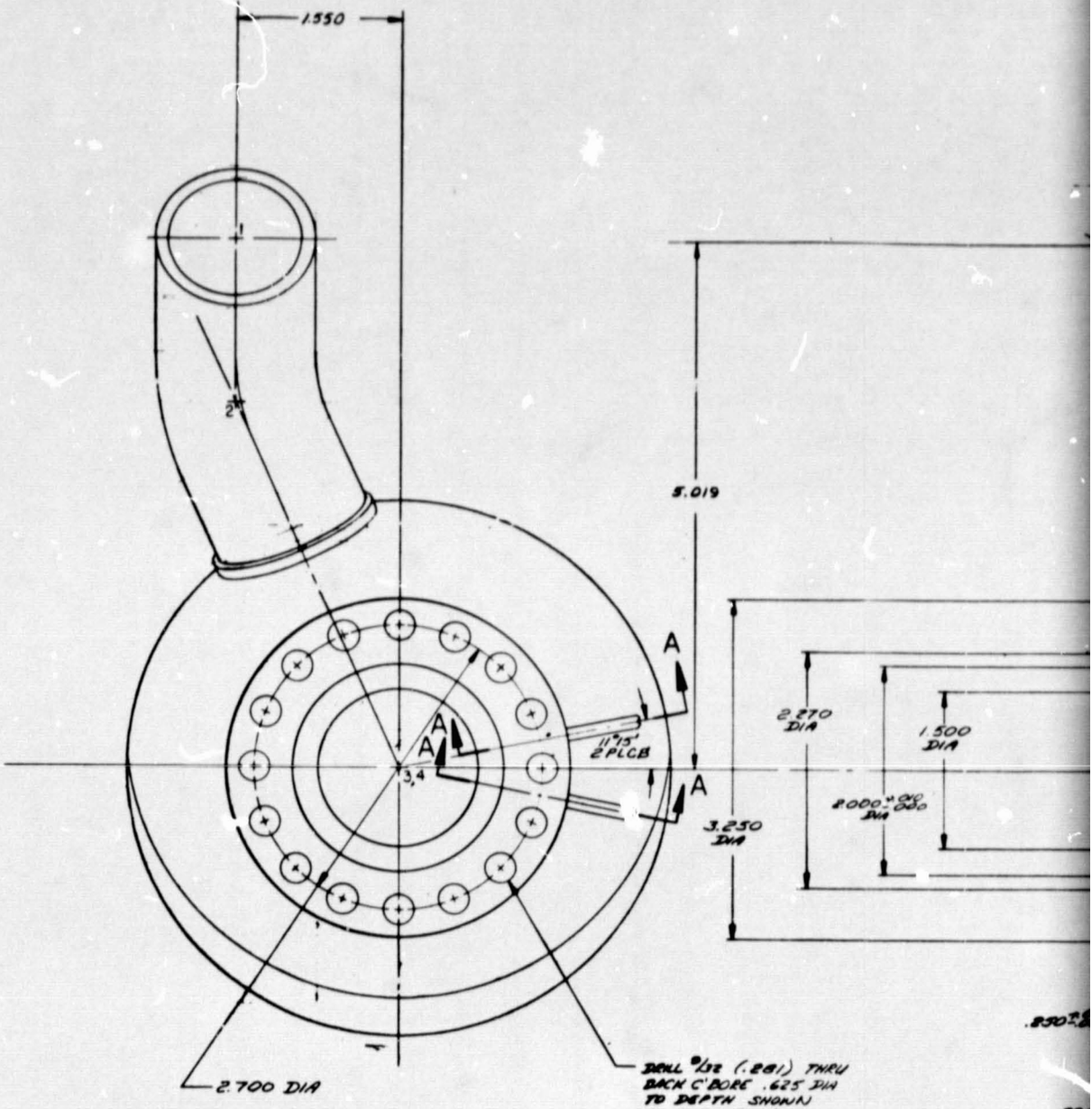

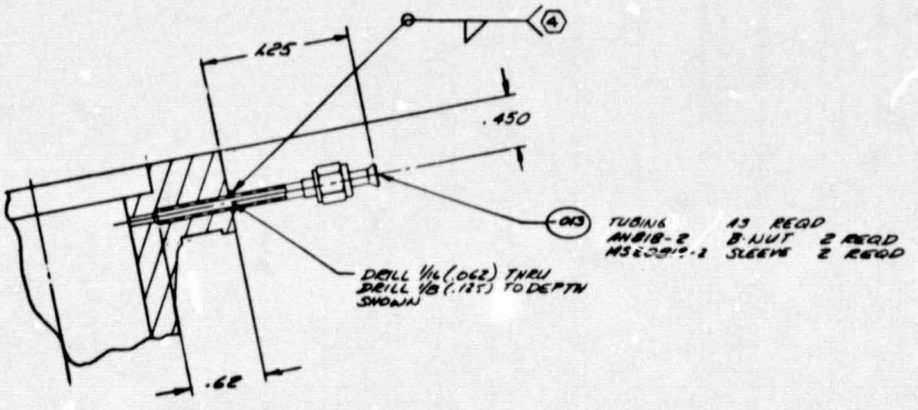

SECTION A-A 2 PLCS

H G F E D C B A

16 15 14 13 12

Rockwell International Corporation
Rocketdyne Division
Canoga Park, California

CODE IDENT 07502	FRAME 1		
99PS010253		CHNG	SHEET

12 11 10 9 8

MICROFILM OVERLAP AREA

[redacted]

3

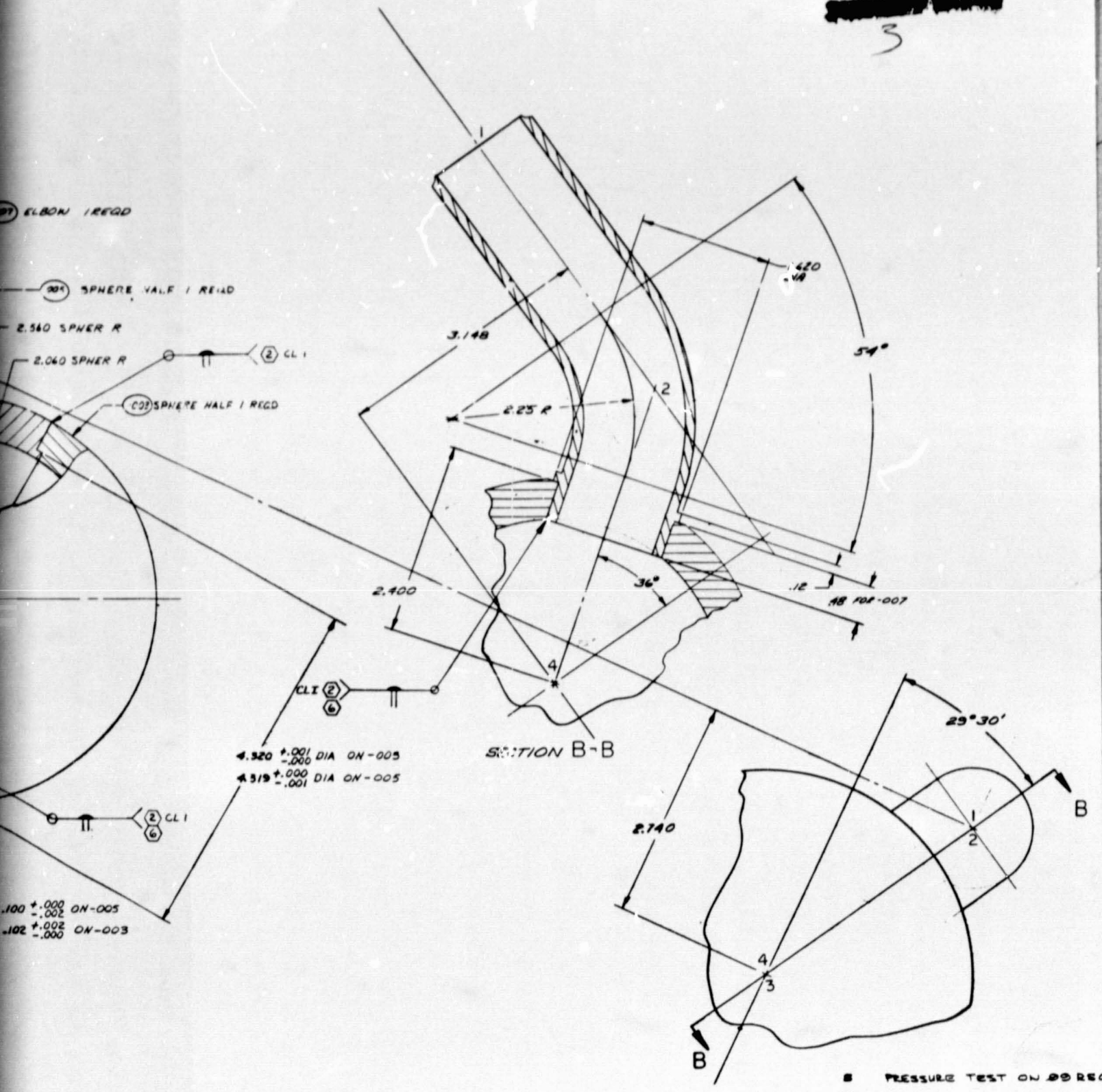

8 PRESSURE TEST ON 99 REQ

7 PREP FOR FULL PENETRATION J WELD

6 GAP BETWEEN -005 & -007, & .000 TO.003 DIAMITRAL CLEARA

5 FLAT WITHIN 4 HELIUM LIGHT BANDS

4 WELD PER RA0107-027

3 IDENTIFY PER RA0104-008.

2 ELECTRON BEAM WELD PER RADIO

1 MACHINE PER RA0103-016.

NOTE: UNLESS OTHERWISE SPECIFIED

[redacted] Corporation
[redacted] Division
[redacted], California

FRAME 1		
253	CHNG	SHEET

8 7 6 5 4

• MICROFILM OVERLAP AREA •

[redacted]

3

[redacted]

4

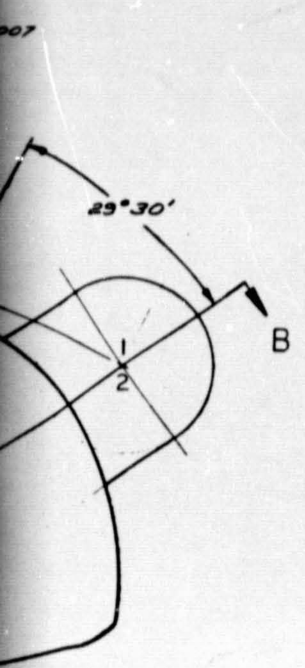

RESSURE TEST ON 99RS010256

REP FOR FULL PENETRATION J-GROVE WELD

AP BETWEEN -005 & -007, & -003 & 007 TO B
000 TO .003 DIAMITRAL CLEARANCE

RAT WITHIN 4 HELIUM LIGHT BANDS

WELD PER RA0107-027

IDENTIFY PER RA0104-008.

ELECTRON BEAM WELD PER RA0107-042.

MACHINE PER RA0103-016.

NOTE: UNLESS OTHERWISE SPECIFIED

--001
NO

Figure 48

81

DASH NO.	MATERIAL	SIZE	SPECIFICATION	ZONE
-013	321 CRES TUBING	.125 OD X .035 WT		
-009	INCONEL 625 BAR	—	AMS 5666	11F
-007	INCONEL 625 BAR	—	AMS 5666	9G
-005	INCONEL 625 BAR	—	AMS 5666	9F
-003	INCONEL 625 BAR	—	AMS 5666	8F

PARTS LIST

HEAT TREAT | FINISH | MATL

UNLESS OTHERWISE SPECIFIED DIMENSIONS ARE IN INCHES AND APPLY PRIOR TO FINISH.
MACH. SURF. ROUGHNESS
TOLERANCES ON ANGLES ± 0° 30'
DECIMALS .XX ± .03 .XXX ± .010
HOLES NOTED "DRILL"

OVER	THRU	TOLERANCE
.000	.0400	+ .0015 − .0010
.0400	.1300	+ .0030 − .0010
.1300	.2750	+ .0045 − .0010
.2750	.5000	+ .0060 − .0010
.5000	.7500	+ .0070 − .0010
.7500	1.0000	+ .0090 − .0010
1.0000	2.0000	+ .0130 − .0010

DO NOT SCALE PRINT

DWN [signature] DATE 11-11-75
CHK [signature] DATE
DSGN [signature]
MATL [signature]
STRUCT [signature]
DESIGN ACTIVITY APVD [signature] DATE

Rockwell International Corporation
Rocketdyne Division
Canoga Park, California

SIMULATOR, OXID PUMP - 20K ADVANCE T/C, ASSY OF

SIZE	CODE IDENT NO.	DRAWING NO.
J	02602	99RS010253

SCALE 2/1 SHEET

FRAME X-1

FORM NO. R138-H-6 REV. 7-73

99RS010253

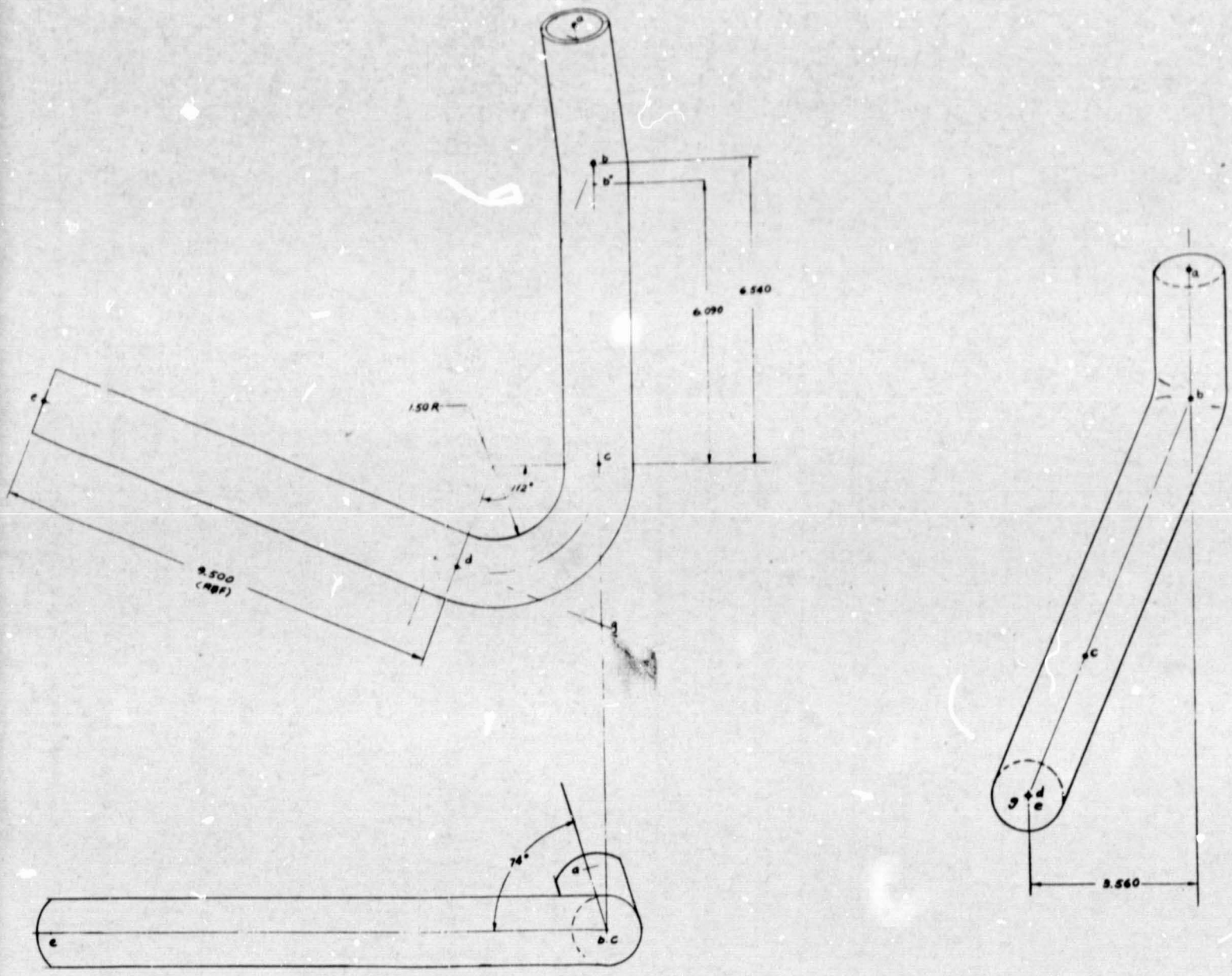

SIDE VIEW

Rockwell International Corporation
Rocketdyne Division
Canoga Park, California
CODE IDENT 03803 | FRAME 1
CHNG | SHEET

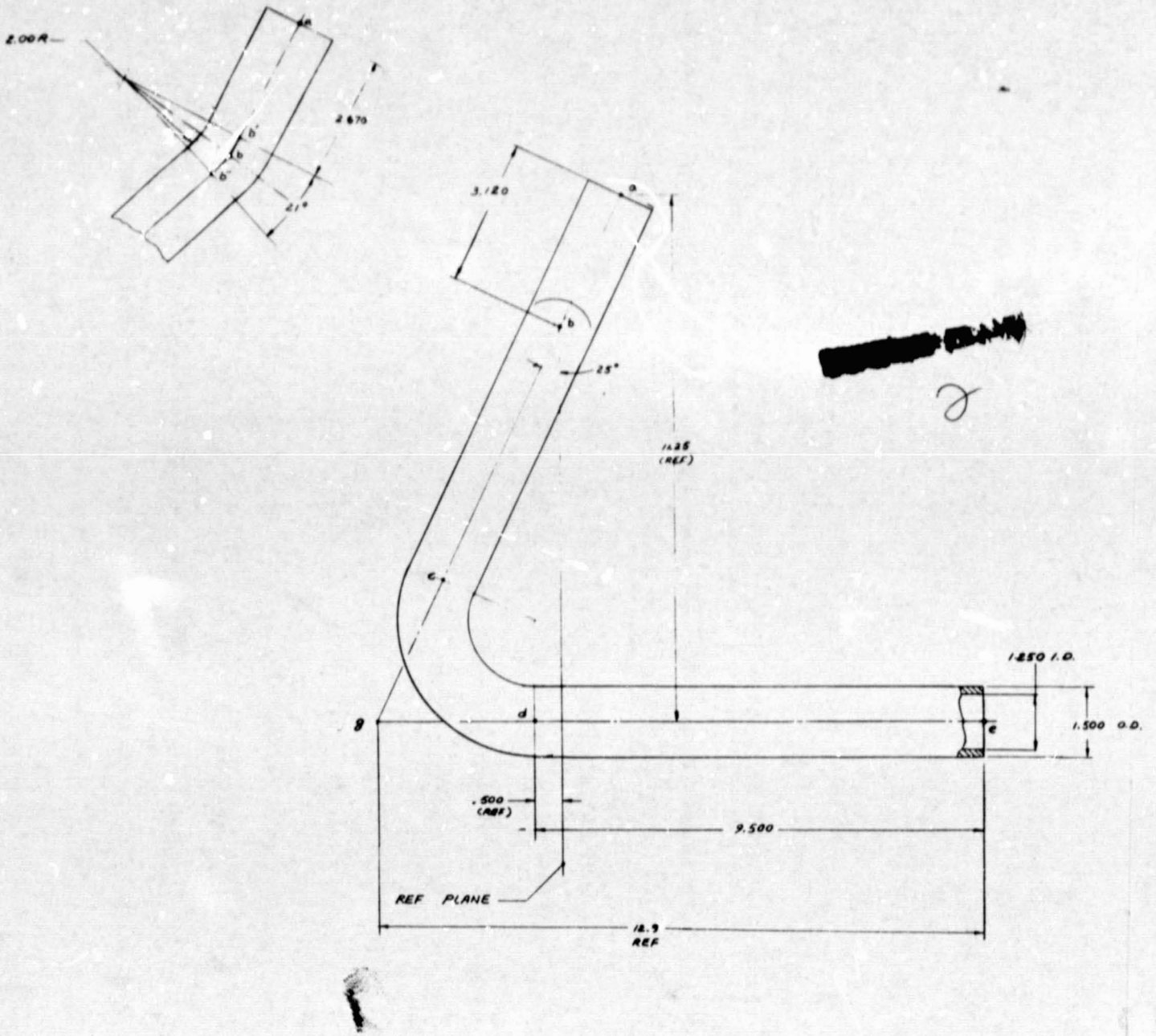

PLAN VIEW

5 PROOF & LEAK TEST PER ENGINEERING INSTRUC
4 PART MAY BE FABRICATED IN SECTIONS & WELDED.
3. CLEAN PER RA0110-018
2. TUBE BENDING PER
1. MACHINE PER RA 0103-016

NOTE: UNLESS OTHERWISE SPECIFIED

The fuel turbine simulator (Fig. 50) was similar to the oxidizer simulator except that the ducting diameter was larger to accommodate the greater hot gas flowrate (68% of the total) and the metering and pressure drop orifice was located further upstream from the main injector. The downstream segment of the simulator and ducting were welded directly to the injector fuel manifold housing (Fig. 51). Inconel 625 was used for this subassembly, as it was for the oxidizer turbine simulator and ducting because of the high temperature strength properties and the resistance to hydrogen embrittlement.

Installation of the preburner and ducting components on the main injector simulator is shown in Fig. 52. This was the configuration utilized for initial testing of the preburner assembly. Use of the injector simulator permitted installation of the preburner into the test stand in the same position, and with the same ducting, that would prevail during the subsequent staged combustion assembly testing. Thus, the operating parameters and the high-pressure feed system ducting, once operational, would not require replacement or re-evaluation for later test series.

Combustion chamber coolant discharge ducts are shown in Fig. 53 and 54. Figure 55 shows the nozzle coolant discharge ducting. All ducting was welded together inplace on the staged combustion assembly prior to transfer of the assembly to the test facility. The balance of the ducting, both for the high-pressure propellant and coolant inlet system and for the lower pressure coolant discharge to the overboard disposal systems were field-fitted on the test stand.

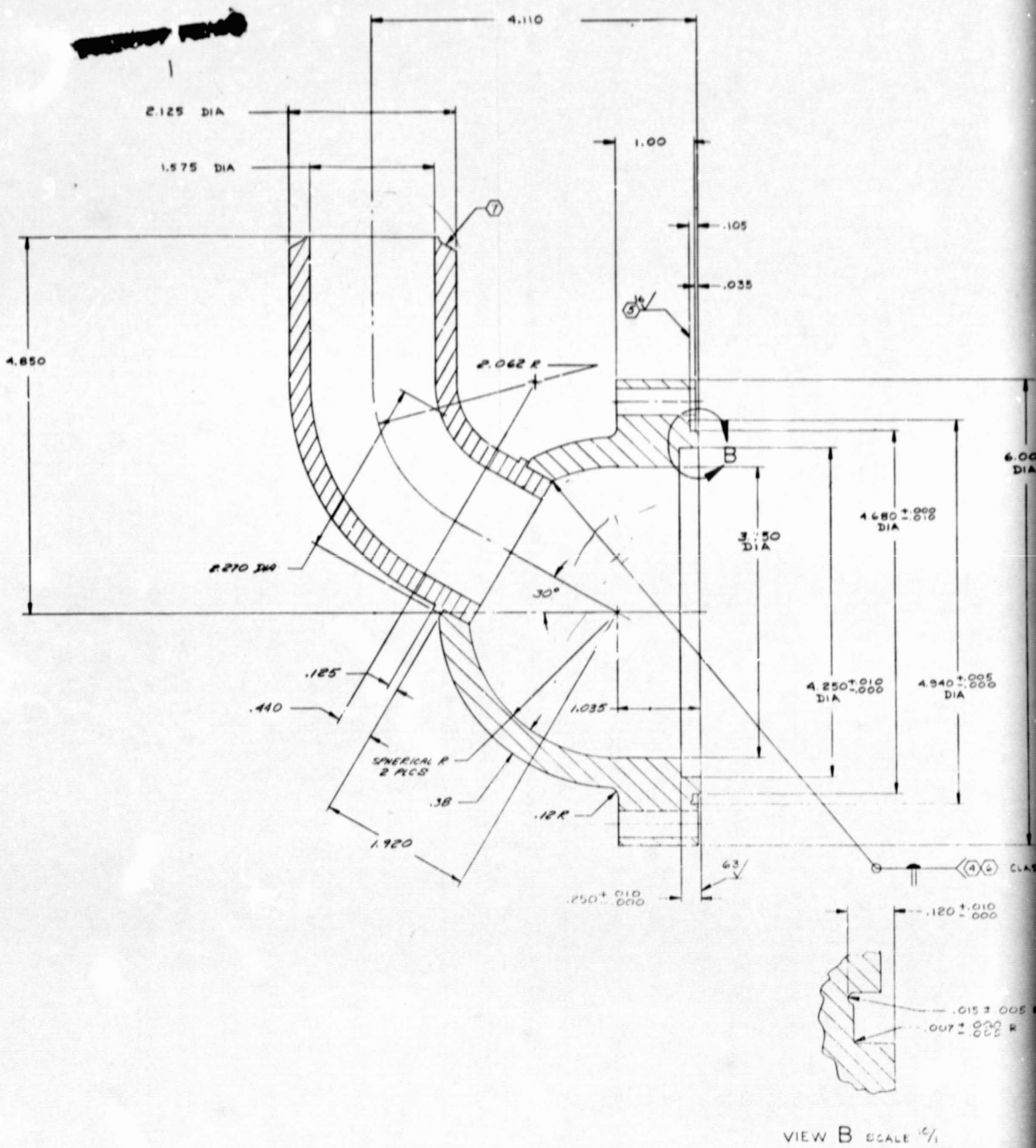
4.110
2.125 DIA
1.575 DIA
1.00
.105
.035
4.850
2.062 R
B
6.00 DIA
4.680 +.000 -.010 DIA
3.750 DIA
R.270 IWA
30°
.125
.440
1.035
4.250 +.010 -.000 DIA
4.940 +.005 -.000 DIA
SPHERICAL R 2 PLCS
.38
.12 R
1.920
63
.250 +.010 -.000
.120 +.010 -.000
.015 ± .005
.007 +.010 -.000 R
VIEW B SCALE 10/1

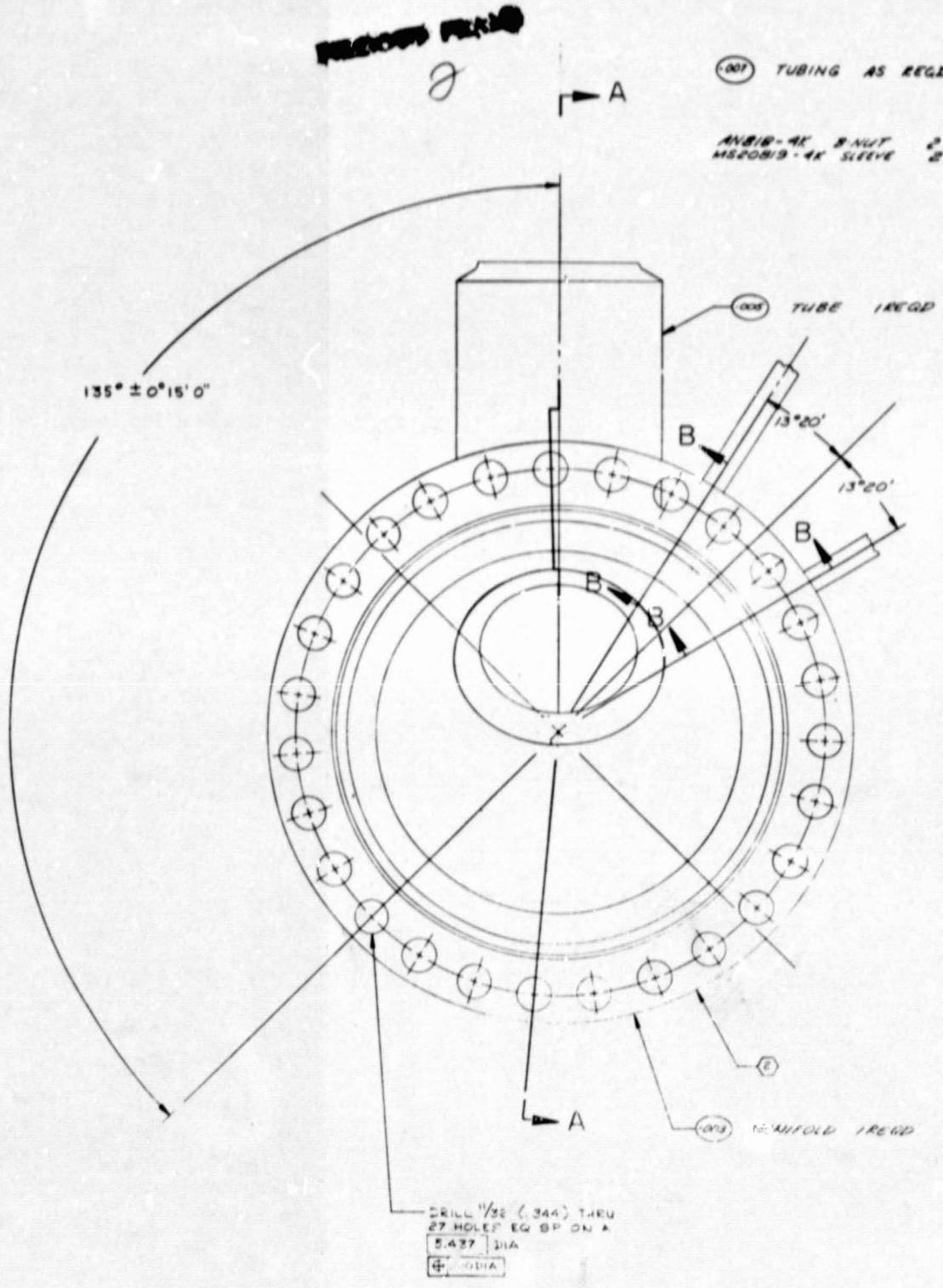

ORIGINAL PAGE IS
OF POOR QUALITY

Rockwell International Corporation
Rocketdyne Division
Canoga Park, California

99RSA10252

• MICROFILM OVERLAP AREA •

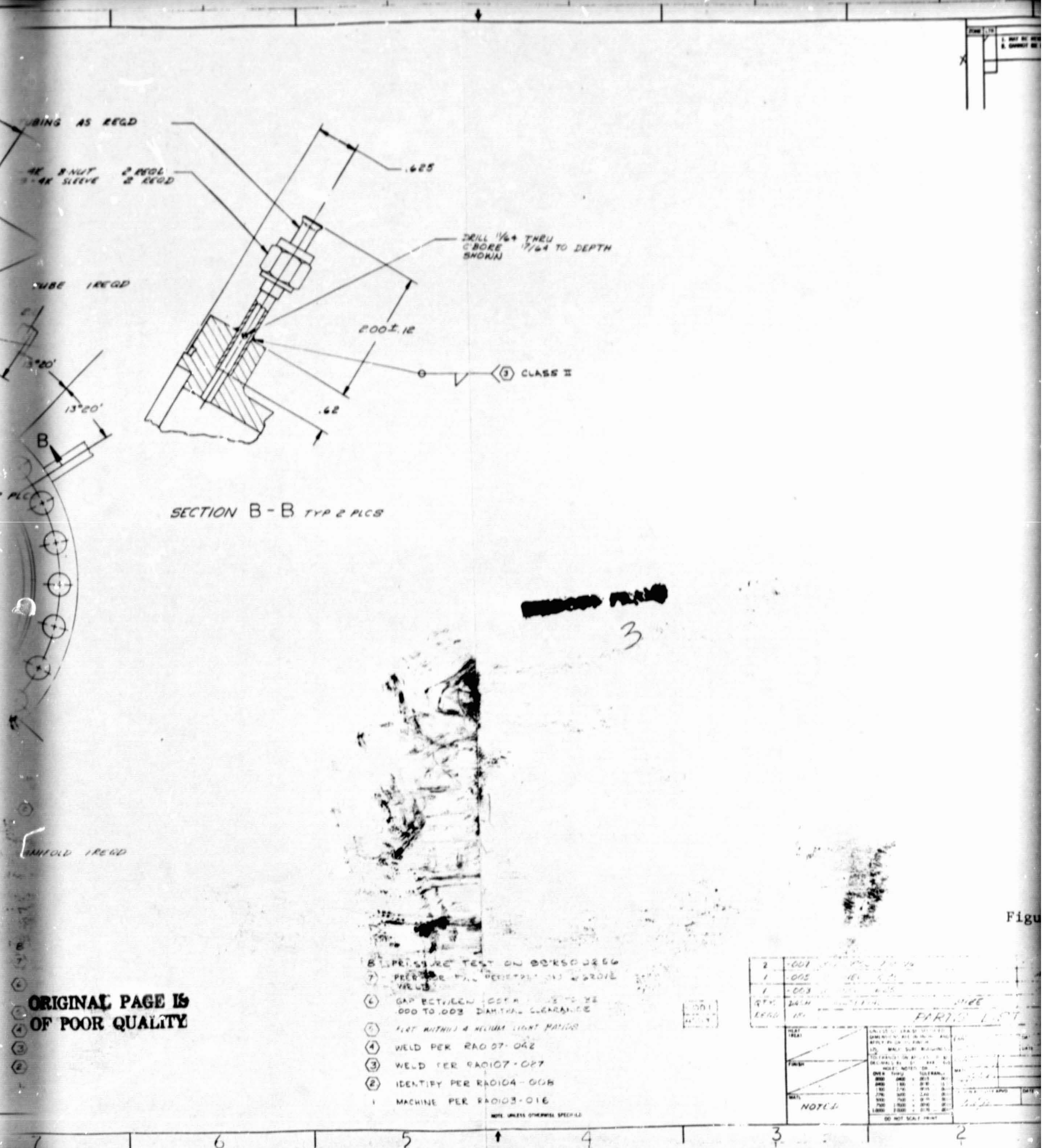

Figu

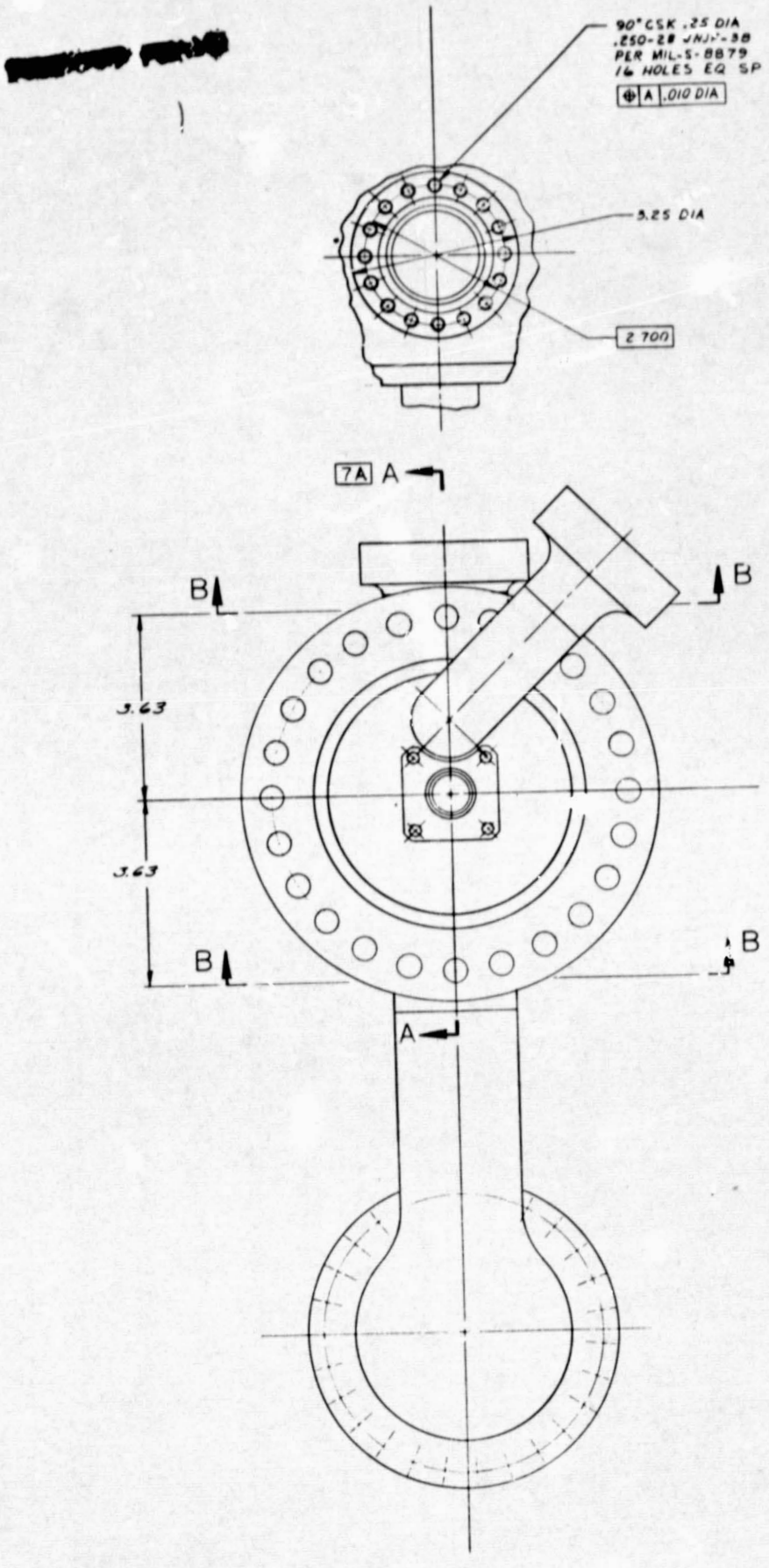

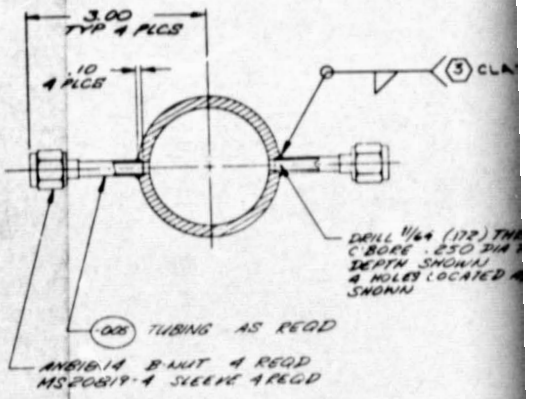

SECTION B-B TYP 2 PLCS

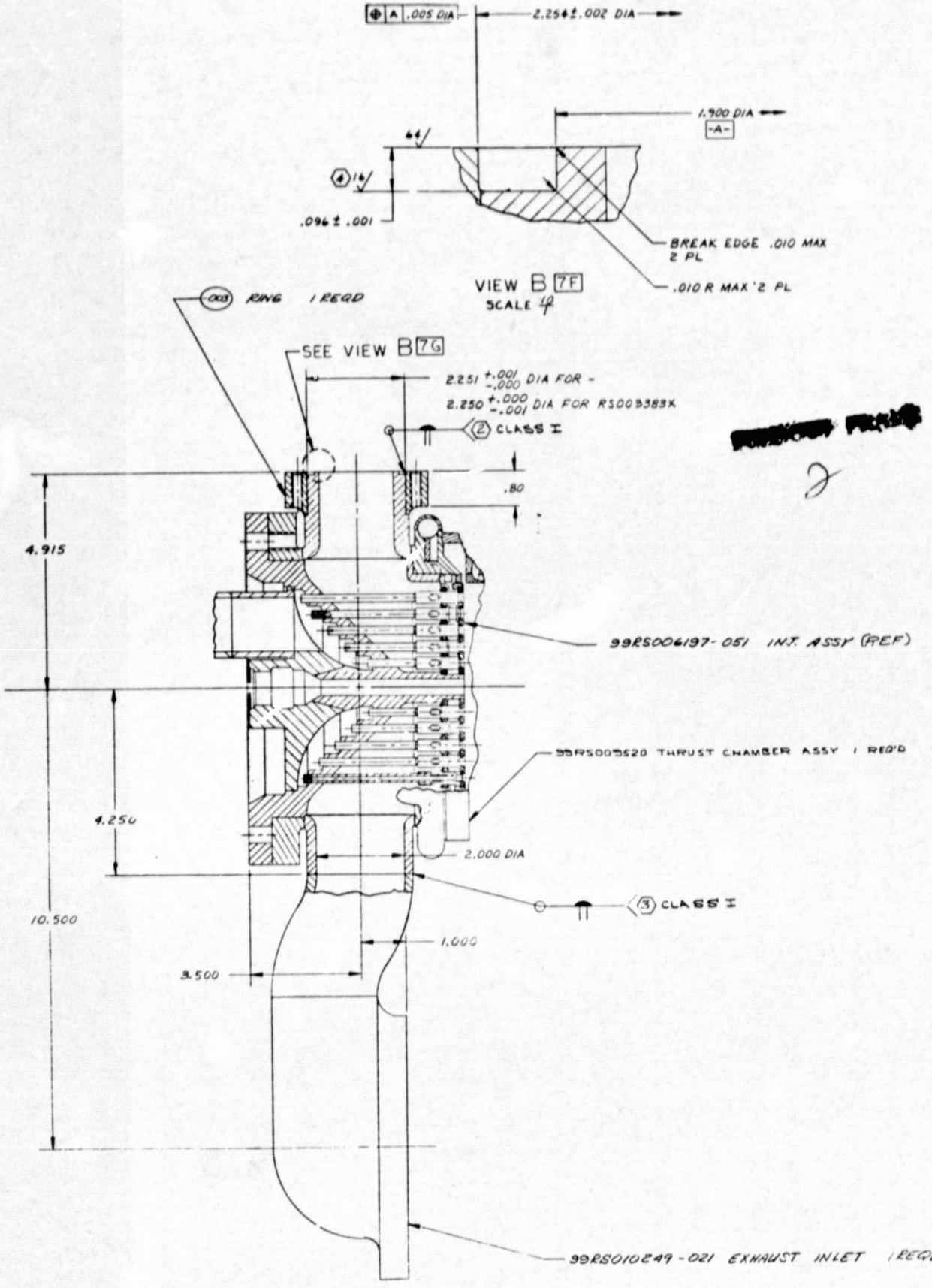

64 (172) THRU .250 DIA TO SHOWN LOCATED AS

GE IS
LITY

Rockwell International Corporation
Rocketdyne Division
Canoga Park, California

CODE IDENT 07602	FRAME 2		
99RS010248		CHNG	SHEET

• MICROFILM OVERLAP AREA •

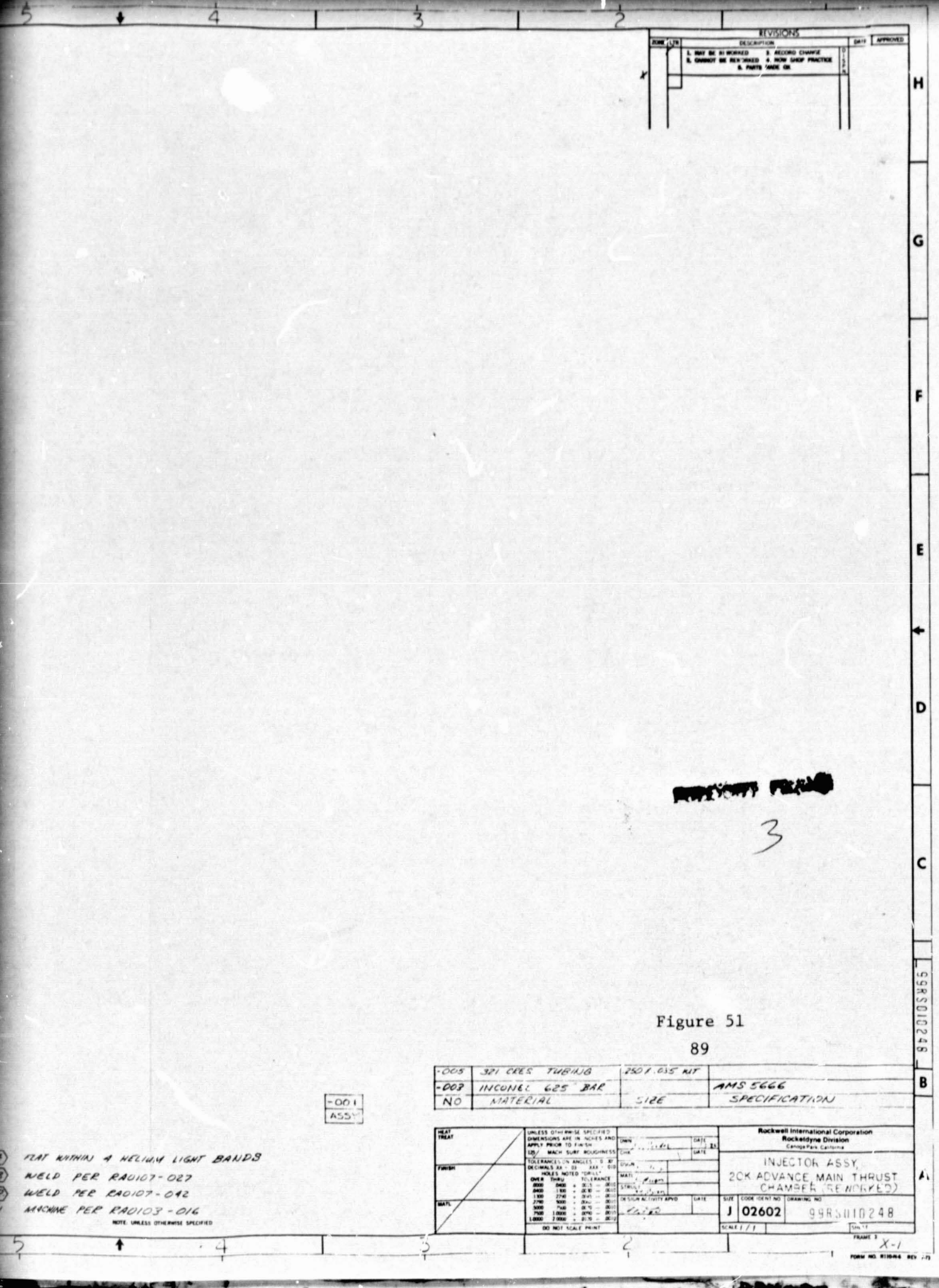
REVISIONS
ZONE (LTR)
DESCRIPTION
DATE
APPROVED
1. MAY BE REWORKED
2. CANNOT BE REWORKED
3. RECORD CHANGE
4. NEW SHOP PRACTICE
5. PARTS MADE OBS.
-005 321 CRES TUBING 250 I.D. .035 WT
-003 INCONEL 625 BAR AMS 5666
NO MATERIAL SIZE SPECIFICATION
-001 ASSY
FLAT WITHIN 4 HELIUM LIGHT BANDS
WELD PER RA0107-027
WELD PER RA0107-042
MACHINE PER RA0103-016
NOTE: UNLESS OTHERWISE SPECIFIED
HEAT TREAT
FINISH
MATL
UNLESS OTHERWISE SPECIFIED DIMENSIONS ARE IN INCHES AND APPLY PRIOR TO FINISH
125/ MACH SURF ROUGHNESS
TOLERANCES ON ANGLES ± 30'
DECIMALS XX ± .03 XXX ± .010
HOLES NOTED "DRILL"
OVER THRU TOLERANCE
.000 .060 ± .003 — .005
.060 1.00 ± .010 — .005
1.00 2.90 ± .015 — .005
2.90 5.00 ± .020 — .005
5.00 7.60 ± .025 — .005
7.60 10.00 ± .030 — .005
10.00 20.00 ± .040 — .005
DO NOT SCALE PRINT
DRWN
CHK
DESIGN ACTIVITY APVD
DATE
Rockwell International Corporation
Rocketdyne Division
Canoga Park California
INJECTOR ASSY,
20K ADVANCE MAIN THRUST
CHAMBER (RENOKED)
SIZE J
CODE IDENT NO 02602
DRAWING NO 99RS010248
SCALE 1/1
SHEET
FRAME 3
X-1
FORM NO. R10846 REV. -(7)
99RS010248
3

Figure 51

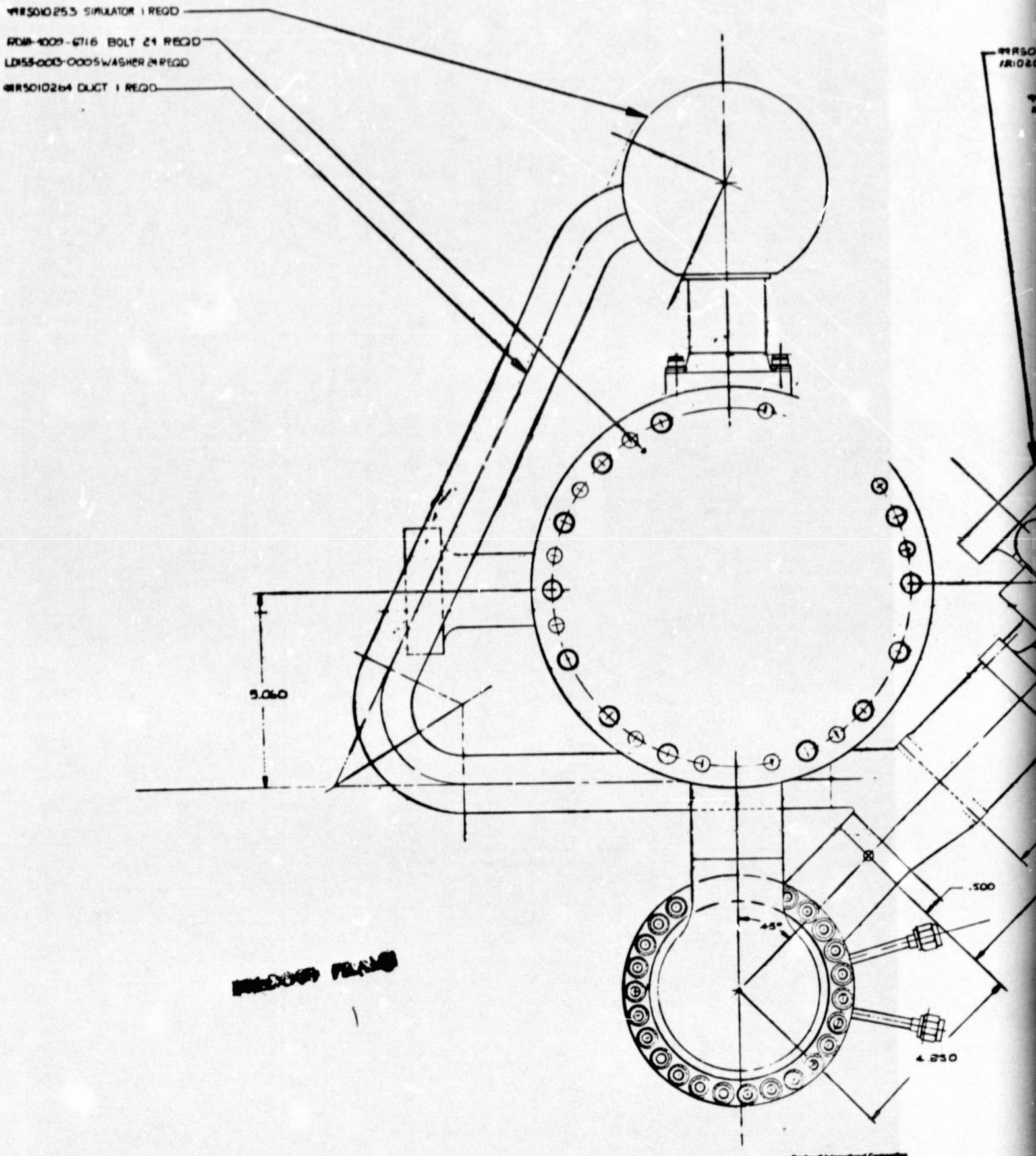

Rockwell International Corporation
Rocketdyne Division

Rocketdyne International Corporation
Rocketdyne Division
Canoga Park, California

	FRAME 1		
		Orig	SHEET

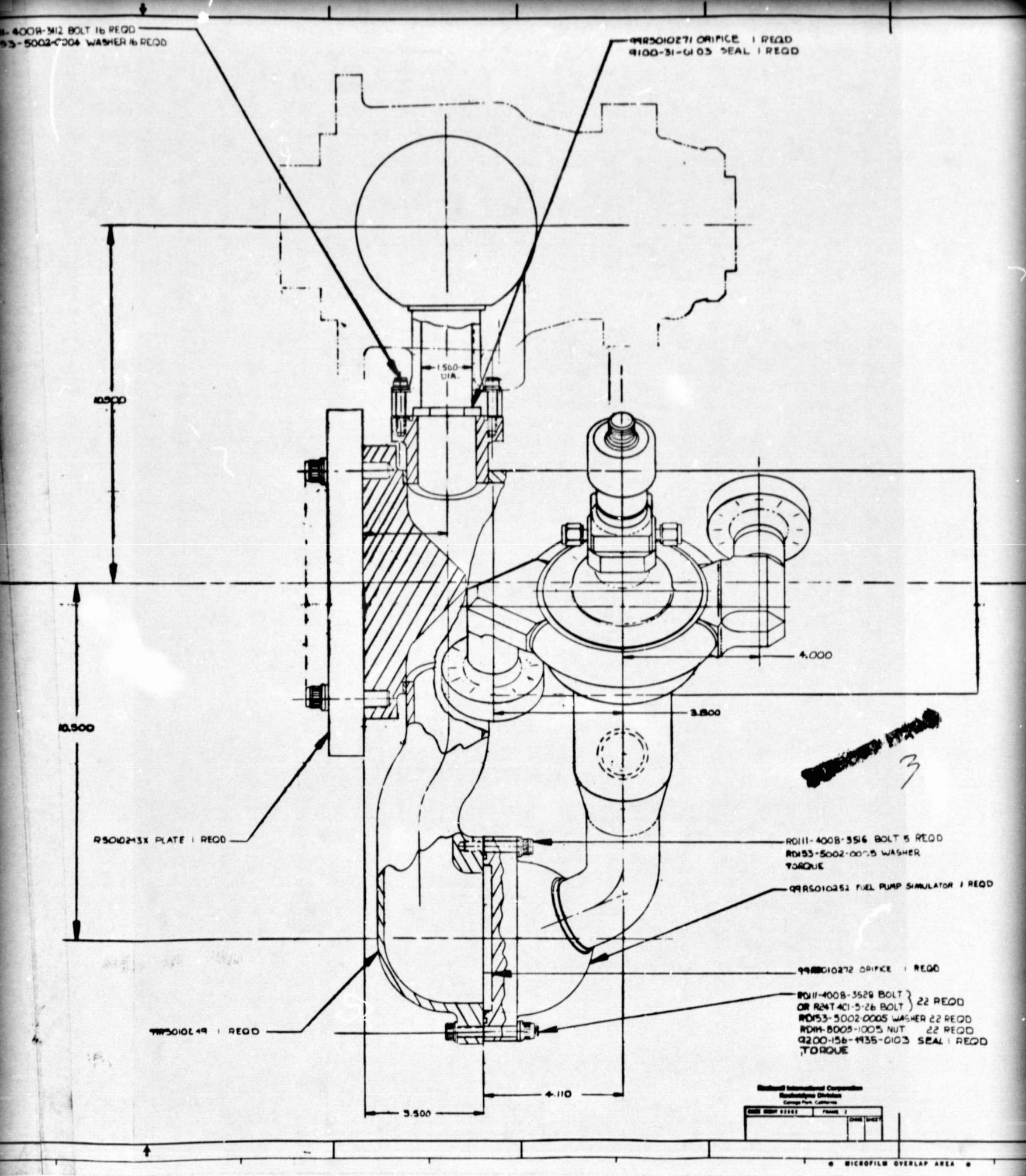

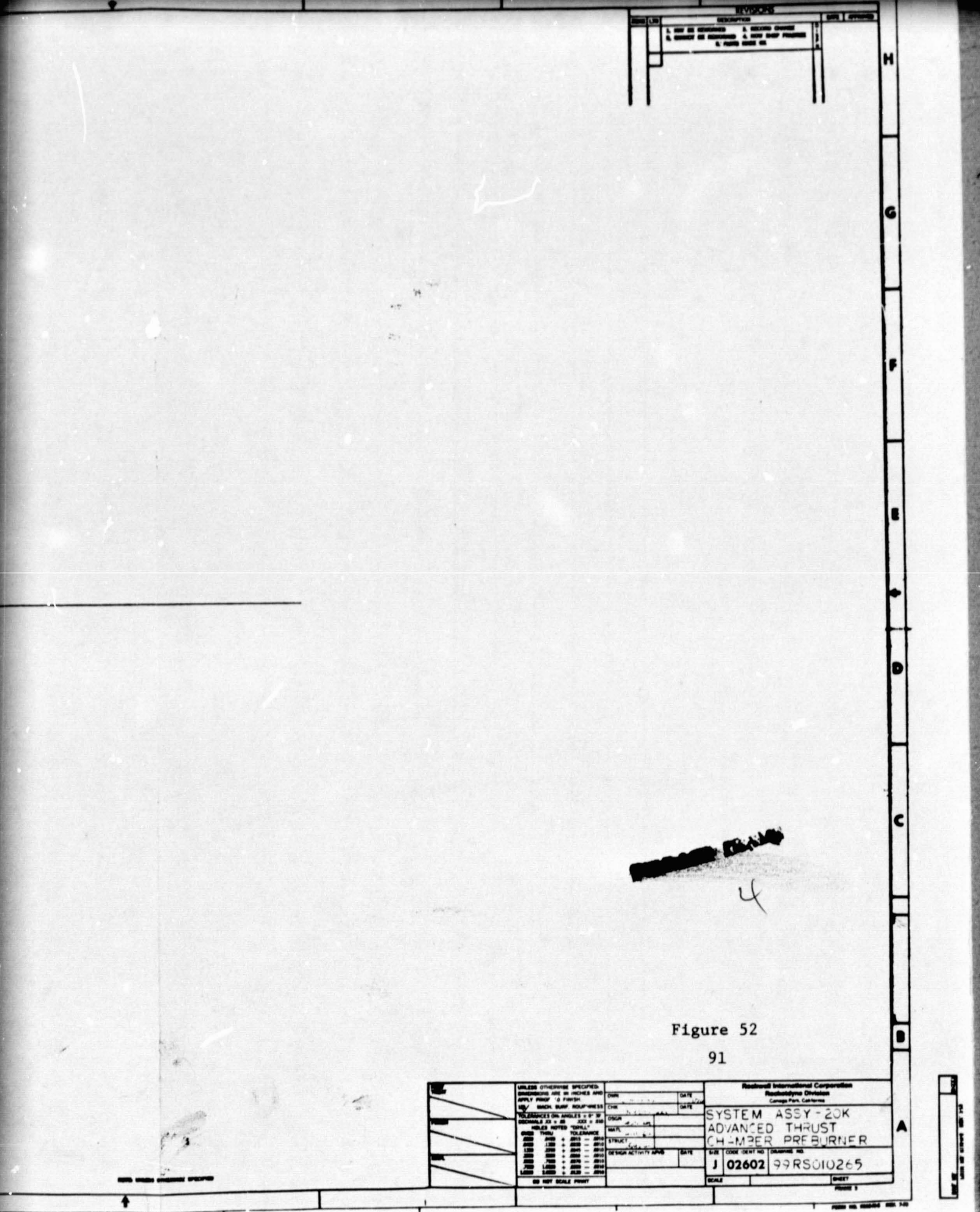
REVISIONS
SYSTEM ASSY - 20K
ADVANCED THRUST
CHAMBER PREBURNER
J
02602
99RS010265

Figure 52

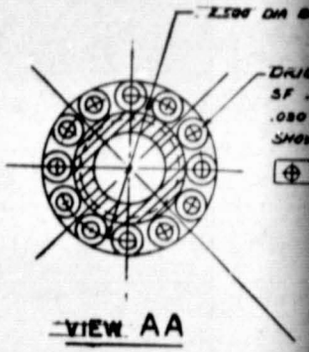

VIEW AA

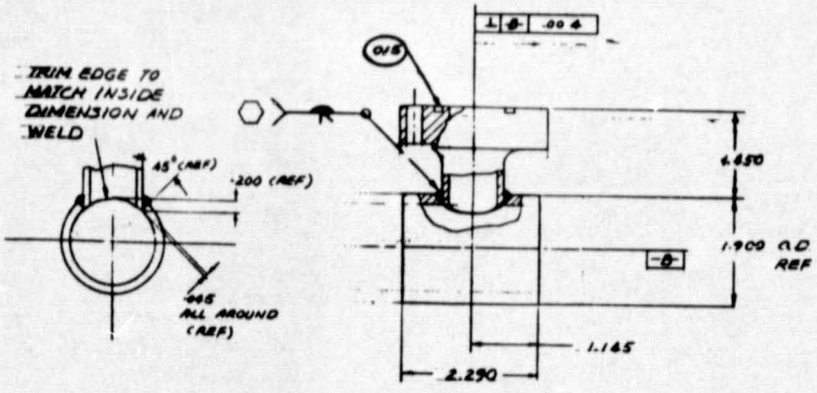

DETAIL B

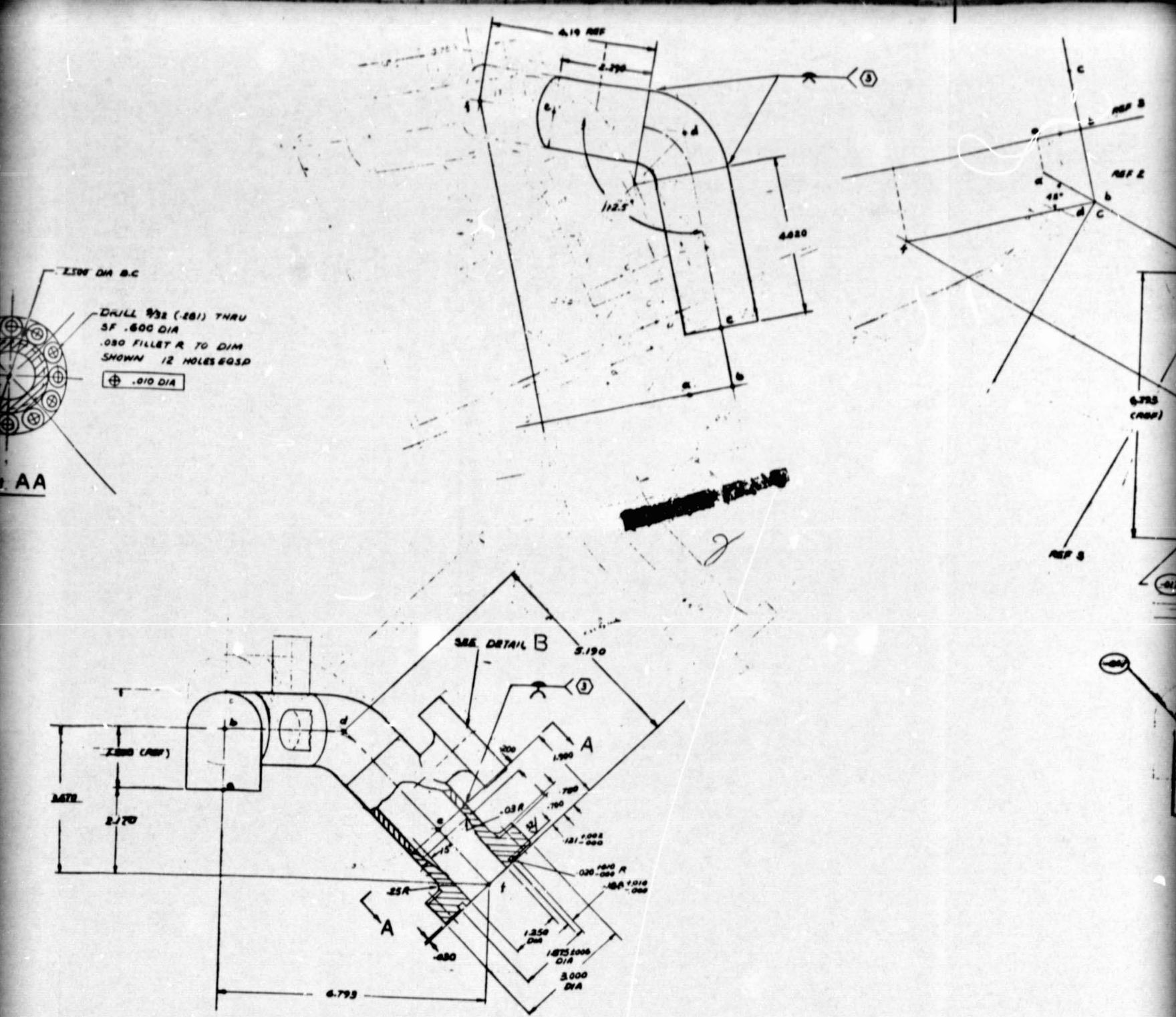
4.19 REF
2.290
112.5°
4.020
2.100 DIA B.C
DRILL 9/32 (.281) THRU
3F .600 DIA
.030 FILLET R TO DIM
SHOWN 12 HOLES EQSP
.010 DIA
AA
REF 3
REF 2
45°
6.375
(REF)
REF 3
SEE DETAIL B
5.190
1.900
.700
.700
.03 R
121 +.005 -.000
.020 +.010 -.000 R
.15
.25R
1.350
DIA
1.875 +.000 -.005
DIA
3.000
DIA
.480
6.793
2.370

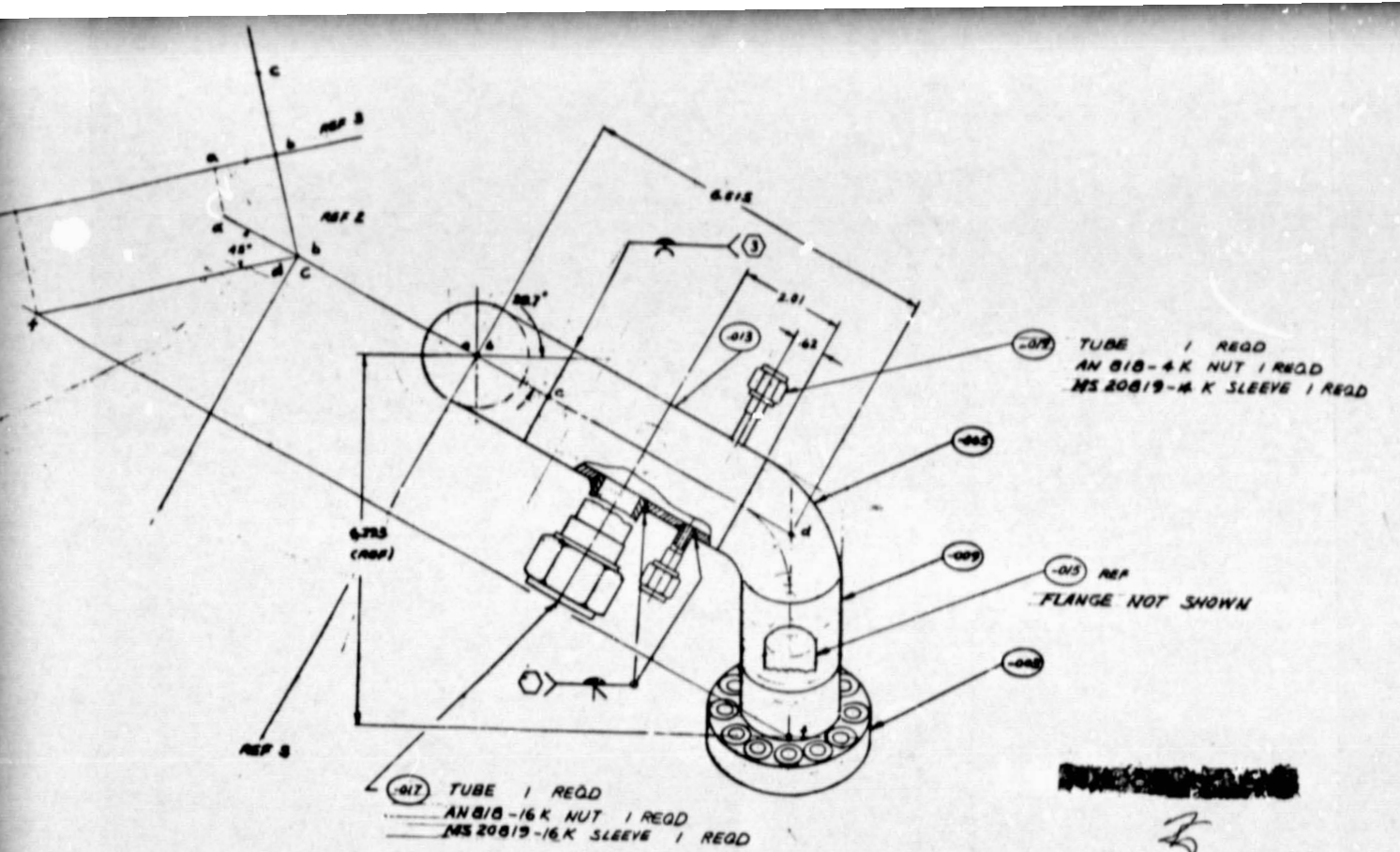

[redacted]

5

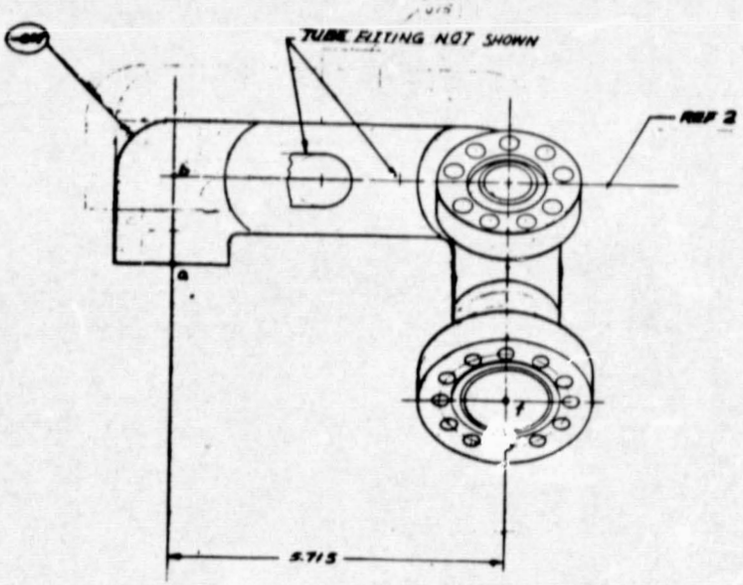

5 PROOF & LEAK TEST PER ENGINE INSTRUCTION
4. IDENTIFY PER RA0104-008
3 WELD PER RA0107-027
2. CLEAN PER RA0110-018
1. MACHINE PER RA0103-002

NOTE: UNLESS OTHERWISE SPECIFIED

MICROFILM OVERLAP AREA

TUBE 1 REQD
AN 818-4K NUT 1 REQD
MS 20819-4K SLEEVE 1 REQD

(BIS) REF
FLANGE NOT SHOWN

[redacted]

3

[redacted]

4

Figure 53

QTY REQD	DASH NO	MATERIAL	SIZE	SPECIFICATION
2	-019	321 CRES	.250 OD x .065 W TUBE x 2" LG	
1	-017	321 CRES	.100 OD x .120W TUBE X 2" LG	
1	-015	321 CRES		MAKE FROM 99RS019547-3
1	-013	321 CRES	1.500 PIPE SCH 80	
1	-009	321 CRES	1.500 PIPE SCH 80	
1	-007	321 CRES	90° EL, S.R. X STRG	
1	-005	321 CRES	45° EL S.R SCH 80	
1	-003	321 CRES		QQ-S-763 COND A

5 PROOF & LEAK TEST PER ENGINEERING INSTRUCTION
4. IDENTIFY PER RA0104-008
3 WELD PER RA0107-027
2. CLEAN PER RA0110-018
1. MACHINE PER RA0103-002

NOTED

Rocketdyne Division
DUCT ASSY OF 20K THRUST CHAMBER H_2 COOLANT DISCHARGE RIGHT

SIZE	CODE IDENT NO.	DRAWING NO.
J	02602	99RS010275

99RS010275 B

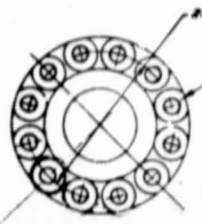

VIEW BB

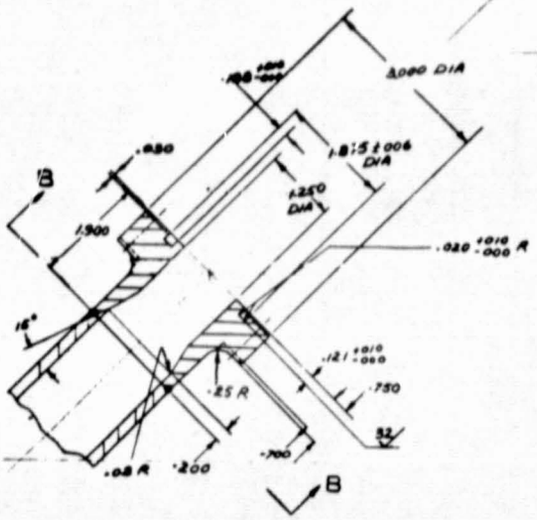

SECTION AA
DETAIL OF -003 FLANGE

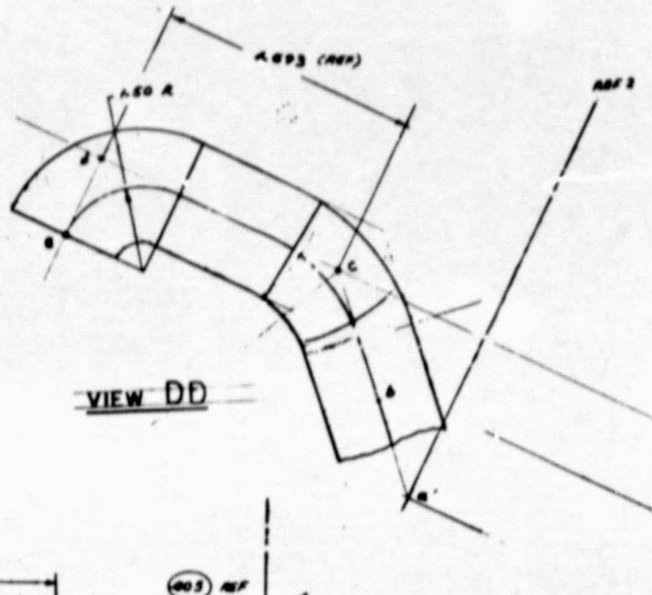

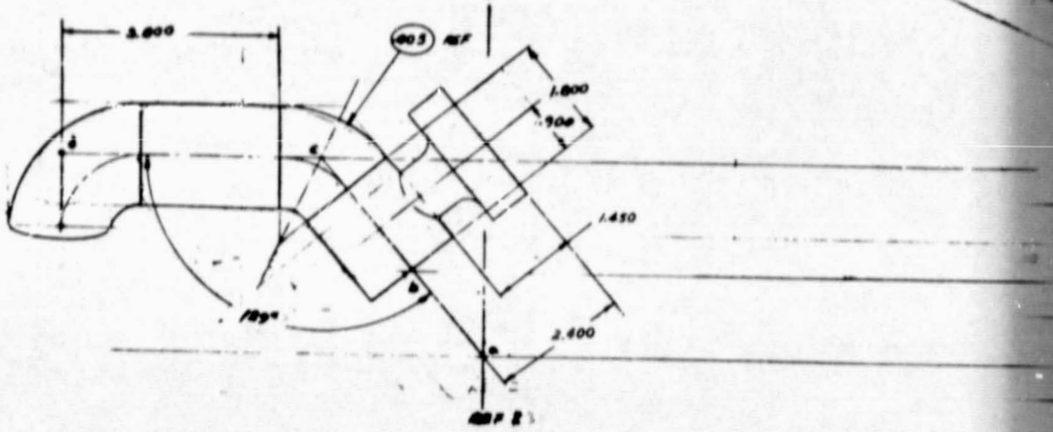

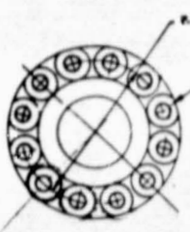

VIEW BB

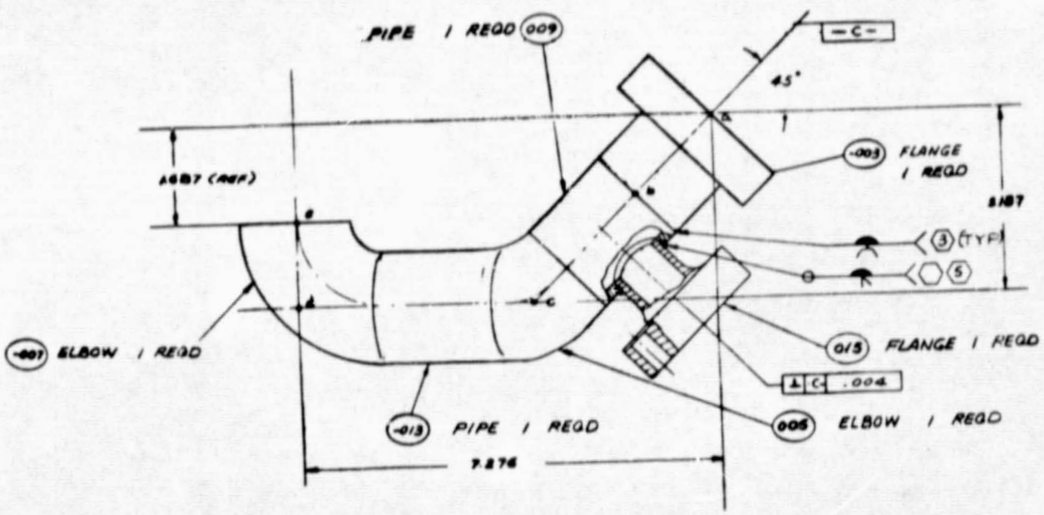

Rocketdyne International Corporation
Rocketdyne Division
Canoga Park, California

DWG IDENT 03853	FRAME 1		
99RS010276		DWG	SIZE

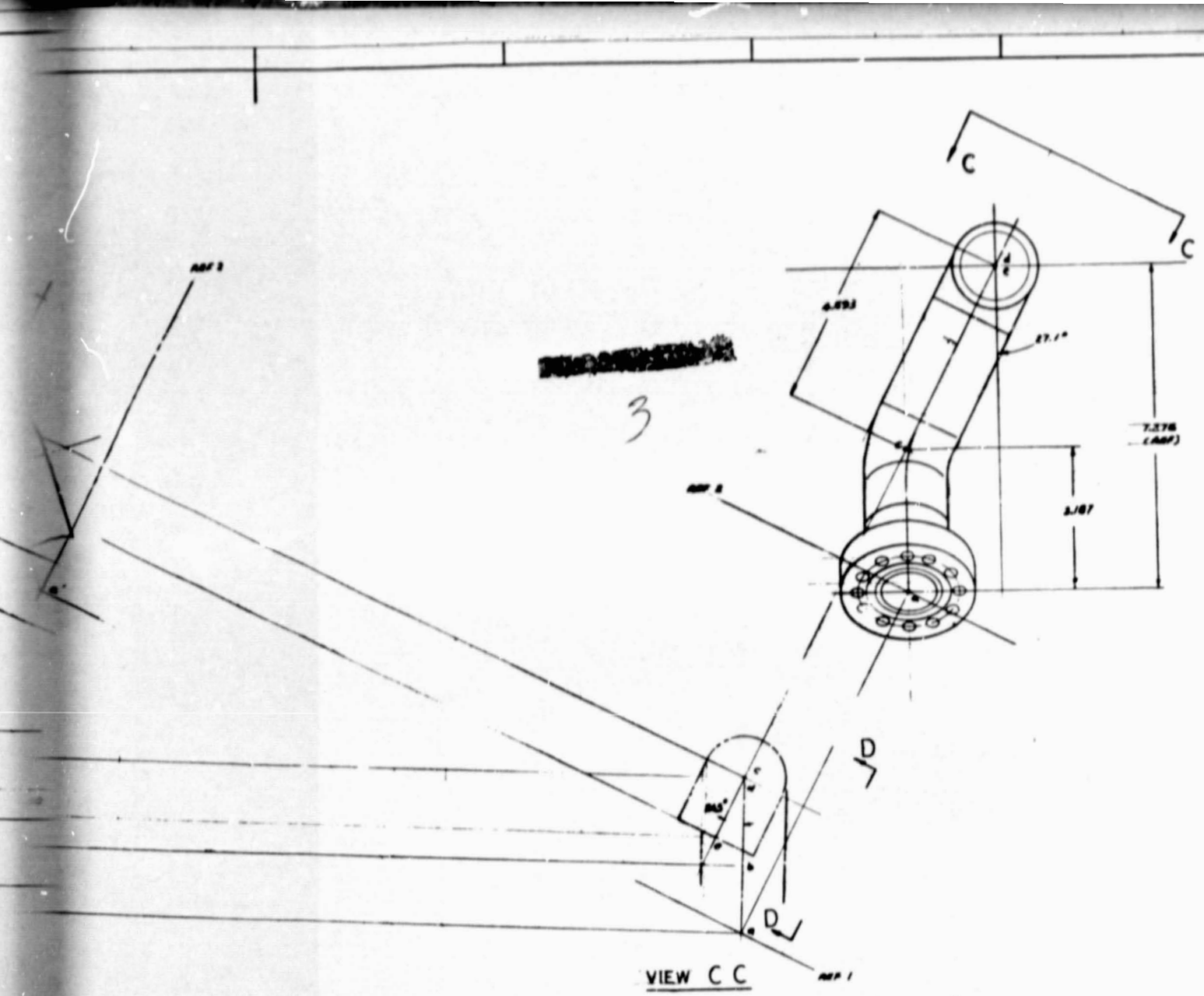

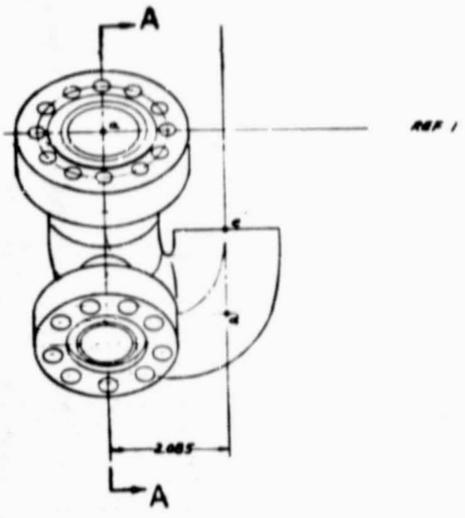

5.187

REQD

6. PROD
5. TRIM
PETA
4. CLEA
3. WELD
2. IDEN
1. MACH

Rockwell International Corporation
Rocketdyne Division

CODE IDENT 07702	FRAME
99RS010276	SHEET 1 OF 1

6. PROOF & LEAK TEST PER ENGINEERING INSTRUCTION
(5) TRIM EDGE AS SHOWN IN DWG 99RS01026 DETAIL B AND WELD.
4. CLEAN PER RA0110-018
(5) WELD PER RA0107-027
2. IDENTIFY PER RA0104-008
1. MACHINE PER RA0103-002

NOTE: UNLESS OTHERWISE SPECIFIED

QTY REQD	DASH NO	MATERIAL	SIZE	SPECIFICATION	
1	-015	321 CRES	FLANGE	MAKE FROM 99RS010567	
1	-013	321 CRES	1.50 PIPE SCH 80		
1	-009	321 CRES	1.50 PIPE SCH 80		
1	-007	321 CRES	90° ELBOW 1.50 SCH 80 SR		
1	-005	321 CRES	45° ELBOW 1.5 SCH 80 SR		
1	-003	321 CRES		QQ-S-763 COND A	

Rockwell International Corporation
Rocketdyne Division
Canoga Park, California

DUCT ASSY OF ·20K THRUST CHAMBER H_2 COOLANT DISCHARGE LEFT

SIZE J | CODE IDENT NO 02602 | DRAWING NO 99RS010276

MATL NOTED

DO NOT SCALE PRINT

99RS010276

Figure 54

FOLDOUT FRAME

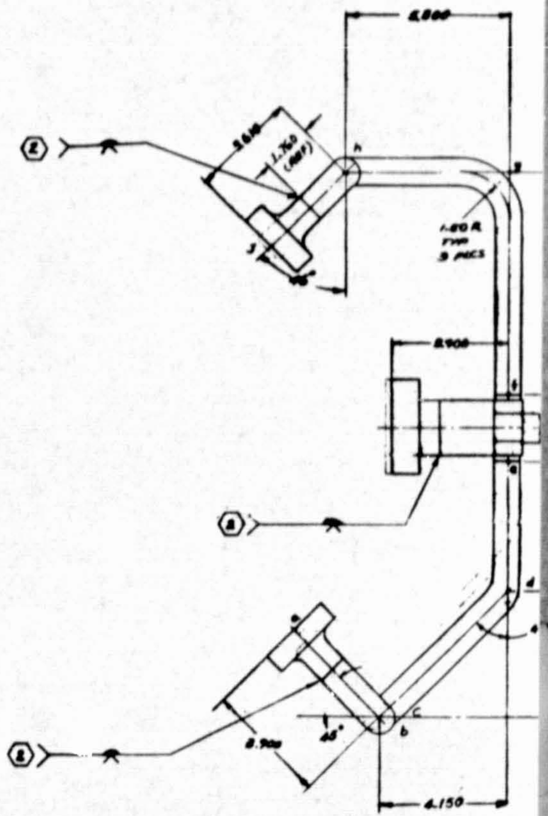

FOLDOUT FRAME 7

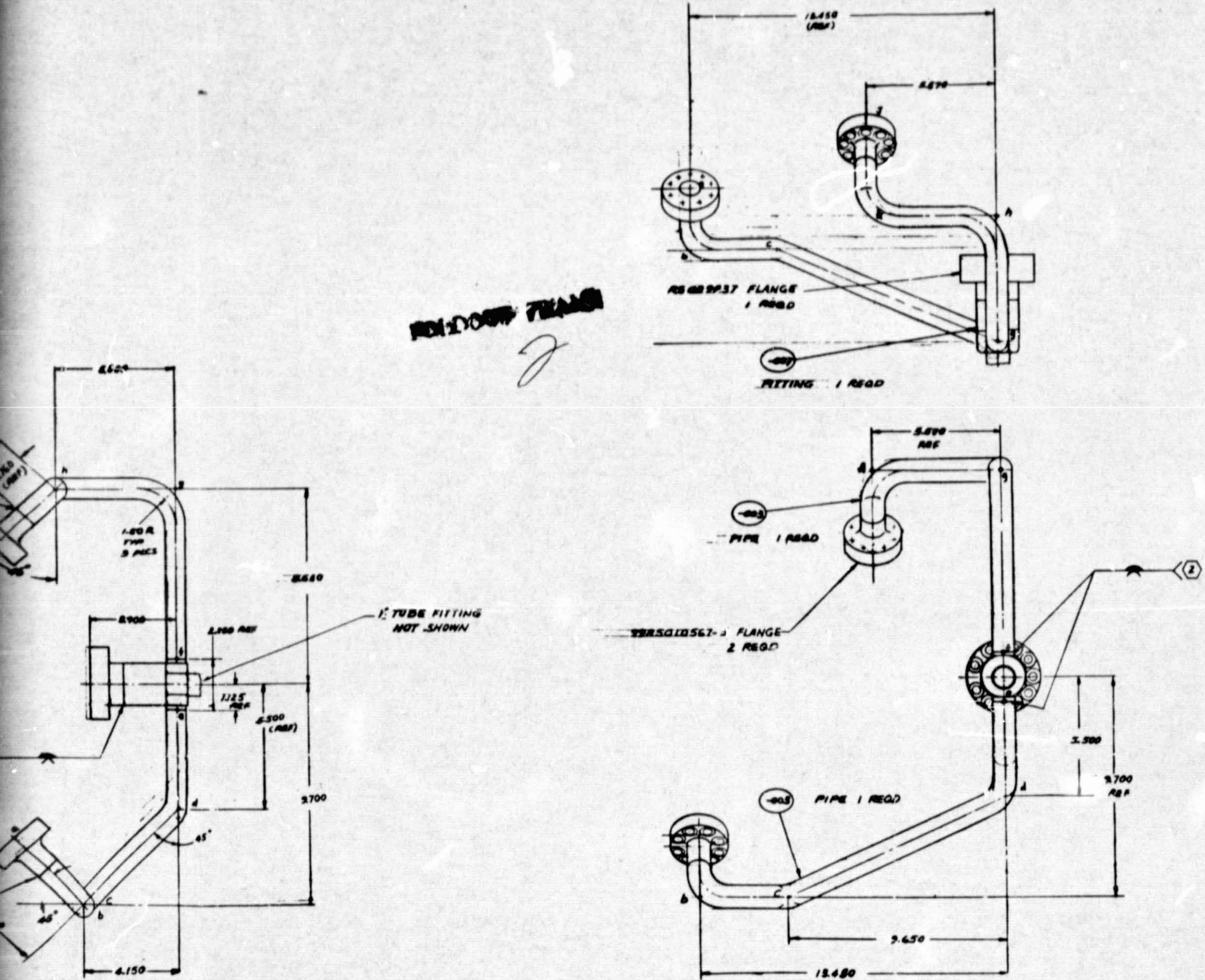

Rockwell International Corporation
Rocketdyne Division
Canoga Park, California

CODE IDENT 02602	FRAME 2	CHNG	SHEET
99R006324			

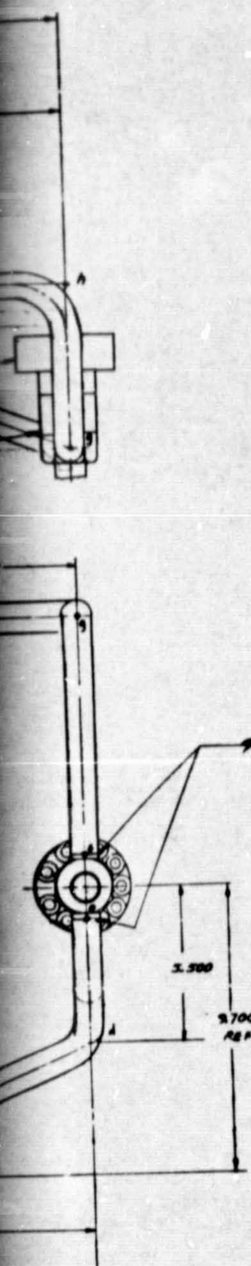

[redacted]
3

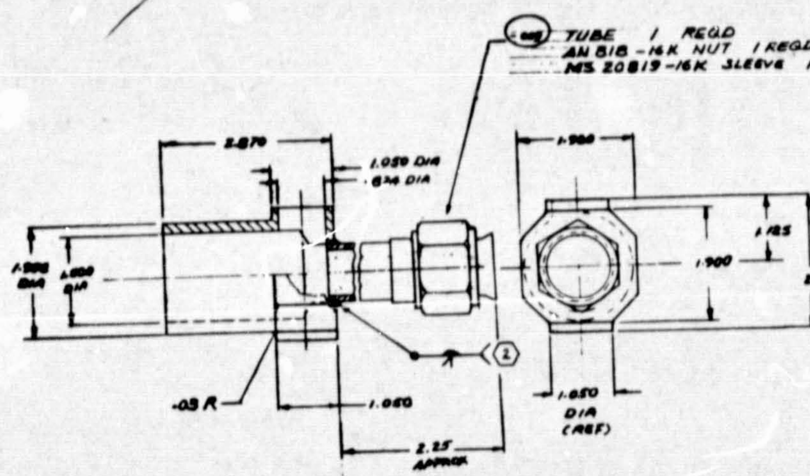

-007 DETAIL DIMENSION

5. PROOF & LEAK TEST
4. CLEAN PER RA
3. IDENTIFY PER
(2) WELD PER RA
1. MACHINE PER

NOTE: UNLESS OTHERWISE SPECIFIED

ll International Corporation
Rocketdyne Division
Canoga Park, California

02602	FRAME 1		
R006324		CHNG	SHEET

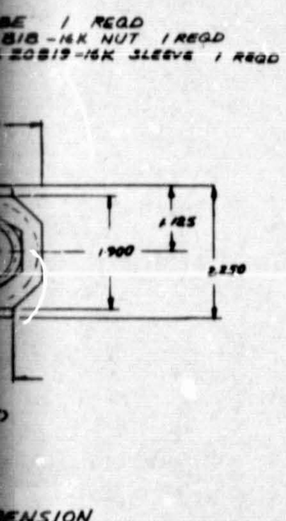

Figure 55

QTY REQD	DASH NO	MATERIAL	SIZE	SPECIFICATION	
1	-009	321 CRES	(1.000 OD x .120 W x 2.75 LG TUBE WITH FLARE END)		
1	AS9003837	INCO 625			
1	-007	321 CRES			
1	-005	321 CRES	1.050 OD x .824 ID		
1	-003	321 CRES	1.050 OD x .824 ID		

5. PROOF & LEAK TEST PER ENGINEERING INSTRUCTION
4. CLEAN PER RA0110-018
3. IDENTIFY PER RA0104-008
(2) WELD PER RA0107-027
1. MACHINE PER RA0103-002

NOTE: UNLESS OTHERWISE SPECIFIED

Rockwell International Corporation
Rocketdyne Division
Canoga Park, California

DUCT ASSY OF 20K THRUST CHAMBER NOZZLE H_2 COOLANT DISCHARGE

SIZE J | CODE IDENT NO 02602 | DRAWING NO 99R006324

DO NOT SCALE PRINT

99R006324

HARDWARE FABRICATION

Upon release of the component and system drawings, component fabrication and/or rework was initiated. To assist in the tracking and coordination of fabrication effort, a complete parts list was generated (Table 16). Components on this list are of four general categories: (1) nuts, bolts, washers, seals, etc., (2) components available from the Advanced Thrust Chamber Technology program with no modification required; (3) components available from the Advanced Thrust Chamber Technology program, but with modification necessary due to the different requirements of the staged combustion system assembly; and (4) newly purchased or fabricated units.

The major components available from the Advanced Thrust Chamber Technology program which did not need modification were the spark igniter assemblies, the combustion chamber, and the regeneratively cooled nozzle. Fabrication processes for these components have been documented in the Advanced Thrust Chamber Technology Final Report (Ref. 1). The major component made available from the Thrust Chamber Technology program which did require alteration was the main propellant injector. The basic fabrication processes for the injector are also reported in the Advanced Thrust Chamber Technology Final Report (Ref. 1) and will not be repeated, although a discussion of the rework effort is described. Pertinent details of the fabrication of the remaining major components and subassemblies is described.

Main Injector Rework

The main propellant injector (Fig. 56) was originally assembled with fuel sleeves designed for gaseous hydrogen as the fuel, because the injector had been fabricated as part of the Advanced Thrust Chamber Technology program. Fuel sleeves with a larger inside diameter, designed to pass the lower density, higher mass flowrate preburner gases were made.

The existing sleeves in the injector were removed by machining out the conical retaining sections, after which the faceplates could be lifted off and the old sleeves could be unthreaded from the LOX posts. The holes in the faceplates were enlarged slightly to pass the new fuel sleeves and reassembly of the injector began. Figure 57 shows the main injector during reassembly after the first set of fuel sleeves has been threaded onto the LOX posts on rows 1, 3, and 5. After these sleeves were properly located with the faceplate support flanges all located in the same plane, the lower faceplate was put into place. The remainder of the fuel sleeves were then threaded through the faceplate onto the LOX posts on rows 2 and 4. These sleeves have a small flange which rests on the first or lower faceplate when they are properly seated, thus holding this plate firmly in position. The second faceplate was then set into place on all 108 sleeves now aligned in the same plane to provide a support for the plate. The ends of all of the sleeves were then swaged over into the conical recesses in the second faceplate, thus retaining this plate firmly in position. No further effort on the injector was required. The water flow testing of the LOX posts had been completed during the Advanced Thrust Chamber Technology program.

TABLE 16. STAGED COMBUSTION SYSTEM ASSEMBLY PARTS LIST

Part Name	Part Number	Quantity/ Assembly	Quantity Ordered	Remarks
• Staged Combustion System Assembly	99RS010250			
Combustor Assembly	99RS010263	1	1	
Injector Assembly	99RS006197-041	1	1	
Injector Seal	9200-156-6245-0103	1	6	Hydrodyne
Mounting Plate	RS010243X	1	1	
Bolts, Injector	RD111-4009-6722	24	30	
Washer	LD153-0013-0005	24	30	
Nozzle, REGEN	99RS006195	1	1	
Bolt, Nozzle Attach	RD111-4008-6408	12	15	
Washer, Nozzle Attach	RD153-5002-0004	12	15	
Seal, Nozzle Attach	9500-7-3-SP-V	1	6	Advanced Product Co.
Body, Preburner	99RS010246	1	2	
Injector, Preburner	99RS010247	1	2	
Seal, Preburner to Injector	9100-40-0103	1	5	Hydrodyne
Bolt, Preburner to Injector	RD111-4008-6620	8	10	
Washer, Preburner to Injector	PL1-6-7.3	8	10	
Simulator, Oxidizer Turbopump	99RS010253	1	1	
Orifice, Oxidizer Turbopump	99RS010271	1	3	
Seal, Oxidizer Simulator	9100-31-0103	1	6	Hydrodyne
Bolt, Oxidizer Simulator to injector	RD111-4008-3412	16	20	

TABLE 16. (Continued)

Part Name	Part Number	Quantity/ Assembly	Quantity Ordered	Remarks
Washer, Oxidizer Simulator to Injector	RD153-5002-0004	16	20	
Simulator, Fuel Turbopump	99RD010252	1	1	
Orifice, Fuel Turbopump Simulator	99RS010272	1	1	Blank Orifice
Bolt, Fuel Turbopump Simulator	RD111-4008-3528	22	25	
Bolt, Fuel Turbopump Simulator	RD111-4008-3516	5	6	
Washer, Fuel Turbopump Simulator	RD153-5002-005	27	30	
Nut, Fuel Turbopump Simulator	RD114-8005-1005	22	25	
Seal, Fuel Simulator to Injector	9200-156-4935-0103	1	5	Hydrodyne
Duct, Preburner to Oxidizer Turbine Inlet	99RS010264	1	1	
Orifice, Preburner Injector Fuel Inlet	99RS010270	2	2	
Seal, Preburner Injector Fuel Inlet	AR10204-223A1Q	4	10	Aeroquip (Omniseal)
Bolt, Preburner Injector Fuel Inlet	RD111-4008-6428	24	30	
Washer, Preburner Injector Fuel Inlet	RD153-5002-0004	24	30	
Nuts, Preburner Injector Fuel Inlet	RD114-8005-2004	24	30	

TABLE 16. (Continued)

Part Name	Part Number	Quantity/ Assembly	Quantity Ordered	Remarks
Adapter, Igniter	99RS010258	2	6	
Seal, Igniter Adapter	RD261-3005-1010	2	10	Sierracin Harrison
Bolt, Igniter Adapter	ND112-0002-0610	8	10	
Spark Plug Insulator, Electrode	99RS010273	1	3	
Spark Plug Electrode	99RS010274	1	3	
Seal, Igniter	RD261-3016-0110	2	5	Naflex
Orifice, Preburner Injector Oxidizer Inlet	99RS010269	1	5	(5) Blank Spares
Seal, Preburner Injector Oxidizer Inlet	AR10204-213A1Q	2	10	Aeroquip (Omniseal)
Duct, Fuel Coolant Discharge	99RS010275	1	1	
Duct, Fuel Coolant Discharge	99RS010276	1	1	
• Exhaust Assembly, Preburner	99RS010249	1	1	
Preburner LOX Valve	AP76005	1	1	
Main LOX Valve	AP76005	1	1	
Nozzle (NASA)	CF622498	1	2	
Combustion Chamber No. 2	99RS009520	1	1	
Fuel, Discharge Manifold	RS009832E-011	1	1	
Injector, Fuel Inlet Manifold	RS0098328-001	1	1	
Spring, Wave	RS006321X	1	2	
Ring, Piston	RS006322X	2	10	

TABLE 16. (Continued)

Part Name	Part Number	Quantity/ Assembly	Quantity Ordered	Remarks
Ring, Piston Retainer	99RS010259	1	1	
Bolts, Retainer	RD111-4009-3304	8	10	
Washer, Retainer	RC153-5002-0003	8	10	
Injector	99RS006197-001	1	1	
Flange, Oxidizer Inlet	99RS010260-003	1	1	
Elbow, Oxidizer Inlet	99RS010260-005	1	1	
Tube, Oxidizer Inlet	99RS010260-007	1	1	
Elbow, Oxidizer Inlet	99RS010260-009-0103	1	1	
Seal, Injector	9200-156-6245	1	1	Hydrodyne
Bolts, Injector Retainer	RD111-4009-6722	24	30	
Washer, Injector Retainer	RD153-5002-0005	24	30	
Plate, Thrust Mount Adapter	RS0102434	1	1	
Adapter, Igniter	99RS010258	1	1	
Bolts, Igniter Attach	ND112-002-0610	4	8	
Seal, Igniter Adapter	RD261-3005-9010	1	10	K Seal
Spark Plug	99RS003397	1	5	
Insulator, Electrode	99RS010273	1	3	
Electrode	99RS010274	1	3	
Seal, Spark Plug	RD261-3016-0110	1	3	Naflex

TABLE 16. (Concluded)

Part Name	Part Number	Quantity/ Assembly	Quantity Ordered	Remarks
• Thrust Mount Installation	RS010268X	1		
Thrust Mount	RS009835X	1	1	Use on All Installations
Bolts, aft Attach	RD111-4008-6618	12	15	
Washers, RD153-5002-0006	RD153-5002-0006	12	15	
Bolts, Forward Attach	RD111-3001-5828	6	10	
Washer	RD153-0013-0008	6	10	
Support, Gimbal Trunion	RS009840X	2	2	
Bolts, Gimbal Support	RD111-3001-5608	8	10	
Washers, Gimbal Support	LD153-0013-0006	8	10	
Trunion, Gimbal	RS009839X	1	1	
Fixture, Gimbal Attach	RS010267X	1	1	
Bolts, Fixture	RD111-3001-5814	5	10	
Washers, Fixture	LD153-0013-0008	6	10	

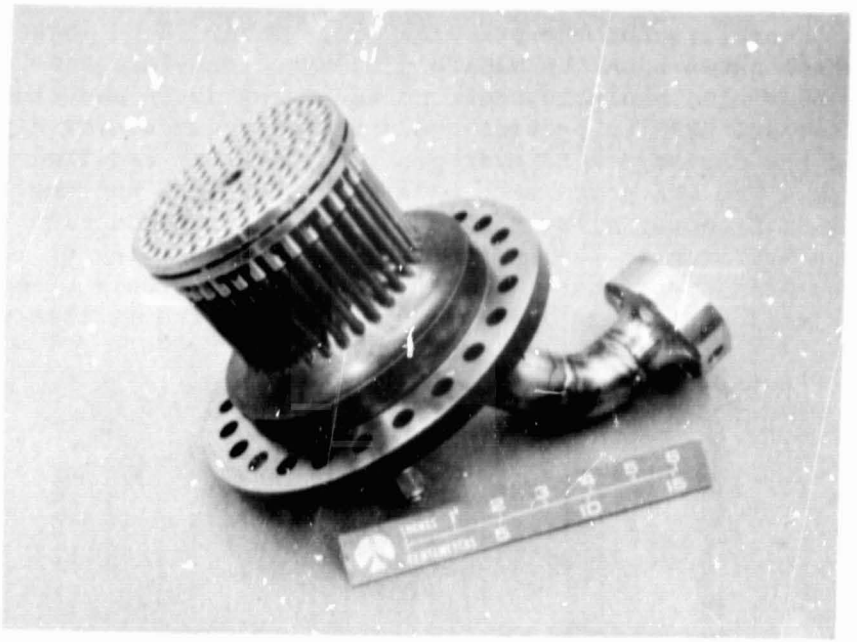

1HS42-2/10/76-C1C*

Figure 56. Main Propellant Injector

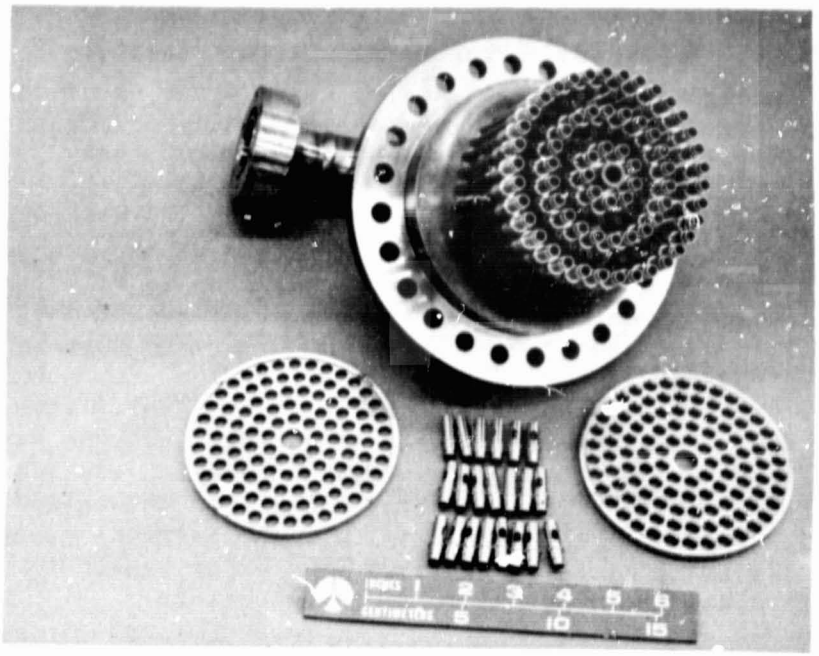

1HS42-2/9/77-C1

Figure 57. Partially Reassembled Main Propellant Injector

Preburner Injector

Two injector assemblies for the preburner were made. Both injectors are shown in Fig. 58 which shows both the manifold side and the face side of the injector. The injector housings, manifold sections and inlet ducts and flanges were fabricated from 321 CRES to provide the strength required for high-pressure operation and the resistance to hydrogen embrittlement required in the fuel manifold areas. The LOX posts were made from 304L CRES and the injector faceplate was NARloy A copper alloy to provide good heat conduction from the face to the gaseous hydrogen in the manifold. The configuration of the injector is similar to the main propellant injector, with two rows only of concentric propellant injection elements and a coaxial spark/torch igniter post.

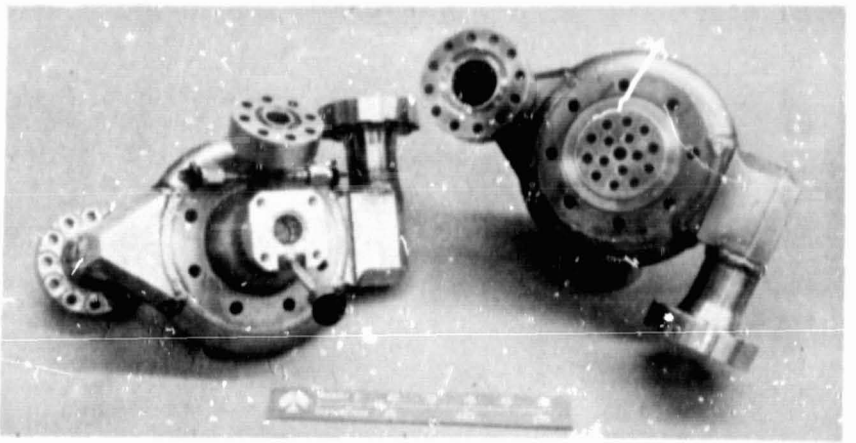

1HS32-5/5/76-C1B*

Figure 58. Preburner Injector Assemblies

The injector faceplate was made of NARloy A, a copper based material alloyed with small amounts of silver and zirconium to enhance the material properties at elevated temperatures.

Assembly was begun by welding the CRES components together to provide a welded body assembly. The fuel sleeves were then brazed to the LOX posts with a high melting temperature, 1310 K (1899 F), braze designated PAL-7 which is a 70 gold-22 nickel-8 palladium alloy. Four 6.35 mm (0.250 inch) lengths of 1.57 mm (0.062 inch) diameter wire were brazed to each post and sleeve assembly to provide positive spacing between the two elements to ensure that the post would at all times remain concentric with the fuel sleeve. In this way, each element would have a uniform field of gaseous hydrogen surrounding the central LOX flow, and hot streaks from fuel starvation could be avoided. The sleeve and post assemblies were then installed into the welded body assembly and brazed with the same PAL-7 braze alloy. The original sleeve-to-post braze was unaffected at this time because the braze remelt temperature is somewhat higher than the original melting temperature.

The subassembly was subjected to a vacuum leak check to verify the integrity of the individual braze joints. Silicone rubber plugs were installed over the ends of the LOX posts and a vacuum was drawn on the LOX manifold side and held for 10 minutes. No decay of the vacuum was observed, thus indicating that there was no leakage past the braze joints. This procedure was repeated for a total of three vacuum checks. If a leak had been detected the units could have been re-brazed by applying braze paste to the joints which were readily accessible at this time and reheating the assemblies.

The NARloy A faceplate was installed on the assembly and brazed to the individual fuel sleeves, the center igniter post, and the welded body assembly with a somewhat lower melting temperature, 1168 K (1643 F) alloy designated as Silcoro Braze, which is a 75 gold-20 copper-5 silver alloy. During the cool-down cycle the parts were held in the furnace at 756 K (900 F) for 3 hours to provide aging treatment to the NARloy A for improved strength.

Following the braze operation the injectors were proof pressure tested with water at 6000 psi for a total of five cycles and again subjected to three vacuum leak check cycles.

Preburner Combustor

The preburner combustor body (Fig. 59) was fabricated from three basic elements, all machined from Inconel 625 alloy: (1) the body and mounting flange, (2) the hydrogen cooled sleeve or inner liner with the integral acoustic cavity, and (3) the exhaust duct connector Y section.

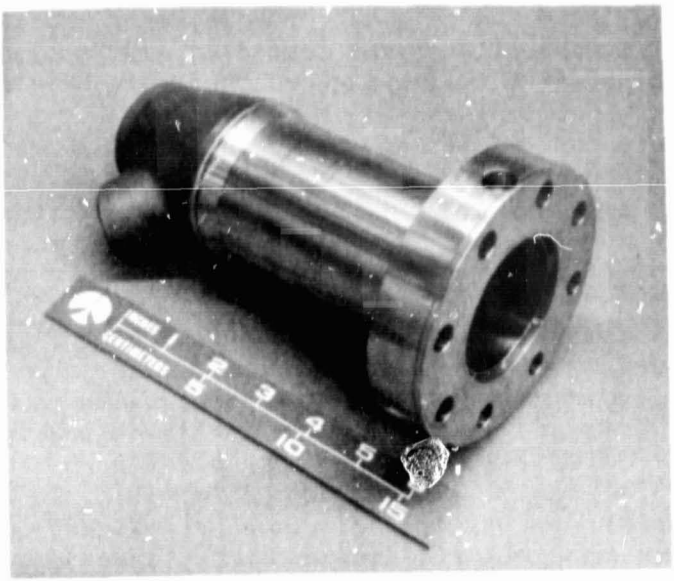

1HS32-4/30/76-C1E*

Figure 59. Preburner Combustor Body

The body and flange were machined by conventional lathe turn machining. No special techniques were required nor were any difficulties encountered.

The inner liner section was also machined by conventional lathe turning procedures, but the acoustic cavities were formed by electrical discharge machining (EDM). This process uses an electrode formed to the desired shape of the cavity which is brought close to the surface of the material to be removed. An interrupted electrical current generates an arc from the electrode to the part which melts a small point on the part. This melted material is then washed away by a circulating kerosene bath in which the part is immersed. Previous application of this technique has demonstrated the ability to machine out small cavities such as these with great accuracy and speed relative to other metal removing techniques.

Upon completion of the liner machining, small lengths of wire were brazed onto the outside wall of the liner at the forward and aft ends of the liner. These wires laid on in the axial direction provided positive control of the spacing uniformity between the liner and the combustor body. A constant width gap between these two elements is required to ensure equal circumferential distribution of the gaseous hydrogen coolant flowing in this gap space.

The liner was installed in the body and the two components were EB welded together at the forward or flange end. EB welding was used to obtain the depth of weld required in a confined location with minimum heat distortion from the welding operation.

The exhaust duct connector was machined on a tape-controlled, three axis milling machine with provision for full penetration J-groove welding to the ducting at a later time. This element was then EB welded to the downstream end of the preburner combustor body. Cleanup maching at the flange end to provide the design mating surfaces to the injector, hydrogen coolant inlet ports, and chamber pressure measurement ports was done at the completion of all welding operations. Proof pressure testing of the assembly was deferred until later assembly with the injector and exhaust ducting. At that time the unit was proof pressure tested to 413.56 N/cm^2 (6000 psi) with water for a total of five cycles with the pressure held for 2 minutes each cycle.

Figures 60 and 61 show the preburner combustor, injector, and igniter units prior to assembly and after assembly. In this configuration, the preburner body is ready to be welded to the exhaust gas ducting.

Turbine Simulators

The turbine simulators, which provided configurational continuity for the staged combustion system assembly, also provided a housing for the orifices used to simulate the pressure drop which would be encountered with actual turbines in the system. The simulator housings are shown in Fig. 62 through 64. They consisted of flanged assemblies machined from Inconel 625. The orifices were initially machined at 6.35 mm (0.25 inch) thick rounded inlet orifice plates. The original orifices were later replaced with 25.4 mm (1.0 inch) thick orifices, still with rounded inlets, but more capable of withstanding the high pressure differential of the hot preburner gases without distortion.

The preburner combustor is shown in Fig. 65 with the two turbine simulators (upstream section of fuel turbine simulator only) and the interconnecting exhaust gas ducting. Final welding of the ducting to the preburner was deferred pending alignment of all components in a final assembly.

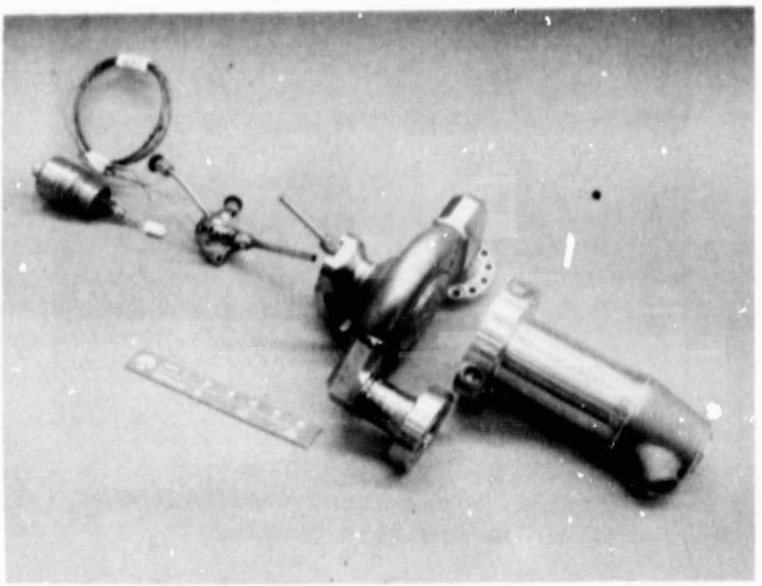

1HS32-5/5/76-C1A*

Figure 60. Preburner Combustor, Injector, and Igniter Prior to Assembly

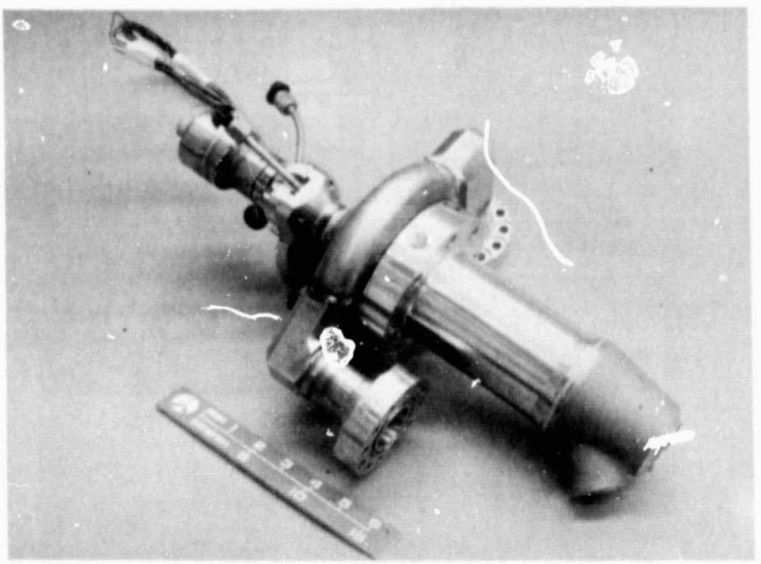

1HS32-5/5/76-C1C*

Figure 61. Preburner Combustor, Injector, and Igniter Assembled

Figure 62. Fuel Turbine Simulator - Upstream Section

Figure 63. Fuel Turbine Simulator - Downstream Section

Figure 64. Oxidizer Turbine Simulator

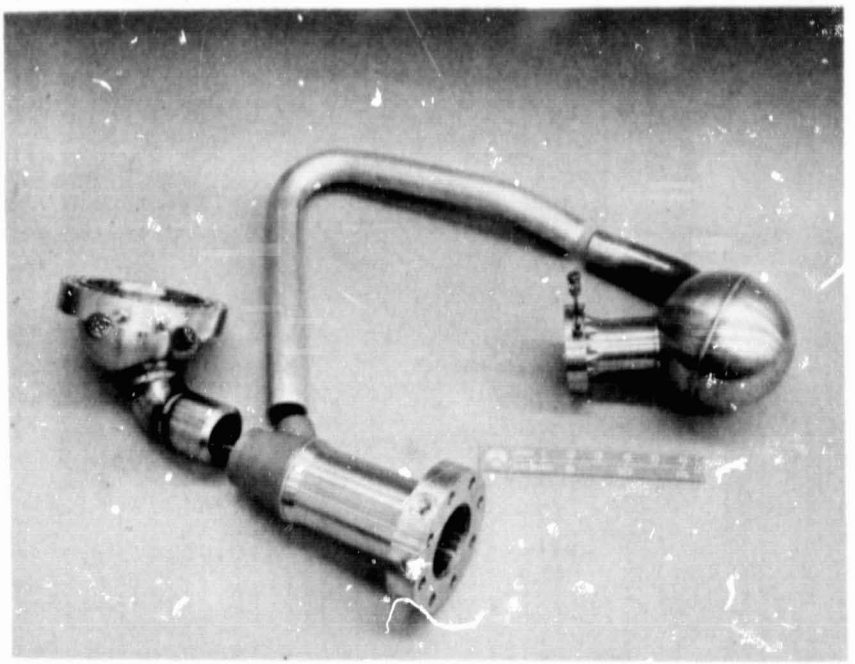

1HS32-4/30/76-C1B*

Figure 65. Preburner Combustor With Turbine Simulators and Exhaust Gas Ducting

Injector Simulator

The injector simulator (Fig. 66) used for initial checkout testing of the preburner was fabricated from 321 CRES bar stock and pipe. Inconel 625 ducting and the downstream section of the fuel turbine simulator were welded to this unit to provide the initial mockup of the duct routing and preburner location. This simulator consists of little more than a pipe to direct the exhaust gases from the preburner in the proper direction during initial preburner testing. Figures 67 and 68 show the final assembly of the preburner injector and igniter, combustor, turbine simulators, and ducting to the injector simulator. Bosses were added to the ducting downstream of the preburner, so that three thermocouples could be inserted into each discharge duct to determine the operating thermal gradient and combustion temperature.

The injector, body, turbine simulators, thrust chamber simulator, and ducting were assembled and successfully proof pressure tested to 3100 N/cm^2g (4500 psig). The proof test consisted of three cycles, each maintained for 3 minutes at maximum pressure. Blank orifice plates were installed in the turbine simulators to contain the pressure for these tests, and the ducting downstream of the simulators was not proof tested. The welds in these areas were subjected to thorough X-ray inspection to verify their integrity.

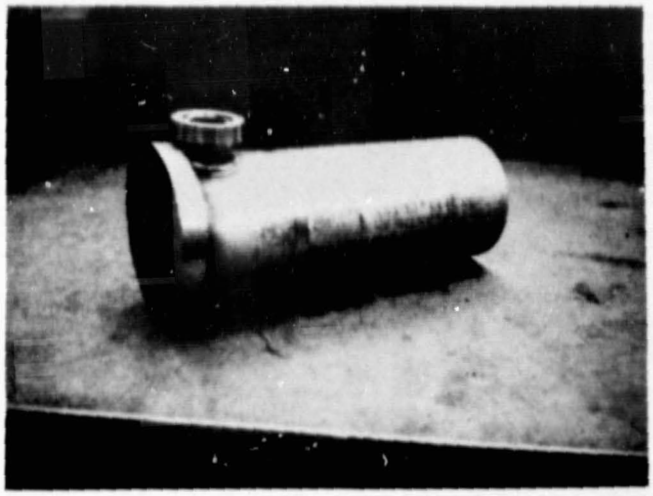

Figure 66. Injector Simulator

LOX Control Valves

Although not a part of the contracted effort, two servocontrolled, hydraulic actuated LOX ball valves were fabricated and assembled for use with the staged combustion system assembly during hot-fire test activities. The valves (Fig. 69) were put together from a combination of newly fabricated components and existing available components. One valve was intended to control the LOX flow to the preburner and one was for control of the LOX flow to the main injector. The two valves were essentially the same, the principal difference being that the main LOX valve, due to the higher main LOX flow-rate, had a larger diameter flow passage and a larger diameter ball with an extension of the exit cone required to mate with injector LOX inlet duct. The hydraulic actuators and the position indicators shown in Fig. 69 were identical for both units.

Two controllers were obtained to provide the position signal and opening and closing ramp rate signals to the valves. One of the controllers is shown in Fig. 70. These controllers, designed for use on the Space Shuttle Main Engine (SSME) program have the capability to signal setpoint changes during a test and to utilize engine operating parameters or valve position feedback for position control, accounting for the large array of setpoint controls displayed. This entire capability was not needed for the staged combustion system assembly testing with only one position setpoint, one opening ramp rate, and one closing ramp rate required for each test.

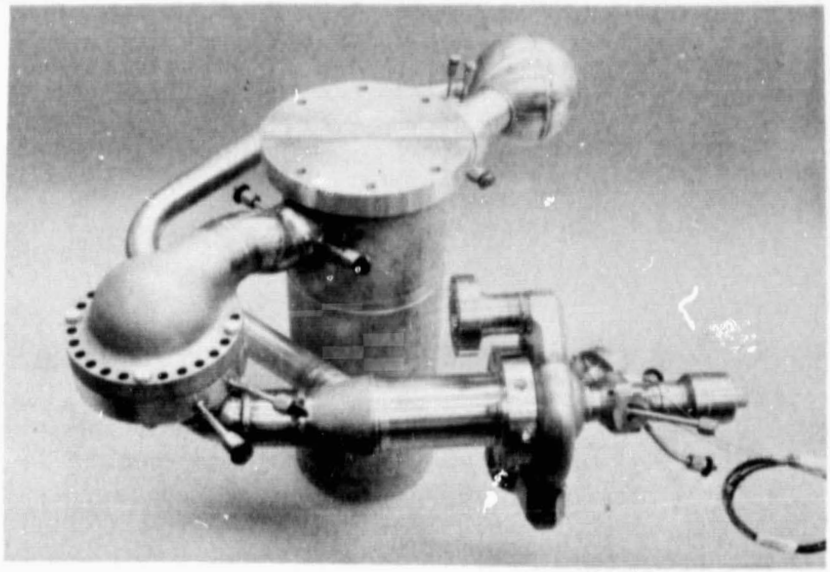

1HS32-5/5/76-C1D*

Figure 67. Preburner, Turbine Simulator and Injector Simulator Assembly

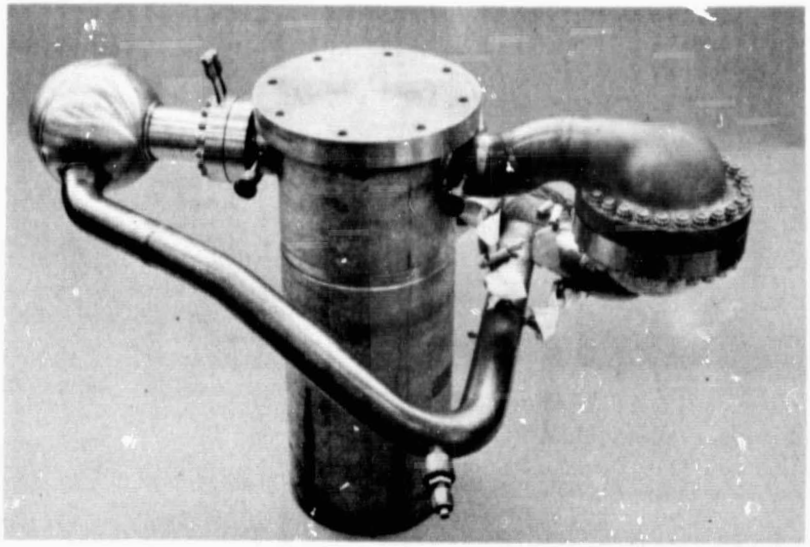

1HS35-9/27/76-C1A*

Figure 68. Preburner, Turbine Simulators and Injector Simulator Assembly

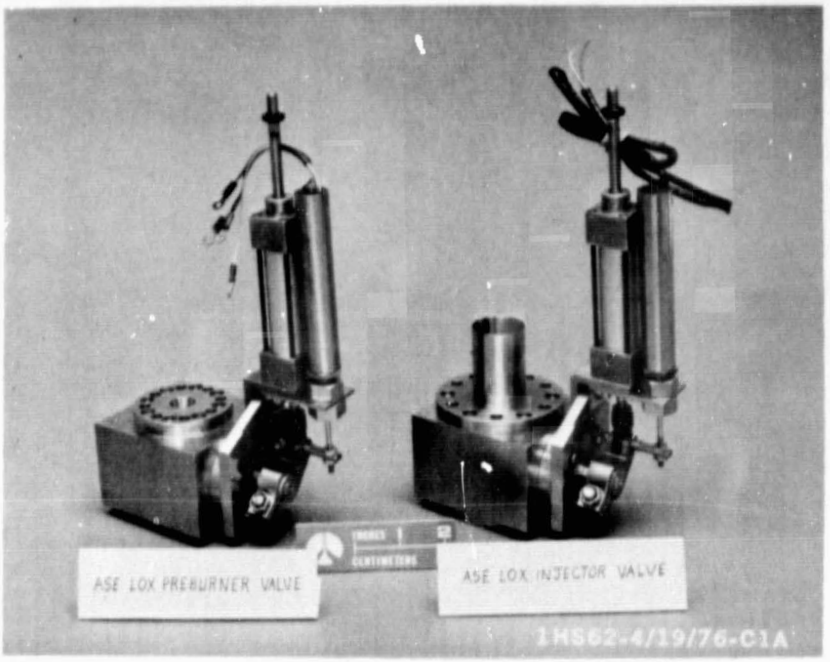

Figure 69. LOX Control Valves

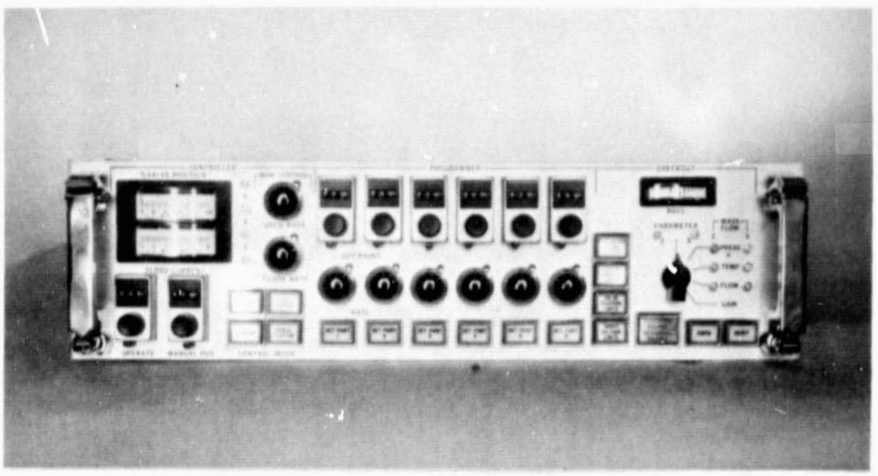

6CE63-7/24/72-S1B

Figure 70. LOX Valve Controllers

400:1 Area Ratio Nozzle Extension

Two 400:1 area ratio nozzle extensions (Fig. 71) were fabricated by NASA and delivered to Rocketdyne for testing with the staged combustion system assembly. The fabrication technique for both nozzles was the same. Plate stock of 12.7 mm (0.50 inch) mild steel (SAE 1010-1030) was brake-rolled and butt-welded together to form five basic truncated conical sections. These were welded together with continuous circumferential welds to form the rough nozzle shape which was then "bumped", or cold-forged into a shape which could be machined to the final contour. This assembly was then welded to the forward flange ring rough machining and the temporary stiffening ring at the aft or exit end of the nozzle. This rough part was stress relieved at 865 to 895 K (1100 to 1150 F) for 1 hour in air and then allowed to air cool. The rough contour was reviewed to determine whether further bumping was required before final machining and welding of the stiffening ring support tabs. The nozzle inner contour was machined to the aerodynamic contour determined by Rocketdyne which matched and extended the contour of the regeneratively cooled, 175:1 area ratio, nozzle. Care was taken to ensure that an unfavorable "step" in the contour would not occur at the joint between the two nozzles.

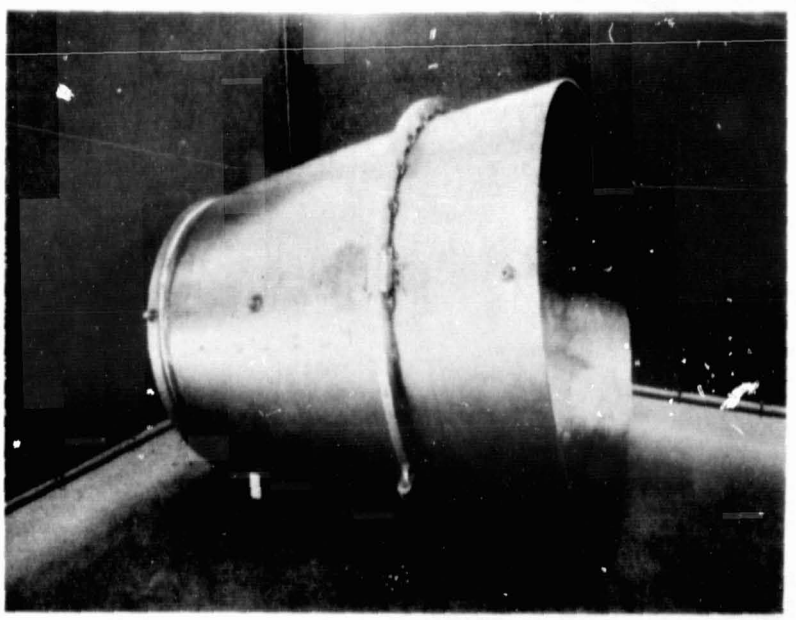

Figure 71. 400:1 Uncooled Nozzle

A total of 16 3.18 mm (0.125 inch) diameter static pressure taps were drilled through the wall, and threaded bosses welded to the wall of the nozzle that was subsequently used during the test program.

System Assembly

The original program plan included the concept of full regenerative cooling of the combustor chamber, with the chamber coolant fed directly to the preburner fuel inlet manifold. The preburner, turbine simulators, and ducting subassembly, which had been previously welded together and aligned with the injector simulator was installed and aligned with the cooled combustion chamber, and the coolant outlet to preburner inlet fuel ducts were welded into place as shown in Fig. 73a and 73b. This system was welded together without the use of hard tooling because it was a "one-of-a-kind" assembly. The downstream section of the fuel turbine simulator does not show in these views because only one unit was fabricated and it was welded onto the injector simulator at this time. For the final assembly of the staged combustion system assembly the turbine simulator was cut off of the injector simulator following the preburner checkout tests and welded into place with this system. In Fig. 73b, the preburner servocontrolled LOX valve can be seen as well as both main chamber and preburner igniter assemblies. Figure 72 shows the staged combustion assembly installed on the regeneratively cooled nozzle with all preburner components and ducting in place.

1XZ21-11/30/77-C1E*

Figure 72. Staged Combustion Assembly and Regeneratively Cooled Nozzle

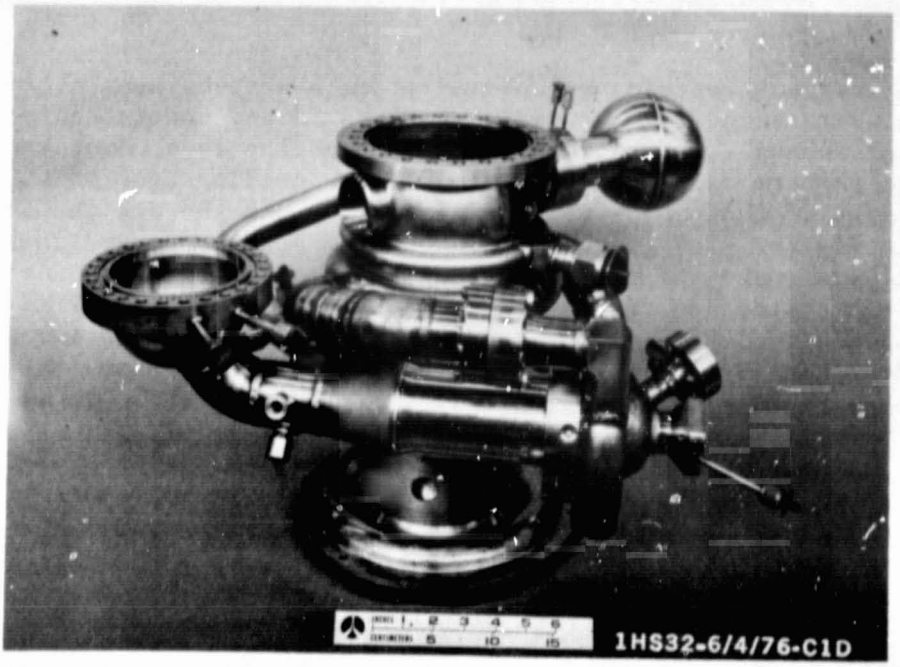

(a)

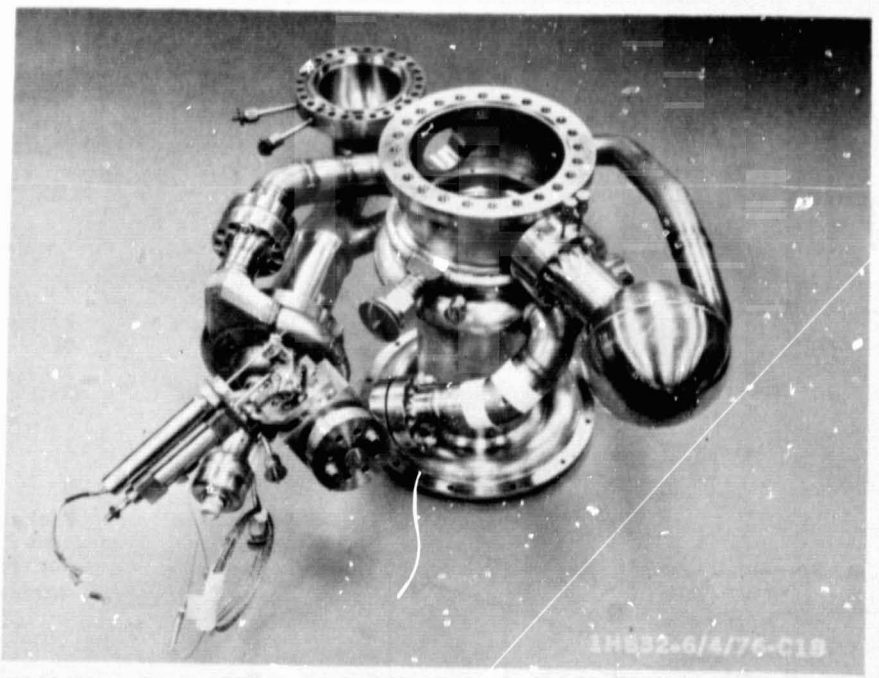

(b)

Figure 73. Staged Combustion Syscem Assembly

TEST

The overall program test plan was conceived as a step-by-step approach to system testing, with each stage providing background and understanding of the component and subsystem operation and ensurance that each component and subsystem would perform as projected during the succeeding test phase. Schematic representatives of the configurations assembled, and the designation of each are shown in Fig.74. The preburner test system and the staged combustion system assemblies were the configuration subjected to hot-fire testing. The preburner test system and the staged combustion system assembly (8:1) were tested in open air with no diffuser. The final staged combustion system assembly with the 175:1 nozzle and the 400:1 nozzle extension installed was tested in the special diffuser/ejector.

The coolant and propellant supply systems and the relationship of the test systems to the altitude capsule and the entrance to the diffuser are shown in the installation drawing (Fig. 75).

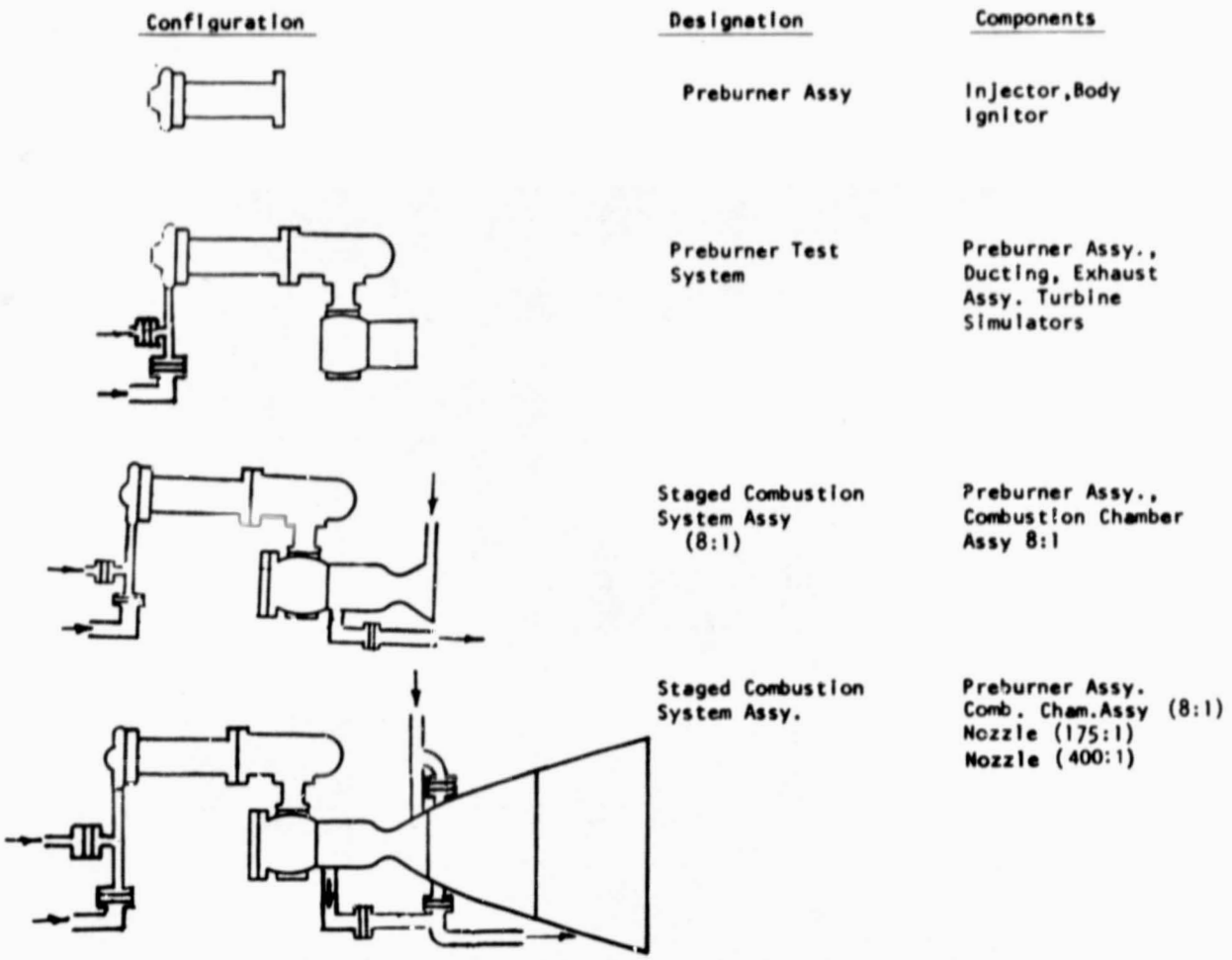

Figure 74. Staged Combustion System - Designations and Configurations

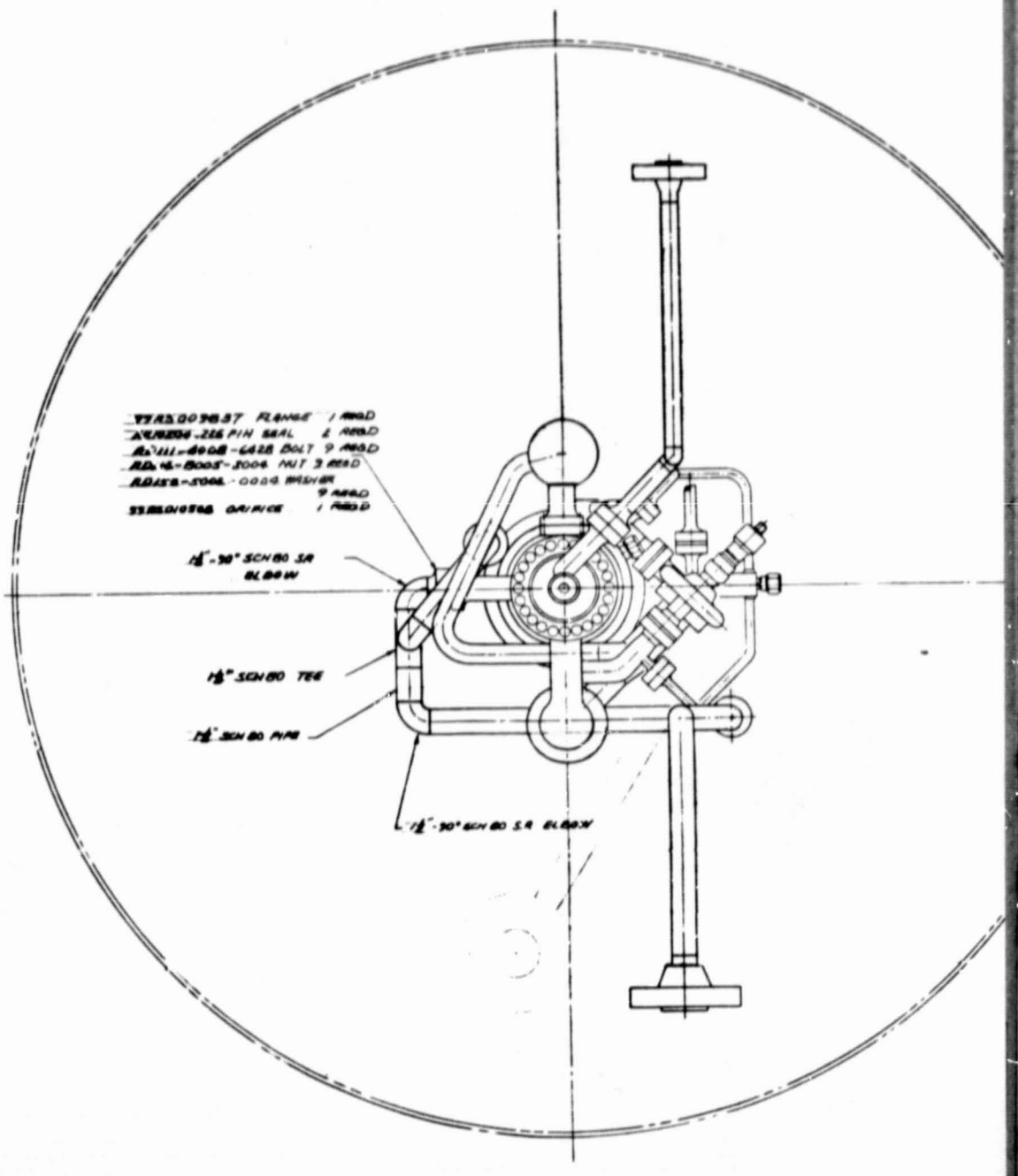

VIEW LOOKING AFT

REDUCE SIZE

2

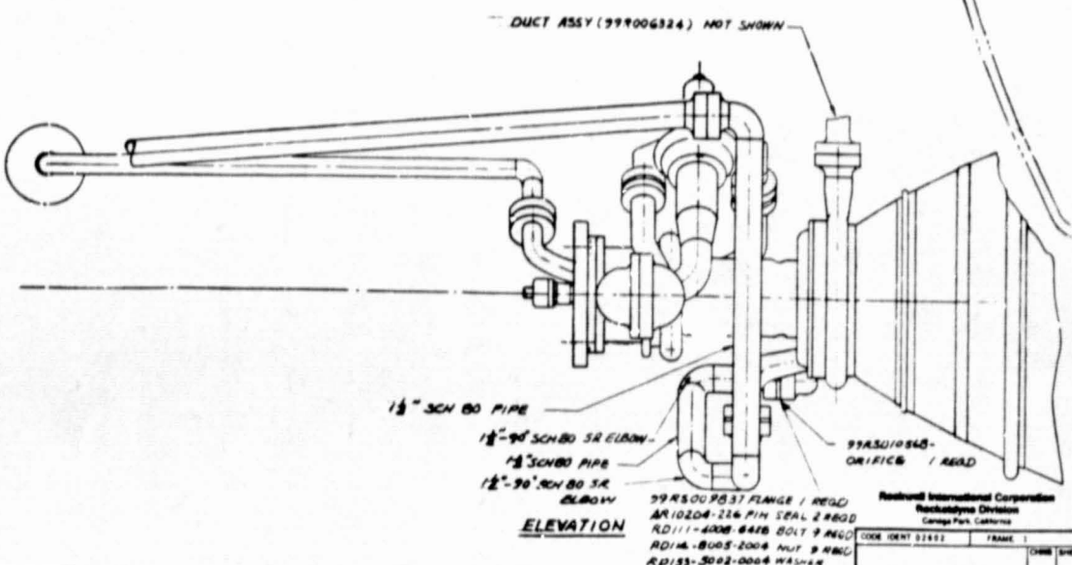

ELEVATION

99A5007837 FLANGE 1 REQD
AR10204-224 PIN SEAL 2 REQD
RD111-4008-6416 BOLT 9 REQD
RD114-8005-2004 NUT 9 REQD
RD133-5002-0004 WASHER 9 REQD

Rocketdyne International Corporation
Rocketdyne Division
Canoga Park, California

CODE IDENT 02602	FRAME 1	
		CHNG SHEET

* MICROFILM OVERLAP AREA *

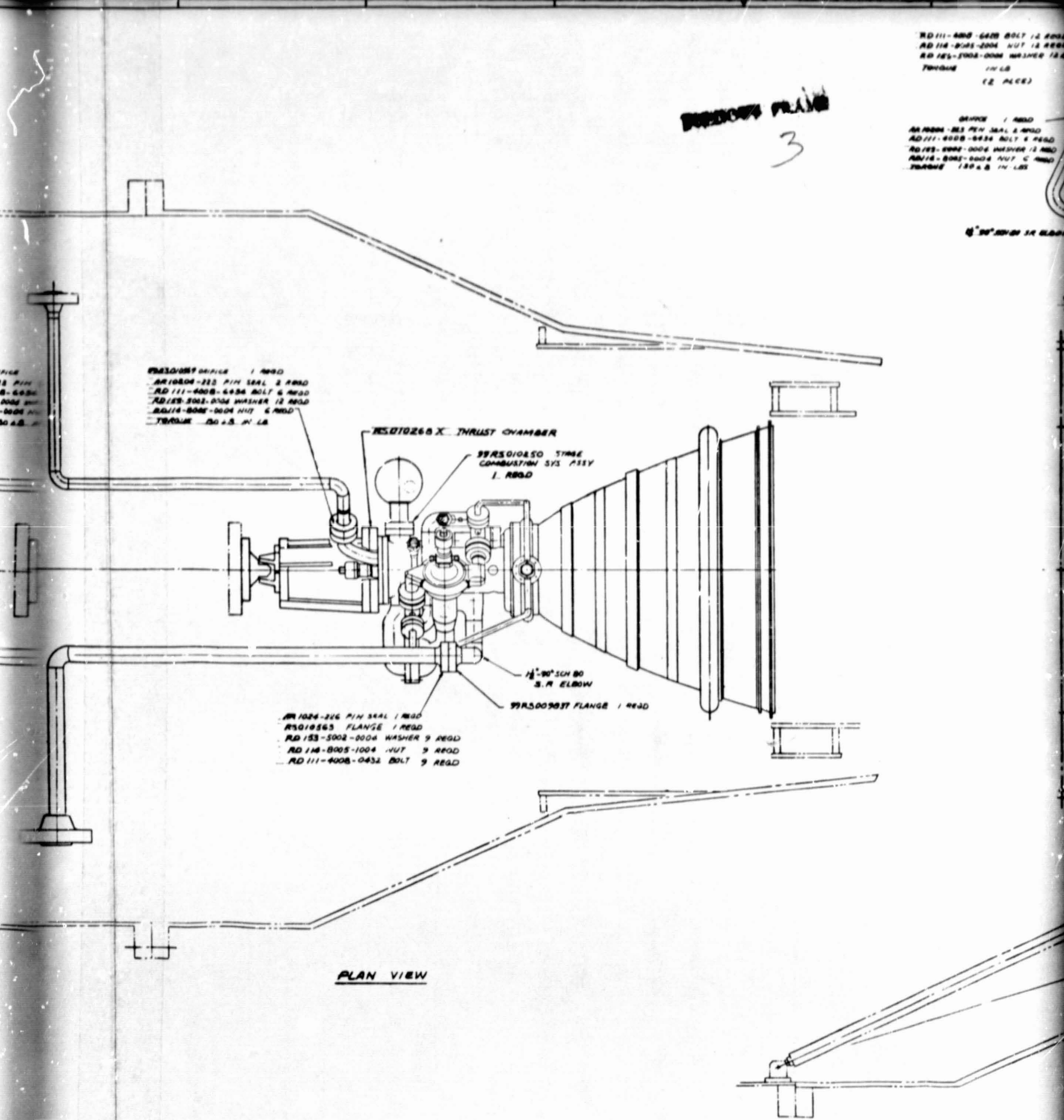
RS010268 X THRUST CHAMBER
99RS010250 STAGE COMBUSTION SYS ASSY 1 REQD
½"-90° SCH 80 S.A ELBOW
99RS009837 FLANGE 1 REQD
AR1024-226 P/N SEAL 1 REQD
RS010363 FLANGE 1 REQD
RD153-5002-0004 WASHER 9 REQD
RD116-8005-1004 NUT 9 REQD
RD111-4008-0432 BOLT 9 REQD

PLAN VIEW

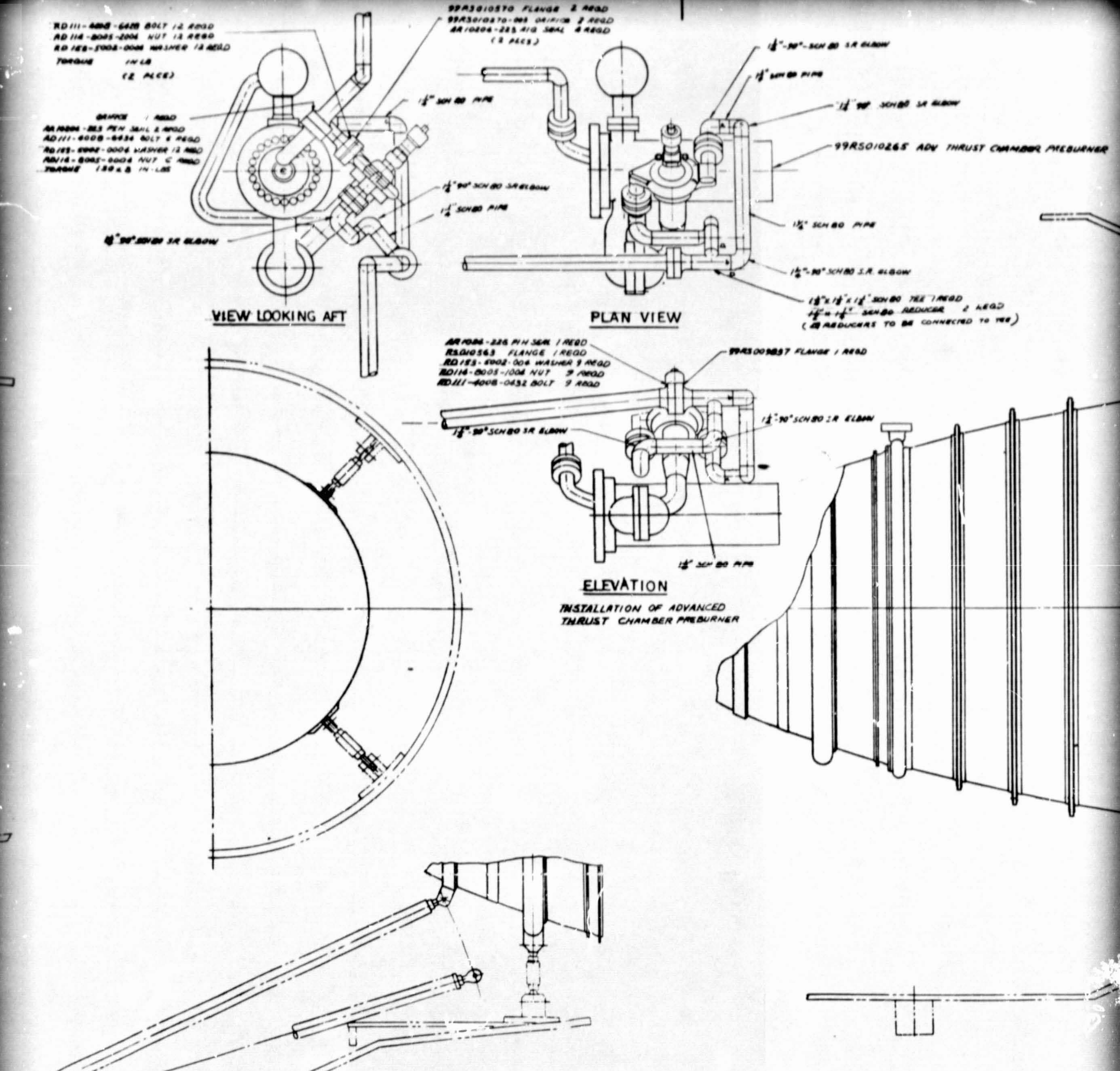

[redacted] FRAME

4

Rockwell International Corporation
Rocketdyne Division
Canoga Park, California

CODE IDENT 02602	FRAME 2		
99RS010565		CHNG	SHEET

● MICROFILM OVERLAP AREA ●

FRAME 4

FRAME 5

UNLESS OTHERWISE SPECIFIED

OVERLAP AREA

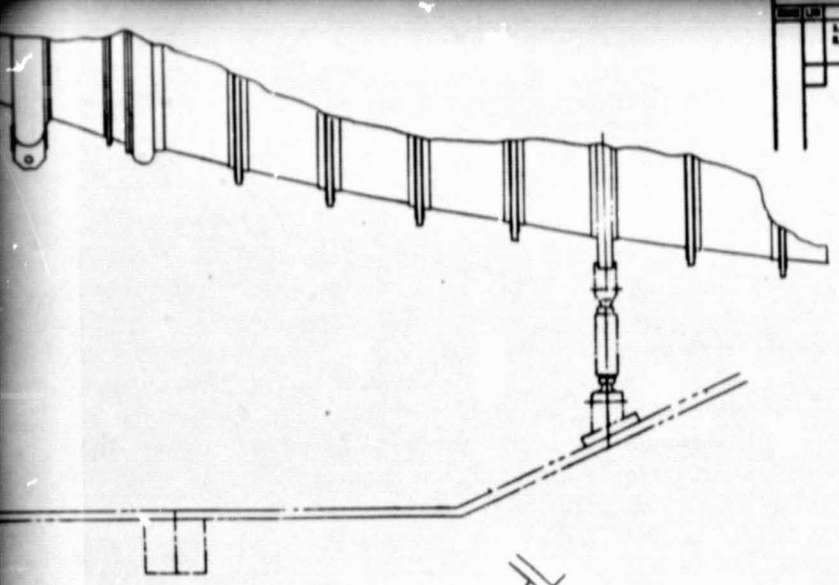

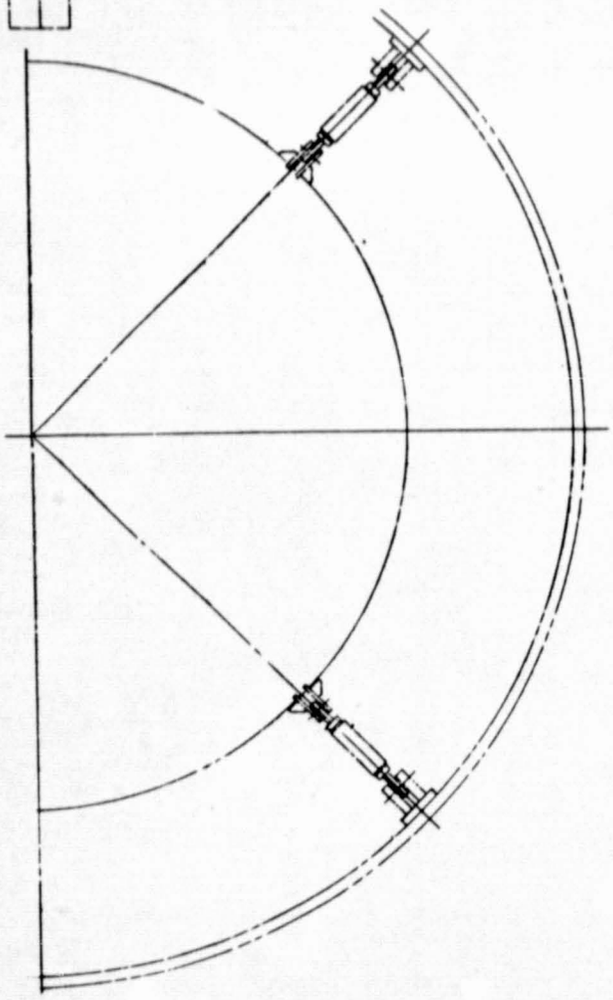

Figure 75

Test Systems and Facility

All hot-fire testing was conducted on Nan stand (test stand No. 017, Fig. 76, in the Propulsion Research Area [PRA]). The facility propellant system schematic diagrams are shown in Fig. 77 through 79, which show the evolution of the facility from preburner test system testing through complete staged combustion system assembly testing with the 400:1 nozzle extension.

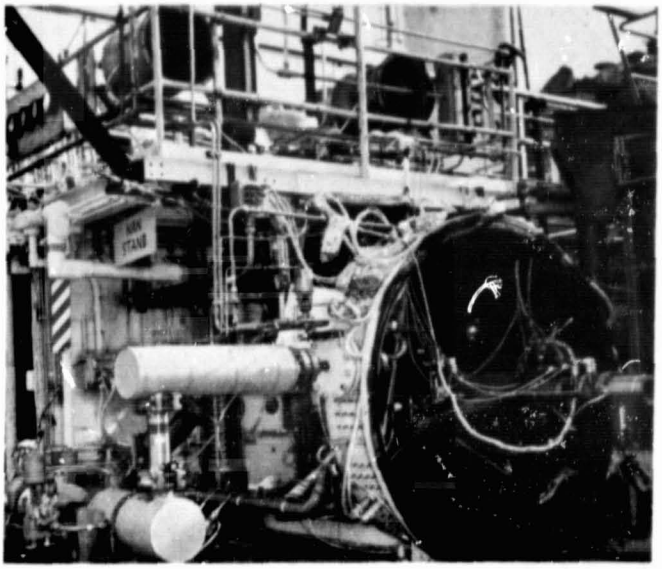

1HS61-1/29/75-S1*

Figure 76. Test Stand Nan, PRA

Liquid oxygen was supplied to the preburner and main injector from a 3450 N/cm^2 (5000 psi) rated 750-liter (200-gallon) liquid nitrogen jacketed tank through 7.6 cm (3 inch) heavy-wall piping. The 7.6 cm (3 inch) hydraulically actuated two-position Annin valve used for flow control during the Advanced Thrust Chamber Technology Program was used as a facility shutoff for this testing. For all testing, the tank was pressurized with helium gas.

The feed system downstream of the valve was reduced to a 2.5 mm (1 inch) pipe which branched inside the capsule; one branch led to the preburner servocontrolled LOX valve and the other branch led to the main injector valve. During the preburner-only testing this latter branch was ducted to the facility LOX bleed dump line with a small, 0.76 mm (0.030 inch) orifice to keep LOX in this line so that gaseous oxygen bubbles would not be bled into the flow stream.

A turbine type flowmeter and an inline venturi meter upstream of the facility LOX valve provided the primary oxidizer flowrate measurement. A venturi meter in the branch line to the preburner metered the flowrate to the preburner for determination of preburner mixture ratio and performance.

Igniter oxidizer flow was tapped from the LOX line upstream of the main valve, but downstream of the flowmeters, and routed through a coil heat exchanger to provide near ambient temperature gaseous oxygen to the two igniters. A separate 2.5 mm (1 inch) Annin valve was used to control the igniter oxidizer flow to permit operation of the igniters independently of

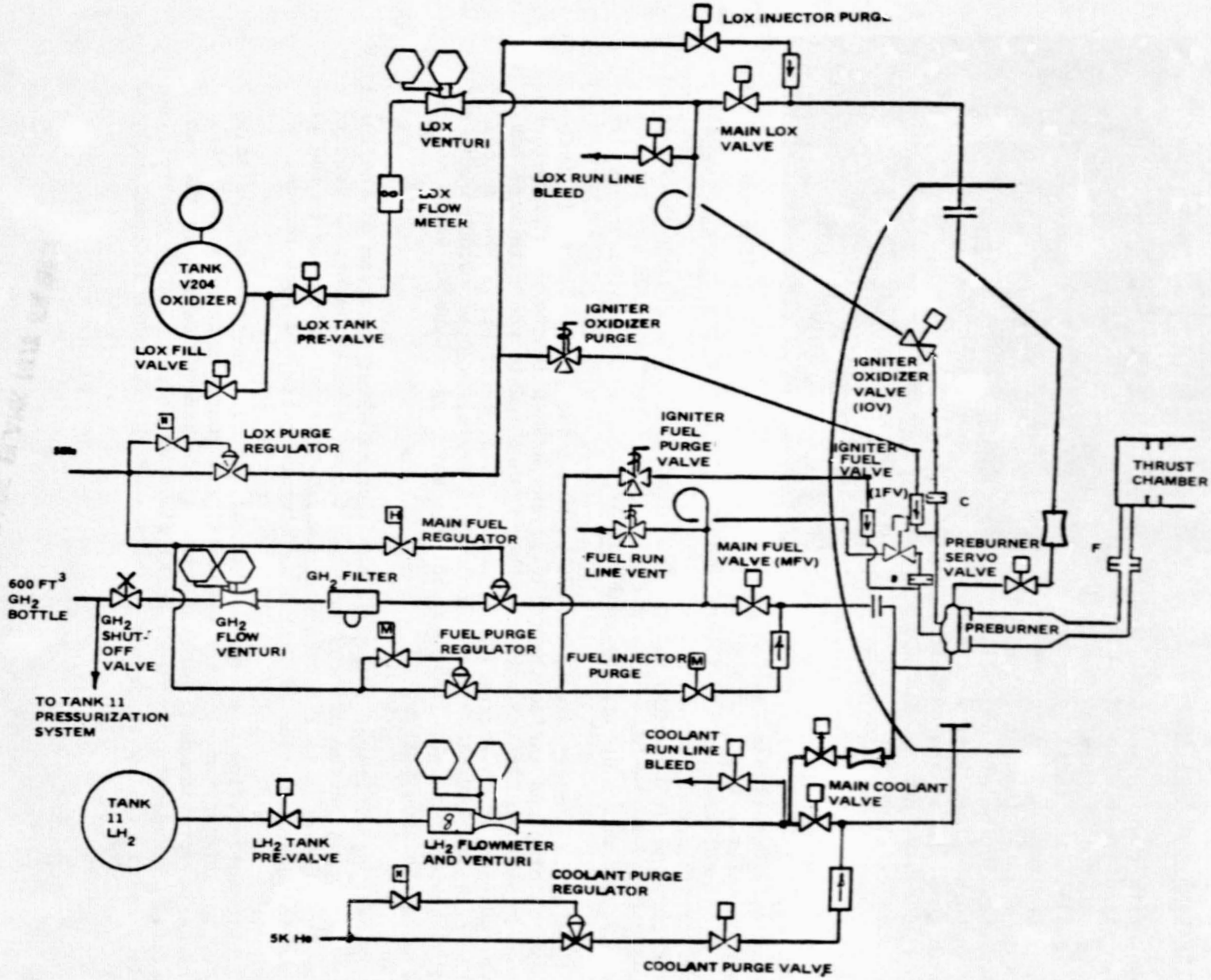

Figure 77. Propellant Feed System Schematic

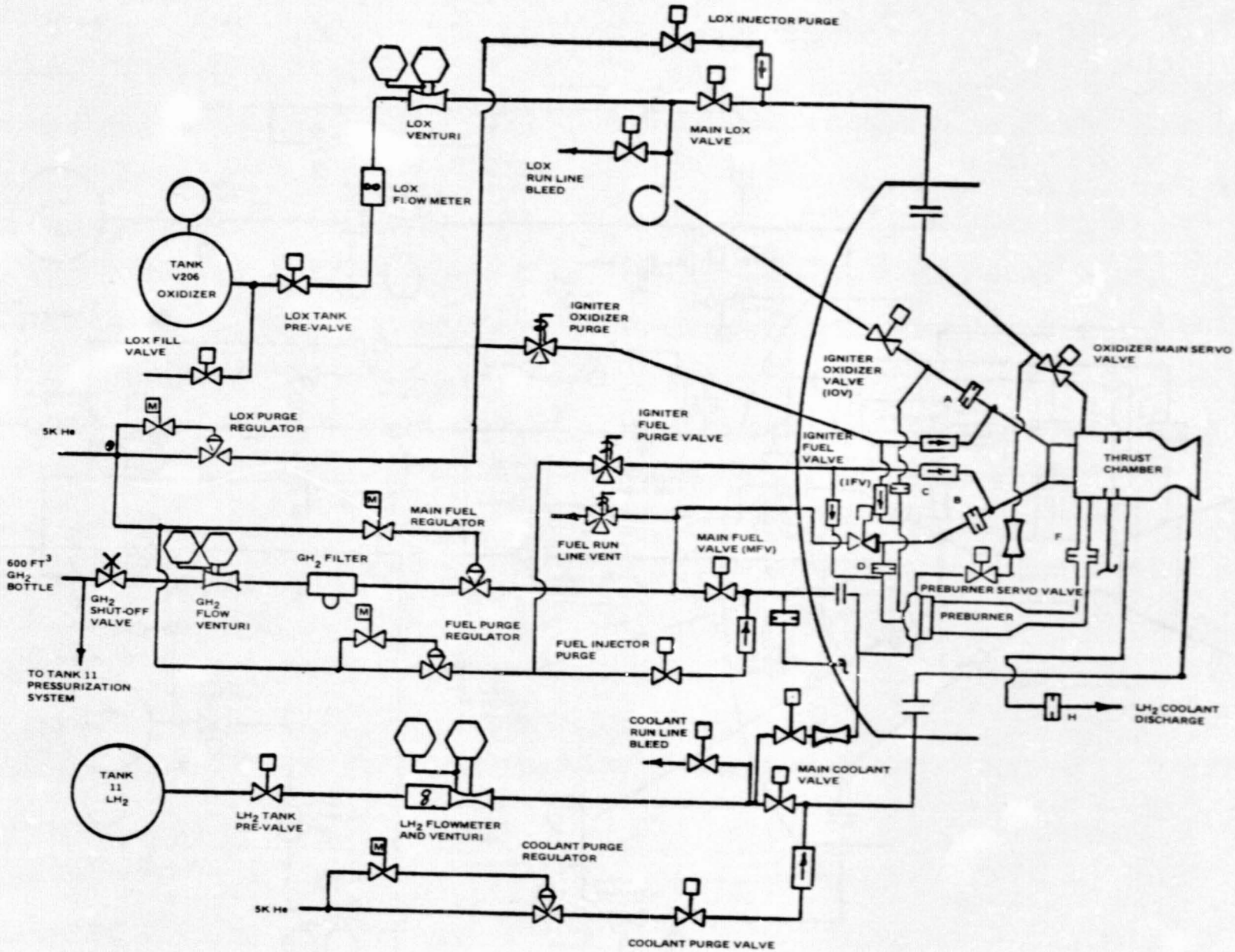

Figure 78. Propellant Feed System Schematic

ORIGINAL PAGE IS
OF POOR QUALITY

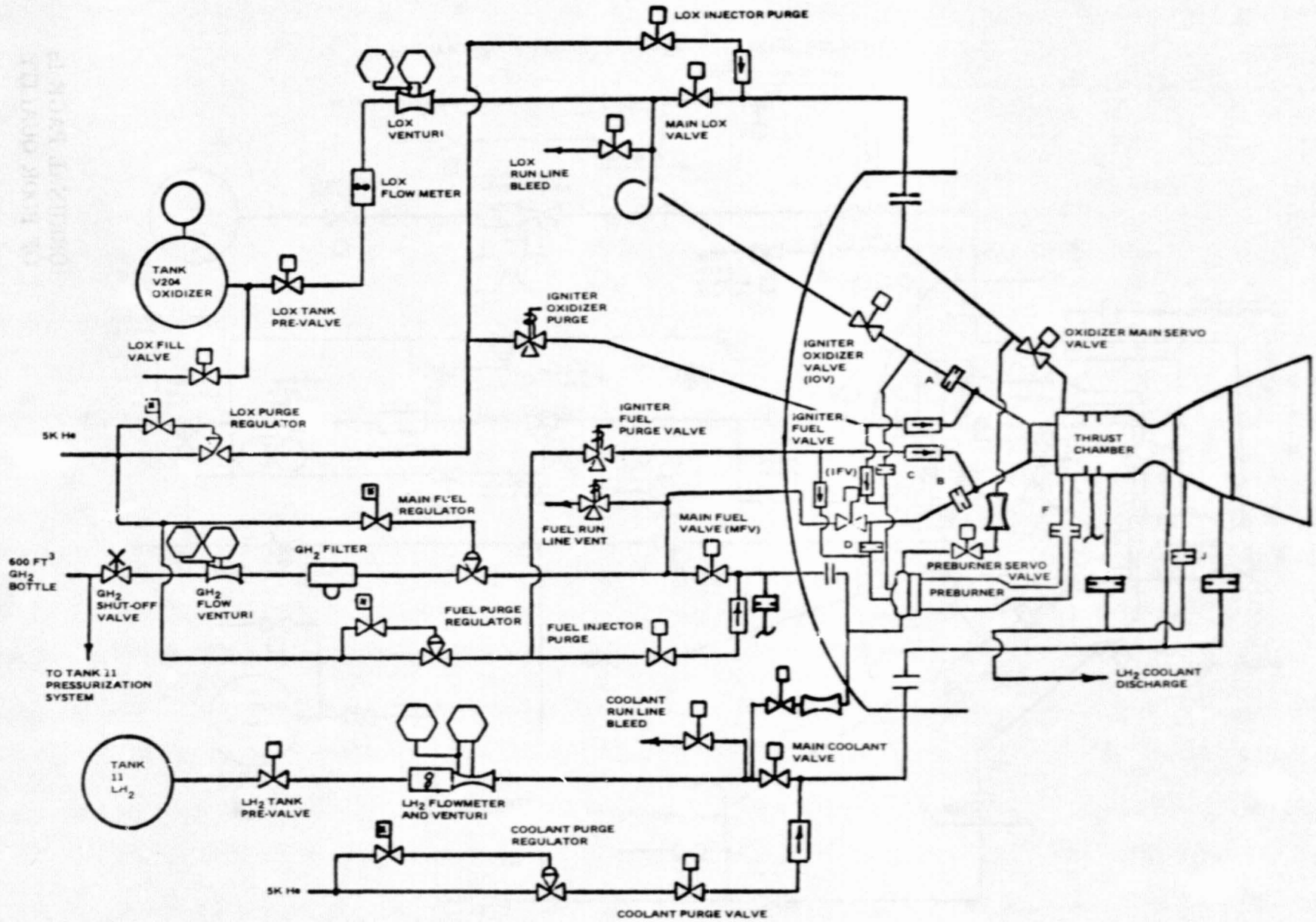

Figure 79. Propellant Feed System Schematic

the preburner or main chamber operation and to permit sequencing of the igniters to fire prior to perburner main chamber operation.

Gaseous hydrogen used for fuel on all tests was supplied from a 3450-N/cm^2 (5000 psi) area supply system, reduced to run line pressure through a Grove regulator. The feed line was a 10 cm (4 inch) pipe from the facility shutoff valve to the main combustion chamber Annin control valve. From the valve to the injector, 5 cm (2 inch) heavy wall pipe was used. A controlled amount of liquid hydrogen tapped off of the LH_2 coolant system line was fed into a tubular mixer, (Fig. 80), to provide hydrogen of the proper temperature to the preburner injector.

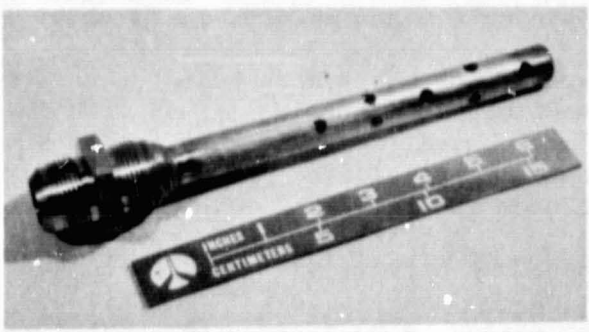

Figure 80. LH_2 - GH_2 Mixer Element

Hydrogen for the igniters was tapped off the gaseous hydrogen line between the regulator and the main propellant valve with a separate 2.5 cm (1 inch) Annin valve for igniter flow and sequencing control. The gaseous hydrogen for both preburner flow and igniter flow was not temperature controlled and the resultant temperature of the gas reflects the local ambient temperature. Little problem was encountered as a consequence of this; the temperature varied generally between 290 K (60 F) and 310 K (100 F), but this span did not cause any observable discrepant operation.

Liquid hydrogen was supplied to the combustion chamber and nozzle coolant systems and to the preburner fuel mixer from a 3450 N/cm^2 (5000 psi) rated 750 liter (200 gallon) vacuum and liquid nitrogen jacketed, insulated tank through 7.6 cm (3 inch) heavy wall vacuum jacketed piping and a 7.6 cm (3 inch) hydraulically actuated, two-position control component valve. The tank was pressurized with hydrogen gas to provide the expulsive force.

Diffuser/Ejector

Sea level testing of a high area ratio nozzle requires a diffuser-ejector system capable of accommodating rocket nozzle exit pressures as low as 0.28 N/cm^{2}a (0.4 psia) with an external ambient pressure of 9.5 N/cm^{2}a (13.8 psia).

The diffuser makes use of the high velocity rocket exhaust gases to achieve an ejector pumping action and to evacuate the test chamber around the engine, thus providing a low pressure environment at the nozzle exit while decreasing the velocity to increase the static pressure at the diffuser system exit. An ejector driven by heated gaseous nitrogen was placed downstream of the diffuser to ensure that the discharge total pressure at the system exit is greater than or equal to the ambient pressure.

Diffuser/Ejector Configuration. A heated gaseous nitrogen ejector augmented diffuser assembly was used to provide the simulated altitude for the high expansion ratio nozzle testing (ϵ = 400:1). Figure 81 shows the diffuser/ejector assembly with the cylindrical capsule section included for the 400:1 nozzle assembly testing. A facility schematic showing the locations of diffuser and ejector pressure measurements, P, is shown in Fig. 82.

Prior to hot-fire test of the nozzle assemblies, the mating sleeve installed inside the diffuser section was properly aligned with the nozzle exit to ensure proper diffuser action and to ensure that no interference would occur during test due to thermal expansion of either the staged combustion system assemblies or the diffuser assembly.

Ejector Operation. Gaseous nitrogen was supplied to the ejector nozzle from two 13.25m^3 (3500 gallon) bottles at an initial pressure of approximately 2000 N/cm^2 (2900 psig) through a multipass tube heater (Fig. 83 through 85), which heated the gas to a temperature of 810 K to 865 K (1000 F to 1100 F) pretest. Heated gaseous nitrogen blowdowns were required to establish the operating pressure requirements and capacities of the ejector system. The design requirements showed that 41 kg/s (90 lb/sec) gaseous nitrogen was required to draw the internal pressure down to 7.6 N/cm^2-a (11 psia), the required pressure for nozzle full-flow starting. The blowdowns established the time required to achieve this capsule starting pressure and the duration of operation at this pressure which established the thrust chamber operating duration and the sequence-start delay margin.

The blowdown tests were conducted with various quantities of air flowing into the diffuser inlet to simulate the rocket nozzle exhaust gases. Air entered the two opened altitude capsule entry ports during the first blowdown (test 017) to permit approximately 48 kg/sec (106 lb/sec) of air to flow. During the second blowdown, the ports were closed and no air flowed; during the third blowdown only one port was opened to permit approximately 27 kg/sec (60 lb/sec) of air to flow. For the last two tests the altitude capsule cylindrical section was removed to allow unimpeded entry of air into the diffuser and the air flow was approximately 134 kg/sec (295 lb/sec). The diffuser/ejector blowdown test results are summarized in Tables 17 and 18. The calculated GN_2 flowrates and measured ejector GN_2 temperatures during these blowdown tests are shown in Fig. 86 and 87 .

Instrumentation

Test parameters from the hot-fire testing were measured by a variety of transducer types, converted to a digital form by a Beckman 210 data acquisition system and forwarded to a central recording location for recording

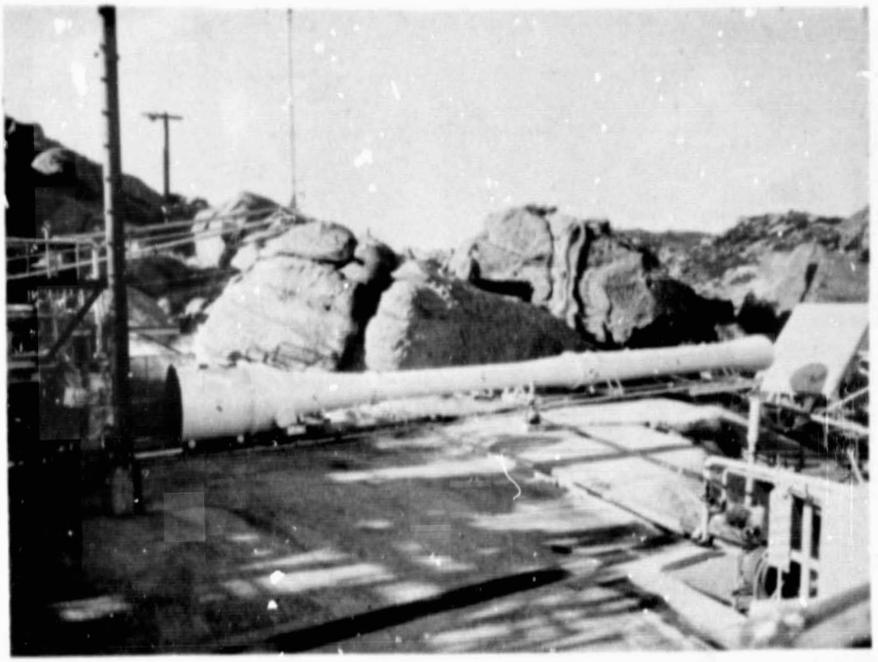

1H34-11/17/75-S1B*

Figure 81. Altitude Test Facility

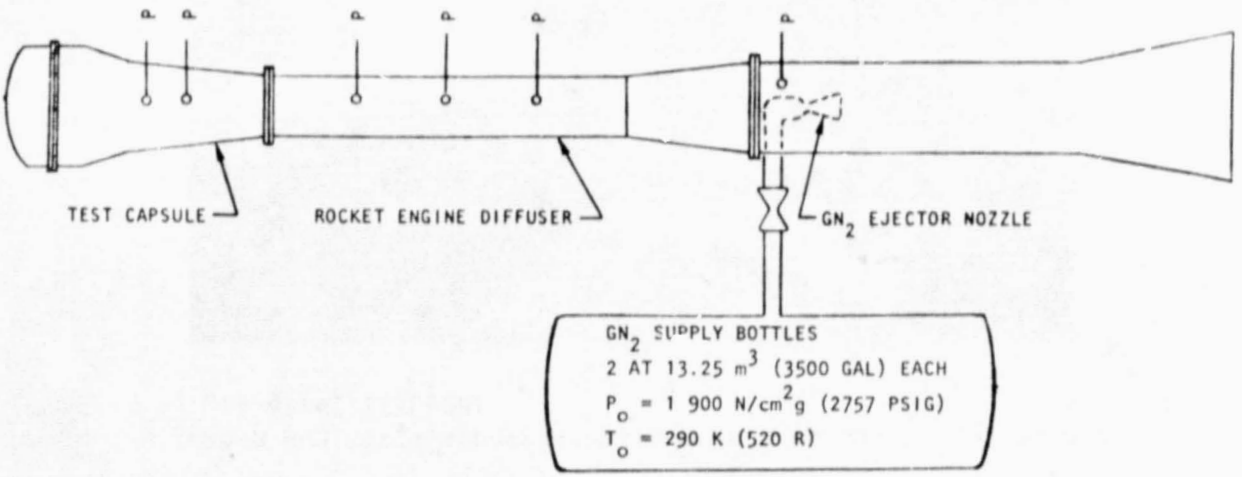

Figure 82. ASE Altitude Test Facility

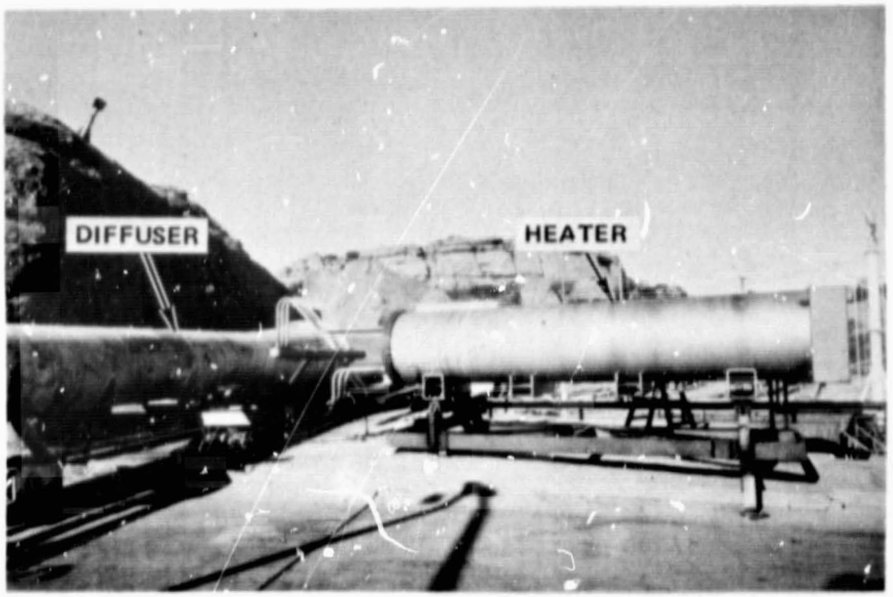

1HS63-11/16/76-S1A

Figure 83. Altitude System Diffuser and Ejector Gas Heater

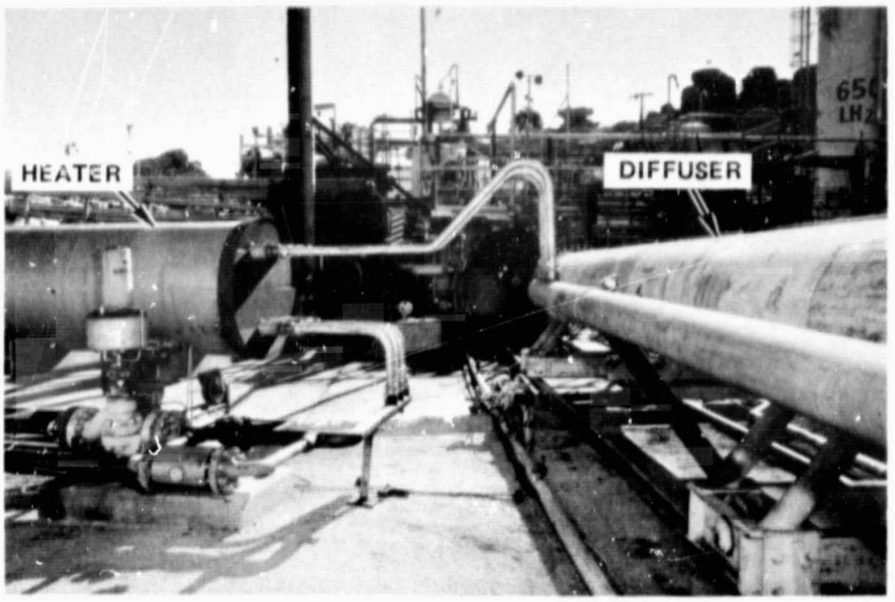

1HS63-11/16/76-S1C

Figure 84. Altitude System Diffuser and Ejector Gas Heater

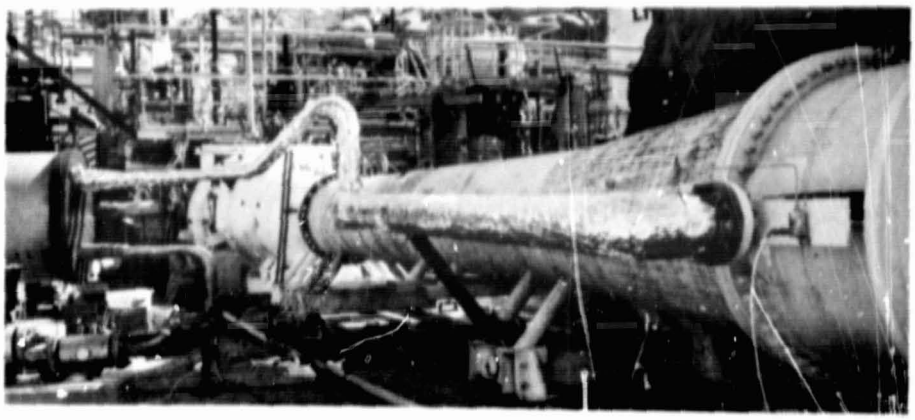

1HS63-2/9/77-S

Figure 85. Combustion Chamber Coolant Side Thermocouple Installation

TABLE 17. DIFFUSER/EJECTOR BLOWDOWN TEST CONDITIONS SUMMARY

	Blowdown Test No.*				
	017	019	021	022	023**
Gaseous Nitrogen Initial Pressure, N/cm^2 (psig)	1980 (2873)	1997 (2897)	1988 (2883)	1980 (2872)	1900 (2756)
Gaseous Nitrogen Initial Temperautre, K (F)	287.1 (56.8)	288.3 (58.9)	290.6 (63.1)	295 (71)	299 (78)
Heater Initial Temperature, K (F)	867 (1100)	867 (1100)	810 (1000)	810 (1000)	810 (1000)
Ejector Maximum Pressure, N/cm^2 (psig)	385 (559)	391 (567)	382 (554)	384 (557)	374 (542)
Ejector Maximum Gaseous Nitrogen Temperature, K (F)	DNR	637 (686)	609 (636)	602 (624)	631 (675)

*Not related to hot-fire test numbers

**Gaseous nitrogen valve cycled for 1 second pretest. All other tests used low-level purge for preheating downstream piping.

TABLE 18. DIFFUSER/EJECTOR BLOWDOWN SUMMARY

Five Blowdowns		
Ejector Operation:		
Maximum GN_2 Temperature, K (F)	=	637 (686)
Maximum GN_2 Pressure, N/cm^2 (psig)	=	391 (567)
Test Durations, s	=	9 to 30
GN_2 Flowrate, kg/s (lb/sec)	=	43 to 44 (95 to 98)
Diffuser Operation		
Minimum "Throat" Pressure N/cm^2 (psig)	=	-3.28 (-4.76)
Minimum Capsule Pressure N/cm^2 (psig)	=	-3.23 (-4.68)
Air Flowrates, kg/s (lb/sec)	=	0, 27, 48, 134 (0, 60, 106, 295)

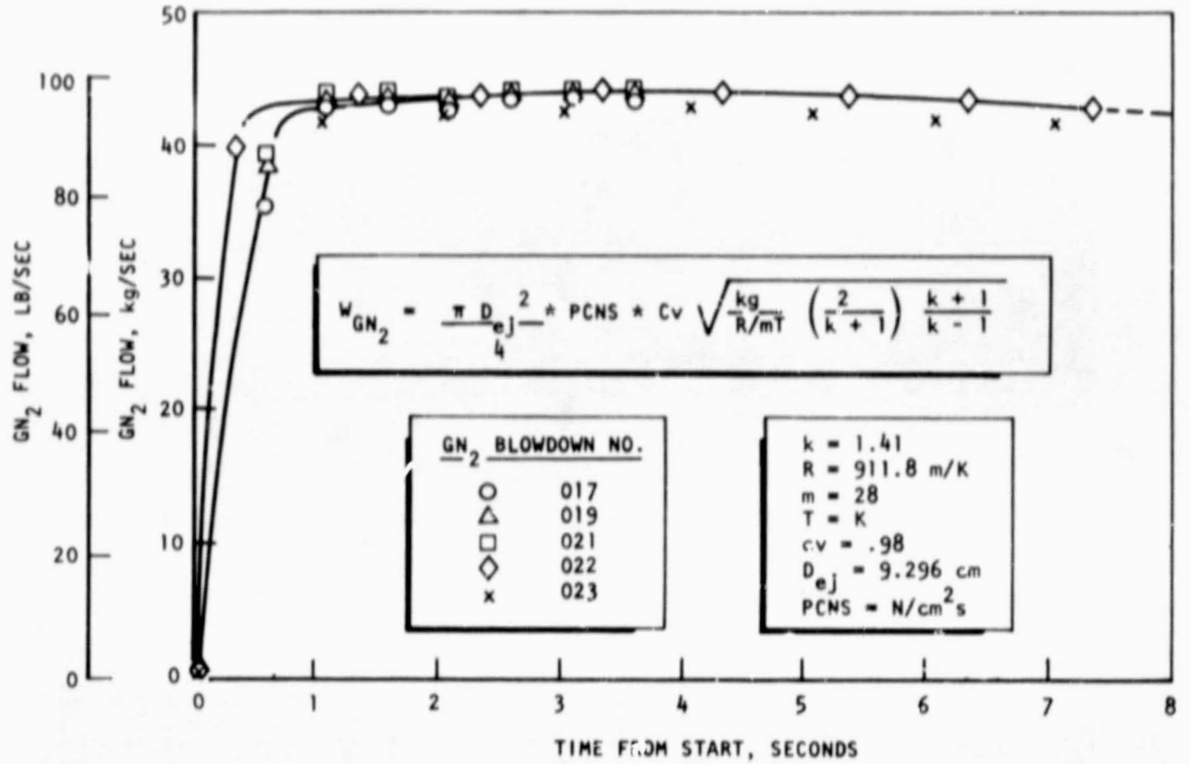

Figure 86. GN_2 Flowrate to Ejector Nozzle vs Flow Time Determined From Sonic Flow Through Ejector Throat

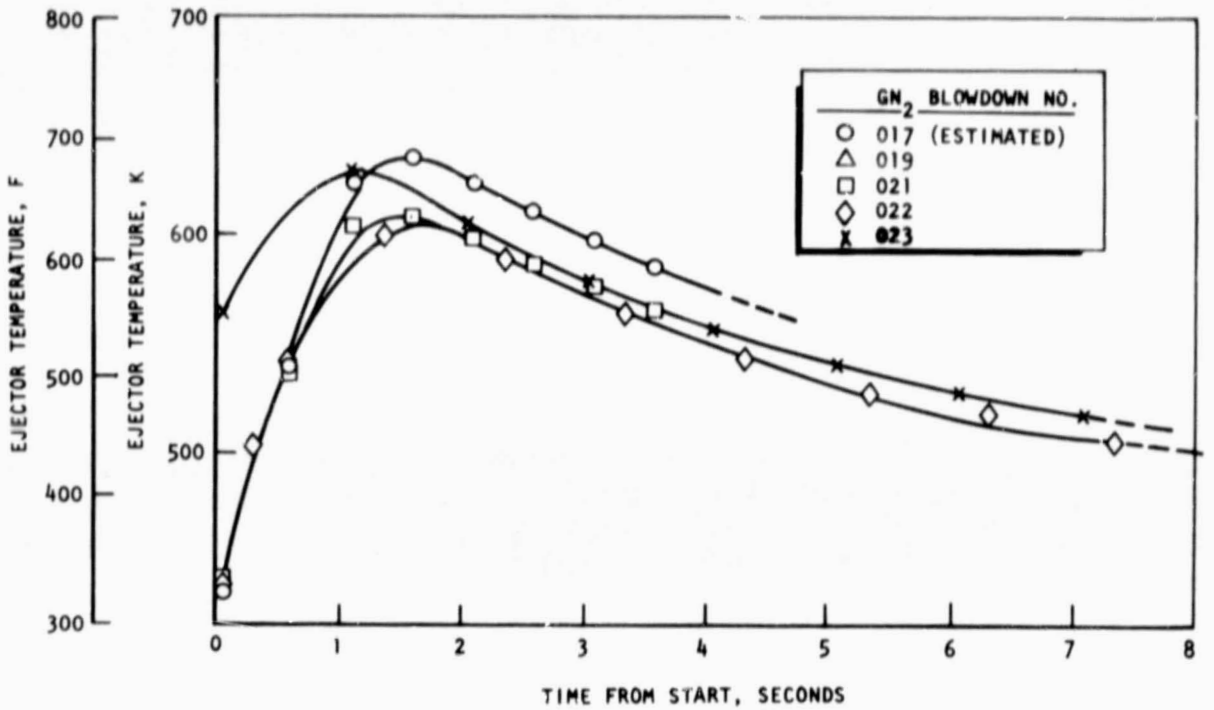

Figure 87. Ejector GN_2 Temperature vs Time From Start

and storing on magnetic tape. The data were then "sliced" and "scaled" at the computing center. The slicing operation consisted of averaging the discrete digitalized outputs of each parameter over a brief time interval selected by the data analyst, usually 200 milliseconds, throughout the test. Each parameter was then scaled by applying the appropriate pretest or posttest zero and calibration span factor to convert the Beckman 210 digital output into the desired engineering units. This result was then printed out in columnar form so that for each time interval (slice) the averaged value of each measured parameter, in the appropriate engineering units, was listed. In addition, CRT (cathode ray tube) printouts of each data point, in engineering units, over the total duration of each test were obtained to provide analog traces of each parameter. These data were then utilized in the performance, thermal, and aerodynamics analysis activities. The data acquisition and analysis flow diagram (Fig. 88) shows these steps in block form.

The Beckman digitalizer system has a capacity of 100 channels of pressure, temperature, and thrust, plus five channels of high level output suitable for recording turbine flowmeter output and valve position indications. The basic allocation of these 105 channels with a note regarding its use or need in the data analysis process is given in Table 19. Changes from the basic list were made from time to time to provide additional measurements of different aspects of the test program. For example, during early testing of the 400:1 nozzle, some preburner and thrust chamber parameters were deleted to provide additional diffuser and ejector measurements. In later testing these measurements were eliminated and more nozzle wall pressure and exit boundary layer measurements were made.

The thermocouples used to measure combustion chamber rib temperatures were a special assembly provided by NASA/LeRC for this testing. The Thermocouples were made of chromel and constantan wire with a silver ball melted onto the junction. The thermocouples were spring loaded into the 0.50 mm (0.020 inch) holes drilled into the copper alloy chamber rib as shown in Fig. 89. The spring loading and the silver globule were intended to provide good contact with the copper wall and to minimize the contact resistance so that the copper wall temperature could be very closely measured. A helium purge was supplied individually to the chamber wall thermocouples and a helium blanket was introduced into the entire cavity surrounding the throat region. This inert atmosphere was intended to prevent liquifaction of air and to minimize surface oxidation at the point of contact.

Special pressure and temperature rakes (Fig. 90) were fabricated to measure boundary layer parameters at the exit of the 400:1 nozzle. The first pressure rake (Fig. 90), was fabricated from molybdenum -50 rhenium tubing to withstand the high exhaust gas temperatures. The first temperature rake was made with tungsten-5 rhenium/tungsten-26 rhenium thermocouples encased in molybdenum sheaths and welded together to form a single rake structure also shown in Fig. 90. The initial testing with these rakes demonstrated the need for greater structural support, and a new pressure rake utilizing the molybdenum-rhenium tubing, press-fit into drilled passages in a heavy CRES support was fabricated; individual thermocouple probes were inserted through the nozzle wall near the exit plane. The new boundary layer probes are shown in Fig. 91 and 92, and the installation on the 400:1 nozzle is shown in Fig. 93. These

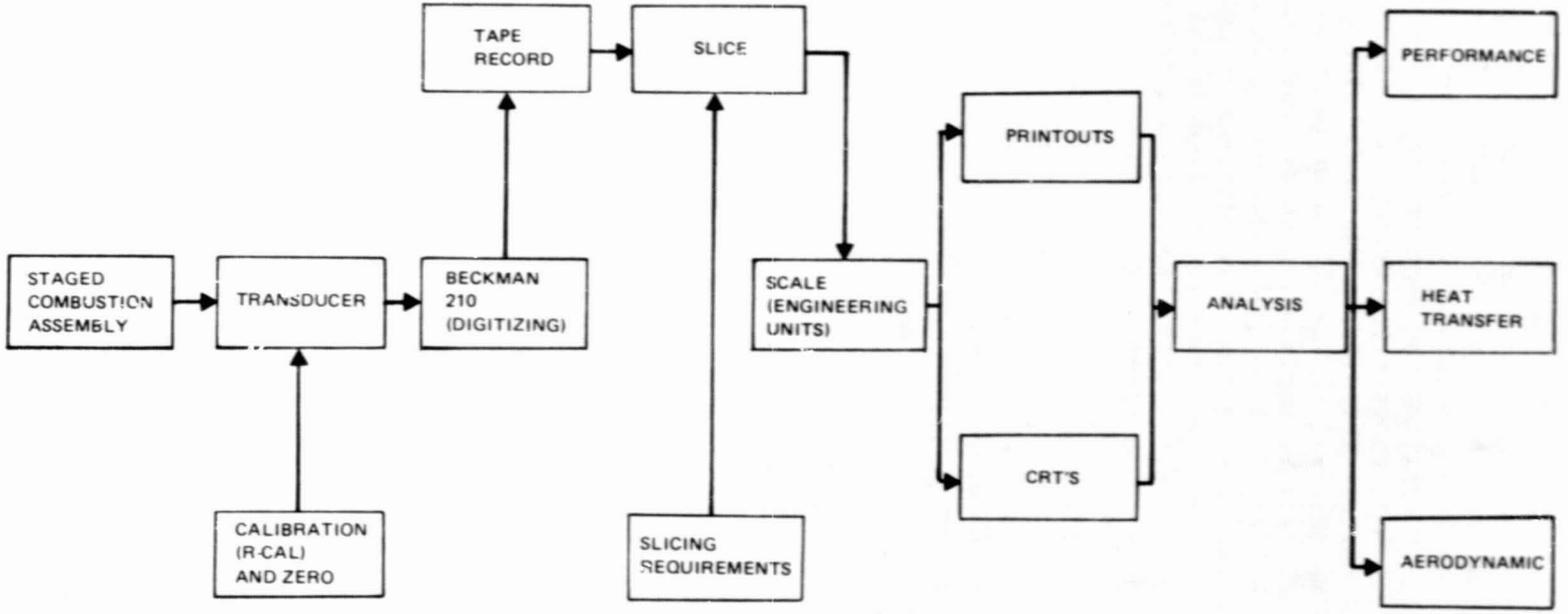

Figure 88. Data Acquisition Flow Diagram

TABLE 19. TESTING INSTRUMENTATION LIST

Beckman Channel	Type	System	Name	Function	Use
11	T-16	Preburner	TPBLHV	Preburner LH_2 Venturi Inlet Temperature	Preburner LH_2 Flow Measurement
12		Thrust Chamber	TNOZCIN	Nozzle Coolant Inlet Temperature	Nozzle Heat Flux
13		Diffuser	TGN$_2$ EJECTOR	Ejector GN_2 Temperature	Ejector Operation
14		Preburner	TPBFINJ	Preburner Fuel Injection Temperature	Preburner Performance
15		↓	TFV1	GH_2 Venturi Temperature	Preburner-GH_2 Flow Measurement
16		↓	TPB GH_2	GH_2 Temperature Upstream of Mixer, (used for face coolant and wall coolant)	Face Coolant and Wall Coolant Operation
17		Thrust Chamber	TC1OCAV	Igniter Oxidizer Cavity Temperature (thrust chamber)	Igniter Operation
18		Preburner	TS-1	Preburner Skin (wall) Temperature	Preburner Performance
19		Thrust Chamber	TCDCH	Main Chamber Coolant Discharge Temperature	Chamber Heat Flux
20		Preburner	TPP1OCAN	Igniger Oxidizer Cavity Temperature (preburner)	Igniter Operation
21	DP(16)	↓	FVDP	GH_2 Venturi Delta P	Preburner GH_2 Flow Measurement
22	DP(16)	↓	PPBODP	Oxidizer Venturi Delta P, Preburner	Preburner LOX Flow Measurement
23	T-40	Thrust Chamber	TCHIDET 1	Igniter Ignition Detect Temperature — Thrust Chamber 1,	Igniter Operation
24	↓	↓	2	↓ 2,	↓
25	↓	↓	3	↓ 3,	↓
26	↓	Preburner	TPBIDET 1	Igniter Ignition Detect Temperature — Preburner 1,	↓
27	↓	↓	2	↓ 2,	↓
28	↓	↓	3	↓ 3,	↓
29	↓	Thrust Chamber	TIC	Coolant Inlet Temperature	Thrust Chamber Coolant Heat Flux
30	↓	Preburner	TLHTIN 3	Fuel Turbine Inlet Temperature 3	Preburner Gas Temperature
31	↓	↓	TLOXTIN 1	LOX Turbine Inlet Temperature 1	↓
32	↓	↓	TLOXTIN 2	LOX Turbine Inlet Temperature 2	↓
33	↓	Thrust Chamber	TCHWALL 1	Combustion Chamber Wall (rib) Temperature 1	Thrust Chamber Wall Temperature

TABLE 19. (Continued)

Beckman Channel	Type	System	Name	Function	Use
34	T-40	Thrust Chamber	TCH WALL 2	Combustion Chamber Wall (rib) Temperature 2	Thrust Chamber Wall Temperatures
35		Preburner	TOPVB	Preburner Oxydizer Venturi Temperature	Preburner LOX Flow Measurement
36		Thrust Chamber	TNOZCOUT	Nozzle Coolant Outlet Temperature	Nozzle Heat Flux
37		Preburner Thrust Chamber	TCFM	LH_2 Flowmeter Temperature	LH_2 Total Flow Measurement
38		Preburner Thrust Chamber	TCTO	LH_2 Tank Outlet Temperature	LH_2 Operation
39		Thrust Chamber	T OCH INJ	LOX Injection Temperature Main Chamber	Thrust Chamber Operation LOX Leak Detect
40		Preburner Thrust Chamber	TOFM	LOX Flowmeter Temperature	LOX Total Flow Measurement
41	T-16	Preburner Thrust Chamber	TiFOUS	Igniter Fuel Orifice Upstream Temperature	Igniter Fuel Flow Measurement
42	T-16	Preburner Thrust Chamber	TIOOUS	Igniter Oxidizer Orifice Upstream Temperature	Igniter Oxidizer Flow Measurement
43	V-16	Test	PSM(LIMA		Instrumentation Troubleshoot
44	T-16		RJT(LIMA)		Thermocouple Reference Junction
45	T-16		RJT(NAN)		Thermocouple Reference Junction
46	V-16		PSM(NAN)		Instrumentation Troubleshoot
47	T-40	Thrust Chamber	T CH WALL 3	Combustion Chamber Wall (rib) Temperature 3	Thrust Chamber Wall Temperatures
48			T CH WALL 4	4	
49			T CH WALL 5	5	
50			T CH WALL 6	6	
51			TFCHIN 2	Main Chamber Fuel (Preburner Gas) Injection Temperature 2	Thrust Combustion Operation
52		Preburner	TLHTiN 2	Fuel Turbine Inlet Temperature 2	Preburner Gas Temperature
53		Thrust Chamber	TRAKE 1	Nozzle Exit Boundary Layer Temperature 1	Nozzle Performance
54			TRAKE 2	2	
55			TRAKE 3	3	
56			TRAKE 4	4	
57			TRAKE 5	5	

TABLE 19. (Continued)

Beckman Channel	Type	System	Name	Function	Use
58	T-40	Thrust Chamber	TFCHIN 1	Main Chamber Fuel (preburner gas) Injection Temperature	Thrust Chamber Operation
59	No RCal		PRAKE 1	Nozzle Exit Boundary Layer Pressure 1	Nozzle Performance
60			PRAKE 2	2	
61		Preburner Thrust Chamber	PRAKE 3	3	
62		Thrust Chamber	PRAKE 4	4	
63		Preburner Thrust Chamber	PRAKE 5	5	
64		Thrust Chamber	PRAKE 6	6	
65	T-40	Preburner	TOPBINJ	Preburner LOX Injection Temperature	Preburner Operation
66			TLOXTIN 3	LOX Turbine Inlet Temperature 3	Preburner Gas Temperature
67			TLHTIN 1	Fuel Turbine Inlet Temperature 1	Preburner Gas Temperature
68		Thrust Chamber	TNOZ 1	Nozzle Temperature 1	400: 1 Nozzle Heat Transfer
69			TNOZ 2	2	
70			TNOZ 3	3	
71	P		PFCHIN 1	Main Chamber Fuel (preburner gas) Injection Pressure 1	Thrust Chamber Injector Operation
72	P	Test-Diffuser	P GN_2BOT BANK	GN_2 Supply Pressure	GH_2 Supply to Ejector
73	F	Test Chamber	THRUST B	Thrust, B Bridge	Thrust Chamber Thrust
74	P		PFCHIN 2	Main Chamber Fuel (preburner gas) Injection Pressure 2	Thrust Chamber Injector Operation
75			PIC	Coolant Inlet Pressure, Thrust Chamber	Thrust Chamber Coolant Operation
76			P NOZ E 1	400:1 Nozzle Static Pressure 1	Nozzle Performance
77		Preburner Thrust Chamber	PPBIOOUS	Igniter Oxidizer Orifice Upstream Pressure	Igniter Oxidizer Flow Measurement
78		Preburner	PPBWCOUS	Preburner Wall Coolant Orifice Upstream Pressure	Preburner Wall Coolant Flow Measurement

TABLE 19. (Continued)

Beckman Channel	Type	System	Name	Function	Use
79	P	Preburner Thrust Chamber	PPBIFOUS	Igniter Fuel Orifice Upstream Pressure	Igniter Fuel Flow Measurement
80		Thrust Chamber	PNOZ E 2	400:1 Nozzle Static Pressure 2	Nozzle Performance
81		↓	PNOZ E 3	400:1 Nozzle Static Pressure 3	Nozzle Performance
82		Preburner	PCPB 1	Preburner Chamber Pressure	Preburner Chamber Pressure
83		Thrust Chamber	P FACE C	Main Injector Face Coolant Injection Pressure	Thrust Chamber Operation - Face Coolant Flow
84		Thrust Chamber	PDC	Combustion Chamber Coolant Discharge Pressure	Thrust Chamber Coolant Operation
85		Preburner Thrust Chamber	PCAP 1	Capsule Pressure	Thrust Correction Measurement
86		↓	↓ 2	↓	↓
87		↓	↓ 3	↓	↓
88		Thrust Chamber	PNOZCIN	Nozzle (175:1) Coolant Inlet Pressure	Nozzle Coolant Operation
89		Diffuser	PDIFF 1	Diffuser Pressure	Diffuser Operation
90		↓	↓ 2	↓	↓
91		↓	↓ 3	↓	↓
92		Thrust Chamber	PNOZ E 4	400:1 Nozzle Static Pressure 4	Nozzle Performance
93		Diffuser	PGN_2 EJECTOR	GN_2 Ejector Inlet Pressure	Diffuser Operation-Ejector GN_2 Flow Measurement
94		Thrust Chamber	PNOZCOUT	Nozzle Coolant Outlet Pressure	Nozzle Coolant Operation
95		Thrust Chamber	POCHIN	LOX Injection Pressure Main Chamber	Thrust Chamber Operation
96		Preburner	PPBWCODS	Preburner Wall Coolant Orifice Downstream Pressure	Preburner Wall Coolant Flow Measurement
97		Thrust Chamber	PC 1	Chamber Pressure Main Chamber	Thrust Chamber Pressure
98	↓	Test	P3KHYD	Hydraulic System Pressure	Facility Operation (2500 psi hydraulics)

TABLE 19. (Concluded)

Beckman Channel	Type	System	Name	Function	Use
99	P	Preburner Thrust Chamber	PTO (TK 206)	LOX Tank Pressure	Test Setup, LOX Tank Set Pressure
100		Preburner Thrust Chamber	PTC	LH_2 Tank Pressure	Test Setup, LH_2 Tank Set Pressure
101		Preburner	PPBLHVUS	Preburner LH_2 Venturi Upstream Pressure	Preburner LH_2 Flow Measurement
102			PFVUS	GH_2 Venturi Upstream, Pressure	Preburner GH_2 Flow Measurement
103	DP		PPBLHVDP	Preburner LH_2 (to mixer) Delta P	Preburner LH_2 Flow Measurement
104	P	Preburner Thrust Chamber	PLGH 2	GH_2 Line (Regulated) Pressure	Test Setup, GH_2 Set Pressure
105	P	Preburner Thrust Chamber	PPBOVU/S	Preburner LOX Venturi Upstream Pressure	Preburner LOX Flow Measurement
106	F	Thrust Chamber	THRUST A	Thrust, A Bridge	Thrust Chamber Thrust
107	P	Thrust Chamber	PC_2	Chamber Pressure, Main Chamber	Thrust Chamber Pressure, Backup
108		Test	P2KHYD	Hydraulic System Pressure	Facility Operation (200 psi) Hydraulics
109		Preburner	PFPBIN	Preburner Fuel Injection Pressure	Preburner Fuel Operation
110		Preburner	POPBIN	Preburner LOX Injection Pressure	Preburner LOX Operation
111	FL	Preburner Thrust Chamber	WOX	LOX Flowmeter	LOX Total Flow Measurement
112	FL	Preburner Thrust Chamber	WLH_2	LH_2 Flowmeter	LH_2 Total Flow Measurement
113	V	Thrust Chamber	POSTCLV	Thrust Chamber LOX Valve Position Indicator	Thrust Chamber LOX Valve Operation
114	V	Preburner	POSPBLV	Preburner LOX Valve Position Indicator	Preburner LOX Valve Operation
115					

NOTE: Test = Facility Requirement

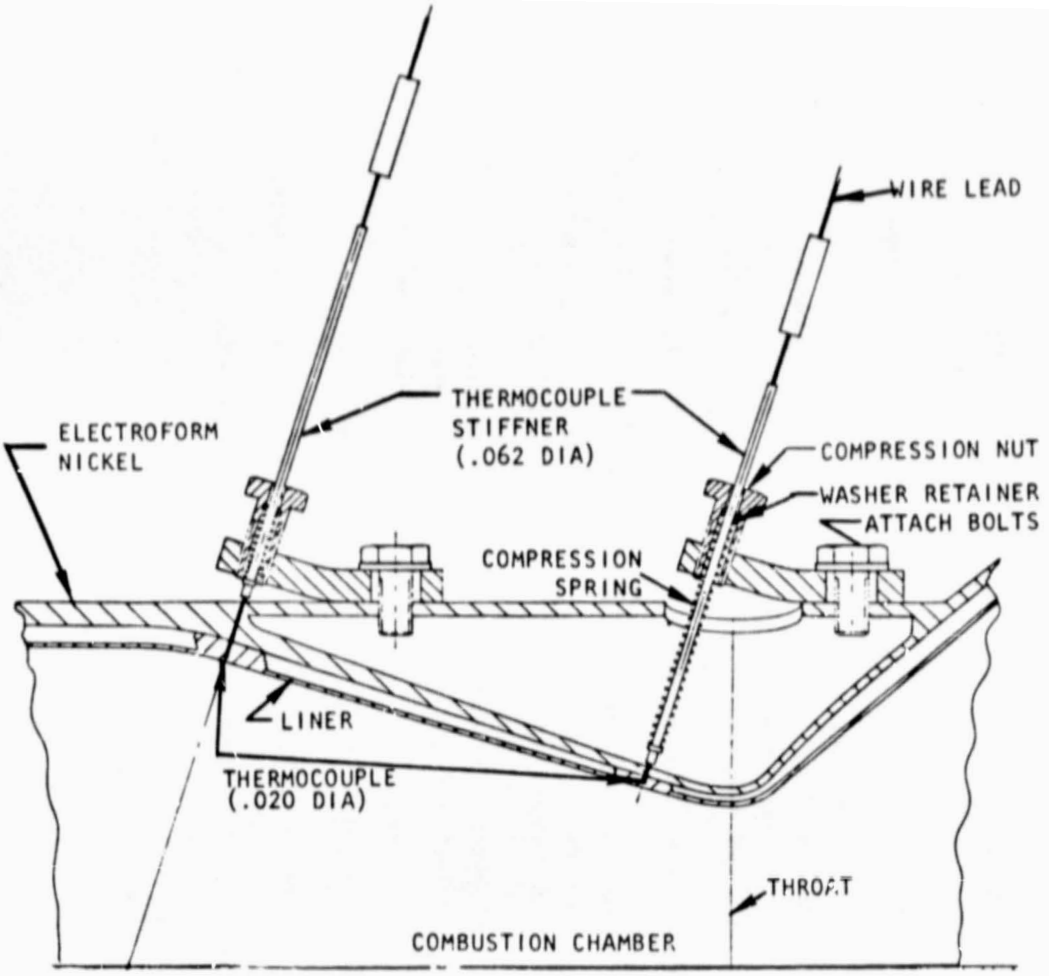

Figure 89. Combustion Chamber Coolant Side Thermocouple Installation

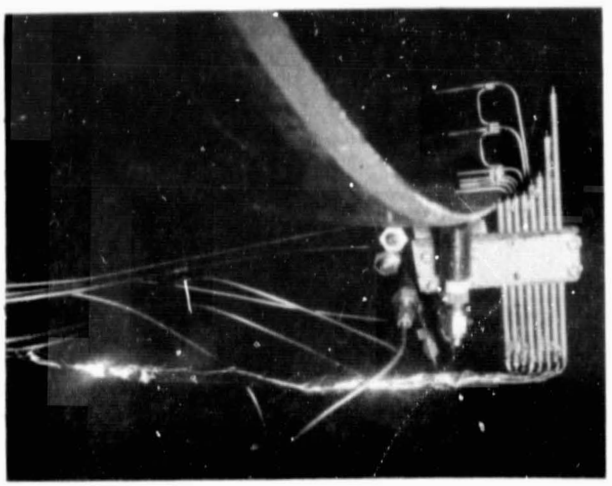

1HS63-5/10/77-S2*

Figure 90. Boundary Layer Pressure and Temperature Rakes

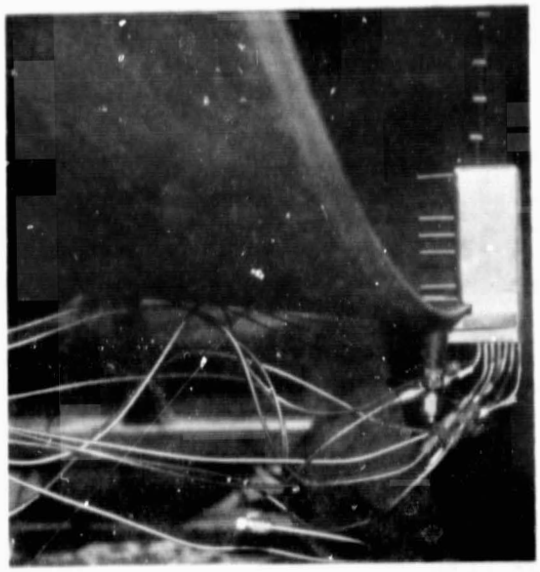

1HS34-10/13/77-S1A*

Figure 91. Improved Boundary Layer Pressure Rake Installed

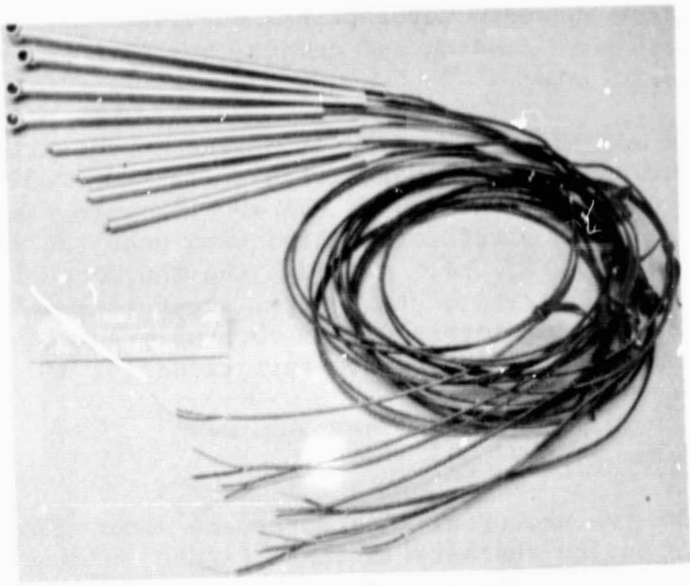

1HS62-10/5/77-C1*

Figure 92. Improved Boundary Layer Temperature Rakes

1HS34-10/13/77-S1B*

Figure 93. Boundary Layer Temperature Measurement Rakes Installed

later boundary layer probes survived the last series of four hot-fire tests with some erosion and damage, but with greater durability than had been anticipated.

An additional measurement of the regeneratively cooled nozzle tube wall temperature was attempted with a 1.59 mm (0.0625 inch) thermocouple fed through a pressure tap boss on the 400:1 nozzle, laid along the nozzle wire contour and tack welded to the A286 tube near the downstream turnaround manifold as shown in Fig. 94. Although the thermocouple sheath was held in place with several strips of thin metal sheet tack welded to the heavier sections of the nozzle, completely within the fully developed boundary layer, it was ripped loose during the first start transient and no measurements of wall temperature were obtained.

Water Flow

The two preburner injectors were water-flow tested to evaluate the flow distribution characteristics. Figure 95 is a diagrammatic representation of the preburner face and shows the numbering or the injection elements with respect to the fuel and oxidizer inlets. Results of the flow tests are detailed in Tables 20 and 21. While the flow distribution is not completely uniform, there is not a discernible pattern related to the inlet manifolds, and the flow variation from element-to-element was within acceptable limits. The one exception was the flow through the fuel side of element 2-1 of injector No. 2. This flow was 15% above the average. Inspection of this element divulged no discrepancies. While the flow through the fuel side of both injectors showed a greater variation, this flow was much more difficult to capture than the flow through the oxidizer side and there is, consequently, a greater uncertainty regarding each data point. The experimental difficulty was manifested by the very complete dispersal of the effluent water while trying to capture the fuel-side flows from the inner row elements, and the attempts were abandoned. The overall flow based on averaging the individual element flows, however, compared favorably and both injectors were accepted; injector No. 1 was chosen for initial testing.

Oxidizer Valve

The two servocontrolled LOX ball valves were tested in the laboratory prior to delivery and installation onto the staged combustion assembly. The purpose of the laboratory tests was to determine the shaft and seal leakages, valve hydraulic resistence, and actuation pressure requirements. The two valves were similar and used similar components except for the differences in ball diameters and related details. The injector LOX valve uses a 2.54 cm (1.0 inch) diameter spherical ball with a 1.27 cm (0.5 inch) diameter flow passage while the preburner LOX valve uses a 1.587 cm (0.625 inch) diameter spherical ball with a 0.762 cm (0.300 inch) diameter flow passage.

The valves were subjected to ball seal leakage and shaft seal leakage tests after actuation at inlet pressures varied from ambient pressure to 2750 N/cm^2 (4000 psi) and ambient and LN_2 temperatures, following cyclic activation. The preburner LOX valve was actuated in excess of 850 cycles, and the main

Figure 94. Nozzle Tube Wall Temperature Measurement

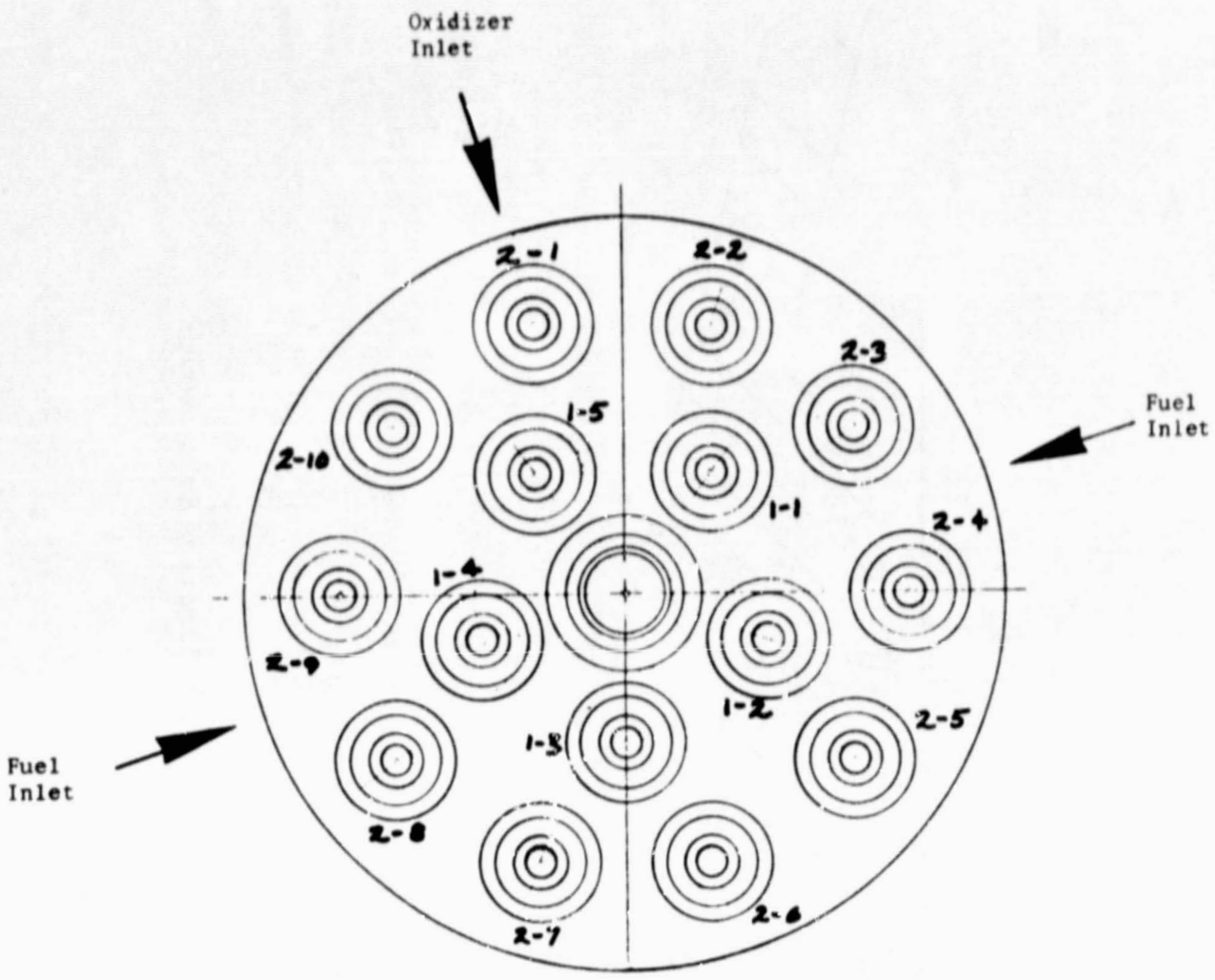

Figure 95. ASE Preburner Injector Face

TABLE 20. PREBURNER INJECTOR NO. 1

Oxidizer Flow = 30 ± 1 cps = .379 ± .020 kg/sec (.835 ± .043 lb/sec) = 378.9 ± 12.5 ml/sec

ΔP = 17-18 N/cm² (25-26 psi)

Fuel Flow = 100 ± 1cps = 1.246 ± .020 kg/sec (2.746 ± .043 lb/sec) = 1246 ± 12.5 ml/sec

ΔP = 1.4 N/cm² (2 psi)

Orifice Number	Oxidizer				Fuel			
	Time Sec	Sample ml	Flow ml/sec	Notes	Time Sec	Sample ml	Flow ml/sec	Notes
1-1	60.1	1470	24.46		-	-	-	
1-2	60.0	1525	25.42		-	-	-	
1-3	60.0	1450	24.17		-	-	-	
1-4	60.0	1525	25.42		-	-	-	
1-5	60.0	1500	25.00		-	-	-	
Average			24.894				-	
2-1	60.0	1500	25.00		18.5	1560	84.32	
2-2	60.0	1460	24.33		18.7	1600	85.56	
2-3	60.4	1470	24.34		20.0	1580	79.00	
2-4	60.2	1470	24.42		20.0	1560	78.00	
2-5	60.0	1460	24.33		18.0	1570	87.22	
2-6	59.9	1465	24.46		20.0	1580	79.00	
2-7	60.0	1505	25.08		19.4	1560	80.41	
2-8	60.0	1450	24.17		20.0	1590	79.50	
2-9	60.0	1485	24.75		20.0	1600	80.00	
2-10	60.0	1430	23.83	Flow Slightly Low	20.5	1590	77.56	
Average			24.471				81.057	1215.9 ml/sec overall
Overall Average			24.612	369.2 ml/sec overall				

Max/Min = 25.42/23.83 = 103.3%/96.8% = 87.22/77.56 = 107.6/95.7

TABLE 21. PREBURNER INJECTOR NO. 2

Oxidizer Flow = 30 ± 1 cps = .379 ± .020 kg/sec (.835 ± .043 lb/sec) = 378.9 ± 12.5 ml/sec

ΔP = 16-17 N/cm² (23-24 psi)

Fuel Flow = 100 ± 1 cps = 1.246 ± .020 kg/sec (2.746 ± .045 lb/sec) = 1246 ± 12.5 ml/sec

ΔP = 2 N/cm² (3 psi)

Orifice Number	Oxidizer				Fuel			
	Time Sec	Sample ml	Flow ml/sec	Notes	Time Sec	Sample ml	Flow ml/sec	Notes
1-1	60.0	1490	24.83		-	-	-	
1-2	60.0	1445+	24.08		-	-	-	
1-3	60.0	1460	24.33		-	-	-	
1-4	60.0	1440	24.00	A little was spilled	-	-	-	
1-5	60.0	1460	24.33					
Average			24.314				-	
2-1	60.0	1490	24.83		14.0	1310	93.57	
2-2	60.0	1500	25.00		18.5	1590	85.95	
2-3	60.0	1455	24.25		18.5	1360	73.51	
2-4	60.1	1415	23.54		19.0	1420	74.74	
2-5	60.0	1475	24.58		18.0	1410	78.33	
2-6	60.0	1435	23.92		18.0	1470	81.67	
2-7	60.0	1535	25.58		18.2	1540	84.62	
2-8	60.2	1515	25.17		19.5	1480	76.41	
2-9	60.0	1460	24.33		18.7	1560	83.42	
2-10	60.0	1575	26.25	Slightly high flow	19.7	1600	81.22	
Average			24.745				81.34	1220 ml/sec overall
Overall Average			24.600	369 ml/sec overall				

Max/Min = 26.25/23.54 = 106.7 %/95.7%

= 93.57(85.95)/73.51 = 115.0 (105.7)%/90.4%

injector LOX valve was actuated in excess of 1000 cycles during these tests. Valve seal leakage, summarized in Table 22, was acceptable and shaft seal leakage was negligible under all conditions.

TABLE 22. LOX VALVE SEAL LEAKAGE TEST SUMMARY

	Test Temperature	Actuations	Maximum Seal Leakage, sccm	
			GN_2	Helium
Injector	Ambient	570	18	-
Valve	LN_2	450	-	172
	Total	1020		
Preburner	Ambient	424	82	-
Valve	LN_2	430	-	492
	Total	854		

The minimum valve actuation (hydraulic) pressure was also determined during these tests. Results are shown in Fig. 96 and 97. The test facility utilizes a 1380 N/cm^2g (2000 psig) hydraulic system so that both valves have an adequate operating margin at the nominal 2760 N/cm^2g (4000 psig) inlet pressure. The required actuation pressure at LN_2 temperature was greater than at ambient temperature, probably because of a changing friction coefficient which increases with decreasing temperature.

The valve was then flow tested with water to establish the valve flow resistence characteristics. Figure 98 shows the effective flow area of the injector valve and preburner valve as a function of valve ball rotation angle. Water flow versus differential pressure data for each valve are summarized in Table 23 which also tabulates the valve resistence determined for each valve from the relationship

$$\text{Resistance} = \frac{\rho \Delta P}{\dot{w}^2}$$

where

ρ = test fluid density
$\Delta\rho$ = valve pressure drop
$\dot{w}$ = test fluid flowrate

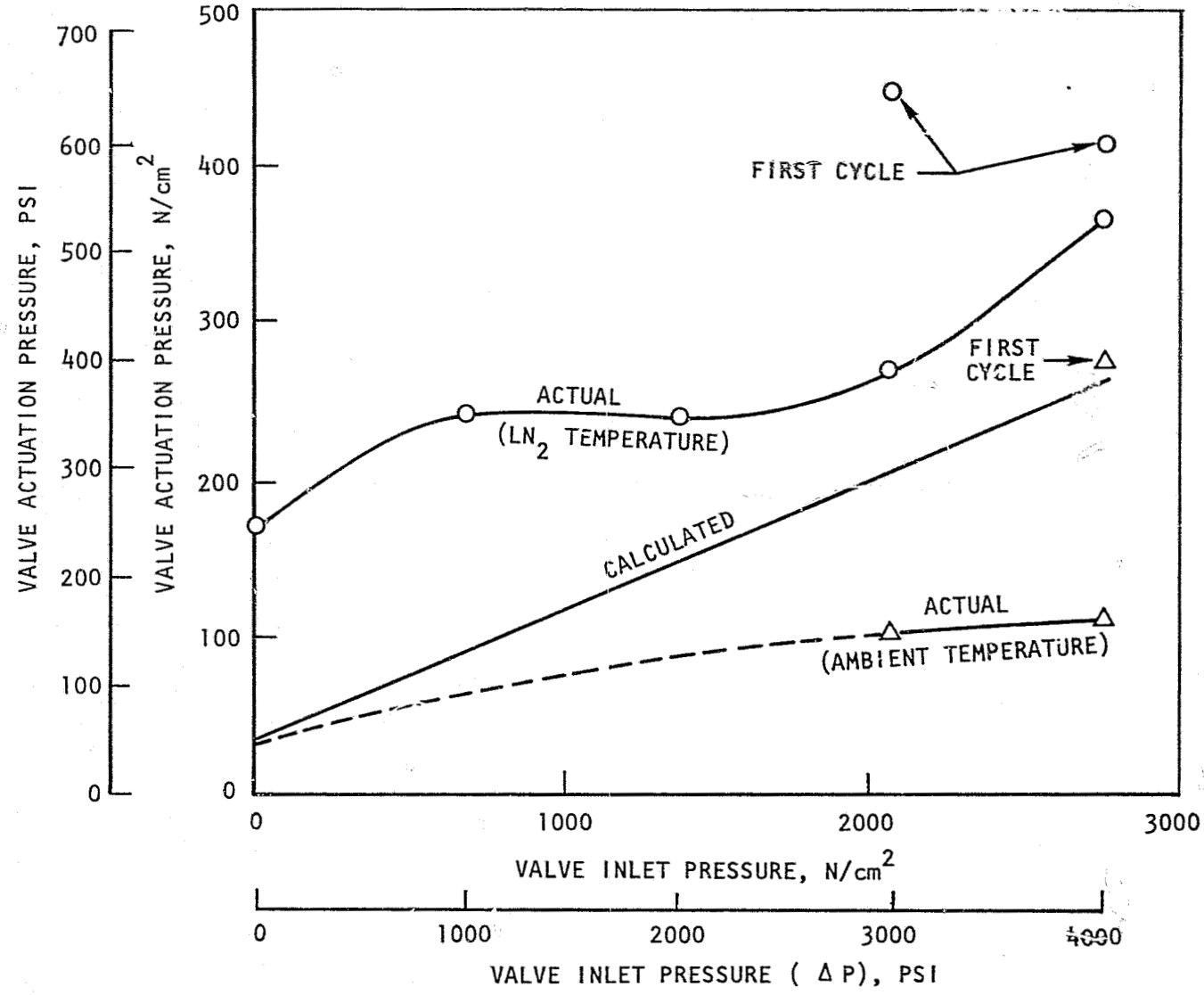

Figure 96. Injector LOX Valve Actuation Pressure Summary

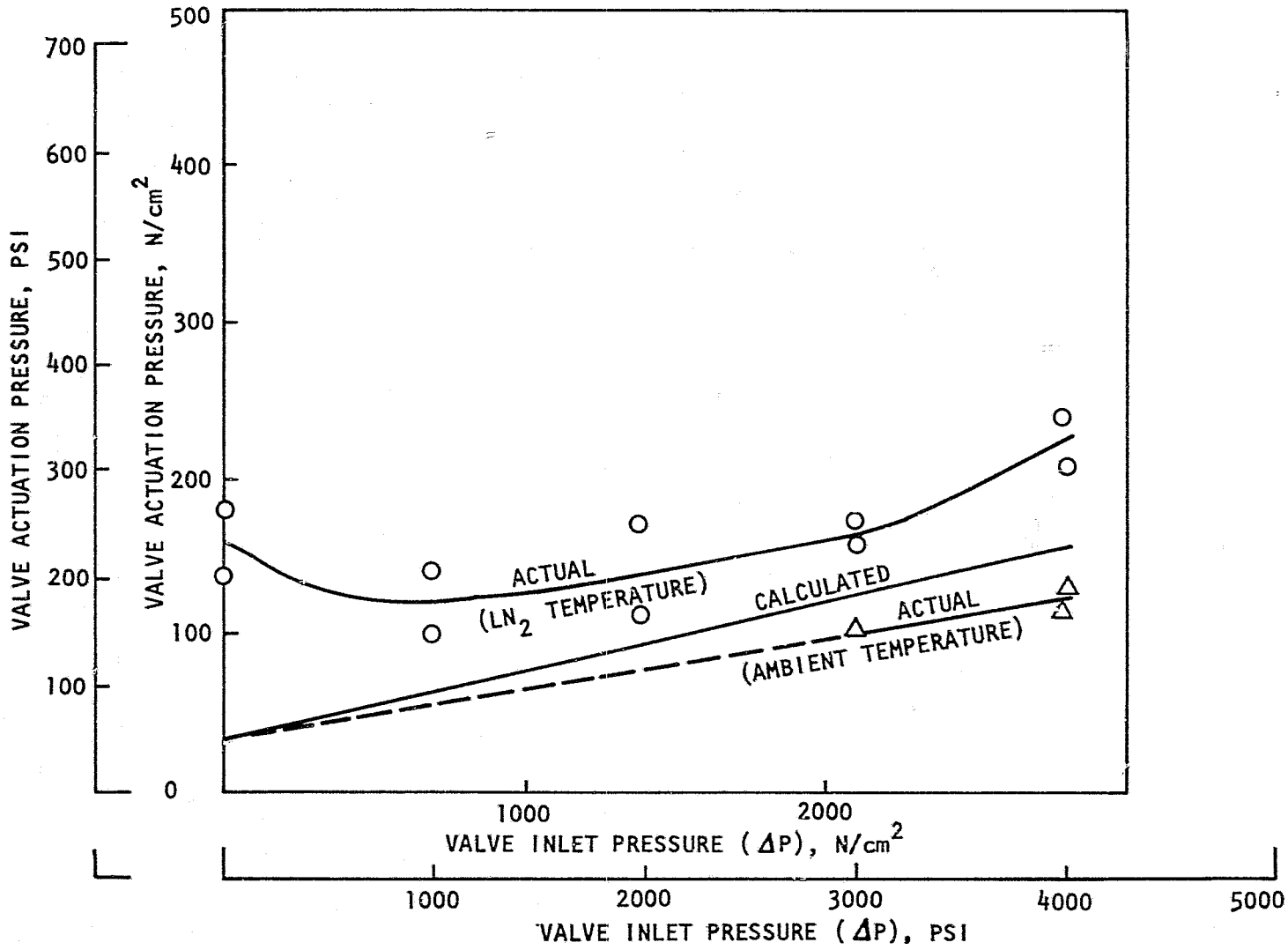

Figure 97. Preburner Valve Actuation Pressure Summary

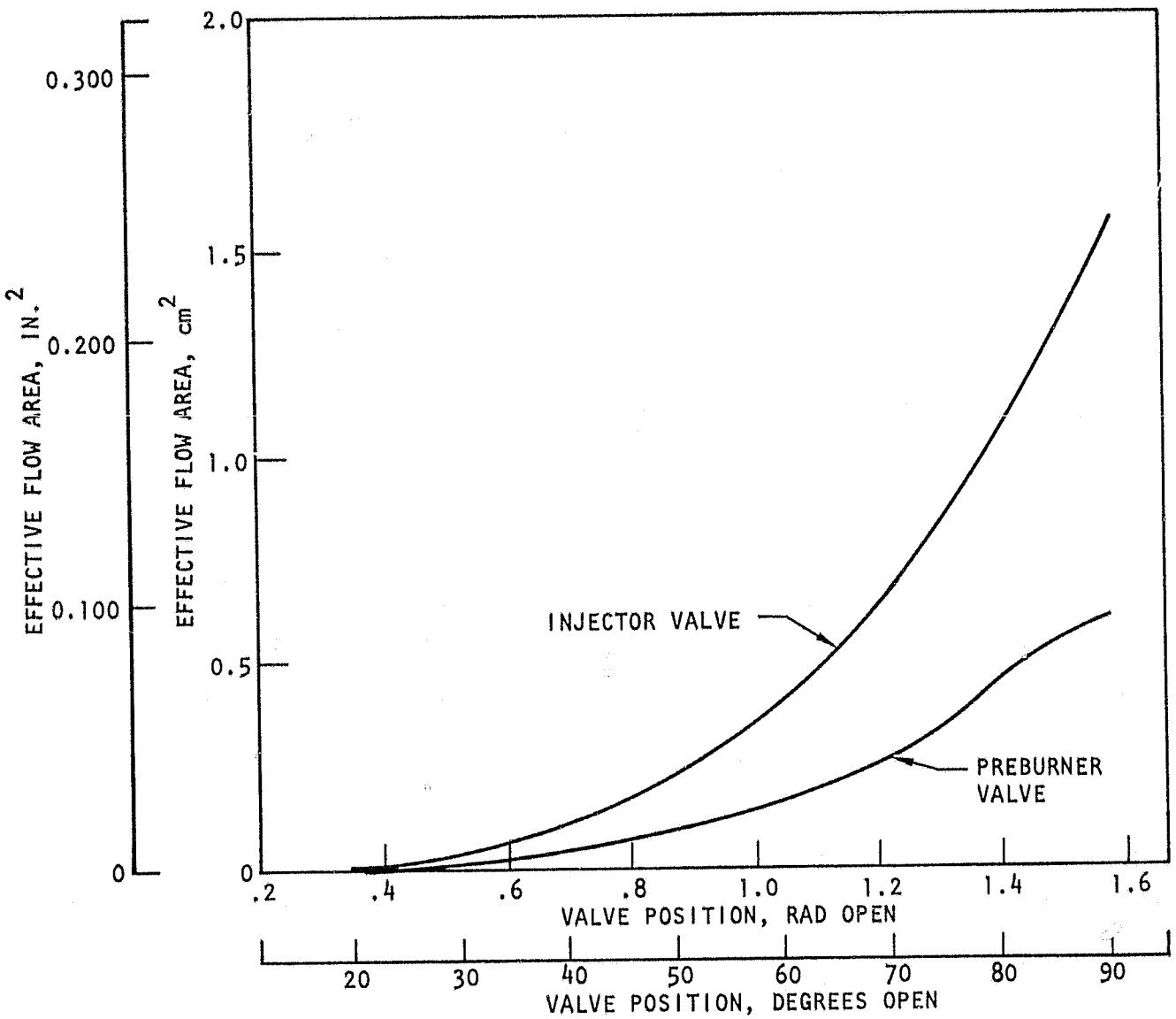

Figure 98. LOX Valve Flow Area vs Open Position

TABLE 23. LOX VALVE FLOW TEST SUMMARY

Valve	Valve Position, Degrees	Flowrate		Effective Open Area		Resistance	
		kg/s	lb/sec	cm^2	$in.^2$	sec^2/dm^2	$sec^2/ft^3\text{-}in.^2$
Injector	90	0.605	1.333	1.568	0.243	21.90	40
	80	0.416	0.917	1.077	0.167	45.16	82.5
	70	0.257	0.567	0.665	0.103	113.85	208
	60	0.152	0.334	0.394	0.061	315.29	576
	50	0.088	0.195	0.230	0.0356	994.04	1.816×10^3
	45	0.062	0.137	0.161	0.0250	1.961×10^3	3.583×10^3
	40	0.041	0.091	0.107	0.0166	4.579×10^3	8.365×10^3
	35	0.028	0.063	0.075	0.0116	11.107×10^3	20.291×10^3
	30	0.015	0.032	0.037	0.0058	35.910×10^3	65.603×10^3
	25	0.007	0.0155	0.018	0.0028	155.359×10^3	283.824×10^3
Preburner	90	0.234	0.516	0.608	0.0942	105.10	192
	80	0.178	0.392	0.459	0.0712	232.64	425
	70	0.104	0.230	0.271	0.042	846.79	1.547×10^3
	60	0.060	0.133	0.157	0.0243	3.208×10^3	5.860×10^3
	50	0.035	0.078	0.092	0.0142	24.109×10^3	44.045×10^3
	45	0.026	0.0575	0.068	0.0105	66.926×10^3	122.266×10^3
	40	0.019	0.042	0.049	0.0076	314.738×10^3	574.993×10^3
	35	0.015	0.032	0.037	0.0058	9.377×10^6	17.130×10^6
	30	0.011	0.024	0.029	0.0045	-	-
	25	0.007	0.016	0.019	0.0029	-	-
	20	0.003	0.007	0.008	0.0012	-	-

NOTE: Valve ($P = 76.2$ cm H_2O) (30 inches H_2O) for all tests

These resistance values were utilized in the system and facility flow balance computer programs to establish facility pressure losses, tank pressure requirements, and orificing requirements for the hot-fire testing phase of the program.

Preburner

The initial testing was undertaken with the preburner assembly and the thrust chamber simulator to minimize exposure of the main combustion chamber and injector during the preburner checkout testing. The installation of the preburner on the test stand with the thrust chamber simulator was made identical to the impending installation of preburner and the main combustion chamber so that no propellant lines or operational procedures needed to be changed for the later testing. Figure 99 shows the preburner and simulator during the installation on the test stand; clearly shown are the thrust chamber simulator in the center, the preburner, the hot gas ducting to the two turbine simulators, and the LH_2 pump turbine simulator to the left center and the oxidizer pump turbine simulator to the right of center. The entire assembly is mounted within the altitude capsule in preparation for the subsequent testing with the high area ratio nozzle.

Table 24 is a summary of the initial testing effort planned with the preburner and thrust chamber simulator. A minimum of six successful tests was projected as needed to verify the ignition operation, start sequence, system pressure drop, and flow characteristics.

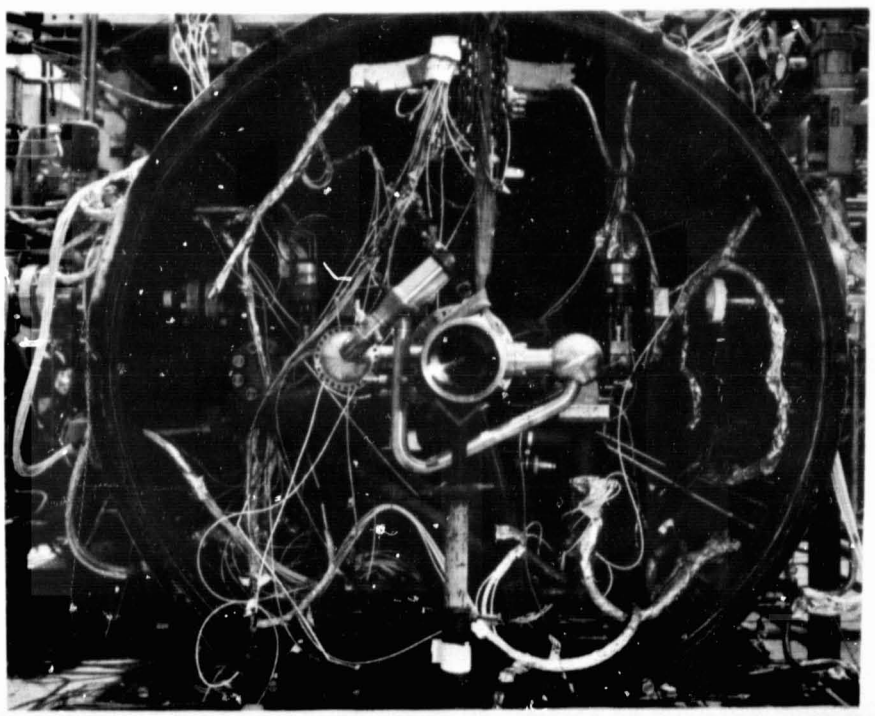

1HS53-7/9/76-S1H

Figure 99. Preburner Installation Nan Stand

TABLE 24. PREBURNER INJECTOR TEST SEQUENCE

Activities Pretest:

1. Install preburner assembly with injector simulator

Activities Posttest:

1. Remove fuel inlets from injector simulator for installation on injector

Potential Problems:

1. Off-design preburner operation instability
2. Igniter ignition-detect system

Hardware Configuration

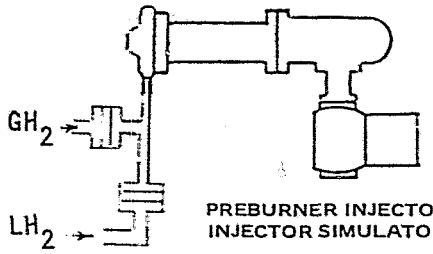

PREBURNER INJECTOR + PREBURNER BODY + INJECTOR SIMULATOR

Test Objectives:

1. Check out preburner injector and body
2. Establish test stand ΔP's and flow characteristics

Components												Test Program					
Main Injector		Combustor Chamber		Nozzle		Nozzle Extension		Preburner Injector		Preburner Body							
S/N	Fluid	S/N	Coolant	S/N	Coolant	S/N	Coolant	S/N	Propellant	S/N	Coolant	Tests	Chamber P_{c_b} N/cm^{2}a (psia)	Chamber MR (o/f)	Preburner P_{c_b} N/cm^{2}a (psia)	Preburner MR (o/f)	Comments
-	-	-	-	-	-	-	-	1	GH_2 and LH_2 + LOX	1	GH_2	6	-	-	- 690 - 2275 (1000 - 3300)	0.6 0.75	Igniter and preburner checkouts

A system flow balance for the preburner testing was performed using the test data obtained during the prior test program for system resistances. The results of this system balance are shown in Table 26. The target preburner chamber pressure was 2366 N/cm^{2}a (3432 psia) at a mixture ratio (o/f) of 0.650. The purpose of the system balance was to establish the proper orifice size and propellant tank pressures to achieve the target igniter and preburner operating points and to ensure that these tank pressures were within the limits of the test facility capabilities. Several iterations were required for each flow balance. The result shown in Table 26 is the final and satisfactory balance.

Testing was initiated as planned, with igniter checkouts as shown in the Test Log (Table 25). During an attempted preburner mainstage test (test No. 18) the oxidizer side of the injector burned out causing a delay in the program schedule.

The oxidizer manifold helium purge setting for this test was too low, and permitted the gaseous hydrogen from the fuel lead to back up into the oxidizer side of the injector. When the oxidizer valve was opened the incoming oxygen mixed with the fuel in the manifold, ignited and burned, and caused extensive damage to the injector face and manifolding, the igniter, and the oxidizer servocontrolled main valve. The purge system regulated (lockup) pressure had been set at a high level, but system restrictions and pressure losses resulted in a low pressure at the injector manifold which was unable to prevent hydrogen backflow into the injector.

TABLE 25. PREBURNER PROGRAM TEST LOG

Test No.	Date	Type
14	8-5-76	No ignition
15	8-5-76	Igniter only
16	8-12-76	Test cut
17	8-12-76	Igniter only
18	8-12-76	Oxidizer manifold fire and detonation
19	9-7-76	Igniter only - cut at GH_2 signal
20	9-7-76	Igniter + GH_2/LH_2 flow
21	9-7-76	No ignition - H_2 + LOX flow
22	9-9-76	No ignition - H_2 + LOX flow
23	9-13-76	No ignition
24	9-13-76	No ignition
25	9-16-76	Igniter only
26	9-16-76	Preburner test: P_c = approximately 1 second 1380 N/cm^{2}a (2000 psia)
27	9-17-76	Ignition detect cutoff
28	9-17-76	Preburner test: P_c = approximately 3 seconds 1380 N/cm^{2}a (2000 psia)
29	9-20-76	Preburner test: P_c = approximately 1 second 2275 N/cm^{2}a (3300 psia)
30	9-22-76	Preburner test: P_c = approximately 3 seconds 2275 N/cm^{2}a (3300 psia)
31	9-22-76	Preburner test: P_c = approximately 8 seconds 2275 N/cm^{2}a (3300 psia)

TABLE 26. COMBUSTION CHAMBER NO. 2 FLOW BALANCE WITH THE PREBURNER BASED ON THRUST CHAMBER NO. 1 TEST DATA

	Last Test		Next Test	
Propellant Tanks				
Oxidizer Tank Pressure, N/cm^2g (psig)	2107.5	(3056.5)	2912.9	(4224.7)
Oxidizer Temperature, K (F)	106.9	(-267.5)	105.6	(-270.0)
GH_2 Line Pressure, N/cm^2g (psig)	2066.3	(2996.8)	2845.5	(4126.9)
GH_2 Line Temperature, K (F)	309.8	(97.7)	294.4	(70.0)
LH_2 Tank Pressure, N/cm^2g (psig)	2881.3	(4178.8)	2769.1	(4016.1)
LH_2 Tank Temperature, K (F)	33.4	(-390.8)	33.9	(-390.0)
System				
Oxidizer Flow Total, kg/s (lb/sec)			13.501	(40.788)
Fuel Total Flow, kg/s (lb/sec)			3.084	(6.798)
System Mixture Ratio (o/f) (includes 0.16 kg/s (0.36 lb/sec) dump nozzle flow and 0.16 kg/s (0.36 lb/sec) face coolant flow)			6.000	(6.000)
Preburner				
Oxidizer Inlet Pressure, N/cm^2g (psig)			2539.8	(3683.6)
Oxidizer Inlet Temperature, K (F)			105.6	(-270.0)
Oxidizer Servovalve P, N/cm^2 (psi)			151.1	(219.2)
Oxidizer Valve Position, rad (deg)			73.9	(73.9)
Oxidizer Valve Resistance, sec^2/dm (sec^2/ft^3-in.^{2})			535.7	(978.6)
Oxidizer Valve P W/O Main Oxidizer, N/cm^2 (psi)			332.2	(481.8)
Oxidizer Valve Position, rad (deg)			64.4	(64.4)
Oxidizer Valve Resistance, sec^2/dm (sec^2/ft^3-in.^{2})			1177.1	(2150.5)
Oxidizer Flowrate, kg/s (lb/sec)			1.792	(3.950)
H_2 Inlet Pressure, N/cm^2g (psig)			2451.0	(3554.8)
LH_2 Mix Orifice Diamger (G), mm (inch)		(Line size this test)		
GH_2 Flowrate, kg/s (lb/sec)			2.292	(5.053)
LH_2 Flowrate, kg/s (lb/sec)			0.628	(1.385)
Sleeve Coolant Flow, kg/s (lb/sec)			0.136	(0.300)
Sleeve Coolant Orifice Diameter, mm (inch)			6.91	(0.272)
Face Coolant Flow, kg/s (lb/sec)			0.163	(0 360)
Total H_2 Flowrate, kg/s (lb/sec)			2.757	(6.078)
Fuel Injection Velocity, m/s (ft/sec)			240.8	(790.1)
Nozzle Stagnation P_c, N/cm^2a (psia)			2366.4	(3432.0)
Injector End P_c, N/cm^2a (psia)			2366.4	(3432.0)
Mixture Ratio (o/f)			0.650	(0.650)
Core Mixture Ratio (o/f)			0.684	(0.684)
Preburner Gas Temperature, K (R)			866	(1594)
Oxidizer Turbine Simulated Diameter (F1), mm (inch)			13.03	(0.513)
H_2 Turbine Simulated Diameter (F2), mm (inch)			19.13	(0.753)
Igniter				
Oxidizer Inlet Pressure, n/cm^2g (psig)	2847.3		2879.0	(4175.5)
Oxidizer Inlet Temperature, K (F)	298.2	(76.7)	294.4	(70.0)
Oxidizer Flowrate, kg/s (lb/sec)	0.019 1	(0.042)	0.023 6	(0.052)
Oxidizer Orifice Diameter (A, C), mm (inch)	0.70	(0.0275)	0.65	(0.0255)
GH_2 Inlet Pressure, N/cm^2g (psig)	1876.2	(2721.1)	2659.7	(3857.4)
GH_2 Inlet Temperature, K (F)	304.8	(88.7)	294.4	(70.0)
GH_2 Flowrate, kg/s (lb/sec)	0.021 8	(0.048)	0.025 4	(0.056)
GH_2 Orifice Diameter (B, D), mm (inch)	1.61	(0.0635)	1.46	(0.0575)
Mixture Ratio (o/f)	0.859	(0.858)	0.929	(0.929)

The damaged components, with the exception of the injector, were reworked and reassembled with injector No. 2 and the testing was resumed. Initial difficulties with the ignition system were overcome, and testing of the preburner proceeded through tests at the planned 1380 N/cm^{2}a (2000 psia) and 2275 N/cm^{2}a (3300 psia) levels was accomplished (Fig. 100). Test results from the data tests are shown in Table 27. During this test series the turbine simulation orifices were gradually being enlarged by scretching of the orifice plates from the pressure and temperature influence. The degree of enlargement occurring during each test could only be estimated as the orifices were not inspected until the completion of the test series. The preburner combustion performance parameter, c*, shown in Table 27 has been corrected for the estimated throat area variation.

The preburner gas temperature is plotted in Fig. 101. The temperature variation shown is the result of individual temperature measurements made in the duct supplying the fuel turbopump and in the duct supplying the oxidizer thrbopump. Approximately 68% of the gas flows to the fuel turbopump and the average temperature has been determined by taking a mass weighted average of the two duct gas temperatures for each test. The extreme temperature difference between the two ducts shown in Fig. 101 was not evidenced in the later testing of the staged combustion assembly and an investigation of the cause of the difference shown here was not pursued.

Two Kistler pressure transducers were installed in the combustor wall for the final two tests to determine whether high-frequency oscillations were present. A typical section of the Statos playback of the taped output recording is shown in Fig. 102. The shorted input trace near the top reveals some 350 to 360 Hz interference superimposed on the Kistler output. With this ignored, the two Kistler traces below show a 80 to 90 N/cm^2 (120 to 130 psi) peak-to-peak oscillation amplitude, which is less than four % of the chamber pressure and satisfactorily meets usual stability criteria. The IRIG trace at the bottom of Fig. 102 is a time signal where each cycle represents 1 millisecond.

Staged Combustion Assembly

Following the successful demonstration of preburner-only testing, the copper alloy (Amzirc) combustion chamber and injector were installed on the test stand with the preburner to form a staged combustion assembly configuration.

The coolant was plumbed as a bypass cooling system to provide greater flexibility during testing as to coolant flowrates and cutoff overrides. Figure 103 and 104 show the assembly installed on the test stand together with both servo-controlled oxidizer valves. The nozzle expansion area ratio of the copper chamber is approximately 8:1 so that this nozzle was expected to flow full during all tests at the site ground level, and no diffuser or ejector operation was planned for this phase of the testing.

Table 28 is a summary of testing effort tests planned with the 8:1 expansion ratio staged combustion assembly. A minimum of six successful tests was projected as needed to verify the ignition, start, and shutdown sequences, combustion chamber cooling characteristics, and main injector operation with the hot gas fuel. The flow balance previously developed for the preburner was found to have been adequate, and a further balance was not required for these tests.

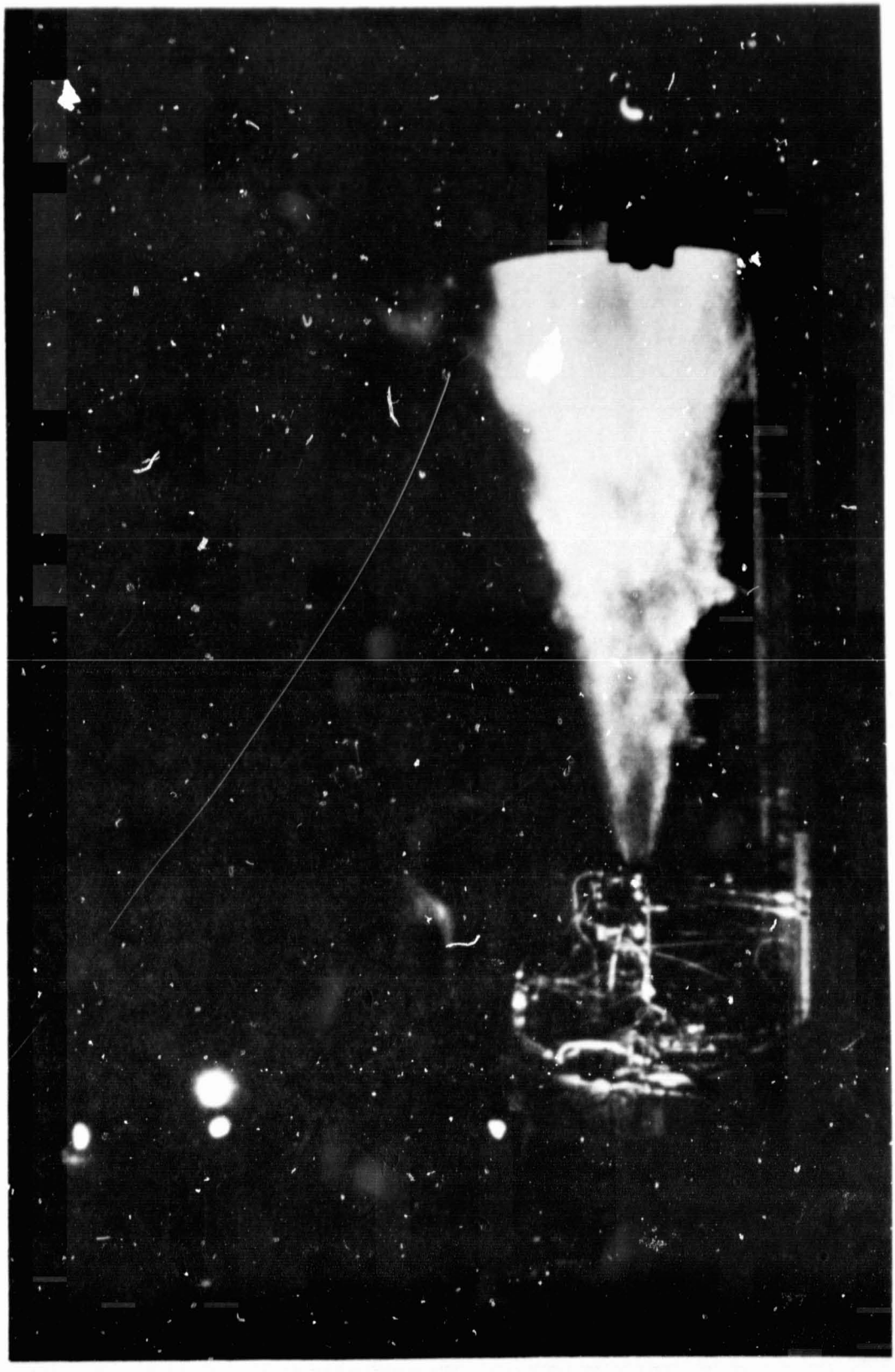

Figure 100. ASE Preburner Test

TABLE 27. PREBURNER TEST SUMMARY

Test No.	Slice	Slice Time, seconds	P_c (Injector End), N/cm^2a (psia)	Mixture Ratio, o/f	Throat Area (Estimated*), cm^2 ($in.^2$)	c* (Corrected), m/s (ft/sec)	Average Gas Temperature, K (F)
026	16.044	1	1461.3 (2119.3)	0.589	4.290 (0.665)	2030 (6661)	703 (805)
028	19.468	3	1507.7 (2186.7)	0.851	4.535 (0.703)	2152 (7060)	1067 (1461)
029	34.852	1	2296.6 (3330.8)	0.648	4.613 (0.715)	2006 (6580)	825 (1025)
030	25.860	3	2312.4 (3353.7)	0.740	4.852 (0.752)	2056 (6744)	952 (1254)
031	28.871	1	2276.8 (3302.1)	0.781	4.935 (0.765)	2128 (6982)	1051 (1432)
	30.067	2	2270.7 (3293.3)	0.798	5.013 (0.777)	2140 (7021)	1071 (1467)
	32.047	4	2259.1 (3276.4)	0.814	5.174 (0.802)	2180 (7152)	1087 (1497)
	34.851	7	2245.9 (3257.3)	0.828	5.419 (0.840)	2262 (7420)	1117 (1551)

*Note: Hydrogen turbine simulator orifice was becoming distorted during test series, and diameter was increasing with each succeeding test.

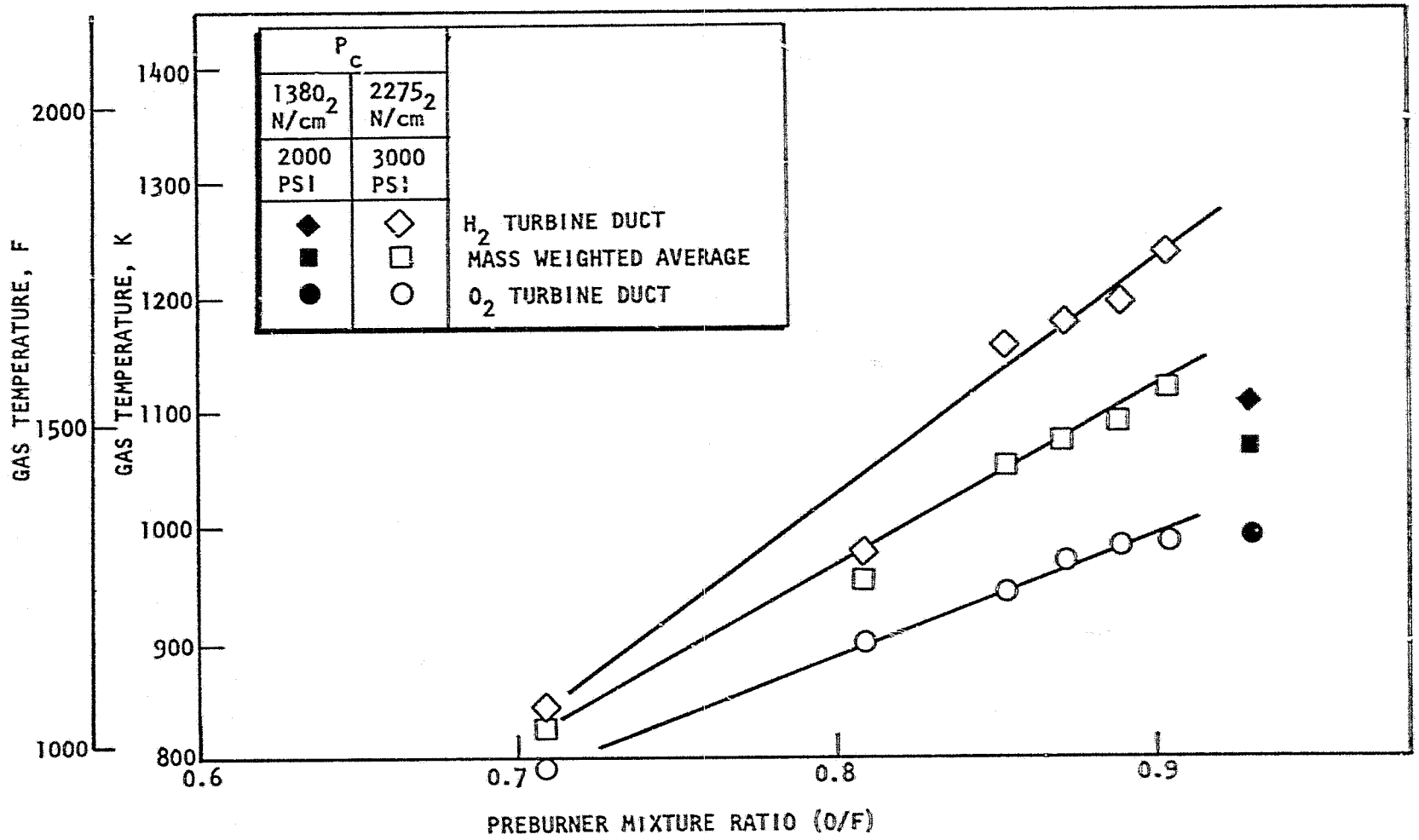

Figure 101. Preburner Gas Temperature vs MR

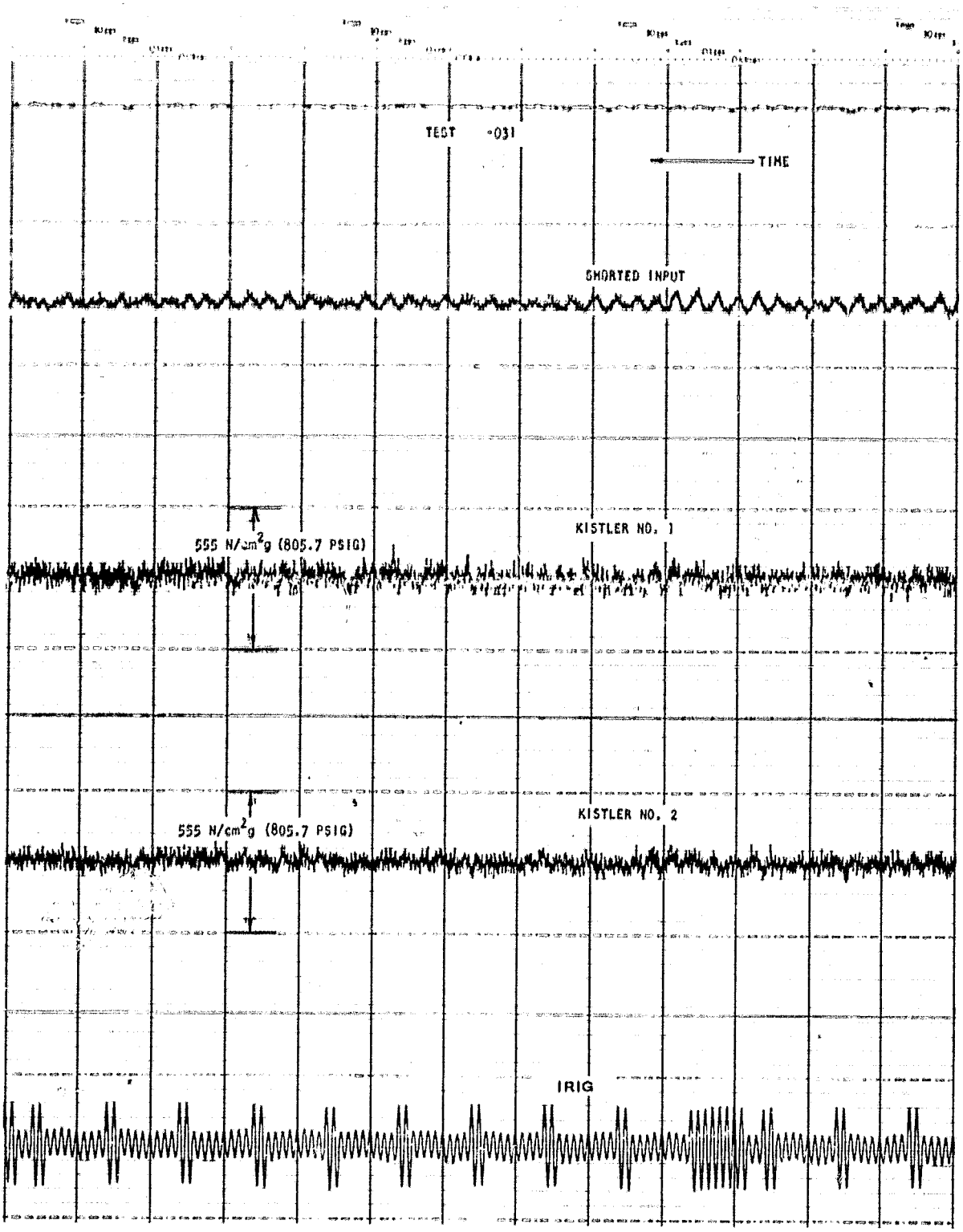

Figure 102. Typical Section of Stator Playback

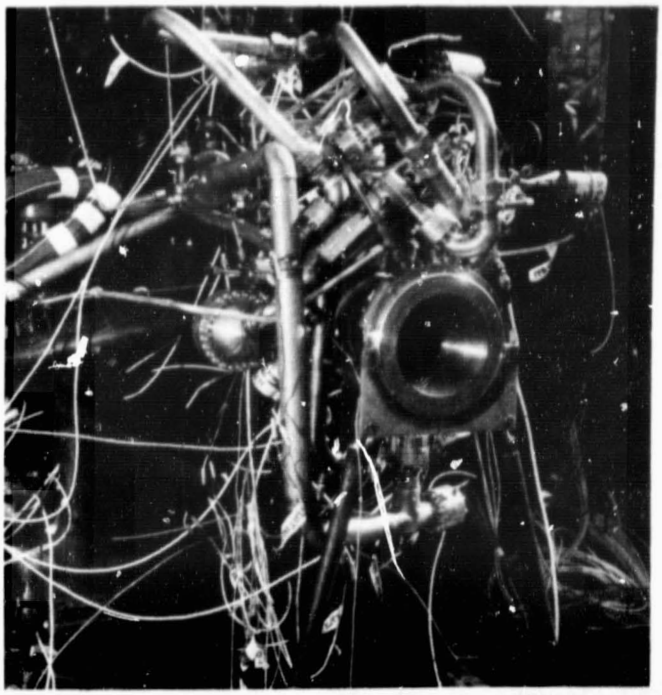

1HS23-10/15/76-S1C*

Figure 103. Staged Combustion Assembly on Nan Stand

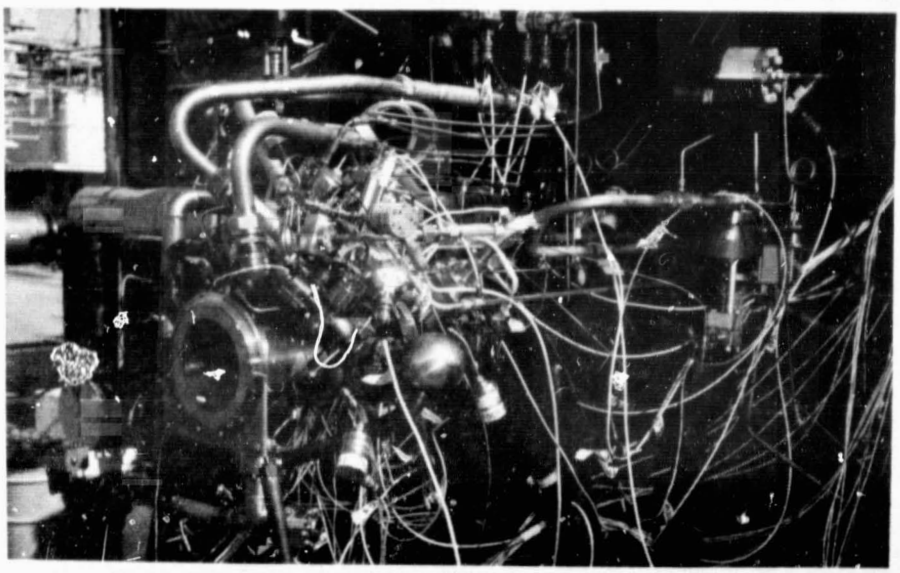

1HS23-10/15/76-S1A*

Figure 104. Staged Combustion Assembly on Nan Stand

TABLE 28. PREBURNER OPERATION TEST SEQUENCE

Activities Pretest:

1. Install cooled chamber and injector
2. Flow test gaseous hydrogen mixer and orifices
3. Install LOX control valve

Activities Posttest:

Potential Problems:

1. Off-design preburner operation
2. Preburner startup

Hardware Configuration:

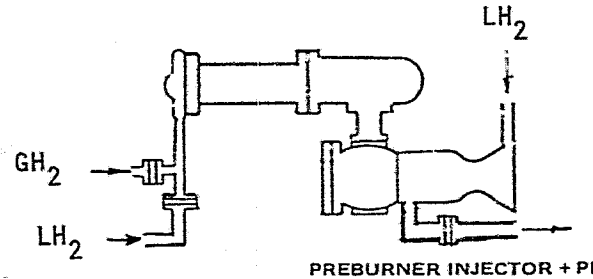

PREBURNER INJECTOR + PREBURNER BODY

COMBUSTION CHAMBER + FUEL MANIFOLD HOUSING + INJECTOR

COMBUSTION CHAMBER ASSEMBLY (COOLED)

Test Objectives:

1. Check out main chamber injector with preburner fuel

Components												Test Program					
Main Injector		Combustor Chamber		Nozzle		Nozzle Extension		Preburner Injector		Preburner Body							
S/N	Fluid	S/N	Coolant	S/N	Coolant	S/N	Coolant	S/N	Propellant	S/N	Coolant	Tests	Chamber P_c, N/cm2a (psia)	Chamber MR (o/f)	Preburner P_{cb} N/cm2a (psia)	Preburner MR (o/f)	Comments
3	Hot Gas	2	LH_2	-	-	-	-	2	GH_2 and LH_2 + LOX	1	GH_2	1	TBD	0	69 (100)	-	ϵ = 8:1 Ignition test duration = 1 second (preburner)
3	Hot Gas	2	LH_2	-	-	-	-	2	GH_2 and LH_2 + LOX	1	GH_2	2	TBD	0	1380 - 2225 (2000 - 3227)	0.685	System transition tests duration = 1 and 3 seconds (preburner)
3	Hot Gas + LOX	2	LH_2	-	-	-	-	2	GH_2 and LH_2 + LOX	1	GH_2	3	690 - 1517 (1000 - 2200)	2.72 - 6.0	2225 (3227)	0.685	Mainstage tests duration = 1, 3, and 8 seconds

Testing was initiated as planned with checkout of the preburner and combustion chamber spark igniters. The early phase of this testing were plagued with spark igniter difficulties which results in repetitious igniter checkout tests. The difficulties were ultimately attributed to breakdown of the high voltage cable insulation which caused the spark current flow to follow a short circuited path rather than jumping the gap in the igniter system. Replacement high voltage cables were procured and the difficulties with the igniters were subsequently minimized.

The tests conducted are summarized in the Test Log, Table 29 and testing of the assembly is shown in Fig. 105. A satisfactory preburner mainstage of 3 seconds duration and main chamber transition test of 0.5 seconds duration, No. 039, was performed before a system electrical malfunction occurred which caused significant damage to the preburner turbine simulators and main injector. The malfunction occurred when the preburner was signalled to shut off because the chamber pressure had not reached the mainstage pressure level in time. The shutoff signal generated an extraneous electrical pulse which overrode other commands and resignaled the preburner LOX valve to open. The LOX valve thus opened while preburner fuel flows were decreasing and the resultant momentary high mixture ratio in the preburner ducting burned off the duct thermocouples. The LOX continued to flow and combined with gaseous hydrogen back-flowing into the main injector manifold from the main injector face coolant circuit. This created a greater fire which burned the main injector fuel turbine simulator and downstream faces of the turbine simulation orifices. The damaged components are shown in Fig. 106 through 108.

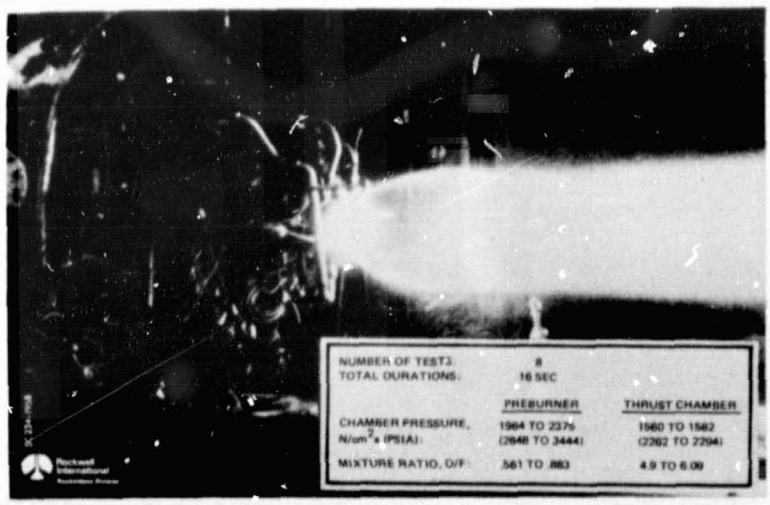

Figure 105. ASE Preburner/Combustion Chamber Test Results

TABLE 29. STAGED COMBUSTION ASSEMBLY TEST LOG

Test No.	Date	Preburner Mixture Ratio (o/f)	Chamber Pressure		Gas Temperature		Duration seconds	Combustion Chamber Mixture Ratio (o/f)	Chamber Pressure		Duration seconds	Test Results
			N/cm^2a	psia	K	F			N/cm^2a	psia		
032	10-15-76	-	-	-	-	-	-	-	-	-	-	Preburner and thrust chamber igniters fired
033	10-19-76	-	-	-	-	-	-	-	-	-	-	Preburner and thrust chamber igniters fired
034	10-21-76	-	-	-	-	-	-	-	-	-	-	Preburner and thrust chamber igniters fired
035	10-22-76	-	-	-	-	-	-	-	-	-	-	Preburner igniter only fired
036	10-22-76	-	-	-	-	-	-	-	-	-	-	Preburner igniter only fired
037	10-29-76	-	-	-	-	-	-	-	-	-	-	Both igniters fired; no preburner operation
038	11-01-76	*	*	*	*	*	1	-	-	-	-	Scheduled 1-second preburner test; data not stabilized
039	11-03-76	0.883	2375	3444	1122	1560	3	*	*	*	0.5	Scheduled 3-second preburner and ½-second main chamber test; chamber data not stabilized
040	11-05-76	-	-	-	-	-	-	-	-	-	-	Spark plugs failed
041	11-10-76	-	-	-	-	-	-	-	-	-	-	Preburner spark plug failed
042	11-10-76	0.361	1964	2848	439	330	2	-	-	-	-	2-second preburner test; main chamber injector burned when preburner LOX valve reopened after shutdown
001	3- 9-77	-	-	-	-	-	-	-	-	-	-	No preburner igniter operation
002	3-16-77	-	-	-	-	-	-	-	-	-	-	Low chamber igniter temperature
003	3-22-77	-	-	-	-	-	-	-	-	-	-	Low chamber igniter temperature
004	3-22-77	0.680	2321	3366	837	1047	0.2	-	-	-	-	Scheduled preburner only operation
005	3-25-77	-	-	-	-	-	-	-	-	-	-	Igniter checkout test
006	3-25-77	-	-	-	-	-	-	-	-	-	-	Igniter checkout test
007	3-25-77	-	-	-	-	-	-	-	-	-	-	Igniter checkout test
008	3-29-77	*	2340	3394	*	*	0.2	-	-	-	-	Scheduled 0.2-seconds preburner test
009	3-29-77	0.697 0.561	2329 2313	3378 3355	971 851	1288 1071	1.3	4.9	1571	2279	0.3	Scheduled duration test; two data slices shown
010	4-20-77	0.594	2275	3299	869	1104	1.7	5.57	1560	2262	0.7	Scheduled duration test
011	4-20-77	0.589	2282	3309	852	1074	3.9	6.09	1582	2294	2.8	Scheduled duration test C*=2532 m/s (7718 ft/sec) c*=99.78

*NOTE Duration too short for data stabilization

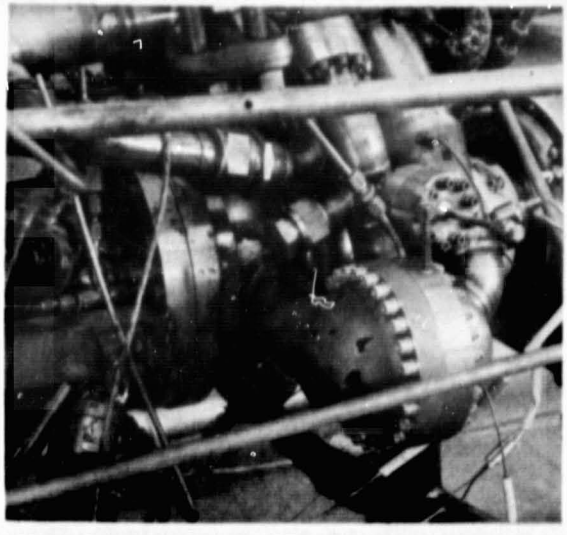

1HS25-11/11/76-S1A

Figure 106. Damaged Fuel Turbine Simulator

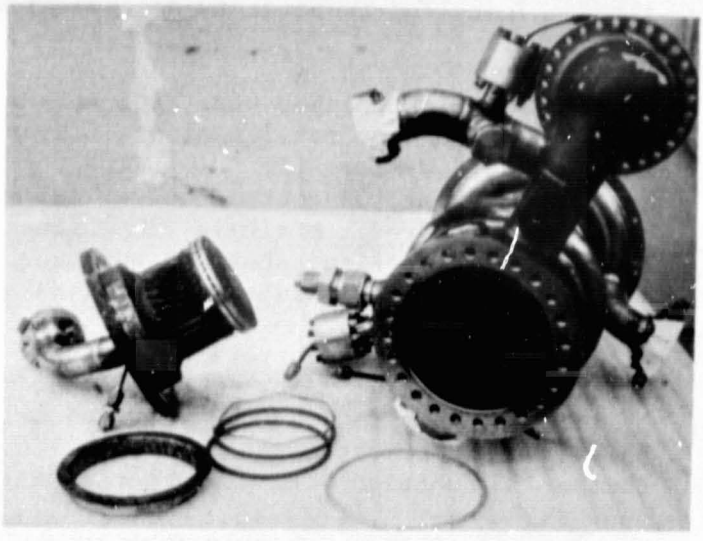

1HS35-11/15/76-C1E

Figure 107. Damaged Combustion Chamber Components

1HS55-11/15/76-C1A

Figure 108. Damaged Turbine Simulation Orifices

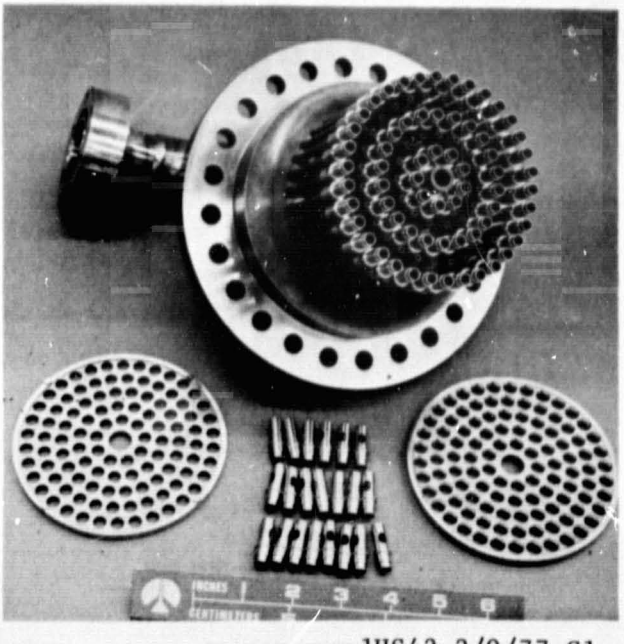

1HS42-2/9/77-C1

Figure 109. Injector Components

The injector, turbine simulators, and orifices were repaired and/or replaced. Figure 109 shows the main injector after repair with the first set of fuel sleeves installed preparatory to assembling the Rigimesh face plates onto the LOX posts.

Several facility changes were made at the same time to provide better start sequencing and more consistent start transients. This included relocation of the LOX bleed system, Fig. 110. With the pretest bleed tapped off just upstream of the preburner LOX control valve, delivery of good quality LOX to the preburner was ensured. A single, 20-channel, solid-state sequencer was installed, and with it, a revised shutdown sequence providing for simultaneous and positive shutoff of all oxidizer control valves at the cutoff signal.

With these reworks incorporated, testing was resumed with a series of igniter checkout tests and one brief, 0.2 second preburner start. Three staged combustion assembly tests, 009, 010, and 011, were performed to verify the system operation and to establish the capability of the main injector and combustion chamber to function with preburner gases.

Measurement of the preburner exhaust gas temperatures indicated a significant difference between the earlier test series (preburner tests 026 through 031 and staged combustion assembly tests 039 and 042) and the later tests (staged combustion assembly tests 009 through 011), as shown in Fig. 111.

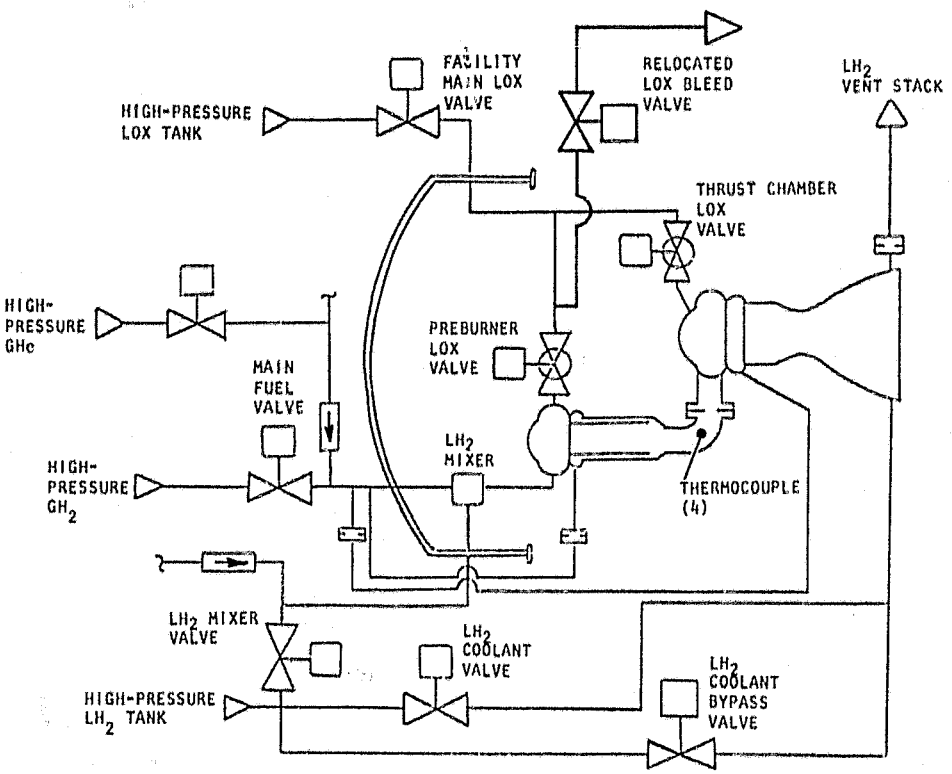

Figure 110. Man Stand Propellant Feed System

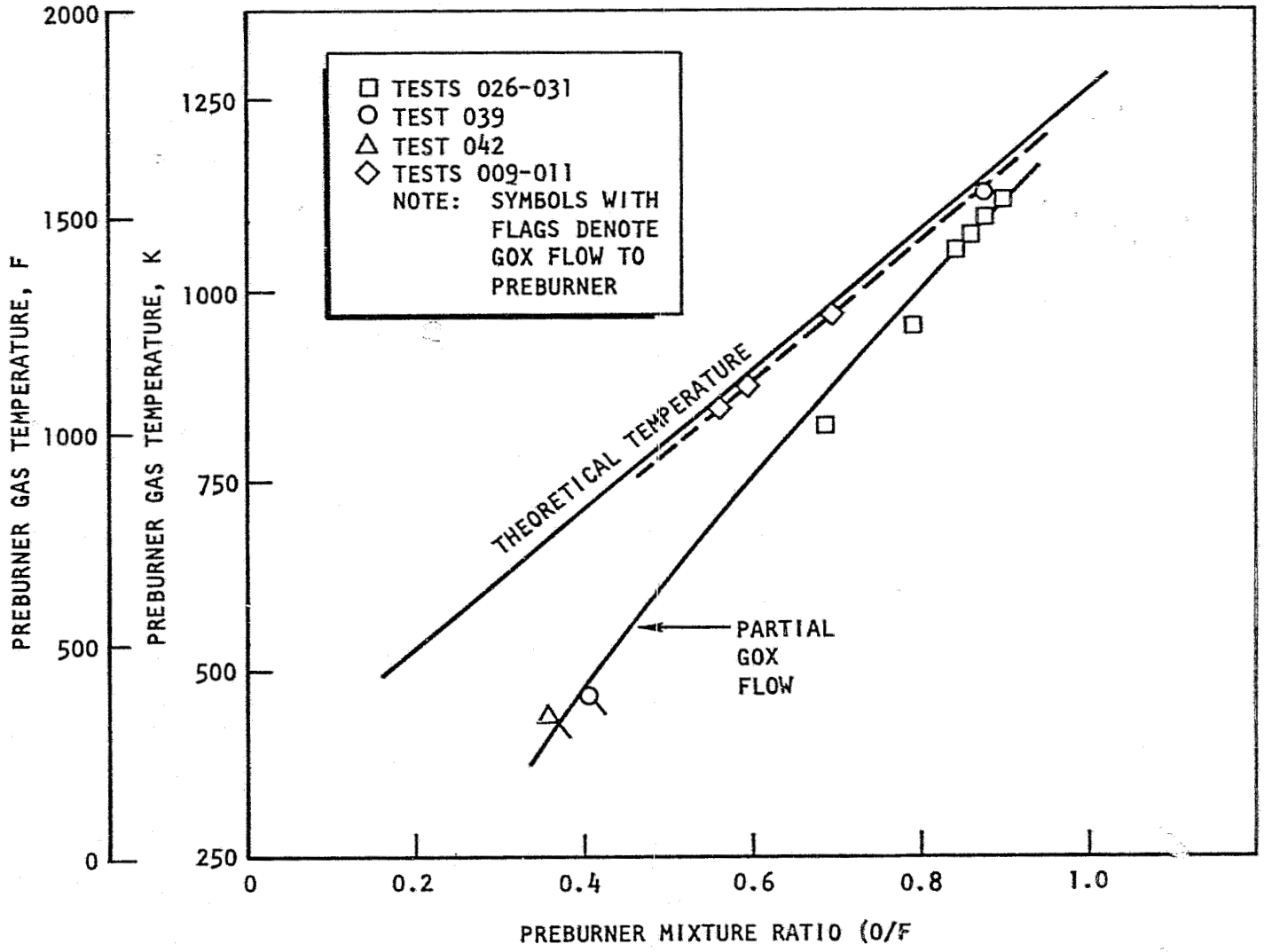

Figure 111. Staged Combustion Assembly Test Preburner Gas Temperature vs MR

Review of the test sequencing and pretest LOX bleed cycles showed that the earlier tests were subject to a mixed phase oxidizer flow. The mixed phase flow resulted in poorer combustion efficiency and, consequently, lower gas temperature than the longer duration tests and the later staged combustion assembly tests (009 through 011).

Preburner-only test 031 was the second test of the day and was therefore subjected to a better LOX bleed and system chill than the other preburner tests; the system replumbing and modified sequencing for the staged combustion assembly tests (009 through 011) resulted in better LOX quality.

Satisfactory determination of the combustion efficiency (c* or ηc^*) could not be made for the staged combustion assembly tests because the flow across the turbine simulation orifices was subsonic because of the downstream backpressure created by the combustion in the main chamber. The purpose of these tests was to demonstrate operation of the preburner with the main combustion chamber and injector, and performance measurements were to be made during later testing with the complete assembly.

Staged Combustion Assembly With 400:1 Nozzle

Successful demonstration of the staged combustion assembly led directly to the next planned phase of testing, which was altitude testing of the assembly with the 400:1 uncooled nozzle extension.

The regeneratively cooled tubular 175:1 nozzle and the 400:1 mild steel uncooled nozzle extension, shown together in Fig. 112 were added to the staged combustion assembly already installed on the test stand, Fig. 113. Facility plumbing was modified to add the nozzle LH_2 coolant flow circuit. To maximize the system flexibility, this coolant flow was installed in parallel with the existing chamber coolant flow circuit as shown schematically in Fig. 114. Thus, coolant flowrates to the chamber and nozzle were established independently by means of the two sonic flow orifices in the two outlet lines. It was important that the nozzle coolant flowrate be high during the start transient because of the high heat fluxes encountered in the nozzle while the gas flow was separated from the nozzle wall. For the second series of tests (019-022) the coolant flow circuit was modified so that the LH_2 coolant flow passed first through the combustion chamber coolant jacket and then through the nozzle tubes as shown in Fig. 115.

Test and Performance. The original test plan was prepared with the intention of conducting the tests with regenerative cooling of the combustion chamber and nozzle. However, as the detailed planning progressed, it was decided to revert to bypass cooling of both components. This modified test plan is summarized in Table 30. Initially two tests of the ignition system and preburner-only were scheduled to verify the operation of these subsystems and ensure that valve sequencing and timing were correct. Of particular concern was the sequencing of the ejector valve to achieve maximum ejector chamber pressure at the instant that the main combustion chamber reaches maximum chamber pressure so that the nozzle would flow full. Because of the excessive LH_2 bypass coolant flow required with the parallel flow system and the limited LH_2 high-pressure tank capacity, mainstage test duration was limited to just under 3 seconds.

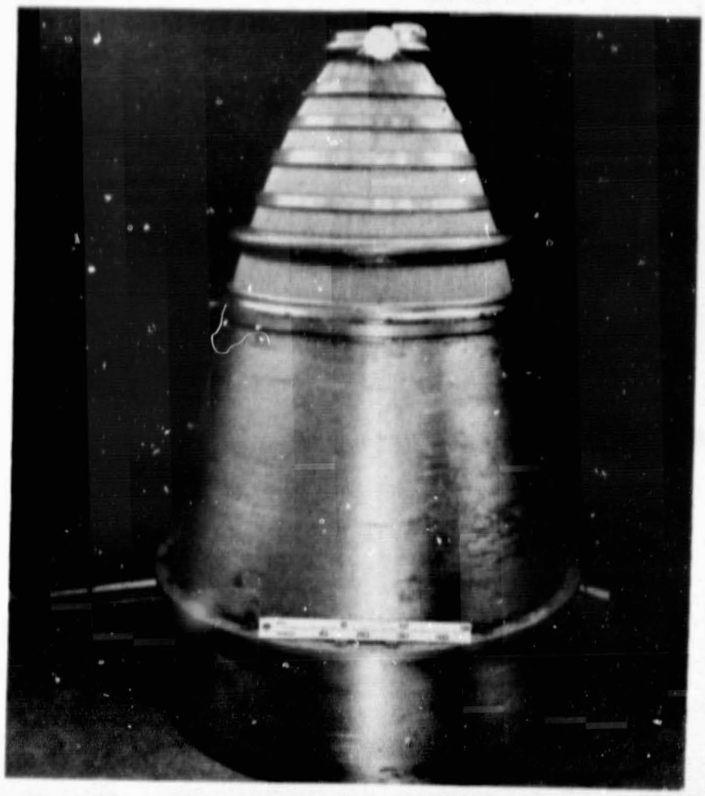

1HS32-1/12/77-C1E

Figure 112. Regeneratively Cooled Nozzle and 400:1 Uncooled Nozzle Stackup

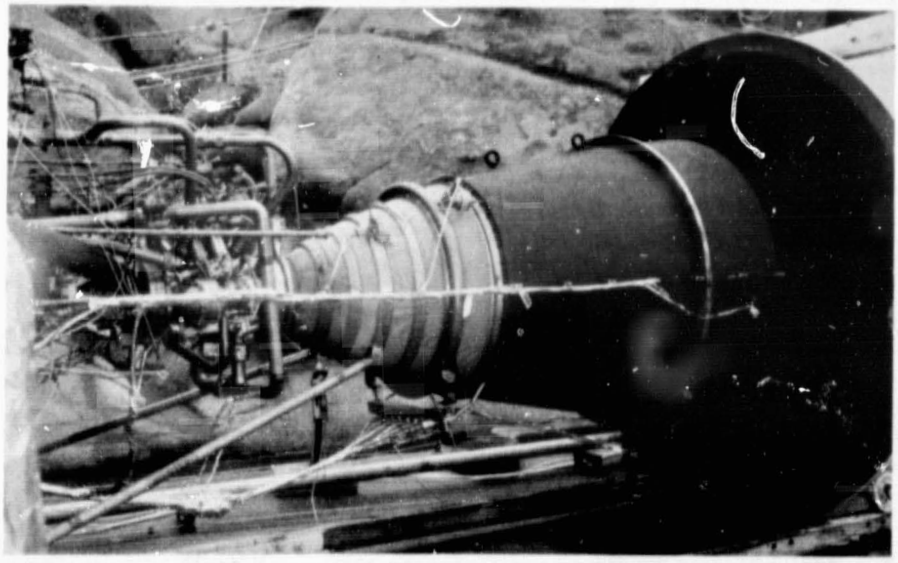

1HS35-5/16/77-S2*

Figure 113. Staged Combustion Assembly and 400:1 Nozzle Assembly on Nan Stand

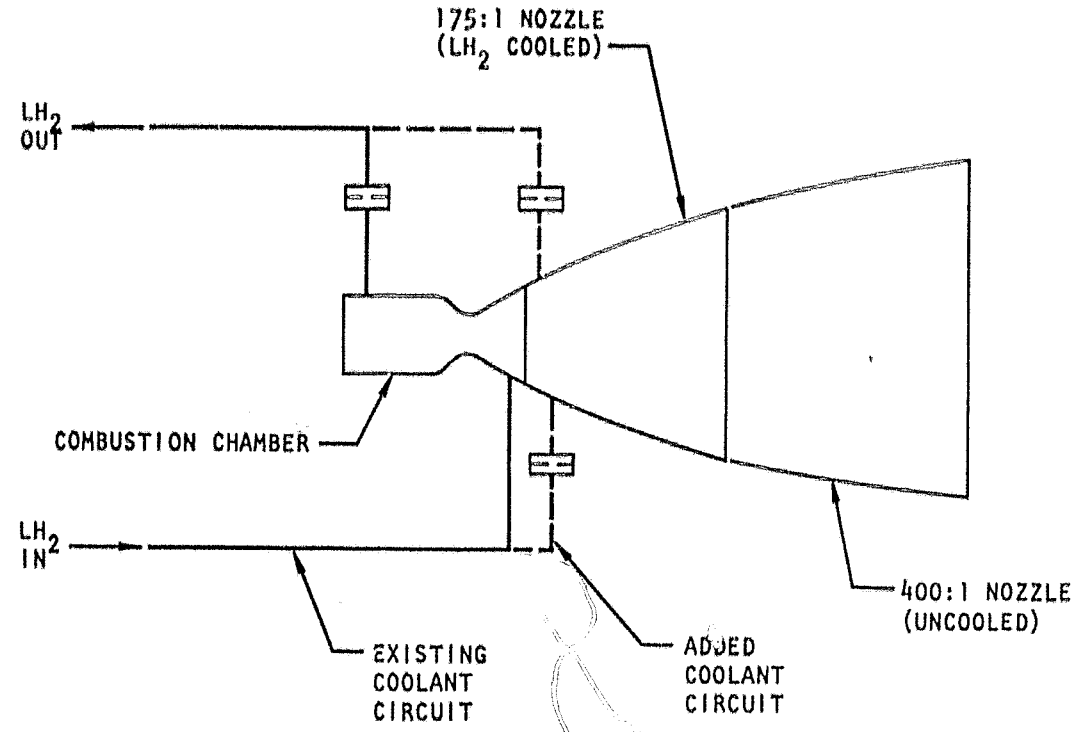

Figure 114. Parallel LH_2 Coolant Circuit for 400:1 Nozzle Testing

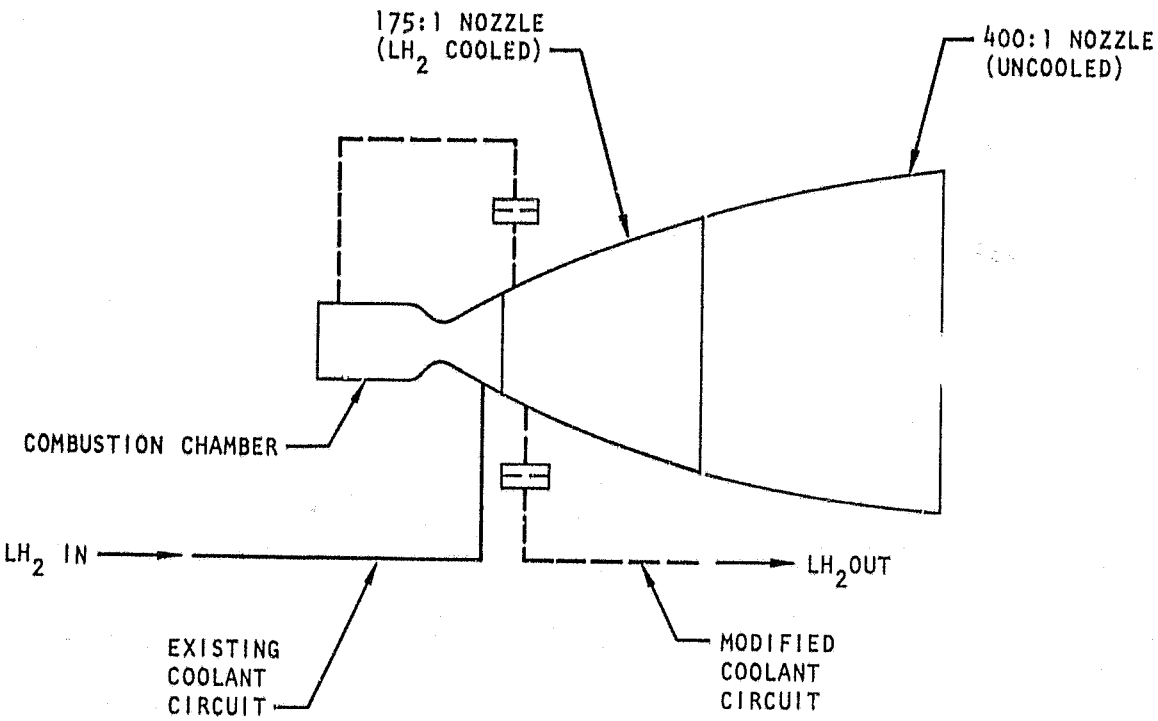

Figure 115. Series LH_2 Coolant Circuit for 400:1 Nozzle Testing

TABLE 30. PREBURNER SYSTEM, SYSTEM OPERATION TEST SEQUENCE

Activities Pretest:

1. Install 175:1 nozzle
2. Plumb nozzle coolant
3. Install 400:1 nozzle
4. Blowdown test diffuser/ejector

Activities Posttest:

1. Final operation

Potential Problems:

1. Preburner startup
2. Diffuser operation

Hardware Configuration:

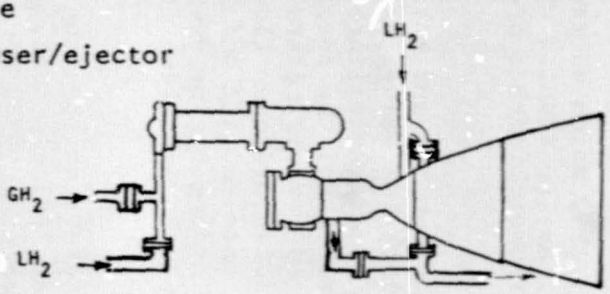

THRUST CHAMBER ASSEMBLY

PREBURNER INJECTOR + PREBURNER BODY

FUEL MANIFOLD HOUSING + COMBUSTION CHAMBER + NOZZLE (175:1) + NOZZLE EXTENSION (400:1)

Test Objectives:

1. Full regenerative cooled operation
2. Performance evaluation
3. Altitude operation

Components												Test Program					Comments
Main Injector		Combustor Chamber		Nozzle		Nozzle Extension		Preburner Injector		Preburner Body							
S/N	Fluid	S/N	Coolant	S/N	Coolant	S/N	Coolant	S/N	Propellant	S/N	Coolant	Tests	Chamber $P_{c_{ss}}$ N/cm²a (psia)	Chamber MR (o/f)	Preburner $P_{c_{ss}}$ N/cm²a (psia)	Preburner MR (o/f)	
3	Hot Gas + LOX	2	LH_2	2	LH_2	2	-	2	GH_2 and LH_2 + LOX	1	GH_2	2	-	-	2225 (3227)	0.685	ϵ = 400:1 Preburner operation with overboard dump of coolant. Duration = 1-3 seconds
3	Hot Gas + LOX	2	LH_2	2	LH_2	2	-	2	GH_2 and LH_2 + LOX	1	GH_2	3	1517 (2200)	5.5 - 6.5	2225 (3227)	0.685	Full-staged combustion assembly operation. Duration = 3-5 seconds

Additional tests with the series coolant flow were subsequently undertaken with test durations of 4 and 5 seconds. A complete test log is shown in Table 31, including the performance and coolant circuit parameter measurements.

Specific impulse for each test data point was computed from the measured thrust and measured propellant flowrates. The thrust was corrected to vacuum conditions by adding a capsule pressure times nozzle exit area.

$$F_{vacuum} = F_{measured} + (P_{capsule} \times A_{nozzle})$$

Figure 116 is a typical thrust and chamber pressure CRT trace with the corresponding capsule pressure and nozzle exit pressure traces. The thrust measured was influenced by the capsule pressure and could not achieve stabilization until the capsule was completely pumped down to a steady-state level which generally required 2 to 2.5 seconds. The nozzle exit pressure tended to reflect the rapid stabilization of the main chamber pressure and indicated that full flow in the nozzle was quickly realized.

Operation of the diffuser/ejector is shown in Fig. 117, which summarizes the pressure measured during tests 015, 016, and 017.. As the results of these tests showed the satisfactory operation of the diffuser, further pressure measurements were not made on the subsequent tests.

The oxidizer flowrate was measured with a turbine flowmeter and a subsonic venturi meter in series upstream of the main facility LOX valve. A series of in-place flow calibrations were performed using a specially calibrated facility flowmeter for a standard to ensure accurate measurement of the total oxidizer flow to the preburner and main injector. Calibrated venturi meters were used for measurement of the gaseous hydrogen and the liquid hydrogen flow to preburner fuel mixer. Gaseous hydrogen for injector face coolant and for the preburner inner liner coolant were taken from the hydrogen line downstream of the venturi meter so that the two meters described were measuring the total hydrogen flow to the test system.

Propellant temperatures were measured at the flowmeters so that the correct propellant density could be utilized in the flowrate calculations. The specific impulse was then computed from these measurements:

$$I_s = F_{vacuum} / (\dot{w}_{oxid} + \dot{w}_{fuel})_{total}$$

The specific impulse was further corrected for the heat loss to the coolant flow, which of course was carried away with the bypass coolant system employed for these tests. This correction was made by comparing the theoretical performance at the actual propellant inlet temperatures with the theoretical performance at the propellant inlet temperatures predicted with a regeneratively cooled system. This difference was applied to the calculated specific impulse and it ranged from 0.98 N-s/kg (0.1 sec) to 14.7 N-s/kg (1.5 sec).

TABLE 31. STAGED COMBUSTION ASSEMBLY (400:1) TEST LOG

Test No.	Date	Preburner					Chamber							Chamber Coolant			Nozzle Coolant			GN_2 Ejector	
		Chamber Pressure, N/cm2a (psia)	Mixture Ratio (o/f)	Fuel Inlet Temperature, K (F)	Gas Temperature K (F)	Duration, seconds	Pressure (Injector End), N/cm2a (psia)	Thrust, Vacuum N (pounds)	Mixture Ratio (o/f)	Duration, seconds	c* m/sec (ft/sec)	c* η, %	Specific Impulse, (Is vac) N-s/kg (seconds)	Flow rate, kg/s (lb/sec)	Inlet Temperature, K (F)	Outlet Temperature K (F)	Flow rate, kg/s (lb/sec)	Inlet Temperature, K (F)	Outlet Temperature, K (F)	Maximum GN_2 Pressure, N/cm2g (psig)	Maximum GN_2 Temperature, K (F)
012	5-6-77	-- (--)	--	-- (--)	-- (--)	--	-- (--)	-- (--)	--	--	-- (--)	--	-- (--)	-- (--)	-- (--)	-- (--)	-- (--)	-- (--)	-- (--)	-- (--)	-- (--)
013	5-10-77	2256.0 (3272)	--	-- (--)	-- (--)	1.1	-- (--)	-- (--)	--	--	-- (--)	--	-- (--)	-- (--)	-- (--)	-- (--)	-- (--)	-- (--)	-- (--)	434 (630)	731 (855)
014	5-12-77	2262.7 (3281.7)	0.545	245.3 (-18.5)	847 (1064)	1.3	-- (--)	-- (--)	--	0.25	-- (--)	--	-- (--)	-- (--)	-- (--)	-- (--)	-- (--)	-- (--)	-- (--)	433 (628)	722 (840)
015	5-25-77	2257.1 (3273.5)	0.553	250.7 (-8.8)	858 (1085)	3.1	1557.1 (2258.3)	98 483 (22,141)	6.084	2.15	2322 (7618)	98.8	4665 (475.7)	2.503 (5.517)	55.3 (-360.4)	189.2 (-119.4)	2.795 (6.161)	55.3 (-360.4)	185.0 (-127.0)	429 (622)	740 (872)
016	5-27-77	2279.8 (3306.4)	0.528	253.1 (-4.4)	840 (1052)	3.6	1570.2 (2277.3)	99 328 (22,331)	5.954	0.65	2344 (7689)	99.3	4698 (480.1)	2.567 (5.660)	53.4 (-363.9)	186.5 (-124.3)	2.504 (5.520)	53.4 (-363.9)	194.7 (-109.5)	427 (619)	745 (881)
017	6-1-77	2300.6 (3336.6)	0.595	252.6 (-5.3)	894 (1150)	3.8	1573.7 (2282.4)	100 680 (22,635)	6.428	2.80	2309 (7577)	99.4	4695 (478.7)	2.585 (5.699)	51.5 (-367.3)	186.7 (-124.0)	2.395 (5.280)	51.5 (-367.3)	200.3 (-99.5)	421 (611)	752 (893)
018	10-5-77	-- (--)	--	-- (--)	-- (--)	--	-- (--)	-- (--)	--	--	-- (--)	--	-- (--)	-- (--)	-- (--)	-- (--)	-- (--)	-- (--)	-- (--)	301 (437)	525 (125)
019	10-14-77	2272.2 (3295.5)	0.512	241.1 (-26.0)	822 (1019)	1.6	1563.9 (2268.2)	-- (--)	--	0.5	-- (--)	--	-- (--)	-- (--)	-- (--)	-- (--)	-- (--)	-- (--)	-- (--)	419 (608)	713 (824)
020	10-20-77	2274.5 (3269.7)	0.530	235.7 (-35.8)	805 (989)	5.0	1540.8 (2234.7)	96 962 (21,799)	5.751	4.0	2368 (7765)	99.7	4723 (481.6)	2.741 (6.042)	54.8 (-361.4)	178.3 (-139.1)	2.382 (5.251)	178.3 (-139.1)	284.3 (51.7)	435 (631)	752 (894)
021	10-25-77	2301.3 (3337.6)	0.596	245.4 (-18.2)	881 (1125)	6.0	1576.6 (2286.6)	100 996 (22,706)	6.378	5.0	2311 (7581)	99.3	4694 (478.6)	2.608 (5.749)	52.7 (-365.2)	186.2 (-124.9)	2.262 (4.986)	186.2 (-124.9)	305.4 (89.8)	429 (622)	752 (894)
022	10-26-77	2248.5 (3261.0)	0.564	244.6 (-19.8)	873 (1112)	6.2	1528.8 (2217.3)	97 469 (21,913)	5.920	5.2	2328 (7637)	98.5	4699 (479.1)	2.548 (5.617)	46.4 (-376.5)	182.8 (-130.9)	2.211 (4.874)	182.8 (-130.9)	298.1 (76.5)	437 (634)	742 (876)

Figure 116. Preburner/Thrust Chamber Test Results

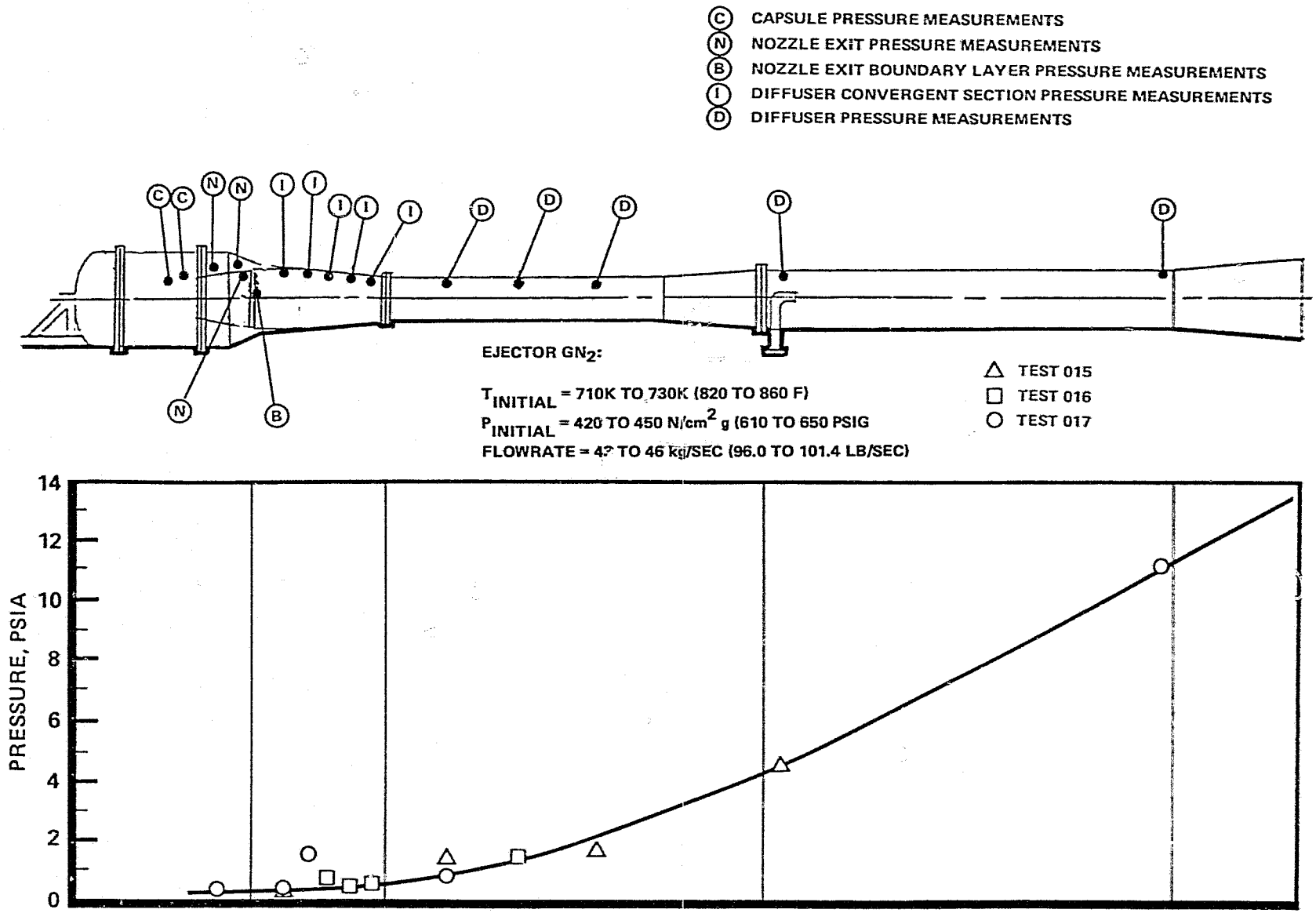

Figure 117. ASE Diffuser/Ejector Operation

Performance calculations were made for several slices from each of the longer duration (more than 2 seconds) tests. A plot of specific impulse versus propellant mixture ratio with all of these slices is shown in Fig. 118. The characteristic velocity efficiency (ηc^*), thrust coefficient efficiency (η_{C_F}), and specific impulse efficiency (η_{I_S}) points for each of these data slices are shown plotted against propellant mixture ratio in Fig. 119. The η_{I_S} is relatively constant over the mixture ratio range tested although the c* efficiency trends slightly higher with a compensating drop in the η_{C_F} at the higher mixture ratio.

Nozzle Boundary Layer. The temperature and pressure rakes were included with the 400:1 nozzle testing of the staged combustion assembly. As previously indicated, two different rake configurations were used for the initial test series (tests 012 through 017) and the second test series (tests 018 through 022).

Temperature Rake Results. Temperature measurements obtained during the initial series are presented in Table 32, and the temperature measurements obtained during the second series are shown in Table 33. During the initial test series, the thermocouples did not have radiation shields and the measured temperature were all corrected for a radiation loss to the surroundings.

The radiation shields attached to the thermocouple sheaths for the final test series were torn off by the force of the nozzle gases at various times during the first two tests, and only limited data not requiring a radiation loss correction were obtained.

Thermocouple correction is necessary to allow for the convection to and the radiation from the exposed thermocouple junction. It is assumed that the correction for conduction loss to the thermocouple sheath and base is small. Based on a balance between the thermocouple element convection and the element reradiation (assuming the incident gas radiation is small) there results:

$$hg\ (T_T - T_P) = \sigma eF\ (T_P^4 - T_S^4)$$

$$\Delta T = (T_T - T_P) = \left(\frac{\sigma eF}{h}\right)\ (T_P^4 - T_S^4)$$

Assuming the sink temperature (T_S) is small with respect to the thermocouple probe temperature (T_P),

$$\Delta T = \left(\frac{\sigma eF}{h}\right)\ T_P^4$$

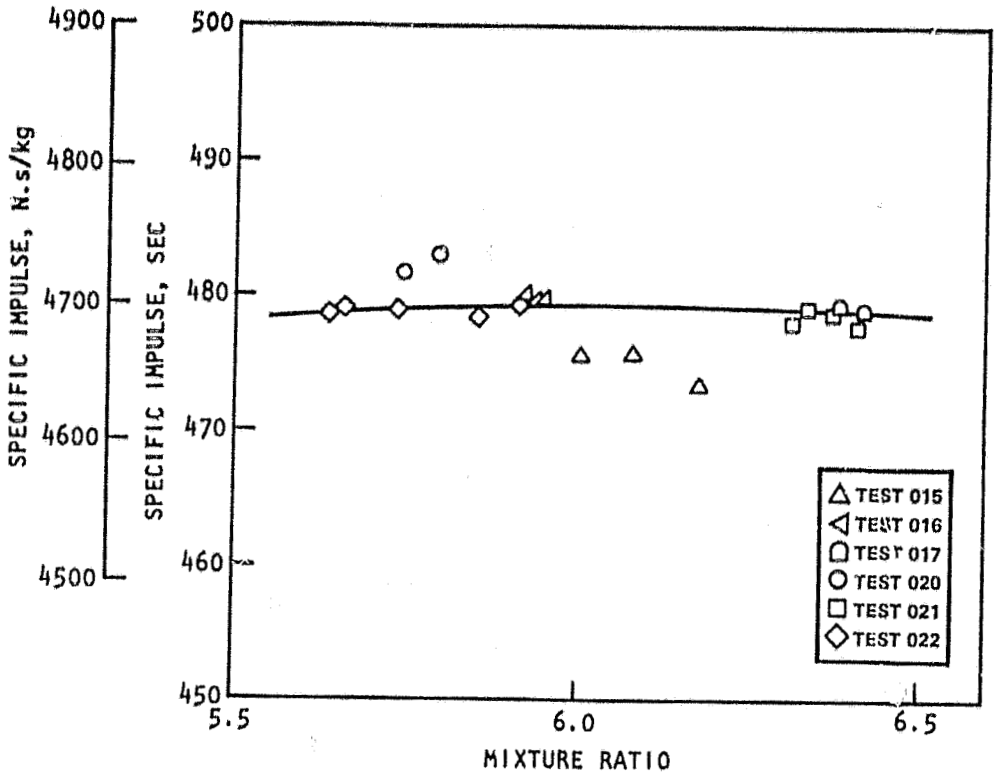

Figure 118. Specific Impulse vs MR

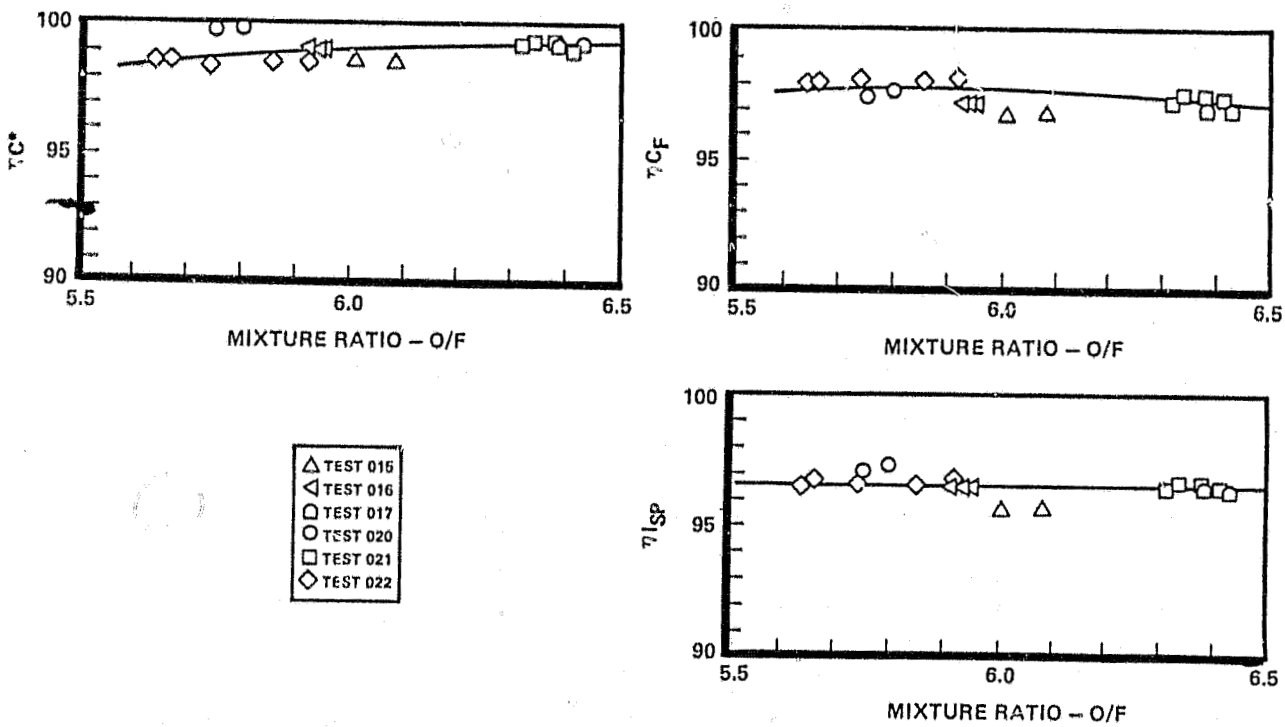

Figure 119. ASE Combustion System Performance Efficiencies

TABLE 32. TEMPERATURE RAKE DATA, INITIAL SERIES

	Thermocouple Position	y, cm (inch)	y/R	Measured Temperature, (T_p), K (F)	Radiation Correction (ΔT_p), K(F)	Total Temperature (T_T), K (F)
Test 014 (Separated Flow)	1	0.127 (0.050)	0.001 99	2278 (3640)	24.6 (44.2)	2303 (3684)
	3	0.445 (0.175)	0.006 98	2058 (3245)	36.2 (65.2)	2094 (3310)
	5	1.240 (0.488)	0.019 5	2644 (4300)	113.9 (205)	2758 (4505)
	6	1.715 (0.675)	0.027 0	2522 (4080)	150.6 (271)	2673 (4351)
	7	4.097 (1.613)	0.064 3	- -	- -	- -
Test 015	1	0.127 (0.050)	0.001 99	1722 (2640)	8.1 (14.5)	1730 (2655)
	3	0.445 (0.175)	0.006 98	1722 (2640)	17.8 (32.0)	1740 (2673)
	5	1.240 (0.488)	0.019 5	2189 (3480)	53.7 (96.6)	2243 (3577)
	6	1.715 (0.675	0.027 0	2158 (3425)	80.7 (145.3)	2239 (3570)
	7	4.097 (1.613)	0.064 3	2467 (3980)	178.6 (321.4)	2646 (4301)
Test 016	1	0.127 (0.050)	0.001 99	1814 (2805)	9.9 (17.8)	1824 (2823)
	2	0.287 (0.113)	0.004 50	1767 (2720)	18.3 (32.9)	1785 (2753)
	4	0.605 (0.238)	0.009 49	1639 (2490)	9.2 (16.5)	1648 (2507)
	6	1.715 (0.675)	0.027 0	2144 (3400)	78.8 (141.8)	2223 (3542)
	7	4.097 (1.613)	0.064 3	2264 (3615)	126.1 (226.9)	2390 (3842)
Test 017	1	0.127 (0.050)	0.001 99	1889 (2940)	11.6 (20.9)	1901 (2961)
	3	0.445 (0.175)	0.006 98	1547 (2325)	11.6 (20.8)	1559 (2346)
	5	1.240 (0.488)	0.019 5	2264 (3615)	85.3 (153.6)	2349 (3769)
	6	1.715 (0.675)	0.027 0	2161 (3430)	81.3 (146.4)	2242 (3576)
	7	4.097 (1.613)	0.064 3	2411 (3880)	125.4 (225.8)	2536 (4106)

TABLE 33. TEMPERATURE RAKE DATA, SECOND SERIES

	Thermocouple Position	y, cm (inch)	y/R	Measured Temperature, (T_p), K(F)	Radiation Correction (ΔT_p), K(F)	Total Temperature (T_T), K(F)
Test 020	1	0.0787	0.001 24 (0.001 24)	1150 (1610)	17 (31)	1167 (1641)
	2	0.119	0.001 88 (0.001 88)	1272 (1830)	26 (46)	1298 (1876)
	3	0.318	0.005 01 (0.005 01)	1558 (2345)	58 (104)	1616 (2449)
	4	1.270	0.020 0 (0.020 0)	1953 (3055)	142 (256)	2095 (3311)
	5	3.373	0.053 2 (0.053 2)	(2447) (3945)	- -	2447 (3945)
	6	5.001	0.078 9 (0.078 9)	2269 (3625)	260 (468)	2529 (4093)
	7	6.271	0.098 9 (0.098 9)	2019 (3175)	163 (293)	2182 (3468)
Test 021	1	0.0787	0.001 24 (0.001 24)	1189 (1680)	19 (35)	1208 (1715)
	2	0.119	0.001 88 (0.001 88)	1333 (1940)	31 (56)	1364 (1996)
	3	0.318	0.005 01 (0.005 01)	1614 (2445)	67 (120)	1681 (2565)
	4	1.270	0.020 0 (0.020 0)	1975 (3095)	149 (268)	2124 (3363)
	5	3.373	0.053 2 (0.053 2)	2228 (3550)	241 (434)	2469 (3984)
	6	5.001	0.078 9 (0.078 9)	2164 (3435)	214 (386)	2378 (3821)
	7	6.271	0.098 9 (0.098 9)	- -	- -	- -
Test 022	1	0.0787	0.001 24 (0.001 24)	1142 (1595)	17 (30)	1159 (1625)
	2	0.119	0.001 88 (0.001 88)	- -	- -	- -
	3	0.318	0.005 01 (0.005 01)	1528 (2290)	53 (96)	1581 (2386)
	4	1.270	0.020 0 (0.020 0)	1997 (3135)	156 (281)	2153 (3416)
	5	3.373	0.053 2 (0.053 2)	2180 (3465)	222 (399)	2402 (3864)
	6	5.001	0.078 9 (0.078 9)	2278 (3640)	264 (475)	2542 (4115)
	7	6.271	0.098 9 (0.098 9)	- -	- -	- -

Based on a 0.81 mm (0.032 in.) diameter junction diameter and the following data:

$$\sigma = 5.68 \times 10^{-12} \text{ W/cm}^2\text{-K}^4/(3.31 \times 10^{-15} \text{ Btu/in.}^2\text{-sec-R}^4)$$

$$\epsilon = 0.85$$

$$F = 1.02$$

$$N_{PR} = 0.65$$

$$C_p = 3766 \text{ J/kg-K}$$

$$\mu = 8.03 \times 10^{-7} \text{ kg/cm-sec}$$

The average heat transfer coefficient becomes approximately

$$N_{ST}\, N_{PR} = \left(\frac{0.32}{N_{RE}^{0.4}}\right) \quad \text{(laminar average)}$$

where

$$N_{ST} = \left(\frac{h}{\rho U C_p}\right) = \frac{0.457}{N_{RE}^{0.4}}$$

$$h = \frac{1854\ \rho U}{N_{RE}^{0.4}}$$

The ΔT correction then becomes

$$\Delta T = \frac{2.604 \times 10^{-11}\ N_{RE}^{0.4}}{\rho U}$$

or

$$\Delta T = \frac{6.562 \times 10^{-11}}{(\rho U)^{0.6}} (T_p)^4$$

Expressing the mass velocity, ρU, in terms of throat mass velocity ($\rho^* U^*$) and gas dynamic equivalent area ratio:

$$\rho U = \frac{(\rho^* U^*)}{\epsilon} = \frac{P_c g}{c^*_\epsilon} = \frac{1572 \times 10\ 000 \times 9.185}{2316\ \epsilon \times 9.806} = \frac{6.357 \times 10^3}{\epsilon}$$

where

$$\epsilon = f(a, M) = 250.6$$

the final correction becomes:

$$\Delta T = 3.428 \times 10^{-13}\ \epsilon^{.016}\ T_p^4$$

The corrections are included in Tables 28 and 29.

The values of temperature corrected for the radiation influences from the probe are shown in Fig. 120. The levels shown at the maximum measured point are deemed low, however, due to the adiabatic wall effect on the temperature recovery from static to total in the boundary layer.

$$\frac{T_{AW}}{T_o} = \frac{1 + (Pr)^a \frac{\gamma - 1}{2} M^2}{1 + \frac{\gamma - 1}{2} M^2}$$

For Prandtl number of unity or Mach number of zero no correction need be made. Based on the following:

$a = 0.42$ (average of turbulent (0.33) and laminar (015)

$\gamma = 1.26$

$Pr = 0.7$

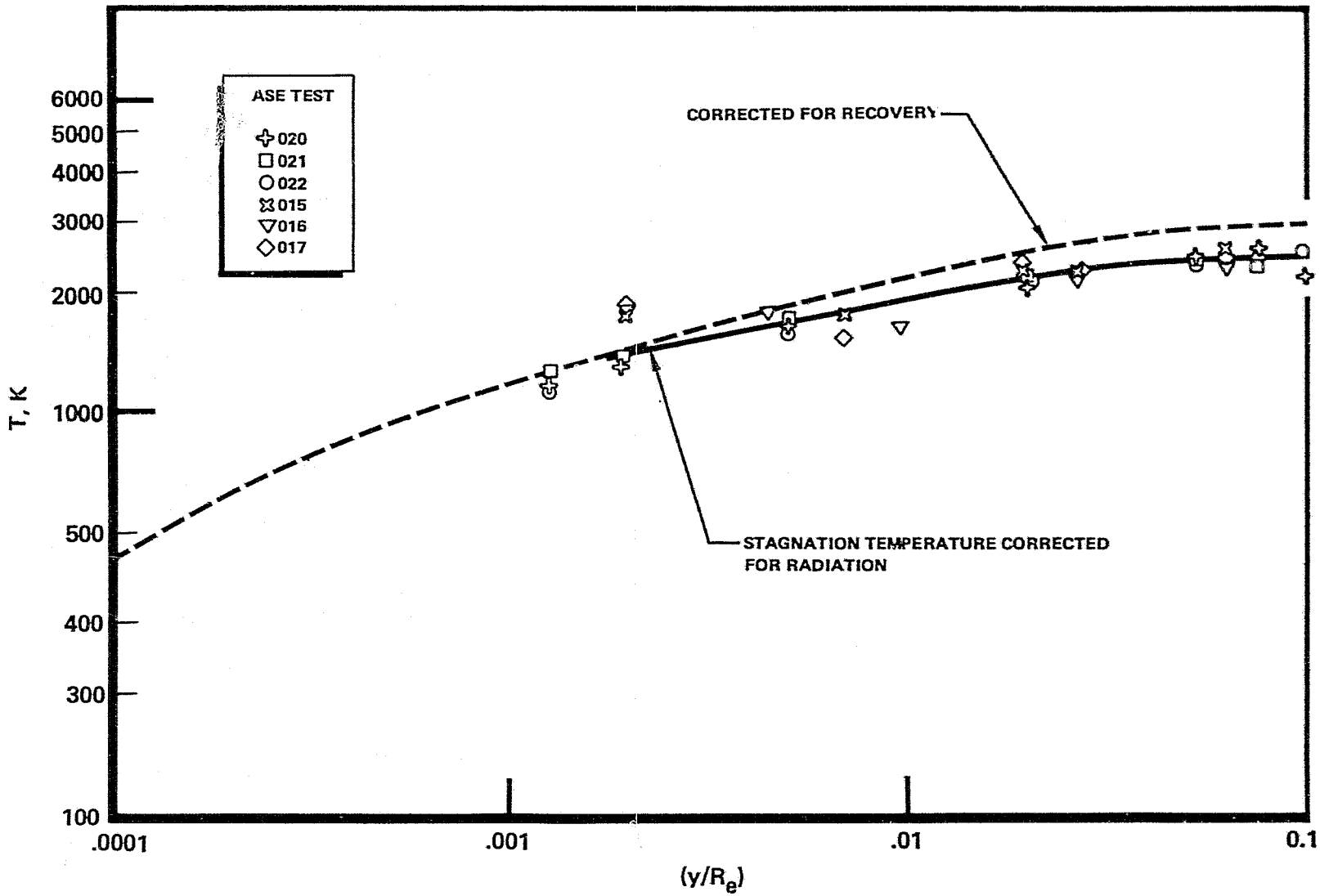

Figure 120. Summary of ASE Temperature Rake Test Data

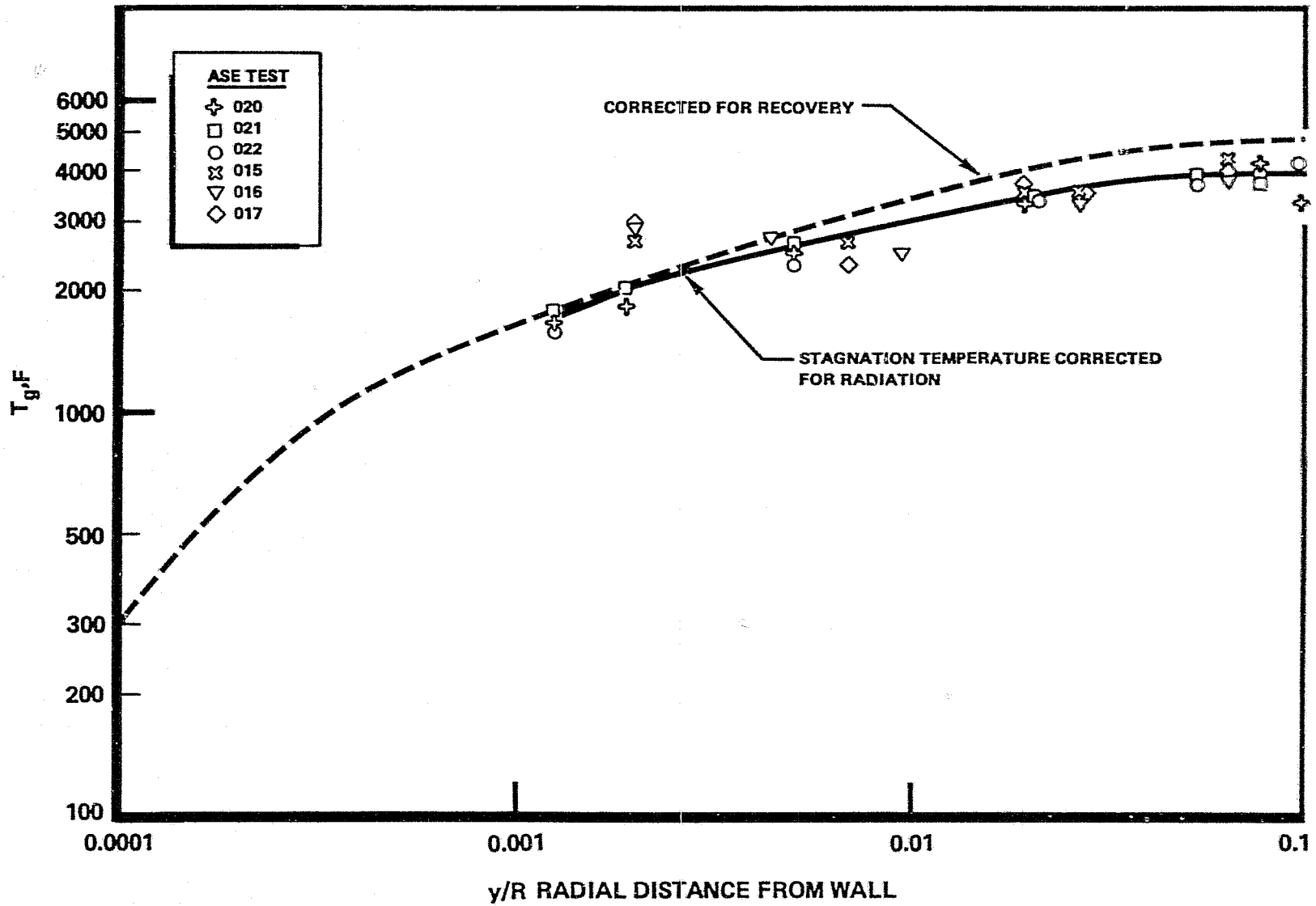

Figure 120. (Concluded)

At a Mach number of 1.0, a 2.0 percent correction is noted. At a Mach number of 5.45, a value of 15.1% correction is shown. At the corrected for radiation measured values of 2478 K (4460 R) the resulting predicted gas temperature at the outer edge becomes 2852 K (5133 R) which is substantially closer to the 100% combustion value of 3483 K (6270 R) at MR = 6.0. This added correction is shown in Fig. 120. The inability to measure a gas temperature more nearly equal to the theoretical temperature may be due to one or more of the following effects:

- Inaccurate measurement of Mach number
- Incomplete combustion near the wall
- Laminar instead of mixed turbulent gas flow
- Actual γ higher than that used for the corrections
- Inaccurate thermocouple indications at high temperatures
- Insufficient correction for radiation
- Total gas temperature lower at lower nozzle shock recover pressure level due to pressure effect

Pressure Rake Results. During the test program the two pressure rake configurations were subjected to erosion and distortion due to the high temperature and high velocity of the exhaust gas stream at the nozzle exit. Figure 121 shows the pressure and temperature rakes at the conclusion of the first test series, tests 012 through 017, while still mounted on the nozzle. Figure 122 shows the second pressure rake after completing testing, tests 018 through 022. The severe erosion noted was cumulative throughout this test series; the molybdenum-rhenium tubes which burned off after each test were carefully replaced by drilling out the damaged tubes and pressing in replacement tubes. Figure 122 indicates the remarkable durability of the stainless steel pitot support.

Table 34 illustrates the various measured values of pitot pressures and the resulting calculated velocities and Mach numbers for computation of boundary layer drag. Satisfactory pitot pressure readings were obtained on the first test series, with some operational difficulties encountered during test 022 which resulted in only limited pressure measurements. The pressure measurements were made with 0 to 15 psia Data Sensor pressure transducers. For tests 018 through 022 these transducers were accurately calibrated in the 0 to 0.7 N/cm^2a (0 to 1 psia) range with precision Wallace and Tiernan vacuum gauges.

To obtain the pressure measurements close to the nozzle wall it was necessary to flatten the open end of the 2.29 mm (0.090 inch) diameter molybdenum-rhenium tubing to about 1.0 mm (0.040 inch) in width.

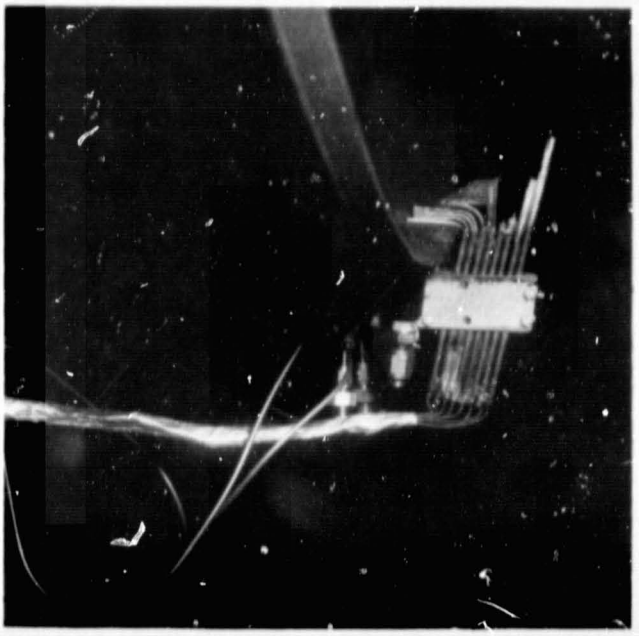

1HS35-6/6/77-S1*

Figure 121. Eroded CRES Pilot Pressure Elements and Temperature Rake Displacement

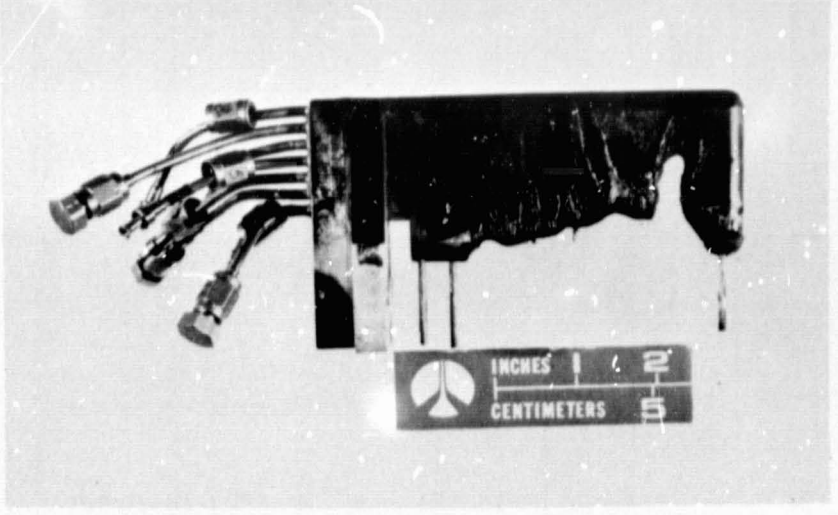

1XZ45-10/27/77-C1

Figure 122. Improved Boundary Layer Pressure Rake After Test

TABLE 34. BOUNDARY LAYER PITOT PRESSURE RAKE TEST RESULTS (TESTS 015 THROUGH 017

	P_T, N/cm^{2}a (P_T, psia)	P_T/P_c	P_T/P_w	Y (y)	Y/R_e	M_y (Y=1.26)	$(M_y)^2$	T_T, K (T_t, R)	T_s, TT	T_s, K (T_s, R)	a, m/s (a, ft/sec)	V, m/s (V, ft/sec)
Test 015: P_c = 1557.1 N/cm^{2}a; P_w = 0.334 N/cm^{2}a; P_w/P_c = 0.000 214 (P_c = 2258.3 psia; P_w = 0.484 psia; P_w/P_c = 0.000 214)												
PRI	-- (--)	-- (--)	-- (--)	-- (--)	-- (--)	-- (--)	-- (--)	-- (--)	-- (--)	-- (--)	-- (--)	-- (--)
2	-- (--)	-- (--)	-- (--)	-- (--)	-- (--)	-- (--)	-- (--)	-- (--)	-- (--)	-- (--)	-- (--)	-- (--)
3	5.41 (7.850)	0.003 48	16.219	2.73 (0.1075)	0.004 3	3.64	13.25	1755 (3160)	0.367	645 (1160)	691.6 (2269)	2520 (8 260)
4	-- (--)	-- (--)	-- (--)	-- (--)	-- (--)	-- (--)	-- (--)	-- (--)	-- (--)	-- (--)	-- (--)	-- (--)
5	9.69 (14.059)	0.006 23	29.048	8.28 (0.326)	0.013 1	4.93	24.30	2345 (4220)	0.240	560 (1010)	645.3 (2117)	3180 (10 440)
6	-- (--)	-- (--)	-- (--)	-- (--)	-- (--)	-- (--)	-- (--)	-- (--)	-- (--)	-- (--)	-- (--)	-- (--)
7	9.43 (13.684)	0.006 06	28.273	38.46 (1.514)	0.060 6	4.86	23.62	2940 (5290)	0.246	720 (1300)	732.1 (2402)	3560 (11 670)
8	-- (--)	-- (--)	-- (--)	-- (--)	-- (--)	-- (--)	-- (--)	-- (--)	-- (--)	-- (--)	-- (--)	-- (--)
Test 016: P_c = 1570.2 N/cm^{2}a; P_w = 0.309 N/cm^{2}a; P_w/P_c = 0.000 197 (P_c = 2277.3 psia; P_w = 0.448 psia; P_w/P_c = 0.000 197)												
PRI	3.95 (5.724)	0.002 51	12.777	2.34 (0.092)	0.003 68	3.20	10.24	1685 (3030)	0.429	720 (1300)	732.1 (2402)	2340 (7 690)
2	3.59 (5.210)	0.002 29	11.629	1.93 (0.076)	0.003 04	3.06	9.36	1595 (2870)	0.451	715 (1290)	729.4 (2393)	2230 (7 320)
3	3.50 (5.078)	0.002 23	11.335	1.93 (0.076)	0.003 04	3.02	9.12	1595 (2870)	0.458	730 (1310)	735.2 (2412)	2220 (7 280)
4	-- (--)	-- (--)	-- (--)	-- (--)	-- (--)	-- (--)	-- (--)	-- (--)	-- (--)	-- (--)	-- (--)	-- (--)
5	6.44 (9.335)	0.004 10	20.837	6.71 (0.264)	0.010 6	4.14	17.14	2230 (4010)	0.310	690 (1240)	715.1 (2346)	2960 (9 710)
6	-- (--)	-- (--)	-- (--)	-- (--)	-- (--)	-- (--)	-- (--)	-- (--)	-- (--)	-- (--)	-- (--)	-- (--)
7	-- (--)	-- (--)	-- (--)	-- (--)	-- (--)	-- (--)	-- (--)	-- (--)	-- (--)	-- (--)	-- (--)	-- (--)
8	9.79 (14.205)	0.006 24	31.708	58.67 (2.310)	0.092 5	5.16	26.63	2965 (5340)	0.224	665 (1200)	703.5 (2308)	3630 (11 910)
Test 017: P_c = 1573.7 N/cm^{2}a; P_w = 0.312 N/cm^{2}a; P_w/P_c = 0.000 198 (P_c = 2282.4 psia; P_w = 0.453 psia; P_w/P_c = 0.000 198)												
PRI	3.05 (4.428)	0.001 94	9.775	2.34 (0.092)	0.003 68	2.81	7.90	1685 (3030)	0.493	830 (1490)	783.9 (2572)	2200 (7 230)
2	-- (--)	-- (--)	-- (--)	-- (--)	-- (--)	-- (--)	-- (--)	-- (--)	-- (--)	-- (--)	-- (--)	-- (--)
3	3.84 (5.611)	0.002 46	12.386	1.93 (0.076)	0.003 04	3.15	9.92	1595 (2870)	0.437	695 (1250)	718.1 (2356)	2260 (7 420)
4	5.44 (7.893)	0.003 46	17.424	4.32 (0.170)	0.006 81	3.78	14.29	1985 (3570)	0.350	695 (1250)	718.1 (2356)	2710 (8 910)
5	6.39 (9.271)	0.004 06	20.466	6.71 (0.264)	0.010 6	4.10	16.81	2230 (4010)	0.314	700 (1260)	720.9 (2365)	2960 (9 700)
6	-- (--)	-- (--)	-- (--)	-- (--)	-- (--)	-- (--)	-- (--)	-- (--)	-- (--)	-- (--)	-- (--)	-- (--)
7	-- (--)	-- (--)	-- (--)	-- (--)	-- (--)	-- (--)	-- (--)	-- (--)	-- (--)	-- (--)	-- (--)	-- (--)
8	4.58 * (6.645)*	-- (--)	-- (--)	37.64 (1.482)	0.059 4	-- (--)	-- (--)	-- (3470)	-- (--)	-- (--)	-- (--)	-- (--)

*Values indicate loose fitting at tap
NOTE: MW assumed 14.1; Y = 1.26; MR = 6.0

TABLE 34. (Concluded)

	P_T, N/cm^{2}a (P_T, psia)	P_T/P_c	P_T/P_w	γ (γ)	γ/R_e	$M_y(\gamma=1.26)$	$(M_y)^2$	T_T, K (T_T, R)	T_s/T_T	T_s, K (T_s, R)	a, m/s (a, ft/sec)	V, m/s (V, ft/sec)
Test 020: P_c = 1549 N/cm^{2}a; P_w/P_c = 0.000 194 (P_c = 2246 psia; P_w = 0.435 psia; P_w/P_c = 0.000 194)												
PRI	2.16 (3.13)	0.001 39	7.20	1.78 (0.070)	0 002 8	2.38	5.66	1560 (2810)	0.585	915 (1644)	824 (2703)	1 960 (6 430)
2	0.96 (1.39)	0.000 619	3.20	1.52 (0.060)	0.002 4	1.50	2.25	1520 (2740)	0.780	1185 (2137)	939 (3082)	1 410 (4 620)
3	3.60 (5.22)	0.002 32	12.0	3.94 (0.155)	0.006 2	3.07	9.42	1910 (3440)	0.449	860 (1545)	798 (2619)	[illegible] (8 040)
4	6.03 (8.75)	0.003 90	20.1	10.80 (0.425)	0.017 0	4.06	16.48	2435 (4380)	0.318	775 (1393)	668 (2192)	2 710 (8 900)
5	8.55 (12.4)	0.005 52	28.5	36.32 (1.43)	0.057 2	4.86	23.62	2950 (5310)	0.246	725 (1306)	734 (2409)	3 570 (11 710)
6	10.69 (15.5)	0.006 90	35.6	49.15 (1.935)	0.077 4	5.44	29.59	2935 (5280)	0.206	605 (1087)	670 (2198)	3 650 (11 960)
7	11.03 (16.0)	0.007 13	36.8	61.72 (2.43)	0.097 2	5.53	30.58	2840 (5112)	0.201	570 (1027)	651 (2136)	3 600 (11 810)
8	10.62 (15.4)	0.006 86	35.4	92.20 (3.63)	0.145	5.42	29.38	2830 (5090)	0.208	590 (1059)	661 (2169)	3 580 (11 760)
Test 021: P_c = 1586 N/cm^{2}a; P_w = 0.317 N/cm^{2}a; (P_w/P_c = 0.000 20 (P_c = 2300 psia; P_w = 0.460 psia; P_w/P_c = 0.000 200)												
PRI	0.55 (0.80)	0.000 348	1.74	1.02 (0.040)	0.001 60	0.97	0.941	1380 (2480)	0.895	1235 (2220)	957 (3140)	930 (3 050)
2	0.55 (0.79)	0.000 344	1.72	1.78 (0.070)	0.002 80	0.96	0.922	1560 (2810)	0.897	1400 (2520)	1019 (3343)	980 (3 210)
3	4.77 (6.92)	0.003 00	14.8	3.94 (0.155)	0.006 20	3.47	12.04	1910 (3440)	0.390	745 (1340)	744 (2440)	2 580 (8 470)
4	1.2* (1.7)*	0.000 738*	--	10.41 (0.410)	0.016 4	--	--	-- (--)	--	-- (--)	-- (--)	-- (--)
5	4.4* (6.4)*	0.002 78*	--	36.83 (1.45)	0.058 0	--	--	-- (--)	--	-- (--)	-- (--)	-- (--)
6	10.55 (15.3)	0.006 64	33.2	48.77 (1.92)	0.076 8	5.25	27.56	2935 (5280)	0.218	640 (1150)	689 (2261)	3 620 (11 870)
7	11.07 (16.05)	0.006 97	34.9	62.74 (2.47)	0.098 8	5.37	28.84	2810 (5060)	0.211	595 (1067)	664 (2178)	3 570 (11 700)
8	10.48 (15.2)	0.006 60	33.0	93.47 (3.68)	0.147 2	5.23	27.35	2755 (4960)	0.220	605 (1090)	671 (2200)	3 510 (11 510)
Test 022: P_c = 1536 N/cm^{2}a; P_w = 0.299 N/cm^{2}a; P_w/P_c = 0.001 95 (P_c = 2227 psia; P_w = 0.434 psia; P_w/P_c = 0.001 95)												
PRI	0.4* (0.6)*	0.000 274*	1.405	1.02 (0.040)	0.001 6	--	--	-- (--)	--	-- (--)	-- (--)	-- (--)
2	-- (--)	--	--	-- (--)	--	--	--	-- (--)	--	-- (--)	-- (--)	-- (--)
3	-- (--)	--	--	-- (--)	--	--	--	-- (--)	--	-- (--)	-- (--)	-- (--)
4	1.7* (2.4)	0.001 12*	--	10.41 (0.410)	0.016 4	--	--	-- (--)	--	-- (--)	-- (--)	-- (--)
5	4.8* (6.9)	0.003*	--	36.83 (1.45)	0.058 0	--	--	-- (--)	--	-- (--)	-- (--)	-- (--)
6	-- (--)	--	--	-- (--)	--	--	--	-- (--)	--	-- (--)	-- (--)	-- (--)
7	-- (--)	--	--	-- (--)	--	--	--	-- (--)	--	-- (--)	-- (--)	-- (--)
8	10.14 (14.7)	0.006 61	33.9	93.47 (3.68)	0.147 2	5.31	28.20	2755 (4960)	0.215	590 (1066)	663 (2176)	3 520 (11 560)

*Values indicate loose fitting at tap

NOTE: MW assumed 14.1; γ = 1.26; MR = 6.0

The pitot pressure to wall pressure ratios from both series of tests are plotted in Fig. 124, with a summary line drawn to best represent the data. Also shown on this plot for comparison purposes are the summary curves from previous subscale model tests performed with other test fluids. A good agreement with these curves is shown. Also plotted are the pitot pressure to chamber pressure ratios, Fig. 124.

The Mach number away from the nozzle wall surface was computed based on the pitot pressure ratio by the normal shock relationship.

$$\frac{P_T}{P_w} = \left(\frac{\gamma+1}{2} M^2\right)^{\frac{\gamma}{\gamma-1}} \Bigg/ \left(\frac{2\gamma}{\gamma+1} M^2 - \frac{\gamma-1}{\gamma+1}\right)^{\frac{1}{\gamma-1}} \quad ; \quad \gamma = 1.26$$

These values are computed in Table 34 and are illustrated in Fig. 125. The Mach number curve has been drawn asymptotic to a 5.45 value.

The deficit in Mach number below the free stream level value just outside the boundary layer represents the accumulated drag resulting from wall shear and cooling losses. An analytical development of the loss percentage is reasoned by the method described below.

The free stream thrust based on an unattenuated exit velocity of uniform potential field value becomes approximately:

$$T = \int_0^{Ac} \rho \frac{V^2}{g} dA = \frac{\rho_\infty V_\infty}{g} \pi R_e^2$$

The boundary layer thrust for a thin fractional layer becomes

$$T_{BL} = \int_0^{\delta} \frac{2\pi R_e}{g} \rho_y V_y^2 dy = \frac{2\pi R_e^2}{g} \int_0^{\delta} \rho_y u_y^2 \, d(y/R_e)$$

For a constant static pressure through the boundary layer

$$\rho_y = \frac{P}{RT_y} \quad , \quad My^2 = \frac{u_y^2}{\gamma g R T_y}$$

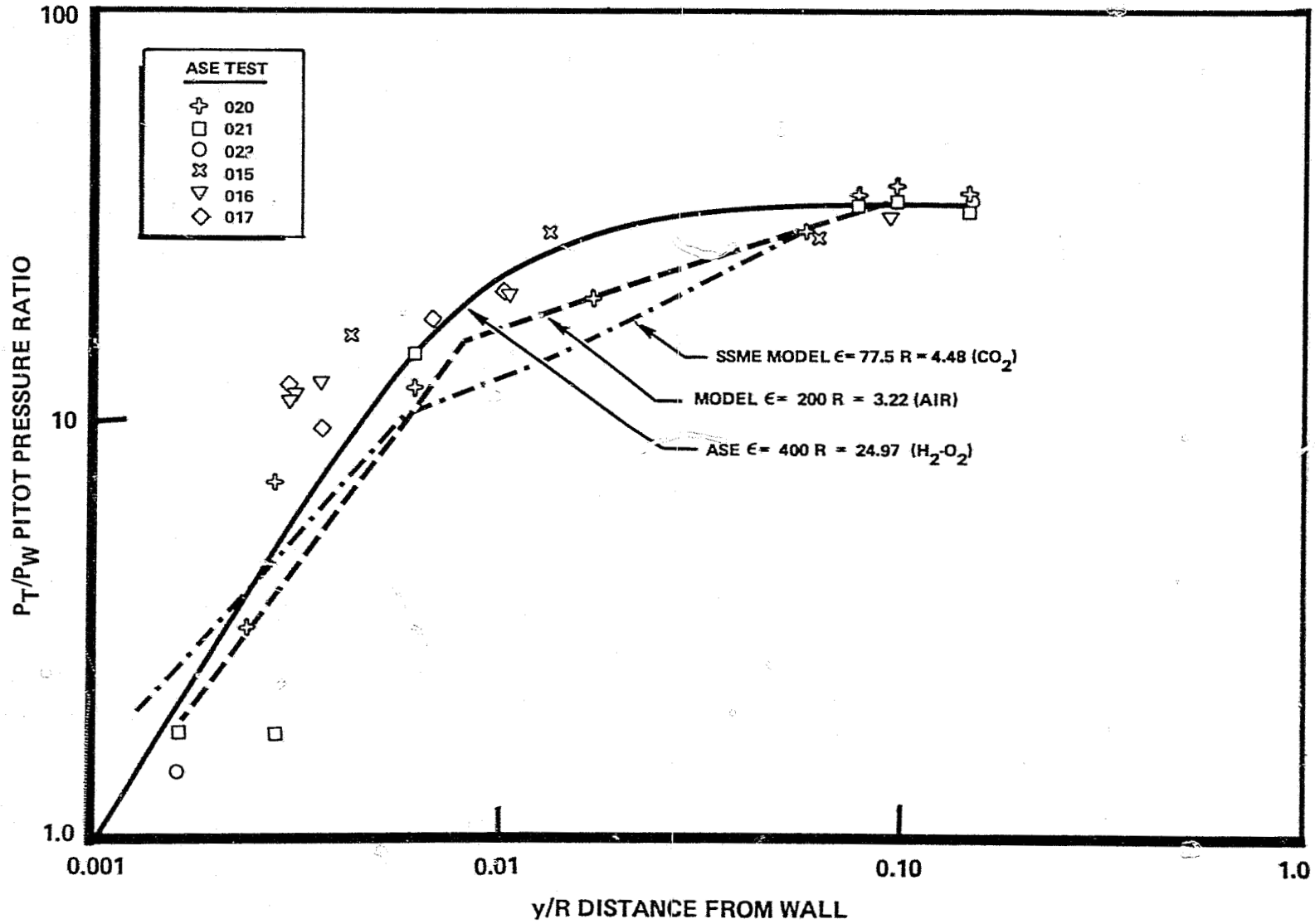

Figure 123. Comparative Summary of ASE Full-Scale Boundary Layer Pitot Pressure With Cold-Flow Model Data

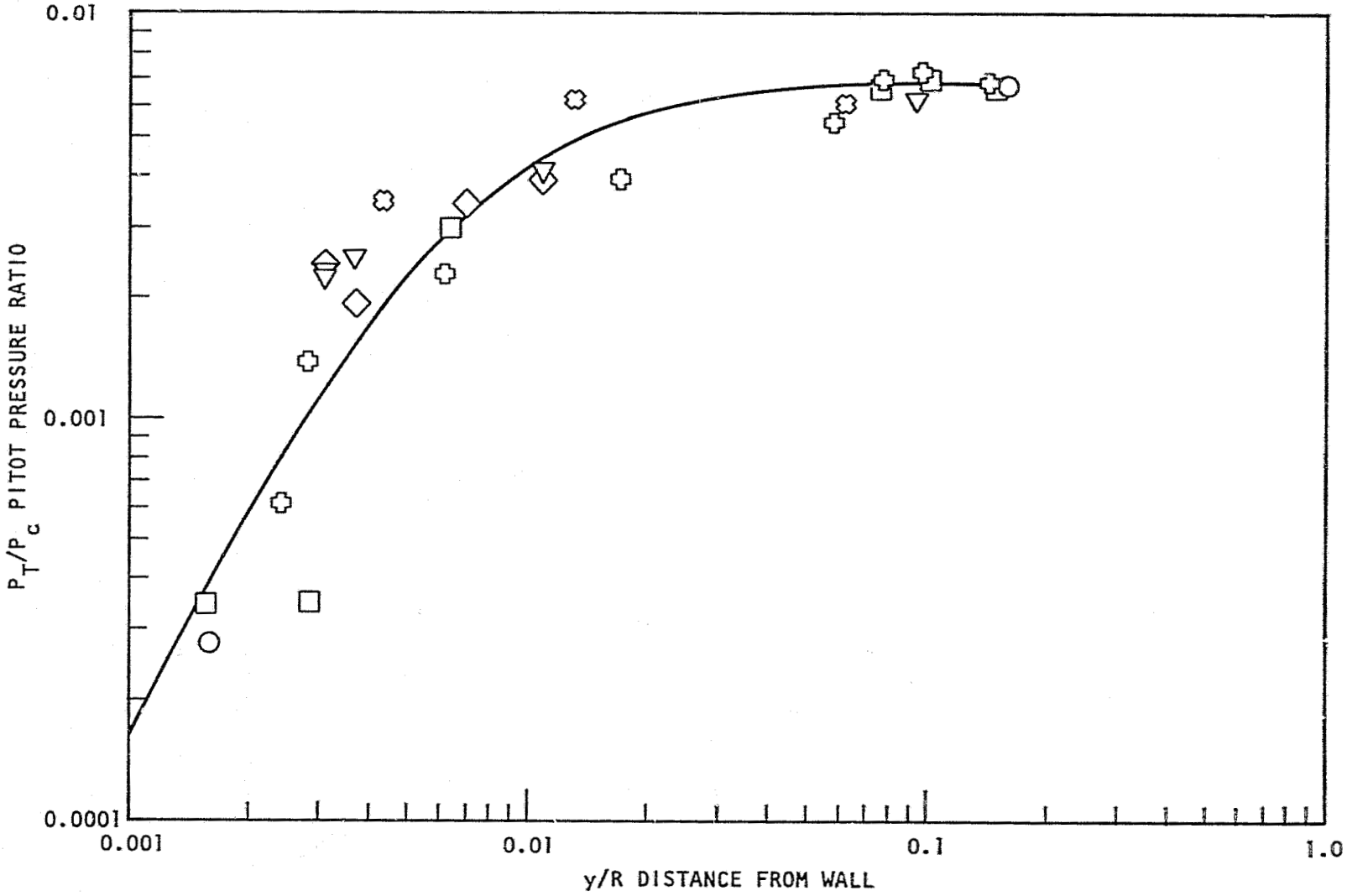

Figure 124. Summary of ASE Pitot Rake Test Data (P_w/P_e = 0.000197)

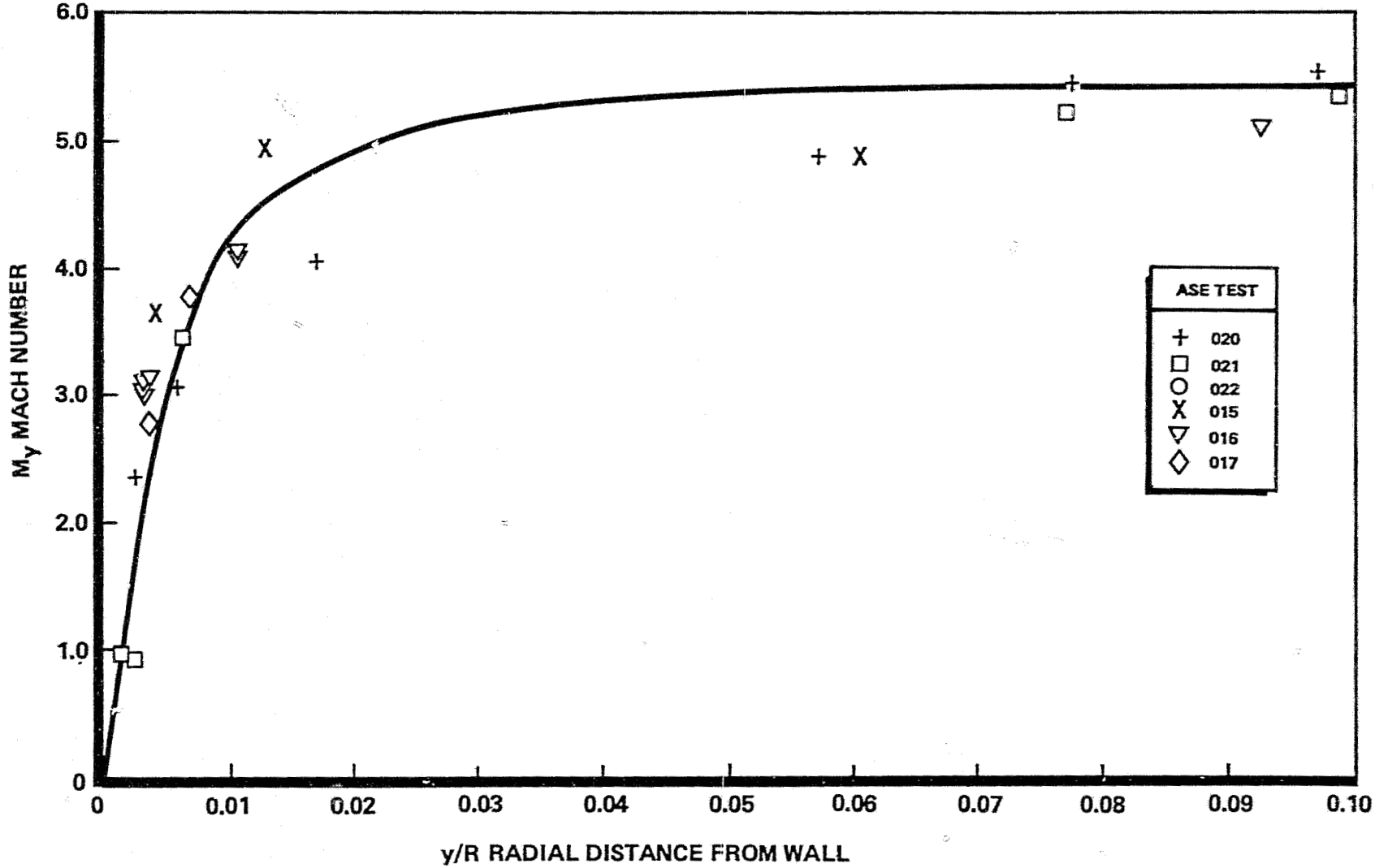

Figure 125. Computed ASE Boundary Layer Mach Number vs y/R

Therefore

$$\frac{\rho_y u_y^2}{\rho_\infty u_\infty^2} = \frac{P\gamma g M_y^2}{P\gamma g M_\infty^2} = \frac{M_y^2}{M_\infty^2}$$

The thrust of the boundary layer consequently results as,

$$T_{BL} = \frac{2\pi R_e^2}{g} \rho_\infty u_\infty^2 \int_0^\delta \frac{M_y^2}{M_\infty} d(y/R_e)$$

Taking the ratio of the boundary layer thrust to mainstream thrust therefore results

$$\frac{\Delta T_{BL}}{T} = 2 \int_0^\delta \left(\frac{M_y}{M_\infty}\right)^2 d(y/R_e)$$

A correction for the potential field Mach nonuniformity in the radial direction at the exit was made as,

$$\frac{\Delta T_{BL}}{T} = 2 \left(\frac{M_\delta}{M_\infty}\right)^2 \int_0^\delta \left(\frac{M_y}{M_\infty}\right)^2 d(y/R_e)$$

A value of 6.14 was used for M_∞ based on a uniform average one-dimensional exit value. A value of 5.45 was used for the boundary layer edge value, M_δ, as shown by the best fit curve of Fig. 125. The deficit shown in Fig. 126 in terms of the reduction of M_y^2 below the free stream value represents the drag loss. Graphical integration of the deficit area resulted in a determination of the drag value for all tests at 2.0% $\pm$0.25%. Further precision of this value could only be derived through a finer net of data in the region close to the nozzle wall.

Nozzle Wall Static Pressure Results. Table 35 lists the nozzle wall pressures measured during tests 020 to 022. Fig. 127 shows a plot of these pressures, normalized as $P_{wall}/P_{chamber}$, compared to the variable properties theoretical curve for the 175:1 to 400:1 nozzle contour. Additional data slices were reduced, and these points are shown on Fig. 127, although not

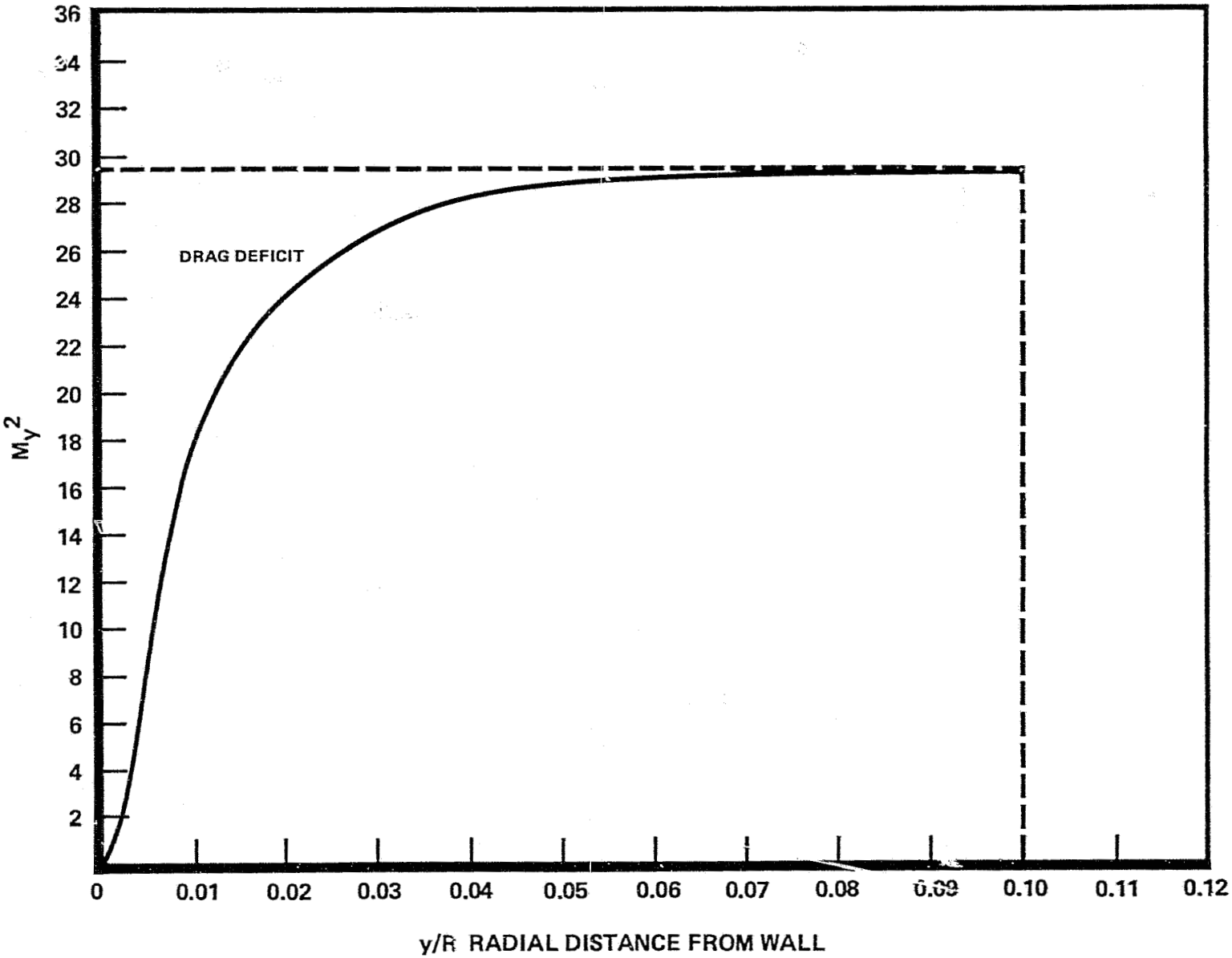

Figure 126. Summary of $(M_y)^2$ for Nozzle Wall Drag Determination

TABLE 35. NOZZLE WALL STATIC PRESSURE MEASUREMENTS

Test No.	Nozzle Wall Static Pressure, N/cm^2a (psia)	Nozzle Wall Pressure Ratio (P_W/P_C)	Nozzle Area Ratio (A/A_{Throat})
020	0.794 (1.152)	0.000 518	221
	0.379 (0.549)	0.000 247	332
	0.301 (0.437)	0.000 195	395
021	0.865 (1.255)	0.000 553	221
	0.416 (0.603)	0.000 266	332
	0.316 (0.458)	0.000 202	395
022	0.836 (1.212)	0.000 563	221
	0.567 (0.823)	0.000 373	298
	0.399 (0.579)	0.000 263	332
	0.299 (0.433)	0.000 196	395

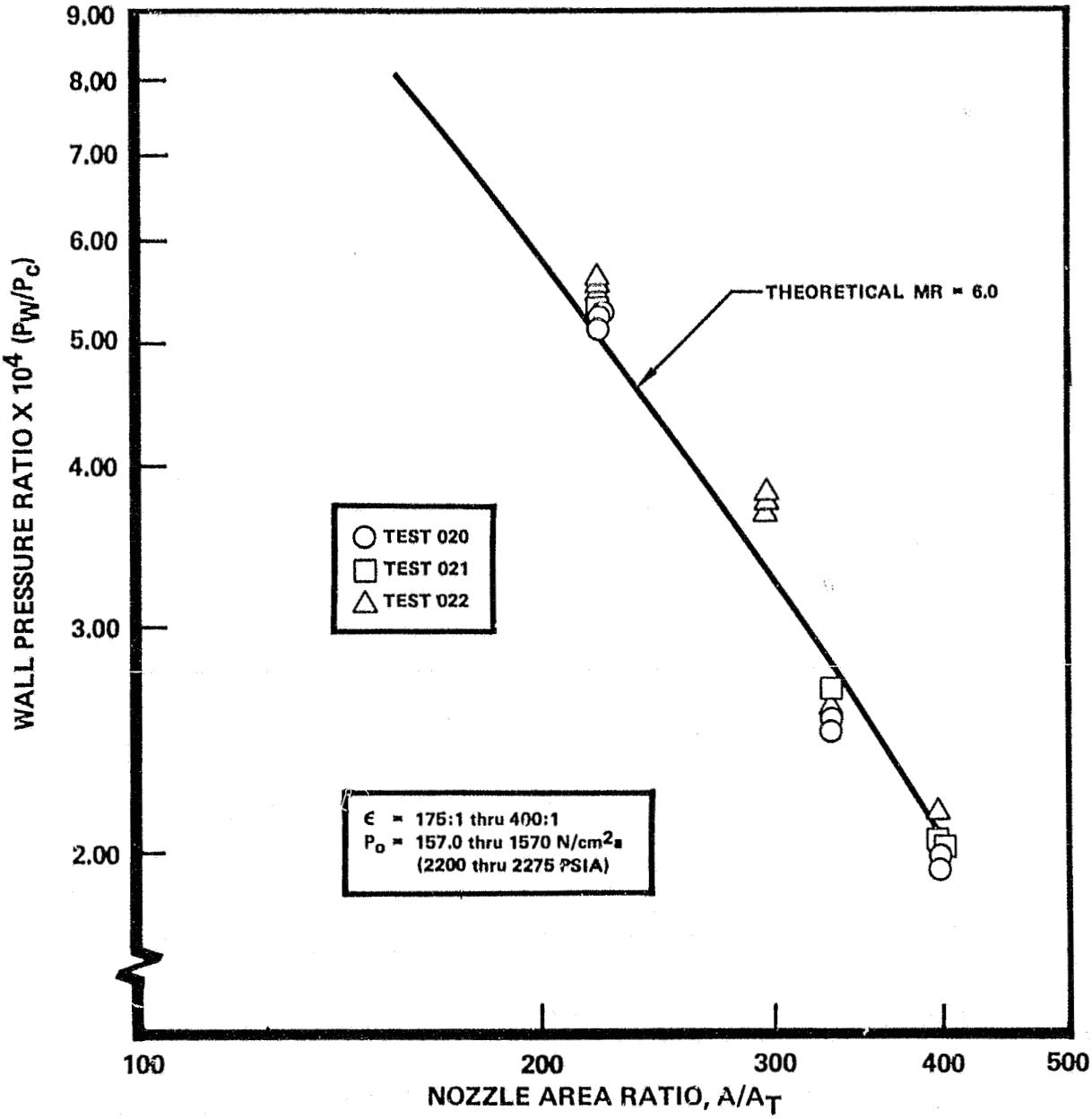

Figure 127. Nozzle Extension Wall Static Pressure Profile

included in the tabular listings. These wall pressure measurements were made with Data Sensor pressure transducers which were also accurately calibrated in the 0 to 0.7 N/cm^{2}a (0 to 1 psia) range with precision Wallace and Tiernan vacuum gauges. These data agree well with the analytical solution, and indicate that no adjustment needs to be made to the variable property method of characteristics solutions for high area ratio nozzles.

Preburner Gas Temperatures

Temperature measurements in the two preburner exhaust ducts were made during all tests. Most of the tests were of short duration, however, and the recorded temperatures were of a transient nature and were, therefore, not included in the data analysis. Figure 128 shows the preburner installed with the main combustion chamber and the thermocouple bosses in the two ducts can be clearly seen. An additional boss was subsequently added in each duct to circumvent interference with some of the system ducting and hardware. The thermocouples were inserted into the duct to varying depths. Figure 129 is a schematic cross section of the ducting showing the different positions of the thermocouples throughout the testing program. Three thermocouples of differing lengths were inserted into each duct and these were interchanged between test series to provide the coverage shown.

Tables 36 and 37 summarize the duct gas temperature recorded. Some of the recordings during these tests were not yet stabilized, as noted in the tables, and the temperature at which the thermocouples would stabilize was indeterminate. Included in Tables 36 and 37 are the main injector inlet temperature, measured by a single thermocouple at each of the two main injector inlet locations. These measurements do not purport to be averages of the upstream duct measurements, but rather indicate the temperature downstream of the turbine simulation orifices and downstream of the ducting passageways which continued to absorb heat from the preburner exhaust gas during these comparatively short duration tests.

The data from Tables 36 and 37 are plotted on Fig. 130 and 131, the oxidizer turbopump duct temperatures and fuel turbopump duct temperatures. On these plots a slight bias can be seen for those temperature measurements taken closer to the duct walls (B, O, U). The temperatures near the wall are lower than the temperatures at other locations, possibly due to the influence of the combustor sleeve coolant flow which may not be fully mixed with the balance of the exhaust gas.

The three data points on Fig. 130 which represent the results from test 031 do not conform to the balance of the data points nor to the slope of the theoretical temperature versus mixture ratio curve. They are included in the interest of completness. It should be noted that these points were derived from test 031, which was a preburner-only test with no combustion chamber downstream of the turbine simulation orifices so that there was sonic flow across these orifices throughout the test. The balance of the points were from staged combustion assembly tests and from a time slice when the main combustion chamber downstream of the turbine simulation orifices was operating at greater than 1380 N/cm^2 (2000 psi) and the flow across these orifices was subsonic.

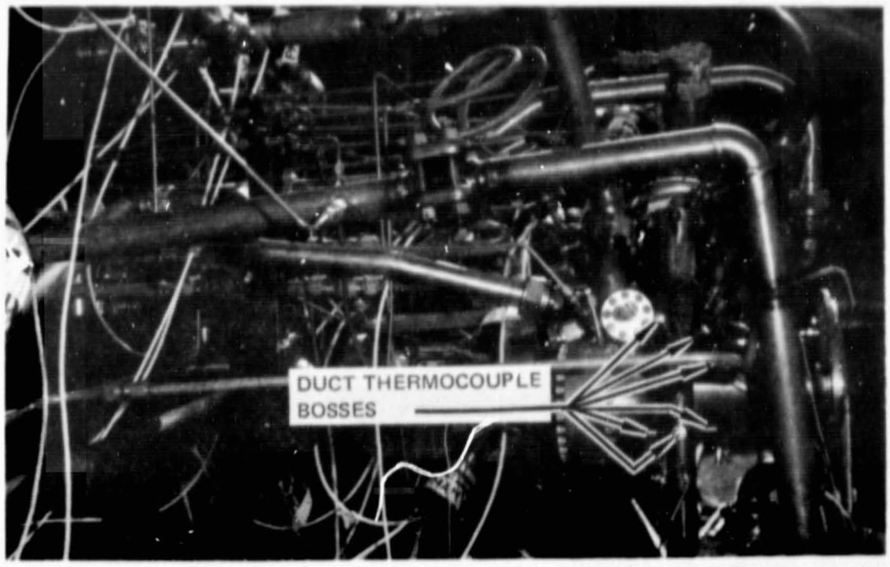

1HS23-10/15/76-S1D*

Figure 128. Stage Combustion Assembly Installation With Duct Thermocouple Bosses

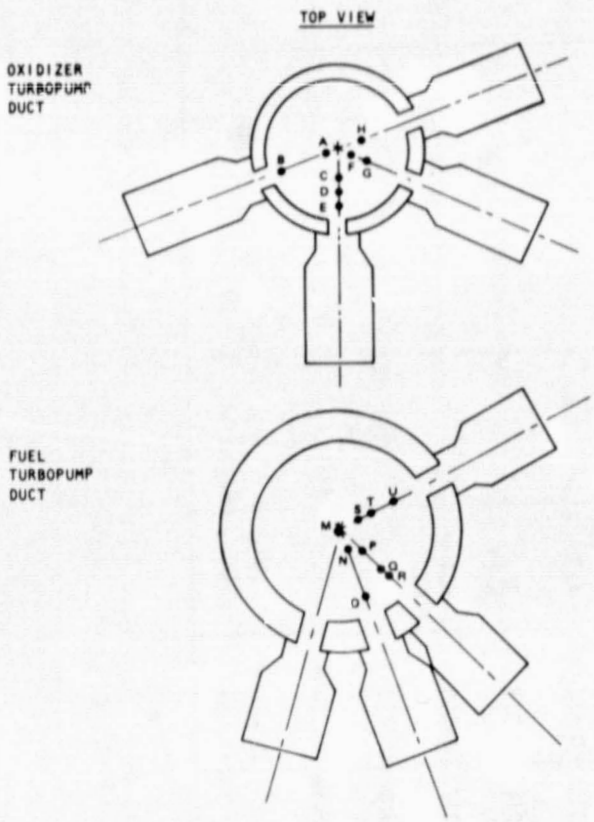

Figure 129. Preburner Duct Thermocouple Locations as Viewed From the Injector

TABLE 36. PREBURNER OXYGEN TURBINE DUCT GAS TEMPERATURES

Test No.	Mixture Ratio (o/F)	Temperature, K (F)								
		A	B	C	D	E	F	G	H	Igniter Inlet
031	0.922	982 (1307)	-	-	994 (1330)	-	-	-	972 (1291)	NG
010	0.584	-	806 (991)	879 (1123)	-	-	839 (1047)	-	-	819 (1015)
011	0.589	-	788 (959)	861 (1090)	-	-	830 (1034)	-	-	805 (989)
015	0.553	817 (1011)	-	-	-	NG	-	831 (1036)	-	808 (994)
016	0.529	797 (974)	-	-	-	NG	-	812 (1002)	-	791 (964)
017	0.595	861 (1090)	-	-	-	NG	-	875 (1115)	-	852 (1074)
020	0.531	-	758 (904)	-	NG	-	791 (964)	-	-	771 (928)
021	0.590	-	827 (1028)	-	NG	-	868 (1103)	-	-	842 (1056)
022	0.564	-	822 (1019)	-	NG	-	853 (1076)	-	-	829 (1033)

TABLE 37. PREBURNER HYDROGEN TURBINE DUCT GAS TEMPERATURE

Test No.	Mixture Ratio (O/c)	Temperature, K (F)									
		M△	N	O	P	Q	R	S	T	U	Igniter Inlet
031	0.922	Not Stabilized	-	-	-	-	Not Stabilized	-	Not Stabilized	-	NG
010	0.584	Not Stabilized	-	-	-	Not Stabilized	-	Not Stabilized	-	-	860 (1088)
011	0.589	Not Stabilized	-	-	-	Not Stabilized	-	876 (1117)	-	-	838 (1049)
015	0.553	Not Stabilized	Not Stabilized	-	-	-	-	-	-	867 (1101)	845 (1061)
016	0.528	Not Stabilized	852 (1073)	-	-	-	-	-	-	850 (1070)	827 (1029)
017	0.595	942 (1236)	930 (1214)	-	-	-	-	-	-	919 (1195)	895 (1151)
020	0.531	873 (1112)	-	Not Stabilized	846 (1063)	-	-	-	-	-	805- (989)
021	0.590	932 (1217)	-	899 (1158)	926 (1206)	-	-	-	-	-	882 (1127)
022	0.564	934 (1221)	-	876 (1116)	917 (1190)	-	-	-	-	-	869 (1105)

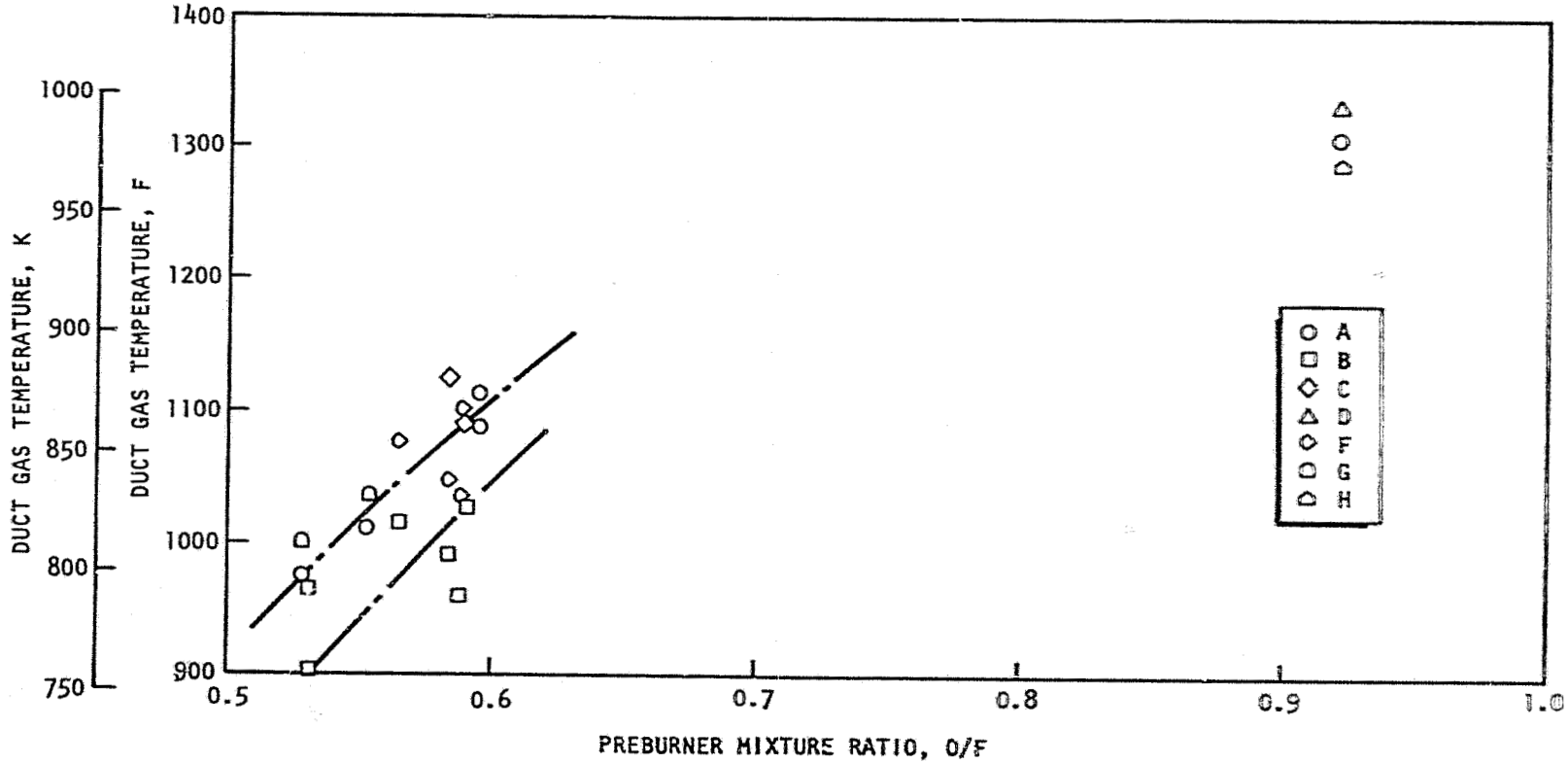

Figure 130. Preburner Oxidizer Turbopump Duct Gas Temperature vs MR

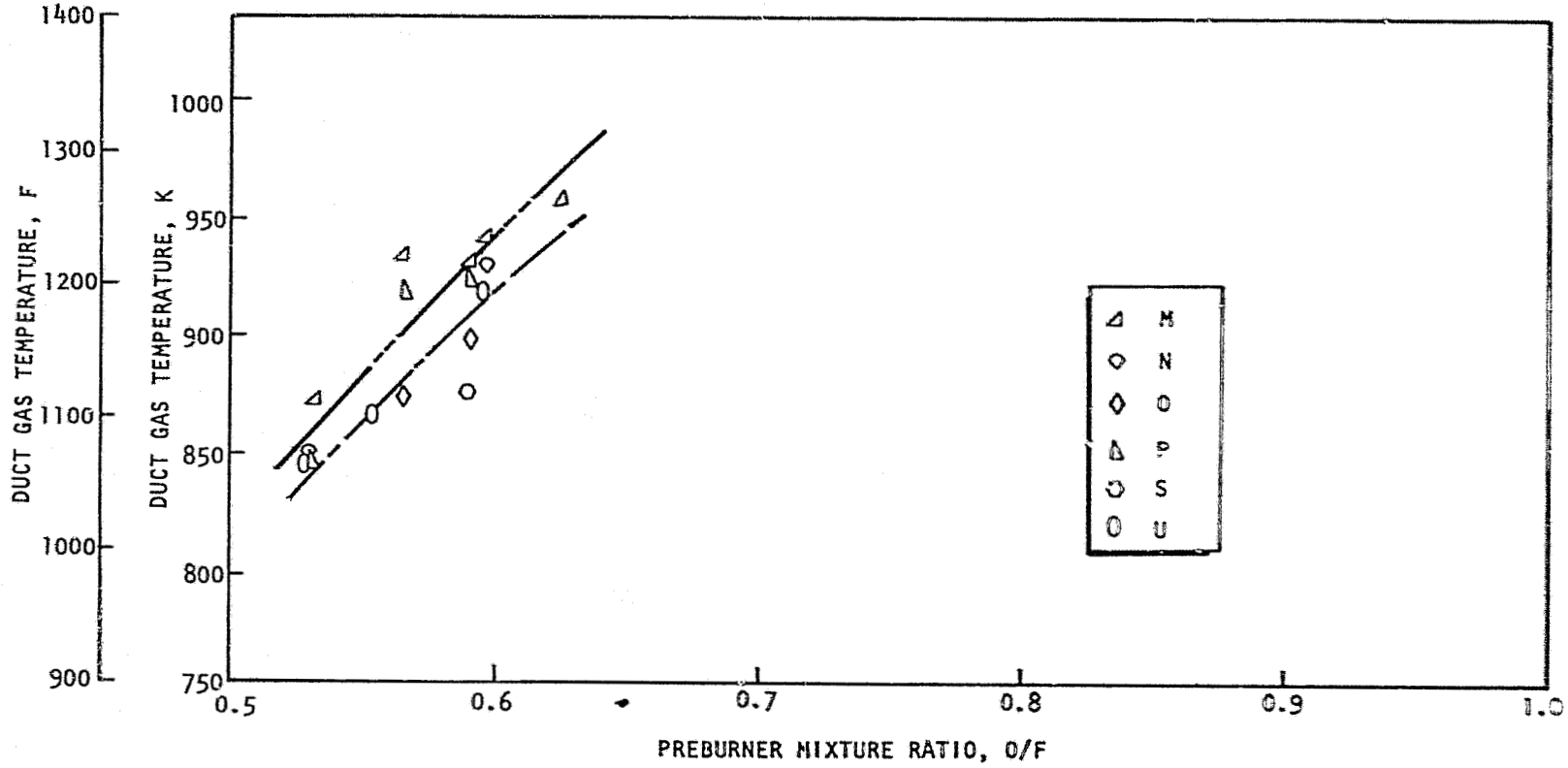

Figure 131. Preburner Fuel Turbopump Duct Gas Temperature vs MR

Heat Transfer

Heat transfer measurements were made during all of the testing. Measurements were of four kinds:

1. Total heat input to the combustion chamber coolant
2. Total heat input to the cooled tubular nozzle
3. Transient heat input to the uncooled nozzle extension
4. Combustion chamber rib wall temperatures

The heat input to the combustion chamber was determined from the coolant total enthalpy increase as evaluated from measurements of the coolant flowrate, coolant inlet temperature, and coolant outlet temperature. The tubular nozzle heat input was similarly determined from the enthalpy increase of the nozzle coolant flowrate, based on the nozzle coolant flowrate and the inlet and outlet coolant temperature. The uncooled 400:1 nozzle section heat transfer rate was determined by the transient method from transient temperatures recorded from thermocouples welded to the outside of the nozzle wall at three locations.

Combustion chamber rib temperature measurements were taken with the special thermocouples previously described. These measurements were intended to complement the other heat input measurements.

Combustion Chamber Heat Input. The combustor heat input measurement results for the longer duration, (more than 2 seconds), tests are summarized in Table 38 and Fig. 132. Figure 133 presents the same data normalized to 1380 N/cm^2a (2000 psia) chamber pressure.

For comparison purposes the heat transfer results from the previous testing of the NARloy-Z chamber, as reported in CR135221, Final Report of Advanced Thrust Chamber Technology (Ref. 1) are plotted on Fig. 132. These tests, identified as test 008 and 043 through 048, utilized ambient temperature hydrogen as the fuel. The heat input to the chamber was about 40% higher during the current test series. Numerous influences which may contribute to this increase were evaluated. The influences calculated to be of significance are:

1. Combustion chamber geometry
2. Chamber pressure and wall temperature
3. Fuel injection velocity

The Zr-Cu combustor tested in the current test series had a lower contraction ratio (3.64 versus 4.02) as a result of a slightly larger throat diameter. This influence and the difference in contour (Fig. 134) resulted in an analytically calculated heat input difference of 4.8%. The influence of chamber pressure and wall temperature difference resulted in a 9.8% increase over the earlier test data.

TABLE 38. COMBUSTION CHAMBER HEAT TRANSFER AND PRESSURE DROP SUMMARY

Test No.	Chamber Pressure, N/cm^2a (psia)	Mixture Ratio, o/f	Coolant					
			Flowrate, kg/s (lb/sec)	Inlet Temperature, K (F)	ΔT, K (F)	Heat Transfer Rate, kW (Btu/sec)	Inlet Pressure, N/cm^2a (psia)	ΔP, N/cm^2 (psi)
011	1581.6 (2293.9)	6.089	2.593 (5.716)	46.2 (-376.8)	132 (238)	5351 (5077)	2793.4 (4051.3)	713.6 (1035.0)
015	1557.1 (2258.3)	6.084	2.503 (5.517)	55.3 (-360.4)	134 (241)	5383 (5107)	2680.6 (3887.7)	764.7 (1109.1)
016	1570.2 (2277.3)	5.954	2.567 (5.660)	53.4 (-363.9)	141 (254)	5456 (5176)	2733.0 (3963.7)	779.1 (1129.9)
017	1573.7 (2282.4)	6.428	2.585 (5.699)	51.5 (-367.3)	135 (243)	5555 (5270)	2753.6 (3993.6)	784.3 (1137.5)
020	1541.4 (2235.5)	5.751	2.741 (6.042)	54.8 (-361.4)	123 (222)	5367 (5092)	2870.9 (4163.8)	785.2 (1138.8)
021	1576.6 (2286.6)	6.378	2.608 (5.749)	52.7 (-365.2)	133 (240)	5547 (5263)	2777.0 (4027.6)	737.3 (1069.3)
022	1528.8 (2217.3)	5.920	2.548 (5.617)	46.4 (-376.5)	137 (246)	5474 (5194)	2662.4 (3861.3)	696.0 (1009.4)

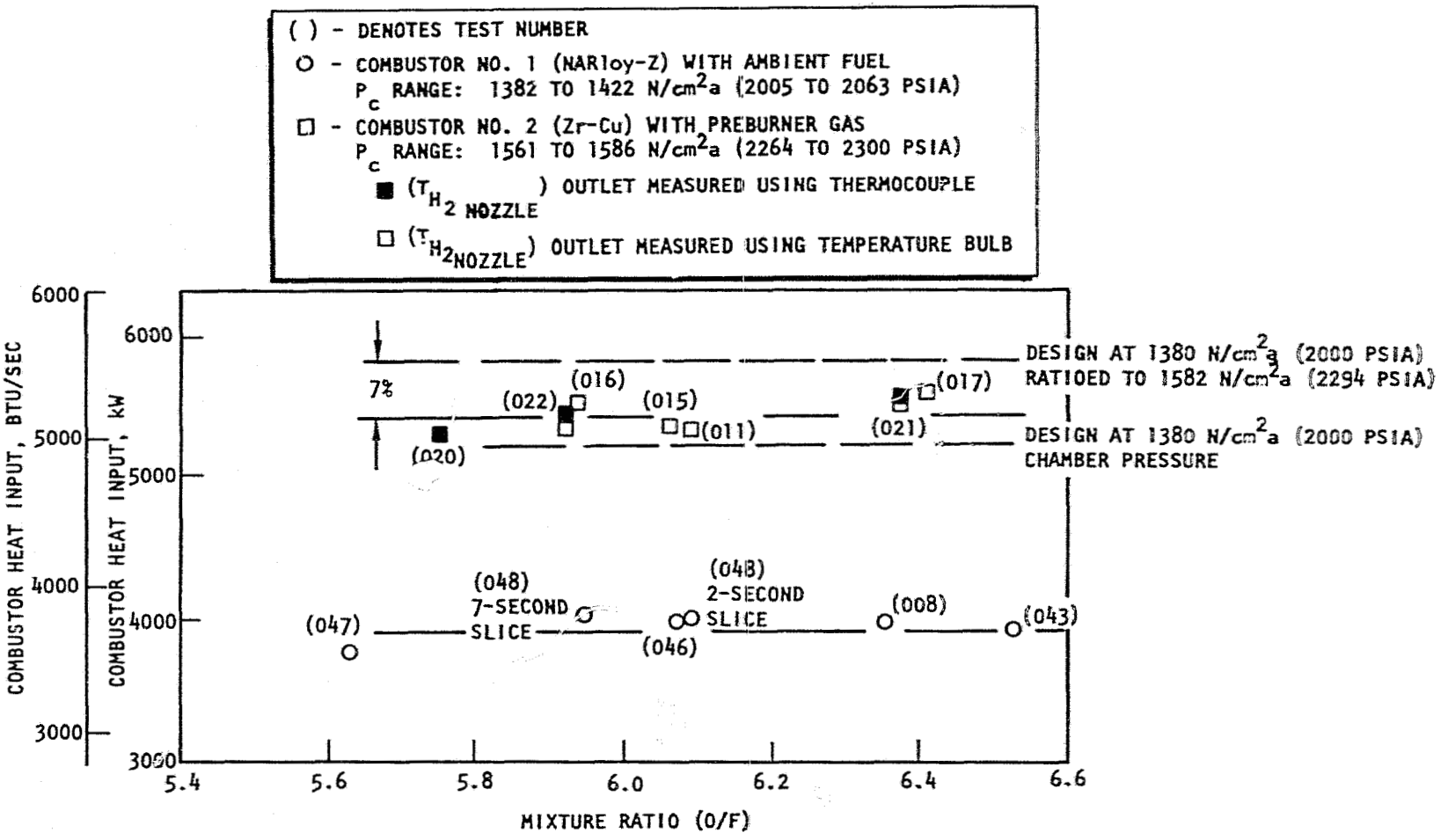

Figure 132. Zr-Cu Combustor Heat Input

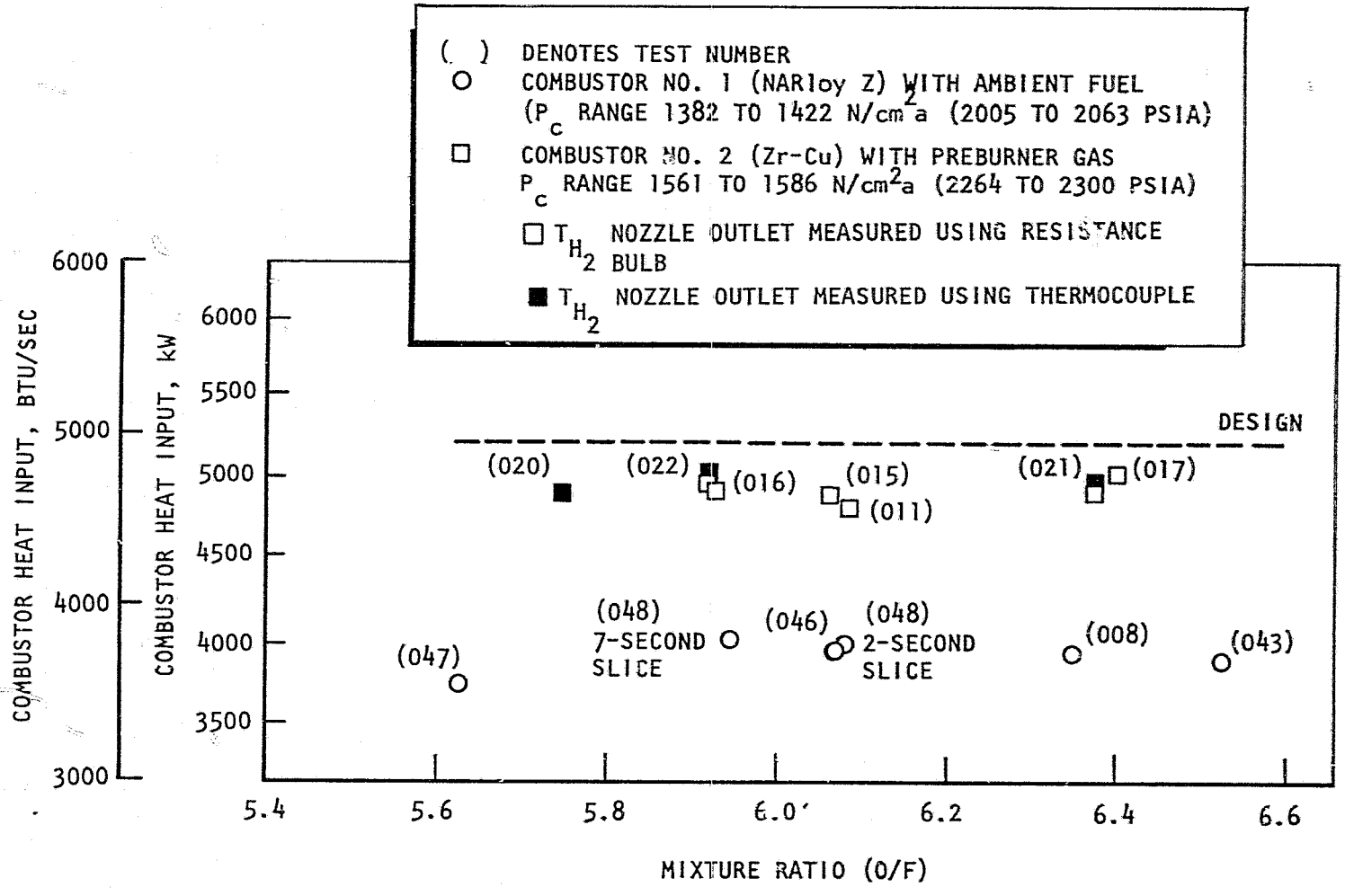

Figure 133. Zr-Cu Combustor Heat Input Normalized to 2000-psia Chamber Pressure

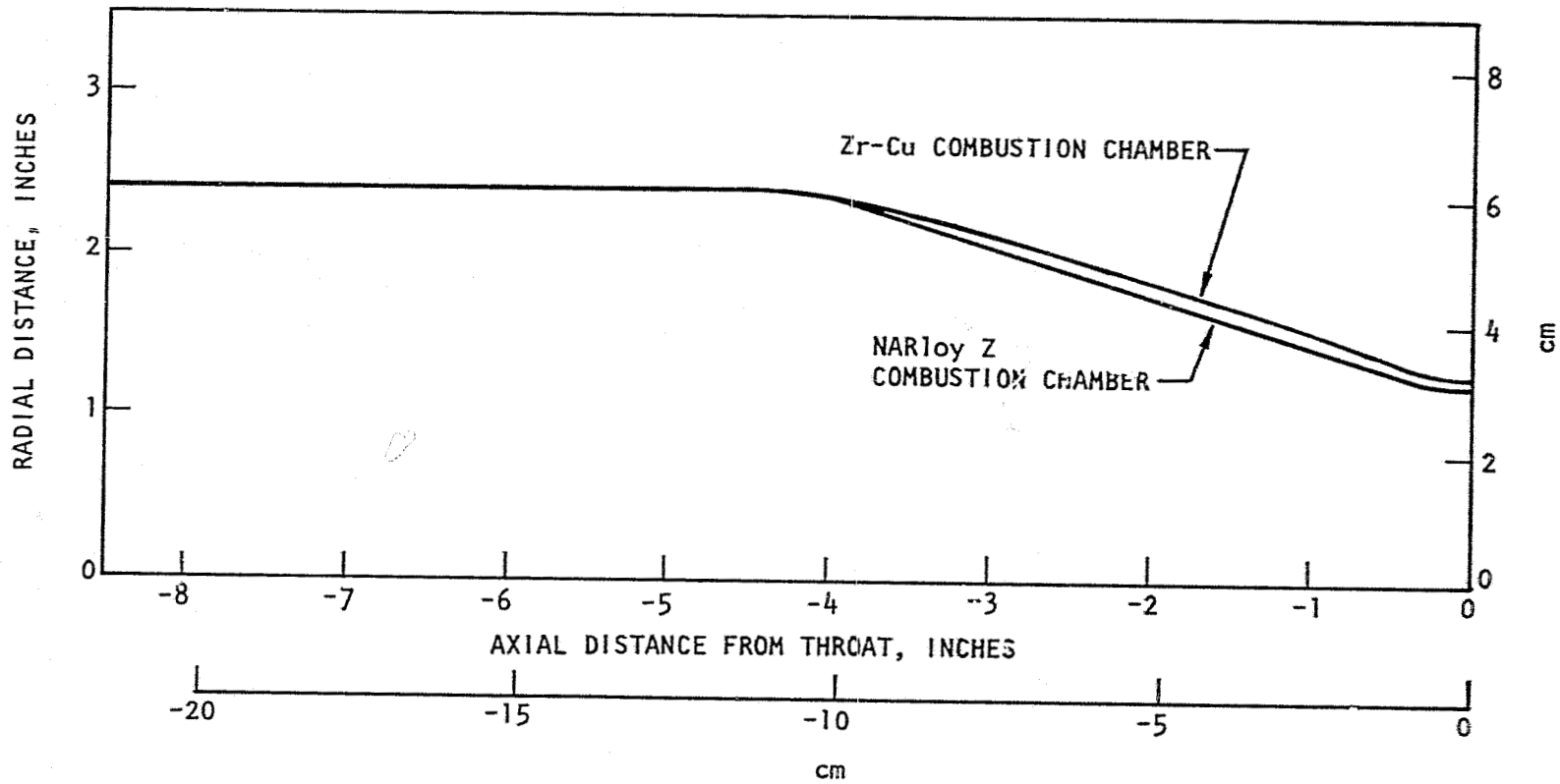

Figure 124. Combustion Chamber Contours

Applying the heat input variation with fuel injection velocity of Ref. 5, a 3.2% increase was determined. The combined effect of these three influences brought the two combustor heat inputs within 18.6% of that shown in Fig. 135.

In addition to the calculable influences, the additional influences were considered, and the magnitude on heat input change was estimated. The three major uncalculable influences considered were:

1. Earlier or enhanced combustion process with preburner gas resulting in higher heat fluxes in the subsonic portions of the chamber

2. Different heat transfer characteristics for the two injectors

   a. Hot preburner gas injector may create a significantly higher turbulence level near the injector increasing injector region heat fluxes.

   b. Change in characteristics of the face coolant flow through the Rigimesh injector face with the two injectors.

3. Higher than predicted combustor geometry influence

As shown in the table in Fig. 135, the magnitude of these unclaculable influences range from a 10 to 30% heat input increase which could easily account for the 18.6% remaining difference.

In the series cooling circuit used for tests 020 through 022, the Zr-Cu combustor was cooled in the same manner as in the parallel cooling circuit. As shown in Fig. 136, the combustor coolant outlet temperature stabilized typically within 1.5 seconds of thrust chamber start. For these tests, two additional thermocouples were installed in the chamber coolant outlet, one in each duct.

The three combustor coolant outlet temperatures differed by 5 K (9 R), which translates into a maximum of a 4% difference in the combustor heat input.

The combustor coolant flowrate during the parallel cooled testing was computed from the sonic flow equation using the combustor coolant outlet properties for the sonic orifice in the outlet duct. For the series cooled testing the combustor coolant flowrate was computed by summing the bypass flow and nozzle coolant flow using sonic flow equations. The nozzle coolant flowrate was calculated using the two different nozzle coolant outlet temperatures so that two different combustor coolant flowrates resulted. Both combustor heat inputs determined using these flowrates are shown in Fig. 132 and the difference only amounted to a maximum of 1.9%. The combustor heat inputs obtained from both of the current test series were essentially identical and were essentially independent with mixture ratio over the 4.7 to 6.4 test range and approximately 7% lower than the design ratioed value.

The Zr-Cu combustion chamber coolant pressure drop vs coolant flowrate data listed in Table 38, are plotted in Fig. 137.

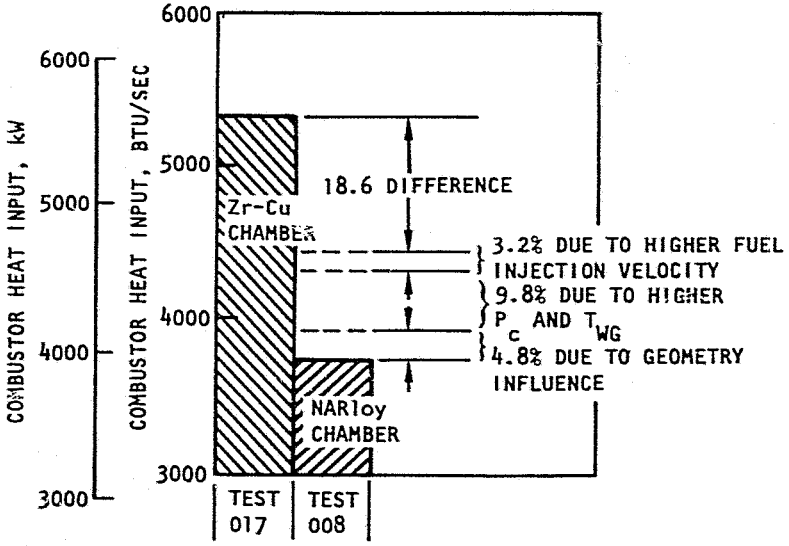

ADDITIONAL INFLUENCES	ESTIMATED MAGNITUDE %
1. EARLIER COMBUSTION WITH PREBURNER GAS.	+5 TO 10%
2. DIFFERENT HEAT TRANSFER CHARACTERISTICS OF DIFFERENT INJECTORS	
a. ADDITIONAL TURBULENCE CREATED BY PREBURNER GAS	+5 TO 10%
b. REDUCED FILM-COOLING INFLUENCE OF FACE COOLING WITH PREBURNER GAS	0 TO 5%
3. HIGHER THAN PREDICTED COMBUSTOR GEOMETRY INFLUENCE	0 TO 5%
TOTAL	+10 TO 30%

Figure 135. Combustor Heat Input Correlation

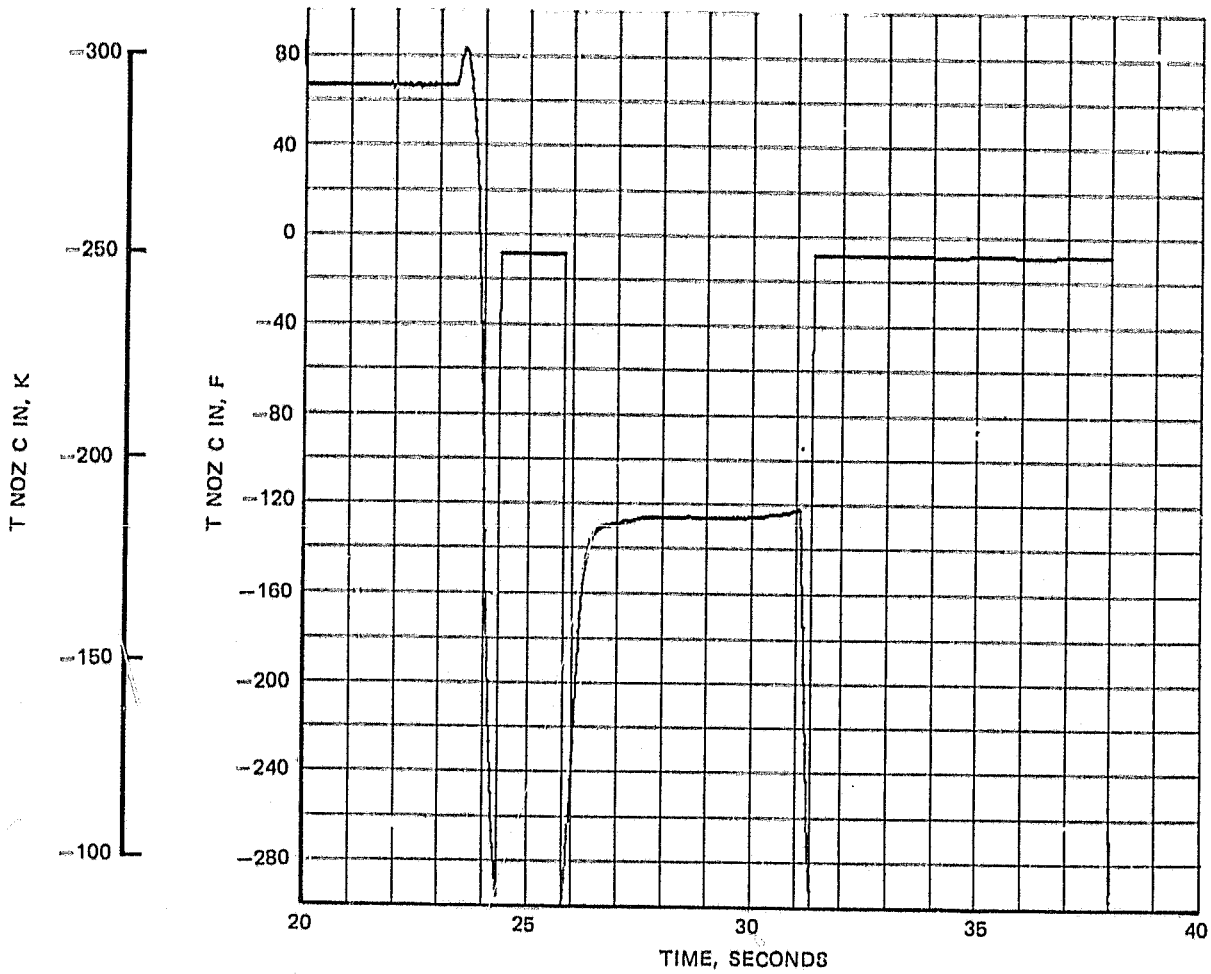

Figure 136. Typical Zr-Cu Combustor Coolant Outlet Temperature History

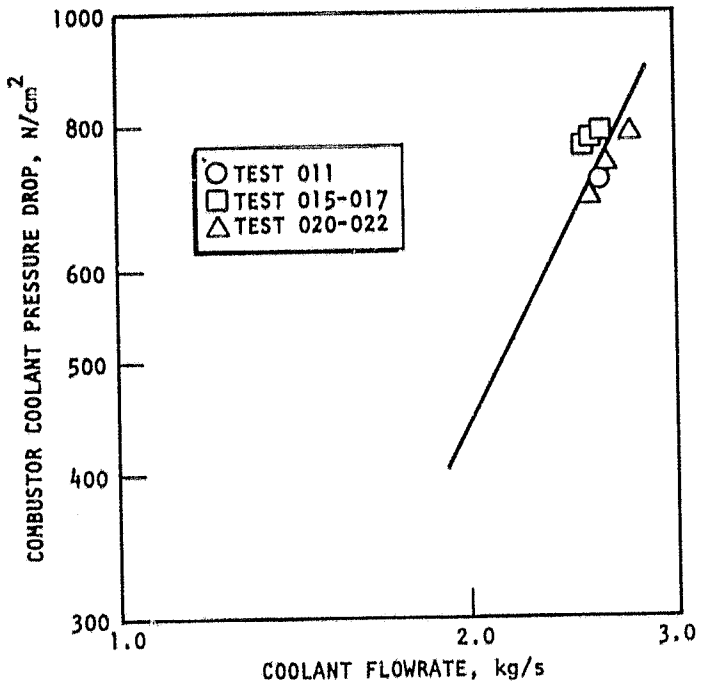

(a)

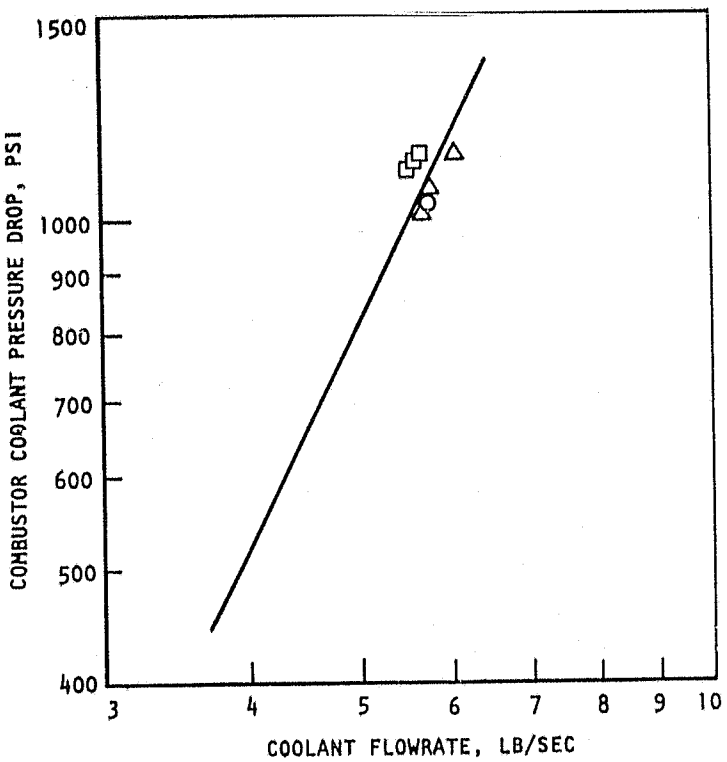

(b)

Figure 137. Zr-Cu Combustor Coolant Pressure Drop vs Coolant Flowrate

The design gas-side heat transfer coefficient distribution was perturbed a constant percentage until the analytical computer run (using the regenerative cooling design/analysis computer program) matched the test data heat input. The resulting cooling pressure drops were compared. The analytically determined combustor coolant pressure drops for the tests were within ±2.1% of the measured value.

Tubular Nozzle Heat Input. The hydrogen cooled nozzle heat input measurement results for these same tests (except 011 which did not have the nozzle installed) are summarized in Table 39 and Fig. 138. Again, for comparison purposes, the heat transfer results from the previous testing of chamber and nozzle, as reported in Ref. 5 CR135221, Final Report of Advanced Thrust Chamber Technology, test 008, is plotted on Fig. 138. Figure 139 shows the data all normalized to 1380 N/cm^2a (2000 psia) chamber pressure by the relationship

$$Q_{1380} = \left(\frac{1380}{P_{noz\ stag}}\right)^{0.8} \times Q_{measured}$$

During all of the tests, the nozzle was dump cooled using hydrogen. The nozzle was over-cooled using coolant flowrates up to four times the rated flow to protect the nozzle from the greater than three times increase in heat flux which is encountered during the nozzle separation which normally occurs during each thrust chamber start and shutdown.

The heat transfer measurements from tests 015 through 017 with the parallel cooling circuits indicated a much higher nozzle heat transfer rate than anticipated (Fig. 138).

Due to the larger combustor throat diameter of the Zr-Cu channel wall combustor, the nozzle, during the current tests, contained a lower combustion gas mass velocity. This influence was calculated to result in a 6.9% heat input increase over that of test 008. The higher chamber pressure and lower wall temperature influence was computed to result in a 16.2% increase over the heat input measured during test of the NARloy-Z chamber.

Figure 140 presents a graphical correlation of the nozzle heat input from test 017 of the current test series and test 008 from the thrust chamber program testing. Figure 140a shows a direct comparison of nozzle heat input from these two tests. As noted, the nozzle heat input during test 017 was 32.7% greater than expected after allowing for the contraction ratio effect (6.9%) and the chamber pressure/wall temperature effect (16.2%).

An extensive analysis of the nozzle hydraulic resistance was performed with both sets of data, and the comparison of the analytical coolant pressure drop was determined and compared to the measured values, (Fig. 141). Fig. 140b shows the comparison of the heat input data assuming that the test 008 data are incorrect. The heat input of test 008 has been increased by the amount necessary, 37.5%, to result in a ΔP correlated to the test 017 ΔP; that is,

TABLE 39. REGENERATIVELY COOLED NOZZLE HEAT TRANSFER AND PRESSURE DROP

Test No.	Chamber Pressure, N/cm^2a (psia)	Mixture Ratio (o/f)	Coolant						
			Flowrate, kg/s (lb/sec)	Inlet Temperature, K (F)	ΔT, K (F)	Heat Transfer Rate, kW (Btu/sec)	Heat Transfer Rate Normalized to 1380 N/cm^2, kW (2000 psi, Btu/sec)	Inlet Pressure, N/cm^2a (psia)	ΔP, N/cm (psi)
015	1557.1 (2258.3)	6.084	2.795 (6.161)	55.3 (-360.4)	129 (233)	5923 (5620)	5401 (5124)	1815.7 (2633.3)	588.9 (854.1)
016	1570.2 (2277.3)	5.954	2.504 (5.520)	53.4 (-363.9)	141 (254)	5800 (5503)	5253 (4984)	1752.3 (2541.4	457.1 (662.9)
017	1573.7 (2282.4)	6.428	2.395 (5.280)	51.5 (-367.3)	149 (268)	5712 (5420)	5139 (4876)	1840.0 (2668.6)	404.7 (587.0)
020	1541.4 (2235.5)	5.751	2.382 (5.251)	178.3 (-139.1)	106 (191)	4028 (3822)	3702 (3513)	1964.0 (2848.5)	774.3 (1123.0)
021	1576.6 (2286.6)	6.378	2.262 (4.986)	186.2 (-124.9)	119 (215)	4242 (4025)	3829 (3633)	1940.0 (2813.7)	750.2 (1088.1)
022	1528.8 (2217.3)	5.920	2.211 (4.874)	182.8 (-130.9)	115 (207)	4027 (3821)	3726 (3535)	1872.1 (2715.1)	724.9 (1051.4)

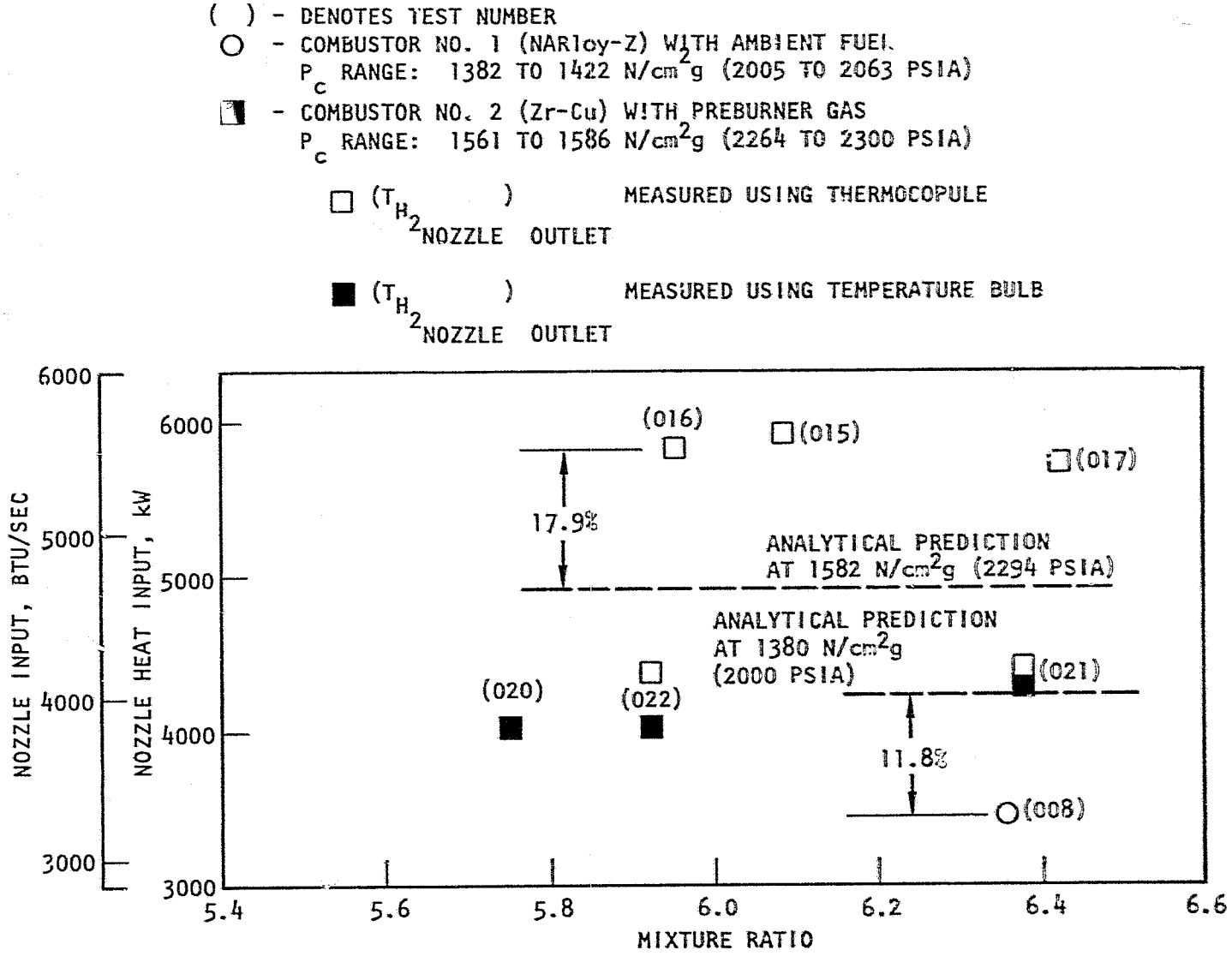

Figure 138. A-286 Regeneratively Cooled Nozzle Heat Input

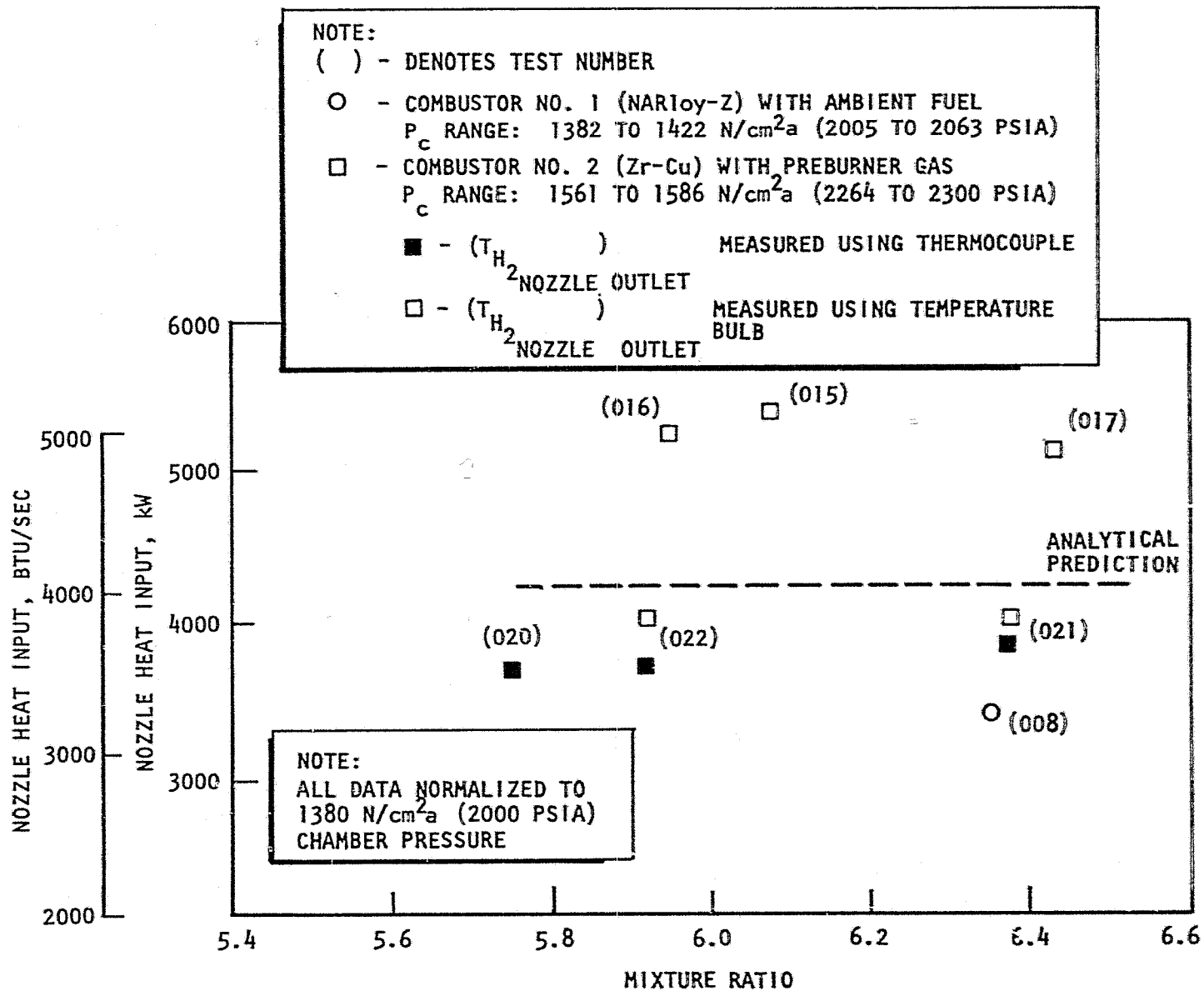

Figure 139. A-286 Regeneratively Cooled Nozzle Normalized Heat Input

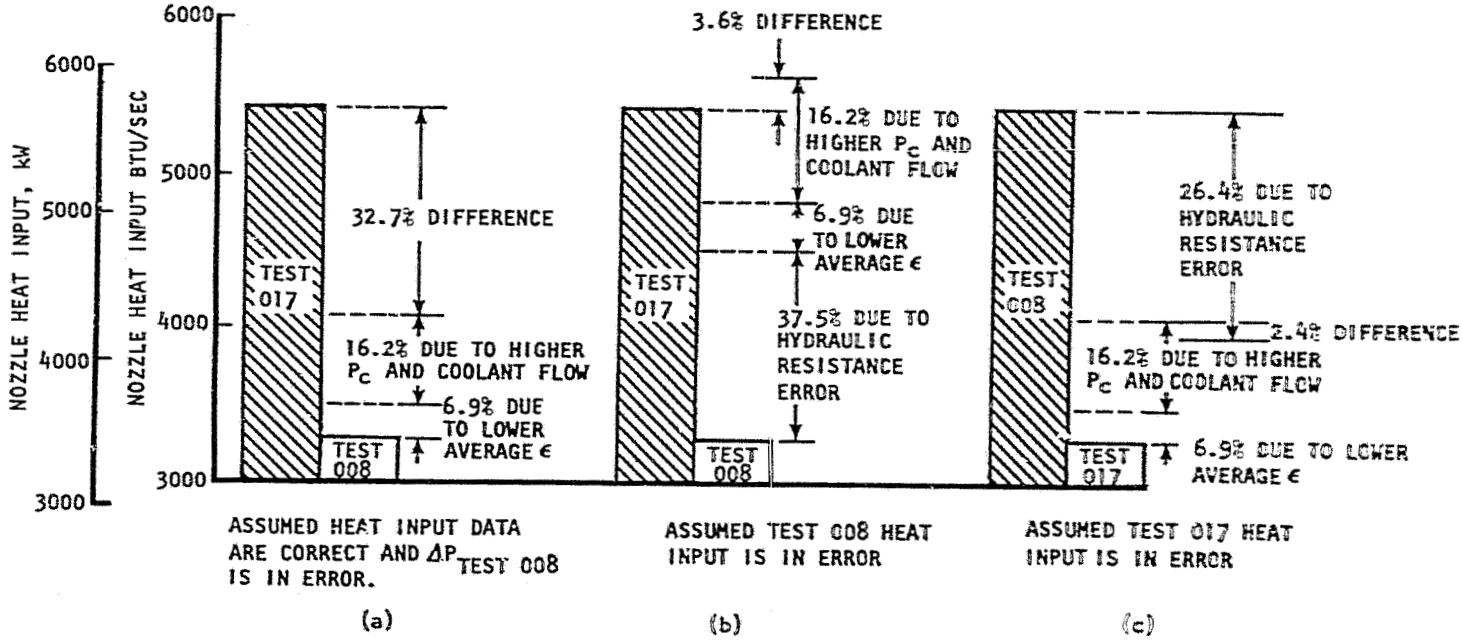

Figure 140. Nozzle Heat Input Correlation

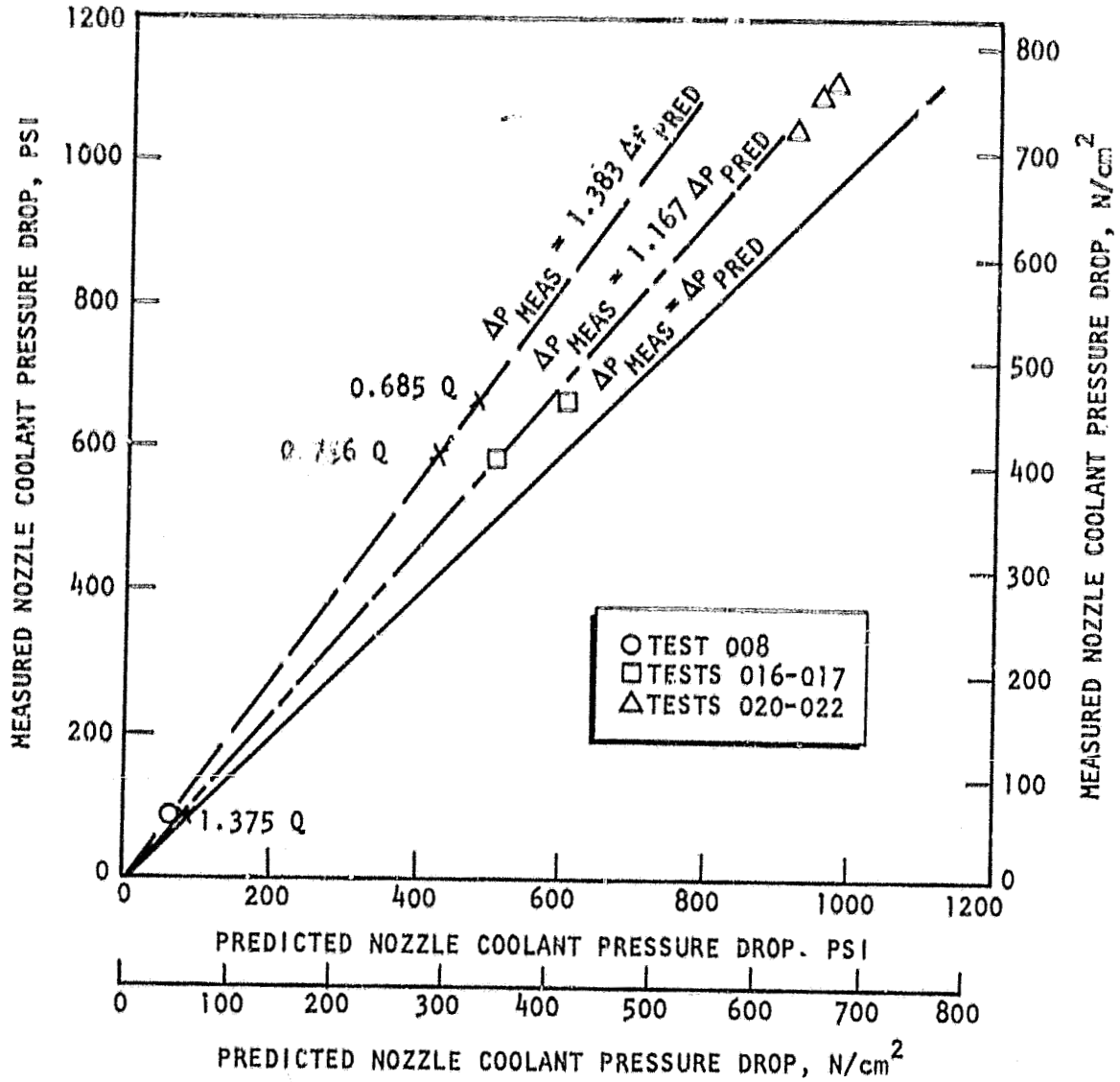

Figure 141. Nozzle Coolant Measured Pressure Drop vs Predicted Pressure Drop

only 16.7% greater than the predicted ΔP. The 6.9% because of the contraction ratio difference and the 16.2% due to the chamber pressure and wall temperature difference have been added. The resultant projected heat input for test 008 was then within 3.6% of that for test 017.

Figure 140c shows the comparison of the heat input data assuming that the test 017 data are incorrect. The heat input of test 017 has been decreased by the amount necessary, 26.4%, to result in a ΔP correlated to the test 008 ΔP; that is, 38.3% greater than the predicted ΔP. The resultant projected heat input for test 017 was then within 2.4% of the test 008 heat input, as modified for the 6.9% contraction ratio difference and the 16.2% chamber pressure and wall temperature difference.

Neither approach provides a clue as to which set of heat transfer data were incorrect and an additional test series, tests 020 through 022, was undertaken. One of the objectives of the final test series, tests 020 through 022, was to resolve the nozzle heat input anomaly and, if possible, to determine the cause of the anomaly. The data presented in Table 39 and Fig. 138 show that on this final series the heat input measurements tended to confirm the earlier (test 008) results. Dual measurement of the nozzle coolant outlet temperature with a thermocouple and a temperature resistance bulb on these tests showed a slight discrepancy but not enough to account for the anomalous results from tests 015 through 017.

The nozzle coolant flowrate was calculated from the sonic flow expression utilizing the nozzle outlet pressure, temperature, and sonic orifice area. As these were two slightly different temperatures recorded for tests 021 and 012, two slightly different flowrates can be calculated and two somewhat different heat transfer rates were determined. These differences are indicated on Fig. 138 although the data tabulated in Table 39 reflects only the results using the thermocouple measurement of the nozzle outlet temperature.

The measured nozzle coolant outlet temperature (Fig. 142) indicated that outlet temperature did not stabilize; however, the coolant flowrate decreased continuously during the test (Fig. 143) as a result of a decreasing LH_2 coolant tank pressure. Computing the nozzle heat input, the heat input did stabilize as shown in Fig. 144. Figure 145 is a plot of the heat flux versus time for test 022, the final 5-second duration test showing the same trend to stabilization. As shown in Fig. 142, the two nozzle coolant outlet temperatures differed by approximately 5 K (9 R), but also differed by 5.5 K (10 R) prior to the thrust chamber start indicating a possible zero shift. A review of the temperatures in the vicinity of the nozzle coolant outlet indicated that the thermocouple pretest value of the outlet temperature was more valid than the temperature resistance bulb pretest value, leading to the greater reliance on the thermocouple.

An attempt was made to determine the transient heat input on the A-286 tubular nozzle by tack welding a thermocouple on the hot-gas side of a nozzle tube as shown in Fig. 94. The thermocouple was introduced through an existing pressure port on the heat sink nozzle extension and fed forward toward the A-286 tubular nozzle. Thermocouples wire were tacked to the crown of a tube. The sheathed portion of the thermocouple was strapped down using strips tack welded to the heat sink nozzle extension.

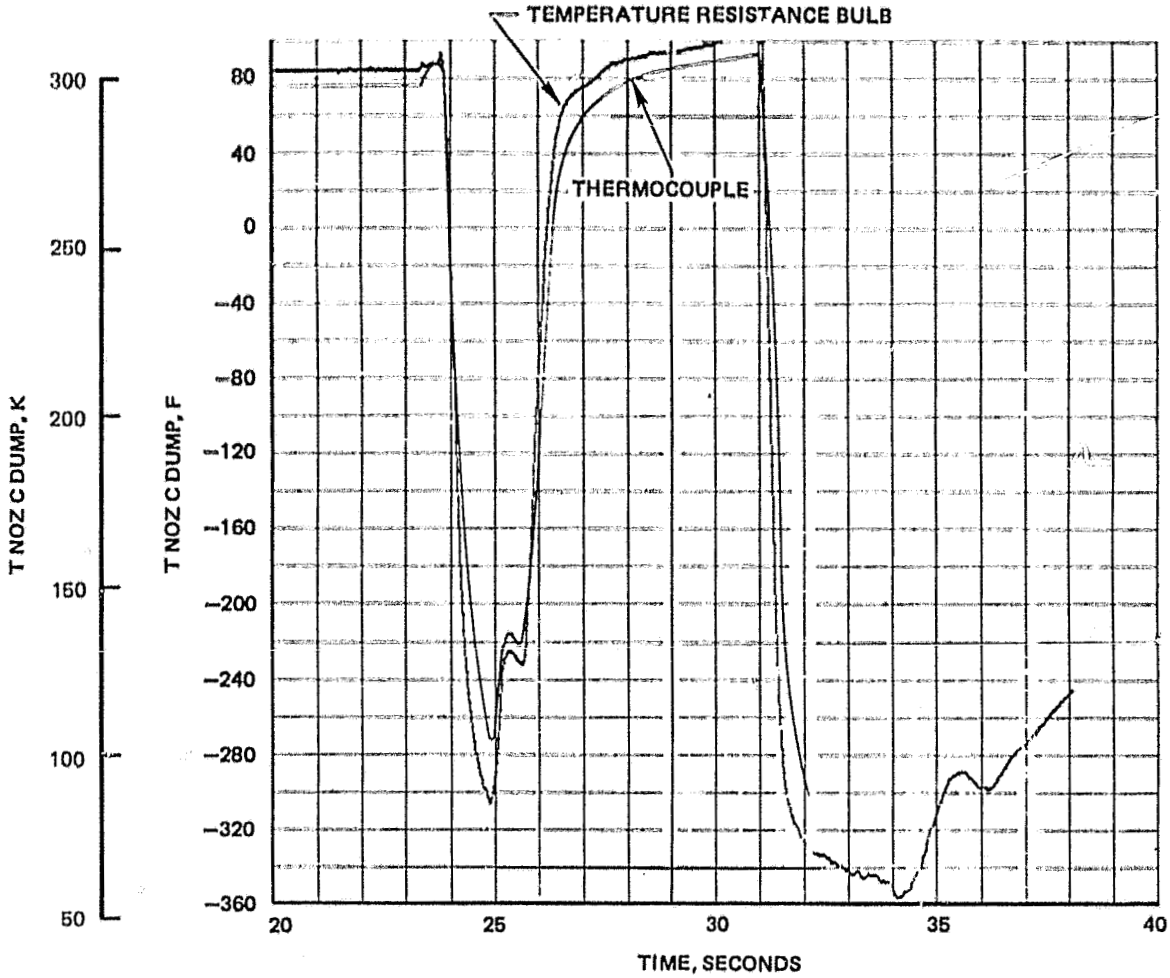

Figure 142. Typical A-286 Tubular Nozzle Coolant Outlet Temperature History

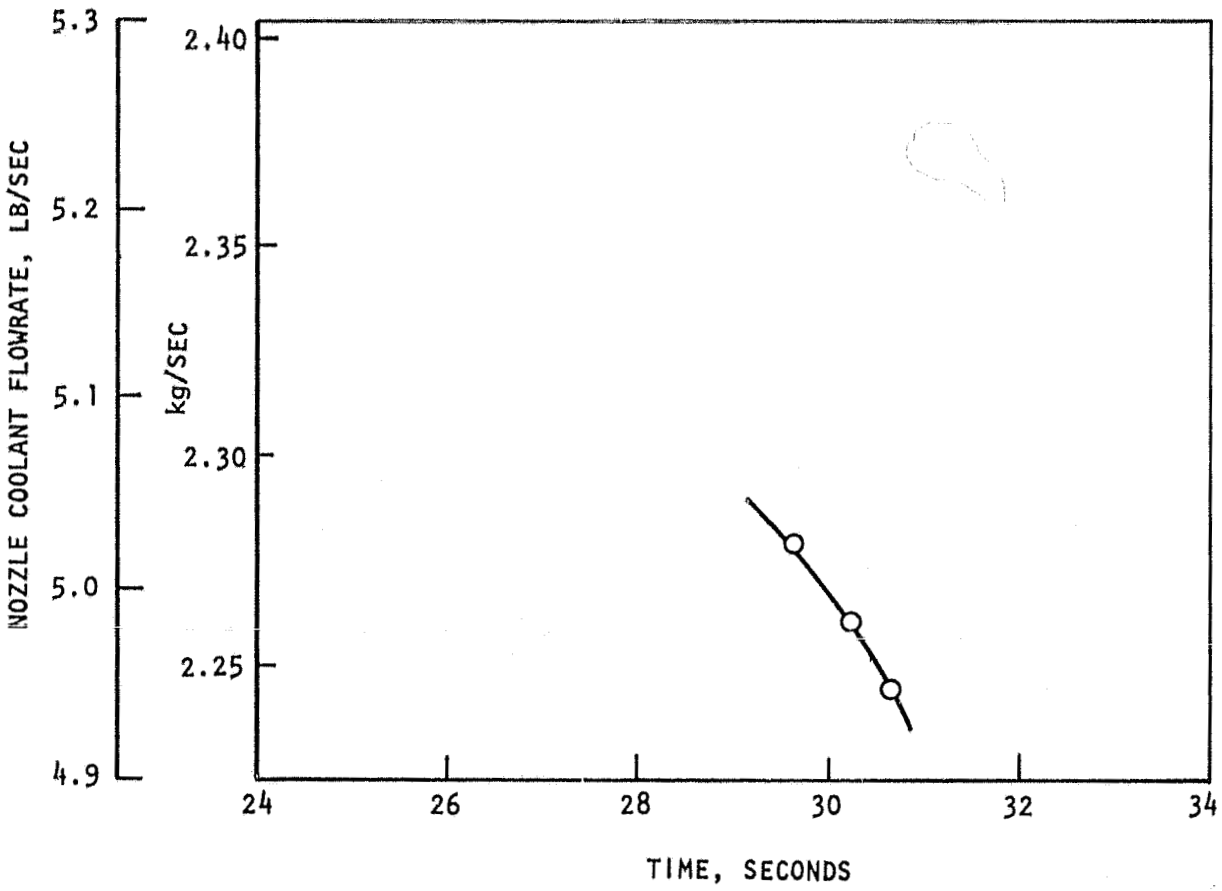

Figure 143. Coolant Flow Variation With Time (Test 021)

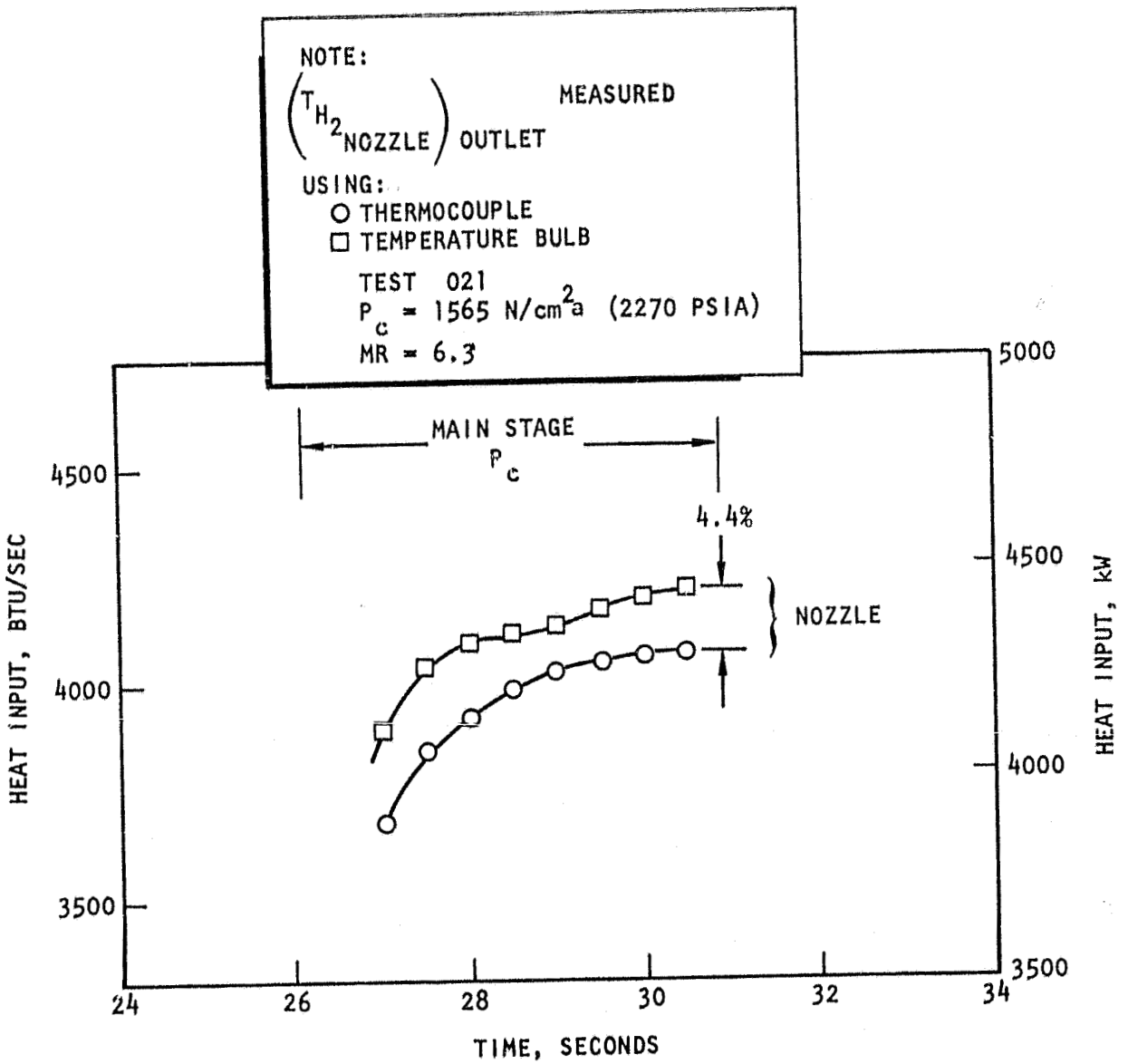

Figure 144. Combustor and Nozzle Heat Input Variation With Time (Test 021)

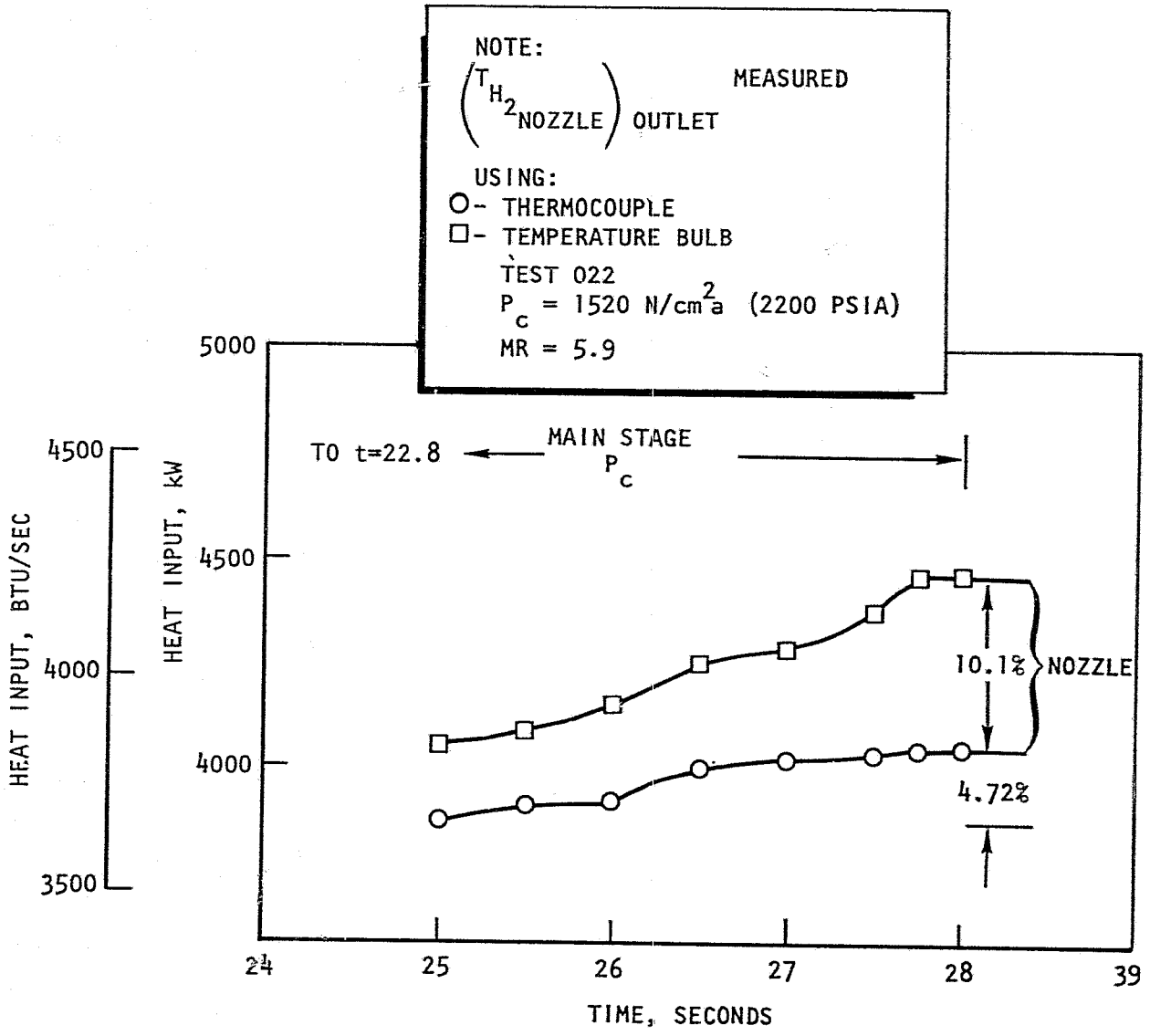

Figure 145. Combustor and Nozzle Heat Input Variation With Time (Test 022)

The gas dynamic forces generated by the combustion gas during thrust chamber start tore the thermocouple loose and no reading was obtained. The thermocouple temperature recording is shown in Fig. 146.

Heat Sink Nozzle Extension ($\epsilon = 175$ to $\epsilon = 400$). The mild steel heat sink nozzle extension was used in place of a tubular dump-cooled nozzle to provide a more durable nozzle extension capable of withstanding the high nozzle flow separation heat fluxes. Three back-side wall thermocouples were installed on the heat sink nozzle and the transient temperature data obtained were reduced to determine transient heat fluxes and steady-state, gas-side heat transfer data. The analysis was performed with the assumption of only natural convection on the nozzle back-side wall.

In the first test series (tests 015 to 017), these back-side wall temperatures were measured; however, convective influences on the back-side wall near these thermocouples affected the measured values and these results were invalidated. On thrust chamber start and shutdown, gas either from the capsule or diffuser flowed past these thermocouples providing convective cooling and heating, alternately. Therefore, metal shields, or "convective hats" were placed over these three thermocouples to attempt to isolate them from these back-side influences (Fig. 147).

Measured wall temperature histories for test 021 are presented in Fig. 148 for the three axial positions. As expected, the temperatures are lower at the higher area ratios because of the lower heat inputs. A comparison of the data for tests 020, 021, and 022 are shown in Fig. 149 through 151, with all data superimposed on one trace. The measured temperatures for a given axial position had essentially the same temperature versus time slope. The steep initial ramp in temperature from 25 to 27 seconds and the increase in slope in temperature at 31 seconds are the result of the increased heat input due to nozzle flow separation at thrust chamber start and shutdown.

The measured transient temperature response of the individual thermocouples was analytically modeled or matched using a one-dimensional model capable of a time dependent adiabatic wall temperature and gas-side heat transfer coefficient. This modeling enables the determination of the thrust chamber start, mainstage, and shutdown gas-side heat transfer coefficients.

The transient gas-side heat transfer coefficients were obtained using the relationship

$$hg = K\, hg_{M/S} \left[\frac{P_c}{P_{c_{M/S}}} \; \frac{\left(P_{c_{M/S}} / P_{noz_{M/S}}\right)}{\left(P_c / P_{noz}\right)} \right]^{0.8}$$

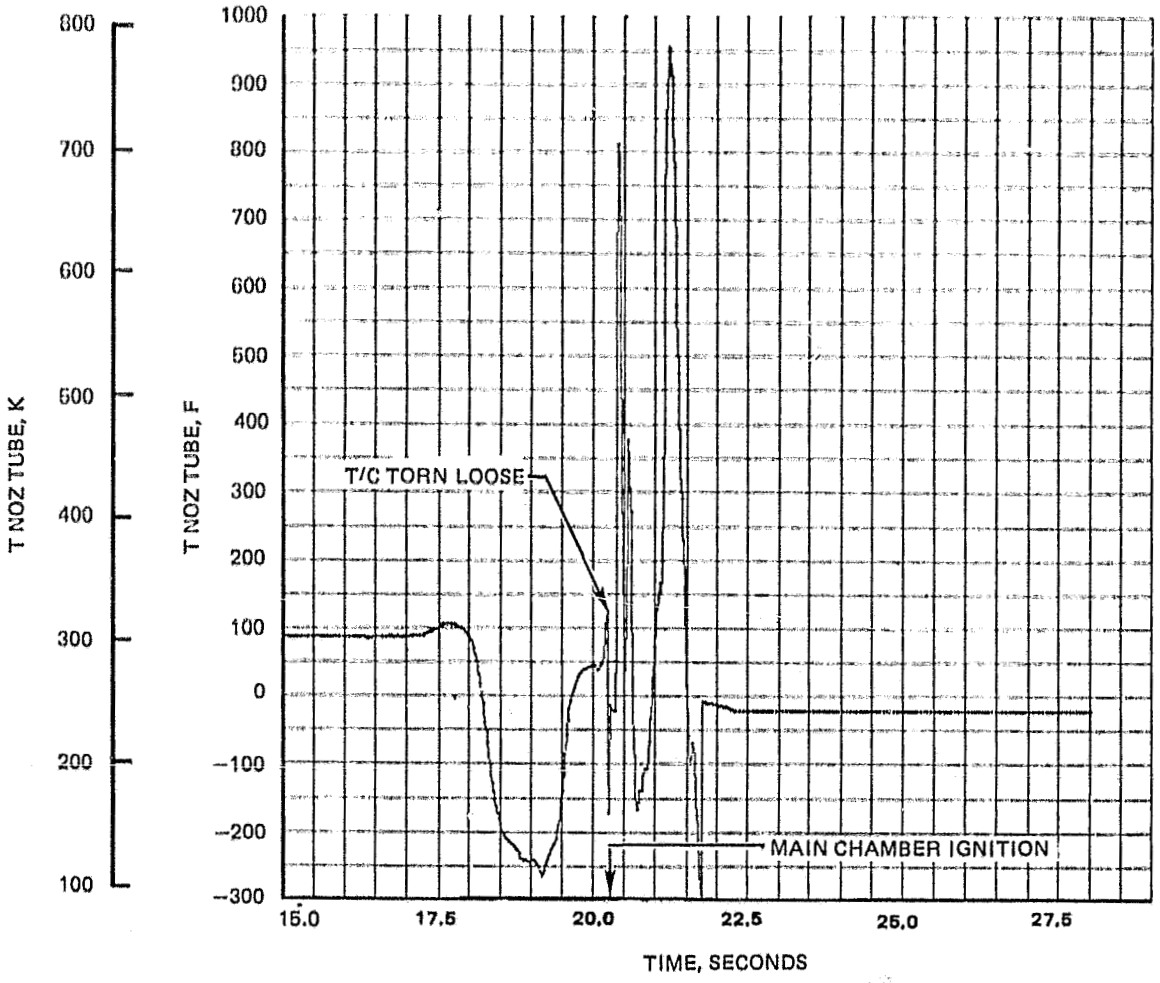

Figure 146. Nozzle Tube Wall Temperature History

1HS36-10/10/77-S1B

Figure 147. Convective Hat Welded Over Uncooled Nozzle Wall Thermocouple

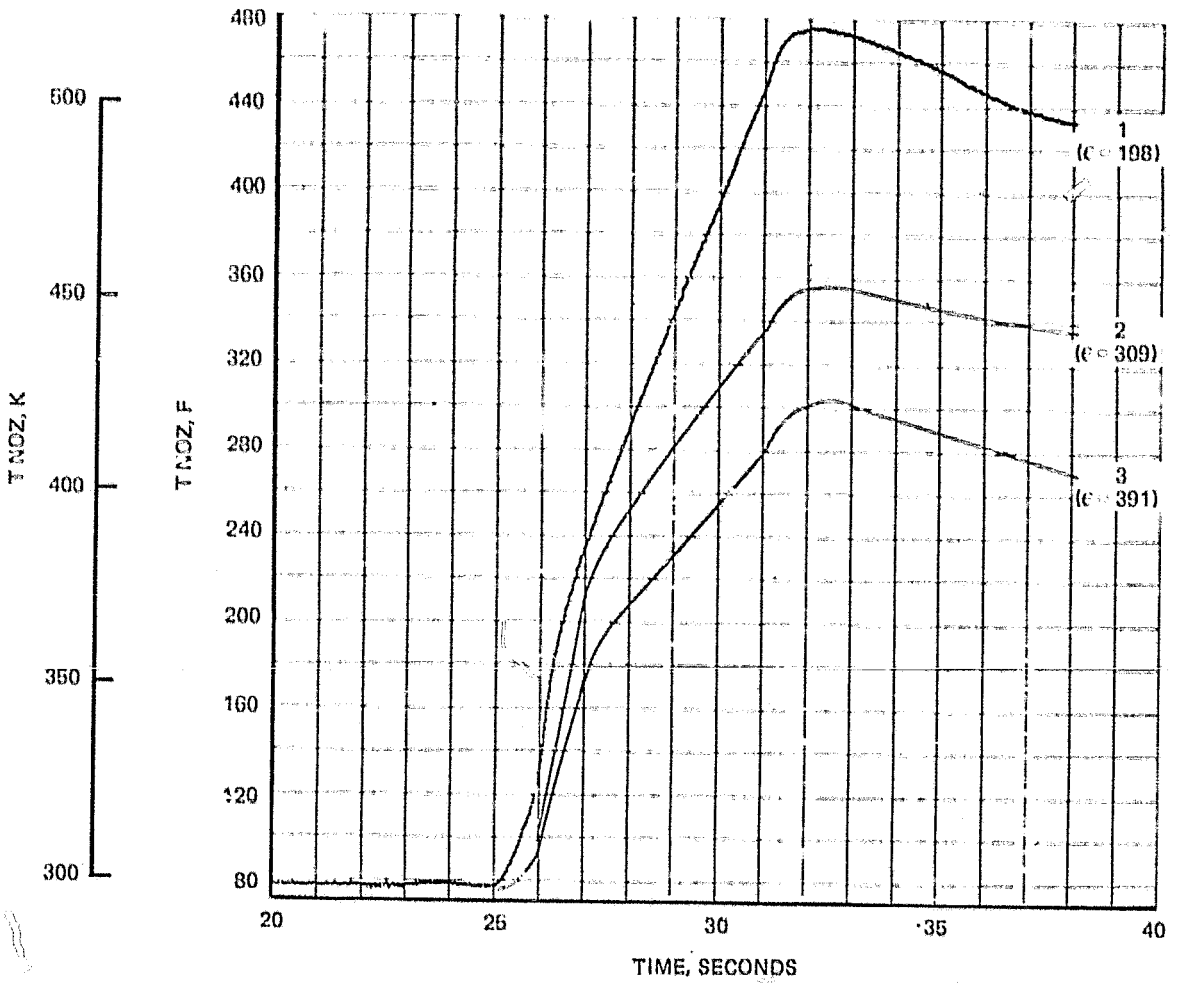

Figure 148. Typical Heat Sink Nozzle Extension Temperature Histories (Test 021)

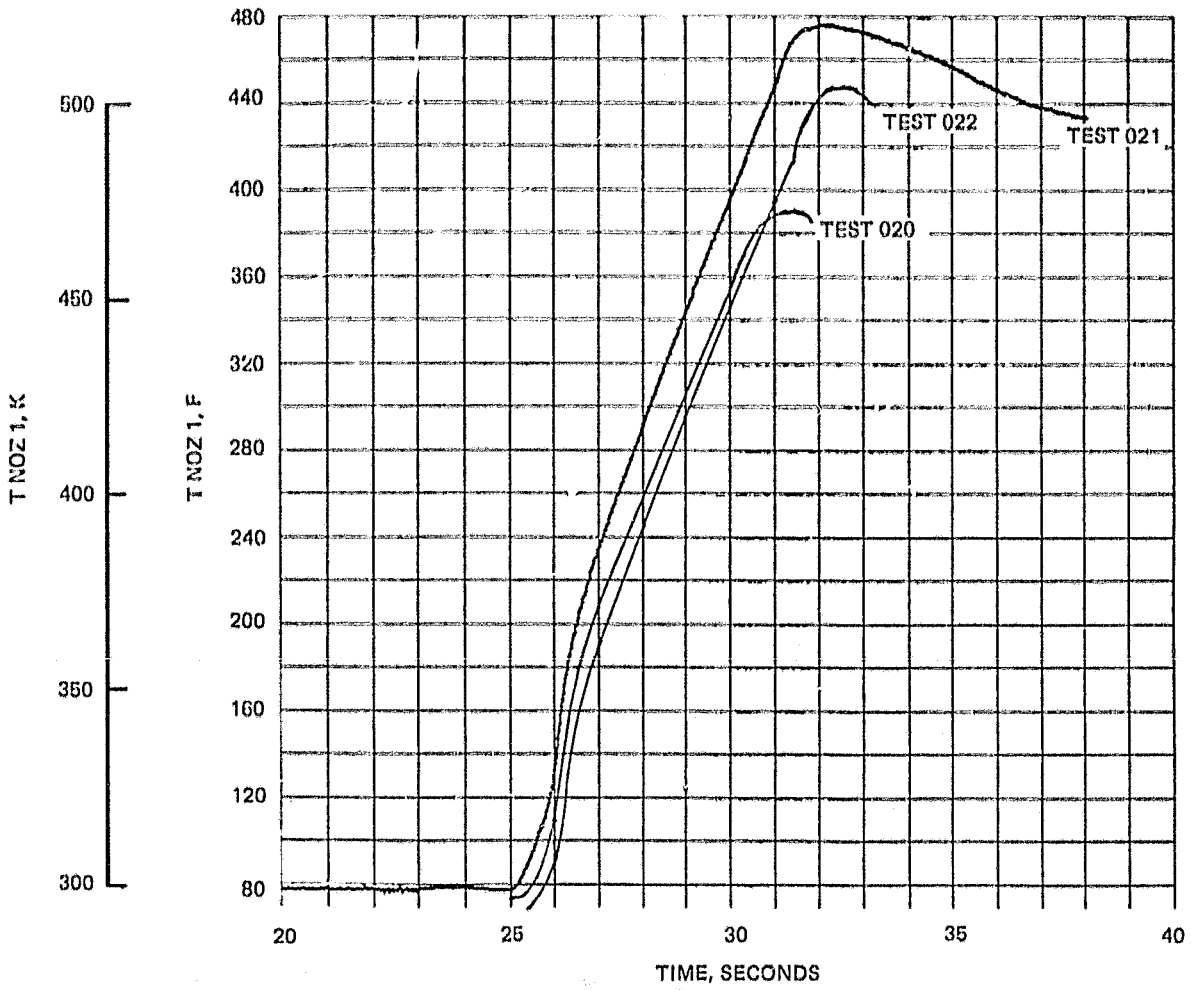

Figure 149. Heat Sink Nozzle Extension Temperature Histories at 198:1 Area Ratio

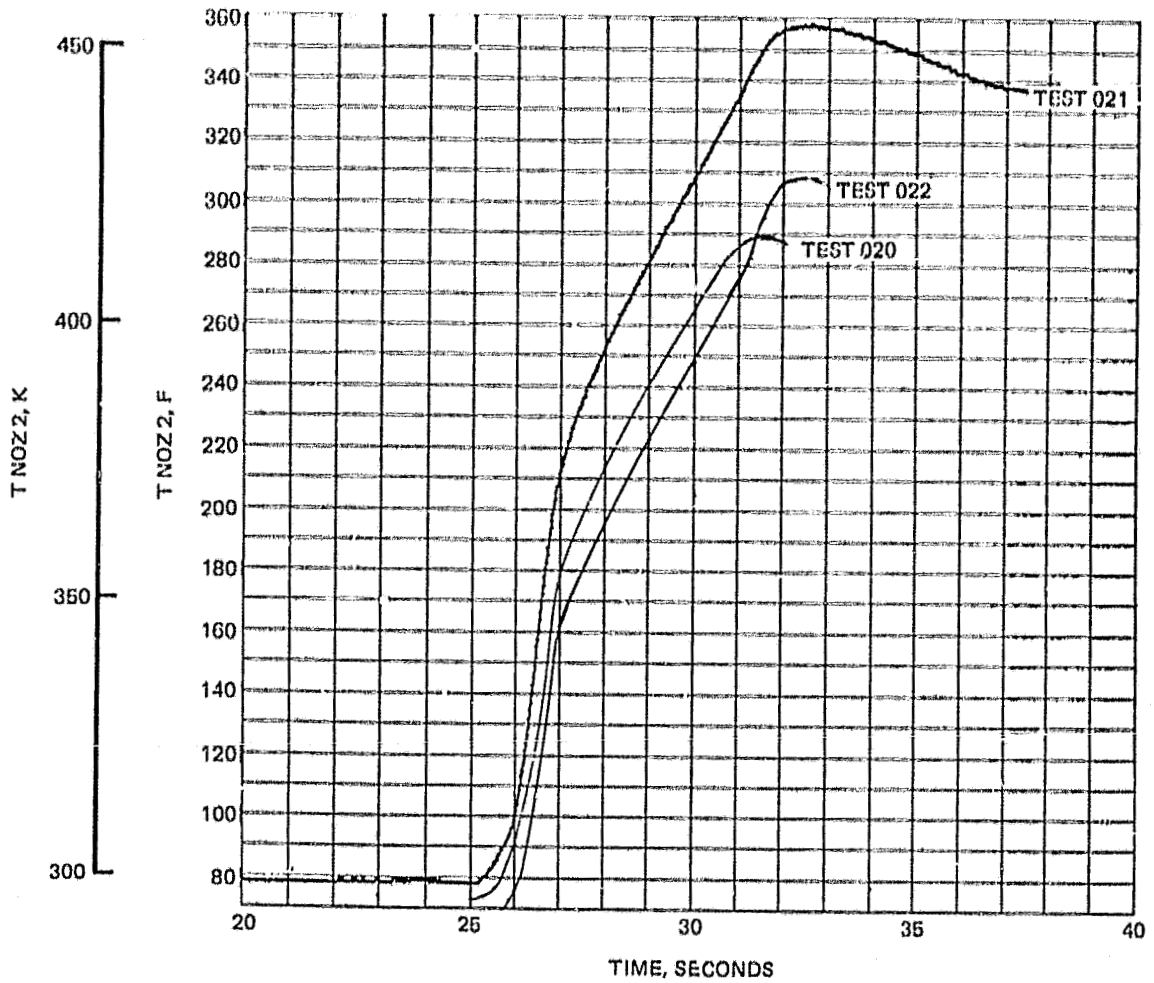

Figure 150. Heat Sink Nozzle Extension Temperature Histories at 309:1 Area Ratio

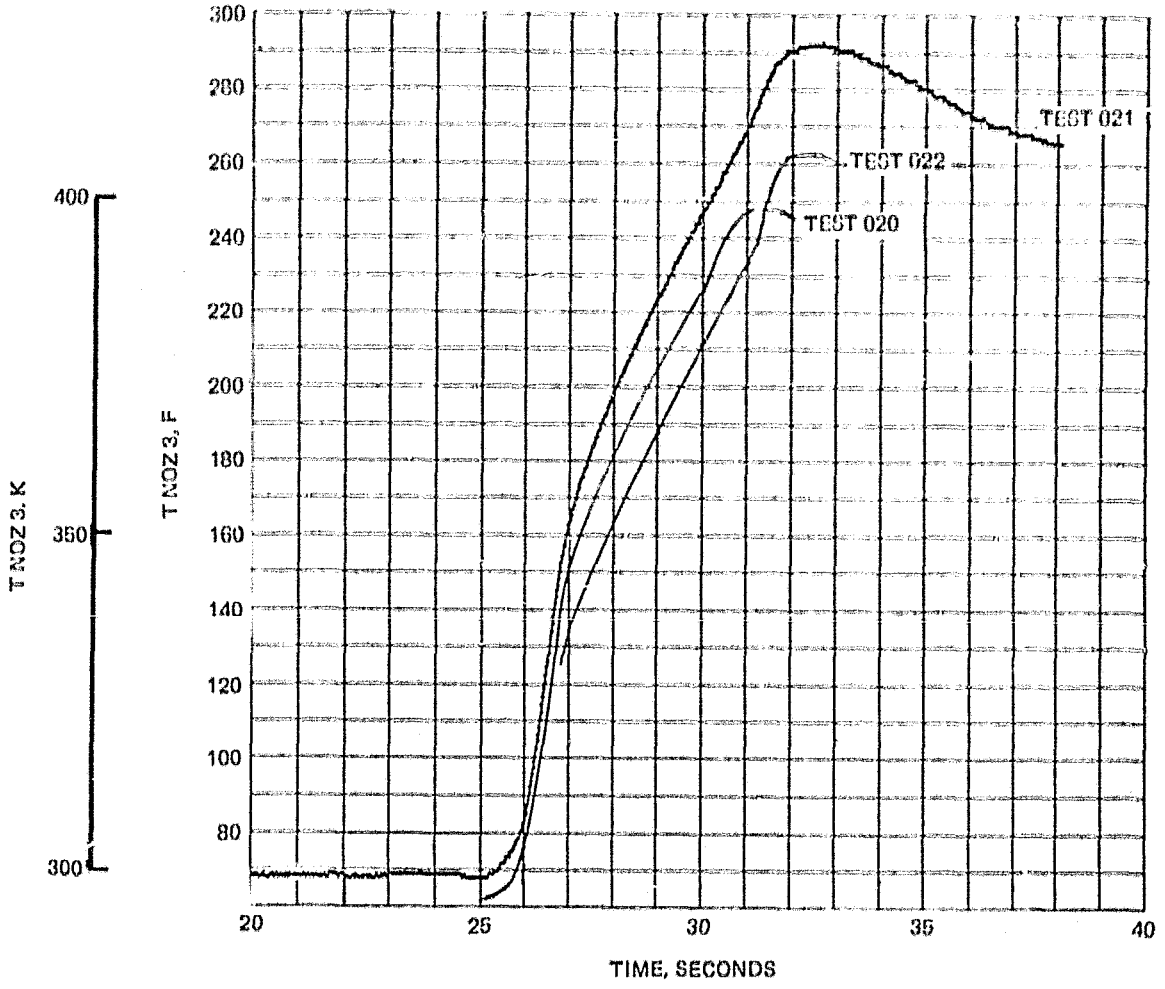

Figure 151. Heat Sink Nozzle, Extension Temperature Histories at 391:1 Area Ratio

where

$hg_{M/S}$ = mainstage gas-side heat transfer coefficient

hg = gas-side heat transfer coefficient at time t

K = constant coefficient required to match test data

P_c = chamber pressure at time t

$P_{c_{M/S}}$ = mainstage chamber pressure

P_{noz} = nozzle wall static pressure at time t

$P_{noz_{M/S}}$ = mainstage nozzle wall static pressure

The resulting value of the coefficient K varied from 1.0 at an area ratio of 198:1 to 0.379 at the nozzle exit.

The data obtained from test 021 were modeled assuming the theoretical gas temperature and the wall thickness measured at the nozzle exit (0.26 inch) and are presented in Fig. 152 through 154. The final match of the test data and the analytical model at area ratio 391:1 is shown in Fig. 152. The analytically determined temperatures through the nozzle wall at this location are shown in Fig. 153. The highest wall temperature is the gas-side value and the lowest is the nozzle back side. The resulting gas-side heat transfer coefficient and heat flux ratios at this location are shown in Fig. 154. It should be noted that the peak heat flux encountered during start was 4.6 times the mainstage value.

Similarly, results of the modeling at area ratios of 309:1 and 198:1 are presented in Fig. 155 and 156. As shown in Fig. 154 through 156, the peak heat flux during start was higher at the lower area ratios, and varied from 4.6 to 6.2 times the mainstage values. At shutdown, the ratio varied from 2.8 to 3.1; of course, the start transients weremuch slower than the shutdown transients.

The calculated mainstage gas-side heat transfer coefficients for the three axial positions are presented in Fig. 157 along with the analytically predicted curves for chamber pressures of 3180 N/cm^2a and 1567 N/cm^2a (2000 psia and 2273 psia). Comparing the test data to the corresponding analytical curve, the experimental gas-side heat transfer coefficients were 3 to 36% lower. Based on these data, the gas-side heat transfer coefficient profile and, therefore, the dump-cooled nozzle heat input appears to be lower than the analytical value.

Combustion Chamber Rib Temperatures. The heat flux at two axial locations in the combustion chamber was to be determined using spring-loaded thermocouples in holes in the lands, or ribs, of the channel wall combustor as shown in Fig. 89. The rib thermocouples were intended to measure the wall temperature at 0.76 mm (0.030 inch) from the hot-gas wall. These thermocouple assemblies were placed 12.7 mm (0.5 inch) upstream of the throat and in the combustion

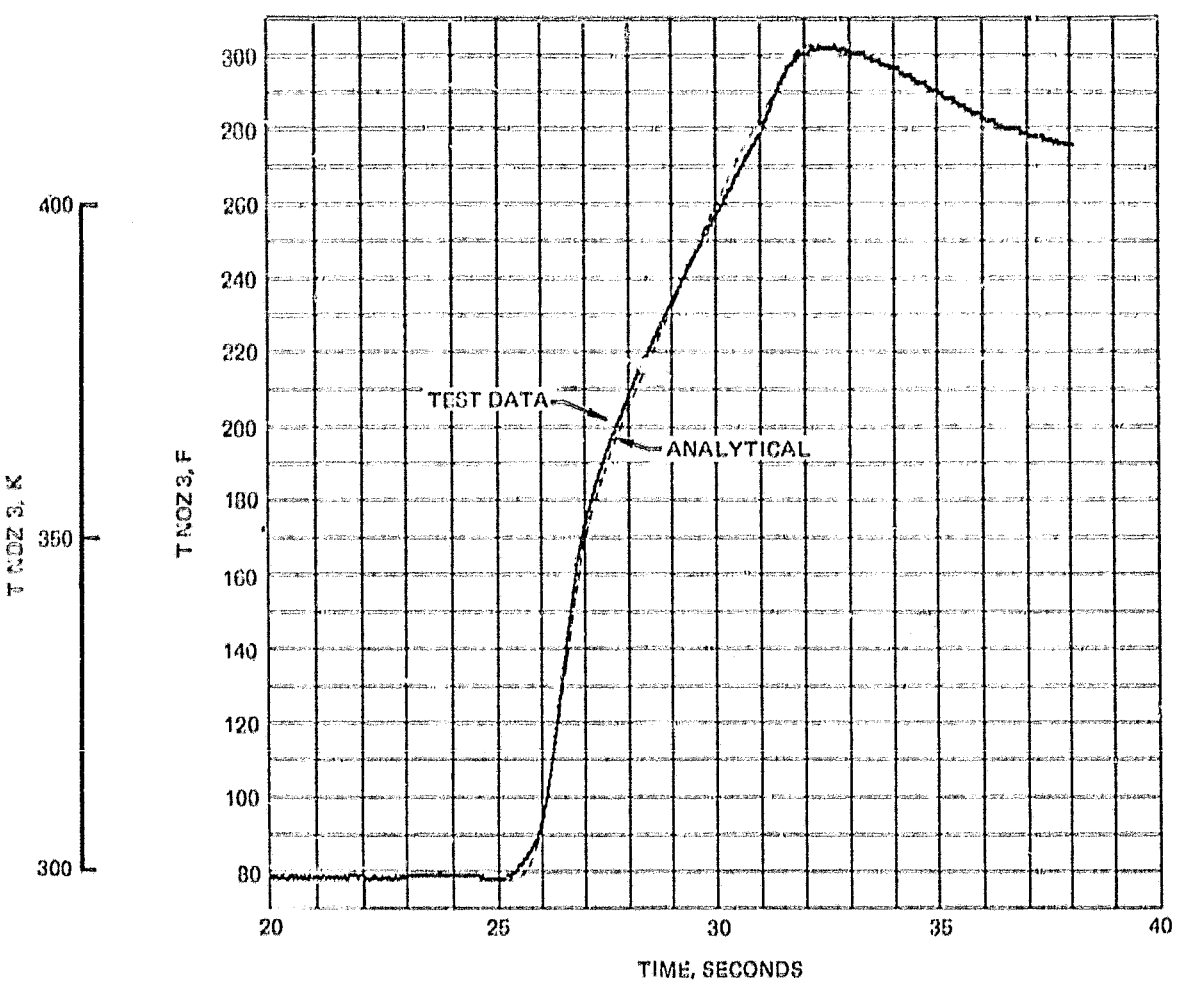

Figure 152. Test Data/Analytical Correlation for 391:1 Area Ratio Location (Test 021)

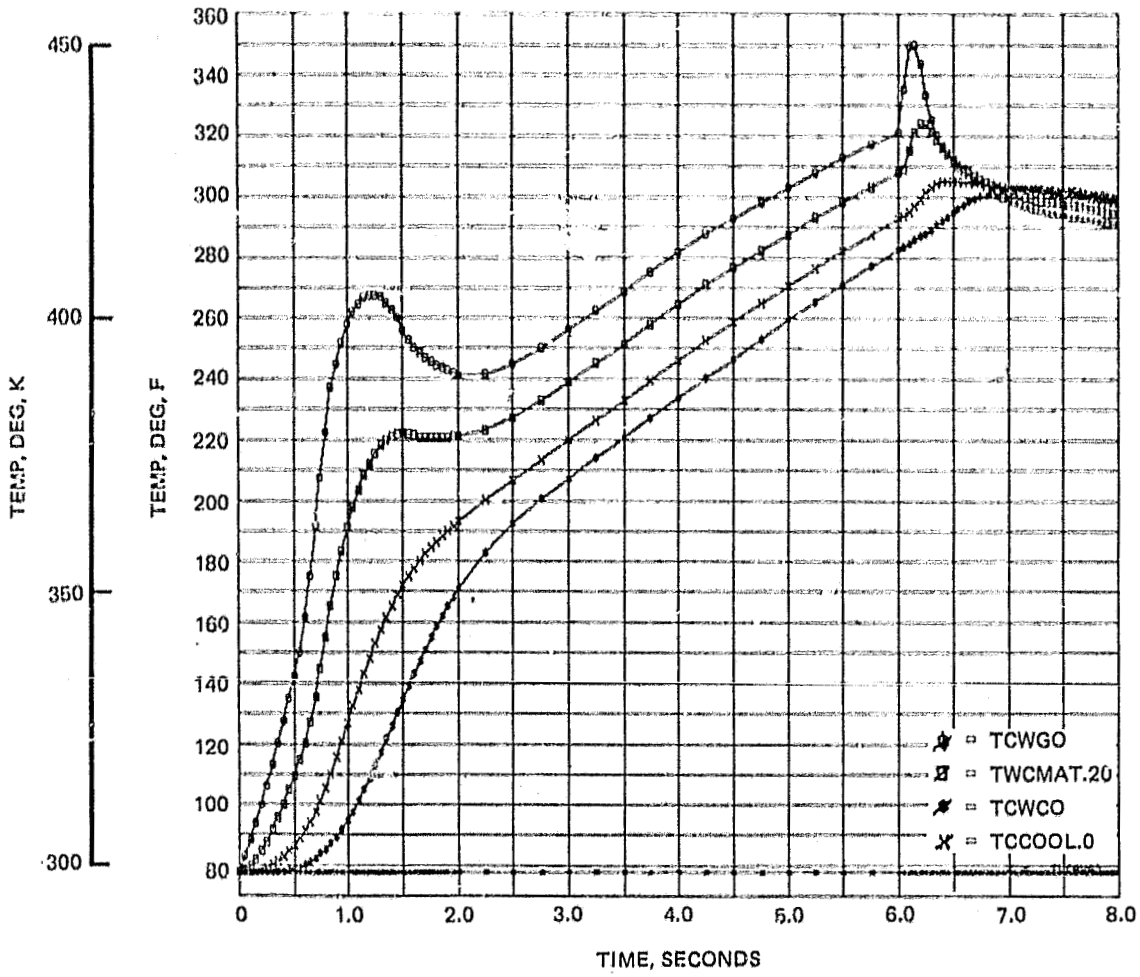

Figure 153. Analytical Correlation for 391:1 Area Ratio Location (Test 021)

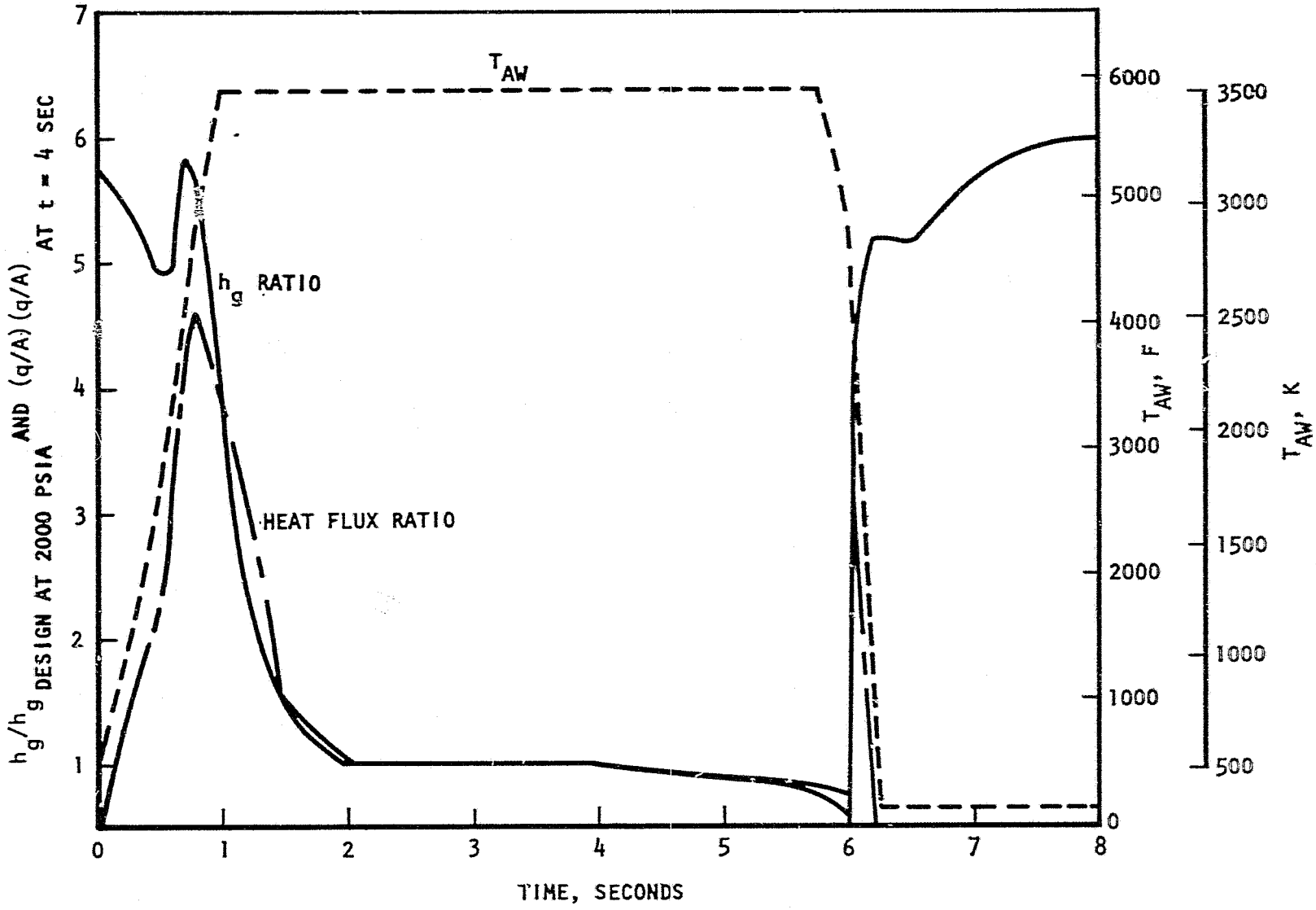

Figure 154. Gas-Side Heat Transfer Coefficient Ratio, Heat Flux Ratio, and Adiabatic Wall Temperature Variation With Time for 395:1 Area Ratio (Test 021)

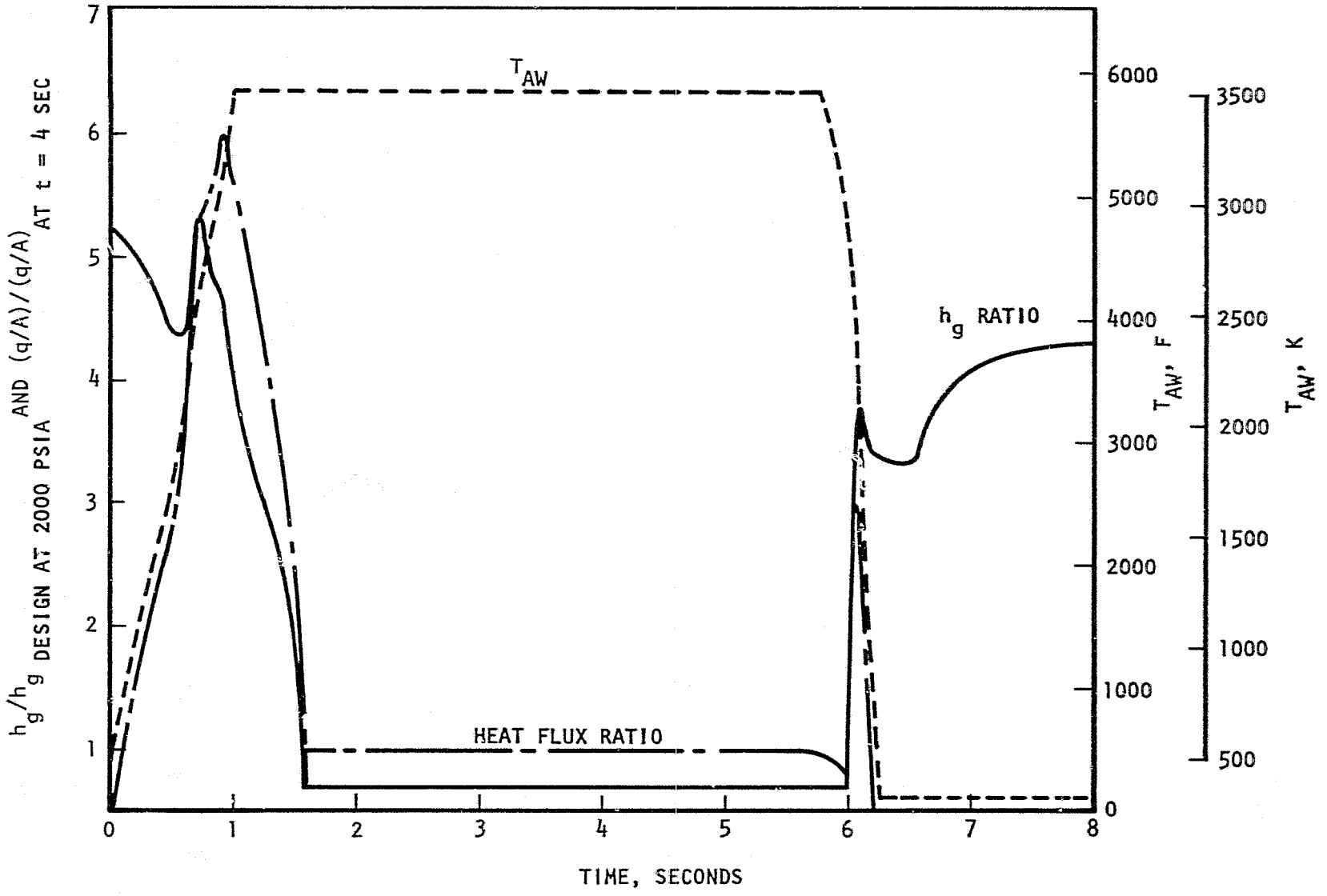

Figure 155. Gas-Side Heat Transfer Coefficient Ratio, Heat Flux Ratio, and Adiabatic Wall Temperature With Time for 309:1 Area Ratio (Test 021)

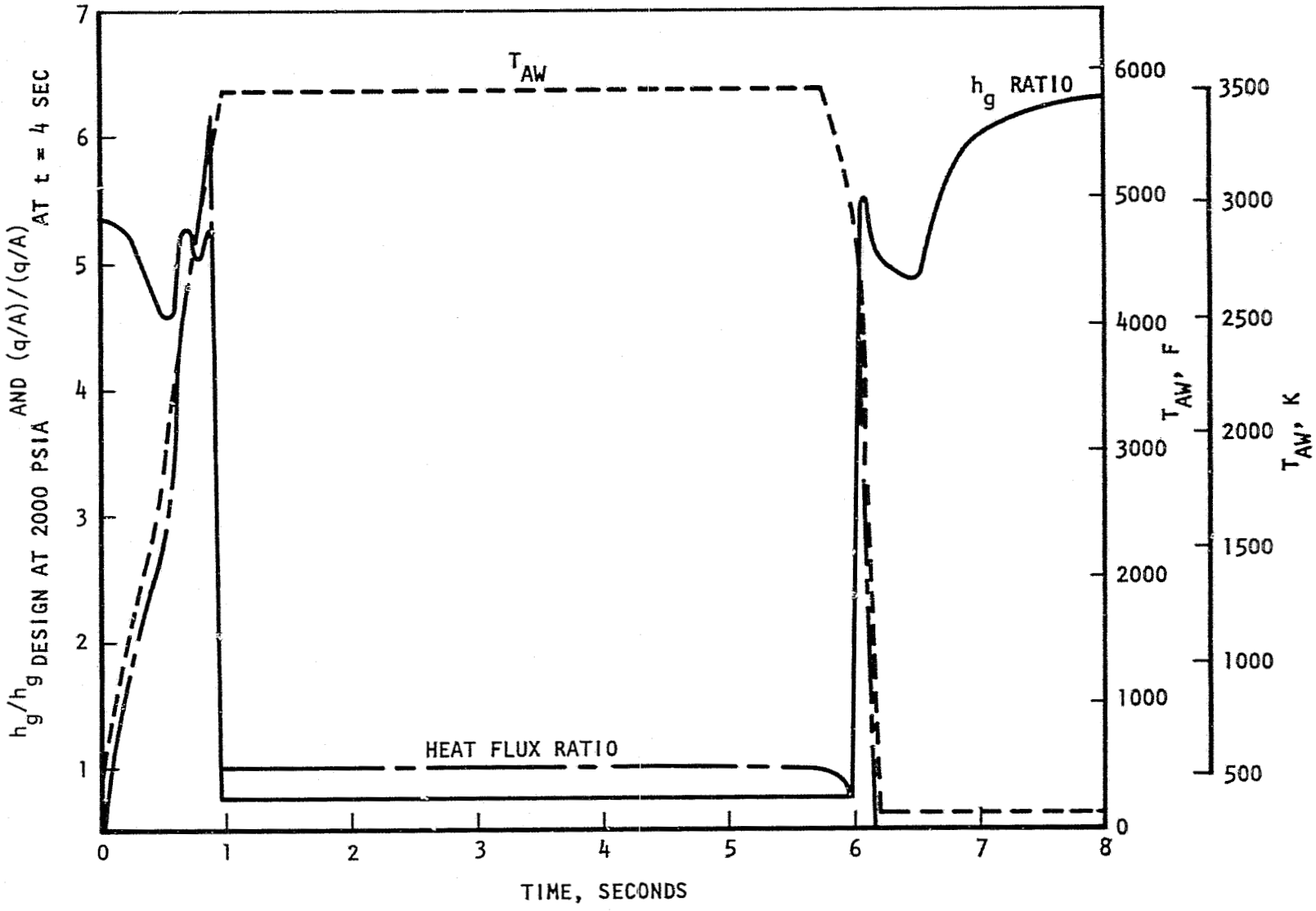

Figure 156. Gas-Side Heat Transfer Coefficient Ratio, Heat Flux Ratio, and Adiabatic Wall Temperature Variation With Time for 198:1 Area Ratio (Test 021)

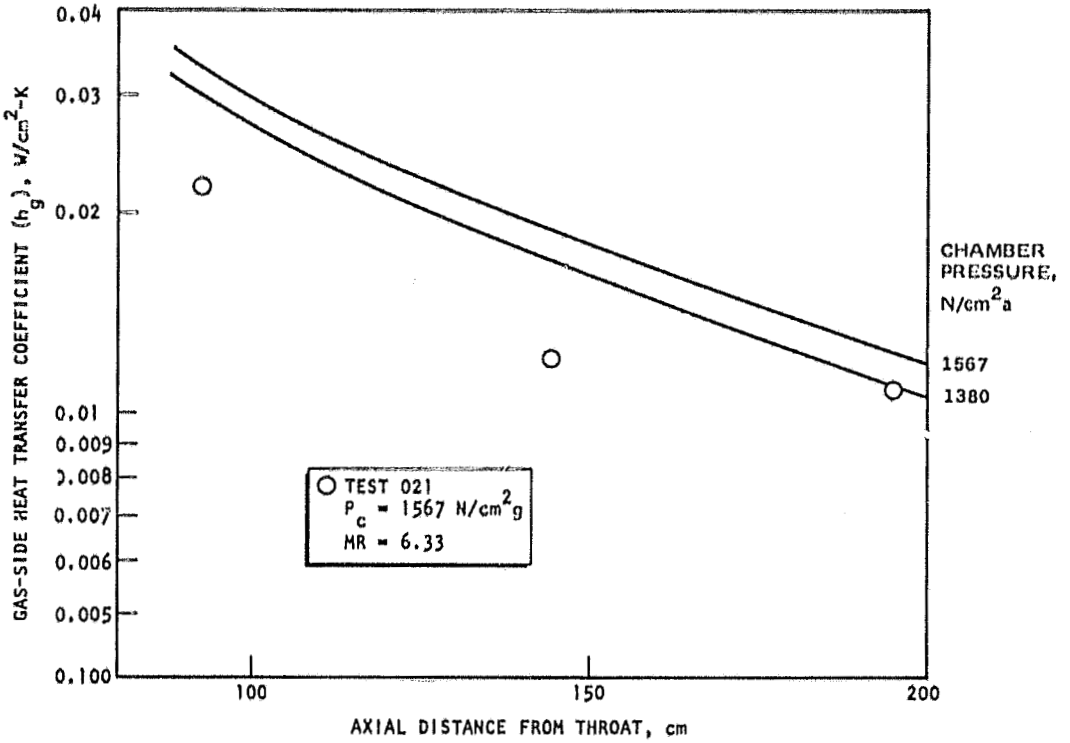

(a)

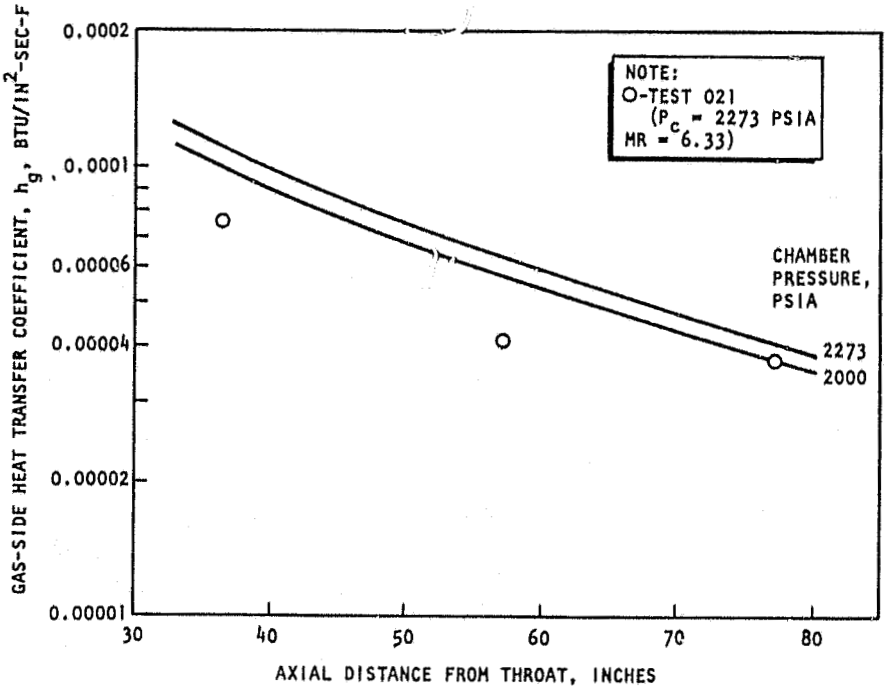

(b)

Figure 157. Heat Sink Nozzle Extension Mainstage Heat Transfer Coefficients

chamber 10 cm (4 inches) from the throat. There were three thermocouples located circumferentially at the combustor location and three thermocouples circumferentially near the throat plane as shown schematically in Fig.158 .

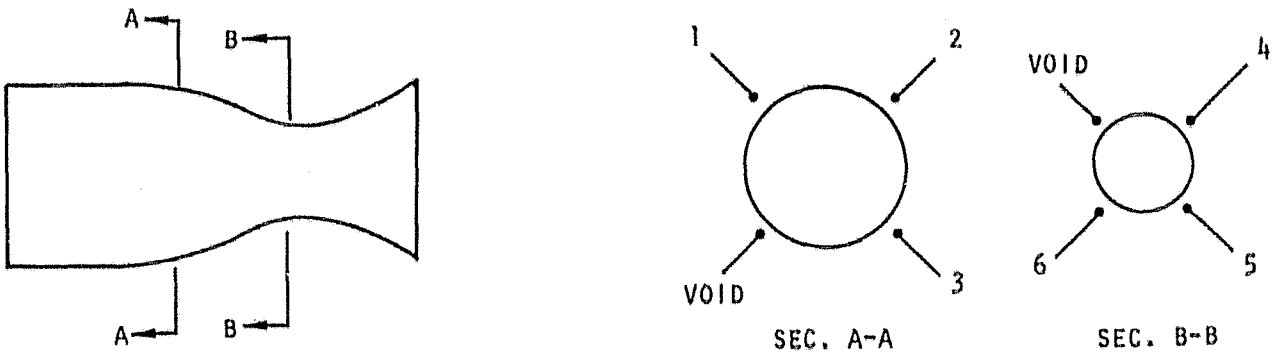

Figure 158. Rib Thermocouple Placement

Typical measured throat region temperature histories are shown in Fig.159 . A 390 to 450 K (700 to 800 F) temperature variation existed for this test. As shown in Fig. 160 through 162, the three throat region temperatures repeated within 15 to 40 K (30 to 70 F) on tests 020 to 022. Thermocouples No. 5 and 6 agreed within 55 K (100 F), although No. 6 exhibited a peculiar behavior of decreasing during mainstage. Thermocouple No. 4 recorded an extraordinarily high temperature throughout and no certain explanation can be made.

Typical measured combustion chamber temperatures are shown in Fig. 163. A 155 K (280 F) temperature variation existed during this test, but thermocouple No. 2 apparently had an excessive contact resistance as evidenced by its slow response. On thrust chamber start (sharp decreases in wall temperature at approximately 23.5 seconds), thermocouples No. 1 and 3 responded similarly and more rapidly than No. 2. This trend occurred during all of the tests. The repeatability of thermocouple No. 1 and 3 is shown in Fig. 164 and 165.

For the throat region thermocouples, two-dimensional thermal analyses were performed using one model with a slot for the thermocouple hole and one without a thermocouple hole. The actual configuration is of course three-dimensional and the measured temperature values should actually lie between the two thermal models analyzed. However, as shown in Fig. 166 and 167, the predicted wall temperatures varied 8 to 40 K (15 to 70 F) between the two models in the range of temperatures measured. The thermocouple hole tends to raise the predicted wall temperature since the hole eliminates a portion of the two-dimensional fin conduction. Figure 168 shows the same model for the combustion chamber location.

The curves shown in Figs. 166 through 168 were obtained analytically by matching the test data measured heat input of test 021. The resulting coolant bulk temperature and coolant-side film coefficient at the two axial thermocouple locations were used in the two-dimensional thermal analysis. The throat region was also analyzed with and without coolant curvature enhancement.

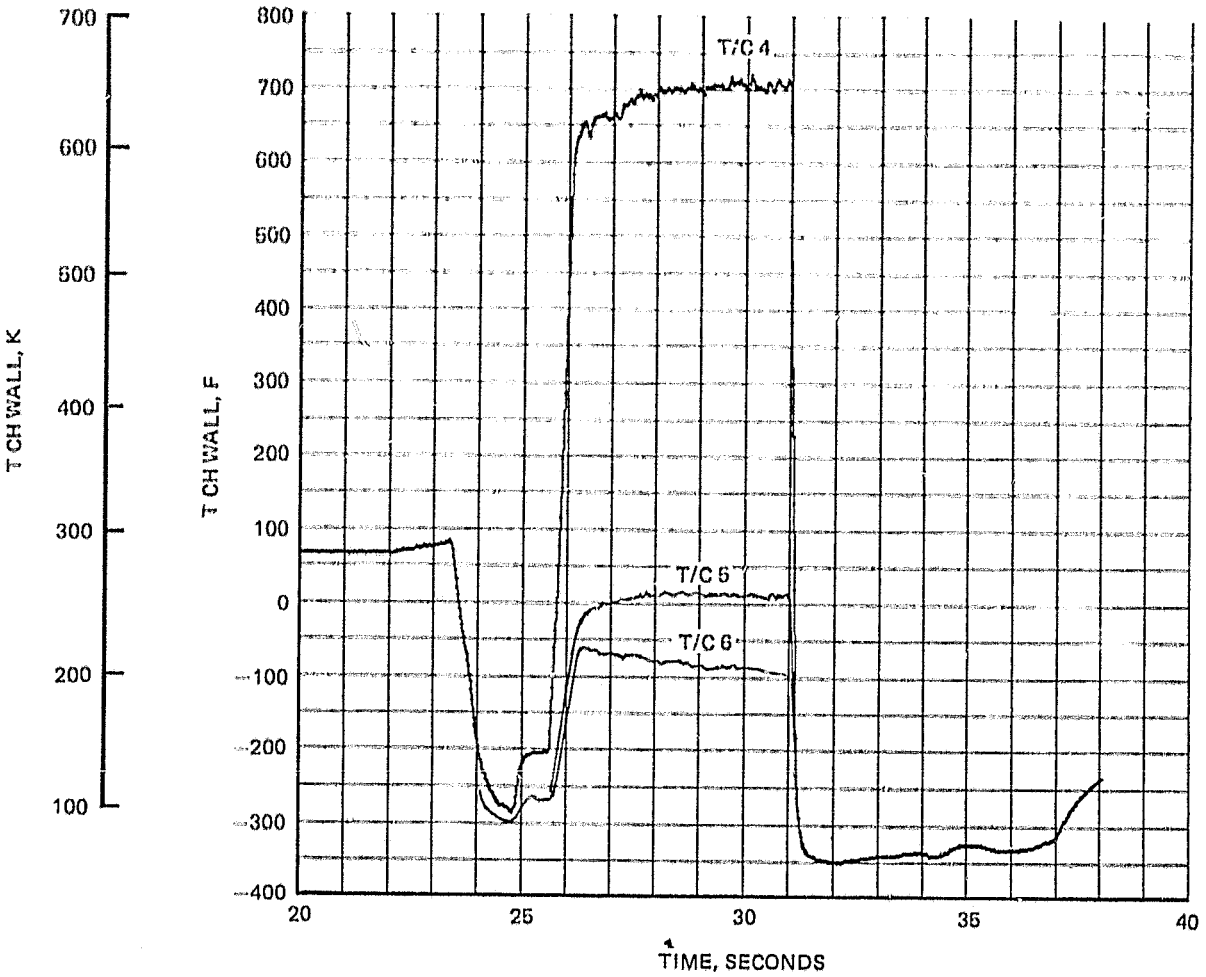

Figure 159. Typical Throat Region Rib Temperature Histories (Test 021)

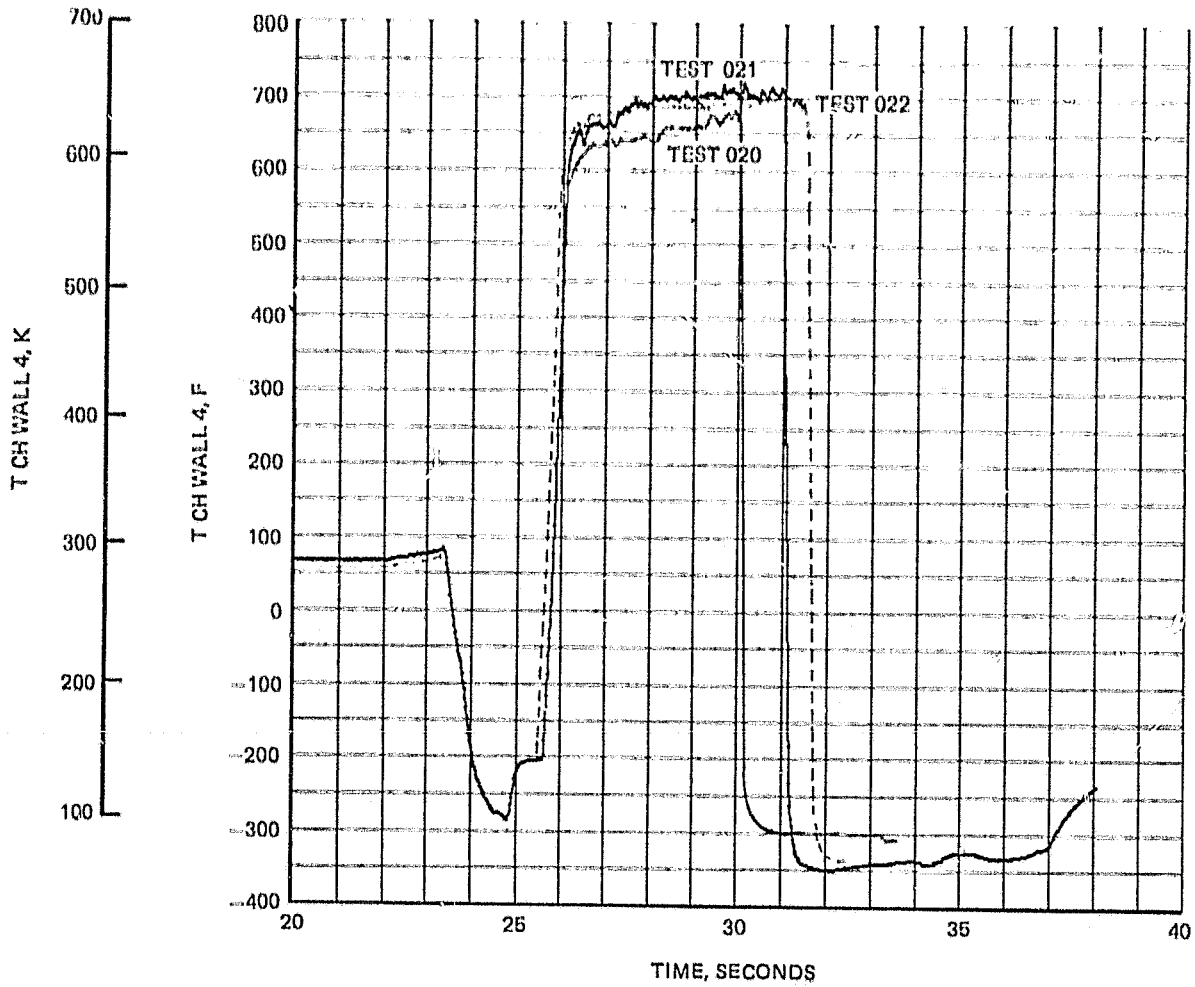

Figure 160. Throat Region Thermocouple No. 4 Temperature Histories

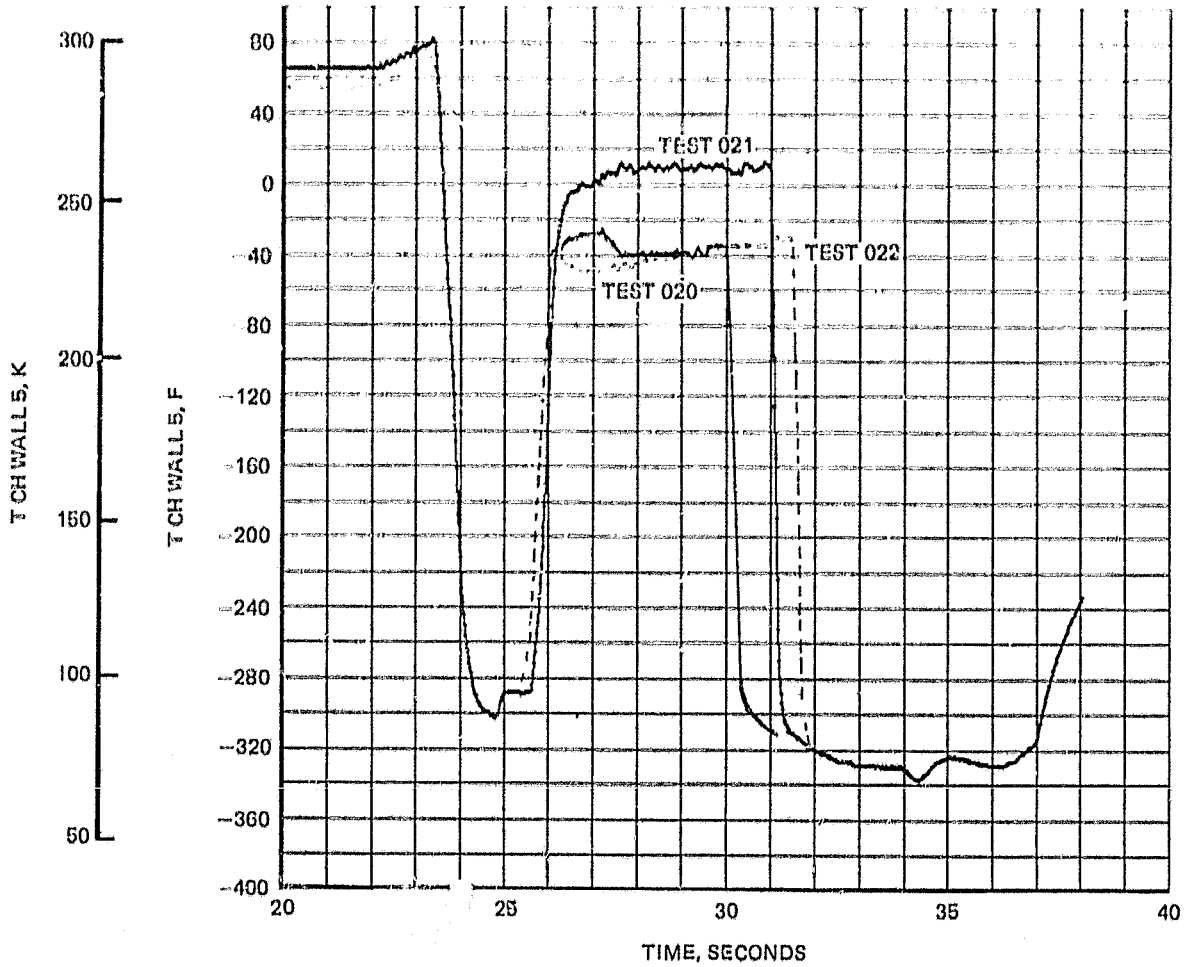

Figure 161. Throat Region Thermocouple No. 5 Temperature Histories

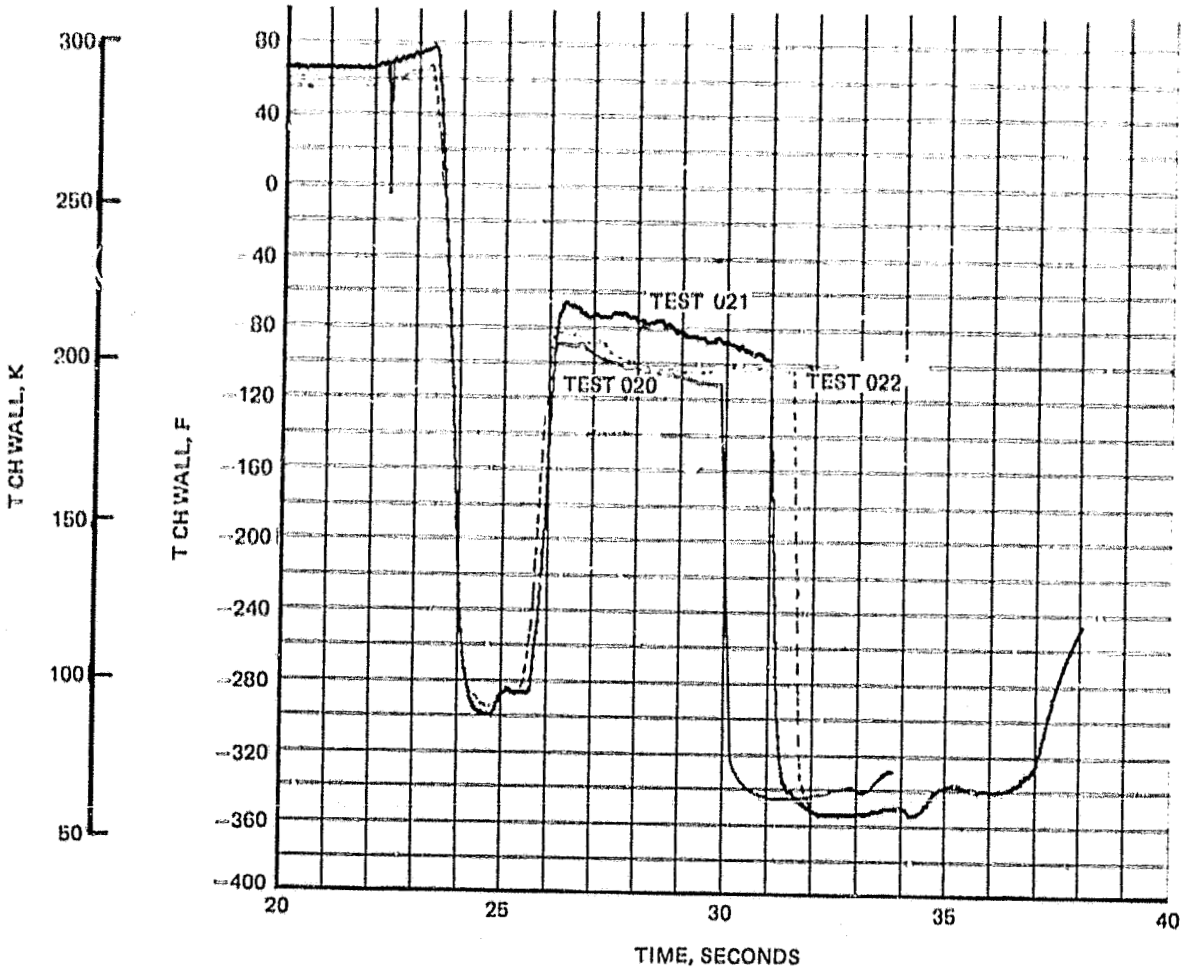

Figure 162. Throat Region Thermocouple No. 6 Temperature Histories

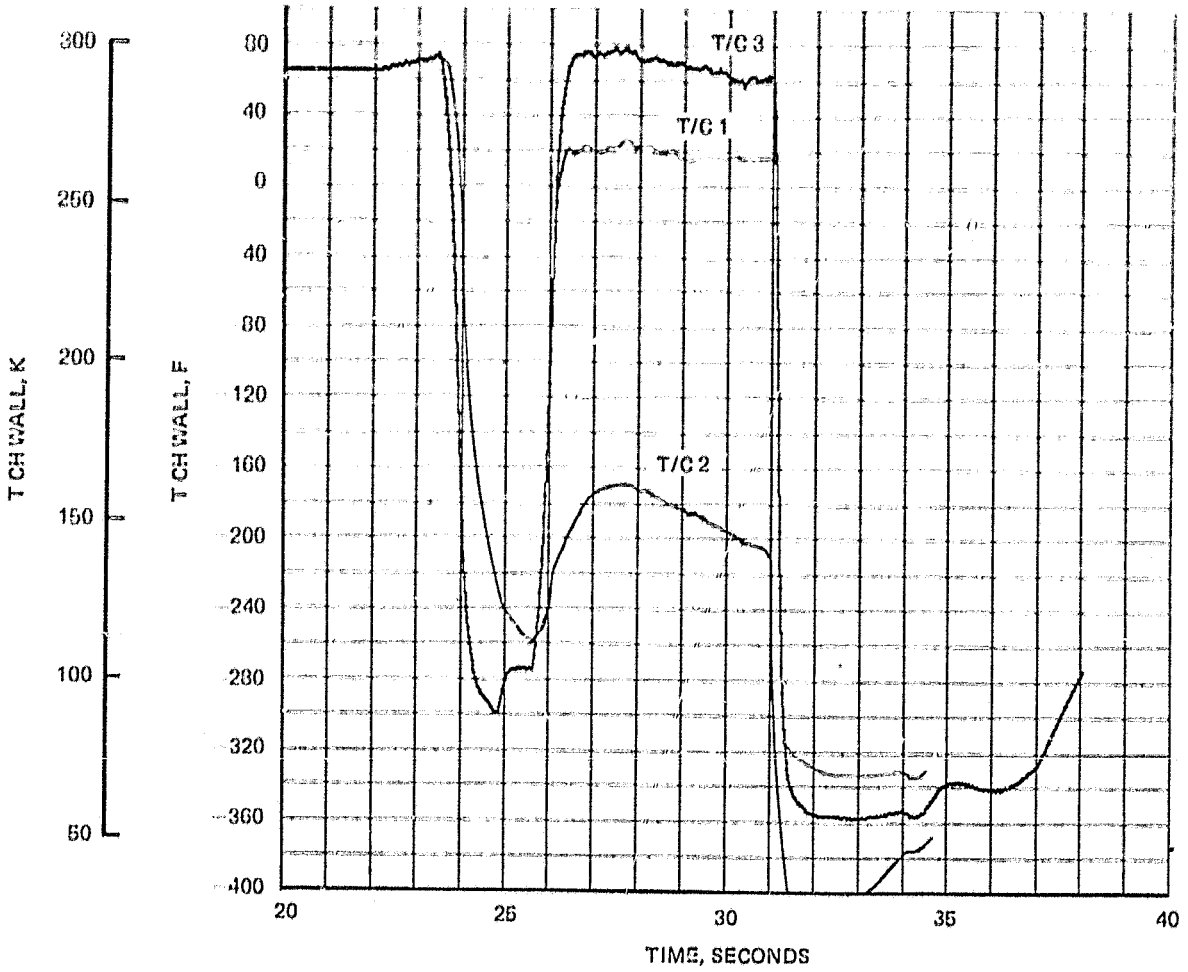

Figure 163. Typical Combustion Chamber Rib Temperature Histories (Test 021)

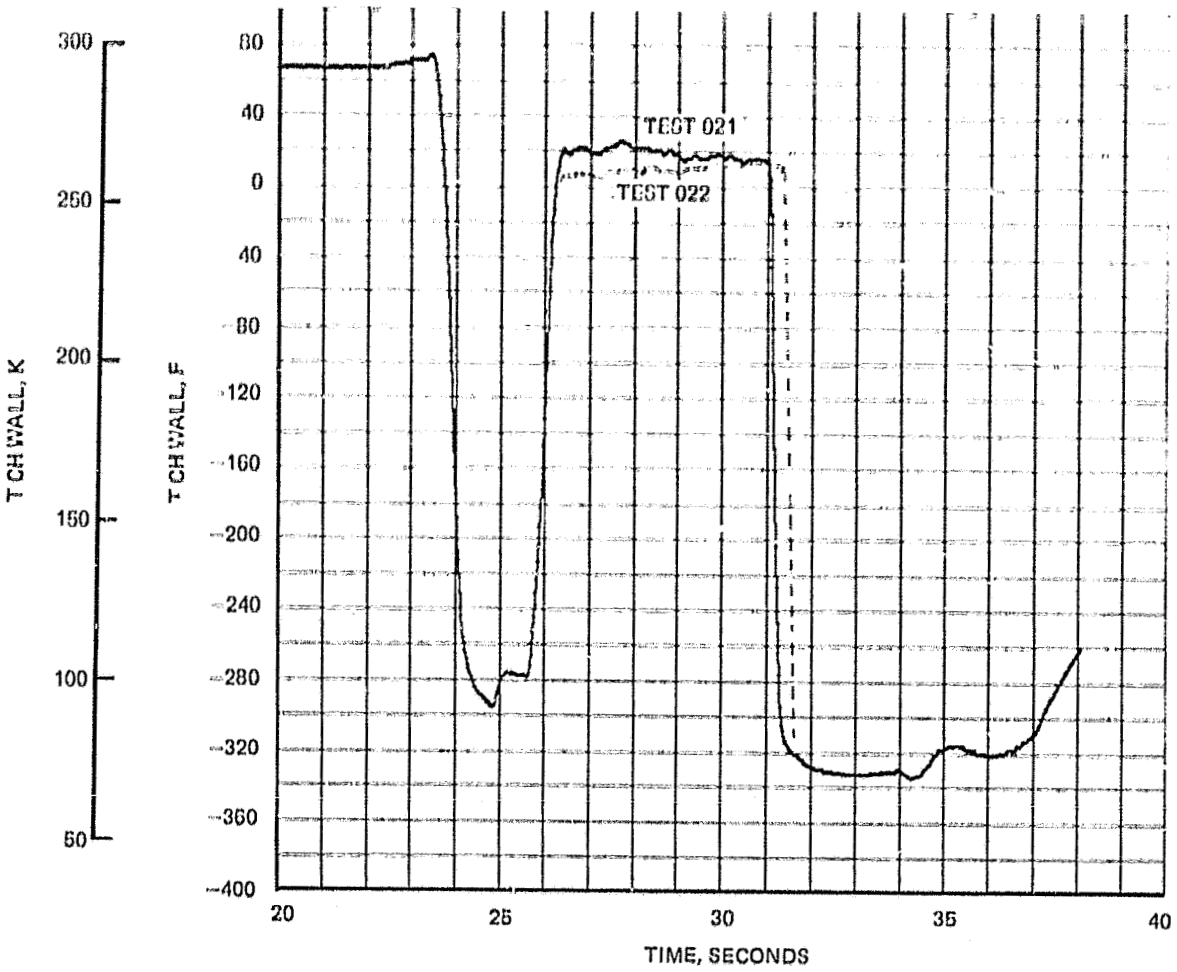

Figure 164. Combustion Region Thermocouple No. 1 Temperature Histories

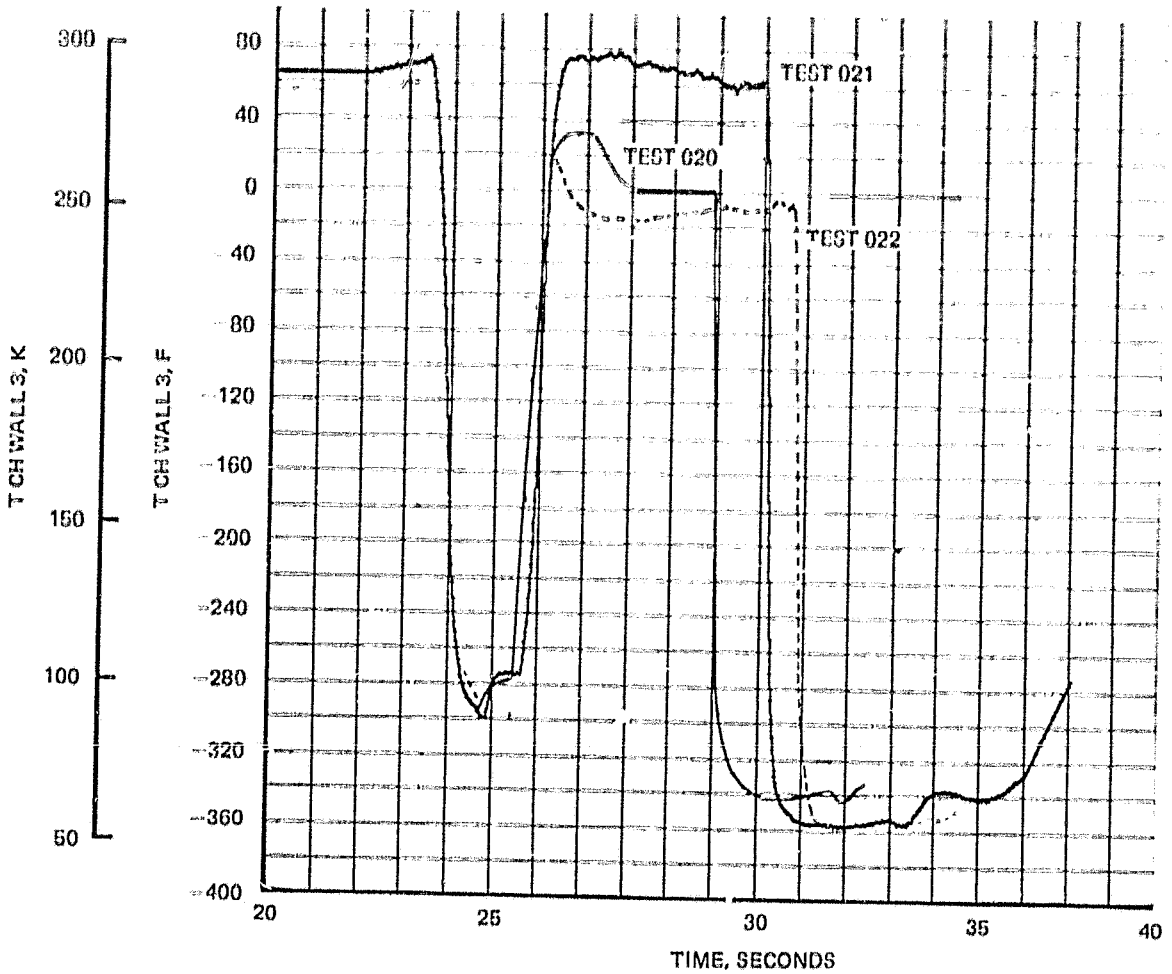

Figure 165. Combustion Chamber Thermocouple No. 3 Temperature Histories

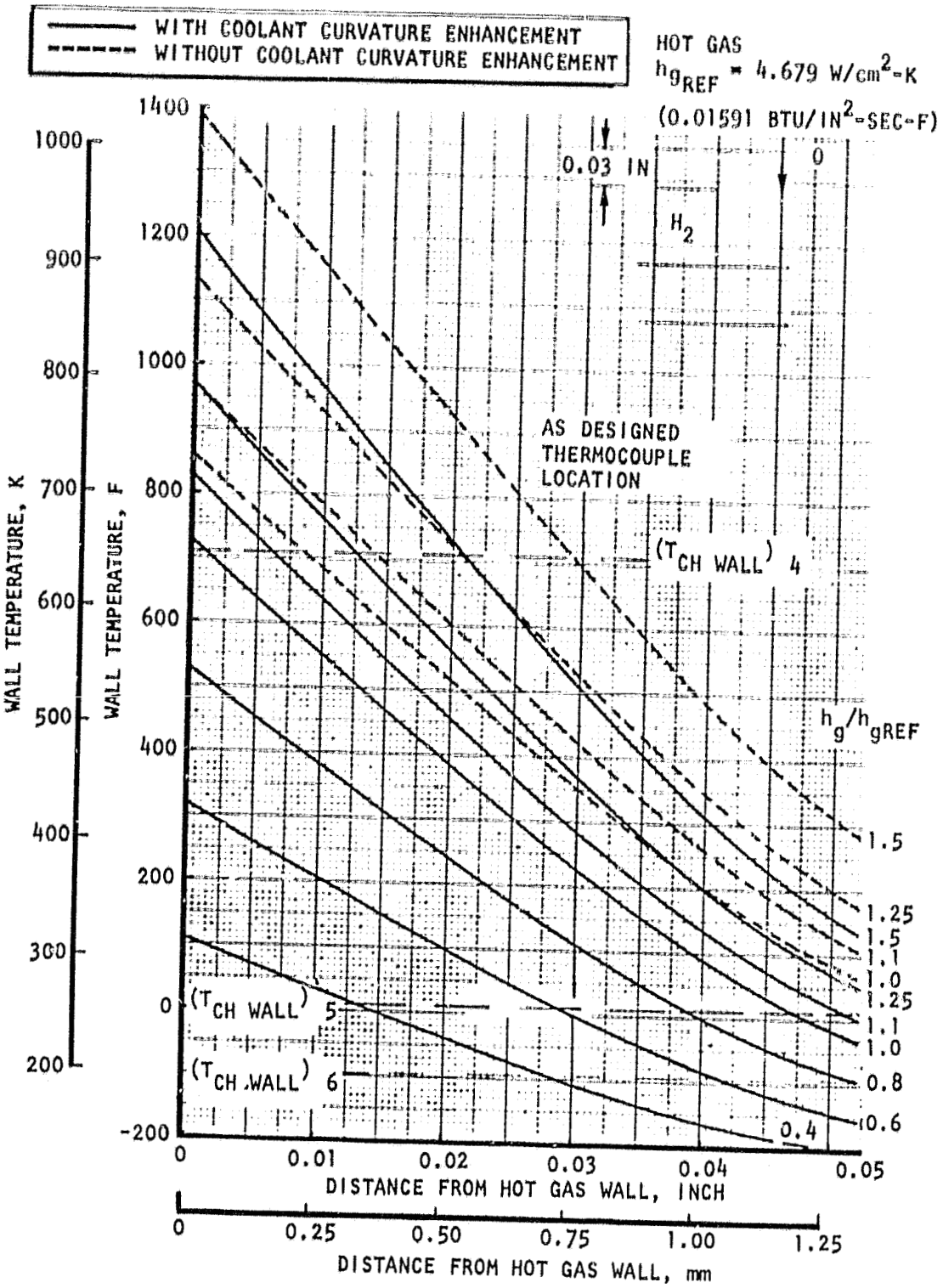

Figure 166. Wall Temperature Variation With Thermocouple Location and Film Coefficient Ratio for Throat Location (Test 021)

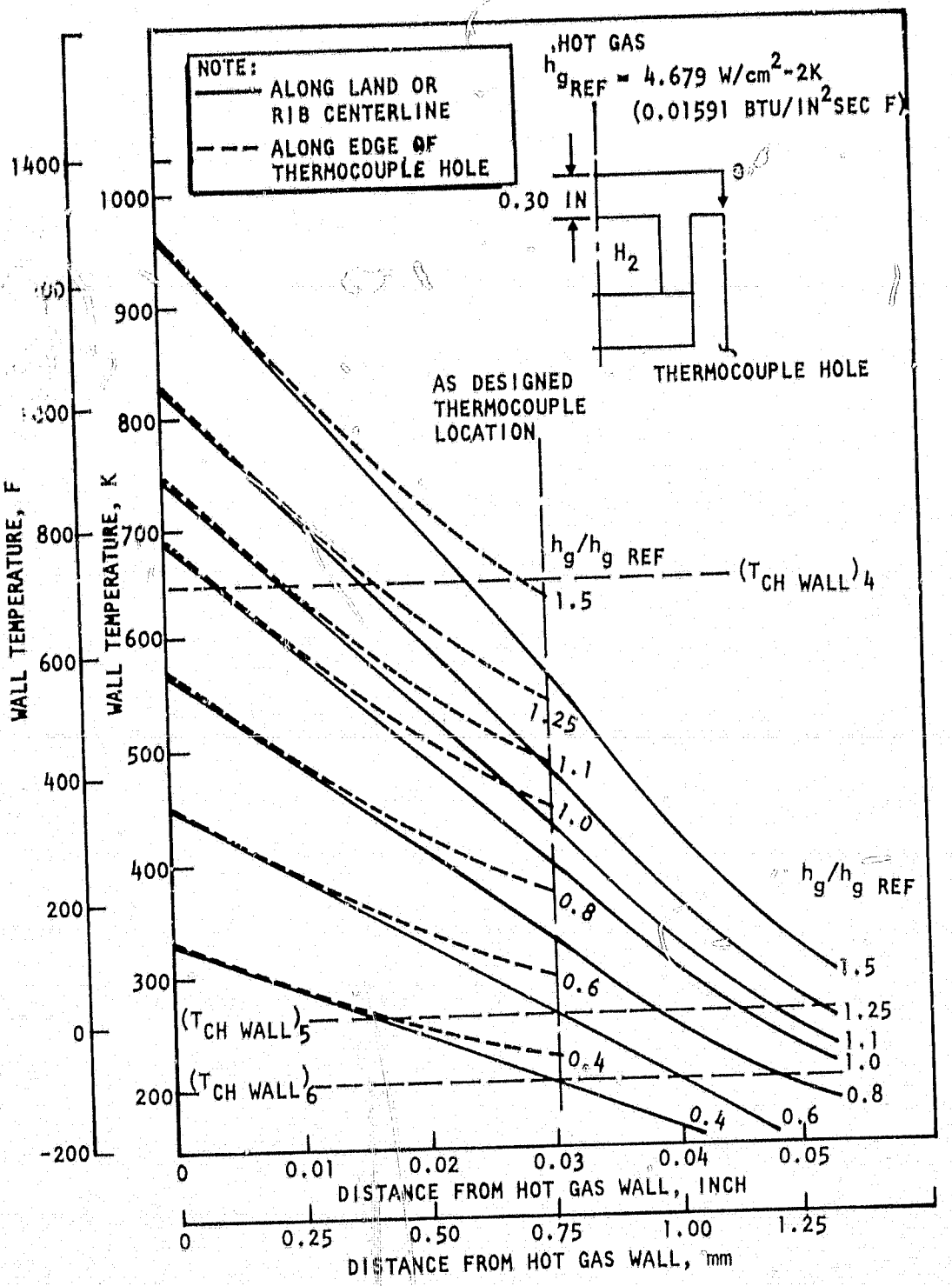

Figure 167. Wall Temperature Variation With Thermocouple Location and Film Coefficient Ratio for Throat Location With Thermocouple Hole (Test 021)

C-4

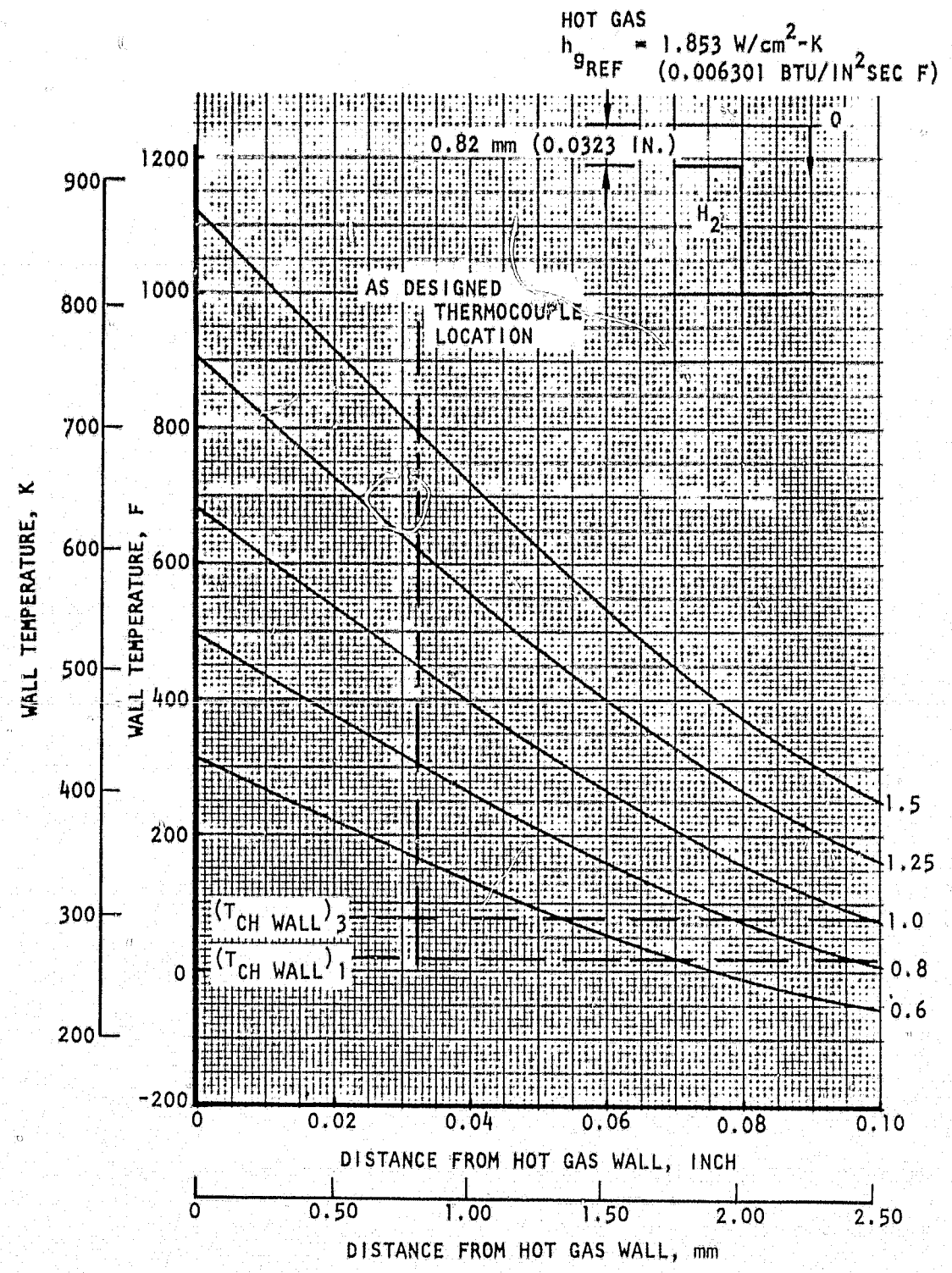

Figure 168. Wall Temperature Variation With Thermocouple Location and Film Coefficient Ratio for Combustion Chamber Location (Test 021)

The analysis of the measured throat rib temperatures result in the following possibilities:

1. With the thermocouples located 0.76 mm (0.03 inch) from the hot-gas wall, the gas-side heat transfer coefficient at the throat varied from 0.4 to greater than 2.0 times the design ratioed reference value. This would indicate a factor of 5 variation in heat flux.

2. Thermocouple No. 5 is located closer to hot-gas wall than thermocouple No. 6 and the gas-side heat transfer is a constant value of approximately 1.1 times the reference value.

3. The high measured value of thermocouple No. 4 is the result of a hot-gas leak and thermocouple No. 5 and 6 are correct. Depending on the thermocouple distance from the hot-gas wall, the gas-side heat transfer coefficient is 0.4 to 1.0 times the reference value.

4. A combination of one or more of the above is possible.

The analysis of the combustion chamber rib temperatures results in the following possibilities:

1. Thermocouple No. 2 had excessive contact resistance and read lower than the actual value.

2. Thermocouples No. 1 and 3 are correct and are located quite far, 2.5 to 3.0 mm (0.10 to 0.12 inch) from the hot-gas wall.

3. Assuming the thermocouples are located 0.82 mm (0.032 inch) from the hot-gas wall, the gas-side heat transfer coefficient would be 0.4 of the reference value.

4. Assuming the gas-side heat transfer is constant, the location of the thermocouple varies from 0.13 mm (0.005 inch) to greater than 2.5 mm (0.1 inch).

5. A combination of one or more of the above is possible.

The Preburner of Staged Combustion Rocket Engine program was conducted to establish the design, to demonstrate the thermal and combustion performance capability of a high chamber pressure preburner, and to combine this with a previously demonstrated 89 000 N (20 000 pound) thrust chamber assembly to test and demonstrate the overall thermal and combustion performance of the staged combustion system. The preburner design points are shown in Table 40 and the thrust chamber operating conditions are shown in Table 41. Analytical studies were conducted to evaluate the preburner injector, combustor, and hot-gas duct temperatures; main injector, chamber and nozzle heat transfer rate, structural and cyclic life features, and combustion performance and stability characteristics were reviewed for compatibility with the preburner gases. In conjunction with these studies, component designs for the injector, combustion chamber, regeneratively cooled nozzle, and dump-cooled nozzle extension were developed. The injector was redesigned to utilize the preburner gases for the fuel while the regeneratively cooled chamber and nozzle section used liquid hydrogen at approximately 50 K (90 R) inlet temperature for coolant.

The preburner assembly (Fig. 169) was designed for liquid oxygen and gaseous hydrogen from the main chamber and nozzle coolant jackets as the propellants. A single preburner is used with the staged combustion assembly and the hot-gas flow branches through two ducts to supply the oxidizer and fuel pump turbines individually (Fig. 170).

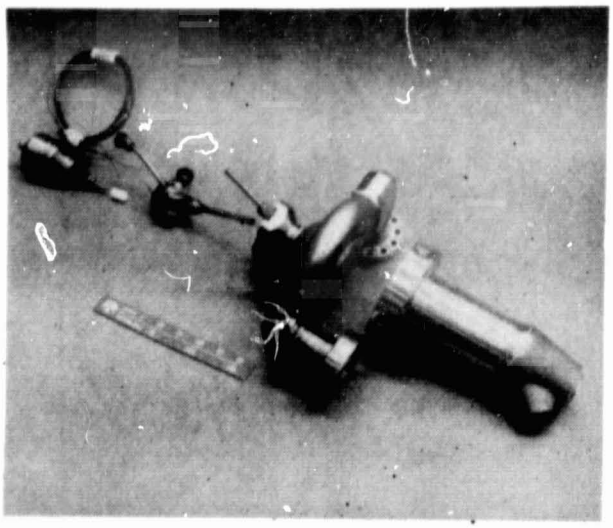

1HS32-5/5/76-C1A*

Figure 169. Preburner Combustor, Injector and Igniter Prior to Assembly

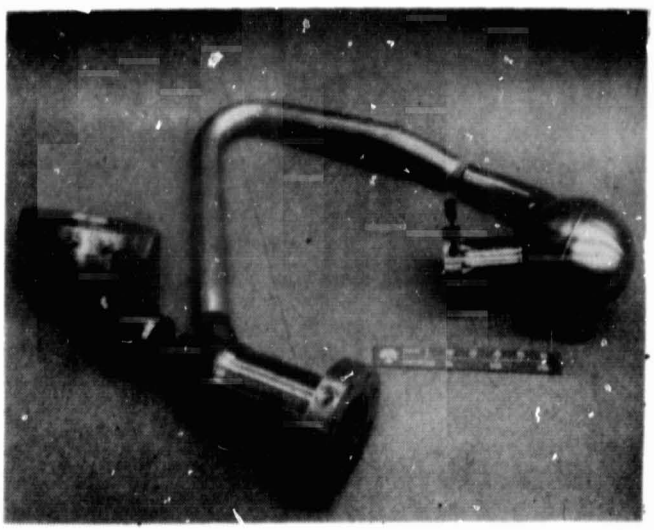

1HS32-4/30/76-C1B*

Figure 170. Preburner Combustor With Simulators and Exhaust Turbine Gas Ducting

TABLE 40. PREBURNER OPERATING CONDITIONS

Chamber Pressure, N/cm^2a (psia)	2328	(3377)
Combustion Temperature, K (R)	1053	(1896)
Mixture Ratio, o/f	0.82	
Total Flowrate, kg/sec (lb/sec)	4.16	(9.18)
Fuel Inlet Temperature, K (R)	239	(431)
Oxidizer Inlet Temperature, K (R)	91	(163)

TABLE 41. THRUST CHAMBER OPERATING CONDITIONS

	Nominal Design Point
Thrust, Newtons (pounds)	88 900 (20 000)
Chamber Pressure, N/cm^2a (psia)	1380 (2000)
Mixture Ratio (overall), o/f	6.0
Nozzle Expansion Ratio	
Regeneratively Cooled	175:1
Uncooled	400:1
Propellant Inlet Temperature, K (R)	
Hydrogen	
To Injector	~278 (~500)
To Chamber	~50 (~90)
Oxygen	78 (140)
Propellant Inlet Pressure	
Hydrogen	TBD
Oxygen	TBD
Energy Release Efficiency (ERE), %	98

The main propellant injector, (Fig. 171) features concentric injector elements, hydrogen-cooled Rigimesh face, and convenient disassembly from the combustion chamber.

The design parameters for this injector were obtained by extrapolating injection element features from other LOX hydrogen injectors (Fig. 172).

The combustion chamber assembly was a channel wall regeneratively cooled zirconium copper alloy assembly with an electroformed nickel closeout. This chamber was designed and fabricated as part of the Advanced Thrust Chamber Technology Program.

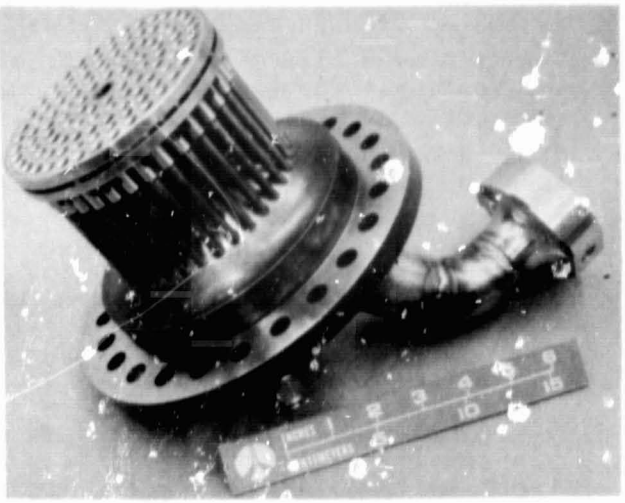

1HS42-2/10/76-C1C*

Figure 171. Injector No. 2

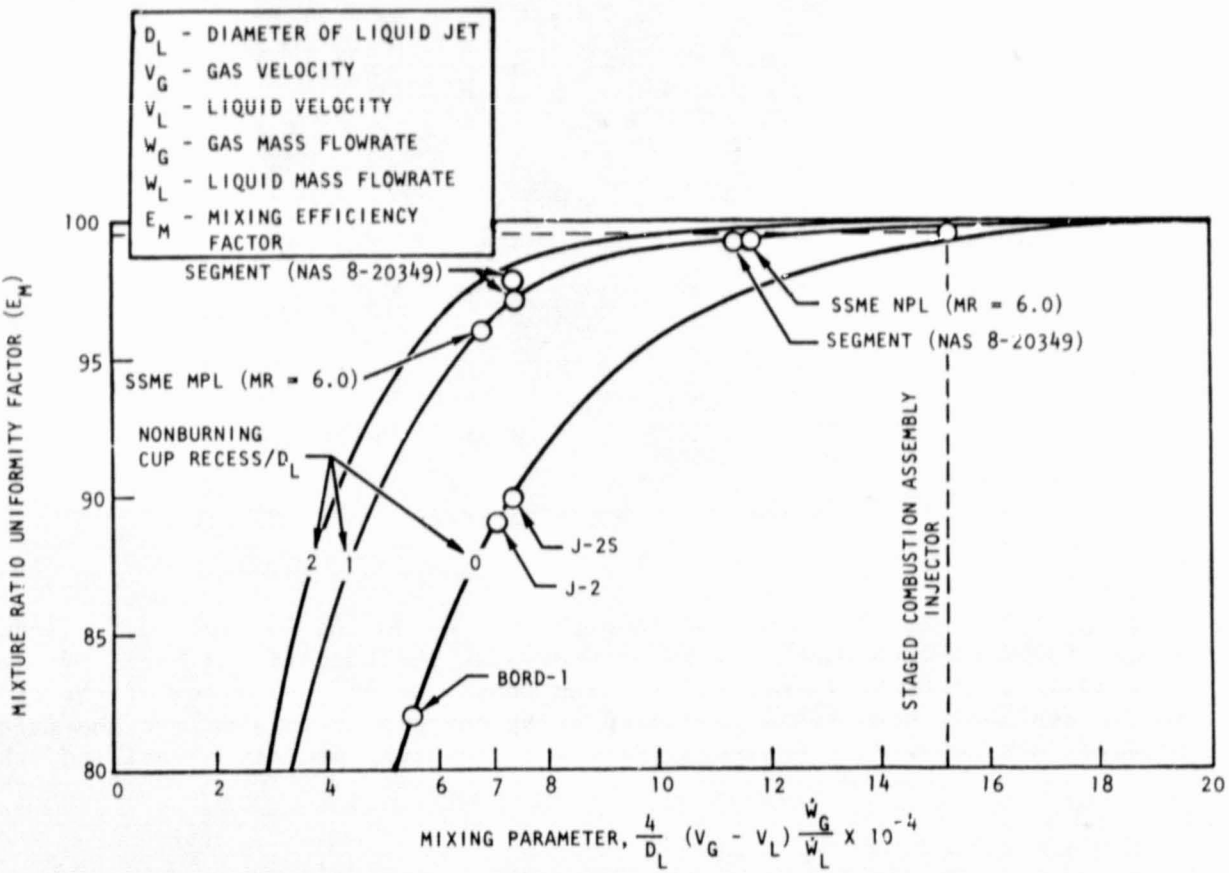

Figure 172. Injector Mixing Efficiency Comparison

The 175:1 expansion area ratio, regeneratively cooled tubular nozzle shown assembled with the combustion chamber (Fig. 173) and a 400:1 expansion area ratio, heavy-wall, mild-steel uncooled nozzle completed the major subassemblies for testing. The regeneratively cooled nozzle which was fabricated as part of the Advanced Thrust Chamber Program used A-286 tapered and formed circular cross-section tubes. The uncooled steel nozzle was fabricated by NASA and supplied to Rocketdyne for this testing.

1XZ21-11/30/77-C1E*

Figure 173. Regeneratively Cooled Nozzle

Testing of the staged combustion assembly was conducted in orderly "building block" fashion, with each test phase providing the support and basis for the succeeding test effort. Initial testing consisted of evaluation of the preburner assembly, with tests conducted using components to simulate the main injector and combustion chamber. With the preburner operation verified, the

main injector and liquid hydrogen cooled combustion chamber were added for testing (Fig. 174). From these tests a combustion efficiency (c*) of 99% for the main injector was first established, and an overall heat flux of 5350 kW (5075 Btu/sec), very close to the predicted heat flux, was measured. Subsequent testing of the staged combustion assembly with the regeneratively cooled and uncooled nozzle components was conducted within a diffuser/ejector (Fig. 175 and 176). Testing of this assembly provided the first performance results with a 400:1 area ratio nozzle (Table 42), demonstrating that the performance goal of 4610 N-s/kg (470 seconds) could be readily achieved with the higher area ratio (400:1) nozzle, while the heat flux to the nozzle (4100 kW (3900 Btu/sec)) was close to the design value (Table 43).

Testing of the 400:1 nozzle with the heated GN_2 driven ejector/diffuser system were successful and full flow in the nozzle was realized on all steady-state duration tests. Heat transfer rates during start and shutdown transients were high, but there was no damage to the regeneratively cooled nozzle tubes because excessive coolant flow was used on all tests. Performance analysis showed that system specific impulse was 4688 N-sec/kg (478 seconds) (Fig. 176).

The fabrication and test programs demonstrated the feasibility of the staged combustion assembly concept as a lightweight, high-performance combustion system suitable for orbital transfer vehicle application. The diffuser/ejector assembly was able to provide the reduced backpressure required to obtain nozzle starting with heated GN_2 supplied to the ejector. Thermal and performance characteristics of the thrust chamber were very close to the theoretically predicted characteristics, thus indicating that the analytical methods utilized are valid in this application.

From the results of the fabrication and testing effort the following conclusions have been made:

- Injector characteristics of main injector for high performance (η_{c*}) = 99%) were demonstrated.
- Fabrication and assembly techniques for small high-performance engines were established.
- A specific impulse of 4688 N-s/kg (478 seconds) is obtainable.
- Altitude testing techniques for high area ratio nozzles using heated nitrogen gas to drive an ejector system have been demonstrated.
- Nozzle heat transfer rates and gas-side film coefficients during separated flow have been measured.
- Preburner hot-gas efflux can be generated which can safely drive the turbopumps for the advanced space engine.
- High area ratio nozzle boundary layer pressure and temperature rakes have been successfully demonstrated and boundary layer drop of 2.0 $\pm$0.25% has been determined.

1HS23-10/15/76-S1C*

Figure 174. Stage Combustion Assembly on NAA Stand

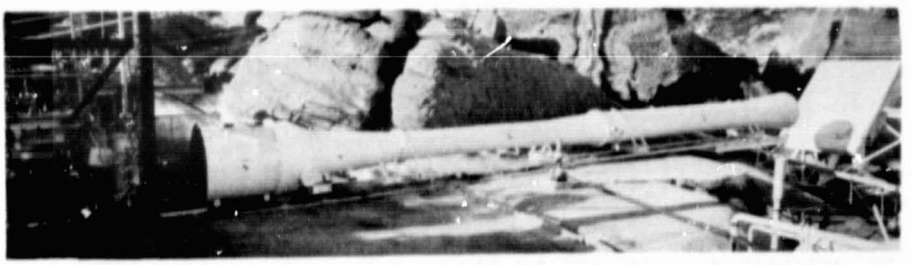

1HS34-11/17/75-S1B*

Figure 175. Altitude Test Facility

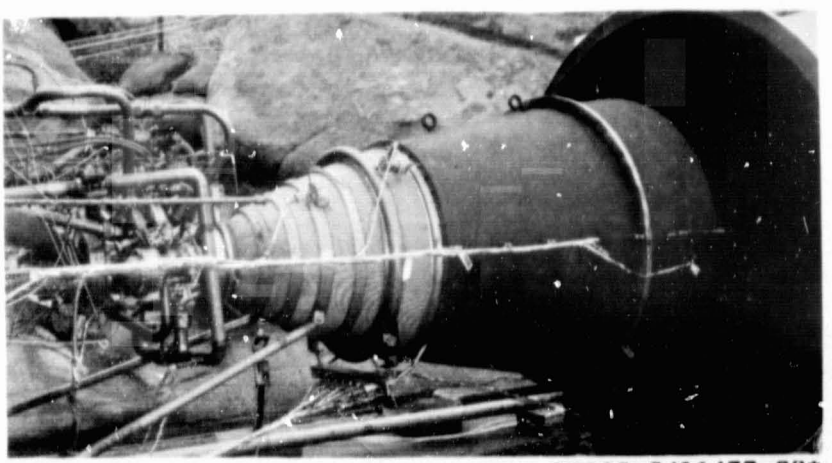

1HS35-5/16/77-S2*

Figure 176. Staged Combustion Assembly and 400:1 Nozzle Assembly on Nan Stand

TABLE 42. TEST RESULTS SUMMARY FOR 400:1 NOZZLE TESTING

Test No.	Preburner			Chamber					
	Chamber Pressure, N/cm^2a (psia)	Mixture Ratio (o/f)	Duration, seconds	Pressure (Injector End), N/cm^2a (psia)	Mixture Ratio (o/f)	Duration, seconds	c*		Specific Impulse, N·s/kg (seconds)
							m/s (ft/sec)	%	
015	2257.1 (3272.5)	0.553	3.1	1557.1 (2258.3)	6.084	2.15	2322 (7618)	98.8	4665 (475.7)
016	2279.8 (3306.4)	0.538	3.6	1570.2 (2277.3)	5.954	2.65	2344 (7689)	99.3	4708 (480.1)
017	2300.6 (3336.6)	0.595	3.8	1573.7 (2282.4)	6.428	2.80	2309 (7577)	99.4	4695 (478.7)
020	2254.4 (3269.7)	0.530	5.0	1541.4 (2235.5)	5.751	4.0	2368 (7769)	99.7	4723 (481.6)
021	2301.3 (3337.6)	0.596	6.0	1576.6 (2286.6)	6.378	5.0	2311 (7581)	99.3	4694 (478.6)
022	2248.5 (3261.0)	0.564	6.2	1582.8 (2217.3)	5.920	5.2	2328 (7637)	98.5	4699 (479.1)

TABLE 43. REGENERATIVELY COOLED NOZZLE HEAT TRANSFER

Test No.	Chamber Pressure, N/cm^2 a (psia)	Mixture Ratio (o/f)	Coolant				
			Flowrate, kg/s (lb/sec)	Inlet Temperature, K (F)	ΔT, K (F)	Heat Transfer Rate, kW	Heat Transfer Rate Normalized to 1380 N/cm^2, kW
015	1557.1 (2258.3)	6.084	2.795 (6.161)	55.3 (-360.4)	129 (233)	5923	5401
016	1570.2 (2277.3)	5.954	2.504 (5.520)	53.4 (-363.9)	141 (254)	5800	5253
017	1573.7 (2282.4)	6.428	2.395 (5.280)	51.5 (-367.3)	149 (268)	5827	5267
020	1541.4 (2235.5)	5.751	2.382 (5.251)	178.3 (-139.1)	106 (191)	5028	3702
021	1576.6 (2286.6)	6.378	2.262 (4.986)	186.2 (-124.9)	119 (215)	4242	3829
022	1528.8 (2217.3)	5.920	2.211 (4.874)	182.8 (-130.9)	115 (207)	4027	3726

REFERENCES

1. R76-116, Advanced Thrust Chamber Technology, Final Report, NASA CR-135221, Contract NAS3-17825, Rocketdyne Division, Rockwell International, Canoga Park, California, July 1977.

2. Sutton, R.D., M.D. Schuman, and W.D. Chadwich: Operating Manual for Coaxial Injection Combustion Model, Final Report, NASA CR-129031, Contract NAS8-29664, Rocketdyne Division, Rockwell International, Canoga Park, California, April 1974.

3. Rupe, J.H.: The Liquid Mixing of a Pair of Impinging Streams, Progress Report 20-195, JPL, Pasadena, California, August 1953.

4. Coultas, T.A., and R.C. Kesselring: "Extension of the Priem Theory and Its Use in Simulation of Instability on the Computer," CPIA Publication No. 105, May 1966.

5. AFRPL-TR-72-25, O_2/H_2 Advanced Maneuvering Propulsion Technology Program; Water-Cooled Segment Testing, Final Report, Rocketdyne Division, Rockwell International, Canoga Park, California, April 1972.

6. McMillion, R.L., and J.A. Nestlerode: "Design Criterion for Acoustic Absorbers," CPIA Publication No. 220, Vol. I, November 1971.

7. Oberg, C.L., T.L. Wong, and W.M. Ford: Final Report: Evaluation of Acoustic Cavities for Combustion Stabilization, NASA CR-115087, Rocketdyne Division, Rockwell International, Canoga Park, California, July 1971.

8. R-8928P-1, Integrated Thruster Assembly Investigation, Rocketdyne Division, Rockwell International, Canoga Park, California, 3 April 1972.

9. R-9258, Advanced Hydrogen Oxygen Chamber Design Analysis, NASA CR-121213, Contract NAS3-16774, Rocketdyne Division, Rockwell International, Conoga Park, California, November 1973.

10. R-9269, Advanced Space Engine Preliminary Design, NASA CR-121236, Contract NAS3-16751, Rocketdyne Division, Rockwell International, Canoga Park, California, October 1973.